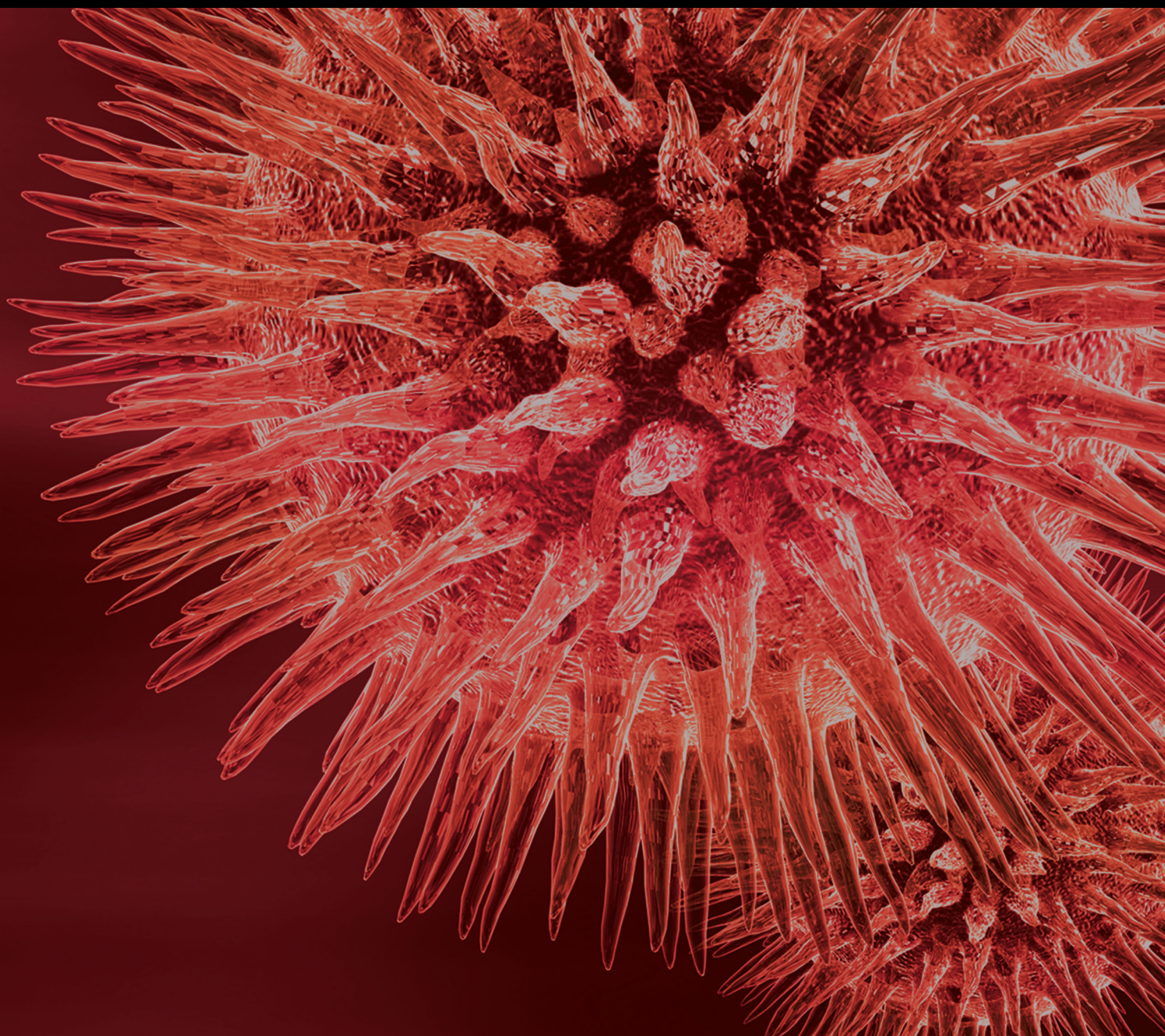


BioMed Research International

Cancer Diagnostic and Predictive Biomarkers 2018

Lead Guest Editor: Franco M. Buonaguro

Guest Editors: Patrizia Caposio, Maria L. Tornesello, Valli De Re, Renato Franco, and Massimo Tommasino






Cancer Diagnostic and Predictive Biomarkers 2018

BioMed Research International

Cancer Diagnostic and Predictive Biomarkers 2018

Lead Guest Editor: Franco M. Buonaguro

Guest Editors: Patrizia Caposio, Maria Lina Tornesello,
Valli De Re, and Renato Franco






Copyright © 2019 Hindawi. All rights reserved.







This is a special issue published in “BioMed Research International.” All articles are open access articles distributed under the Creative Commons Attribution License, which permits unrestricted use, distribution, and reproduction in any medium, provided the original work is properly cited.

Contents



Cancer Diagnostic and Predictive Biomarkers 2018

Franco M. Buonaguro , Patrizia Caposio, Maria Lina Tornesello , Valli De Re, and Renato Franco 
Editorial (3 pages), Article ID 3879015, Volume 2019 (2019)

Effect of Neoadjuvant Hormone Therapy on Resection Margin and Survival Prognoses in Locally Advanced Prostate Cancer after Prostatectomy Using Propensity-Score Matching

Sung Han Kim , Eun Young Park, Jungnam Joo , Jae Young Joung , Ho Kyung Seo ,
Jinsoo Chung , and Kang Hyun Lee 
Research Article (7 pages), Article ID 4307207, Volume 2018 (2019)




Gene Expression Profile Signature of Aggressive Waldenström Macroglobulinemia with Chromosome 6q Deletion

Naohiro Sekiguchi , Junko Nomoto, Akihisa Nagata, Masahiro Kiyota, Ichiro Fukuda, Kazuaki Yamada,
Naoki Takezako, and Yukio Kobayashi 
Research Article (8 pages), Article ID 6728128, Volume 2018 (2019)

A Bioinformatic Profile of Gene Expression of Colorectal Carcinoma Derived Organoids

Peng A , Xinyi Xu, Chenglin Wang, Ling Ye, and Jing Yang 
Research Article (12 pages), Article ID 2594076, Volume 2018 (2019)




Efficient Synthesis of Glutamate Peptide-Estradiol Conjugate for Imaging Estrogen Receptor-Positive Diseases

Ming-Chi Shih , Sergio Daniel Simon, Zhiming Jin, Yuan Gui, Bohua Xu, Zhihong Xu,
Paulo Henrique Rosado-de-Castro , Ana Maria Silveira Braghirolli, Lea Mirian Barbosa da Fonseca ,
Tomio Inoue, and David J. Yang 
Research Article (14 pages), Article ID 5208964, Volume 2018 (2019)



CT Perfusion in Patients with Lung Cancer: Squamous Cell Carcinoma and Adenocarcinoma Show a Different Blood Flow

Alessandro Bevilacqua , Giampaolo Gavelli, Serena Baiocco, and Domenico Barone
Research Article (10 pages), Article ID 6942131, Volume 2018 (2019)




PAX3: A Molecule with Oncogenic or Tumor Suppressor Function Is Involved in Cancer

Ashok Arasu, Sengottuvelan Murugan, Musthafa Mohamed Essa , Thirunavukkarasu Velusamy ,
and Gilles J. Guillemin 
Review Article (12 pages), Article ID 1095459, Volume 2018 (2019)

Rectal Cancer: Redox State of Venous Blood and Tissues of Blood Vessels from Electron Paramagnetic Resonance and Its Correlation with the Five-Year Survival

A. P. Burlaka , A. V. Vovk, A. A. Burlaka, M. R. Gafurov , K. B. Iskhakova, and S. N. Lukin
Research Article (7 pages), Article ID 4848652, Volume 2018 (2019)

Histogram Analysis of Perfusion Parameters from Dynamic Contrast-Enhanced MR Imaging with Tumor Characteristics and Therapeutic Response in Locally Advanced Rectal Cancer

Dong Myung Yeo , Soon Nam Oh , Moon Hyung Choi, Sung Hak Lee, Myung Ah Lee,
and Seung Eun Jung 
Research Article (9 pages), Article ID 3724393, Volume 2018 (2019)

Bioinformatics Analysis Reveals Most Prominent Gene Candidates to Distinguish Colorectal Adenoma from Adenocarcinoma

Nina Hauptman , Emanuela Boštjančič , Margareta Žljapah, Branislava Ranković, and Nina Zidar



Research Article (10 pages), Article ID 9416515, Volume 2018 (2019)

Plasma Chemokine CCL2 and Its Receptor CCR2 Concentrations as Diagnostic Biomarkers for Breast Cancer Patients

Emilia Lubowicka , Andrzej Przyłipiak, Monika Zajkowska , Barbara Maria Piskór, Paweł Malinowski, Wojciech Fiedorowicz, and Sławomir Ławicki

Research Article (9 pages), Article ID 2124390, Volume 2018 (2019)

Mutational Profile of Metastatic Breast Cancer Tissue in Patients Treated with Exemestane Plus Everolimus

Claudia Omarini , Maria Elisabetta Filieri, Stefania Bettelli, Samantha Manfredini, Shaniko Kaleci, Cecilia Caprera, Cecilia Nasso, Monica Barbolini, Giorgia Guaitoli, Luca Moschetti, Antonino Maiorana, Pier Franco Conte, Stefano Cascinu, and Federico Piacentini 

Research Article (8 pages), Article ID 3756981, Volume 2018 (2019)

The Thomsen-Friedenreich Antigen-Specific Antibody Signatures in Patients with Breast Cancer

Oleg Kurtenkov , Kaire Innos, Boris Sergejev, and Kersti Klaamas 

Research Article (8 pages), Article ID 9579828, Volume 2018 (2019)

Targeting CD36 as Biomarker for Metastasis Prognostic: How Far from Translation into Clinical Practice?

Ana-Maria Enciu , Eugen Radu , Ionela Daniela Popescu , Mihail Eugen Hinescu , and Laura Cristina Ceafalan 

Review Article (12 pages), Article ID 7801202, Volume 2018 (2019)

Mutational Analysis of Oncogenic AKT1 Gene Associated with Breast Cancer Risk in the High Altitude Ecuadorian Mestizo Population

Andrés López-Cortés , Paola E. Leone , Byron Freire-Paspuel, Nathaly Arcos-Villacís, Patricia Guevara-Ramírez , Felipe Rosales, and César Paz-y-Miño 



Research Article (10 pages), Article ID 7463832, Volume 2018 (2019)

Clinically Correlated MicroRNAs in the Diagnosis of Non-Small Cell Lung Cancer: A Systematic Review and Meta-Analysis

Min Jiang , Xuelian Li, Xiaowei Quan , Xiaoying Li , and Baosen Zhou 








Review Article (14 pages), Article ID 5930951, Volume 2018 (2019)

Cystathionine β -Synthase in Physiology and Cancer

Haoran Zhu, Shaun Blake, Keefe T. Chan, Richard B. Pearson , and Jian Kang 


Review Article (11 pages), Article ID 3205125, Volume 2018 (2019)

PATRI, a Genomics Data Integration Tool for Biomarker Discovery

G. Ukmar , G. E. M. Melloni , L. Radrizzani , P. Rossi, S. Di Bella , M. R. Pirchio, M. Vescovi, A. Leone, M. Callari , M. Cesarini, A. Somaschini, G. Della Vedova , M. G. Daidone, M. Pettenella, A. Isacchi, and R. Bosotti 

Research Article (13 pages), Article ID 2012078, Volume 2018 (2019)

Alkaline Phosphatase Kinetics Predict Metastasis among Prostate Cancer Patients Who Experience Relapse following Radical Prostatectomy

Carolyn A. Salter, Jennifer Cullen , Claire Kuo, Yongmei Chen, Lauren Hurwitz, Adam R. Metwalli, Jordan Dimitrakoff, and Inger L. Rosner


Research Article (7 pages), Article ID 4727089, Volume 2018 (2019)

HSP90: A Novel Target Gene of miRNA-628-3p in A549 Cells

Jieli Pan, Fusheng Jiang , Jia Zhou, Dehong Wu, Zhenhua Sheng, and Meiya Li 

Research Article (10 pages), Article ID 4149707, Volume 2018 (2019)

A Predictive Model to Determine the Pattern of Nodal Metastasis in Oral Squamous Cell Carcinoma

B. S. M. S. Siriwardena , I. K. Rambukewela, T. N. Pitakotuwaage, M. N. G. P. K. Udagama, P. V. R. Kumarasiri, and W. M. Tilakaratne


Research Article (7 pages), Article ID 8925818, Volume 2018 (2019)

A Comparative Study for Detection of EGFR Mutations in Plasma Cell-Free DNA in Korean Clinical Diagnostic Laboratories

Yoonjung Kim , Saeam Shin , and Kyung-A Lee 

Research Article (11 pages), Article ID 7392419, Volume 2018 (2019)

Mutational Profiling of Non-Small-Cell Lung Cancer Resistant to Osimertinib Using Next-Generation Sequencing in Chinese Patients

Keke Nie, Haiping Jiang, Chunling Zhang, Chuanxin Geng, Xiajuan Xu, Ling Zhang, Hao Zhang, Zhongfa Zhang, Ketao Lan, and Youxin Ji 

Research Article (6 pages), Article ID 9010353, Volume 2018 (2019)

Editorial

Cancer Diagnostic and Predictive Biomarkers 2018

Franco M. Buonaguro ¹, **Patrizia Caposio**,² **Maria Lina Tornesello** ¹,
Valli De Re,³ and **Renato Franco** ⁴

¹Unit of Molecular Biology and Viral Oncology, Department of Research, Istituto Nazionale Tumori IRCCS Fondazione Pascale, 80131 Napoli, Italy

²Vaccine and Gene Therapy Institute, Oregon Health & Science University, Beaverton, OR 97006, USA

³Immunopathology and Cancer Biomarkers/Bio-Proteomics Facility, Centro di Riferimento Oncologico, IRCCS, 33081 Aviano, Italy

⁴Division of Pathology, Department of Mental and Physical Health and Preventive Medicine, Università degli Studi della Campania “Luigi Vanvitelli”, 80131 Napoli, Italy

Correspondence should be addressed to Franco M. Buonaguro; fm.buonaguro@istitutotumori.na.it

Received 20 December 2018; Accepted 20 December 2018; Published 8 January 2019

Copyright © 2019 Franco M. Buonaguro et al. This is an open access article distributed under the Creative Commons Attribution License, which permits unrestricted use, distribution, and reproduction in any medium, provided the original work is properly cited.

Substantial advances have been achieved in the knowledge of the complex mechanisms regulating development and progression of human cancers. The employment of high throughput techniques allowed the identification of deregulated pathways and altered cellular molecules, including mutation signatures, noncoding RNAs, protein expression profiles, and metabolites, which have a significant impact in the early diagnosis, choice of treatment, and prediction of therapeutic response in many cancer types.

This special issue comprises relevant articles focused on the identification of innovative cancer biomarkers based on the analysis of genes containing driver somatic mutations, the quantitation of microRNAs expression levels, and the characterization of gene expression profiles in different types of cancer. Moreover, several authors investigated the efficacy of circulating biomarkers and molecular imaging techniques for noninvasive diagnosis of cancers.

C. Omarini et al. in Italy in the paper titled “Mutational Profile of Metastatic Breast Cancer Tissue in Patients Treated with Exemestane Plus Everolimus” investigated the mutational status of breast cancer biopsies in patients treated with Exemestane and Everolimus and observed that mutations affecting the PI3K/AKT/mTOR pathway were significantly associated with Everolimus resistance and disease relapse. K. Nie et al. in China in the paper titled “Mutational Profiling of Non-Small-Cell Lung Cancer Resistant to Osimertinib Using Next-Generation Sequencing in Chinese Patients”

performed a next-generation sequencing analysis in non-small-cell lung cancer (NSCLC) cases resistant to Osimertinib to identify somatic mutations and new therapeutic targets. The authors observed that EGFR C797S/G and EGFR T790M mutations were the most common in Osimertinib resistant NSCLC patients. A. López-Cortés et al. in Ecuador in the paper titled “Mutational Analysis of Oncogenic AKT1 Gene Associated with Breast Cancer Risk in the High Altitude Ecuadorian Mestizo Population” analyzed the distribution of polymorphic variants of the AKT1 gene in women of the Mestizo population affected by breast cancer and living at high altitudes. The authors found a possible association between the intronic variant rs3803304 GG and the risk of breast cancer in the Mestizo population.

A large number of short noncoding micro RNAs (miRNAs) have been shown to bind the 3'UTR of mRNAs and to selectively deregulate protein translation in many types of cancer. M. Jiang et al. in China in the paper titled “Clinically Correlated MicroRNAs in the Diagnosis of Non-Small Cell Lung Cancer: A Systematic Review and Meta-Analysis” performed a meta-analysis of 71 studies to evaluate the importance of miRNA levels in the diagnosis of NSCLC. They observed that multiple miRNAs have higher diagnostic value than single miRNA in all populations included in the study (Asian, Caucasian, and African populations). The authors concluded that some miRNAs, such as miR-21 and miR-210, could be used as diagnostic biomarkers for NSCLC.

J. Pan et al. in China in the paper titled “HSP90: A Novel Target Gene of miRNA-628-3p in A549 Cells” investigated the effect of miR-628-3p on migration and apoptosis of A549 cells. They performed in silico analysis to identify the heat shock protein 90a (HSP90) gene as target of the miR-628-3p in lung cancer. Then they confirmed by molecular studies that miR-628-3p promotes apoptosis and inhibits migration in A549 cells and concluded that miR-628-3p could be a novel strategy for lung cancer treatment.

The study of gene expression by microarray allows simultaneously comparing the transcription of thousands of genes in cancer versus normal tissues. N. Hauptman et al. in Slovenia in the paper titled “Bioinformatics Analysis Reveals Most Prominent Gene Candidates to Distinguish Colorectal Adenoma from Adenocarcinoma” performed an in silico study of gene expression datasets and identified biomarkers able to distinguish the colorectal adenoma, characterized by pseudoinvasion, from early adenocarcinomas. They identified 16 genes differentially expressed (COL12A1, COL1A2, COL3A1, DCN, PLAU, SPARC, SPON2, SPP1, SULF1, FADS1, G0S2, EPHA4, KIAA1324, LITDI, PCKS1, and C11orf96) which may be used to discriminate colorectal adenoma from carcinoma. Moreover, A. Peng et al. in the paper titled “A Bioinformatic Profile of Gene Expression of Colorectal Carcinoma Derived Organoids” compared the gene expression profiles of colorectal organoids with those of colorectal cancer biopsies obtained by publicly available datasets. They identified common alterations in WNT, MAPK, TGF- β , SHH, ECM-receptor interaction, and FGF pathways suggesting that organoids recapitulate original colon cancer tissues.

N. Sekiguchi et al. in Japan in the paper titled “Gene Expression Profile Signature of Aggressive Waldenström Macroglobulinemia with Chromosome 6q Deletion” performed a microarray analysis to investigate the differences in gene expression in the Waldenström macroglobulinemia with and without the chromosome 6q deletion. Their analysis suggested that the BCR signaling pathway and IL21R expression were activated in 6q del cases. Moreover, FOXP1 and CBLB were found to be positive regulators of the BCR pathway with consequences on the aggressiveness of the Waldenström macroglobulinemia with 6q del expression signature. G. Ukmar et al. in Italy in the paper titled “PATRI, a Genomics Data Integration Tool for Biomarker Discovery” developed a bioinformatics tool named “Platform for the Analysis of TRanslational Integrated data” (PATRI) conceived for the integration of clinical and genomics data. The PATRI workflow identifies statistically significant baseline genomics signatures, sensitive and resistant preclinical models, and then prediction of drugs treatment sensitivity in clinical samples.

Several studies have shown that specific biomarkers are released by cancer tissues in the body fluids, such as blood serum, thus reflecting the molecular spectrum of the tumor cells. Y. Kim et al. in Republic of Korea in the paper titled “A Comparative Study for Detection of EGFR Mutations in Plasma Cell-Free DNA in Korean Clinical Diagnostic Laboratories” performed a quality-assurance pilot study to harmonize the testing of circulating tumor DNA among laboratories. The authors observed that the cobas assay was

a useful method for detecting EGFR mutations in plasma circulating free DNA and that there is a need for each laboratory to optimize the performance to meet the clinical utility.

H. Zhu et al. in Australia in the paper titled “Cystathionine β -Synthase in Physiology and Cancer” reviewed recent literature on the physiological functions of cystathionine β -synthase, which plays multifunctional roles in the regulation of cellular energetics, redox status, DNA methylation, and protein modification in cancer cells. They discussed the possible use of cystathionine β -synthase and its key metabolites, such as homocysteine, as biomarkers for cancer diagnosis or therapeutic targets. E. Lubowicka et al. in Poland in the paper titled “Plasma Chemokine CCL2 and Its Receptor CCR2 Concentrations as Diagnostic Biomarkers for Breast Cancer Patients” evaluated the plasma levels of CCL2, CCR2, and tumor marker CA 15-3 in breast cancer patients and controls and their findings suggested that CCL2 and CCR2 may be used in the diagnosis of breast cancer in conjunction with CA 15-3. O. Kurtenkov et al. in Estonia in the paper titled “The Thomsen-Friedenreich Antigen-Specific Antibody Signatures in Patients with Breast Cancer” analyzed the serum samples of breast carcinoma patients for the levels of Thomsen-Friedenreich antigen-specific antibody isotypes considering that the serum total immunoglobulins glycosylation has been shown to have a diagnostic potential for some type of cancer. The authors demonstrated that the levels of anti-Thomsen-Friedenreich antigen antibodies, their sialylation profile, isotype distribution, and avidity displayed specific changes that could be used as noninvasive Ab-based biomarkers for early detection of breast cancer. A.-M. Enciu et al. in Romania in the paper titled “*Targeting CD36 as Biomarker for Metastasis Prognostic: How Far from Translation into Clinical Practice?*” in their review summarized many pieces of data to support the role of CD36 as a potential prognostic biomarker in cancer. CD36 is a scavenger receptor for fatty acid uptake which modulates cell-to-extracellular matrix attachment, stromal cell fate (for adipocytes, endothelial cells), TGF β activation, and immune signaling. It has been proposed as a prognostic marker in various cancers of epithelial origin. A. Arasu et al. in India in the paper titled “PAX3: A Molecule with Oncogenic or Tumor Suppressor Function Is Involved in Cancer” reviewed current literature on the activity of the transcription factor PAX3/Pax3, which contributes to diverse cell lineages during embryonic development and plays a major role in tumorigenesis. The authors highlighted the oncogenic and tumor suppressor role of PAX3 in different cancer types. C. A. Salter et al. in USA in the paper titled “Alkaline Phosphatase Kinetics Predict Metastasis among Prostate Cancer Patients Who Experience Relapse following Radical Prostatectomy” studied the alkaline phosphatase velocity in order to predict distant metastasis-free survival in a retrospective cohort of prostate cancer patients. They observed that rapid alkaline phosphatase velocity was a strong predictor of distant metastasis-free survival.

Predicting the cancer outcome from histological analysis may provide guidance for surgeons and oncologists on the appropriate treatment, particularly in developing countries.

B. S. M. S. Siriwardena et al. in Sri Lanka in the paper titled “A Predictive Model to Determine the Pattern of Nodal Metastasis in Oral Squamous Cell Carcinoma” have developed a histological prediction model to estimate the probability of developing metastasis in patients affected by oral cancer. They performed a multivariate analysis and observed that the level of differentiation, the pattern of invasion, and stage are the most important predictors of metastasis in oral cancer. S. H. Kim et al. in Republic of Korea in the paper titled “Effect of Neoadjuvant Hormone Therapy on Resection Margin and Survival Prognoses in Locally Advanced Prostate Cancer after Prostatectomy Using Propensity-Score Matching” investigated the effect of neoadjuvant hormone therapy on resection margin positivity, biochemical-recurrence-free survival, and overall survival in patients with locally advanced prostate cancer treated with radical prostatectomy using propensity-score matching. They concluded that neoadjuvant hormone therapy was not a significant factor for resection margin positivity in these patients.

Molecular imaging enables the *in vivo* visualization and quantification of biologic processes in normal tissues and cancers. M.-C. Shih et al. in Brazil in the paper titled “Efficient Synthesis of Glutamate Peptide-Estradiol Conjugate for Imaging Estrogen Receptor-Positive Diseases” used radiolabelled estrogen receptor ligand to quantify estrogen receptor tissue uptake for staging and restaging of cancers as well as endometriosis. The *in vivo* PET imaging studies indicated that ⁶⁸Ga-GAP-EDL could identify estrogen receptor positive tumors in MCF-7 tumor-bearing mice. A. P. Burlaka et al. in the paper titled “Rectal Cancer: Redox State of Venous Blood and Tissues of Blood Vessels from Electron Paramagnetic Resonance and Its Correlation with the Five-Year Survival” analyzed the redox state of venous blood and tissues in patients with rectal cancer by the spin-trapping electron paramagnetic resonance measuring the intensity of the signals from ceruloplasmin, transferrin, and labile iron pool. The results showed that the intensities of the signals from the “native” and “trapped” paramagnetic centres can be potentially used for the study of the rectal cancer molecular mechanisms. D. M. Yeo et al. in Republic of Korea in the paper titled “Histogram Analysis of Perfusion Parameters from Dynamic Contrast-Enhanced MR Imaging with Tumor Characteristics and Therapeutic Response in Locally Advanced Rectal Cancer” performed histogram analysis of perfusion parameters from dynamic contrast-enhanced magnetic resonance imaging (DCE-MRI) evaluating the entire tumor volume and correlated with EGFR expression, KRAS mutation, and therapy response to determine the overall tumor characteristics in rectal cancer. A. Bevilacqua et al. in Italy in the paper titled “CT Perfusion in Patients with Lung Cancer: Squamous Cell Carcinoma and Adenocarcinoma Show a Different Blood Flow” characterized the tumor baseline blood flow in two lung cancer subtypes, the adenocarcinoma and squamous cell carcinoma. They observed a different hemodynamic behaviour between adenocarcinoma and squamous cell carcinoma, suggesting that such parameter could be considered as a biomarker supporting treatment planning to select the patients that would benefit from antiangiogenic therapies.







Conflicts of Interest

The Guest Editors declare that there are no conflicts of interest regarding the publication of this special issue.

*Franco M. Buonaguro
Patrizia Caposio
Maria Lina Tornesello
Valli De Re
Renato Franco*

Research Article

Effect of Neoadjuvant Hormone Therapy on Resection Margin and Survival Prognoses in Locally Advanced Prostate Cancer after Prostatectomy Using Propensity-Score Matching

Sung Han Kim ¹, Eun Young Park,² Jungnam Joo ², Jae Young Joung ¹,
Ho Kyung Seo ¹, Jinsoo Chung ¹ and Kang Hyun Lee ¹

¹Department of Urology, Center for Prostate Cancer, Research Institute and Hospital of National Cancer Center, Goyang, Republic of Korea

²Biometrics Research Branch, Division of Cancer Epidemiology and Prevention, Research Institute and Hospital of National Cancer Center, Goyang, Republic of Korea

Correspondence should be addressed to Kang Hyun Lee; uroonco@ncc.re.kr

Received 14 February 2018; Accepted 13 November 2018; Published 6 December 2018

Guest Editor: Franco M. Buonaguro

Copyright © 2018 Sung Han Kim et al. This is an open access article distributed under the Creative Commons Attribution License, which permits unrestricted use, distribution, and reproduction in any medium, provided the original work is properly cited.

This study aimed to investigate the effect of neoadjuvant hormone therapy (NHT) on resection margin positivity, biochemical-recurrence- (BCR-) free survival, and overall survival (OS) in 176 patients with locally advanced prostate cancer (LAPC) treated with radical prostatectomy using propensity-score matching, including 79 (44.9%) patients treated with the NHT. Fifty pairs of one-to-one propensity-score matching were matched to investigate the pure effect of NHT on resection margin positivity, BCR, and OS with a statistical significance of $p < 0.050$. Before matching, NHT, tumor volume percentage, and extracapsular extension were significant factors for resection margin positivity ($p \leq 0.001$); however, after matching, NHT became insignificant in the multivariate analysis ($p = 0.084$). In the survival analysis, NHT was not associated with BCR or OS before and after matching (BCR: hazard ratio, 1.35 and 0.84, respectively; OS: hazard ratio, 1.05 and 0.77, respectively; $p \geq 0.539$ for all). Conversely, PSA level (HR, 2.23), extracapsular extension (HR, 2.10), and lymphovascular invasion (HR, 1.85) were significant factors for BCR ($p \leq 0.001$ for all), but none were significant factors for OS in the propensity-score matching analysis ($p \geq 0.948$). Therefore, NHT was not a significant factor for resection margin positivity, BCR-free survival, and OS before and after propensity-score matching in patients with LAPC.

1. Introduction

Prostate cancer (PC) results from an androgen-dependent tumor in males. The androgen-producing mechanism is a key therapeutic objective in the treatment of PC. In 1964, Scott and colleagues introduced the idea of encouraging recurrence-free survival in men with advanced PC by treating with radical prostatectomy (RP) and androgen deprivation therapy or androgen blocking hormonal therapy (HT). Presently, HT is one of the standard therapeutic options for PC in order to inhibit the growth of PC, especially for recurrent PC after prostatectomy or advanced PC [1].

The rationale for using HT in the neoadjuvant setting (NHT) is to reduce the size of the tumor before surgery in an effort to improve surgical treatment for locally advanced

PC. In combination with RP, NHT has been shown to result in improvements in both clinical and local pathological outcomes, including achieved pathologic T0 with RP [2]. Improvements include downstaging and organ confinement, with a reduction in positive resection margin (RM) rates and a decrease of lymph node involvement [3, 4]. However, because of existing differences in enrolled patients' baseline characteristics in prior studies [1, 4], there still remains uncertainty as to NHT's direct clinical and pathological impact in locally advanced PC prior to RP, especially in the aspects of overall survival (OS) and disease-free survival [1] that the current EAU guideline 2017 does not recommend NHT [3, 4].

To the best of our knowledge, no studies have evaluated the pure effect of NHT itself on RM positivity and disease-free survival in the aspect of prostate-specific antigen (PSA)

outcome, called biochemical recurrence (BCR), after all of the preoperative and intraoperative variables were conditionally corrected using matching. Therefore, this study aimed to evaluate the effect of NHT on RM positivity, BCR, and OS in patients with locally advanced PC who underwent RP. Patients were allocated into groups based on whether they were or were not administered NHT, and we used the propensity-score (PS) matching method to adjust for the different baseline clinicopathological variables between the two groups.

2. Materials and Methods

2.1. Ethical Statements. All study protocols were conducted according to the ethical guidelines of the “World Medical Association Declaration of Helsinki-Ethical Principles for Medical Research Involving Human Subjects.” This study was approved by the Institutional Review Board (IRB) of the Research Institute and Hospital National Cancer Center (IRB No. NCCNCS 05-049). All enrolled patients’ informed consents were waived by the IRB.

2.2. Patients and Tissue Samples. From March 2004 to December 2015, 176 consecutive locally advanced patients with PC who underwent RP and were clinically staged at either $\geq T3$ or N+ at the Prostate Cancer Center within the National Cancer Center in Goyang, Korea, were retrospectively identified. Patients had complete medical records that included clinicopathological and prognostic information, such as follow-up duration of >6 months and survival outcomes. Those who did not reach a postoperative undetectable PSA level of <0.2 ng/mL were not included, as well as those who had a history of being treated with NHT for at least 3 months. Patients were then divided into NHT and non-NHT groups. Locally advanced PC was defined as having one or more of the following parameters: stage $\geq T3$ and/or PSA > 20 ng/mL and/or Gleason score sum 8-10; any stage T with pelvic nodal involvement; and clinical stage T3b or T4 disease without evidence of nodal involvement or metastasis [5, 6]. All final prostatectomy specimens were also reviewed according to the guidelines of the 2005 International Society of Urological Pathology (ISUP) by a single uropathologist (Dr. WSP) with 15 years of experience [7].

2.3. Statistical Analysis. The clinicopathological differences between NHT and non-NHT groups were evaluated using Pearson’s χ^2 test. The effect of NHT was evaluated by adjusting for significant clinicopathological variables, such as tumor volume percentage and extracapsular extension (ECE). One-to-one nearest neighbor matching using the PS matching technique was conducted with initial PSA level (<40 or ≥ 40 ng/dL), biopsied tumor volume percentage (<50 or $\geq 50\%$), age (<65 or ≥ 65 y), and Gleason score sum (<7 or ≥ 7) as matching variables. The effect of NHT was then re-evaluated in 50 matched pairs within the NHT and non-NHT group.

To investigate the effect of NHT on RM positivity, a univariable logistic regression analysis was performed before PS matching to identify variables with a significant

association. Then, a multivariable logistic regression model was conducted using backward variable selection with an elimination criterion of $p > 0.05$ applied. NHT and other clinical variables with p -value < 0.2 in univariable analysis were entered the multivariable model. Last, a univariable logistic regression was performed after PS matching. To analyze survival, the Cox proportional hazards model was performed to examine the effect of NHT on BCR-free survival and OS. In this study, BCR was defined as a postoperative serum PSA elevation of >0.2 ng/mL assessed on two different occasions following a decrease to nondetectable level [8]. The first PSA value of ≥ 0.2 ng/mL was used to define the time of recurrence. The Cox proportional hazards models were also performed before and after PS matching.

The results were considered statistically significant when two-sided p values were < 0.050 . All analyses were performed using R project version 3.3.3 (The R Foundation, Vienna, Austria) and SAS version 9.4 (SAS Institute Inc., Cary, NC, USA).

3. Results

3.1. Patient Demographics. The overall median follow-up period, median BCR-free survival duration, and OS were 49.1 (range, 7.1-148.3) months, 42 (range, 1-48) months, and were not yet achieved, respectively. In the NHT group, the median treatment duration of NHT was 4 months. Table 1 shows the distribution of clinicopathological variables in the NHT and non-NHT groups before and after PS matching. The results showed no differences in the distribution of preoperative clinicopathological factors between the two groups before PS matching, except for initial PSA level, ECE, lymphovascular invasion (LVI), perineural invasion, neurovascular bundle saving, and positive RM. After PS matching, only ECE, LVI, and neurovascular bundle saving were significantly different between the two groups. Other baseline patient demographics by group before and after the PS matching are summarized in Table 1.

3.2. Prognostic Factors for Resection Margin Positivity. The results from the univariable logistic regression model showed that before PS matching, NHT was a significant factor for predicting RM positivity (Table 2); however, it was no longer associated with RM positivity in the multivariate model. Conversely, tumor volume $\geq 50\%$ and ECE were significant factors for RM positivity in both the univariable and multivariable models. After PS matching, NHT was no longer a significant factor for RM positivity.

3.3. Prognostic Factors for Biochemical Recurrence and Overall Survival. Before PS matching, NHT was not a significant prognostic factor for BCR in both univariable and multivariable Cox proportional hazards model results (Table 3). The initial PSA level, ECE, and LVI remained significant independent factors for BCR in the multivariable model. Even after matching, NHT was not a significant factor for BCR ($p=0.554$). As for OS, there were no significantly associated clinical variables before or after PS matching. Surprisingly, NHT failed to show a significant association with OS (Table 4).

TABLE 1: Baseline characteristics before and after propensity score matching.

Characteristic	Before propensity score matching			After propensity score matching		
	RRP N(%)	RRP+NHT N(%)	<i>p</i> value	RRP N(%)	RRP+NHT N(%)	<i>p</i> value
No. of patients	97 (55.1)	79 (44.9)		50 (50.0)	50 (50.0)	
Age			0.710			0.410
<65	33 (34.0)	29 (36.7)		17 (34.0)	21 (42.0)	
≥65	64 (66.0)	50 (63.3)		33 (66.0)	29 (58.0)	
PSA			<.001			1.000
<40	84 (86.6)	37 (46.8)		37 (74.0)	37 (74.0)	
≥40	13 (13.4)	42 (53.2)		13 (26.0)	13 (26.0)	
Biopsy Gleason score sum			0.476			0.401
<7	16 (16.5)	10 (12.7)		9 (18.0)	6 (12.0)	
≥7	81 (83.5)	69 (87.3)		41 (82.0)	44 (88.0)	
Tumor volume			0.178			1.000
<50%	62 (63.9)	58 (73.4)		31 (62.0)	31 (62.0)	
≥50%	35 (36.1)	21 (26.6)		19 (38.0)	19 (38.0)	
Clinical T stage						
2	1 (1.0)	3 (3.8)		1 (2.0)	1 (2.0)	
≥3	96 (99.0)	76 (96.2)		49 (98.0)	49 (98.0)	
Clinical N stage						
0	90 (92.8)	57 (72.1)		45 (90.0)	34 (68.0)	
1	7 (7.2)	22 (27.9)		5 (10.0)	16 (32.0)	
Extracapsular extension	60 (61.9)	30 (38.0)	0.002	34 (68.0)	22 (44.0)	0.016
Seminal vesicle invasion	37 (38.1)	33 (41.8)	0.625	21 (42.0)	20 (40.0)	0.839
Lymphovascular invasion or emboli	32 (33.0)	9 (11.4)	0.001	17 (34.0)	6 (12.0)	0.009
Perineural invasion	79 (81.4)	52 (65.8)	0.018	40 (80.0)	37 (74.0)	0.476
Apex involvement	25 (25.8)	11 (13.9)	0.053	13 (26.0)	7 (14.0)	0.134
Lymph node dissection	86 (88.7)	76 (96.2)	0.066	43 (86.0)	49 (98.0)	0.059
Neurovascular bundle saving	47 (48.5)	17 (21.5)	<.001	25 (50.0)	12 (24.0)	0.007
Resection margin	36 (37.1)	16 (20.3)	0.015	19 (38.0)	11 (22.0)	0.081
Death	7 (7.2)	11 (13.9)	0.144	6 (12.0)	7 (14.0)	0.766

The *p* value was calculated using Pearson's chi-squared test between NHT and non-NHT groups.

TABLE 2: Logistic regression model for resection margin positivity before and after propensity score matching.

Variables	Before propensity score matching				After propensity score matching	
	Univariable analysis		Multivariable analysis		Univariable analysis	
	OR (95% CI)	<i>p</i> value	OR (95% CI)	<i>p</i> value	OR (95% CI)	<i>p</i> value
NHT plus RRP versus RRP alone	0.43 (0.22-0.86)	0.016	0.59 (0.27-1.30)	0.188	0.46 (0.19-1.11)	0.084
Age ≥65	0.82 (0.42-1.60)	0.561			0.73 (0.30-1.74)	0.473
PSA ≥40	1.41 (0.71-2.79)	0.328			4.23 (1.64-10.93)	0.003
Biopsy Gleason score sum ≥7	1.47 (0.56-3.91)	0.436			1.86 (0.49-7.15)	0.365
Tumor volume ≥50%	6.67 (3.26-13.62)	<.001	3.68 (1.67-8.09)	0.001	5.78 (2.28-14.63)	<.001
Extracapsular extension	9.33 (4.04-21.53)	<.001	5.26 (2.13-12.96)	<.001	6.29 (2.16-18.33)	0.001
Seminal vesicle invasion	2.86 (1.47-5.58)	0.002			3.07 (1.27-7.42)	0.013
Lymphovascular invasion or emboli	4.67 (2.23-9.80)	<.001			4.59 (1.71-12.28)	0.002
Perineural invasion	5.93 (2.00-17.57)	0.001			2.42 (0.75-7.86)	0.141
Apex involvement	253.23 (32.55-)	<.001			NA	
Lymph node dissection	1.05 (0.32-3.52)	0.934			0.69 (0.15-3.10)	0.631
Neurovascular bundle saving	0.55 (0.27-1.11)	0.094			0.51 (0.20-1.31)	0.165

TABLE 3: Cox proportional hazards model for biochemical recurrence before and after propensity score matching.

Variables	Before propensity score matching				After propensity score matching	
	Univariable analysis		Multivariable analysis		Univariable analysis	
	HR (95% CI)	p value	HR (95% CI)	p value	HR (95% CI)	p value
NHT plus RRP versus RRP alone	1.05 (0.69-1.61)	0.809	1.03 (0.62-1.72)	0.906	0.84 (0.47-1.49)	0.554
Resection margin	1.51 (0.97-2.36)	0.071			2.14 (1.18-3.86)	0.012
Age ≥ 65	0.72 (0.46-1.10)	0.128			0.61 (0.34-1.08)	0.091
PSA ≥ 40	2.14 (1.40-3.29)	0.001	2.23 (1.38-3.60)	0.001	3.19 (1.77-5.76)	<.001
Biopsy Gleason score sum ≥ 7	2.35 (1.13-4.87)	0.022			2.77 (0.99-7.73)	0.052
Tumor volume $\geq 50\%$	1.78 (1.15-2.75)	0.010			2.50 (1.41-4.44)	0.002
Extracapsular extension	2.47 (1.59-3.85)	<.001	2.10 (1.30-3.41)	0.003	5.04 (2.48-10.23)	<.001
Seminal vesicle invasion	2.20 (1.44-3.36)	<.001			2.42 (1.36-4.30)	0.003
Lymphovascular invasion or emboli	2.35 (1.50-3.68)	<.001	1.85 (1.13-3.05)	0.015	3.32 (1.83-6.00)	<.001
Perineural invasion	2.04 (1.18-3.51)	0.011			3.61 (1.43-9.17)	0.007
Apex involvement	1.71 (1.05-2.78)	0.031			2.39 (1.26-4.54)	0.008
Lymph node dissection	1.09 (0.47-2.49)	0.845			2.28 (0.55-9.41)	0.256
Neurovascular bundle saving	0.62 (0.39-0.99)	0.045			0.56 (0.30-1.05)	0.070

TABLE 4: Cox proportional hazards model for overall survival before and after propensity score matching.

Variables	Before propensity score matching		After propensity score matching	
	Univariable analysis		Univariable analysis	
	HR (95% CI)	p value	HR (95% CI)	p value
NHT plus RRP versus RRP alone	1.35 (0.52-3.51)	0.539	0.77 (0.25-2.38)	0.650
Resection margin	1.62 (0.60-4.38)	0.338	1.94 (0.63-5.98)	0.250
Age ≥ 65	1.27 (0.45-3.55)	0.654	1.29 (0.40-4.22)	0.669
PSA ≥ 40	1.04 (0.39-2.77)	0.943	0.67 (0.15-3.04)	0.599
Biopsy Gleason score sum ≥ 7	1.36 (0.39-4.75)	0.630	0.84 (0.23-3.10)	0.795
Tumor volume $\geq 50\%$	2.17 (0.82-5.77)	0.120	3.01 (0.97-9.28)	0.056
Extracapsular extension	1.03 (0.41-2.62)	0.948	1.22 (0.41-3.65)	0.717
Seminal vesicle invasion	1.84 (0.71-4.77)	0.210	1.53 (0.48-4.86)	0.471
Lymphovascular invasion or emboli	0.45 (0.10-1.95)	0.286	0.70 (0.16-3.17)	0.644
Perineural invasion	2.69 (0.77-9.34)	0.119	2.22 (0.49-10.09)	0.301
Apex involvement	1.59 (0.51-4.94)	0.421	3.02 (0.87-10.53)	0.083
Lymph node dissection	NA		NA	
Neurovascular bundle saving	0.62 (0.22-1.75)	0.370	0.69 (0.21-2.23)	0.532

4. Discussion

Discussions regarding the efficacy of NHT on RM and survival prognoses are typically met with the issue of different and heterogeneous baseline characteristics of enrolled patients with different tumor burdens in PC [9]. Our research group published two retrospective studies about the efficacy of NHT in PC [2, 10], showing that 75.4% of patients had pathologic RM negative, 19.5% had undergraded Gleason score, 50.0-57.1% of BCR rate, and 3.0-5.6% had nonrecurrent statuses with pT0 until a median follow-up of 59 months. However, both of these studies had a limitation of heterogeneous baseline characteristics.

In order to adjust for this imbalance in the baseline clinicopathological variables between patients with and without NHT, this study evaluated the effect of NHT on three main comparative endpoints (RM positivity, BCR, and OS)

between NHT and non-NHT groups using PS matching in patients with locally advanced PC who underwent RP. Utilization of PS matching corrected the baseline differences for disease state and tumor burdens within the two groups and revealed the inefficacy of NHT on decreasing RM positivity, BCR, and OS, which was contrary to previous reports [2, 10, 11], and which was accorded to the current EAU guideline of PC [3]. The current EAU guideline recommended NHT only for patients with intermediate or high risk PC if receiving definitive radiation therapy.

The rationale for using NHT in PC was to decrease the size of the prostate volume by inhibiting the growth of hormone sensitive prostate cells and cancer cells. Decreasing prostate size might help clinicians to resect the prostate more efficiently and easily, with less intraoperative comorbidities during RP. However, the results of this study were consistent with those of previous studies that showed that HT did not

completely eliminate the PC cells. Additionally, the disease states and the survival prognoses (BCR-free survival and OS) were not affected by NHT [12, 13]. Once androgen deprivation stops after discontinuing HT during intermittent HT, PSA level increases and the tumor may eventually regrow in the resection site. Other studies observed this process in patients with clear RM and without HT, who experienced recurrences at the operative site [1, 14]. However, some studies, including ours, have reported that patients achieved complete pathological response (about 0.2-5.4%) after HT, reflecting potential eradication of advanced prostate cancer with androgen deprivation therapy [2, 15, 16]. Patients with pT0 stage PC are expected to have an extremely favorable prognosis, especially in high risk or locally advanced PC. Further studies should be conducted in patients with pT0 after HT.

Previous systemic reviews and meta-analysis reports showed comprehensive assessments of the efficacy of HT when used as NHT with RP for treatment of PC [1]. Similar to this study, there was no improvement in clinically important outcomes for OS, disease-specific survival, or BCR-free survival when NHT was used with RP. This finding was observed despite improvements in putative pathologic surrogate outcomes, such as RM-free positive status (overall incidence in this study, 74.4%) and pathological downstaging (16.1%), particularly when NHT was maintained for >3 months (data not shown) [17].

In this study, the efficacy of NHT was not statistically significant; however, other studies have shown significant results for prognosis and RM, as well as some specific indicators for those patients with large tumor burdens [18–21]. In these circumstances, NHT should be cautiously discussed with patients and caregivers to make optimal treatment decisions, particularly because there are no phase III randomized controlled trials for NHT. For example, the use of NHT only prior to RP should be discussed in those patients with PC who have a larger prostate adenocarcinoma and a highly expected intraoperative and postoperative morbidity. A recent prospective 10-year NHT phase II study comparing large bulky PC (defined as a tumor >4 cm in diameter) or tumor involvement >50% of the gland with cancer and nonbulky PC evaluated this issue [21]. The study included 62 patients with T3 or T4N0M0 who were administered NHT with goserelin acetate and flutamide followed by RP. The patients achieved longer progression-free survival (7.5 years) and unreached OS (68% of 10-year OS) during a median follow-up time of 10.6 years. This result suggested that NHT might have a role in high volume locally advanced PC as an alternative to combined radiation and HT. In contrast, the present study had 90% of patients staged >T3, and PS matching showed no significant efficacy of NHT (Tables 2–4). The different results and interpretations between the two studies might be influenced by the androgen blocking agents, durations of NHT, and the adjuvant multidisciplinary and multimodal therapeutic options, such as long-term HT and external beam radiation therapy used after RP, which were not matched between the NHT and non-NHT groups in this study [22–24].

Additionally, administration of RP with NHT for 3 months might not be sufficient for improvement in disease-free survival compared with RP alone. Meyer et al. demonstrated that patients receiving NHT for more than 3 months had a significantly lower risk of PSA failure than the RP alone group [19]. In the work from the Canadian Urologic Oncology Group in 500 patients [25], a significant difference in BCR rates was not observed at 4 years, whereas continued pathologic benefit and BCR of PC were observed when NHT was used between 3 and 8 months. In the present study, we were unable to control the duration of NHT usage due to the retrospective design.

Another important factor affecting prognoses is the type of drugs used for NHT. In a recent phase II, randomized, open-label study of NHT with degarelix (gonadotropin-releasing hormone [GnRH] receptor antagonist) versus luteinizing hormone-releasing hormone (LHRH) agonist in patients with PC prior to RP, neoadjuvant degarelix alone was associated with higher levels of intratumoral dihydrotestosterone compared to the use of LHRH agonist and bicalutamide, despite similar testosterone levels [26]. Another randomized phase II trial in patients with intermediate and high risk PC who were administered NHT using LHRH agonists alone versus LHRH agonists plus abiraterone acetate prior to RP found that intraprostatic androgen levels of the prostate specimens were significantly reduced in the abiraterone plus LHRH agonist group than in the LHRH agonist alone group. Additionally, a 71% of pT0 rate and a 55.4% of residual cancer burden/minimal residual disease were reported for the entire cohort [27]. Heterogeneity of NHT drugs might be a confounding factor in the present study, and as such, future randomized controlled trials are required to clarify this issue.

Last important consideration for the use of HT is HT-associated complications. HT has its own local and systemic side effects, secondary to the blockade of androgen hormone [28, 29]. The side effects from HT are related to the duration of HT use. Even though short-term NHT before RP is typically used, the beneficiary effect of HT has been shown to occur after more than 3 months [1, 4, 18, 19, 25]. Clinicians should remain aware of the potential long-term side effects of HT, as severe liver function abnormality (17%), bowel problems (8%), and urinary and sexual (36%) problems have led to discontinuation of HT [30]. Therefore, further prospective, large-scale studies are needed to determine the true efficacy of NHT; however, the findings from this study do not support the use of NHT in locally advanced PC who underwent RP.

This study had limitations. First, this study had a small sample from a single institution with a short follow-up period. Second, the variations of the specific hormonal treatments, the duration of NHT, timing of treatments, the different antiandrogen agents and no adjustment of lymph node status or other pathological parameters in PS matching might have affected the results from the analyses. However, the clinical significance of this study is the potential to minimize the different baseline clinicopathological characteristics of tumor burden and disease status between groups using PS matching. Further studies with a large number of subjects and long-term follow-up are required, and the effect

of secondary hormonal agents should also be investigated for their prognostic efficacy with and without androgen deprivation therapy.

5. Conclusion

This study showed that NHT was not a significant factor in predicting RM positivity, BCR-free survival, and OS before and after PS matching in patients with locally advanced or high risk localized PC who underwent RP.

Data Availability

The datasets used and/or analysed during the current study available from the corresponding author (Kang Hyun Lee, uroonco@ncc.re.kr) on reasonable request. The IRB and ethical committee of the National Cancer Center (in Korea) will review the requests because of the patients' information. After the approval of the committee with confirmation of the reasonable requests, the dataset will be freely available. The other contact e-mail besides the corresponding author's e-mail is irb@ncc.re.kr.

Conflicts of Interest

None of the authors had anything to declare about the conflicts of interest.

Acknowledgments

This study was supported by the Korean National Cancer Center (grants no. 1810021-1).

References

- [1] M. D. Shelley, S. Kumar, B. Coles, T. Wilt, J. Staffurth, and M. D. Mason, "Adjuvant hormone therapy for localised and locally advanced prostate carcinoma: A systematic review and meta-analysis of randomised trials," *Cancer Treatment Reviews*, vol. 35, no. 7, pp. 540–546, 2009.
- [2] J. Y. Joung, J. E. Kim, S. H. Kim et al., "The prevalence and outcomes of pT0 disease after neoadjuvant hormonal therapy and radical prostatectomy in high-risk prostate cancer," *BMC Urology*, vol. 15, no. 1, 2015.
- [3] N. Mottet, J. Bellmunt, M. Bolla, E. Briers, M. G. Cumberbatch, and M. De Santis, "Guideline on Prostate Cancer," *European Urology*, vol. 71, no. 4, pp. 618–629, 2017, <http://Uroweb.org/guideline/prostate-cancer/#6>.
- [4] C. C. Schulman, F. M. J. Debruyne, G. Forster, F. P. Selvaggi, A. R. Zlotta, and W. P. J. Witjes, "4-Year follow-up results of a European prospective randomized study on neoadjuvant hormonal therapy prior to radical prostatectomy in T2-3N0M0 prostate cancer," *European Urology*, vol. 38, no. 6, pp. 706–713, 2000.
- [5] *NCCN Clinical Practice Guidelines in Oncology™ Prostate Cancer V.1.2011*© 2011 National Comprehensive Cancer Network I, 2011.
- [6] S. A. Rosenthal and H. M. Sandler, "Treatment strategies for high-risk locally advanced prostate cancer," *Nature Reviews Urology*, vol. 7, no. 1, pp. 31–38, 2010.
- [7] J. I. Epstein, W. C. Allsbrook Jr., M. B. Amin et al., "The 2005 International Society of Urological Pathology (ISUP) consensus conference on Gleason grading of prostatic carcinoma," *The American Journal of Surgical Pathology*, vol. 29, no. 9, pp. 1228–1242, 2005.
- [8] M. S. Cookson, G. Aus, A. L. Burnett et al., "Variation in the definition of biochemical recurrence in patients treated for localized prostate cancer: the American urological association prostate guidelines for localized prostate cancer update panel report and recommendations for a standard in the reporting of surgical outcomes," *The Journal of Urology*, vol. 177, no. 2, pp. 540–545, 2007.
- [9] A. J. Chang, K. A. Autio, M. Roach, and H. I. Scher, "High-risk prostate cancer-Classification and therapy," *Nature Reviews Clinical Oncology*, vol. 11, no. 6, pp. 308–323, 2014.
- [10] S. H. Kim, W. S. Park, S. H. Kim et al., "Prostate stem cell antigen expression in radical prostatectomy specimens predicts early biochemical recurrence in patients with high risk prostate cancer receiving neoadjuvant hormonal therapy," *PLoS ONE*, vol. 11, no. 3, p. e0151646, 2016.
- [11] M. E. Gleave, S. E. La Bianca, S. L. Goldenberg, E. C. Jones, N. Bruchofsky, and L. D. Sullivan, "Long-term neoadjuvant hormone therapy prior to radical prostatectomy: evaluation of risk for biochemical recurrence at 5-year follow-up," *Urology*, vol. 56, no. 2, pp. 289–294, 2000.
- [12] K.-H. Chang, C. E. Ercole, and N. Sharifi, "Androgen metabolism in prostate cancer: from molecular mechanisms to clinical consequences," *British Journal of Cancer*, vol. 111, no. 7, pp. 1249–1254, 2014.
- [13] A. Katzenwadel and P. Wolf, "Androgen deprivation of prostate cancer: leading to a therapeutic dead end," *Cancer Letters*, vol. 367, no. 1, pp. 12–17, 2015.
- [14] M. L. Cher, K. Shinohara, S. Breslin, J. Vapnek, and P. R. Carroll, "High failure rate associated with long-term follow-up of neoadjuvant androgen deprivation followed by radical prostatectomy for stage C prostatic cancer," *British Journal of Urology*, vol. 75, no. 6, pp. 771–777, 1995.
- [15] R. Mazzucchelli, F. Barbisan, A. Tagliabracci et al., "Search for residual prostate cancer on pT0 radical prostatectomy after positive biopsy," *Virchows Archiv*, vol. 450, no. 4, pp. 371–378, 2007.
- [16] J. Park, I. G. Jeong, J. K. Bang et al., "Preoperative clinical and pathological characteristics of pT0 prostate cancer in radical prostatectomy," *Korean Journal of Urology*, vol. 51, no. 6, pp. 386–390, 2010.
- [17] L. H. Klotz, S. L. Goldenberg, M. A. S. Jewett et al., "Long-term followup of a randomized trial of 0 versus 3 months of neoadjuvant androgen ablation before radical prostatectomy," *The Journal of Urology*, vol. 170, no. 3, pp. 791–794, 2003.
- [18] L. Vaillancourt, B. Têtu, Y. Fradet et al., "Effect of neoadjuvant endocrine therapy (combined androgen blockade) on normal prostate and pro static carcinoma: a randomized study," *The American Journal of Surgical Pathology*, vol. 20, no. 1, pp. 86–93, 1996.
- [19] F. Meyer, L. Moore, I. Bairati, L. Lacombe, B. Têtu, and Y. Fradet, "Neoadjuvant hormonal therapy before radical prostatectomy and risk of prostate specific antigen failure," *The Journal of Urology*, vol. 162, no. 6, pp. 2024–2028, 1999.
- [20] L. Klotz, M. Gleave, and S. L. Goldenberg, "Neoadjuvant hormone therapy: the Canadian trials," *Molecular Urology*, vol. 4, pp. 233–237, 2000.

- [21] R. K. Berglund, C. M. Tangen, I. J. Powell et al., "Ten-year follow-up of neoadjuvant therapy with goserelin acetate and flutamide before radical prostatectomy for clinical T3 and T4 prostate cancer: Update on southwest oncology group study 9109," *Urology*, vol. 79, no. 3, pp. 633–637, 2012.
- [22] A. E. Marciscano, M. E. Hardee, and N. Sanfilippo, "Management of high-risk localized prostate cancer," *Advances in Urology*, vol. 2012, Article ID 641689, 11 pages, 2012.
- [23] M. Bolla, L. Collette, L. Blank et al., "Long-term results with immediate androgen suppression and external irradiation in patients with locally advanced prostate cancer (an EORTC study): A phase III randomised trial," *The Lancet*, vol. 360, no. 9327, pp. 103–108, 2002.
- [24] M. Bolla, G. van Tienhoven, P. Warde et al., "External irradiation with or without long-term androgen suppression for prostate cancer with high metastatic risk: 10-year results of an EORTC randomised study," *The Lancet Oncology*, vol. 11, no. 11, pp. 1066–1073, 2010.
- [25] M. E. Gleave, S. L. Goldenberg, J. L. Chin et al., "Randomized comparative study of 3 versus 8-month neoadjuvant hormonal therapy before radical prostatectomy: Biochemical and pathological effects," *The Journal of Urology*, vol. 166, no. 2, pp. 500–506, 2001.
- [26] R. K. Sayyid, A. Evans, K. Hersey et al., "A phase II, randomized, open-label study of neoadjuvant degarelix versus LHRH agonist in prostate cancer patients prior to radical prostatectomy," *Clinical Cancer Research*, vol. 23, no. 8, pp. 1974–1980, 2017.
- [27] E. A. Mostaghel, S. T. Page, D. W. Lin et al., "Intraprostatic androgens and androgen-regulated gene expression persist after testosterone suppression: Therapeutic implications for castration-resistant prostate cancer," *Cancer Research*, vol. 67, no. 10, pp. 5033–5041, 2007.
- [28] H. Isbarn, L. Boccon-Gibod, P. R. Carroll et al., "Androgen deprivation therapy for the treatment of prostate cancer: consider both benefits and risks," *European Urology*, vol. 55, no. 1, pp. 62–75, 2009.
- [29] A. S. Neto, M. Tobias-Machado, M. A. P. Esteves et al., "Bisphosphonate therapy in patients under androgen deprivation therapy for prostate cancer: a systematic review and meta-analysis," *Prostate Cancer and Prostatic Diseases*, vol. 15, no. 1, pp. 36–44, 2012.
- [30] D. S. Lamb, J. W. Denham, H. Mameghan et al., "Acceptability of short term neo-adjuvant androgen deprivation in patients with locally advanced prostate cancer," *Radiotherapy & Oncology*, vol. 68, no. 3, pp. 255–267, 2003.

Research Article

Gene Expression Profile Signature of Aggressive Waldenström Macroglobulinemia with Chromosome 6q Deletion

Naohiro Sekiguchi ¹, Junko Nomoto,² Akihisa Nagata,¹ Masahiro Kiyota,¹ Ichiro Fukuda,³ Kazuaki Yamada,⁴ Naoki Takezako,¹ and Yukio Kobayashi ²

¹Division of Hematology, National Hospital Organization Disaster Medical Center, Tachikawa, Tokyo 190-0014, Japan

²Department of Hematology, National Cancer Center Hospital, Tsukiji, Tokyo 104-0045, Japan

³Division of Radiology, National Hospital Organization Disaster Medical Center, Tachikawa, Tokyo 190-0014, Japan

⁴Division of Laboratory and Pathology, National Hospital Organization Disaster Medical Center, Tachikawa, Tokyo 190-0014, Japan

Correspondence should be addressed to Yukio Kobayashi; ykkobaya@iuhw.ac.jp

Received 23 March 2018; Revised 21 August 2018; Accepted 10 September 2018; Published 4 October 2018

Academic Editor: Maria L. Tornesello

Copyright © 2018 Naohiro Sekiguchi et al. This is an open access article distributed under the Creative Commons Attribution License, which permits unrestricted use, distribution, and reproduction in any medium, provided the original work is properly cited.

Background. Waldenström macroglobulinemia (WM) is a rare, indolent B-cell lymphoma. Clinically, chromosome 6q deletion (6q del) including loss of the B lymphocyte-induced maturation protein 1 gene (BLIMP-1) is reported to be associated with poor prognosis. However, it remains unclear how the underlying biological mechanism contributes to the aggressiveness of WM with 6q del. **Methods.** Here, we conducted oligonucleotide microarray analysis to clarify the differences in gene expression between WM with and without 6q del. Gene ontology (GO) analysis was performed to identify the main pathways underlying differences in gene expression. Eight bone marrow formalin-fixed paraffin-embedded samples of WM were processed for interphase fluorescence in situ hybridization analysis, and three were shown to have 6q del. **Results.** GO analysis revealed significant terms including “lymphocyte activation” (corrected p value=6.68E-11), which included 31 probes. Moreover, *IL21R* and *JAK3* expression upregulation and activation of the B-cell receptor signaling (BCR) pathway including *CD79a*, *SYK*, *BLNK*, *PLCγ2*, and *CARD11* were detected in WM with 6q del compared with WM without 6q del. **Conclusion.** The present study suggested that the BCR signaling pathway and *IL21R* expression are activated in WM with 6q del. Moreover, *FOXPI* and *CBLB* appear to act as positive regulators of the BCR signaling pathway. These findings might be attributed to the aggressiveness of the WM with 6q del expression signature.

1. Background

Waldenström macroglobulinemia (WM) is a rare, indolent type of B-cell lymphoma with monoclonal IgM gammopathy. B-cells, lymphoplasmacytic cells, and plasma cells (PCs) form neoplasms in WM, with the bone marrow (BM) being the main site of infiltration [1]. The disease has an overall annual incidence of three per million in the United States (US) [2, 3].

Cytogenetic analysis previously detected chromosome 6q deletion (del), including loss of the B-lymphocyte-induced maturation protein 1 gene (*BLIMP-1*) and *TNFAIP3/A20*, in 40%–55% of WM patients in the US and European countries [4–8]. Furthermore, this aberration is recognized as one of the factors associated with poor prognosis, higher serum IgM

levels, and a higher International Prognostic Scoring System for WM (ISSWM) level [4–8].

However, it remains unclear how the underlying biological mechanism contributes to the observed aggressiveness of WM with 6q del. The present study therefore conducted an oligonucleotide microarray analysis to clarify the biological differences between WM with and without 6q del.

2. Methods

2.1. Patients. Newly diagnosed symptomatic WM patients attending the National Hospital Organization Disaster Medical Center from January 2010 to March 2014 were enrolled in this study. Samples of cases whose comprehensive agreement

had been obtained were subject for the study. The WM diagnostic criteria used in the present study were according to the revised 4th edition of World Health Organization (WHO) classification of tumours of haematopoietic and lymphoid tissues [1]. Briefly, these included detection of the IgM monoclonal protein and BM neoplastic cells including lymphocytes, CD20-positive lymphoplasmacytic cells, and some PCs more than 10 % and presence of symptoms.

Patient clinical data were obtained from their medical charts and included age, sex, performance status (PS), hemoglobin level, platelet count, serum β 2-microglobulin level, ISSWM [9], serum M-protein, B symptoms, hepatomegaly, splenomegaly, and lymphadenopathy. PS was determined according to the Eastern Cooperative Oncology Group scale [10].

2.2. Pathological Review. A pathological review confirmed that all cases were IgM-WM according to the revised 4th edition of WHO classification [1]. MALT lymphoma or CLL with monoclonal IgM protein were carefully excluded from the study. Using BM biopsied specimens, the infiltration pattern of neoplastic cells was divided into four groups: diffuse, interstitial, paratrabeular, and nodular. Additionally, the PC%, lymphoplasmacytic cell %, lymphocyte %, and total neoplastic cells% in BM were evaluated from BM smears.

2.3. Fluorescence In Situ Hybridization Analyses (FISH). Cytogenetic aberrations were obtained by FISH analysis using the A20/BLIMP-1/SHGC-79576 Three Color Probe (Cancer Genetics Italia™ SRI, Mila, Italy) to detect 6q del. A20 and BLIMP-1 are located at 6q23 and 6q21, respectively, and the 6q deletion can be easily detected by comparing the signal intensity of this region with that of the chromosome 6 centromere [11]. Interphase FISH was performed using stored BM aspirate patient specimens, and results were recorded according to ISCN 2016 [12]. The normal cut-off values for deletions in the chromosomal region were defined as means + 3SD of the results for 20 normal controls.

2.4. Oligonucleotide Microarray Analyses. cDNA microarray analysis was performed following the manufacturer's instruction. Briefly, formalin-fixed paraffin-embedded BM biopsied samples were deparaffinized and total RNA was extracted using the RNeasy FFPE kit (Qiagen, Venlo, the Netherlands). Isolated total RNA was converted into cDNA, followed by cDNA amplification. After this, 4 μ g of cDNA was fragmented at 37°C for 30 min and then biotinylated using the Encore cDNA (Nugen, San Carlos, CA). Biotin-labeled cDNA was hybridized to the Human Genome U133 Plus 2.0 Array (Affymetrix, Santa Clara, CA). The array was incubated for 18 h at 45°C, then automatically washed, and stained using the GeneChip Hybridization, Wash, and Stain Kit (Affymetrix). The array was scanned using a GeneChip Scanner 3000 7G.

2.5. Immunohistochemistry. Paraffin-embedded BM specimens underwent heat-induced antigen retrieval in pH 6.0 citrate buffer. Polyclonal antibodies against IL-21R (1:500, NBPI-87502, Novus Biological, Littleton, CO) were used.

After incubation with the primary antibody, slides were incubated with the secondary antibody, One-Step Polymer-HRP (BioGenex, Fremont, CA), for visualization. The IL-21R staining pattern was categorized into three groups: <30%, 30%–70%, and >70% of lymphoplasmacytic cells and PCs.

2.6. Statistical Analysis. Descriptive statistics of each clinical data were calculated by IBM SPSS Statistics for Windows 24.0J. Oligonucleotide microarray analyses were carried out using GeneSpring GX software version 13.0 (Agilent Technologies, Santa Clara, CA). Briefly, described as follows, the expression values were calculated from the raw data using the MBEI algorithm [13]. Only probes that signal intensity were within 20 to 100 percentile in each array which were included in the comparative analysis. The genes corresponding to probes having a change in intensity exceeding a ratio of four were considered as genes with a significant differential expression pattern. In parallel, unpaired t-test with unequal variance (Welch's t-test) was performed to compare the means of the two groups of replicates. Probes with a p value less than 0.05 were considered having significant different signal value. GO analysis was then performed on the sets of probes above the 4-fold ratio that passed the t-test to identify the main pathways underlying differences in gene expression. We arbitrary selected 4-fold different expression as a cut-off ratio instead of considering false discovery rate, because of the small sample size, and we performed the oligonucleotide microarray analysis as an exploratory research. Ontologies with corrected p-values <0.1 were considered significant. The microarray datasets used in the present study were deposited in the Gene Expression Omnibus under accession number GSE70511 (<http://www.ncbi.nlm.nih.gov/geo/query/acc.cgi?acc=GSE70511>).

3. Results

3.1. Clinical Features. Eight patients were enrolled in the study, and characteristics are shown in Table 1. Briefly, the median age was 71.5 years, and the male/female ratio was 5/3. ISSWM low/int/high was observed as 0/4/4. Median monoclonal M-protein levels were 2.65 g/dL (range: 0.8–4.28 g/dL). A total of two patients were observed to have constitutional B symptoms; one had hepatomegaly, and another had splenomegaly. Adenopathy and cold agglutinin disease were found in two patients each. Diffuse, interstitial, paratrabeular, and nodular patterns of neoplastic cell invasion into the BM were seen in seven, zero, one, and zero patients, respectively. The median small lymphocyte %, lymphoplasmacytic cell %, and PC% were 39.0 %, 3.3%, and 1.9 %, respectively, with total neoplastic cells accounting for 45.7%.

3.2. Cytogenetic Analysis and Correlations between 6q del and Individual Characteristics. To detect 6q del, fluorescent in situ hybridization (FISH) analysis was performed (Figures 1(a) and 1(b)). The cut-off value for loss of BLIMP-1 and A20 was 3%. Three of the eight cases had 6q del, in which both genes were deleted, and the other five cases did not have 6q del. Median serum M-protein levels were 3.14 g/dL in patients with 6q del, compared with 2.25 g/dL in those without 6q

TABLE 1: Patient characteristics.

	all (N=8)	6q del (+) (N=3)	6q del (-) (N=5)
Median Age (old, range)	71.5 (58-79)	76 (70-79)	71 (58-76)
Sex (M/F) (%)	5/3	2/1	3/2
PS>1 (%)	5	2	3
Hb <11.5 g/dL (%)	6	3	3
plt <10×10 ⁹ /L (%)	1	0	1
β2MG>3mg/L (%)	3 (64.3)	2	2
Median M-protein (g/dL)	2.65 (0.8-4.28)	3.14 (2.13-4.28)	2.25 (0.8-3.87)
ISSWM(Low/Int/High) (%)	0/4/4 (9/36/55)	0/1/2	0/3/2
B-symptom (%)	2 (29.4)	1	1
Hepatomegaly (%)	1 (23.8)	0	1
Splenomegaly (%)	1 (23.8)	0	1
Lymphadenopathy (%)	2(25)	0	2
Cold agglutinin disease	2	0	2
Infiltration pattern (D/P)	7/1	3/0	4/1
Plasma cell (%)	1.9 (1-3.6)	2.0 (1-2.2)	1.8 (1.2-3.6)
Lymphoplasmacytic cell (%)	3.3 (2.4-8.6)	7.1 (2.6-8.6)	3.0 (2.4-5.2)
Small lymphocyte (%)	39.0 (29.4-62.8)	41.6 (35.9-62.8)	36.4 (29.4-46.8)
Total neoplastic cell (%)	45.7 (36-72.4)	46.4 (45-72.4)	41.4 (36-50.4)

PS: performance status; Hb: hemoglobin; plt: platelets; β2MG: β2-microglobulin; cCa: calculated Ca; ISSWM: International Prognostic Scoring System for Waldenström Macroglobulinemia.

del. ISSWM low/int/high was 0/1/2 in patients with 6q del, compared with 0/3/2 in patients without 6q del. The median small lymphocyte %, lymphoplasmacytic cell %, PC %, and total neoplastic cell % were 41.6 %, 7.1%, 2.0%, and 46.4%, respectively, in those with 6q del, versus 36.4%, 3.0%, 1.8%, and 41.4%, respectively, in those without 6q del.

3.3. Oligonucleotide Microarray. All the eight cases' samples were subjected for oligonucleotide microarray analysis. To clarify the differences in gene expression between WM with and without 6q del, we performed oligonucleotide microarray analyses and detected that a total of 428 probes, corresponding to 324 annotated genes, were upregulated (p value < 0.05 and fold change > 4.0), and a total of 112 probes, corresponding to 96 annotated genes, were downregulated (p value < 0.05 and fold change < 0.25) in WM with 6q del (Supplementary Tables 1 and 2). Among genes located on chr 6q, 4 genes were upregulated, and 5 genes were downregulated, while both *BLIMP-1* and *A20* were neither upregulated nor downregulated.

Consecutively, gene ontology (GO) analysis was performed, and GO terms including "lymphocyte activation" (corrected p value=6.68E-11) and "B-cell activation" (corrected p value=2.15E-08) were statistically significant in the upregulated gene lists relative to the all genes on the microarray (Table 2). A network analysis of GO terms associated with "lymphocyte activation" included 31 probes and 30 genes, listed in Table 3. Genes involved in the B-cell receptor (BCR) signaling pathway, including *CD79a*, *SYK*, *BLNK*, *PLCγ2*, and *CARD11*, were shown to be activated in WM with 6q del compared with WM without 6q del. Other upregulated genes included *IL-21R*, *JAK3*, *IFNγ*, and *FOXPI*. In contrast, the

GO term "plasma cell differentiation" was not statistically significant (data not shown).

3.4. Immunohistochemistry of Interleukin (IL)-21R. To confirm the upregulation of the IL21R protein in WM with 6q del, we performed immunostaining analysis. Figures 1(c) and 1(d) show that all three patients with 6q del had >70% positivity of IL-21R in lymphoplasmacytic cells and PCs. In WM without 6q del, one case was categorized as 30%–70% positivity, while the remaining four cases showed <30% positivity.

4. Discussion

WM is a rare entity of low-grade B-cell lymphoma with IgM monoclonal gammopathy according to classification by the WHO [1]. The most commonly involved site of infiltration is the BM, and some patients have adenopathy, hepatomegaly, and splenomegaly [1]. Neoplastic cells consist of CD20-positive B-cells and lymphoplasmacytic cells, while some PCs are also considered to be neoplastic [14]. Recently, Treon et al. [15] reported that the *MYD88* L265P mutation has been recognized in about 90% of WM cases in the US and in 70%–90% of cases worldwide [16]. This mutation is also found in 47% of patients with IgM monoclonal gammopathy of undetermined significance (IgM-MGUS) and is associated with a higher risk of disease progression to WM and splenic marginal zone lymphoma [17]. It is known to be a major mechanism of oncogenesis and is linked with Toll-like receptor (TLR) signaling pathway activation [15]. Furthermore, Yang et al. identified Bruton tyrosine kinase (BTK) complexed to *MYD88* in L265P-expressing WM cells, with preferential binding of *MYD88* to phosphorylated BTK [18].

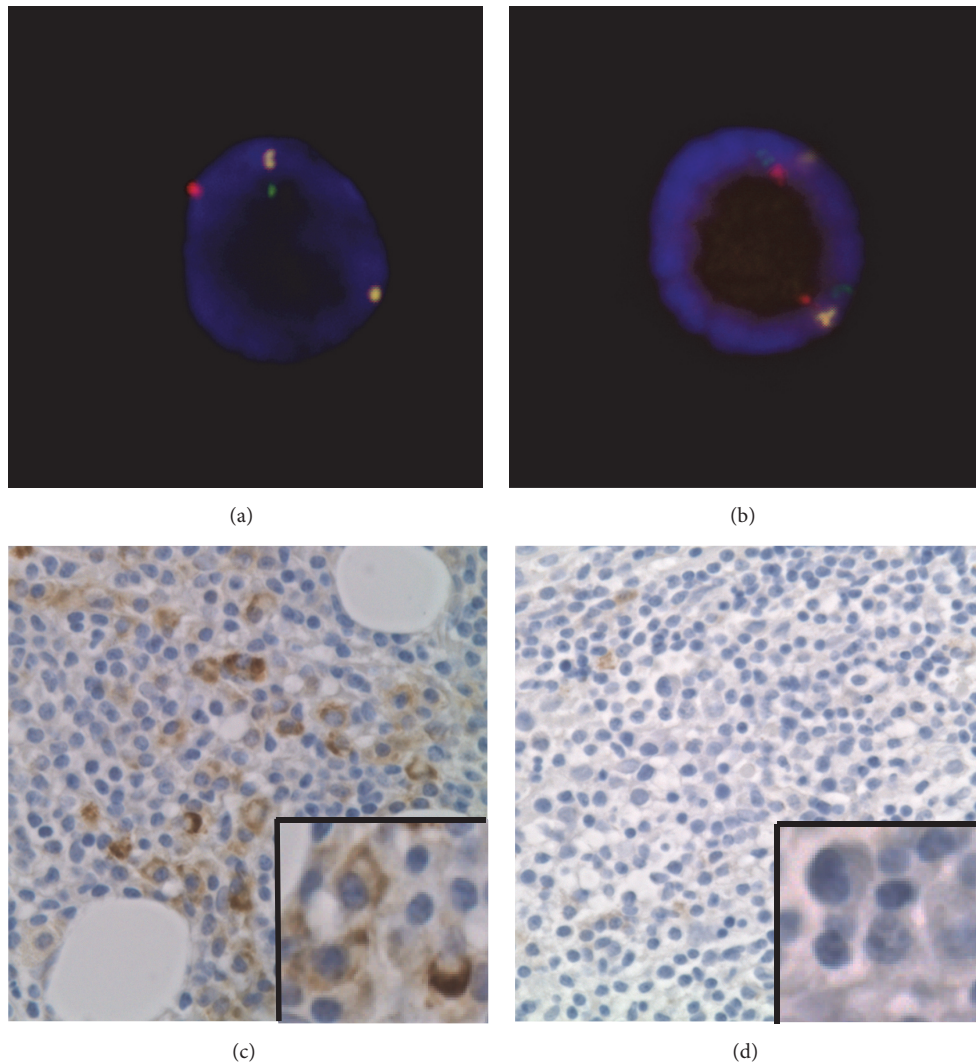


FIGURE 1: FISH analysis of BM aspirates using the A20/BLIMP1/SHGC-79576 Three Color Probe (Cancer Genetics Italia™) and IL21R staining of a BM biopsied specimen. Green, red, and yellow signals represent BLIMP1, A20, and SHGC-79576, respectively. (a) 6q del pattern. One green, one red, and two yellow signals were detected, showing nuc ish (SHGC-79576 x2, BLIMP-1x1, A20 x1). (b) Normal pattern. Two green, two red, and two yellow signals are recognized, showing nuc ish (SHGC-79576, BLIMP-1, A20) x2. (c) >70% positivity of IL-21R in lymphoplasmacytic cells and plasma cells (original magnification $\times 600$). (d) <30% positivity of IL-21R in lymphoplasmacytic cells and plasma cells (original magnification $\times 600$).

In contrast, 6q del, including loss of *BLIMP-1* [19–21] and *A20* [22, 23], is recognized in 40%–55% of WM cases in the US and European countries [4–8, 14]. However, it is not recognized in IgM-MGUS, suggesting that it is a secondary event [7]. 6q del has long been thought to be involved in oncogenesis and is also reported to be associated with poor prognostic factors, such as higher levels of IgM and C-reactive protein and poor-risk patients with high ISSWM levels [4–6]. Nevertheless, the underlying biological mechanism of 6q del in WM is unclear.

Several studies regarding genes expression analyses in WM were performed, and these studies contributed to elucidate the biology and activated pathway in WM [24–26]. Chng et al. firstly conducted genes expression analyses in WM [24]. They reported that the most significantly upregulated

gene was *IL6*, and the most significantly associated pathway for genes-set was MAPK signaling in WM compared to chronic lymphocytic leukemia (CLL) and multiple myeloma (MM). San Miguel and colleagues found deregulation of genes involved in plasma cell differentiation including *PAX5*, which was overexpressed, while *BLIMP-1* and *IRF4* were underexpressed in WM in comparison with CLL and MM. In addition, they hypothesized that lack of *PAX5* repression contributed to the upregulation of 3 genes of BCR signaling pathway including *CD79*, *BLNK*, and *SYK* in WM [25]. Jiménez et al. reported that *CD79A* (B cell activation), *IRF3*, *MYD88*, *MEK1*, *P38* (TLR pathway), and *WNK1* (MAPK pathway) were overexpressed in WM compared to IgM-MGUS, in which pathways might be responsible for WM cell growth and survival [26].

TABLE 2: Significant terms on the gene ontology list.

GO Number	GO term	P-value	Numbers of probes
GO:0046649	lymphocyte activation	6.68E-11	31
GO:0043486	histone exchange	1.81E-10	14
GO:0034508	centromere complex assembly	3.22E-10	14
GO:0043044	ATP-dependent chromatin remodeling	1.02E-09	14
GO:0045321	leukocyte activation	2.49E-09	32
GO:1903706	regulation of hemopoiesis	9.44E-09	27
GO:0042113	B cell activation	2.15E-08	18

GO, gene ontology.

TABLE 3: Genes up-regulated in WM with 6q del compared with WM without 6q del.

Function categories	Up-regulated gene
B-cell receptor signaling pathway	<i>CD79a, SYK, BLNK, PLCγ2, CARD11</i>
IL21/21R signaling pathway	<i>IL21R, JAK3</i>
NF-κB activator	<i>FOXP1</i>
Ubiquitin ligase	<i>CBLB</i>
Ikaros zinc finger family	<i>IFZF3</i>
Cytokines	<i>IFNγ</i>
Other genes	<i>MSH6, IMPDH2, AKAP17A, CCR7, MEF2C, POU2F2, ITPKB, BANK1, IL7R, LAX1, ERCCI, PRKCB, KLRC4-KLRK, HDAC9, ITGAL, GON4L, PSENI, RHOH, PSENI</i>

WM, Waldenstrom macroglobulinemia.

One of the unique findings of the present study was that genes involved in the BCR signaling pathway [23], including *CD79a*, *SYK*, *BLNK*, *PLCγ2*, and *CARD11* are upregulated in WM with 6q del patients compared with those without 6q del. Little is known about BCR pathway upregulation in WM [25], although various subtypes of B-cell lymphomas are associated with BCR pathway activation [27]. However, Argyropoulos et al. suggested that the BCR pathway is activated in WM following phosphoproteomic analysis [28]. Moreover, it is widely accepted that *BLIMP-1* suppresses B-cell proliferation and activation, including the BCR signaling pathway, and orchestrates mature PC differentiation by suppressing the expression of genes necessary for commitment and maintenance of the B-cell identity, including *PAX5* and *XBP-1* [29, 30].

During preparation for this manuscript, Staudt and colleague reported that MYD88, TLR9, and BCR complexes (My-T-BCR Complexes) exist in activated B-cell like diffuse large B-cell lymphoma and in WM, which might play a role in tumor growth and survival [31] (Figure 2). In the present study, the BCR signaling pathway was activated in WM with 6q del patients, which might result from the decreased inhibition occurring through the loss of *BLIMP-1*. However, no difference in the proportion of PCs in the BM was observed between WM with and without 6q deletion. Furthermore, *BLIMP-1* was not among downregulated genes in the present study, suggesting that loss of *BLIMP-1* does not affect PC differentiation. Considering these results, the loss of *BLIMP-1* did not appear to act as a loss of heterozygosity regarding PC differentiation.

We also observed *IL21R* and *JAK3* overexpression in WM with del 6q. Investigators from the Mayo Clinic previously reported that the IL21/21R pathway contributes to IgM secretion and WM cell proliferation via the JAK/STAT signaling pathway in a WM cell line and WM patient samples [32]. Considering these results, it is conceivable that increased IgM levels in WM with 6q del are attributable to IL21/21R pathway activation. In the present cohort, the median M-protein level was higher in patients with 6q del than those without 6q del, although the result was not statistically significant because of the small sample size.

Our cDNA microarray analysis of WM with 6q del. also revealed the overexpression of *FOXP1* and the Casitas B-lineage lymphoma b gene (*CBLB*). *FOXP1* overexpression is widely accepted to be a factor of poor prognosis in activated B-cell-like subtype diffuse large B-cell lymphoma and marginal zone B-cell lymphoma, mucosa-associated lymphoid tissue type [33, 34]. Its overexpression was also shown to lead to the constitutive activation of the nuclear factor-κB pathway as well as BCR, CD40, and TLR signaling pathways [35]. *CBLB* encodes a protein involved in the ligand-induced clustering of BCR on the cell surface and delivery of BCR-captured ligands to TLR9 [36]. Considering these findings, *FOXP1* and *CBLB* might act as positive regulators for the BCR signaling pathway in WM with 6q del. patients (Figure 2).

Our present findings might represent an aggressive expression signature of WM with 6q del., although it should be noted that the study was rather exploratory and the sample size was very small.

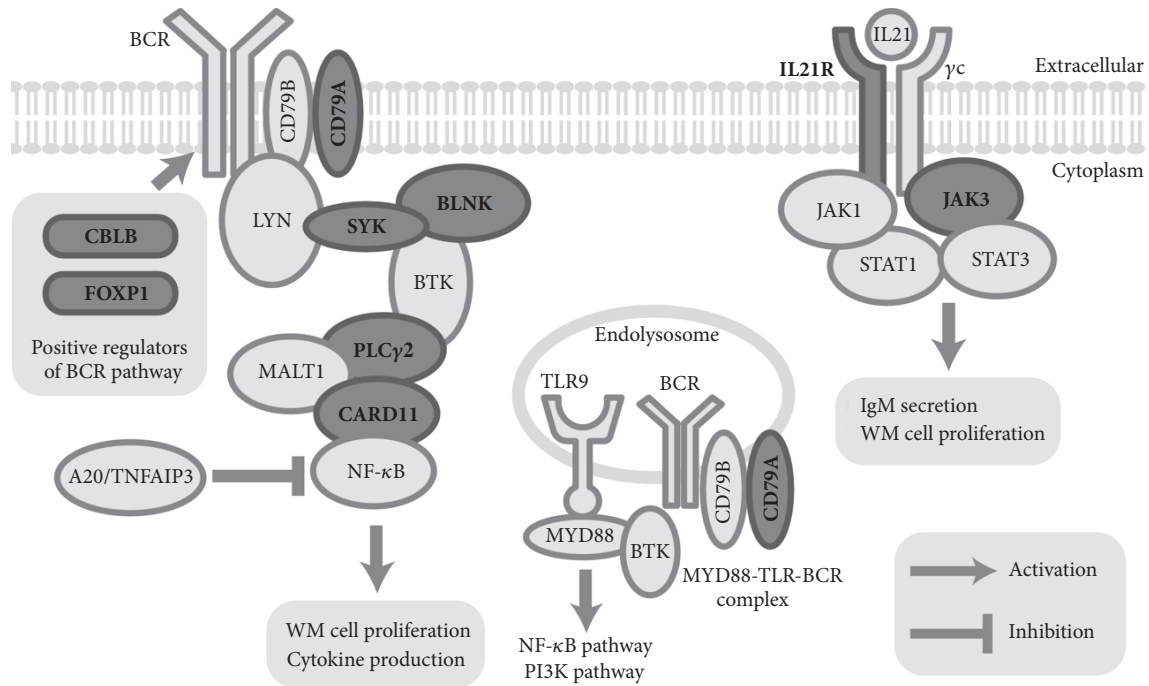


FIGURE 2: Schema of putative biological mechanisms of aggressiveness in Waldenström macroglobulinemia with 6q deletion. Upregulated genes in the present study are represented by bold font and dark shapes.

5. Conclusion

The present study suggested that the BCR signaling pathway and *IL21R* expression are activated in WM with 6q del., and *FOXP1* and *CBLB* appear to act as positive regulators of the BCR signaling pathway. Thus, our present findings might represent an aggressive expression signature of WM with 6q del.

Data Availability

The microarray data sets used in the present study were deposited in the Gene Expression Omnibus under accession number GSE70511 (<http://www.ncbi.nlm.nih.gov/geo/query/acc.cgi?acc=GSE70511>).

Ethical Approval

Investigation has been conducted in accordance with the ethical standards and according to the Declaration of Helsinki and according to national and international guidelines and has been approved by the authors' institutional review board. Institutional Review Board approval was obtained (Disaster Medical Center IRB-2014-8, National Cancer Center Hospital IRB-2013-142).

Disclosure

Masahiro Kiyota Current address is Internal Medicine, The University of Tokyo Hospital, Hongo, Bunkyo-ku, Tokyo 113-8655, Japan.

Conflicts of Interest

The authors have no conflicts of interest to disclose.

Authors' Contributions

Naohiro Sekiguchi and Yukio Kobayashi participated in study design. Naohiro Sekiguchi performed Oligonucleotide microarray analysis. Akihisa Nagata, Naohiro Sekiguchi, Masahiro Kiyota, Ichiro Fukuda, Kazuaki Yamada, and Naoki Takezako prepared the tumor specimens and patient' information. Naohiro Sekiguchi and Yukio Kobayashi wrote the manuscript. All authors discussed the results and commented on the manuscript.

Acknowledgments

The authors would like to thank the members of the research group for useful discussions. This work was supported in part by Grants-in-Aid for Cancer Research from the Ministry of Health, Labour and Welfare of Japan (Clinical Cancer Research 22-014, 22-031, and 23-004), the National Cancer Center Research and Development Fund (23-A-17, 23-A-23, 26-A-4, 26-A-24, and 23-C-7), and a Japan Society for the Promotion of Science, Grant-in-Aid for Scientific Research (C) (25461442, 15K21647, and 16K09865).

Supplementary Materials

Supplementary Table 1. Upregulated gene sets in WM with 6q del compared with WM without 6q del. The sheet contains

428 probe sets. Among them, the first 342 probes that were allocated to genes or loci are shown according to Entrez Gene number in ascending order, and the remaining 86 probes that were not allocated to loci are shown according to fold changes in descending order. **Supplementary Table 2.** Downregulated gene sets in WM with 6q del compared with WM without 6q del. The sheet contains 112 probe sets. Among them, the first 98 probes that were allocated to genes or loci are shown according to Entrez Gene number in ascending order, and the remaining 14 probes that were not allocated to loci are shown according to fold changes in ascending order. (*Supplementary Materials*)

References

- [1] S. H. Swerdlow, A. R. Cook Sohani Jr., S. A. Pileri et al. et al., "Lymphoplasmacytic lymphoma," in *World Health Organization Classification of Tumour of Hematopoietic and Lymphoid Tissues*, S. H. Swerdlow, E. Campo, and N. L. Harris, Eds., IARC Press, Lyon, 2017.
- [2] G. C. Issa, H. Leblebjian, A. M. Roccaro, and I. M. Ghobrial, "New insights into the pathogenesis and treatment of Waldenström macroglobulinemia," *Current Opinion in Hematology*, vol. 18, no. 4, pp. 260–265, 2011.
- [3] A. Vijay and M. A. Gertz, "Waldenström macroglobulinemia," *Blood*, vol. 109, no. 12, pp. 5096–5103, 2007.
- [4] F. Nguyen-Khac, J. Lambert, E. Chapiro et al., "Chromosomal aberrations and their prognostic value in a series of 174 untreated patients with Waldenström's macroglobulinemia," *Haematologica*, vol. 98, no. 4, pp. 649–654, 2013.
- [5] H. Chang, C. Qi, Y. Trieu et al., "Prognostic relevance of 6q deletion in Waldenström's macroglobulinemia: A multicenter study," *Clinical Lymphoma, Myeloma & Leukemia*, vol. 9, no. 1, pp. 36–38, 2009.
- [6] E. M. Ocio, R. F. J. Schop, B. Gonzalez et al., "6q deletion in Waldenström macroglobulinemia is associated with features of adverse prognosis," *British Journal of Haematology*, vol. 136, no. 1, pp. 80–86, 2007.
- [7] R. F. J. Schop, S. A. Van Wier, R. Xu et al., "6q deletion discriminates Waldenström macroglobulinemia from IgM monoclonal gammopathy of undetermined significance," *Cancer Genetics and Cytogenetics*, vol. 169, no. 2, pp. 150–153, 2006.
- [8] E. Braggio, J. J. Keats, X. Leleu et al., "Identification of copy number abnormalities and inactivating mutations in two negative regulators of nuclear factor- κ B signaling pathways in Waldenström's macroglobulinemia," *Cancer Research*, vol. 69, no. 8, pp. 3579–3588, 2009.
- [9] P. Morel, A. Duhamel, P. Gobbi et al., "International prognostic scoring system for Waldenström macroglobulinemia," *Blood*, vol. 113, no. 18, pp. 4163–4170, 2009.
- [10] M. M. Oken, R. H. Creech, and D. C. Tormey, "Toxicity and response criteria of the Eastern Cooperative Oncology Group," *American Journal of Clinical Oncology*, vol. 5, no. 6, pp. 649–655, 1982.
- [11] J. A. Kim, K. Im, S. N. Park, J. Kwon, Q. Choi et al., "MYD88 L265P Mutations Are Correlated with 6q Deletion in Korean Patients with Waldenström Macroglobulinemia," *BioMed Research International*, vol. 2014, Article ID 363540, 7 pages, 2014.
- [12] J. McGowan-Jordan, A. Simons, and M. Schmid, *An International System for Human Cytogenomic Nomenclature*, Cytogenetic and Genome Research, 2016.
- [13] C. Li and W. H. Wong, "Model-based analysis of oligonucleotide arrays: expression index computation and outlier detection," *Proceedings of the National Academy of Sciences of the United States of America*, vol. 98, no. 1, pp. 31–36, 2001.
- [14] S. M. Ansell, R. A. Kyle, C. B. Reeder et al., "Diagnosis and management of Waldenström macroglobulinemia: Mayo stratification of macroglobulinemia and risk-adapted therapy (mSMART) guidelines," *Mayo Clinic Proceedings*, vol. 85, no. 9, pp. 824–833, 2010.
- [15] S. P. Treon, L. Xu, G. Yang et al., "MYD88 L265P somatic mutation in Waldenström's macroglobulinemia," *The New England Journal of Medicine*, vol. 367, no. 9, pp. 826–833, 2012.
- [16] S. P. Treon and Z. R. Hunter, "A new era for Waldenström macroglobulinemia: MYD88 L265P," *Blood*, vol. 121, no. 22, pp. 4434–4436, 2013.
- [17] M. Varettoni, L. Arcaini, S. Zibellini et al., "Prevalence and clinical significance of the MYD88 (L265P) somatic mutation in Waldenström's macroglobulinemia and related lymphoid neoplasms," *Blood*, vol. 121, no. 13, pp. 2522–2528, 2013.
- [18] G. Yang, Y. Zhou, X. Liu et al., "A mutation in MYD88 (L265P) supports the survival of lymphoplasmacytic cells by activation of Bruton tyrosine kinase in Waldenström macroglobulinemia," *Blood*, vol. 122, no. 7, pp. 1222–1232, 2013.
- [19] S. L. Nutt, K. A. Fairfax, and A. Kallies, "BLIMP1 guides the fate of effector B and T cells," *Nature Reviews Immunology*, vol. 7, no. 12, pp. 923–927, 2007.
- [20] J. Monge, E. Braggio, and S. M. Ansell, "Genetic Factors and Pathogenesis of Waldenström's Macroglobulinemia," *Current Oncology Reports*, vol. 15, no. 5, pp. 450–456, 2013.
- [21] G. Bianchi, A. Sacco, S. Kumar, G. Rossi, I. Ghobrial, and A. Roccaro, "Candidate genes of Waldenström's macroglobulinemia: Current evidence and research," *The Application of Clinical Genetics*, vol. 6, pp. 32–42, 2013.
- [22] M. Kato, M. Sanada, I. Kato et al., "Frequent inactivation of A20 in B-cell lymphomas," *Nature*, vol. 459, no. 7247, pp. 712–716, 2009.
- [23] U. Novak, A. Rinaldi, I. Kwee et al., "The NF-kappaB negative regulator TNFAIP3 (A20) is inactivated by somatic mutations and genomic deletions in marginal zone lymphomas," *Blood*, vol. 113, no. 20, pp. 4918–4921, 2009.
- [24] W. J. Chng, R. F. Schop, T. Price-Troska et al., "Gene-expression profiling of Waldenström macroglobulinemia reveals a phenotype more similar to chronic lymphocytic leukemia than multiple myeloma," *Blood*, vol. 108, no. 8, pp. 2755–2763, 2006.
- [25] N. C. Gutiérrez, E. M. Ocio, J. de las Rivas et al., "Gene expression profiling of B lymphocytes and plasma cells from Waldenström's macroglobulinemia: Comparison with expression patterns of the same cell counterparts from chronic lymphocytic leukemia, multiple myeloma and normal individuals," *Leukemia*, vol. 21, no. 3, pp. 541–549, 2007.
- [26] C. Jiménez, M. I. Prieto-Conde, M. García-Álvarez et al., "Unraveling the heterogeneity of IgM monoclonal gammopathies: a gene mutational and gene expression study," *Annals of Hematology*, vol. 97, no. 3, pp. 475–484, 2018.
- [27] C. U. Niemann and A. Wiestner, "B-cell receptor signaling as a driver of lymphoma development and evolution," *Seminars in Cancer Biology*, vol. 23, no. 6, pp. 410–421, 2013.

- [28] K. V. Argyropoulos, R. Vogel, C. Ziegler et al., "Clonal B cells in Waldenström's macroglobulinemia exhibit functional features of chronic active B-cell receptor signaling," *Leukemia*, vol. 30, no. 5, pp. 1116–1125, 2016.
- [29] A. L. Shaffer, K.-I. Lin, T. C. Kuo et al., "Blimp-1 orchestrates plasma cell differentiation by extinguishing the mature B cell gene expression program," *Immunity*, vol. 17, no. 1, pp. 51–62, 2002.
- [30] A. L. Shaffer, A. Rosenwald, and L. M. Staudt, "Lymphoid malignancies: the dark side of B-cell differentiation," *Nature Reviews Immunology*, vol. 2, no. 12, pp. 920–932, 2002.
- [31] J. D. Phelan, R. M. Young, D. E. Webster et al., "A multiprotein supercomplex controlling oncogenic signalling in lymphoma," *Nature*, vol. 560, no. 7718, pp. 387–391, 2018.
- [32] L. S. Hodge, S. C. Ziesmer, Z. Z. Yang et al., "IL-21 in the bone marrow microenvironment contributes to IgM secretion and proliferation of malignant cells in Waldenstrom macroglobulinemia," *Blood*, vol. 120, no. 18, pp. 3774–3782, 2012.
- [33] A. H. Banham, J. M. Connors, P. J. Brown et al., "Expression of the FOXP1 transcription factor is strongly associated with inferior survival in patients with diffuse large B-cell lymphoma," *Clinical Cancer Research*, vol. 11, no. 3, pp. 1065–1072, 2005.
- [34] X. Sagaert, P. De Paepe, L. Libbrecht et al., "Forkhead box protein P1 expression in mucosa-associated lymphoid tissue lymphomas predicts poor prognosis and transformation to diffuse large B-cell lymphoma," *Journal of Clinical Oncology*, vol. 24, no. 16, pp. 2490–2497, 2006.
- [35] M. van Keimpema, L. J. Grueneberg, and M. Mokry, "FOXP1 directly represses transcription of pro-apoptotic genes and cooperates with NF-kappaB to promote survival of human B-cells," *Blood*, vol. 124, no. 23, pp. 3431–3440, 2014.
- [36] M. Veselits, A. Tanaka, S. Lipkowitz et al., "Recruitment of Cbl-b to B cell antigen receptor couples antigen recognition to toll-like receptor 9 activation in late endosomes," *PLoS ONE*, vol. 9, no. 3, 2014.

Research Article

A Bioinformatic Profile of Gene Expression of Colorectal Carcinoma Derived Organoids

Peng A ¹, Xinyi Xu,^{1,2} Chenglin Wang,^{1,2} Ling Ye,^{1,2} and Jing Yang ^{1,2}

¹State Key Laboratory of Oral Diseases, West China School of Stomatology, Sichuan University, Chengdu 610041, Sichuan, China

²National Clinical Research Center for Oral Diseases & Department of Cariology and Endodontics, West China Hospital of Stomatology, Sichuan University, Chengdu 610041, Sichuan, China

Correspondence should be addressed to Jing Yang; yangj7@qq.com

Received 19 March 2018; Revised 29 May 2018; Accepted 15 August 2018; Published 27 September 2018

Academic Editor: Maria L. Tornesello

Copyright © 2018 Peng A et al. This is an open access article distributed under the Creative Commons Attribution License, which permits unrestricted use, distribution, and reproduction in any medium, provided the original work is properly cited.

Colorectal carcinoma is one of the common cancers in human. It has been intensely debated whether the *in vitro* cancer cell lines are closely enough for recapitulating the original tumor in understanding the molecular characteristic of CRC. Organoid as a new *in vitro* 3D culture system has sprang out in CRC study for the capability in reviving the original tissue. The aim of this study is to profile the gene expression of CRC organoid. The gene expression GSE64392 was from GEO database contained 20-patients-derived 37 organoid samples, including 22 colorectal tumor organoid samples and 15 paired healthy samples. Gene ontology (GO) and Kyoto Encyclopedia of Genes and Genomes (KEGG) were applied for classifying differentially expressed genes (DEGs). Protein interaction among DEGs was analyzed by Search Tool for the Retrieval of Interacting Genes (STRING) and Cytoscape software. In total, 853 gene sequences were identified. GO analysis revealed that DEGs were extensively involved in various biological process (BP), like proliferation, cell cycle, and biosynthesis. KEGG pathway analysis showed that WNT, MAPK, TGF- β , SHH, ECM-receptor interaction, and FGF pathways were altered. DEGs which were identified with protein interactions were major response for extracellular matrix organization and the GPCR pathway. In conclusion, our study profiled the DEGs in CRC organoids and promotes our understanding of the CRC organoids as a new model for colorectal cancer research.

1. Introduction

Colorectal carcinoma (CRC) is one of the major cancers and is a contributor to cancer mortality and mobility in human. A variety of studies have revealed critical mutations of genes and the dysregulation of signaling pathways is important for the development of CRC [1]. Nevertheless, like other cancers, CRC presents the instability in genome, which usually leads to the diversity of cancer cell phenotype [1]. The genomic instability consisting of gene mutation and chromosomal hyperchange has been investigated as an important contributor of CRCs [1, 2]. To date, cancer cell lines are still mainly used in tumor research, as the accessibility and ease in manipulation [3], whereas cancer cell lines can be representative of tumors as an *in vitro* system is controversial [4, 5]. Recently, the Cancer Cell Line Encyclopedia (CCLE) characterized nearly 1,000 cancer cell lines via larger-scale genomic application [6]. Most cancer cell lines exhibited

a relatively positive correlation in representing the original tumors from which cancer cell lines were derived. However, most cancer cell lines were derived from highly aggressive and fast growing tumor [3]; they tend to possess more genomic alterations than primary tumor, leading to be partial in representing the initiation or development of tumor [3]. Cancer cell line apparently limits in representing clinical attributes, like diagnosis, drug response, and treatment. A recent developed 3D culture system, organoid technology, demonstrated the maintenance of primary crypt physiology [7]. Then a long-term culture system was established for human intestinal and colonic epithelium organoid, indicating the application in development, pharmacology, and tumorigenesis of colon [8]. In addition, a large scale sequencing has been performed to characterize the developmental lineage tree on the organoid platform, reviving several features of normal mouse development [9]. Most recently, an established organoid bank of CRC patients resembled the primary tumor

tissue physiologically [10]. Moreover, the genomic feature of tumor organoid mimics the primary tissue extensively [10]. Thus, analyzing the gene expression profile and the interaction of differentially expressed genes (DEGs) network of CRC organoid is crucial for understanding the biomedical application of organoid technology in CRCs and sustains that organoid is promising in personalized CRC therapy.

In this study, we analyzed gene expression profiles of healthy and tumor organoids of CRC patients with the GEO2R supported by Gene Expression Omnibus (GEO, <http://www.ncbi.nlm.nih.gov/geo/>). Subsequently, the DEGs were subjected to DAVID, to perform the gene ontology (GO) and pathway enrichment analysis. Then, we investigated the protein interaction among the DEGs. Our study may provide insight of organoids derived from patients as a potential 3D system for investigating the development of CRCs.

2. Materials and Methods

2.1. Microarray Data. The gene expression array of patients-derived healthy and tumor organoids GSE64392 was from GEO database. GSE64392, which was based on Affymetrix Human Gene 2.0 ST Arrays, was submitted by Marc van de Wetering et al. The GSE64392 dataset contained 37 organoid samples derived from 20 patients, including 22 colorectal tumor organoid samples and 15 paired healthy samples.

2.2. Gene Expression Profile Analysis. Differentially expressed genes were analyzed with the GEO2R, which accompanies with the GEO dataset and is supported by GEO database and available at <https://www.ncbi.nlm.nih.gov/geo/>. Data were analyzed with default parameters. Genes with Log₂-fold change between tumor and healthy samples ≥ 1 or ≤ -1 were classified as differentially expressed genes (DEGs) and the adjusted P-value (adj.P.Val) < 0.05 was considered as statistical significance.

2.3. Gene Ontology and Pathway Analysis. Database for Annotation, Visualization, and Integrated Discovery (DAVID: <https://david.ncifcrf.gov/>) is a web application integrated various annotation sources including Gene ontology (GO) and Kyoto Encyclopedia of Genes and Genomes (KEGG) and is essential for the interpretation of high-throughput datasets. DAVID was applied for analyzing the enrichment of GO and KEGG pathway of DEGs. $P < 0.05$ was considered as statistical significance.

2.4. Protein-Protein Interactions (PPIs) Analysis. Search Tool for the Retrieval of Interacting Genes (STRING) is a web-accessible database of protein-protein interactions (PPIs). STRING (version 10.5) currently covers 9'643'763 proteins from 2'031 organisms, including Homo sapiens. To evaluate the protein associations among DEGs, we mapped the DEGs to STRING; interactions with combined score ≥ 0.4 (medium confidence) were considered significant. Cytoscape (3.5.1) was used to visualize the interaction network. The plugin

Molecular Complex Detection (MCODE) was performed to screen the network, with the MCODE score > 3 . Pathway enrichment was analyzed for clusters; $P < 0.05$ was considered as significant difference.

3. Results

3.1. Differentially Expressed Genes. Tissue derived organoids profoundly preserved the basic morphology and organization of primary tissues [7, 8, 10]. Moreover, tumor derived organoids profoundly revealed the genomic features of primary tumors [10]. Marc van de Wetering et al. compared the transcriptome profile of organoids with paired tumor tissues from nine patients. The gene expression profile of organoids displayed a high correlation (Pearson correlation 0.918 ± 0.040) with original paired biopsies, suggesting that organoids successfully recaptured the primary tumors on the scale of gene expressions [10]. Thus, it is grounded to analyze the organoids-based transcriptome profile. In this study, the total 37 organoid samples consisting with 22 tumors and 15 healthy samples were analyzed. Based on the GEO2R analysis, 853 gene sequences were identified. Only genes with GeneBank accession number according to National Center for Biotechnology Information (NCBI) database were listed as differentially expressed genes. Thus, a total of 405 genes were classified, 100 genes were upregulated in tumor organoid samples, and 305 genes were downregulated (Data not shown). The expression of top 50 upregulated and top 50 downregulated genes is listed (Figure 1).

3.2. Gene Ontology (GO) Enrichment Analysis. GO analysis was performed with the DAVID web application. Biological processes (BP) essential for the tumorigenesis exhibited the extensive mRNA expression change in tumor organoid samples. We grouped cell cycle, cell proliferation, and growth to the capability of tumor for doubling its population; both upregulated and downregulated genes enriched in tumor population process (Table 1). In addition, in tumor samples gene expression alteration was found enriched in metastasis and angiogenesis which are characters of cancer [11] (Table 1). Upregulated genes also enriched in the process of biosynthesis. Processes which are important for the survival of cancer cells including cell death evasion, inflammation process, and immune system all exhibited the genes downregulation (Table 1). In addition, downregulated genes showed enrichment in extracellular matrix organization, homeostasis, and secretion process. For cell component (CC), hyperexpressed genes only enriched in the plasma membrane. However, genes those downregulated in tumor samples were found in various aspects of cells, which could be mainly grouped to extracellular part, cell-cell communication (cell junction), plasma membrane, and cytoplasm organelles (Table 2). For molecular function (MF), overexpressed genes exhibited significant enrichments in nucleotide binding, including DNA binding and RNA polymerase activity (Table 3). Genes exhibiting the decrease in mRNA expression dramatically enriched in signaling molecular binding, including ion binding and ligand-receptor binding (Table 3).

TABLE 1: Gene ontology (GO) enrichment analysis of differentially expressed genes (DEG) in tumor organoids. Genes' enrichment of biological processes (BP), EMT: Epithelial-mesenchymal transition; ECM: Extracellular matrix.

Category	Group	Term	GenesCount	GenesCount ratio of Total genes	P-Value	Benjamini	
Upregulated	Population	Cell cycle (GO:0051726)	10	10	4.80E-02	3.20E-01	
		Cell proliferation (GO:0042127)	20	20	1.40E-04	4.80E-03	
		Growth (GO:0040007)	16	16	3.90E-05	2.10E-03	
	Metastasis	Cell migration (GO:0016477)	15	15	1.70E-03	2.90E-02	
		Cell motility (GO:0048870)	16	16	1.80E-03	3.00E-02	
		Locomotion (GO:0040011)	17	17	2.70E-03	4.00E-02	
		EMT (GO:0001837)	8	8	7.40E-07	2.00E-04	
	Agiogenesis	Cell adhesion (GO:0007155)	15	15	3.50E-02	2.70E-01	
		Agiogenesis (GO:0001525)	8	8	4.00E-03	5.50E-02	
	Others	Vasculogenesis (GO:0001570)	4	4	5.10E-03	6.40E-02	
		Biosynthetic process (GO:0009889)	37	37	2.90E-04	7.90E-03	
	GOTERM_BP_ALL	Metastasis	Cell migration (GO:0016477)	34	11.5	2.70E-04	1.70E-02
			Cell motility (GO:0048870)	36	12.2	5.10E-04	2.50E-02
		Locomotion (GO:0040011)	39	13.2	8.70E-04	3.50E-02	
		Localization of cell (GO:0051674)	36	12.2	5.10E-04	2.50E-02	
Cell adhesion; GO:0007155		37	12.5	1.50E-02	2.10E-01		
Cell death (GO:0008219)		49	16.6	2.20E-04	1.50E-02		
Apoptosis (GO:0006915)		44	14.9	4.60E-04	2.30E-02		
Growth (GO:0040007)		27	9.1	1.30E-03	4.30E-02		
Cell proliferation (GO:0008283)		42	14.2	5.00E-03	1.00E-01		
Downregulated		Inflammatory response	Chronic inflammatory response (GO:002544)	3	1	4.10E-02	3.60E-01
	Inflammatory response (GO:0006954)		19	6.4	6.10E-03	1.20E-01	
	Agiogenesis	Agiogenesis (GO:0001525)	12	4.1	4.10E-02	3.60E-01	
		ECM orgnization (GO:0030198)	20	6.8	5.10E-07	2.20E-03	
	Others	Homeostatic process (GO:0042592)	35	11.8	2.50E-02	2.80E-01	
		Secretion (GO:0046903)	33	11.1	1.50E-04	1.20E-02	
		Immune system process (GO:0002376)	50	16.9	1.50E-02	2.10E-01	

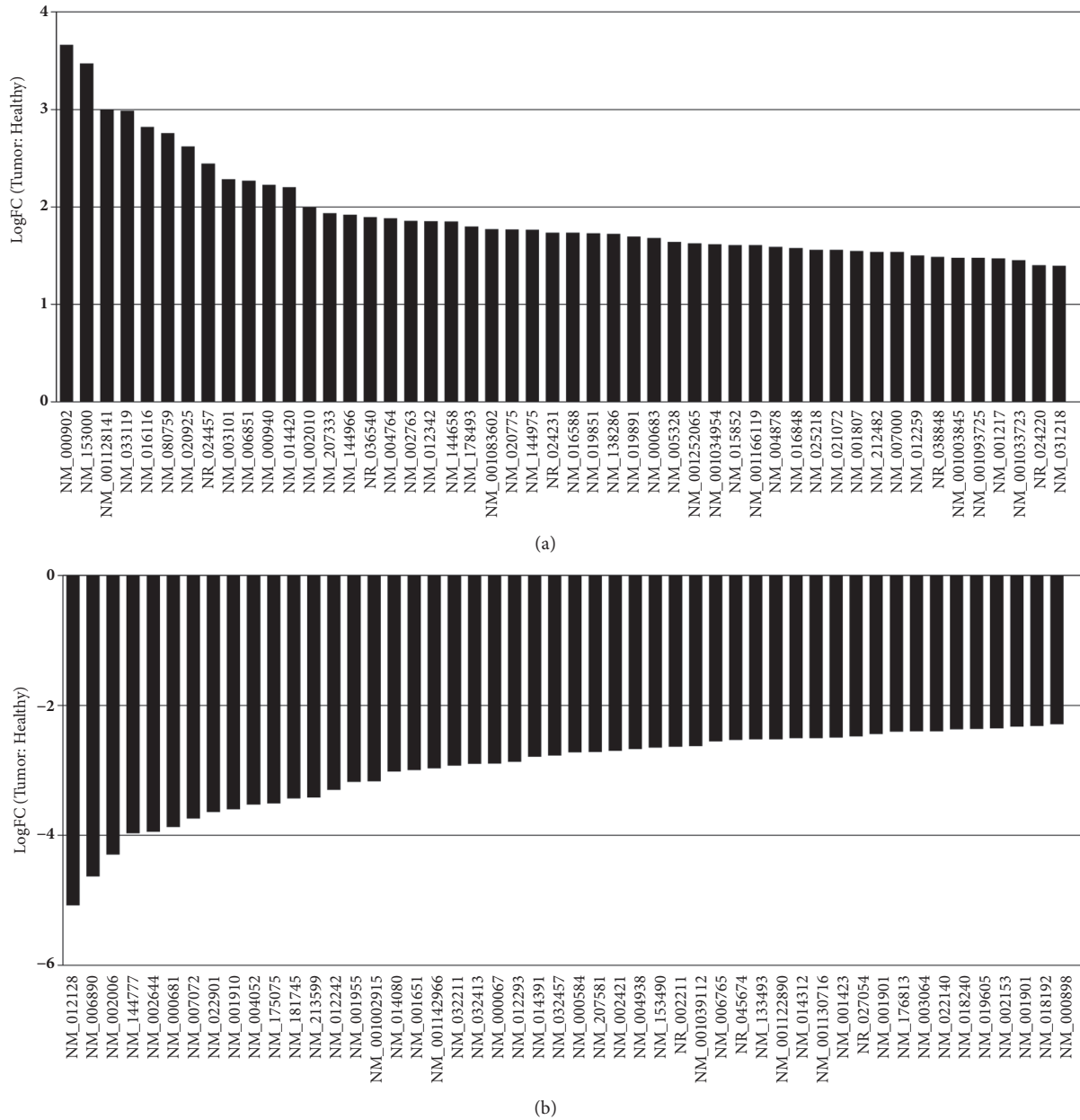


FIGURE 1: The top 100 differentially expressed genes (DEGs), 50 upregulated genes (a) and 50 downregulated genes (b).

3.3. KEGG Pathway Analysis. In the work by Marc van de Wetering et al., it is presented that the mutation rates per Mb of tumor organoids exhibited the similarity of paired biopsies. Mutations in organoids were predominantly CpG to T transitions, consistent with original tumor tissues. Moreover, somatic variants within the coding regions in organoids were highly concordant with the corresponding biopsies for both hypermutated and nonhypermutated patients (median = 0.88 frequency of concordance, range 0.62–1.00). Furthermore, combine the analysis of somatic copy number alterations (SCNAs) and single nucleotide variants (SNVs) to infer Cancer Fractions (CCF) between tumor organoids and biopsies, revealing that CRC driver mutations were maintained in organoids and most commonly altered genes and were

all represented in organoids, including *APC*, *TP53*, *KRAS*, *PIK3CA*, *FBXW7*, and *SMAD4*. These results suggested that there were no distinct CRC driver mutations in organoids which may lead to the variation in pathways. Next, in order to identify the pathway enrichment of DEGs in tumor organoid samples, we investigated the KEGG pathway enrichment of DEGs using DAVID (Table 4). Thus, alteration of gene expression can be found in well-defined CRC related pathway including WNT, MAPK, and TGF- β pathways [1, 2]. We also grouped SHH, ECM-receptor interaction, and FGF signaling pathways. Hyperexpressed genes were also found to regulate cell adhesion. Interestingly, three upregulated genes in colorectal cancer organoid samples were also associated with basal cell carcinoma. Repressed genes were found to

TABLE 2: Gene ontology (GO) enrichment analysis of differentially expressed genes (DEGs) in tumor organoids. Genes' enrichment of cell component (CC).

Category	Group	Term (GO)	GenesCount	%	P-Value
GOTERM_CC_ALL	Upregulated	Plasma membrane part (GO:0044459)	21	21	2.20E-02
		Extracellular region part (GO:0044421)	111	37.5	1.90E-13
		Extracellular region (GO:0005576)	120	40.5	1.00E-11
		Extracellular space (GO:0005615)	52	17.6	4.00E-09
		Extracellular exosome (GO:0070062)	76	25.7	1.10E-07
		Vesicle (GO:0031982)	93	31.4	1.20E-07
		Extracellular vesicle (GO:1903561)	76	25.7	1.30E-07
		Extracellular organelle (GO:0043230)	76	25.7	1.40E-07
		Proteinaceous extracellular matrix (GO:0005578)	21	7.1	4.50E-07
		Extracellular matrix component (GO:0044420)	12	4.1	3.10E-06
		Extracellular matrix (GO:0031012)	24	8.1	4.20E-06
		Cell periphery (GO:0071944)	111	37.5	1.40E-05
		Plasma membrane (GO:0005886)	108	36.5	2.50E-05
		Plasma membrane part (GO:0044459)	65	22	2.90E-05
		Plasma membrane region (GO:0098590)	31	10.5	5.60E-05
		Basement membrane (GO:0005604)	9	3	8.10E-05
		Microvillus (GO:0005902)	8	2.7	1.10E-04
		Cell surface (GO:0009986)	26	8.8	1.80E-04
		Intrinsic component of plasma membrane (GO:0031226)	43	14.5	6.30E-04
		Apical part of cell (GO:0045177)	15	5.1	1.00E-03
		Integral component of plasma membrane (GO:0005887)	41	13.9	1.00E-03
	Membrane part (GO:0044425)	130	43.9	1.20E-03	
	Downregulated	Actin-based cell projection (GO:0098858)	10	3.4	1.40E-03
		Intrinsic component of membrane (GO:0031224)	113	38.2	1.40E-03
		Apical plasma membrane (GO:0016324)	13	4.4	1.40E-03
		Anchored component of membrane (GO:0031225)	9	3	2.30E-03
		Integral component of membrane (GO:0016021)	110	37.2	2.40E-03
		Membrane raft (GO:0045121)	12	4.1	2.80E-03
		Membrane microdomain (GO:0098857)	12	4.1	2.90E-03
		Brush border (GO:0005903)	7	2.4	4.00E-03
		Cluster of actin-based cell projections (GO:0098862)	8	2.7	5.40E-03
		Membrane region (GO:0098589)	13	4.4	6.60E-03
		Endomembrane system (GO:0012505)	75	25.3	8.70E-03
		Basolateral plasma membrane (GO:0016323)	9	3	1.10E-02
		Membrane (GO:0016020)	158	53.4	1.90E-02
		Caveola (GO:0005901)	5	1.7	2.30E-02
		Microvillus membrane (GO:0031528)	3	1	3.10E-02
		Plasma membrane raft (GO:0044853)	5	1.7	3.30E-02
		Cytoplasmic vesicle (GO:0031410)	28	9.5	4.00E-02
		Intracellular vesicle (GO:0097708)	28	9.5	4.10E-02
		Spanning component of membrane (GO:0089717)	2	0.7	4.40E-02
		Spanning component of plasma membrane (GO:0044214)	2	0.7	4.40E-02
Actin cytoskeleton (GO:0015629)		13	4.4	4.50E-02	
Cytoplasmic, membrane-bounded vesicle (GO:0031410)	26	8.8	4.50E-02		

be tightly associated with Rap1 signaling and regulating Pantothenate and CoA biosynthesis, cytoskeleton, and renin-angiotensin system. In addition, downregulated genes were indicated to contribute the formation of bladder cancer in human.

3.4. Protein Interaction Network Analysis. Protein-protein interactions (PPIs) are critical for the signaling transduction and the biological process. Thus, to investigate the protein interactions among the DEGs, we screened the protein interaction within the STRING database. Nodes with combined

TABLE 3: Gene ontology (GO) enrichment analysis of differentially expressed genes (DEGs) in tumor organoids. Genes' enrichment of molecular function (MF).

Category	Group	Term	Count	%	P-Value
		sequence-specific double-stranded DNA binding (GO:1990837)	14	14	3.40E-05
		transcription regulatory region sequence-specific DNA binding (GO:0000976)	13	13	9.60E-05
		double-stranded DNA binding (GO:0003690)	14	14	9.80E-05
		transcription factor activity, sequence-specific DNA binding (GO:0003700)	16	16	5.90E-04
		nucleic acid binding, sequence-specific DNA binding (GO:0001071)	16	16	6.00E-04
		transcription regulatory region DNA binding (GO:0044212)	13	13	6.50E-04
		regulatory region DNA binding (GO:0000975)	13	13	6.70E-04
		regulatory region nucleic acid binding (GO:0001067)	13	13	6.80E-04
		sulfur compound binding (GO:1901681)	7	7	8.30E-04
		RNA polymerase II transcription factor activity, sequence-specific DNA binding (GO:0000981)	11	11	1.10E-03
		transcription factor activity, RNA polymerase II core promoter proximal region sequence-specific binding (GO:0000982)	8	8	1.20E-03
		receptor binding (GO:0005102)	17	17	1.20E-03
		RNA polymerase II core promoter proximal region sequence-specific DNA binding (GO:0000978)	8	8	1.50E-03
		transcriptional repressor activity, RNA polymerase II transcription regulatory region sequence-specific binding (GO:0001227)	6	6	1.50E-03
		sequence-specific DNA binding (GO:0043565)	14	14	1.60E-03
Upregulated		transcriptional repressor activity, RNA polymerase II core promoter proximal region sequence-specific binding (GO:0001078)	5	5	1.90E-03
		carbonate dehydratase activity (GO:0004089)	3	3	1.90E-03
		core promoter proximal region sequence-specific DNA binding (GO:0000987)	8	8	2.00E-03
		core promoter proximal region DNA binding (GO:0001159)	8	8	2.10E-03
		RNA polymerase II regulatory region sequence-specific DNA binding (GO:0000977)	10	10	2.10E-03
		RNA polymerase II regulatory region DNA binding (GO:0001012)	10	10	2.20E-03
		activating transcription factor binding (GO:0033613)	4	4	2.80E-03
		DNA binding (GO:0003677)	23	23	3.20E-03
		metal ion binding (GO:0046872)	32	32	3.70E-03
		ion binding (GO:0043167)	33	33	4.20E-03
		cation binding (GO:0043169)	32	32	4.40E-03
		RNA polymerase II activating transcription factor binding (GO:0001102)	3	3	1.40E-02
		kinase binding (GO:0019900)	8	8	2.30E-02
		hydro-lyase activity (GO:0016836)	3	3	2.50E-02
		carboxyl-O-methyltransferase activity (GO:0010340)	2	2	3.30E-02
		protein carboxyl O-methyltransferase activity (GO:0051998)	2	2	3.30E-02
		binding (GO:0005488)	75	75	3.80E-02
		protein kinase binding (GO:0019901)	7	7	4.00E-02
		heparin binding (GO:0008201)	4	4	4.00E-02
		enzyme binding (GO:0019899)	15	15	4.10E-02
		modified amino acid binding (GO:0072341)	3	3	4.40E-02
		carbon-oxygen lyase activity (GO:0016835)	3	3	4.70E-02
		alcohol binding (GO:0043178)	3	3	4.80E-02
GOTERM_MF_ALL					

TABLE 3: Continued.

Category	Group	Term	Count	%	P-Value
		calcium ion binding (GO:0005509)	32	10.8	8.80E-08
		growth factor binding (GO:0019838)	11	3.7	2.10E-05
		laminin binding (GO:0043236)	5	1.7	9.50E-04
		NADH pyrophosphatase activity (GO:0035529)	3	1	2.10E-03
		phospholipid binding (GO:0005543)	14	4.7	2.50E-03
		collagen binding (GO:0005518)	6	2	2.60E-03
		cytokine activity (GO:0005125)	10	3.4	6.00E-03
		fibronectin binding (GO:001968)	4	1.4	6.50E-03
		metal ion binding (GO:0046872)	80	27	7.60E-03
		extracellular matrix binding (GO:0050840)	5	1.7	7.80E-03
		sulfur compound binding (GO:1901681)	10	3.4	8.10E-03
		lipid binding (GO:0008289)	19	6.4	9.10E-03
		receptor antagonist activity (GO:0048019)	3	1	9.10E-03
		receptor binding (GO:0005102)	34	11.5	9.80E-03
		heparin binding (GO:0008201)	8	2.7	9.90E-03
		cation binding (GO:0043169)	80	27	1.00E-02
		calcium-dependent phospholipid binding (GO:0005544)	5	1.7	1.10E-02
		glycosaminoglycan binding (GO:0005539)	9	3	1.30E-02
		ion binding (GO:0043167)	82	27.7	1.30E-02
		enzyme inhibitor activity (GO:0004857)	13	4.4	1.40E-02
		receptor inhibitor activity (GO:0030547)	3	1	1.80E-02
		nucleotide diphosphatase activity (GO:0004551)	3	1	2.30E-02
		transforming growth factor beta binding (GO:0050431)	3	1	2.30E-02
		metalloendopeptidase inhibitor activity (GO:0008191)	3	1	2.30E-02
		protein homodimerization activity (GO:0042803)	19	6.4	2.40E-02
		binding (GO:0005488)	225	76	2.60E-02
		receptor regulator activity (GO:0030545)	4	1.4	3.20E-02
		actin binding (GO:003779)	12	4.1	3.50E-02
		protein binding (GO:0005515)	175	59.1	3.60E-02
		interleukin-1 receptor antagonist activity (GO:0005152)	2	0.7	4.40E-02
		fibroblast growth factor binding (GO:0017134)	3	1	4.50E-02
		cytoskeletal protein binding (GO:0008092)	20	6.8	4.70E-02
	Downregulated				

TABLE 4: Kyoto Encyclopedia of Genes and Genomes (KEGG) pathway analysis of differentially expressed genes (DEGs) in tumor organoids.

Category	KEGG pathway	Genes Count	%	P-Value	Gene members
Upregulated	Wnt signaling pathway	5	5	3.20E-03	NM_012342, NM_004655, NM_014420, NM_001166119, NM_033119
	Basal cell carcinoma	3	3	2.50E-02	NM_004655, NM_001166119, NM_001083602
	Pathways in cancer	6	6	2.90E-02	NM_004655, NM_019851, NM_002010, NM_212482, NM_001166119, NM_001083602
	Adherens junction	3	3	4.00E-02	NM_001166119, NM_005985, NM_001034954
Downregulated	Rap1 signaling pathway	9	3	1.40E-02	NM_000899, NM_003253, NM_021116, NM_001992, NM_001962, NM_002006, NM_022970, NM_057159, NM_003246
	Bladder cancer	4	1.4	2.40E-02	NM_000584, NM_004938, NM_002421, NM_003246
	Pantothenate and CoA biosynthesis	3	1	3.00E-02	NM_006208, NM_005021, NM_004666
	Pathways in cancer	12	4.1	3.60E-02	NM_000584, NM_000899, NM_004991, NM_021116, NM_001200, NM_001992, NM_004938, NM_002006, NM_022970, NM_057159, NM_002421, NM_000958
	Regulation of actin cytoskeleton	8	2.7	4.10E-02	NM_006633, NM_003253, NM_001992, NM_002006, NM_022970, NM_001127663, NM_053025, NM_001112706
	Renin-angiotensin system	3	1	4.70E-02	NM_001150, NM_021804, NM_000537

score ≥ 0.4 (medium confidence) were subjected to Cytoscape to visualize the protein interaction (Figure 2). Total nodes were subjected to analyze the interaction modules by using MCODE. Four modules were extracted from the network (Figures 3(a)~3(d)). Pathway enrichment analysis of modules showed that proteins were mainly involved in extracellular matrix organization and the GPCR signaling pathway.

4. Discussion

Colorectal cancer development is a complex process of accumulation of genetic mutations, epigenetic alteration, and dysregulation of signaling pathways [1]. Despite numerous progress has been made in elucidating the molecular mechanism of the development of CRC, the underlying mechanism remains vagueness. Cancer cell lines have been applied as the main workforce for cancer research [3, 6]. Nevertheless, like other tumors, CRC exhibits a high genomic instability which contributes to the various phenotypes and pathologies of CRCs [2]. Cancer cell lines limit in the capability of resembling the characteristics of the primary tumor tissue. Studies have reported the difference in gene expression and genomic alteration between cell line and tumors [4, 5, 12, 13]. Resulting from the identification of Lgr5+ stem cell in intestine and colon [14], a new 3D in vitro system, organoid [7], has made great impact on the colorectal research [10, 15, 16]. As organoids resemble the characteristics of primary tissue, organoids have been widely applied for studying organ

development, tissue homeostasis, tumorigenesis, and disease [17–19]. As a promising *ex vivo* 3D culture system for studying CRC, profiling genes expression level of CRC organoids is important for understanding the development of CRC. In the present study, we analyzed the data from GSE64392 and identified 100 upregulated genes and 305 downregulated genes in tumor organoids. DEGs were identified to involve in main capabilities of cancer, including cell renew, metastasis, angiogenesis, and cell death escaping. By analyzing the protein interaction of DEGs, we classified genes that may provide new insight for understanding the development of CRC.

In order to have a better view about the function of DEGs, GO analysis and KEEG pathway were performed. Upregulated genes were mainly involved in biological processes consisting of cell cycle, the cell proliferation controlling, tumor metastasis, and angiogenesis, which are essential for the sustentation of tumor [11]. For downregulated genes, in addition to involving the retaining of tumor, genes were also accumulated in biological processes which serves as barriers to cancer [11]. For example, programmed cell death, apoptosis, which is the most important physiologic processes in body to eliminate deteriorated cells [11], was another downregulated gene-enriched biological process. Moreover, downregulated genes were also found to participate in the following process, like extracellular matrix (ECM) organization, secretion process, immune-response, and homeostasis, alteration of which is acquired by cancer to escape the

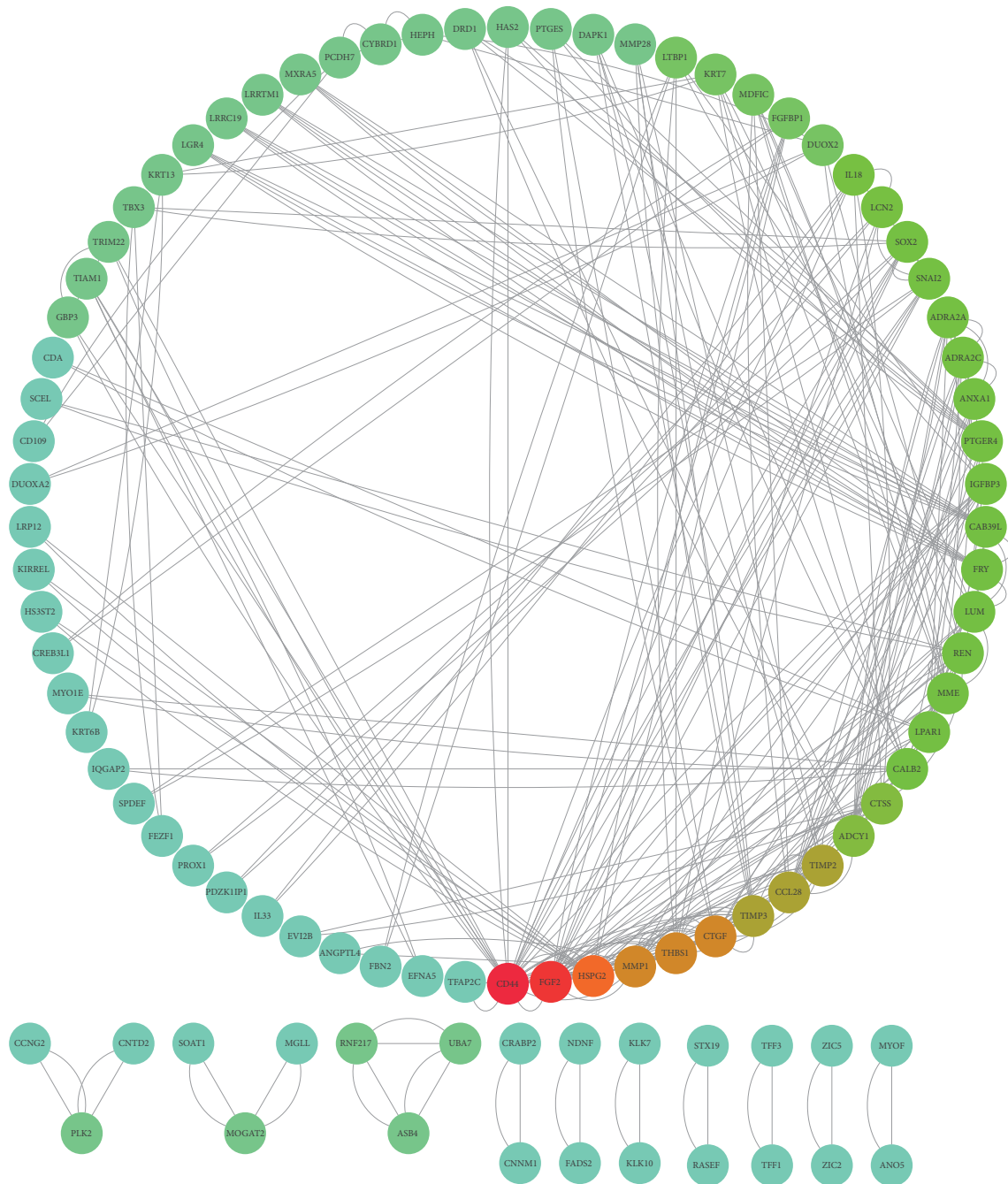


FIGURE 2: The protein-protein interaction (PPI) network of differentially expressed genes (DEGs).

tethering of surrounding tissue and the chasing of immune system [11]. Organoid culture system has been proved to recapitulate the *in vivo* counterpart [20]; specifically, established CRC organoid cultures displayed a highly agreement with the primary tumor tissue, in genomic mutation, chromosomal alterations, and epigenetic modifications [1, 2, 10]. The KEGG pathway enrichment analysis revealed that genes in WNT pathway are upregulated, including *AXIN2*, *DKK4*, and *NK1*, which are target of WNT/ β -catenin signaling pathway and also antagonize WNT pathway. In addition,

LEF1, which activates gene transcription in the axis of WNT signaling, was upregulated as well. The hyperexpression of WNT target genes corresponds with the hyperactivated WNT pathway in primary CRC and CRC cancer cell lines, most likely resulting from the biallelic inactivation mutation of *APC*, *FBXW7*, *AXIN2*, and *FAM123B* or the activating mutations in *CTNNB1* [2, 6]. Besides, overexpressed genes were identified to involve in other pathways, including FGF signaling, SHH signaling, and that are commonly found in various types of cancers [6, 21–23]. What is more, upregulated

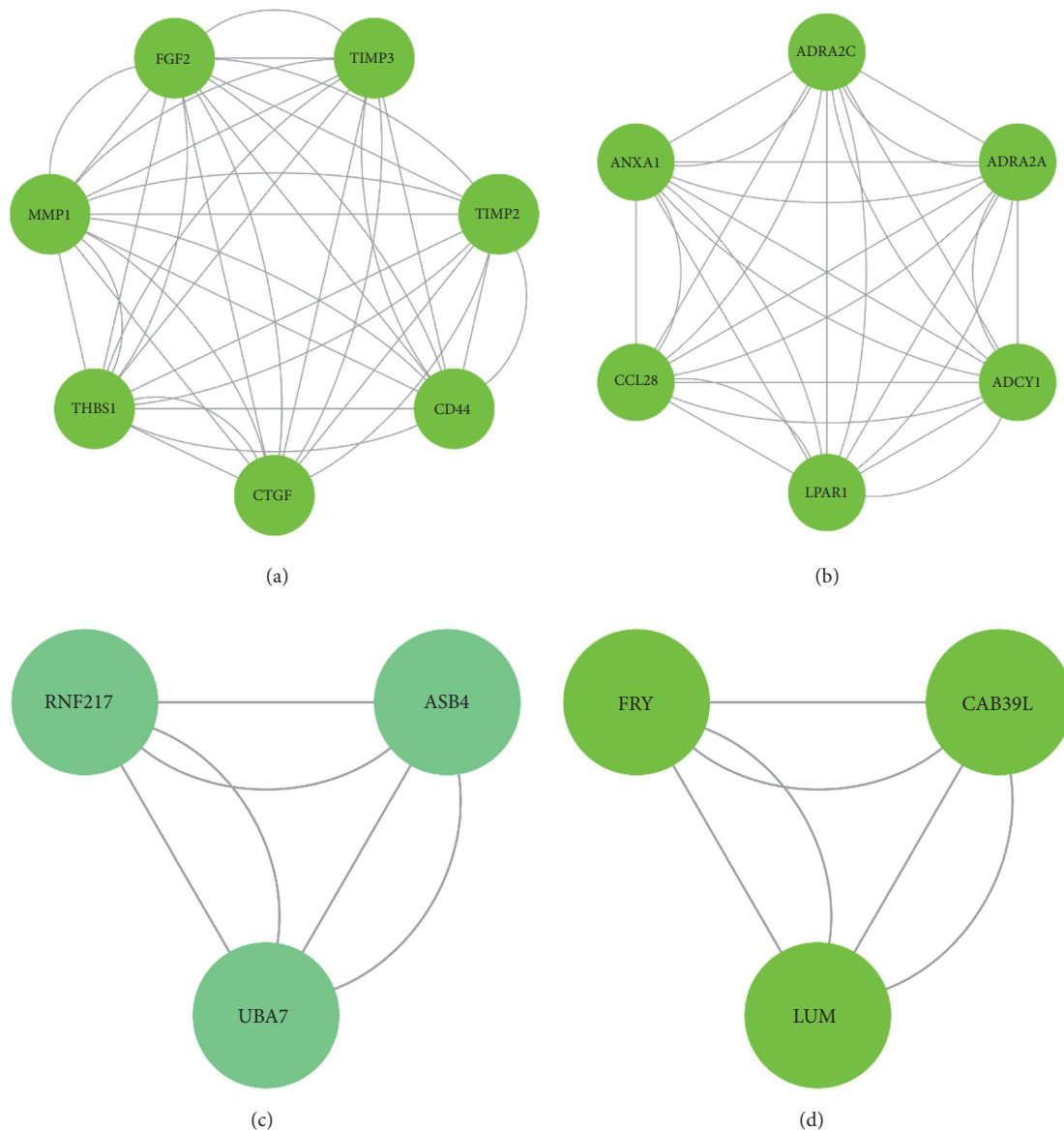


FIGURE 3: Top 4 modules of the protein-protein interaction (PPI) network were listed.

genes were related to cell-cell adhesion, alteration of which is widely reported in cancer [11, 24]. For downregulated genes, besides carcinoma common pathways, altered genes were identified in Rap1 pathway, which regulates various cancer tightly related biological processes, including angiogenesis control, cell movements, intercellular interaction, and cell expansion [6, 25]. Genes associated with CoA synthesis were also identified hypoexpressed, indicating the alteration of metabolism in CRCs [26, 27]. Also, downregulated genes were classed in regulating cytoskeleton, this is correlated with the dysregulation of signaling transduction intracellularly. Additionally, downregulated genes were identified in renin-angiotensin system which is an important pathway in regulating plasma sodium concentration and blood pressure, indicating that the development of CRCs may affect the

homeostasis via the hormone system. Surveying alterations of these pathways may help us to understand the development of CRCs.

Protein interactions are essential for the signaling transduction within cells and communicating intercellularly and environmentally. The protein interaction module analysis of DEGs revealed that, in tumor organoid samples, PPIs were identified and enriched in extracellular matrix organization, GPCR signaling pathway. GPCRs are the largest receptor in eukaryotes; they are coupled with G proteins triggering signaling cascades to regulate various physiological processes [28]. The alteration of GPCRs signaling pathway, in cancer cells, promotes the proliferation, angiogenesis, and metastasis, aids to escape from apoptosis, and sustains the survive. Moreover, PPIs were also identified to involve in

other signaling pathways, including AMPK signaling, mTOR signaling, and DNA damage, which are frequently altered in CRCs [2].

In conclusion, our study shows a bioinformatic analysis of differentially expressed genes in CRCs organoids. The study supports the fact that organoid technology as a promising *in vitro* 3D system recapitulates the property of tumors. Our study will encourage the exploration of the application of organoid as a more convenient resource for CRC therapy studies.

Data Availability

The data used to support the findings of this study are available from the corresponding author upon request.

Disclosure

This article does not contain any studies with human participants or animals performed by any of the authors.

Conflicts of Interest

The authors declare that they have no conflicts of interest.

Authors' Contributions

A. Peng formed the conception and designed the experiments. A. Peng, Xinyi Xu, Chenglin Wang, Ling Ye, and Jing Yang drafted and revised the article. Jing Yang revised the work critically. All authors have approved the manuscript and agreed with this publication.

Acknowledgments

The authors would like to thank Xin Li and Fanyuan Yu for revising this article. This work was supported by the National Natural Science Foundation of China (81600859) and Science Foundation of Sichuan Province under Grant no. 17-YCG053 (2017036).





References

- [1] E. R. Fearon, "Molecular genetics of colorectal cancer," *Annual Review of Pathology: Mechanisms of Disease*, vol. 6, no. 6, pp. 479–507, 2011.
- [2] The Cancer Genome Atlas Network, "Comprehensive molecular characterization of human colon and rectal cancer," *Nature*, vol. 487, no. 7407, pp. 330–337, 2012.
- [3] J. R. W. Masters, "Human cancer cell lines: fact and fantasy," *Nature Reviews Molecular Cell Biology*, vol. 1, no. 3, pp. 233–236, 2000.
- [4] D. T. Ross, U. Scherf, M. B. Eisen et al., "Systematic variation in gene expression patterns in human cancer cell lines," *Nature Genetics*, vol. 24, no. 3, pp. 227–235, 2000.
- [5] R. Sandberg and I. Ernberg, "The molecular portrait of *in vitro* growth by meta-analysis of gene-expression profiles," *Genome Biology*, vol. 6, p. R65, 2005.
- [6] J. Barretina, G. Caponigro, N. Stransky et al., "The Cancer Cell Line Encyclopedia enables predictive modelling of anticancer drug sensitivity," *Nature*, vol. 483, pp. 603–607, 2012.
- [7] T. Sato, R. G. Vries, H. J. Snippert et al., "Single Lgr5 stem cells build crypt-villus structures *in vitro* without a mesenchymal niche," *Nature*, vol. 459, no. 7244, pp. 262–265, 2009.
- [8] T. Sato, D. E. Stange, M. Ferrante et al., "Long-term expansion of epithelial organoids from human colon, adenoma, adenocarcinoma, and Barrett's epithelium," *Gastroenterology*, vol. 141, no. 5, pp. 1762–1772, 2011.
- [9] S. Behjati, M. Huch, R. Van Boxtel et al., "Genome sequencing of normal cells reveals developmental lineages and mutational processes," *Nature*, vol. 513, no. 7518, pp. 422–425, 2014.
- [10] M. van de Wetering, H. E. Francies, J. M. Francis et al., "Prospective derivation of a living organoid biobank of colorectal cancer patients," *Cell*, vol. 161, no. 4, pp. 933–945, 2015.
- [11] D. Hanahan and R. A. Weinberg, "The hallmarks of cancer," *Cell*, vol. 100, no. 1, pp. 57–70, 2000.
- [12] D. J. Smiraglia, L. J. Rush, M. C. Frühwald et al., "Excessive CpG island hypermethylation in cancer cell lines versus primary human malignancies," *Human Molecular Genetics*, vol. 10, no. 13, pp. 1413–1419, 2001.
- [13] S. Houshdaran, S. Hawley, C. Palmer et al., "DNA Methylation Profiles of Ovarian Epithelial Carcinoma Tumors and Cell Lines," *PLoS ONE*, vol. 5, no. 2, p. e9359, 2010.
- [14] N. Barker, J. H. van Es, J. Kuipers et al., "Identification of stem cells in small intestine and colon by marker gene *Lgr5*," *Nature*, vol. 449, no. 7165, pp. 1003–1007, 2007.
- [15] M. Matano, S. Date, M. Shimokawa et al., "Modeling colorectal cancer using CRISPR-Cas9-mediated engineering of human intestinal organoids," *Nature Medicine*, 2015.
- [16] J. Drost, R. Van Boxtel, F. Blokzijl et al., "Use of CRISPR-modified human stem cell organoids to study the origin of mutational signatures in cancer," *Science*, vol. 358, no. 6360, pp. 234–238, 2017.
- [17] J. Drost and H. Clevers, "Translational applications of adult stem cell-derived organoids," *Development*, vol. 144, no. 6, pp. 968–975, 2017.
- [18] J. Roper, T. Tammela, N. M. Cetinbas et al., "In vivo genome editing and organoid transplantation models of colorectal cancer and metastasis," *Nature Biotechnology*, vol. 35, no. 6, pp. 569–576, 2017.
- [19] M. Huch, S. F. Boj, and H. Clevers, "Lgr5⁺ liver stem cells, hepatic organoids and regenerative medicine," *Journal of Regenerative Medicine*, vol. 8, no. 4, pp. 385–387, 2013.
- [20] M. Huch and B.-K. Koo, "Modeling mouse and human development using organoid cultures," *Development*, vol. 142, no. 18, pp. 3113–3125, 2015.
- [21] M. Touat, E. Ileana, S. Postel-Vinay, F. André, and J.-C. Soria, "Targeting FGFR signaling in cancer," *Clinical Cancer Research*, vol. 21, no. 12, pp. 2684–2694, 2015.
- [22] I. S. Babina and N. C. Turner, "Advances and challenges in targeting FGFR signalling in cancer," *Nature Reviews Cancer*, vol. 17, no. 5, pp. 318–332, 2017.
- [23] L. L. Rubin and F. J. de Sauvage, "Targeting the Hedgehog pathway in cancer," *Nature Reviews Drug Discovery*, vol. 5, no. 12, pp. 1026–1033, 2006.
- [24] U. Cavallaro and G. Christofori, "Cell adhesion and signalling by cadherins and Ig-CAMs in cancer," *Nature Reviews Cancer*, vol. 4, no. 2, pp. 118–132, 2004.

- [25] B. Vaill e, D. Vittet, and J.-J. Feige, “*In vitro* models of vasculogenesis and angiogenesis,” *Laboratory Investigation*, vol. 81, no. 4, pp. 439–452, 2001.
- [26] M. G. V. Heiden, L. C. Cantley, and C. B. Thompson, “Understanding the warburg effect: the metabolic requirements of cell proliferation,” *Science*, vol. 324, no. 5930, pp. 1029–1033, 2009.
- [27] M. Agathocleous and W. A. Harris, “Metabolism in physiological cell proliferation and differentiation,” *Trends in Cell Biology*, vol. 23, no. 10, pp. 484–492, 2013.
- [28] R. T. Dorsam and J. S. Gutkind, “G-protein-coupled receptors and cancer,” *Nature Reviews Cancer*, vol. 7, no. 2, pp. 79–94, 2007.

Research Article

Efficient Synthesis of Glutamate Peptide-Estradiol Conjugate for Imaging Estrogen Receptor-Positive Diseases

Ming-Chi Shih ¹, Sergio Daniel Simon,² Zhiming Jin,³ Yuan Gui,³
Bohua Xu,³ Zhihong Xu,³ Paulo Henrique Rosado-de-Castro ^{4,5},
Ana Maria Silveira Braghirolli,⁶ Lea Mirian Barbosa da Fonseca ⁵,
Tomio Inoue,⁷ and David J. Yang ⁸

¹Department of Internal Medicine, School of Medicine, Federal University of Rio De Janeiro, Rio De Janeiro, Brazil

²Brazilian Breast Cancer Study Group (GBECAM), Brazil

³Jiangsu Huayi Technology Co., Ltd, Jiangsu, China

⁴Institute of Biomedical Sciences, Federal University of Rio de Janeiro, Rio de Janeiro, Brazil

⁵Department of Radiology, School of Medicine, Federal University of Rio de Janeiro, Rio de Janeiro, Brazil

⁶Nuclear Engineering Institute, National Nuclear Energy Commission, Rio de Janeiro, Brazil

⁷Director of Advanced Medical Center, Shonan Kamakura General Hospital, Kamakura, Japan

⁸Vyripharm Biopharmaceuticals LLC, Houston, Texas, USA

Correspondence should be addressed to Ming-Chi Shih; mingchi.shih@gmail.com

Received 14 February 2018; Revised 19 June 2018; Accepted 16 August 2018; Published 25 September 2018

Academic Editor: Franco M. Buonaguro

Copyright © 2018 Ming-Chi Shih et al. This is an open access article distributed under the Creative Commons Attribution License, which permits unrestricted use, distribution, and reproduction in any medium, provided the original work is properly cited.

Molecular imaging of estrogen receptor-positive (ER+) pathway-activated system serves the basis of ER+ disease management such as cancers and endometriosis. ER+ patients have better response to endocrine therapy and survive twice as long as negative ER patients. However, tumor resistance resulting from clinical used aromatase inhibitors and antiestrogens is unpredictable. Radiolabeled ER+ ligand could quantify ER+ tissue uptake which helps to stage and restage of the cancer as well as endometriosis. The differential diagnosis of ER+ lesions by using a labeled ligand helps to select the patients for optimal response to endocrine therapy and to discontinue the treatment when resistance occurs. In addition, radiolabeled ER+ ligand serves as basis for image-guided response follow-up. Glutamate receptors are cell surface receptors which are overexpressed in inflammation and infection. Using glutamate peptide as a drug carrier helps to target intracellular genes via glutamate receptor-mediated process. Reports have shown that polyglutamate is a drug carrier that could alter drug solubility and enhance estrogen receptor-ligand binding pocket. However, polyglutamate was a blend of mixed polymer with a wide range of molecular weight. Thus, the structural confirmation and purity of the conjugates were not optimized. To overcome this problem, the efficient synthesis of glutamate peptide-estradiol (GAP-EDL) conjugate was achieved with high purity. EDL was conjugated site-specific at the first glutamate of GAP. The average cell uptake of ⁶⁸Ga-GAP-EDL was 5-fold higher than the previous reported synthesis. The efficient synthesis of GAP-EDL has greatly enhanced sensitivity and specificity in cell uptake studies. In vivo PET imaging studies indicated that ⁶⁸Ga-GAP-EDL could image ER (+) tumors in MCF-7 tumor-bearing mice. Therefore, GAP-EDL makes it possible to image ER-enriched endometriosis and cancer.

1. Introduction

Estrogen leads to genomic effects on transcription through α and β estrogen receptors (ERs), which are primarily found in the nucleus. The function of ER α in the mediation of gene transcription is widely documented, and reports with mouse

models and human breast cancer cell lines have indicated that ER α has a part in cell proliferation. On the other hand, the function of ER β as a transcriptional regulator continues to be ambiguous. Reports indicate that ER β can reduce ER α activity, possibly by heterodimerization [1, 2]. Estrogen may elicit rapid ‘non-genomic’ actions on different cellular processes

through membrane ERs. ER modulators including tamoxifen are valuable instruments for the evaluation the mechanisms of action of estrogen. ER intermediates inhibition of NF- κ B activity at numerous levels. This cross-talk among central regulators of endocrine and immune systems might be used for treating oncologic, inflammatory, and autoimmune disorders [3]. Oxidative stress is related to an excess of reactive oxygen species (ROS). ROS induce DNA injury and lead to overactivation of poly-ADP ribose polymerase-1 (PARP-1), which results in depletion of cytosolic NAD⁺. ROS also increase proinflammatory transcription factor NF- κ B leading to neuroinflammation. Reduction of NAD⁺ inhibits glycolysis and yielding inadequate levels of pyruvate and reducing mitochondrial ATP production. Furthermore, NAD⁺ reduction causes ineffective conversion of lactate to pyruvate and lactate cannot be the energy substrate, leading to cell apoptosis. There are three principal paths for the elimination of ROS, including reduced thioredoxin (TXN), glutathione (GSH), and catalase, which have key enzymes that may be aimed to reduce antioxidant effects within cancer cells. Amid such pathways, GSH is influenced by increased cysteine and glutamate transporter systems, as well as NADPH. GSH is derived from cysteine and glutamate. Glutaminase 1 (GLS1) and GLS2 produce glutamate, and cysteine is provided by the cystine/glutamate transporter XCT for the production of GSH through the action of the glutamate-cysteine ligase modifier subunit (GCLM) and the GCL catalytic subunit (GCLC). GSH has direct action on the elimination of ROS through glutathione peroxidase and glutathione *S*-transferase [4–6]. Glutamate leads to cellular overload with Ca²⁺ ions during ROS which induces the production of GSH. Thus, glutamate receptor/transporter system is associated with intracellular GSH production. The excitatory amino acid glutamate exerts its action through different glutamate receptors. Metabotropic glutamate receptors may interact with membrane ERs and, more specifically, the mGlu5 receptor subtype. mGlu5 and 17 β -estradiol antagonists have neuroprotective effects in the 1-methyl-4-phenyl-1,2,3,6-tetrahydropyridine (MPTP) mouse model of Parkinson disease [7]. Therefore, estradiol (EDL), an ER ligand, was selected as a molecule for conjugation to glutamate peptide.

It has been described that glutamate peptide (GAP) stimulates bone resorption in vitro and specific to glutamate receptors [8]. GAP has shown its ability to target renal tissue [9]. It would be amenable to conjugate estradiol (EDL) to GAP and GAP-EDL may increase binding efficacy to cytosolic ERs. With acid residue from GAP, GAP could chelate radiometallic isotopes for imaging and radio therapeutic applications. Previously it has been reported that ^{99m}Tc-GAP-EDL and ⁶⁸Ga-GAP-EDL are useful compounds for imaging functional ER via ER-mediated process by planar scintigraphy and PET [10, 11]. However, EDL was conjugated to GAP using aqueous purification [10–12]. However, the cell uptake was low. This is probably due to its purity. In receptor-based imaging, the agent needs to achieve high specific activity (Ci/umol). If the labeled agent is contaminated with different molecular weight, the image quality assurance would be

problematic. In addition, it is unknown at which position the drug is conjugated to GAP. Regulatory compliance of detailed Chemistry, Manufacturing, and Control (CMC) information during clinic trials is required by governmental agency. Thus, it is amenable to develop pure glutamate peptide-estradiol (GAP-EDL). With sufficient purity, the overexpressed glutamate systems could enhance cell uptake of labeled GAP-EDL. Once GAP-EDL internalized, GAP-EDL could target ER pathways. Here, we report the efficient synthesis of GAP-EDL that allows EDL to be conjugated to the first glutamate of glutamate peptide.

2. Material and Methods

2.1. Synthesis of (8R,9S,13S,14S)-3-Cyanomethoxy-13-methyl-7,8,9,11,12,14,15,16-octahydro-6H-cyclopenta[a]phenanthren-17-one (GAP-EDL-1). (8R,9S,13S,14S)-3-Hydroxy-13-methyl-7,8,9,11,12,14,15,16-octahydro-6H-cyclopenta[a]phenanthren-17-one (Estrone, 2.00g, 7.40 mmol) was dissolved in anhydrous tetrahydrofuran (THF, 25ml) under nitrogen atmosphere. Sodium methoxide (0.80g, 14.82mmol) was then added. Bromoacetonitrile (1.78g, 14.84 mmol) dissolved in 12mL THF was dropwisely added. The mixture was stirred at room temperature for 1h. The additional sodium methoxide (0.60g, 11.11mmol) and bromoacetonitrile (1.21g, 10.89 mmol) in 4mL THF were added. The reaction mixture was continued to stir at room temperature for 0.5 h. Saturated ammonium chloride solution (100ml) and ethyl acetate (100mL) was added to the reaction mixture. The organic layer was collected. The aqueous phase was extracted with additional ethyl acetate (2x50mL). The organic layer was combined and washed with saturated sodium chloride solution. The organic extract was dried over magnesium sulfate and filtered. The solvent was evaporated under reduced pressure. The crude solid product was washed with diethyl ether and obtained 2.11g (6.82mmol) solid product with 92.2% yield. ¹H-NMR (300MHz, DMSO): 7.27 (d, J=8.6Hz, 1H), 6.83 (dd, J=8.8Hz,2.6Hz, 1H), 6.78(d, J=2.5Hz, 1H), 5.11(s, 2H), 2.80-2.86(m, 2H), 2.36-2.50(m, 2H), 2.16-2.26(m, 1H), 1.84-2.15(m, 3H),1.74-1.80(m, 1H), 1.33-1.46(m, 3H), and 1.46-1.60(m, 3H),0.84 (s, 3H). LC-MS was calculated for C₂₀H₂₃NO₂, 309.2, and found [M+H]⁺ 310.1. The spectrum is shown in Figure 1.

2.2. Synthesis of (8R,9S,13S,14S,17S)-3-Aminoethoxy-13-methyl-6,7,8,9,11,12,14,15,16,17-decahydrocyclopenta[a]phenanthrene-17-ol (GAP-EDL-2). Under nitrogen atmosphere GAP-EDL-1 (2.10g, 6.79mmol) was dissolved in anhydrous THF (90 ml). The mixture was cooled down to 0-5°C and lithium aluminum hydride (1.70g, 44.80mmol) was portion wisely added. The reaction mixture was stirred at 0-5°C for 5-10min and then at room temperature 2 hours. After reaction was ended, the mixture was cooled down to 0-5°C again and quenched with water. The suspension was filtered and washed with THF. The filtrate was evaporated and concentrated under reduced pressure. The crude compound was purified by the silica gel-packed column chromatography eluted with methanol/dichloride (MeOH/DCM; 1/30) to afford 3-aminoethoxy estradiol (GAP-EDL-2) as off-white solid

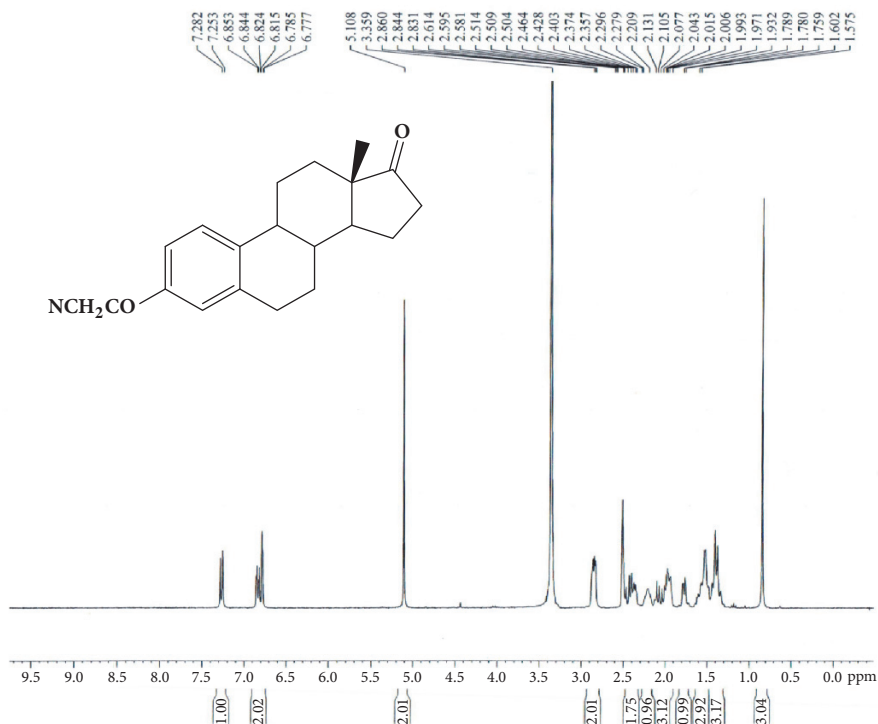


FIGURE 1: Synthesis of GAP-EDL-1.

(1.22 g, 3.87 mmol, 57.0 % yield). ¹H-NMR (300 MHz, CDCl₃): 7.20 (d, J=8.6 Hz, 1H), 6.71 (dd, J=8.6 Hz, 2.7 Hz, 1H), 6.64 (d, J=2.7 Hz, 1H), 3.98 (t, J=5.2 Hz, 2H), 3.73 (t, J=8.4 Hz, 1H), 3.06 (t, J=5.2 Hz, 2H), 2.80-2.85 (m, 2H), 2.26-2.36 (m, 1H), 2.06-2.23 (m, 2H), 1.83-1.98 (m, 2H), 1.65-1.76 (m, 2H), 1.65-1.76 (m, 1H), and 1.14-1.48 (m, 7H), 0.78 (s, 3H). LC-MS was calculated for C₂₀H₂₉NO₂, 315.2, and found [M+H]⁺ 316.1. The spectrum is shown in Figure 2.

2.3. Synthesis of 5- N- [Amino-3-ethoxyestradiol]-1-Benzyl-N-tert-butoxycarbonyl-L-Glutamate 5-Amide (GAP-EDL-3). 1-Benzyl-N-tert-butoxycarbonyl-L-glutamic acid ester (0.50 g, 1.48 mmol), 1,2,3-benzotriazol-1-ol (0.215 g, 1.59 mmol) and benzotriazol-1-yloxy-tris(dimethylamino)phosphonium hexafluoro-phosphate (BOP, 0.700 g, 1.58 mmol) were dissolved in anhydrous dimethylformamide (DMF, 15 mL) under nitrogen atmosphere. N,N-Diisopropylethylamine (DIPEA, 0.205 g, 1.59 mmol) was then added. The reaction mixture was stirred at 0-5 °C and then added with GAP-EDL-2 (0.50 g, 1.585 mmol). The reaction was stirred at 0-5 °C for 10 min and at room temperature for 1 hour. After completion of reaction, DMF was removed under reduced pressure and ethyl acetate (250 mL) was added. The organic phase was washed with 4% sodium bicarbonate solution (200 mL), dried over magnesium sulfate, filtered, and concentrated under reduced pressure. The crude compound was purified by a column chromatography over silica gel eluted with ethyl acetate/dichloromethane (EtOAc/DCM; 5/1) to afford GAP-EDL-3 as white solid (0.40 g, 0.63 mmol, 42.5% yield). ¹H-NMR (300 MHz, CDCl₃): 7.31-7.38 (m, 5H), 7.19 (d, J=8.7 Hz, 1H), 6.69 (dd, J=8.6 Hz, 2.7 Hz, 1H), 6.61 (d, J=2.6 Hz,

1H), 6.27 (br, 1H), 5.27-5.34 (m, 1H), 5.19 (d, J=12.2 Hz, 1H), 5.11 (d, J=12.2 Hz, 1H), 4.28-4.47 (m, 1H), 3.99 (t, J=5.1 Hz, 2H), 3.73 (t, J=8.5 Hz, 1H), 3.62 (q, J=5.7 Hz, 2H), 2.78-2.88 (m, 2H), 2.06-2.34 (m, 6H), 1.84-1.98 (m, 3H), 1.65-1.76 (m, 1H), 1.14-1.54 (m, 16H), and 0.77 (s, 3H). LC-MS was calculated for C₃₇H₅₀N₂O₇, 634.4, and found [M+H]⁺ 335.2. The spectrum is shown in Figure 3.

2.4. Synthesis of 5- N- [Amino-3-ethoxyestradiol]- N-tert-butoxycarbonyl-L-Glutamic acid 5-Amide (GAP-EDL-4). To a solution of GAP-EDL-3 (0.39 g, 0.61 mmol) in THF (40 mL) and methanol (8 mL) under nitrogen atmosphere, 0.080 g of 5% Pd/C was added. The reaction mixture was stirred at room temperature under hydrogen atmosphere for 1 hour. The suspension was then filtered over Celite and concentrated under reduced pressure. The de-ester product was obtained as white solid (0.30 g, 0.55 mmol, 89.7% yield). ¹H-NMR (300 MHz, CDCl₃): 7.19 (d, J=8.7 Hz, 1H), 6.69 (dd, J=8.6 Hz, 2.7 Hz, 1H), 6.61 (d, J=2.6 Hz, 1H), 6.49 (br, 1H), 5.64-5.66 (m, 1H), 4.26 (q, J=6.6 Hz, 1H), 4.02 (t, J=5.1 Hz, 2H), 3.73 (t, J=8.4 Hz, 1H), 3.62-3.70 (m, 2H), 2.81-2.86 (m, 2H), 2.38-2.60 (m, 2H), 2.26-2.36 (m, 1H), 2.06-2.22 (m, 3H), 1.82-2.04 (m, 3H), 1.64-1.76 (m, 1H), 1.17-1.55 (m, 16H), 0.77 (s, 3H). LC-MS was calculated for C₃₀H₄₄N₂O₇, 544.3, and found [M+H]⁺ 545.2. The spectrum is shown in Figure 4.

2.5. Synthesis of 5- N- [Amino-3-ethoxyestradiol]-N-tert-butoxycarbonyl-L-Glutamoyl-1,5-di-t-butyl-L-Glutamate pentapeptide ester (GAP-EDL-5). GAP-EDL-4 (0.580 g, 1.06 mmol), 1-Hydroxybenzotriazole (0.146 g, 1.08 mmol), and BOP (0.470 g, 1.06 mmol) were dissolved in anhydrous DMF

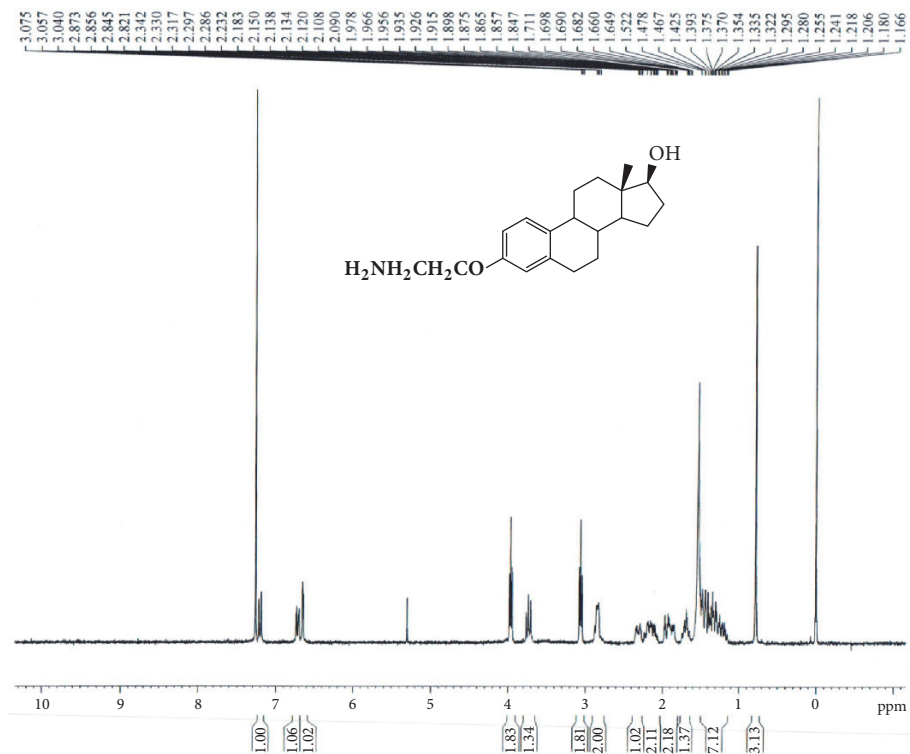


FIGURE 2: Synthesis of GAP-EDL-2.

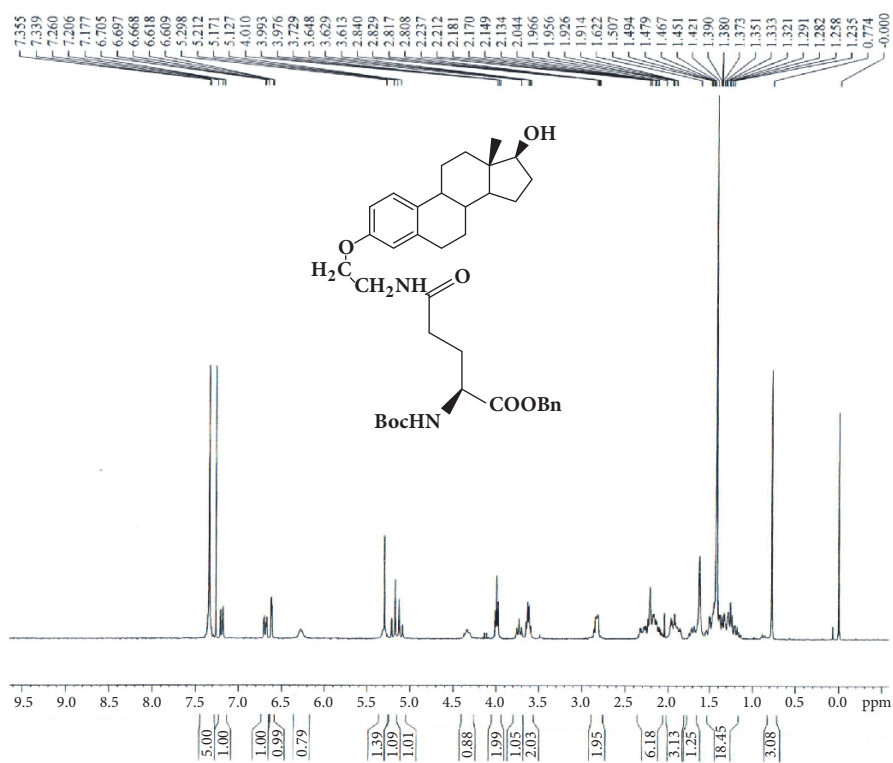


FIGURE 3: Synthesis of GAP-EDL-3.

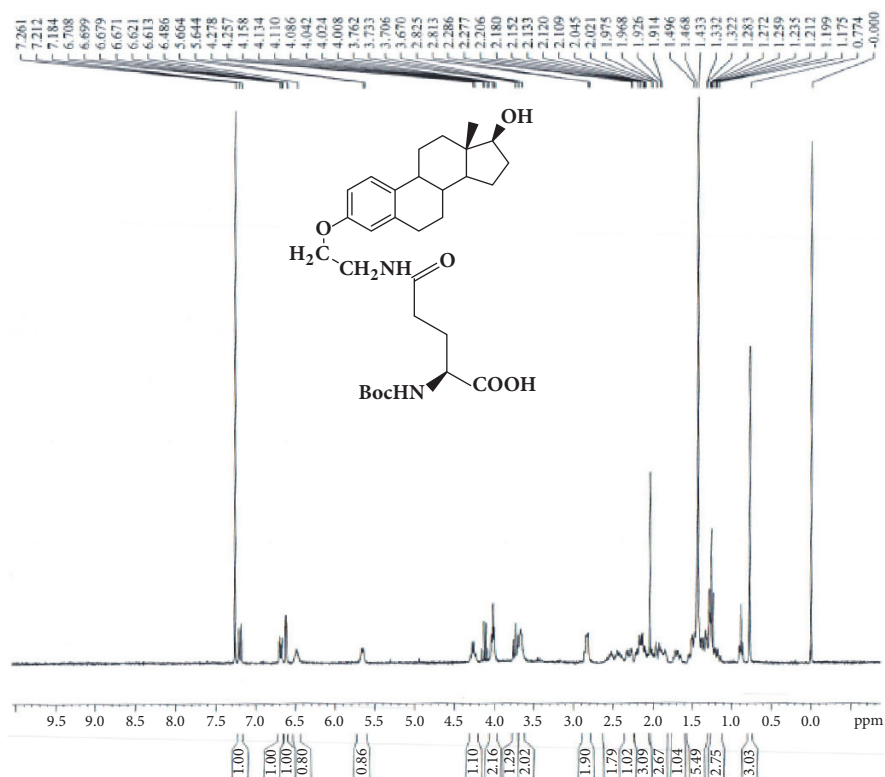


FIGURE 4: Synthesis of GAP-EDL-4.

(10 mL). The mixture was stirred under nitrogen atmosphere with temperature cooled down to 0°C. N,N-Diisopropylethylamine (DIPEA, 0.140g, 1.08mmol) and 1,5-di-t-butyl-L-Glutamate pentapeptide ester (GAP ester, 1.260g, 1.06mmol) (Zhejiang Ontores Biotechnologies Co., Ltd, Hangzhou, Zhejiang, China) were then added. The reaction mixture was continued to stir for 16-18h at 50°C and monitored by TLC. When TLC analysis showed the reaction completion, DMF was removed under reduced pressure and DCM (250ml) was added. The organic phase was washed with saturated sodium chloride solution (200mL), dried over magnesium sulfate, filtered, and concentrated under reduced pressure. The crude compound was purified by a silica gel-packed column eluted with gradient DCM and DCM/MeOH (100:0-100:1) to afford GAP-EDL-5 as foam white solid (0.96g, 0.56mmol, 52.8% yield). ¹H-NMR(300MHz, DMSO+D₂O):7.80-8.20(m, 7H),7.12 (d, J=8.6Hz, 1H), 7.03 (brs, 1H), 6.64 (d, J=8.6Hz,1H), 6.58(s,1H), 4.04-4.28 (m,6H), 3.77-3.93(m, 3H), 3.45-3.54(m,1H), 3.30-3.44 (m, 2H), 2.66-2.78 (m, 2H), 2.00-2.32(m, 16H), 1.50-2.00(m,18H), 1.35(s, 72H), 1.05-1.28(m, 7H), and 0.63(s, 3H). The spectrum is shown in Figure 5. To ascertain the structure of GAP-EDL-5, the proton NMR of 1,5-di-t-butyl-L-Glutamate pentapeptide ester (GAP ester) was performed (shown in Figure 6). The proton NMR of GAP-EDL-5 was compared to GAP ester (Figure 7). There were chemical shifts at 7ppm seen in GAP-EDL-5, but not in GAP ester. The chemical shift was the aromatic protons from GAP-EDL-5.

2.6. Synthesis of 5-N-[Amino-3-ethoxyestradiol]-Glutamoyl-L-Glutamic acid pentapeptide (GAP-EDL). GAP-EDL-5 (0.560g, 0.327 mmol) was dissolved in anhydrous DCM (11mL) at 0-5°C under nitrogen atmosphere. Trifluoroacetic acid (2.8mL, 37.702mmol) was added. The mixture was stirred at room temperature for 16-18h. The solvent was removed under reduced pressure and the residue was washed with diethyl ether to obtain the crude product. The crude product was purified by prep-HPLC using the gradient elution VA:VB=95:5-70:30 (A phase: 0.1% TFA in water solution; B phase: 0.1% TFA in acetonitrile). After lyophilization, GAP-EDL was obtained as white solid (0.214g, 0.176mmol, 53.7%yield). ¹H-NMR (300MHz, DMSO+D₂O): 7.12 (d, J=8.6Hz,1H), 6.64 (d, J=8.6Hz, 1H), 6.57 (s, 1H), 4.10-4.26 (m, 6H), 3.85-3.94 (m, 2H), 3.76-3.80 (m,1H), 3.47-3.53(m, 1H), 3.32-3.41(m, 2H), 2.66-2.76 (m, 2H), 2.00-2.34 (m, 16H), 1.48-1.98 (m, 18H), 1.00-1.40 (m, 7H), and 0.61(s, 3H); LC-MS was calculated for C₅₅H₇₈N₈O₂₃, 1218.5, and found [M+H] 1219.7. The proton NMR and mass spectrum are shown in Figures 8 and 9. To ascertain the structure of GAP-EDL, the proton NMR of GAP-EDL-4 (monomer) was compared to GAP-EDL (Figure 10). There were chemical shifts from the aromatic protons at 7ppm seen both in GAP-EDL-4 and GAP-EDL. HPLC analysis showed that there were differences of the absorption (210nm vs 239nm) and retention time between GAP-EDL and GAP-EDL-4 (Figure 11).

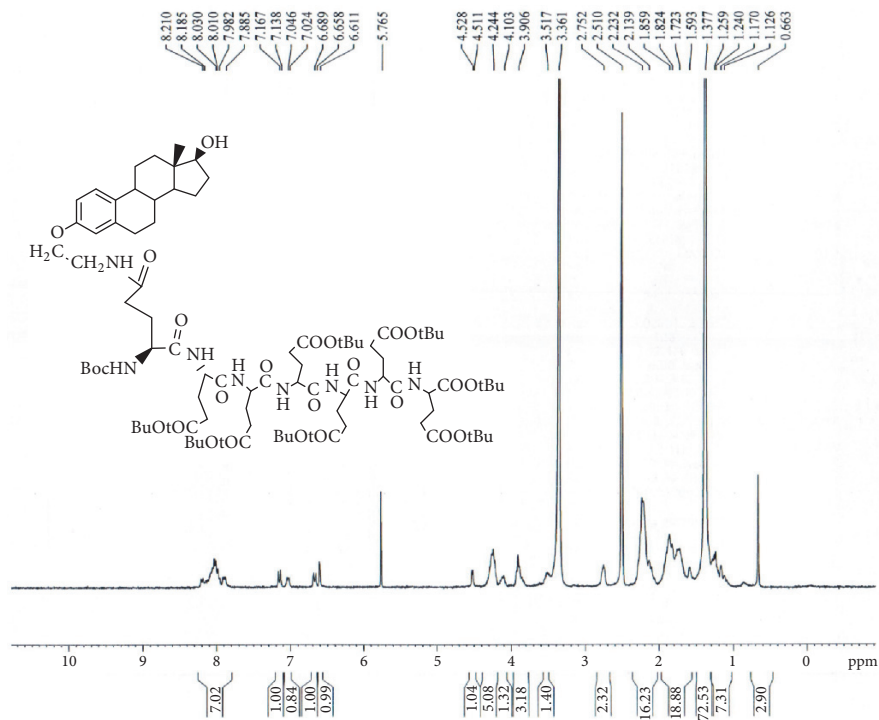
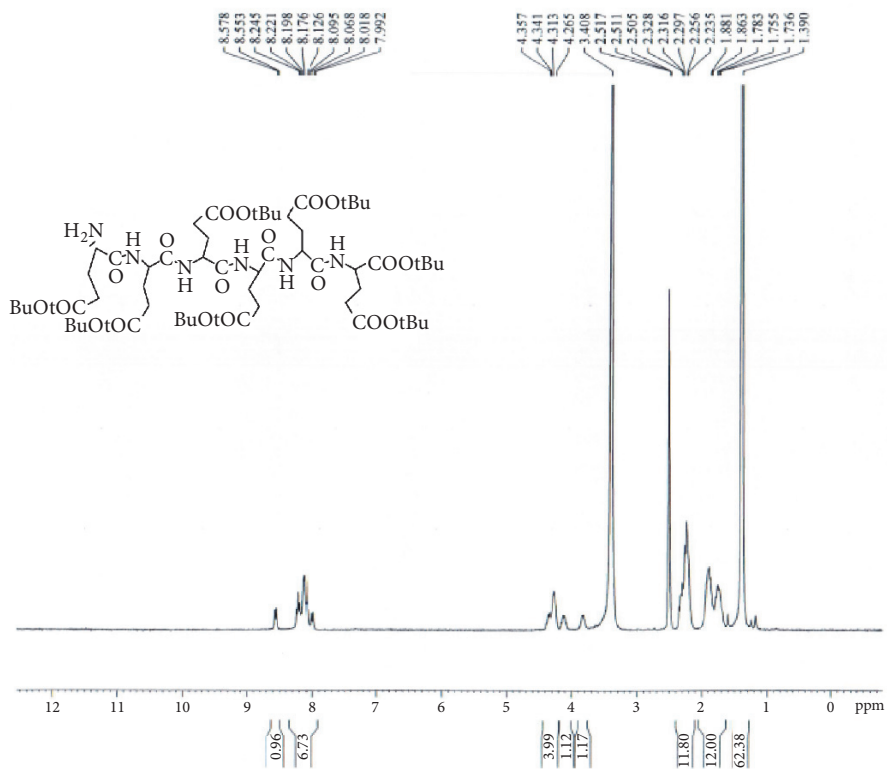


FIGURE 5: Synthesis of GAP-EDL-5.

FIGURE 6: $^1\text{H-NMR}$ of 1,5-di-tert-butyl GAP ester.

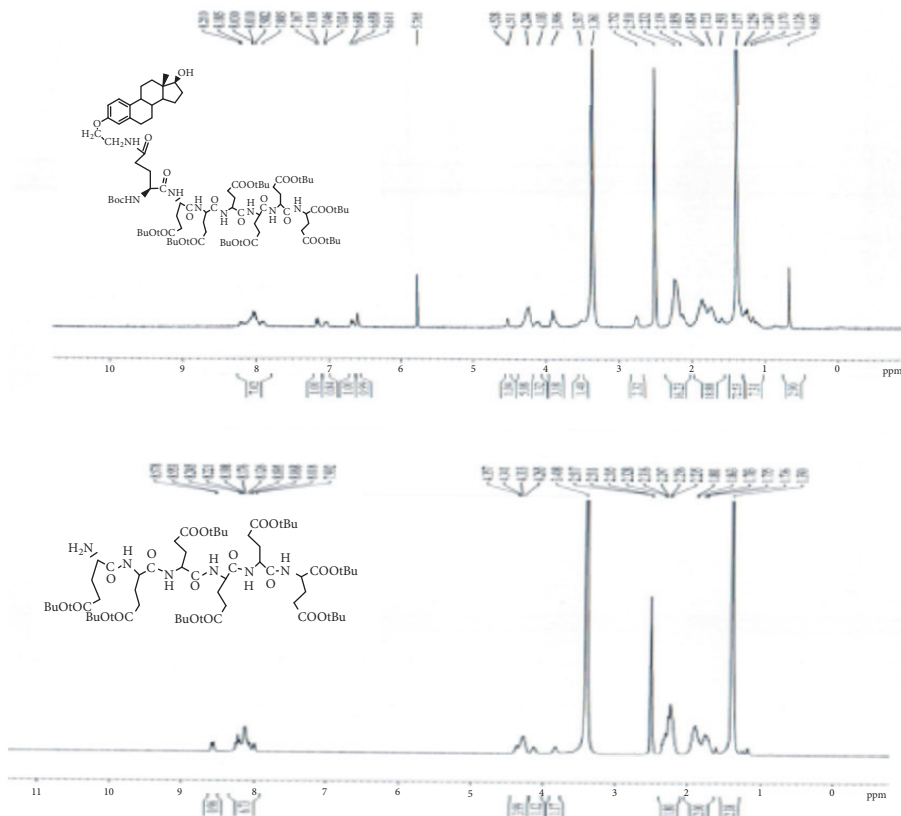


FIGURE 7: ¹H-NMR of 1,5-di-t-butyl GAP ester and GAP-EDL-5.

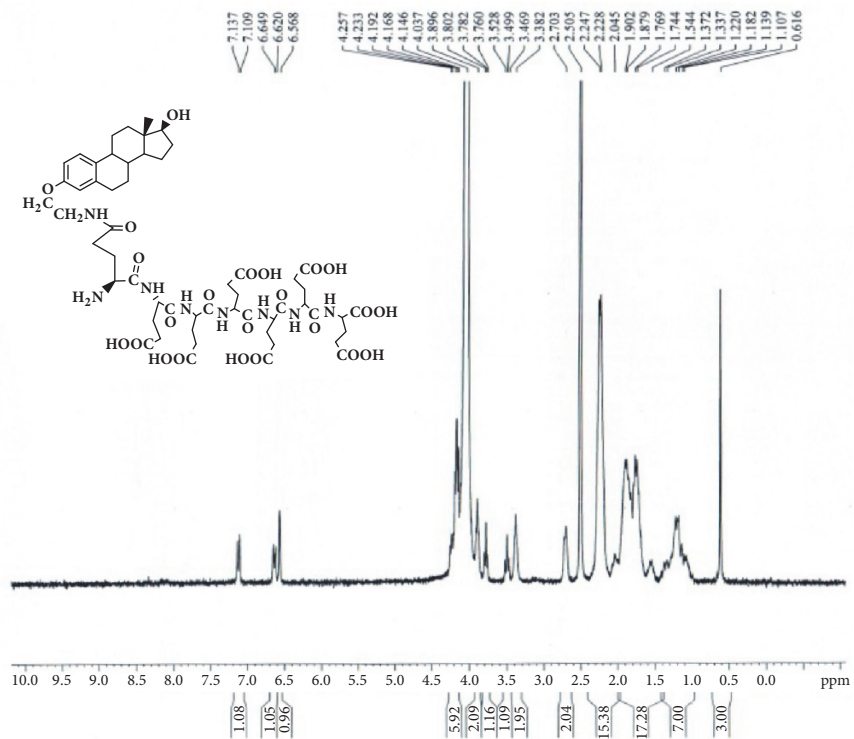


FIGURE 8: Synthesis of GAP-EDL.

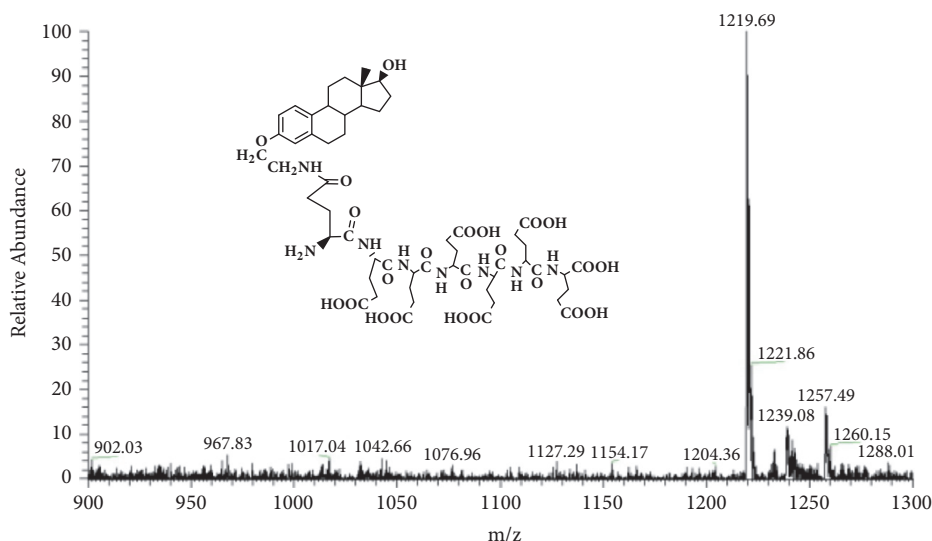


FIGURE 9: Mass Spectrum of GAP-EDL ($C_{55}H_{78}N_8O_{23}$, 1218.5; found $[M+H]$ 1219.7).

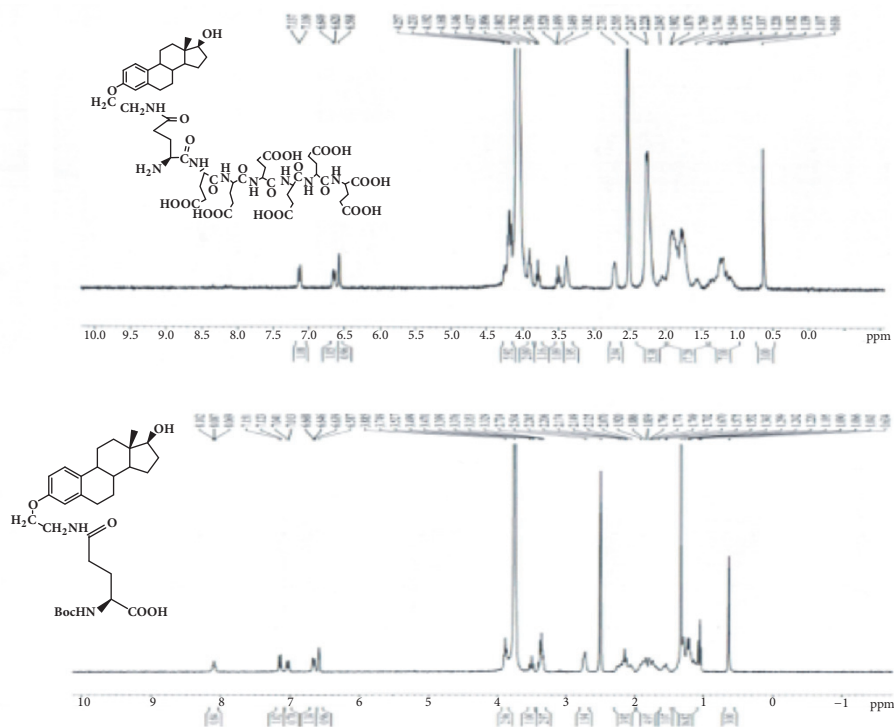


FIGURE 10: 1H -NMR of GAP-EDL and GAP-EDL-4.

2.7. Synthesis of ^{68}Ga -GAP-EDL. $^{68}GaCl_3$ was obtained from a $^{68}Ge/^{68}Ga$ generator eluted with HCL (ranging from 0.01N-1N). For instance, $^{68}GaCl_3$ was eluted from a $^{68}Ge/^{68}Ga$ generator (Ithemba, South Africa) with 0.3N and 0.6NHCL (10mL). On the following day, the elution volume (0.3N or 0.6NHCL, 6 mL) was distributed in a 12-tube (0.5mL/tube). Each tube was counted for its radioactivity. The highest activities in the fractions between 4 and 6 were combined. In the consecutive cycle, the generator is eluted again with 6mL HCL and collected at these specific fractions. Based

upon previous elution profile, an aliquot of $^{68}GaCl_3$ (0.5ml in 0.6NHCL, 6.70 mCi) was added to the solution of GAP-EDL (0.1mg) in 0.8 ml NaOAc (2.5M), and pH value was 4-5. The solution was heated at 70°C for 10 min. After cooling, radiochemical yield and purity were determined by ITLC (Polyamide-6-layer sheets, cat. 30149864, Sinopharm Chemical Reagent Co., Shanghai, China), eluted with saline. Radiochemical yield and purity were 100% with Rf value 0.01. Under the same ITLC conditions, the Rf value for ^{68}Ga was more than ^{68}Ga -GAP and ^{68}Ga -GAP-EDL (Figure 12). ^{68}Ga

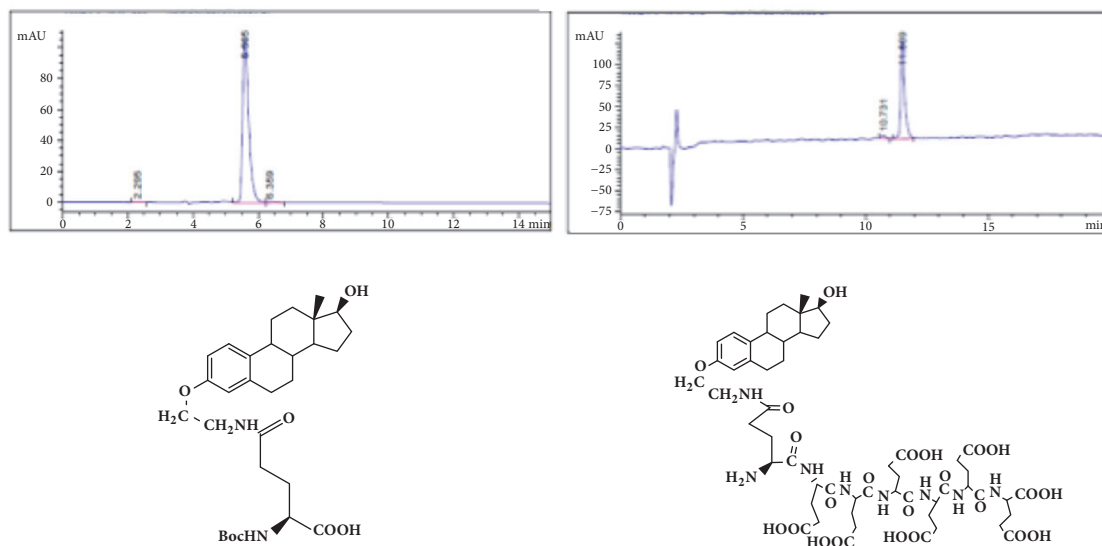


FIGURE 11: HPLC of GAP-EDL-4 (left) and GAP-EDL (right).

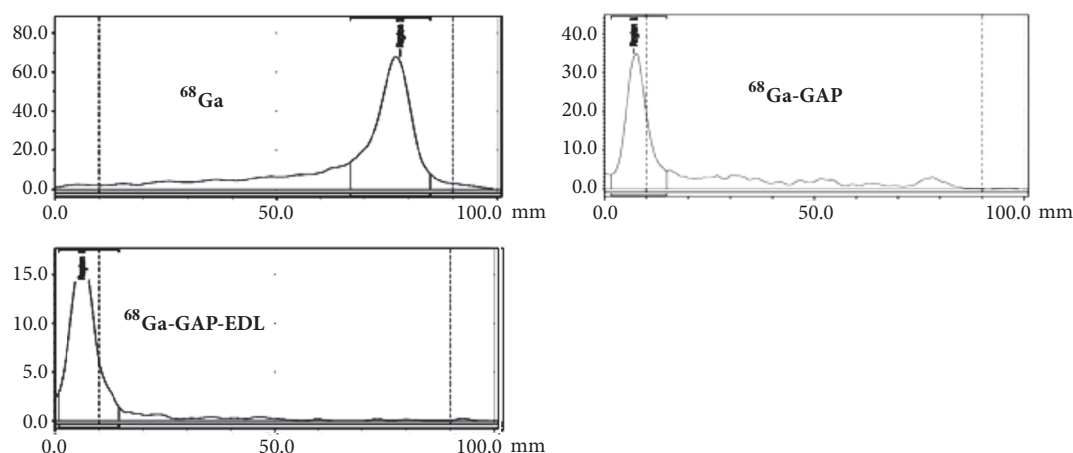


FIGURE 12: ITLC analysis of $^{68}\text{GaCl}_3$, $^{68}\text{Ga-GAP}$ and $^{68}\text{Ga-GAP-EDL}$ (Polyamide, eluant: saline).

chloride eluted from a generator remains as ^{68}Ga chloride form under pH 2. ^{68}Ga chloride migrates using saline as a mobile phase. However, ^{68}Ga chloride forms colloidal when pH changes due to dilution. The colloidal ^{68}Ga (Ga_2O_3) stays at origin using saline as a mobile phase.

2.8. In Vitro Cellular Uptake Assays. In vitro cellular uptake studies of $^{68}\text{Ga-GAP-EDL}$ in breast tumor cells were performed. Breast cancer cell lines with high (MCF7; ER+) and low (SK-BR-3; ER-) estrogen receptor densities were used to determine the sensitivity and specificity for the cellular uptake assay. Briefly, for sensitivity assay, breast tumor cells (50,000 cells/well, 12 wells) were added with $^{68}\text{GaCl}_3$, $^{68}\text{Ga-GAP}$, and $^{68}\text{Ga-GAP-EDL}$ (4 uCi/80uL/well, 4ug/well). The cells were incubated for 0.5-2 hrs. To demonstrate that cellular uptake of $^{68}\text{Ga-GAP-EDL}$ was via an ER-mediated process (specificity assay), breast tumor cells (50,000 cells/well) were treated with 0, 15, 150, and 300 $\mu\text{mol/L}$ of cold estrone (in

DMSO) for 30 minutes followed by adding $^{68}\text{Ga-GAP-EDL}$ (4ug/well, 4uCi/well) and incubated up to 90 minutes. After incubation, the supernatant was collected. The cells were washed twice with ice cold PBS (1 ml) and trypsin EDTA (0.1 ml). After 2 min, the cells were collected. The wells were washed twice with cold PBS (0.5ml). The total volume of cell supernatant and the total volume containing cells were transferred to test tube to count the activity separately. Each piece of data represents an average of three measurements. Percentage of uptake (%) = $\frac{\text{cell activity}}{\text{cell supernatant} + \text{cell activity}} \times 100\%$ was calculated.

2.9. Micro-PET/CT Imaging Studies in MCF-7 Breast Tumor-Bearing Mice. To assure stability of $^{68}\text{Ga-GAP-EDL}$, $^{68}\text{Ga-GAP-EDL}$ was incubated at 37°C in saline up to 120 min, followed by ITLC analysis. $^{68}\text{Ga}_2\text{O}_3$ could form colloidal particles during $^{68}\text{Ga-GAP-EDL}$ synthesis which decreased tumor uptake, thus, fresh ^{68}Ga chloride (pH<2) was used as a control

TABLE 1: In vitro cell uptake assays (an average of three measurements).

	MCF-7			SK-BR-3		
	$^{68}\text{GaCl}_3$	$^{68}\text{Ga-GAP-EDL}$	$^{68}\text{Ga-GAP}$	$^{68}\text{GaCl}_3$	$^{68}\text{Ga-GAP-EDL}$	$^{68}\text{Ga-GAP}$
30min	1.35±0.35	12.91±0.4*	2.20±0.73	1.74±0.21	3.63±1.02	1.84±0.27
1h	1.79±0.28	10.61±2.34	3.20±1.17	1.80±0.20	9.28±0.49	3.11±1.29
2h	1.63±0.33	10.17±1.38	2.43±0.71	2.21±0.11	10.65±0.78	2.45±0.21

* Significant difference between corresponding groups (t-test, $P < 0.05$).

in ITLC system. For in vivo stability, athymic MCF-7 tumor-bearing nude mice ($n=2$) were administered $^{68}\text{Ga-GAP-EDL}$ (0.14mg per $30\mu\text{Ci}$, 0.1 mL, iv) and the tissue biodistribution was conducted at 90 min post-administration. The selected tissues were excised, weighed and counted for radioactivity by gamma counter. Each sample was calculated as percentage of the injected dose per gram of tissue wet weight (%ID/g). Counts from a diluted sample of the original inject were used for reference.

For PET imaging studies, athymic nude mice ($n=2$ per compound) inoculated with MCF-7 cells (s.c. 10^6 cells/mouse) at the left hind legs. When tumor reached 0.7cm, the tumor-bearing mice were anesthetized with 2% isoflurane on prone position. ^{68}Ga chloride (5mCi) was obtained by eluting a $^{68}\text{Ge}/^{68}\text{Ga}$ generator (20mCi size from Eckert Ziegler, Germany) with HCL (0.1N, 1.5 mL). Labeling GAP (1 mg) and GAP-EDL (1mg) was achieved by dissolving both compounds in sodium acetate (0.4 mL, 0.1N, pH 5.4), followed by adding ^{68}Ga chloride (1mCi, 0.3mL). Both compounds were sat at 37°C for 20 min. For animal imaging studies, the concentrations were diluted to 1.5mL/mg by adding saline (0.9%). Each mouse was administered with $^{68}\text{Ga-GAP}$ and $^{68}\text{Ga-GAP-EDL}$ (0.14mg per $100\mu\text{Ci}$, 0.2 mL, iv). $^{68}\text{Ga-GAP}$ and $^{68}\text{Ga-GAP-EDL}$ imaging studies were performed with a Siemens Inveon micro-PET/CT scanner (Siemens Medical Systems, Hoffman Estates, IL). Three serial 30-minute trans-axial PET images were obtained. All corrections for attenuation, scatter, and dead time were applied to generate quantifiable images. Regions of interests were then drawn on the tumor tissue and muscle regions and time activity curves were generated, the counts per pixel were used to determine tumor tissue-to-muscle tissue count density ratios.

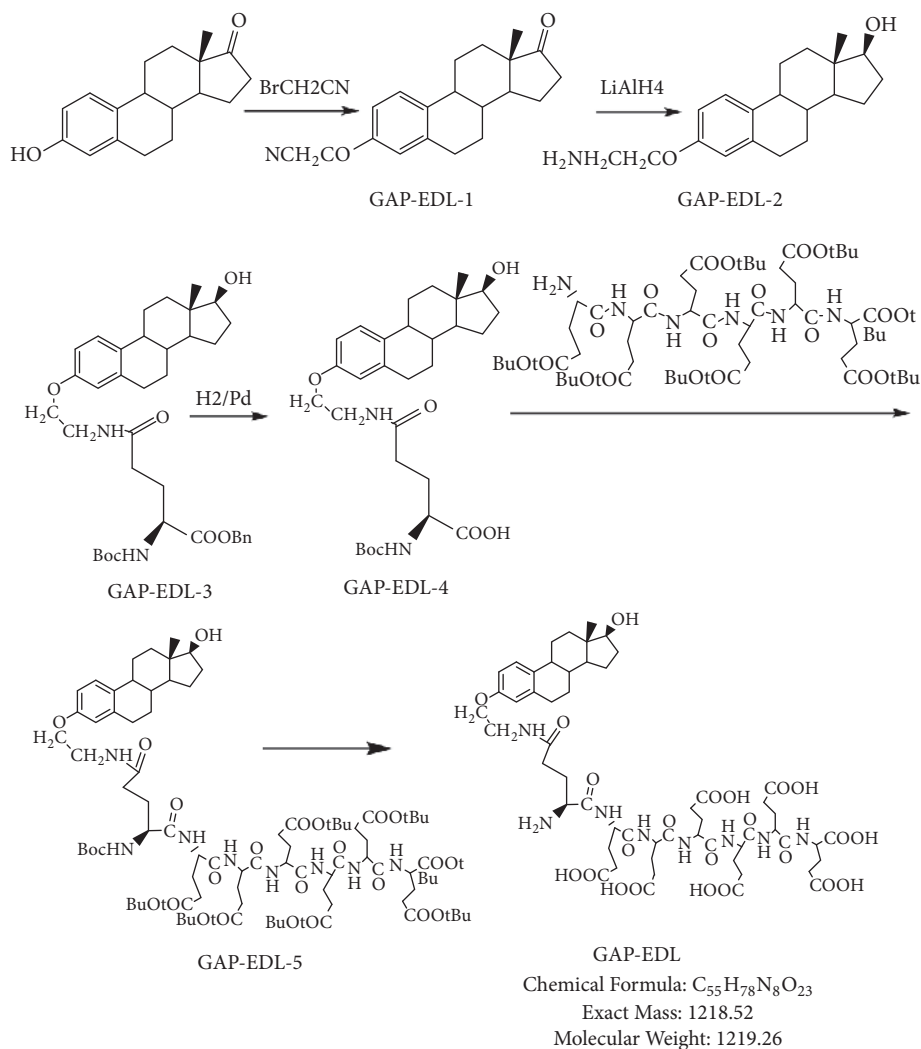
3. Results

3.1. Chemistry. The synthetic scheme of GAP-EDL is shown in Scheme 1. The analytical data for structural determination of GAP-EDL analogues was shown in Figures 1–12. Aspects of the efficient synthesis provide novel methods for preparing a glutamate-estradiol conjugate and a glutamate peptide-estradiol conjugate. To initiate the efficient synthesis, the position-3 of estrone was reacted with bromoacetonitrile to yield cyano analogue of estrone (GAP-EDL-1). GAP-EDL-1 was then reduced to afford 3-aminoethoxy estradiol (GAP-EDL-2). For preparing a glutamate-estradiol conjugate, the method used an amino estradiol with an

amino and l-carboxylic acid protected glutamate in organic solvent, thereby producing the gamma glutamoyl-estradiol conjugate (GAP-EDL-4). For preparing a glutamate peptide-estradiol conjugate, the method used was by reacting the gamma glutamoyl-estradiol (GAP-EDL-4) with all carboxylic acid protected glutamate pentapeptide comprising coupling agents. Thus, estradiol is positioned at the first glutamate of the glutamate peptide-estradiol in the finished product (GAP-EDL). During the synthesis of GAP-EDL-3, it is unlikely that protected glutamate might be conjugated with 17-OH group of amino-EDL. However, the NMR data showed the conjugation produced an amide bond, not an ester bond. Also, the ester group could not sustain at the hydrogenation process in the next step (GAP-EDL-4). The total synthesis of GAP-EDL was six steps with overall yield 5.7%. The GAP-EDL was analytically pure as proven by NMR (Figure 8), mass spectra (Figure 9), and HPLC (Figure 11).

3.2. Cell Uptake Assays. There was a marked increase in the uptake of $^{68}\text{Ga-GAP-EDL}$ compared with the uptake of $^{68}\text{GaCl}_3$ and $^{68}\text{Ga-GAP}$ in breast cancer cells (Table 1). The improved synthetic method makes a pure GAP-EDL and has greatly enhanced specificity in cell uptake studies. The uptake of $^{68}\text{Ga-GAP-EDL}$ was higher than $^{68}\text{Ga-GAP}$ both in ER (+) MCF7 cells and ER (-) SK-BR-3 cells. At 30 min, the uptake of $^{68}\text{Ga-GAP-EDL}$ in ER (+) MCF7 cells was significantly higher than ER (-) SK-BR-3 cells but not at 1 and 2hrs. The average cell uptake of $^{68}\text{Ga-GAP-EDL}$ of the improved synthesis (Table 1) was at least 5-fold higher than the previous reported synthesis [11]. In specificity assay, the cell uptake of $^{68}\text{Ga-GAP-EDL}$ could be blocked by estrone, particularly at 15, 150, 300 $\mu\text{mol/L}$. Again, MCF-7 has more decreased uptake than ER (-) SKBR-3 particularly at $15\mu\text{mol/L}$ of estrone (Table 2). The decreased uptake demonstrated the cellular uptake of $^{68}\text{Ga-GAP-EDL}$ was via an ER-mediated process.

3.3. Micro-PET/CT Imaging and Biodistribution Studies in MCF-7 Breast Tumor-Bearing Mice. MCF 7 cell line was well established for ER (+) cells and was used in cell uptake studies; thus, it was selected for an animal imaging model. In vitro ITLC stability analysis revealed that $^{68}\text{Ga-GAP-EDL}$ stayed at origin (Figure 12) whereas free ^{68}Ga chloride migrates from 30min to 120 min. PET imaging studies showed that $^{68}\text{Ga-GAP}$ had less tumor uptake than $^{68}\text{Ga-GAP-EDL}$ at 30-90 min post-administration in breast tumor model by



SCHEME 1: Efficient Synthesis of GAP-EDL.

TABLE 2: In vitro cell blocking assays with ^{68}Ga -GAP-EDL (an average of three measurements).

Estrone (umol/L)	MCF-7	SK-BR-3
0	14.78±3.10	9.38±1.95
15	7.96±2.09	8.55±3.55
150	2.95±0.56	2.68±1.00
300	2.95±0.43	2.84±1.00

visualization (Figure 13). Preliminary biodistribution of ^{68}Ga -GAP-EDL at 90 min revealed the comparable (tumor-to-muscle) data to imaging findings (Table 3).

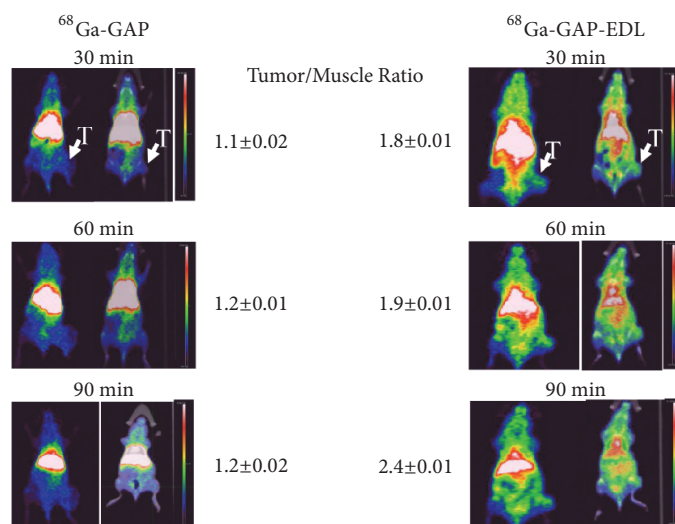
4. Discussion

The discovery of ERs in binding and responding to individual hormonal pathways benefits patients in the treatment of oxidative stress induced ROS, inflammation, and cancer. High ERs were overexpressed in the cytosol during cancerous progression. Glutamate receptor/transporter systems were

known to have overexpressions due to high demand of GSH in disease status. Poly-L-glutamic acid (PG) with repeated glutamate units has been used as a tumor-aiming drug carrier for different hydrophobic cancer chemotherapeutic agents [13–21]. PG have other advantages such as excellent water solubility, biocompatibility, nonimmunogenicity, biodegradability to glutamate, and a high drug loading capability due to their multiple carboxyl side groups [22–25]. In order to enhance specificity in targeting ER (+) system, conjugation of EDL to GAP would provide a dual target purpose. First, an enhanced uptake of ^{68}Ga -GAP-EDL may occur through

TABLE 3: Biodistribution of ^{68}Ga -GAP-EDL at 90 min in MCF-7 tumor-bearing mice (n=2).

Tissue	Mouse 1 (%ID/g)	Mouse 2 (%ID/g)	Mean \pm SD (%ID/g)
Uterus	9.08	9.85	9.47 \pm 0.55
Ovary	10.26	8.53	9.39 \pm 1.23
Kidney	7.55	7.60	7.58 \pm 0.04
Tumor	6.42	8.42	7.42 \pm 1.41
Bone	6.94	7.33	7.14 \pm 0.28
Liver	6.57	7.22	6.89 \pm 0.45
Lung	7.59	6.13	6.86 \pm 1.03
Heart	6.01	6.27	6.14 \pm 0.18
Spleen	4.56	5.47	5.02 \pm 0.64
Muscle	3.20	2.95	3.07 \pm 0.18
Blood	2.32	2.33	2.33 \pm 0.01
Brain	0.63	0.75	0.69 \pm 0.08

FIGURE 13: Micro-PET/CT analysis showed that ^{68}Ga -GAP-EDL had higher tumor-to-muscle ratios than ^{68}Ga -GAP in breast tumor-bearing mice.

cell surface glutamate transporter/receptor system. Secondly, ^{68}Ga -GAP-EDL may target ERs faster due to enhanced internalization.

Regarding synthetic production of GAP-EDL for ^{68}Ga labeling, when conjugation was produced in aqueous conditions, purification of the GAP-EDL may sometimes present a challenge. Purification in aqueous conditions can be achieved using, for example, size exclusion chromatography, or dialysis with membranes of particular molecular weight cut-offs; for instance, dialysis is generally most effective when separating species of molecular weights of 1000 g/mol or higher. Nevertheless, this method of purification often isolates not only the desired agent but also any other species that may pass through the membrane. Receptor-based imaging agents require high specific activity (>0.1 Ci/ μmol) in order to overcome nonspecific protein binding. Therefore, introduction of impurities into receptor-based imaging agents may be problematic in their clinic uses. For instance, if an imaging agent incorporating a radionuclide is thought to be pure

but actually contains impurities that also incorporate a radionuclide, the proper measurement or detection of the imaging agent may be obscured or rendered false due to the presence of the impurity. This is particularly true when using polypeptide such as polyglutamate as a drug carrier. Commercially available polyglutamate has a wide range molecular weight which contains a mixture of various polyglutamate. This makes difficulty in the structure determination of the EDL position in the molecule. In addition, the conjugation reaction is frequently done in an aqueous condition in which the product purity is not optimized.

For preparing a glutamate peptide-estradiol conjugate, the protected carboxylic acid of glutamate-estradiol conjugate is selectively deprotected and reacted with all acid protected glutamate pentapeptide ester using coupling chemicals such as DIPEA and BOP. These coupling agents are able to conjugate estradiol to the glutamate peptide at the first glutamate using the synthetic route described in Scheme 1. In some aspects, these synthetic methods may obviate the

need of adding protecting groups to glutamate and glutamate pentapeptide and increase process efficiency and purify of the final product as compared to other methods as described in US Patent application 20060246005, WO 2006107794 A2 [10–12]. To generate a metal ion labeled-glutamate peptide-estradiol conjugate, the metal ion selected was a gallium ion, a radionuclide for PET imaging. The site to be imaged may be a tumor or endometriosis or an ER-enriched tissue such as ovaries and uterine tissue. ER (+) cancers are breast cancer, lung cancer, prostate cancer, ovarian cancer, uterine cancer, cervical cancer, and endometrial cancer. To demonstrate that GAP-EDL is suitable for commercialized generators, we have used two different generators to label GAP-EDL. Both generators were able to synthesize ^{68}Ga -GAP-EDL. ^{68}Ga -GAP-EDL was stable in saline at least up to 120 min. Our in vitro cellular uptake assays demonstrated that the uptake of ^{68}Ga -GAP-EDL was higher than ^{68}Ga -GAP both in ER (+) MCF7 cells and ER (-) SK-BR-3 cells. MCF-7 showed early binding that is retained, whereas SKBR-3 shows higher binding as a function of time. However, the increased uptake of ^{68}Ga -GAP-EDL in ER (+) MCF7 cells could be significantly blocked by estrone at $15\mu\text{mol/L}$, but not ^{68}Ga -GAP, indicating the uptake mechanism was via an ER-mediated process. In vivo imaging findings indicated that ^{68}Ga -GAP-EDL could image ER (+) tumors. Further studies warrant evaluation of whether ^{68}Ga -GAP-EDL remains intact and associates with ER once internalized.

In summary, the efficient synthesis of GAP-EDL conjugate for molecular imaging of ER (+) disease was achieved. GAP-EDL integrating diagnostic imaging instrument helps to understand the dynamic changes in ER (+) pathway-activated systems leading to tissue degeneration, inflammatory, and proliferative disorders and to improve patient diagnosis, therapy, and prognosis. The efficient synthetic methods can be further prepared in pharmaceutical formulations and kits using chemical procedures. This precision imaging agent allows delivering personalized therapeutics on the basis of individual genetic make-up, biochemistry, and molecular blueprint associated to each patient's disease.

Data Availability

The data used to support the findings of this study are available from the corresponding author upon request.

Conflicts of Interest

The authors declare that they have no conflicts of interest.

References

- [1] V. Speirs, P. J. Carder, S. Lane, D. Dodwell, M. R. Lansdown, and A. M. Hanby, "Oestrogen receptor β : what it means for patients with breast cancer," *The Lancet Oncology*, vol. 5, no. 3, pp. 174–181, 2004.
- [2] S. Hayashi, H. Eguchi, K. Tanimoto, T. Yoshida et al., "The expression and function of estrogen receptor alpha and beta in human breast cancer and its clinical application," *Endocrine-Related Cancer*, vol. 10, no. 2, pp. 193–202, 2003.
- [3] L. Sas, F. Lardon, P. B. Vermeulen et al., "The interaction between ER and NF κ B in resistance to endocrine therapy," *Breast Cancer Research*, vol. 14, no. 4, 2012.
- [4] H. Chen, X. Tang, B. Zhou, Z. Zhou, N. Xu, and Y. Wang, "A ROS-mediated mitochondrial pathway and Nrf2 pathway activation are involved in BDE-47 induced apoptosis in Neuro-2a cells," *Chemosphere*, vol. 184, pp. 679–686, 2017.
- [5] M. R. Akanda, M. J. Kim, I. S. Kim et al., "Neuroprotective effects of sigesbeckia pubescens extract on glutamate-induced oxidative stress in HT22 cells via downregulation of MAPK/caspase-3 pathways," *Cellular and Molecular Neurobiology*, pp. 1–9, 2017.
- [6] E. Habib, K. Linher-Melville, H.-X. Lin, and G. Singh, "Expression of xCT and activity of system xc- are regulated by NRF2 in human breast cancer cells in response to oxidative stress," *Redox Biology*, vol. 5, pp. 33–42, 2015.
- [7] S. Al-Sweidi, M. Morissette, and T. Di Paolo, "Estrogen receptors modulate striatal metabotropic receptor type 5 in intact and MPTP male mice model of Parkinson's disease," *The Journal of Steroid Biochemistry and Molecular Biology*, vol. 161, pp. 84–91, 2016.
- [8] C. Chenu, C. M. Serre, C. Raynal, B. Burt-Pichat, and P. D. Delmas, "Glutamate receptors are expressed by bone cells and are involved in bone resorption," *Bone*, vol. 22, no. 4, pp. 295–299, 1998.
- [9] H. Chai, L. Kiew, Y. Chin et al., "Renal targeting potential of a polymeric drug carrier, poly-L-glutamic acid, in normal and diabetic rats," *International Journal of Nanomedicine*, vol. Volume 12, pp. 577–591, 2017.
- [10] N. Takahashi, D. J. Yang, S. Kohanim et al., "Targeted functional imaging of estrogen receptors with $^{99\text{mTc}}$ - GAP-EDL," *European Journal of Nuclear Medicine and Molecular Imaging*, vol. 34, no. 3, pp. 354–362, 2007.
- [11] N. Takahashi, D. J. Yang, H. Kurihara et al., "Functional Imaging of Estrogen Receptors with Radiolabeled-GAP-EDL in Rabbit Endometriosis Model," *Academic Radiology*, vol. 14, no. 9, pp. 1050–1057, 2007.
- [12] D. J. Yang, C. S. Oh, S. Kohanim, D. F. Yu, A. Azhdarinia, and E. E. Kim, "Poly(peptide) as a chelator: methods of manufacture and uses," U.S. Patent application 20060246005, WO 2006107794 A2, 2006.
- [13] H. G. Batz, H. Ringsdorf, and H. Ritter, "Pharmacologically active polymers, 7. Cyclophosphamide- and steroid hormone containing polymers as potential anticancer compounds," *Die Makromolekulare Chemie*, vol. 175, no. 8, pp. 2229–2239, 1974.
- [14] E. Hurwitz, M. Wilchek, and J. Pitha, "Soluble macromolecules as carriers for daunorubicin," *Journal of Applied Biochemistry*, vol. 2, no. 1, pp. 25–35, 1980.
- [15] Y. Kato, M. Saito, H. Fukushima, Y. Takeda, and T. Hara, "Antitumor Activity of 1- β -D-Arabinofuranosylcytosine Conjugated with Polyglutamic Acid and Its Derivative," *Cancer Research*, vol. 44, no. 1, pp. 25–30, 1984.
- [16] C. J. T. Hoes, W. Potman, W. A. R. van Heeswijk et al., "Optimization of macromolecular prodrugs of the antitumor antibiotic adriamycin," *Journal of Controlled Release*, vol. 2, no. C, pp. 205–213, 1985.
- [17] E. Mochizuki, Y. Inaki, and K. Takemoto, "Synthesis of poly-L-glutamates containing 5-substituted uracil moieties," *Nucleic Acids Symposium Series*, no. 16, pp. 121–124, 1985.
- [18] F. Zunino, G. Pratesi, and A. Micheloni, "Poly(carboxylic acid) polymers as carriers for anthracyclines," *Journal of Controlled Release*, vol. 10, no. 1, pp. 65–73, 1989.

- [19] C. J. T. Hoes, J. Grootoank, R. Duncan et al., "Biological properties of adriamycin bound to biodegradable polymeric carriers," *Journal of Controlled Release*, vol. 23, no. 1, pp. 37–53, 1993.
- [20] L. V. Kiew, S. K. Cheong, E. Ramli, K. Sidik, T. M. Lim, and L. Y. Chung, "Efficacy of a poly-L-glutamic acid-gemcitabine conjugate in tumor-bearing mice," *Drug Development Research*, vol. 73, no. 3, pp. 120–129, 2012.
- [21] Y. Morimoto, K. Sugibayashi, S. Sugihara, K.-I. Hosoya, S. Nozaki, and Y. Ogawa, "Antitumor agent poly (amino acid) conjugates as a drug carrier in cancer chemotherapy," *Journal of Pharmacobio-Dynamics*, vol. 7, no. 9, pp. 688–698, 1984.
- [22] C. Li, "Poly(L-glutamic acid)-anticancer drug conjugates," *Advanced Drug Delivery Reviews*, vol. 54, no. 5, pp. 695–713, 2002.
- [23] A. D. Kenny, "Evaluation of sodium poly-alpha," *L-Glutamate as a Plasma Expander*, vol. 100, no. 4, pp. 778–780, 1959.
- [24] L. A. McCormick-Thomson, D. Sgouras, and R. Duncan, "Poly(amino acid) Copolymers as a Potential Soluble Drug Delivery System. 2. Body Distribution and Preliminary Bio-compatibility Testing In Vitro and In Vivo," *Journal of Bioactive and Compatible Polymers*, vol. 4, no. 3, pp. 252–268, 1989.
- [25] H. Sumi, K. Kawabe, and N. Nakajima, "Effect of various polyamino acids and d- and l-amino acids on the blood fibrinolytic system," *Comparative Biochemistry and Physiology – Part B: Biochemistry and*, vol. 102, no. 1, pp. 159–162, 1992.

Research Article

CT Perfusion in Patients with Lung Cancer: Squamous Cell Carcinoma and Adenocarcinoma Show a Different Blood Flow

Alessandro Bevilacqua ^{1,2}, Giampaolo Gavelli,³ Serena Baiocco,^{2,4} and Domenico Barone³

¹DISI (Department of Computer Science and Engineering), University of Bologna, Viale Risorgimento 2, Bologna 40136, Italy

²ARCES (Advanced Research Center on Electronic Systems), University of Bologna, Via Toffano 2/2, Bologna 40125, Italy

³Istituto Scientifico Romagnolo per lo Studio e la Cura dei Tumori (IRST) IRCCS, Meldola 47014, Italy

⁴DEI (Department of Electrical, Electronic and Information Engineering), University of Bologna, Viale Risorgimento 2, Bologna 40136, Italy

Correspondence should be addressed to Alessandro Bevilacqua; alessandro.bevilacqua@unibo.it

Received 19 March 2018; Revised 4 July 2018; Accepted 16 August 2018; Published 3 September 2018

Academic Editor: Franco M. Buonaguro

Copyright © 2018 Alessandro Bevilacqua et al. This is an open access article distributed under the Creative Commons Attribution License, which permits unrestricted use, distribution, and reproduction in any medium, provided the original work is properly cited.

Objectives. To characterize tumour baseline blood flow (BF) in two lung cancer subtypes, adenocarcinoma (AC) and squamous cell carcinoma (SCC), also investigating those “borderline” cases whose perfusion value is closer to the group mean of the other histotype. **Materials and Methods.** 26 patients (age range 36-81 years) with primary Non-Small Cell Lung Cancer (NSCLC), subdivided into 19 AC and 7 SCC, were enrolled in this study and underwent a CT perfusion, at diagnosis. BF values were computed according to the maximum-slope method and unreliable values (*e.g.*, arising from artefacts or vessels) were automatically removed. The one-tail Welch’s t-test (p -value < 0.05) was employed for statistical assessment. **Results.** At diagnosis, mean BF values (in [mL/min/100g]) of AC group [(83.5 ± 29.4)] are significantly greater than those of SCC subtype [(57.0 ± 27.2)] (p -value = 0.02). However, two central SCCs undergoing artefacts from vena cava and pulmonary artery have an artificially increased mean BF. **Conclusions.** The different hemodynamic behaviour of AC and SCC should be considered as a biomarker supporting treatment planning to select the patients, mainly with AC, that would most benefit from antiangiogenic therapies. The significance of results was achieved by automatically detecting and excluding artefactual BF values.

1. Introduction

Tumorigenesis involves angiogenesis, a complex mechanism consisting in the generation of a vascular network nourishing the tumour that is highly disorganized [1]. Studying abnormal vascular patterns, and their temporal changes, may be essential for tissue characterization [2]. To this purpose, the interest in CT perfusion (CTp) methodologies has been recently confirmed [3], since CTp supplies both high spatial and temporal resolution and allows computing perfusion parameters from the analysis of the time concentration curves (TCCs) [4], generated by the contrast agent reaching the tumour. Among the most effective perfusion parameters allowing angiogenesis evaluation [5], the blood flow (BF) arises [6] mainly because of its high correlation with the tissue biomarker microvessel density (MVD) [7]. BF can be measured by considering only the first passage of the

contrast medium, this requiring a short-time examination permitting to minimize the radiation dose given to the patient [8, 9]. Clinical applications of BF information computed at diagnosis include the lesion characterization [10], especially relevant for inoperable patients, who need to schedule non-surgical treatments [11]. Or else, higher baseline BF values in patients with advanced lung carcinoma could suggest a better response to therapy [12].

The differences in BF values between responders and nonresponders have prompted a tumour hemodynamic characterization, which also embodies cancer histological subtypes. Characterizing the perfusion of non-small cell lung cancer (NSCLC) has shown to provide useful information concerning their status, in particular as regards their hypoxia degree, deeply affecting tumour response to treatment [13]. In particular, it was shown that the adenocarcinoma (AC) subtype has a significantly lower hypoxia degree than the

squamous cell carcinoma (SCC) one [14]. Various perfusion parameters have been reported to differ between lung cancer subtypes [13, 15], showing discordant results [16–21]. However, when considering these discordant findings, we must bear in mind that BF computation of lung tumours is exposed to several sources of error [22], arising from respiratory motion [23], CTP artefacts [24], and, not to forget, tumour location [25], which can affect the reliability of BF values [26], thus dimming the real nature of tumours and hampering development and standardization of biomarkers. As regards tumour location, its influence on BF values is rarely considered in CTP studies. Nonetheless, it has been shown that perfusion in central carcinomas is significantly lower than in peripheral ones, due to the different recruitment of vessels [27]. Nevertheless, also anatomical structures inside lesion, such as vessels and bronchi, can be responsible for jeopardizing perfusion analyses [26].

The aim of this study was to evaluate the characteristics of lung tumour at diagnosis (i.e., at baseline condition), newly investigating possible significant differences in perfusion between AC and SCC, the two predominant NSCLC phenotypes. Nevertheless, as previously shown, the literature presents discordant results in AC and SCC perfusion characterization, caused by too a high measurement variability, stemming from clinical and physiological factors as well as external causes (e.g., patient movements and artefacts). To reduce such a variability, we automatically detected and removed unreliable perfusion values. In addition, we examined lesions' position, central or peripheral, and their proximity to large vessels, studying whether and how this external factor could artificially affect histotype perfusion. Finally, for each histotype we also analyse the less representative lesions, whose perfusion values are shifted to the group mean value characterizing the other histotype.

2. Materials and Methods

Study Population. This study was approved by the Institutional Review Board (IRB) that waived informed consent for the retrospective data analysis of the patients. In addition, a written consensus was obtained by all patients before each study. Between September 2010 and April 2013, a total of 32 consecutive patients (22 men, 10 women; age range 36–81 years) with primary NSCLC, subdivided in 24 AC and 8 SCC, were identified and enrolled for data analysis. Tumour stage was determined in all patients according to the TNM classification of malignant tumours (seventh edition): 1 patient was diagnosed with stage IB, 3 patients with stage IIIA, 5 patients with stage IIIB, and 23 patients with stage IV.

The patients included in this study were selected according to the following criteria: over eighteen years old, with histologically verified NSCLC, and no prior history of chemotherapy, surgery, or thoracic radiation therapy. Patients were excluded if the longest axial lesion diameter was less than 10 mm in at least one slice ($n=2$), if the examination was severely affected by physics-based artefacts ($n=4$), in case of a clinically significant cardiovascular disease and a known history of deep vein thrombus or pulmonary embolus.

The final population included 26 patients, 19 AC, and 7 SCC. Besides subtypes and staging, Table 1 includes lesion's location and position as the cancer features. For the sake of completeness, we also report the widest axial tumour section.

CTp Protocol. At diagnosis, the patients underwent axial CT perfusion (CTp) performed on a 256-slice CT system (Brilliance iCT, Philips Medical System, Best, The Netherlands), feet first in the supine position. Initially, an unenhanced low-dose full-body CT scan was performed to identify the target lesion at baseline conditions. Then, a 50 mL intravenous bolus of contrast agent (Iomeron, Bracco, Milan, Italy) was injected at 5 mL/s for axial cine contrast-enhanced CT, followed by a flush with physiological saline solution (30 mL), 5 mL/s. Five seconds later, each patient underwent a single acquisition of duration 25 seconds under breath-hold condition. This protocol yields 20 scans, each corresponding to different sampling instants, with 55 mm of z-coverage (11 slices \times 5-mm slice thickness, 0.4-sec rotation time, at 80 kV, 250 mA, 100 mAs). Image data are reconstructed to 220 cine images (512 \times 512 pixel, 11 slices, 350 mm \times 350 mm, 5-mm slice spacing, 1.25-sec temporal resolution).

Perfusion Maps. A region of interest (ROI) in the descending aorta was selected as the input function. A second ROI was manually drawn in consensus [27] by two experienced radiologists (D.B. and G.G., 25-year experience each) on a reference slice, where the tumour showed the widest area, similar to what was done in [20, 27, 28]. Then, for each lesion, the radiologists performed a 3D alignment according to the procedure described in [29]. In order to obtain the TCCs relative to each voxel, the values of the temporal sequence were fitted using the sigmoid-shape model, arising from the Hill Equation [30], and the random sampling method described in [31]. The curve fitting is achieved employing an in-house fitting algorithm based on the nonlinear, least squares, Levenberg-Marquardt minimization algorithm (lsqcurvefit, MATLAB[®]; MathWorks, Natick, MA, USA). After TCCs computation, BF values, expressed in mL/min/100 g, were computed for AC and SCC subtypes using the maximum-slope method [32, 33] by considering the first-pass phase only [34] and representing each voxel with a one-compartment model, including both the intravascular and the extravascular spaces [35]. This allowed performing short-time examinations with great benefits for patients, in terms of absorbed radiation dose and examination quality, since motion artefacts were reduced by the possibility for patients to hold their breath.

Nonetheless, in this paper, we propose two methodological approaches to improve the reliability of results, that is, removing potential artefacts from perfusion maps through an accurate data analysis and separately analysing the “borderline cases”.

Data Analysis. Unreliable BF values were excluded from the analysis and highlighted in the colour map with the pink colour. In particular, BF values strictly lower than 1 mL/min/100 g were automatically removed, being considered unlikely compliant with physiological values and rather ascribable to numerical errors. Similarly, BF values

TABLE 1: Summary of the histological diagnosis, tumour stage, position, location, and area of the widest tumour slice relative to each lesion.

Patient ID	Diagnosis	Stage	Position	Location	Size [cm^2]
ID1	AC	IV	Left	Peripheral	2.4
ID2	AC	IV	Left	Extended	15.9
ID3	AC	IV	Left	Peripheral	4.6
ID4	AC	IV	Right	Extended	7.0
ID5	AC	IV	Right	Extended	16.1
ID6	AC	IV	Right	Peripheral	15.0
ID7	AC	IIIA	Right	Extended	5.9
ID8	AC	IV	Left	Peripheral	1.5
ID9	AC	IV	Right	Extended	29.0
ID10	AC	IIIA	Right	Peripheral	2.5
ID11	AC	IV	Right	Extended	20.3
ID12	AC	IV	Right	Extended	3.9
ID13	AC	IV	Right	Peripheral	0.6
ID14	AC	IV	Left	Extended	2.5
ID15	AC	IV	Left	Extended	10.8
ID16	AC	IV	Right	Extended	1.9
ID17	AC	IV	Left	Peripheral	1.5
ID18	AC	IV	Left	Central	3.8
ID19	AC	IIIB	Right	Central	10.7
ID20	SCC	IB	Left	Peripheral	2.1
ID21	SCC	IV	Left	Central	7.2
ID22	SCC	IV	Right	Peripheral	5.2
ID23	SCC	IIIB	Right	Central	10.3
ID24	SCC	IIIB	Right	Extended	22.8
ID25	SCC	IV	Right	Central	8.2
ID26	SCC	IIIB	Right	Central	16.1

undergoing high TCC fitting errors due to the presence of structures, such as blood vessels and bronchi, or dynamic artefacts, were automatically detected as unreliable through the method presented in [26]. Finally, mean BF values were computed for each examination and considered to identify hemodynamic differences between the two histological NSCLC subtypes, AC and SCC.

To better understand the implications of the denoising methods we used, in Figure 1 we report two BF maps related to ID15, obtained with the denoising method we used [26] (a) and by manually removing (i.e., clipping) the highest BF values (b), supposedly out of the physiological range, as it is normally done. The removed values are shown in the pink colour in both maps. As one can see, the denoising method removes unreliable regions, including the outer ones, that is, those suffering from partial volume effect, which pure clipping normally keeps. Nevertheless, this method preserves a range of BF values wider than clipping does. This behaviour is underlined by the BF histogram of Figure 2(b), showing that, by clipping, the highest BF values (in red) are removed independently from their reliability, and the range of values narrowed. On the other side, the BF histogram of Figure 2(a) highlights the clear advantage of the denoising method, which “saves” those high values which are generated with no appreciable errors. Furthermore, one can see how this

method is able to even automatically remove unreliable low values falling within the physiological BF range. This explains why the range of BF values is wider, though the regions removed have a wider extent. Although these two maps are apparently very similar, the real benefit of the denoising method definitely arises in the subsequent analysis. For instance, as regards the perfusion analysis, the mean BF value of the clipped map (mean BF = 44.1 mL/min/100 g) is smaller than that of the corresponding denoised map (mean BF = 47.7 mL/min/100 g) by almost 10%. This underestimation of the mean BF value, due to the inclusion of unreliable BF values and exclusion of high BF values regardless of their reliability, could severely affect the statistical analysis of all perfusion studies. Of course, in the presence of bronchi, vessels, and, above all, artefacts this difference can be even larger.

The “Borderline” Examinations. After performing the automatic error analysis to detect and exclude unreliable values, we looked for the causes that could affect the perfusion of the “borderline” cases. Indeed, these are the most aspecific lesions of the two classes, whose parameter values are nearest to each other, which negatively affect the statistical significance of the study. If from one side they could simply originate from artefacts, from the other side, more interestingly, they

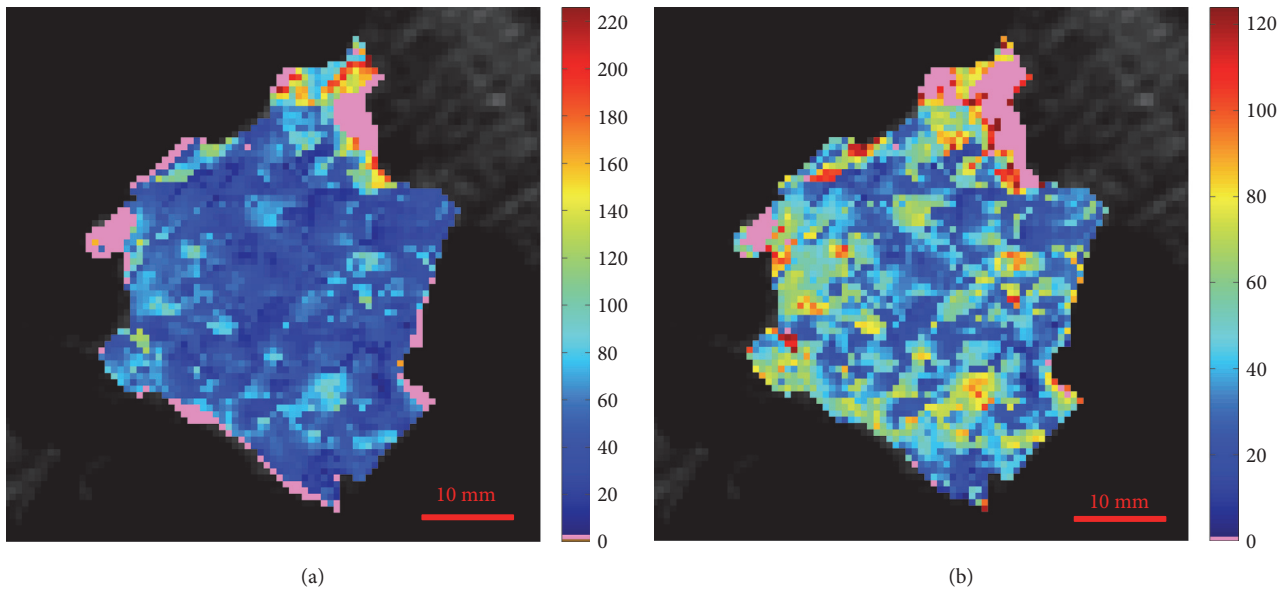


FIGURE 1: Perfusion maps of ID15 achieved through the use of the automatic denoising method (a) and by hand clipping the highest BF values (b). In pink, the unreliable values.

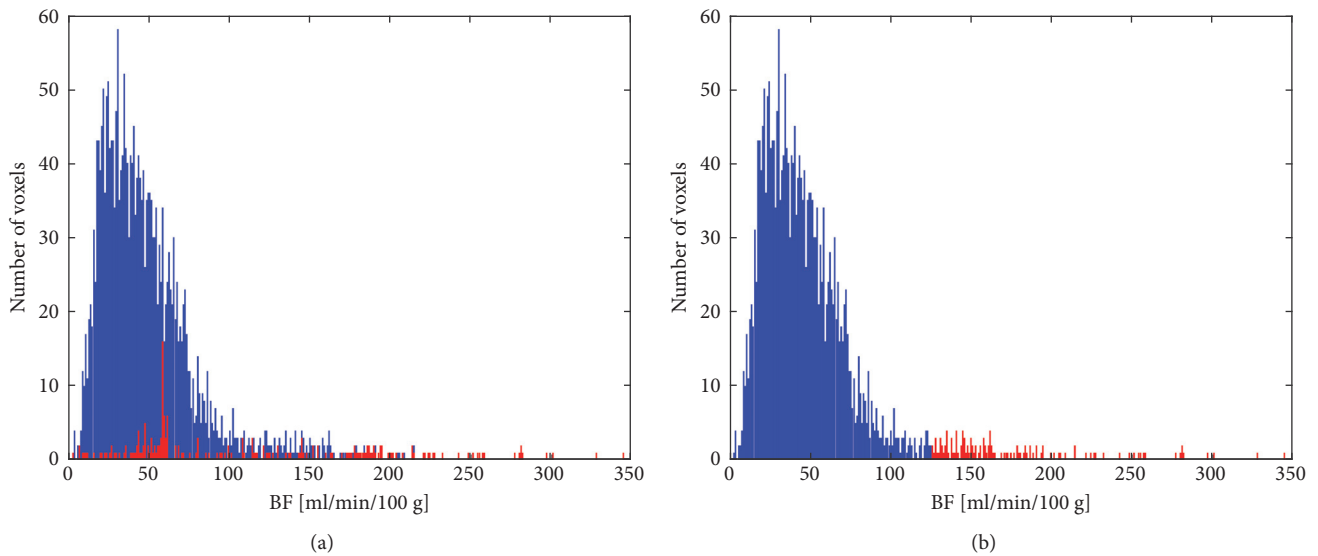


FIGURE 2: In blue, the histograms related to the original ID15 BF map and, in red, the BF values that were removed through the use of the automatic denoising method (a) and by hand clipping the highest BF values (b).

can reflect the inherent variability of data and the intrinsic tumour properties.

2.1. Assessment of Results. The main purpose of this work is to determine whether AC and SCC are characterized by a different baseline perfusion. In order to assess the statistical significance of the differences in BF between AC and SCC subtypes, the one-tail Welch's t-test was used for mean, while the one-tail Wilcoxon Rank Sum test (also known as Mann-Whitney U-test) was used for median. For both, the statistical significance is achieved with $p\text{-value} < 0.05$. Statistical

analysis was performed using R software (version 3.0.1, The R Foundation for Statistical Computing).

As regards the analysis of the borderline cases, we examined several factors that may cause perfusion variability. We considered where tumours arose, right or left lung, since it is proved that they drain to different lymph node groups according to their position [36]. In this context, we also considered the tumour location, central or peripheral, since central tumours can almost completely be fed by the bronchial circulation, while the peripheral tumours, mainly at their early growth stage, can have a significant pulmonary contribution [20]. Finally, we looked for the extrinsic effects on

TABLE 2: BF stratified by NSCLC subtypes.

NSCLC Subtypes	BF [mL/min/100 g]				
	Mean	Median	Minimum	Maximum	SD
AC	83.5	79.2	33.0	141.3	29.4
SCC	57.0	44.3	28.0	98.4	27.2

Note: SD = standard deviation.

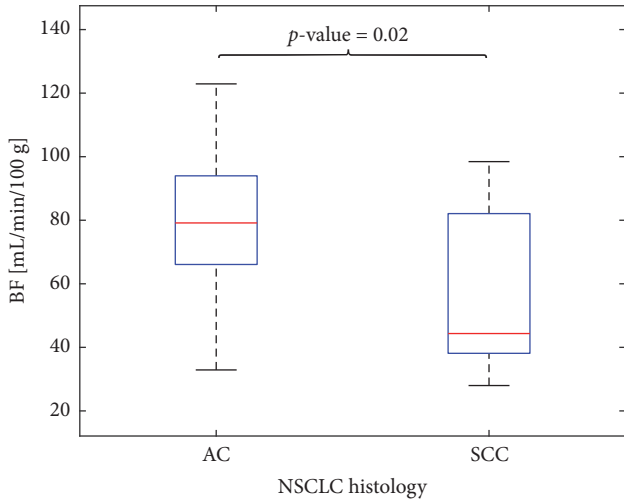


FIGURE 3: Box plots showing the BF values of AC (left) and SCC (right) lesions. The median is indicated as a red line in the boxes, whereas the vertical size gives the interquartile range.

perfusion computation of beam hardening artefacts which, for instance, occur in tumour localized near bony regions of the chest and, also, where the contrast medium is highly concentrated [24].

2.1.1. Tumour Location. For each examination, two radiologists examined the entire scan sequence so as to form in their mind the morphological structure of the lesion, also exploiting dynamic information. They divided tumours into three groups according to their locations, also reporting if they are in the left or right lung. A tumour was considered peripherally located if it is 20 mm of the costal pleura, within the pulmonary parenchyma without direct connection to mediastinal structures. A tumour is centrally located if it is 20 mm of the mediastinal structures, in a close relationship with the central airways. Otherwise, it is considered as an extended tumour (that could be either large or small). The two radiologists started by performing this analysis in double blind and, then, they reviewed together all cases to reach an agreement. This information is reported in Table 1.

3. Results

Table 2 resumes the main BF parameter values for AC and SCC subtypes, while Figure 3 graphically shows the distribution of BF values for the two subtypes. The outcome

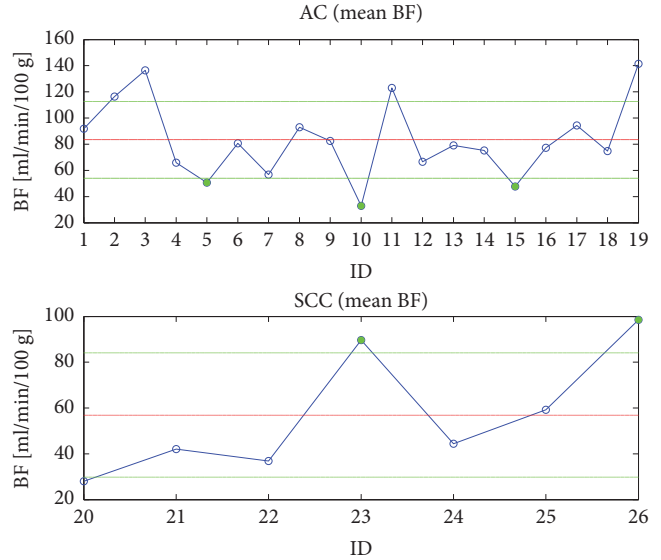


FIGURE 4: Mean BF values of AC (top) and SCC (bottom) examinations (blue circles), along with the corresponding group mean (solid red line) and SD (solid green line) values. The green circles highlight the examinations for each subtype that are closer to the mean value of the other subtype.

highlights that the baseline BF mean value of AC examinations is definitely greater than that of SCC ones (p -value = 0.02), as well as the BF median value (p -value = 0.03). Figure 4 shows the averaged BF values of each AC (top) and SCC (bottom) examination. For reader's convenience, the samples have been joined and displayed with solid blue lines, whereas the group mean and standard deviation (SD) values are shown with solid red and green lines, respectively. As one can see, as it often happens each subtype may have some borderline examinations nearer to the group mean value of the other subtype (the green disks in Figure 4), which are responsible for reducing the statistical significance of the between-group mean difference. In particular, ID5 (mean BF = 50.5 mL/min/100 g), ID10 (mean BF = 32.9 mL/min/100 g), and ID15 (mean BF = 47.7 mL/min/100 g) are three AC examinations whose BF values are closer to the SCC group mean value, while ID23 (mean BF = 89.7 mL/min/100 g) and ID26 (mean BF = 98.5 mL/min/100 g) are two SCCs with mean values closer to AC group mean. In the next section, we consider other studies aiming at assessing perfusion values of AC and SCC, besides these borderline cases, which are analysed to assess whether their mean value really reflects phenotypical features.

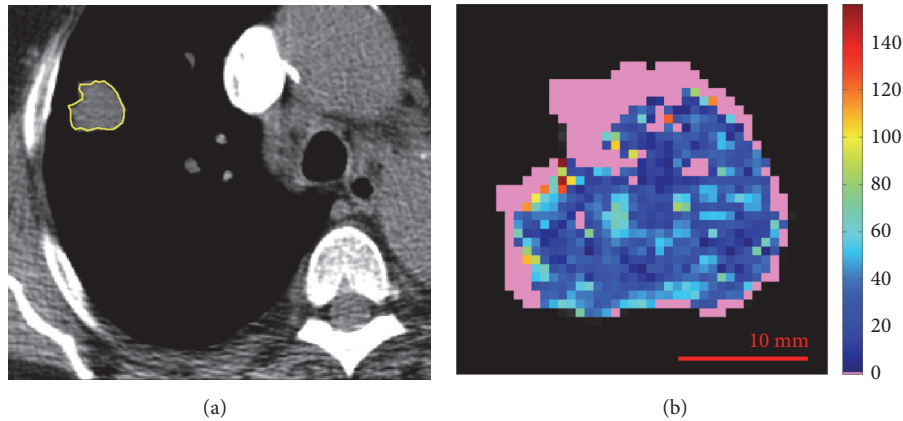


FIGURE 5: Reference slice (a) and perfusion map (b) related to ID10. In pink, the unreliable values.

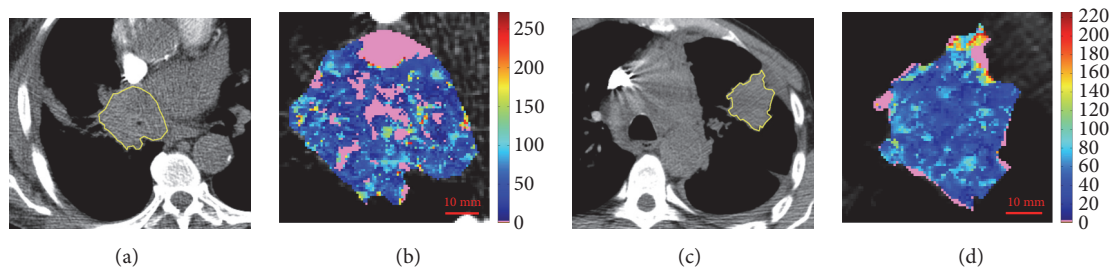


FIGURE 6: Reference slice and perfusion map related to ID5 (a, b) and ID15 (c, d). In pink, the unreliable values.

4. Discussion

In the literature, studies concerning the perfusion characterization of AC and SCC report contrasting results. The authors in [16] indicate that AC is characterized by a more abundant blood supply than SCC, as the higher peak of their TCCs suggested. Moreover, also blood volume and flow-extraction product are significantly higher in AC than in SCC [14]. The authors in [17] also found that AC has apparently a higher perfusion than SCC, but these results were not statistically significant, although MVD is significantly more intense in AC than in SCC. Other studies [18–20] highlighted no differences in perfusion parameters among these two histological subtypes, also finding that they are characterized by a similar MVD [21].

Among the possible causes for these discordant results, we propose to consider also those borderline cases whose perfusion values might be ascribed to motivation other than their phenotypical features. The first comment concerns ID10, the AC lesion characterized by the lowest perfusion and shown in Figure 5. This lesion is a very small peripheral carcinoma, one of the smallest examined, located in the subpleural parenchyma, probably characterized by a predominant pulmonary circulation, which could not have activated the angiogenesis process yet [37]. As regards the other two AC lesions with a low perfusion, ID5 in Figure 6(a) and ID15 in Figure 6(b), these share similar properties that could explain their low perfusion. In fact, both of them are large and extended lesions, presenting wide low-perfusion regions,

maybe suggesting hypoxia, which lower the mean BF values. Altogether, these three cases seem not showing any external characteristic artificially altering their BF. For instance, ID19 (mean BF = 141.4 mL/min/100 g) is a central carcinoma, as large as ID15, with a high perfusion value (the highest one). As a matter of fact, lesions of such a dimension are often characterized by a hypoxic core, due to the presence of weak and disorganized capillaries characterizing tumour angiogenesis. These vessels, being more permeable than normal, increase the liquid of the extravascular space, causing the adjacent cells moving away from the vessels and, consequently, the low oxygenation of the surrounding tissue. However, the presence of segmental vessels inside ID19 still nourished the core of the lesion.

As far as SCC are concerned, the two examinations ID23 and ID26 (Figure 7), showing a higher perfusion compared to the others SCC, share a common feature. Indeed, they are both central SCC lesions positioned at the right lung, directly connected to the vena cava and the pulmonary artery, respectively. This particular location, in proximity of these large blood vessels, may yield several artefacts during image acquisition, as shown in the original slices of Figure 7, which are responsible for an artificial increasing of BF values. A detail of six artefactual slices of ID23, referred to the same couch position, is shown in Figure 8. Nonetheless, one other central lesion, ID25 (mean BF = 59.3 mL/min/100 g) in Figure 9(a), suffers from moderate artefacts, while the last one, ID21 (mean BF = 42.0 mL/min/100 g) in Figure 9(b), is not artefactual. It is worth mentioning that if the artefacts

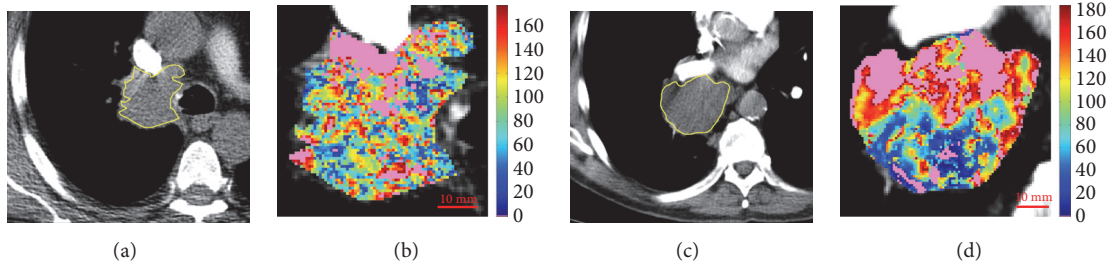


FIGURE 7: Reference slice and perfusion map related to ID23 (a, b) and ID26 (c, d). In pink, the unreliable values.

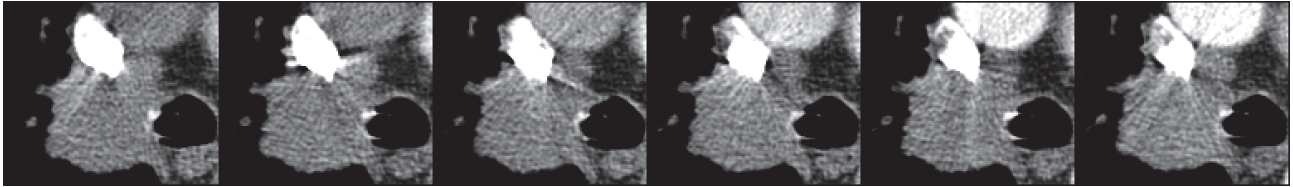


FIGURE 8: A sequence of six slices of ID23, referring to same couch position, shows the effect of beam hardening artefacts on lesions.

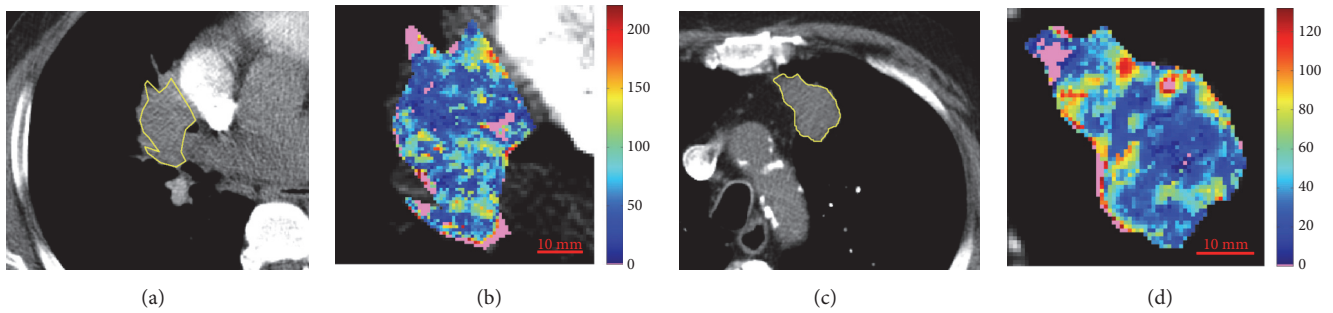


FIGURE 9: Reference slice and perfusion map related to ID25 (a, b) and ID21 (c, d). In pink, the unreliable values.

in ID23, ID25, and ID26 were removed manually, BF values for SCCs would rise to mean BF = 63.5 mL/min/100 g and SD BF = 36.9 mL/min/100 g, this yielding the difference between the overall means of the histotypes not to be statistically significant (p-value = 0.08). As a marginal note, it is interesting to see how the SCC lesion characterized by the lowest mean BF value in our court, ID20 (mean BF = 28.0 mL/min/100 g), shown in Figure 10, is staged IB.

At the end, we analysed the mean BF values of each lesion in relation to position and location. We report that each of the four peripheral ACs in the left lung has a mean value greater than the group mean, and the three right peripheral lesions have a lower mean BF, probably because of two bronchial arteries usually running to the left lung, while one only to the right lung. Similarly, all the extended AC lesions, neglecting their position, have a mean value lower than the group mean, except for ID2 and ID11 (Figures 11(a) and 11(b), respectively), that represent large lesions undergoing light beam hardening artefacts, from left and right atrium, respectively.

The present study newly investigated the perfusion baseline characteristics of AC and SCC, the two major NSCLC subtypes, after that the literature has reported discordant outcomes. We addressed the BF mean value, commonly used

as significant statistical parameter in several studies [7, 38]. Our results show that, before treatments, the AC histological type has a BF mean value significantly greater than SCC subtype, which generally shows a lower perfusion associated with an increased presence of necrotic areas. These results arise from the reliability analysis of the BF maps and are enforced by the analysis of borderline cases.

The reliability assessment, carried out through an automatic and objective error detection method [26], allowed removing the anatomical structures (mainly blood vessels and bronchi) and regions undergoing artefacts that could compromise the correct interpretation of perfusion maps, thus considerably improving their reliability. In particular, automatically removing and excluding all the artefactual regions from the subsequent analysis is probably the main reason why this study found a clear statistical significance of the different BF properties of AC and SCC histotypes.

Besides improving perfusion reliability, we analytically examined the borderline cases, that is, those most aspecific examinations of the two histotypes, whose perfusion values are so near to the mean value of the other histotype as to partly lose their representativeness. In particular, we looked for some external causes, besides phenotypical properties,

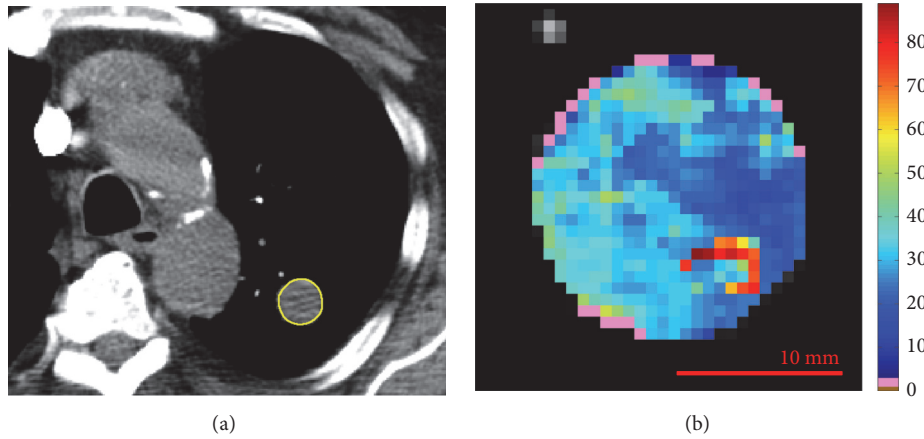


FIGURE 10: Reference slice (a) and perfusion map (b) related to ID20. In pink, the unreliable values.

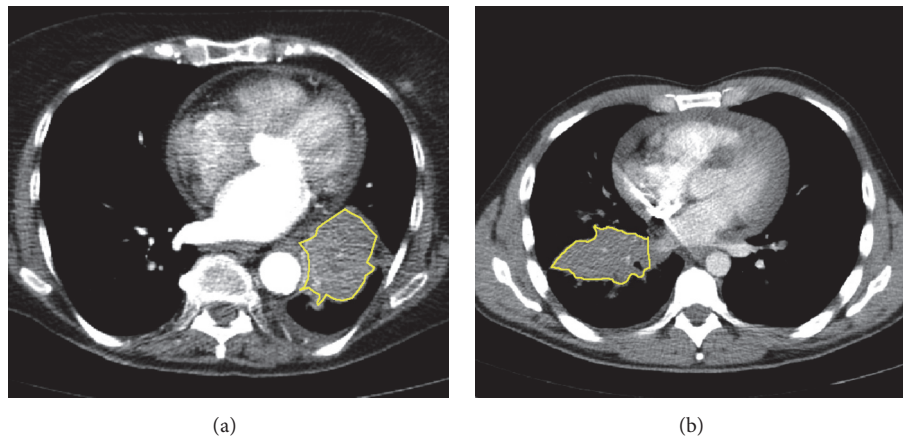


FIGURE 11: AC examinations ID2 (a) and ID11 (b) undergoing beam hardening artefacts.

which could motivate the mean BF value of each borderline case. As far as the three ACs are concerned, we could not find any external cause that could explain their lower BF values. Rather, the wide range covered by the AC histotype could be suggestive of the existence of subpopulations with different perfusion behaviours. Although there is no statistical evidence regarding probable effects of tumour's position and location on the BF mean values, we found some interesting tendencies regarding subgroups of the AC histotypes that could support this hypothesis and are worth investigating separately in a dedicated study. On the contrary, the predominantly central position of SCCs makes them prone to beam hardening artefacts, due to high contrast medium concentration in large neighbouring vessels, such as vena cava and the pulmonary artery. Indeed, it is known that artefacts may yield false results in tumours localized near to large central vessels [27]. In particular, we proved that without automatically removing those artefactual regions from perfusion computation in two borderline SCCs, their BF mean values would expectedly be higher so as that the difference between AC and SCC means would not be significant any more. This could explain the discordant results emerging

in the literature regarding the perfusion characterization of these lung cancer subtypes, since the “noise” emerging from the colour maps was almost disregarded. As an example, the study carried out in [15] reports group mean and SD BF values for AC (74.7 ± 28.2 mL/min/100 g) and SCC (68.7 ± 32.1 mL/min/100 g) that are so near to each other as to conclude that their difference is not statistically significant. However, a deep analysis of SCCs could highlight that they underwent artefacts and using our same method to remove them could have led to the opposite conclusion.

As an added value of this research, we want to stress how these results have been achieved using a short-time, dose-saving, protocol that could foster other studies aiming at investigating the peculiarities of AC subgroups, as far as BF is concerned. Nonetheless, increasing the examination time would jeopardize the possibility for patients to hold their breath, and motion artefacts introduced after a 25-sec period would worsen the quality of the image sequence [27].

This study has also some limitations. The first is the relatively small cohort of patients. However, other works in the literature reported a similar number of examinations, such as that in [38] (22 AC, 8 SCC), or smaller, like in [18]

(14 AC, 9 SCC), [20] (18 AC, 5 SCC), and [14] (6 AC, 8 SCC). Nonetheless, removing the unreliable perfusion values improved the statistical significance of the examinations at our disposal. The second limitation stems from the first one, as the number of examinations prevented us from exploring BF properties of possible AC subgroups. Finally, we have studied the BF only. However, considering other parameters was beyond the purpose of this research.

5. Conclusions

The main purpose of this work was to investigate the BF properties of AC and SCC at diagnosis, before treatment, and clear perfusion differences emerged from these NSCLC cancer subtypes that should be considered during their treatment planning. Nonetheless, we introduced two methodological contributions that allowed this study, with a non-large size cohort and a short-time protocol, to achieve a clear outcome. These contributions, which could benefit other cancer perfusion studies, consist in the use of a method to improve the reliability of single examinations and the accurate analysis of those borderline lesions less characterizing for the histotype they belong to. In particular, we believe it is important to explicitly investigate the causes that may be responsible for those values because, besides permitting to detect values that are artificially high (or low), the borderline lesions could contain even more valuable information than the other ones.

Among the practical advantages, the capability of achieving more accurate results could prevent the need of using a higher tube voltage, for instance, when investigating central carcinomas, which reduces the sensitivity to the contrast medium and increases the exposure of the patient [27].

We encourage the authors of all the previous studies on AC and SCC to review their analysis in the light of the methodological approaches presented in this research. In this age of personalised medicine, a non-invasive profiling of the tumour in terms of perfusion characteristics, apparently an independent surrogate biomarker, could have important implications in treatment strategy, particularly in the identification of the patients, mainly with AC, that will most benefit from antiangiogenic therapies.

Data Availability

The data used to support the findings of this study are included within the article.

Conflicts of Interest

The authors declare that there are no conflicts of interest regarding the publication of this paper.




References

- [1] R. N. Eskander and K. S. Tewari, "Incorporation of anti-angiogenesis therapy in the management of advanced ovarian carcinoma—Mechanistics, review of phase III randomized clinical trials, and regulatory implications," *Gynecologic Oncology*, vol. 132, no. 2, pp. 496–505, 2014.
- [2] A. Bevilacqua and S. Baiocco, "Automatic classification of lung tumour heterogeneity according to a visual-based score system in dynamic contrast enhanced CT sequences," *International Journal of Modern Physics C*, vol. 27, no. 9, Article ID 1650106, 14 pages, 2016.
- [3] B. Romain, L. Rouet, D. Ohayon, O. Lucidarme, F. d'Alché-Buc, and V. Letort, "Parameter estimation of perfusion models in dynamic contrast-enhanced imaging: a unified framework for model comparison," *Medical Image Analysis*, vol. 35, pp. 360–374, 2017.
- [4] A. B. Gill, N. J. Hilliard, S. T. Hilliard, M. J. Graves, D. J. Lomas, and A. Shaw, "A semi-automatic method for the extraction of the portal venous input function in quantitative dynamic contrast-enhanced CT of the liver," *British Journal of Radiology*, vol. 90, no. 1075, p. 20160875, 2017.
- [5] S. Malavasi, D. Barone, G. Gavelli, and A. Bevilacqua, "Multi-slice Analysis of Blood Flow Values in CT Perfusion Studies of Lung Cancer," *BioMed Research International*, vol. 2017, Article ID 3236893, 11 pages, 2017.
- [6] G. D'Assignies, A. Couvelard, S. Bahrami et al., "Pancreatic endocrine tumors: Tumor blood flow assessed with perfusion CT reflects angiogenesis and correlates with prognostic factors," *Radiology*, vol. 250, no. 2, pp. 407–416, 2009.
- [7] A. Kambadakone, S. S. Yoon, T.-M. Kim et al., "CT perfusion as an imaging biomarker in monitoring response to neoadjuvant bevacizumab and radiation in soft-tissue sarcomas: comparison with tumor morphology, circulating and tumor biomarkers, and gene expression," *AJR. American journal of roentgenology*, vol. 204, no. 1, pp. W11–W8, 2015.
- [8] A. So, E. Stewart, C. d'Esterre et al., "CT Perfusion: Principles, Implementation, and Clinical Applications," in *Multi-detector CT Imaging: Principles, Head, Neck, and Vascular Systems*, J. Fagerberg, D. C. Mowery, and R. N. Nelson, Eds., p. 29, CRC Press, Boca Raton, FL, USA, 2013.
- [9] K. A. Miles, T.-Y. Lee, V. Goh et al., "Current status and guidelines for the assessment of tumour vascular support with dynamic contrast-enhanced computed tomography," *European Radiology*, vol. 22, no. 7, pp. 1430–1441, 2012.
- [10] R. García-Figueiras, V. J. Goh, A. R. Padhani et al., "CT perfusion in oncologic imaging: a useful tool?" *American Journal of Roentgenology*, vol. 200, no. 1, pp. 8–19, 2013.
- [11] F. Shan, Z. Zhang, W. Xing et al., "Differentiation between malignant and benign solitary pulmonary nodules: Use of volume first-pass perfusion and combined with routine computed tomography," *European Journal of Radiology*, vol. 81, no. 11, pp. 3598–3605, 2012.
- [12] F. Fraioli, M. Anzidei, F. Zaccagna et al., "Whole-tumor perfusion CT in patients with advanced lung adenocarcinoma treated with conventional and antiangiogenetic chemotherapy: initial experience," *Radiology*, vol. 259, no. 2, pp. 574–582, 2011.
- [13] E. E. Graves, A. Maity, and Q.-T. Le, "The tumor microenvironment in non-small-cell lung cancer," *Seminars in Radiation Oncology*, vol. 20, no. 3, pp. 156–163, 2010.
- [14] H. C. Mandeville, Q. S. Ng, F. M. Daley et al., "Operable non-small cell lung cancer: correlation of volumetric helical dynamic contrast-enhanced CT parameters with immunohistochemical markers of tumor hypoxia," *Radiology*, vol. 264, no. 2, pp. 581–589, 2012.
- [15] J. Shi, G. Schmid-Bindert, C. Fink et al., "Dynamic volume perfusion CT in patients with lung cancer: Baselineperfusion characteristics of different histological subtypes," *European Journal of Radiology*, vol. 82, no. 12, pp. e894–e900, 2013.

- [16] S.-H. Ma, K. Xu, Z.-W. Xiao et al., "Peripheral lung cancer: relationship between multi-slice spiral CT perfusion imaging and tumor angiogenesis and cyclin D1 expression," *Clinical Imaging*, vol. 31, no. 3, pp. 165–177, 2007.
- [17] Y. Li, Z.-G. Yang, T.-W. Chen, H.-J. Chen, J.-Y. Sun, and Y.-R. Lu, "Peripheral lung carcinoma: Correlation of angiogenesis and first-pass perfusion parameters of 64-detector row CT," *Lung Cancer*, vol. 61, no. 1, pp. 44–53, 2008.
- [18] A. W. Sauter, S. Winterstein, D. Spira et al., "Multifunctional profiling of non-small cell lung cancer using 18F-FDG PET/CT and volume perfusion CT," *Journal of Nuclear Medicine*, vol. 53, no. 4, pp. 521–529, 2012.
- [19] W. van Elmpt, C. M. L. Zegers, B. Reymen et al., "Multiparametric imaging of patient and tumour heterogeneity in non-small-cell lung cancer: quantification of tumour hypoxia, metabolism and perfusion," *European Journal of Nuclear Medicine and Molecular Imaging*, vol. 43, no. 2, pp. 240–248, 2016.
- [20] S. Nakano, J. Gibo, Y. Fukushima et al., "Perfusion evaluation of lung cancer: Assessment using dual-input perfusion computed tomography," *Journal of Thoracic Imaging*, vol. 28, no. 4, pp. 253–262, 2013.
- [21] D. Spira, H. Neumeister, S. M. Spira et al., "Assessment of tumor vascularity in lung cancer using volume perfusion CT (VPCT) with histopathologic comparison: A further step toward an individualized tumor characterization," *Journal of Computer Assisted Tomography*, vol. 37, no. 1, pp. 15–21, 2013.
- [22] A. Bevilacqua, D. Barone, S. Baiocco, and G. Gavelli, "A novel approach for semi-quantitative assessment of reliability of blood flow values in DCE-CT perfusion," *Biomedical Signal Processing and Control*, vol. 31, pp. 257–264, 2017.
- [23] T. S. Koh, C. H. Thng, S. Hartono et al., "Dynamic contrast-enhanced CT imaging of hepatocellular carcinoma in cirrhosis: Feasibility of a prolonged dual-phase imaging protocol with tracer kinetics modeling," *European Radiology*, vol. 19, no. 5, pp. 1184–1196, 2009.
- [24] J. F. Barrett and N. Keat, "Artifacts in CT: Recognition and avoidance," *RadioGraphics*, vol. 24, no. 6, pp. 1679–1796, 2004.
- [25] E. Kang, K. Lee, J. Han, M. S. Roh, and C. Son, "Evaluation of Dual-Input Perfusion in Lung Cancer Using a 320-Detector CT: Its Correlation with Tumor Size, Location, and Presence of Metastasis," *Journal of the Korean Society of Radiology*, vol. 75, no. 5, p. 354, 2016.
- [26] A. Bevilacqua, D. Barone, S. Malavasi, and G. Gavelli, "Automatic detection of misleading blood flow values in CT perfusion studies of lung cancer," *Biomedical Signal Processing and Control*, vol. 26, pp. 109–116, 2016.
- [27] F. Kiessling, J. Boese, C. Corvinus et al., "Perfusion CT in patients with advanced bronchial carcinomas: A novel chance for characterization and treatment monitoring?" *European Radiology*, vol. 14, no. 7, pp. 1226–1233, 2004.
- [28] D. H. Lee, S. H. Kim, I. Joo, and J. K. Han, "CT Perfusion evaluation of gastric cancer: correlation with histologic type," *European Radiology*, vol. 28, no. 2, pp. 487–495, 2018.
- [29] A. Bevilacqua, D. Barone, S. Malavasi, and G. Gavelli, "Quantitative assessment of effects of motion compensation for liver and lung tumors in CT perfusion," *Academic Radiology*, vol. 21, no. 11, pp. 1416–1426, 2014.
- [30] S. Goutelle, M. Maurin, F. Rougier et al., "The Hill equation: a review of its capabilities in pharmacological modelling," *Fundamental & Clinical Pharmacology*, vol. 22, no. 6, pp. 633–648, 2008.
- [31] A. Gibaldi, D. Barone, G. Gavelli, S. Malavasi, and A. Bevilacqua, "Effects of guided random sampling of TCCs on blood flow values in CT perfusion studies of lung tumors," *Academic Radiology*, vol. 22, no. 1, pp. 58–69, 2015.
- [32] K. A. Miles and M. R. Griffiths, "Perfusion CT: a worthwhile enhancement?" *British Journal of Radiology*, vol. 76, no. 904, pp. 220–231, 2003.
- [33] D. Ippolito, G. Querques, S. Okolicsanyi, C. T. Franzesi, M. Strazzabosco, and S. Sironi, "Diagnostic value of dynamic contrast-enhanced CT with perfusion imaging in the quantitative assessment of tumor response to sorafenib in patients with advanced hepatocellular carcinoma: A feasibility study," *European Journal of Radiology*, vol. 90, pp. 34–41, 2017.
- [34] Y. Ohno, Y. Fujisawa, H. Koyama et al., "Dynamic contrast-enhanced perfusion area-detector CT assessed with various mathematical models: Its capability for therapeutic outcome prediction for non-small cell lung cancer patients with chemoradiotherapy as compared with that of FDG-PET/CT," *European Journal of Radiology*, vol. 86, pp. 83–91, 2017.
- [35] E. A. Bretas, U. S. Torres, L. R. Torres et al., "Is liver perfusion CT reproducible? A study on intra- and interobserver agreement of normal hepatic haemodynamic parameters obtained with two different software packages," *British Journal of Radiology*, vol. 90, no. 1078, p. 20170214, 2017.
- [36] D. Lardinois, P. De Leyn, P. Van Schil et al., "ESTS guidelines for intraoperative lymph node staging in non-small cell lung cancer," *European Journal of Cardio-Thoracic Surgery*, vol. 30, no. 5, pp. 787–792, 2006.
- [37] L. Eldridge, A. Moldobaeva, Q. Zhong et al., "Bronchial artery angiogenesis drives lung tumor growth," *Cancer Research*, vol. 76, no. 20, pp. 5962–5969, 2016.
- [38] T. D. L. Nguyen-Kim, T. Frauenfelder, K. Strobel, P. Veit-Haibach, and M. W. Huellner, "Assessment of bronchial and pulmonary blood supply in non-small cell lung cancer subtypes using computed tomography perfusion," *Investigative Radiology*, vol. 50, no. 3, pp. 179–186, 2015.

Review Article

PAX3: A Molecule with Oncogenic or Tumor Suppressor Function Is Involved in Cancer

Ashok Arasu,¹ Sengottuvelan Murugan,² Musthafa Mohamed Essa ³,
Thirunavukkarasu Velusamy ¹ and Gilles J. Guillemin ⁴

¹Department of Biotechnology, School of Biotechnology and Genetic Engineering, Bharathiar University, Coimbatore 641046, Tamil Nadu, India

²Endocrine Research Facility, Department of Animal Science, Rutgers University, New Brunswick-08901, NJ, USA

³Department of Food Science and Nutrition, CAMS, Sultan Qaboos University, Muscat, Oman

⁴Neuroinflammation Group, Faculty of Medicine and Health Sciences, Deb Bailey MND Research Laboratory, Macquarie University, NSW, 2109, Australia

Correspondence should be addressed to Musthafa Mohamed Essa; drmdessa@gmail.com,
Thirunavukkarasu Velusamy; bharathiarasu@gmail.com, and Gilles J. Guillemin; gilles.guillemin@mq.edu.au

Received 8 February 2018; Accepted 2 July 2018; Published 16 August 2018

Academic Editor: Franco M. Buonaguro

Copyright © 2018 Ashok Arasu et al. This is an open access article distributed under the Creative Commons Attribution License, which permits unrestricted use, distribution, and reproduction in any medium, provided the original work is properly cited.

Metastasis is the most deadly aspect of cancer and results from acquired gene regulation abnormalities in tumor cells. Transcriptional regulation is an essential component of controlling of gene function and its failure could contribute to tumor progression and metastasis. During cancer progression, deregulation of oncogenic or tumor suppressive transcription factors, as well as master cell fate regulators, collectively influences multiple steps of the metastasis cascade, including local invasion and dissemination of the tumor to distant organs. Transcription factor PAX3/Pax3, which contributes to diverse cell lineages during embryonic development, plays a major role in tumorigenesis. Mutations in this gene can cause neurodevelopmental disease and the existing literature supports that there is a potential link between aberrant expression of PAX3 genes in adult tissues and a wide variety of cancers. PAX3 function is tissue-specific and could contribute to tumorigenesis either directly as oncogene or as a tumor suppressor by losing its function. In this review, we discuss comprehensively the differential role played by PAX3 in various tissues and how its aberrant expression is implicated in disease development. This review particularly highlights the oncogenic and tumor suppressor role played by PAX3 in different cancers and underlines the importance of precisely identifying tissue-specific role of PAX3 in order to determine its exact role in development of cancer.

1. Introduction

Cancer is a disease that is characterized by uncontrolled cell growth, proliferation, migration, and invasion of abnormal cells resulting in aggregation of these cells to form tumors in organ. There are several etiologies for the development of cancer, ranging from environmental to genetic causes. Mutations that inhibit the normal function of oncogenes, tumor suppressor genes, and apoptosis genes can lead to uncontrollable cell growth. Changes in molecular mechanisms that regulate stem cell differentiation were also known to be a strong factor associated with development of cancer [1]. The paired box (PAX: human)/(Pax: mouse)

gene family is known to be associated with developmental functions and play a crucial role in cellular proliferation, differentiation, migration, and tissue development [2]. PAX proteins are subclassified according to the additional DNA-binding homeodomain or octapeptide region, which can serve as a binding motif for the protein cofactor for effective inhibition of downstream gene transcriptions [3]. The role of PAX/Pax protein as transcriptional activators or repressors has been demonstrated through their interaction with other transcription factors to induce target promoters [4]. There is a possible link between the anomalous expression of PAX genes in adult tissues and a wide class of cancers by promoting tumorigenesis as an oncogene or by failing to perform its role

as a tumor suppressor [5, 6]. PAX proteins may be useful as a biomarker in the diagnosis of cancers. PAX genes have an oncogenic ability when constitutively expressed, either as a part of a fusion gene or as a whole gene [7–12].

PAX3, a member of PAX gene family, plays a critical role in cell proliferation, differentiation, and migration during embryonic development of cells [13]. PAX3 contains all three complete structural domains: a paired domain, homeodomain, and octopeptide, which is a characteristic of PAX family of proteins. PAX3 interacts with other transcription factors through its paired domain (PD) and recruits them to target promoters [14, 15]. PAX3 is expressed as several isoforms such as PAX3a, PAX3b, PAX3c, PAX3d, PAX3e, PAX3g, and PAX3h [16–19]. Each of these isoforms are generally involved in developmental function, however, with specific functions that are unique to them in different tissues [19]. PAX3 expression is necessary for proliferation and migration of neural crest (NC) cells and muscle cell precursors in the dorsal dermomyotome. It is also involved in developmental pathways that lead to melanocytes and neurons originating from the NC and mature skeletal myocytes from the dorsal dermomyotome. Acceleration of proliferation, migration, and survival of neural crest cells are also regulated by PAX3 [20]. PAX3/Pax3 (human/mouse) is a developmentally expressed transcription factor in embryo and is rapidly switched off during terminal differentiation [21–23]. PAX3 is necessary not only for the proper specification of these developing tissues, but also for cell survival. Homozygous loss of PAX3 in mouse leads to several neural crest and neural tube defects, attributable to induction of p53-dependent apoptosis [5, 24–28]. PAX3 is necessary for neural crest-derived peripheral nervous system development (PNS) and its reexpression in differentiated neural crest cells is suspected to be involved in the development of peripheral nervous system tumor, neuroblastoma. A gain of function mutation in PAX3 is associated with several diseases such as Waardenburg syndromes, craniofacial-deafness-hand syndromes, alveolar rhabdomyosarcomas, and neuroblastomas [3, 29]. Being an important developmental factor, the expression of PAX3 gradually decreases as the tissues differentiate. However, its reexpression in differentiated adult tissues that require PAX3 function during embryonic development leads to several tumors [3, 15].

More recently, PAX3 was observed to be overexpressed in various types of cancer tissues and cell lines like neuroblastomas, glioblastomas, melanomas, and gastric cancers, suggesting that it may function as an oncogene in these cancers [30–36]. In rhabdomyosarcomas, PAX3-FOXO1 fusion increases the transcriptional activity of PAX3 by constitutive nuclear localization [37]. However, in thyroid cancer, it plays a completely different role as a tumor suppressor. Loss of function of PAX3 due to decreased expression caused by hypermethylation is reasoned out as an underlying cause for development of thyroid cancer [36]. Based on these facts, it is important to determine the functions of PAX3 specific to tissue type and then understand its role in disease pathogenesis. This review will mainly discuss about the specific roles played by PAX3 in different tissue types and then will focus on specific examples where PAX3 has contradictory

function as either oncogene or tumor suppressor, and is implicated in development of cancer.

2. PAX3 and Its Role in Development and Diseases

PAX3 is a very well-characterized protein that is expressed in the neural crest (NC) [38]. It is also one of the most well-characterized transcription factors of the NC and has been extensively studied in NC induction during development, cardiac NC, and melanocyte lineages [38]. The physiological function of PAX3 has been well understood through characterizing the mutations that are reported in mice and humans. PAX3 plays a major role during early skeletal muscle formation in the embryo, while PAX7 predominates during postnatal growth and muscle regeneration in the adult [39]. PAX3 is expressed during early migration of NC and in somitic cells along the neuronal crest cell migratory path [40]. PAX3 is generally extinguished in migratory neural crest cells as they differentiate but maintained in the melanocyte lineage and also sustained in cultured neural crest-derived stem cells [41], in later stages of development in various lineages. The timing of expression in early neural crest and subsequent downregulation as neural crest-derived cells differentiate also implicates PAX3 as an important factor for maintaining progenitor populations. In fact, persistent PAX3 misexpression in cranial neural crest cells resulted in cleft palate and other craniofacial defects, ocular defects, and perinatal lethality [42]. Another phenotype associated with persistent PAX3 expression is that bone morphogenetic protein- (BMP-) induced osteogenesis is blocked via upregulation of the PAX3 target *Sostdc1*, a soluble BMP inhibitor. This highlights the role PAX3 plays in maintaining an undifferentiated state by blocking responsiveness to differentiation signals [42]. PAX3 function well-characterized in the neural crest is the availability of a series of mutations in the murine *PAX3* gene. These alleles represent a range of null, severely hypomorphic, and mildly hypomorphic forms of PAX3. In addition to neural crest defects, PAX3 and PAX7 mutants display neurulation defects and altered somitogenesis [39]. PAX3 and *versican* have mutually exclusive expression pattern and when PAX3 is lost, the *versican* (VCAN) expression domain is expanded, correlating with an absence of migrating neural crest cells lateral to the neural tube [43]. Where PAX3 and *Zic1* expression overlap, they act together to specify the neuroectoderm to adopt a neural crest fate [44, 45] and activate *Slug* expression in a Wnt-dependent manner [24]. Multiple experiments demonstrate that PAX3 and *Zic1* together are both necessary and sufficient to specify neural crest [44, 45]; PAX3 is upregulated in the dorsal neural crest in response to Wnt signaling and also depends on bone morphogenetic protein (BMP) signaling. Downregulation of PAX3 occurs when the neural crest migration starts [46, 47].

In the absence of functional PAX3 (PAX3 mutants), the neural crest cells migrating to the peripheral nervous system undergo premature neurogenesis (evidenced by increased *Brn3* positive staining in neural tube explants), perhaps due to a change in the regulation of genes such as *Hes1* and

Ngn2 (needed for differentiation and proliferation), which PAX3 regulates by directly binding to their promoters. In this role, PAX3 may couple migration with neural crest cells maintenance and neurogenesis [48]. *In vitro*, a different phenomenon is seen. PAX3 is initially expressed in all neural crest cells from culture but is subsequently only retained in neurons. PAX3 homozygous mutant neural crest cultures had an 80% reduction in the capacity to generate sensory-like neurons. Downregulation of PAX3 in dorsal root ganglia inhibited 80–90% of newly generated sensory neurons but had no effect on survival of sensory neurons or precursors [49]. Mutation of PAX3, as occurs in PAX3 homozygotes, results in development of heart defects including persistent truncus arteriosus (PTA), signs of cardiac failure [25, 50, 51], and defects of the aortic arches, in addition to thymus, thyroid, and parathyroid defects, ultimately leading to embryonic lethality. PAX3 inhibits p53-dependent apoptosis in the dorsal neural tube to regulate its closure [28] and is also important for normal development and migration of the cardiac NC to the developing heart [25]. In addition to its function as a standalone transcription factor, several downstream molecules of other important pathways can act as a coactivator in mediating the transcriptional effects of PAX3. The downstream effector molecules of the Hippo pathway Taz and Yap65 play an important role in neural crest development and deletion of these proteins in neural crest resulted in embryo-lethal neural crest defects and decreased expression of the Pax3 target gene, *Mitf* [52].

The role of PAX3 as a transcription factor is well established in the development of melanocytes during embryogenesis and has recently been characterized as a molecular switch in the initiation of mature melanocytes formation [32]. Interestingly, PAX3 is one of the key molecules in melanogenesis that is absent or greatly reduced in the bulbs of white hair when compared to black hair, further reinforcing its role in melanocyte stem cell populations [53]. Among various PAX3 isoforms, PAX3c is the most studied and well-characterized isoform; in mouse melanocytes *in vitro*, the effect of PAX3 on proliferation, migration, survival, and transformation varies depending on the isoform, with some isoforms having opposite effects [20].

Evidence supports a role for PAX3 as a controller of a cascade of transcriptional events that are necessary and sufficient for skeletal myogenesis [54, 55]. PAX3 is downregulated when muscle tissue begins to differentiate and the muscle specific transcription factors are activated [54, 56]. Ectopic expression of PAX3 prevents the myogenic differentiation of myoblasts into myotubes, which might involve the cooperation of *Mx1* and *Notch* genes [57, 58].

Aberrant expression of PAX proteins is implicated in developmental defects. Specific mutations within a number of PAX/ Pax (human/mouse) genes lead to a range of developmental abnormalities in both human beings and mouse. Many studies proved that PAX3 loss of function mutations are involved in either type 1 or type 3 Waardenburg syndrome [59–65]. PAX3/Pax3 (human/mouse) mutations are associated with limb muscle hypoplasia in Waardenburg syndrome patients and *Splotch* phenotype mice, respectively [54, 55].

Interestingly, PAX3 mutations were typically not found in families with other neurocristopathies [64]. Mutations that partially abolish the activity of PAX2, PAX3, and PAX6 were known to cause dysmorphic syndromes with developmental abnormalities [66–70]. PAX2 and PAX8 double mutants show a complete lack of kidney formation due to reduced activity of these proteins [71].

3. PAX3 Plays an Oncogenic Role in Various Types of Tumors

Several members of the PAX family, especially subgroups II (PAX2, PAX5, and PAX8) and III (PAX3 and PAX7), play key roles in human malignancies, such as renal tumors, lymphoma, medullary thyroid carcinoma, rhabdomyosarcoma (RMS), and melanoma [5, 72–74]. Transfection of 3T3 cells with wild-type Pax1, Pax2, Pax3, Pax6, or Pax8 produced tumors in the nude mice within 2 to 6 weeks; the tumors were well vascularized and resembled spindle cell sarcomas, with high and a typical mitotic activity and infiltration into nerve and muscle tissues and blood vessels [75]. PAX genes in subgroups I (PAX1 and PAX9) are less often involved in cancer or their expression is indicative of a more favorable outcome [5]. PAX/Pax (human/mouse) proteins, therefore, serve as tumor markers in several cancers such as rhabdomyosarcoma, melanoma, neuroblastoma, and Ewing's sarcoma [2, 6, 76]. While PAX expression is very rare in adult tissues, findings support that its expression may be involved in maintaining pluripotency and survival of stem cell populations. Either continuing or recurring PAX expression is essential to provide pools of progenitor cells for tissue regeneration upon injury. In cancer cells, achieving self-sufficiency in growth signals and unrestricted replicative potential are required to be able to survive in potentially adverse microenvironments during tumor progression. There are numerous studies that prove that PAX genes play important roles in conferring growth and survival advantages to cancer cells and that they regulate cell plasticity [2]. Conceptually, cell proliferation and differentiation are placed at opposite ends of the "spectrum" of tumor progression. PAX genes, such as PAX8, could play a key role in balancing these processes [2].

PAX3, which plays a critical role during neural crest development, especially in progenitor cell populations, also plays a role in tumor formation in these tissue types. Many human neuroectodermal tumors express PAX3 [18, 34, 77, 78]. The role of PAX3 and its isoforms in myogenesis, melanogenesis, neurogenesis, and related oncogenesis have been well established (Figure 1). PAX3 is specifically detected in most neural crest-derived Ewing's family tumors and in most peripheral neuroectodermal tumors [34], small cell lung cancer [18], and most primary cultured melanomas [18, 34, 79]. Screening of Ewing's sarcoma and peripheral neuroectodermal tumor specimens and its derived cell lines showed elevated PAX3 expression [34]. Deactivation of p53 during neural tube closure and cardiac neural crest development by stimulating its ubiquitination and degradation requires PAX3 function, but not as a transcriptional regulator

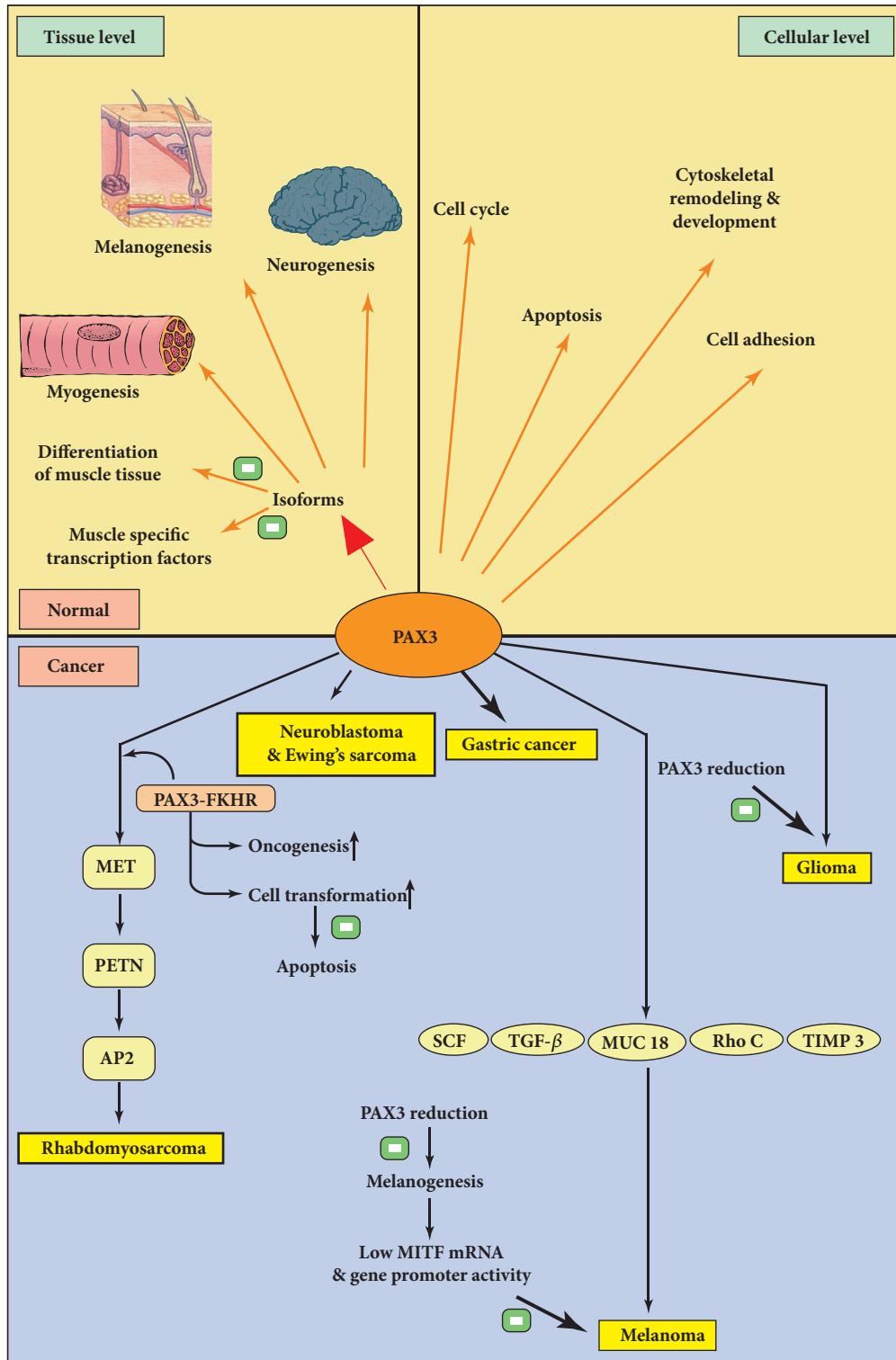


FIGURE 1: Oncogenic role of PAX3 in various types of cancer. PAX3 isoforms play a role in myogenesis, melanogenesis, and neurogenesis. PAX3 is involved in physiological events such as cell cycle, apoptosis, cell adhesion, and cytoskeletal remodeling and development. Overexpression of PAX3 inhibits the differentiation of muscle tissues and muscle specific transcription factors. While overexpression of PAX3 was observed in various types of cancers, PAX3-FKHR leads to tumorigenesis in rhabdomyosarcoma through altering the MET, PTEN, or AP2 signaling pathways. PAX3-FKHR can induce cellular transformation and prevent apoptosis. Reduction of PAX3 prevents development of glioma and also induces a loss of melanogenesis in melanoma. MITF mRNA and gene promoter activity is also decreased because of the PAX3 reduction. Melanoma susceptibility and progression genes like SCF, TGF-β, MUC18, RhoC, and TIMP3 can be regulated by PAX3 and it leads to melanoma.

TABLE 1: Pax3 transcription factor plays a dual role in various types of cancers.

Cancer Type	Effects	Role of PAX3
Rhabdomyosarcoma		PAX3-FKHR can induce cellular transformation and prevent apoptosis by altering the MET, PTEN or AP2 signalling pathways [55, 57, 58, 87, 89, 90, 92].
Melanoma		Regulating the expression of a variety of melanocytic genes, followed by a decrease in MITF mRNA and gene promoter activity and progression genes SCF, TGF- β , MUC18, RhoC and TIMP [84, 85]
Neuroblastoma	Oncogenic effects	Inhibition of PAX3 expression significantly decreased the attachment of S-type SH-EPI cells to extra-cellular matrix proteins, fibronectin, laminin and collagen IV and therefore downregulation of PAX3 reduces migration and invasion [31].
Glioblastoma		PAX3 was upregulated in the glioma SHG-44 cells promoted tumor formation <i>in vivo</i> cell lines, while its knockdown resulted in decreased cell proliferation, invasion and induced apoptosis in these cells. PAX3 expression in glioblastoma U-87MG cells suppressed tumorigenicity [30].
Gastric cancer		MiR-206 significantly suppressed gastric cancer cell invasion and metastasis both <i>in vitro</i> and <i>in vivo</i> by down regulating PAX3. <i>In vivo</i> metastasis assay shows that overexpression of PAX3 promotes invasiveness and pulmonary metastasis [35].
Urothelial cancer		FOXO3a negatively regulates Twist1 and Y-box-binding protein 1 (YB-1), and positively regulated E-cadherin in With FOXO3a PAX3 acts as a prognostic factor [94].
Thyroid cancer	Suppressor	PAX3 a tumor suppressor in thyroid cancer, through inhibiting the activities of PI3K/Akt and MAPK signaling pathways and promoting transcription factor FOXO3a.). The ectopic expression of PAX3, up-regulated the expression of ZIC1, a zinc-finger transcription factor, which in turn increases FOXO3a transcriptional activity [36].
Rhabdomyosarcoma		Overexpression of miR-29 and 206 downregulates the expression of cell cycle genes, induce cell cycle arrest through stabilizing PAX3 [6].
Alveolar rhabdomyosarcoma		PAX3-FOXO1 up-regulate <i>Noxa</i> (Promote activation of <i>caspases</i> and apoptosis) [95].

indicating a novel role for PAX3 in human diseases, such as in neural crest-derived cancers and Waardenburg syndrome types 1 and 3 [80].

Neuroblastoma is an extracranial solid tumor that occurs in children. Abnormally elevated levels of PAX3 expression has also been found in some neuroblastoma cell lines and tumors [81]. PAX-3 is overexpressed in glioma tissues compared to normal brain tissues; however, the pathogenic role of PAX-3 in human glioma cells remains to be elucidated. PAX3 was upregulated in the glioma cell lines, while its knockdown resulted in decreased cell proliferation and invasion and induced apoptosis in these cells (Figure 1). Inhibition of PAX3 expression in glioblastoma U-87MG cells suppressed tumorigenicity and upregulation of PAX3 expression in glioma SHG-44 cells promoted tumor formation *in vivo*. These results indicate that PAX3 in glioma is essential for gliomagenesis; thus, targeting PAX3 or its downstream targets may lead to novel therapies for this disease [30]; this data has been represented in Table 1. PAX3 contributes to various cell lineages during embryonic development and is also important in tumorigenesis. Reexpression of PAX3 was found in neuroblastoma cells, and the malignant neuroblastic (N-type) neuroblastoma cells expressed significantly higher PAX3 protein expression in comparison to their benign substrate-adherent (S-type) counterparts. PAX3 knockdown resulted in persistent cell growth inhibition in neuroblastoma cell, through G1 cell cycle arrest, and leads to progressive apoptosis.

Inhibition of PAX3 expression significantly decreased the attachment of S-type SH-EPI cells to extracellular matrix proteins, fibronectin, laminin, and collagen IV. Migration and invasion of both neuroblastoma cell types were markedly reduced after PAX3 downregulation. Microarray analyses revealed that signaling pathways involving cell cycle, apoptosis, cell adhesion, cytoskeletal remodelling, and development were altered in particular, by PAX3 downregulation (Table 1). These novel findings emphasize that PAX3 might contribute to oncogenic characteristics of neuroblastoma cells by regulating a variety of crucial signaling pathways [31].

While PAX3 promotes melanocyte phenotype, it plays an indispensable role in stem cell maintenance and actively promotes lesion survival, while BRAF mutations support tumor proliferation in melanoma [32]. PAX3 also plays a main role, in the pathogenesis of melanoma by influencing pathways through its transcriptional activity [82] and also by inducing p53 loss of function by promoting its ubiquitination [80]. PAX3 is a key transcription factor in regulating the expression of a variety of melanocytic genes [22, 83]. Inhibiting the expression of PAX3 using antisense RNA in melanoma cell lines resulted in dose dependent reduction of proliferation of melanoma cells and induction of apoptosis, suggesting role for PAX3 in melanoma cell survival [78, 79]. Pax3 reduction also induces a loss of melanogenesis in melanoma cells, followed by a sharp decrease in MITF mRNA and

gene promoter activity. Using microarray analyses PAX3 was identified as a regulator of the melanoma susceptibility and progression genes SCF, TGF- β , MUC18, RhoC, and TIMP3 [84–86], and this data has been represented in Figure 1 and Table 1.

PAX3 involved in muscle development is also implicated in tumorigenesis of muscle, rhabdomyosarcoma. Rhabdomyosarcoma is the most frequent soft tissue tumor in children under 15 years old. It develops as a consequence of disruption to the regulation of the growth and differentiation of myogenic precursor cells. PAX3 promotes tumorigenesis by influencing downstream MET pathway [87]. Rhabdomyosarcoma cells that undergo apoptosis due to specific antisense treatment is rescued from death by ectopic expression of PAX3, which indicates the prosurvival properties promoted by PAX3 [88]. PAX3 expression was markedly higher in gastric cancer tissues than in adjacent noncancerous tissues. MiR-206 significantly suppressed gastric cancer cell invasion and metastasis both *in vitro* and *in vivo* by downregulating PAX3. *In vivo* metastasis assay demonstrates that overexpression of PAX3 significantly promotes invasiveness and pulmonary metastasis of gastric cancer cells [35] (Table 1).

The above-mentioned studies clearly establish the oncogenic role of aberrant expression of PAX3 as a whole molecule in various cancers. Interestingly, PAX3 gene is involved in gene translocations which results in fusion proteins involving PAX3 that offers them oncogenic potential [89]. PAX3-FKHR (forkhead in rhabdomyosarcoma) fusion proteins are involved in promoting different molecular pathogenesis of alveolar rhabdomyosarcoma and embryonal rhabdomyosarcoma by inducing cellular transformation and preventing apoptosis [89, 90]. The tumor promoting effects of PAX3 and PAX3-FKHR in rhabdomyosarcoma tumorigenesis are suggested to be through altering the MET, PTEN, or AP2 signaling pathways (Figure 1, Table 1). PAX3-FKHR mutants through gain of function promote tumor development in myoblasts, which again shows the oncogenic potential of PAX3 transcriptional activity [91]. Interestingly, PAX3-FKHR shows oncogenic effects, predominantly at relatively low levels, while at higher expression levels it induces suppression of growth in 3T3 L1 fibroblasts [92]. This particular study highlighted domain specific function of PAX3 at different levels of activity. At low levels, through its homeo domain and its associated function induced the transformation of 3T3L1 fibroblasts, while at higher levels they inhibited the transformation and growth potential of these cells, by its activity through paired domain. These studies clearly indicate a multifaceted dynamic function of PAX3 depending on the level of activity and cell type.

4. Tumor Suppressing Role of PAX3

The proliferation promoting characteristics of PAX3 have been well established in several cancers as discussed above. However, designating PAX3 as an oncogene has been impaired by contradicting reports available that highlight the growth inhibiting potential of PAX3. The ectopic expression

of PAX3 dramatically inhibited thyroid cancer cell proliferation, colony formation, migration and invasion, induced cell cycle arrest, and apoptosis and retarded tumorigenic potential in nude mice [36]. These reports implicate PAX3 as a novel functional tumor suppressor in thyroid cancer, through inhibiting the activities of PI3K/Akt and MAPK signaling pathways and promoting transcription factor FOXO3a. The study also highlighted that epigenetic alteration such as promoter methylation as a major mechanism by which PAX3 is inactivated in this cancer (Figure 2 and Table 1). Further, PAX3 is a member that belongs to a group of transcription factors that are regulated by posttranslational modification such as acetylation. Pax3 acetylation decreased its transcriptional activity, thereby modulating the activity of downstream effectors Hes1 and increased Neurog2, resulting in sensory neuron differentiation [93]. Overexpression of miR-29 and 206 downregulates the expression of cell cycle genes and induces cell cycle arrest through stabilization of PAX3 in rhabdomyosarcoma, suggesting a tumor suppressor role for PAX3 [6].

5. FOXO-PAX3 Association in Tumor Suppression

PAX3, in addition to its tumor suppressor function, can also combine with other transcription factors and can regulate the expression of a wide variety of proteins that can act as tumor suppressors. FOXO1 transcription factors belong to the FOXO family and are involved in regulating key physiological pathways. In ARMS, gene translocations between PAX3 and FOXO1 resulted in a fusion protein PAX3-FOXO1 which promoted the growth suppressive activity by upregulating the expression of gremlin 1 (GREM1) and death associated protein kinase-1 (DAPK1) tumor suppressor genes [96] (Figure 2). This study also characterized four downstream targets of PAX3-FOXO1 that contribute to the biological activities of growth suppression and myogenic differentiation [96]. PAX3-FOXO1 upregulated Noxa, which in turn promoted the activation of caspases and induced apoptosis. This particular signaling axis is considered as an important aspect of ARMS tumor biology that provides opportunity to create a therapeutic window by induction of apoptosis in ARMS cells [95] (Figure 1 and Table 1).

Similarly, PAX3 can modulate the expression of FOXO3, another type of transcription factor that belongs to the FOXO family that are involved in multiple signaling pathways and plays critical roles in a number of physiologic and pathologic processes [97]. Cancer patients with low FOXO3a expression had poor disease-free survival, cancer-specific survival, and overall survival [94].

FOXO3a negatively regulated Twist1 and Y-box-binding protein 1 (YB-1) and positively regulated E-cadherin in KK47 and TCCsup cells that expressed Twist1, but not in T24 cells that did not express Twist1 (Table 1). This suggests that FOXO3a could act as a prognostic factor in urothelial cancer and could represent a promising molecular target for cancer therapeutics [94]. Interestingly, FOXO3 partners with PAX3/7 to coordinately recruit RNA polymerase II

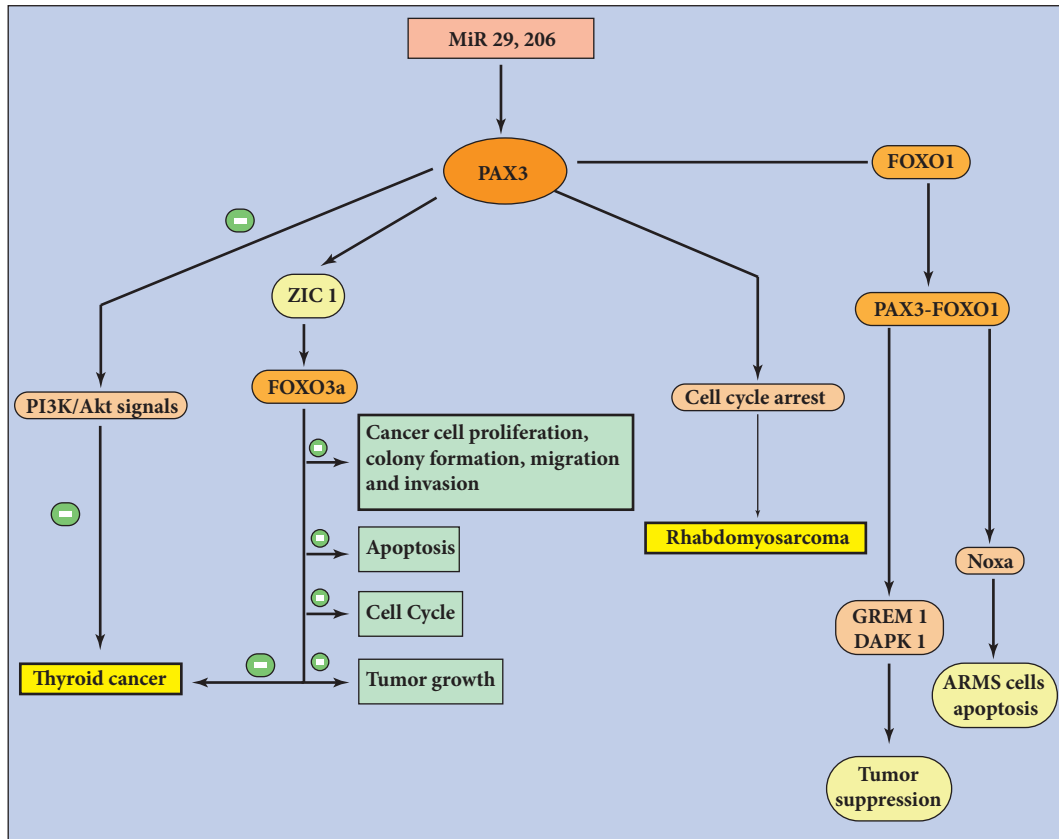


FIGURE 2: Tumor suppressor role of PAX3 in various types of cancer. Ectopic expression of PAX3 inhibits thyroid cancer cell proliferation, colony formation, migration, and invasion, and induced cell cycle arrest and leads to apoptosis through inhibiting the activities of PI3K/Akt and MAPK signaling pathways and promoting transcription factor FOXO3a. MiR 29 and 206 stabilize the PAX3 expression and induce the cell cycle arrest in the rhabdomyosarcoma cell lines. Fusion between the PAX3-FOXO1 induces the tumor cell suppression by inducing the expression of GERM1 and DAPK1 genes which in turn upregulate NOXA (promote activation of caspases and apoptosis) and induce apoptosis in ARMS cells.

and form a pre initiation complex (PIC) to activate MyoD transcription in myoblasts leading to its differentiation [98]. The ectopic expression of PAX3, upregulated the expression of ZIC1, a zinc-finger transcription factor, which in turn increases FOXO3a transcriptional activity in thyroid cancer cells. The regulation of ZIC1 by PAX3 suggests that PAX3 regulates the expression and activity of FOXO3a through multiple mechanisms in thyroid cancer [99]. These studies clearly indicate that, in addition to its own tumor suppressor role, PAX3 can promote tumor suppressor function by interplaying FOXO family of transcription factors to promote the expression of tumor suppressor genes that are controlled by them.

6. Conclusion

PAX3 is a pivotal gene involved in organ development and is also known to play a very important role in development of cancer. PAX3 regulates cell differentiation, proliferation, migration, and the survival of different cell types through activating several target genes. Majority of studies on PAX3

clearly indicate a crucial role for it in the oncogenesis of several human tumors. Interestingly, the studies involving ectopic expression of PAX3 in thyroid cancers show that it can act as a tumor suppressor. Further, PAX3 in association with FOXO3a transcription factor modulates several pathways that lead to cellular differentiation and growth inhibition in cancer. These facts clearly prevent us from designating PAX3 as an oncogene, as there are results pointing in other direction (Figure 3). The possibility of PAX3 having dual functions as oncogenic and tumor suppressor based on the cell type, context, and physiologic stimuli cannot be ignored. While the oncogenic role has been well established, more studies are required that can strengthen its tumor suppressor role. Studies reporting their antiproliferative effect should not be ignored and should be considered seriously. Due to the existing discrepancies, it is important to understand the exact role of PAX3 in diseases, where PAX3 expression is altered. Future studies should focus on determining the tissues specific functions of PAX3, where it is either mutated or aberrantly expressed. This vital information is important and will be very useful in developing therapeutic strategies targeting PAX3.

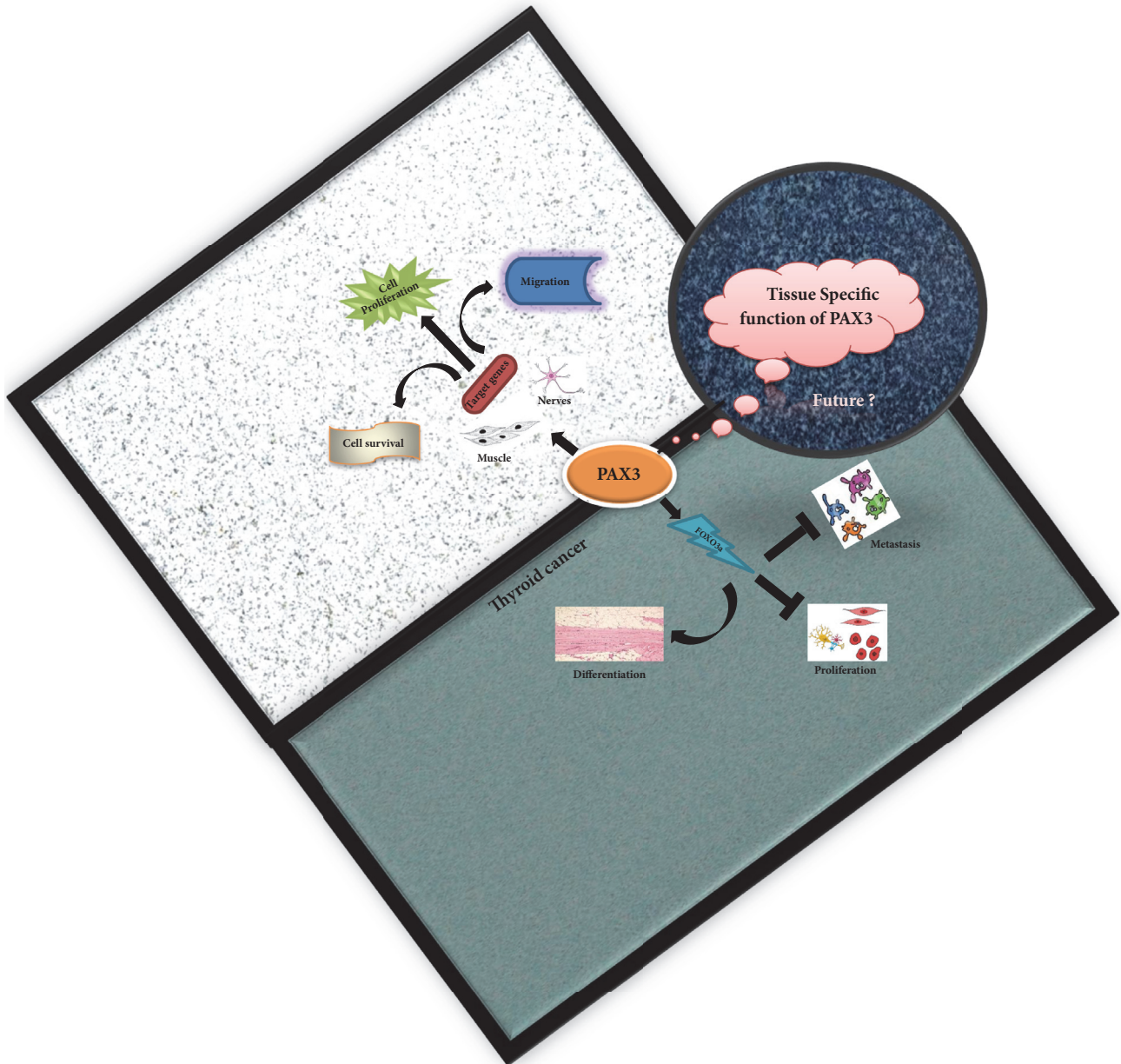


FIGURE 3: Schematic model explaining various tissue-specific cellular functions of PAX3 in normal and disease conditions. PAX3 regulates cell differentiation, proliferation, migration, and the survival of different cell types through activating several target genes. Ectopic expression of PAX3 in thyroid cancers shows that it can act as a tumor suppressor. PAX3 in association with FOXO3a leads to cellular differentiation and growth inhibition in cancer. Determining tissue-specific effects of PAX3 is necessary to understand its role in disease pathogenesis.

Abbreviations

PAX3:	Paired box gene3
FKHR (FOXO1a):	Forkhead transcription factor
MTIF:	Microphthalmia-associated transcription factor
SCF:	Stem cell factor
TGF- β :	Transforming growth factor beta 1
MUC 18:	Melanoma cell adhesion molecule
RhoC:	Ras Homolog Family Member C
TIMP3:	Tissue inhibitor of metalloproteinase 3

YB-1:	Y-box Binding Protein-1
FOXO3a:	Forkhead box O3
PI3K:	Phosphoinositide 3-kinase
Akt:	Protein Kinase B
MAPK:	Mitogen-activated protein kinase
ZIC1:	Zinc-finger transcription factor.

Conflicts of Interest

The authors declare that they have no conflicts of interest.

Acknowledgments

University Grants Commission-Basic Science Research (UGC-BSR) student fellowship in sciences for supporting Mr. Ashok Arasu is highly acknowledged. Department of Biotechnology (DBT), Ramalingaswami Reentry Fellowship Program for supporting Dr. Thirunavukkarasu Velusamy is gratefully acknowledged.

References

- [1] L. V. Nguyen, R. Vanner, P. Dirks, and C. J. Eaves, "Cancer stem cells: an evolving concept," *Nature Reviews Cancer*, vol. 12, no. 2, pp. 133–143, 2012.
- [2] C. G. Li and M. R. Eccles, "PAX genes in cancer; friends or foes?" *Frontiers in Genetics*, vol. 3, 2012.
- [3] Q. Wang, W.-H. Fang, J. Krupinski, S. Kumar, M. Slevin, and P. Kumar, "Pax genes in embryogenesis and oncogenesis: Genes..." *Journal of Cellular and Molecular Medicine*, vol. 12, no. 6A, pp. 2281–2294, 2008.
- [4] A. Buchberger, D. Freitag, and H.-H. Arnold, "A homeo-paired domain-binding motif directs Myf5 expression in progenitor cell of limb muscle," *Development*, vol. 134, no. 6, pp. 1171–1180, 2007.
- [5] E. J. D. Robson, S. He, and M. R. Eccles, "A PANorama of PAX genes in cancer and development," *Nature Reviews Cancer*, vol. 6, no. 1, pp. 52–62, 2006.
- [6] L. Li, A. L. Sarver, S. Alamgir, and S. Subramanian, "Down-regulation of microRNAs miR-1, -206 and -29 stabilizes PAX3 and CCND2 expression in rhabdomyosarcoma," *Laboratory Investigation*, vol. 92, no. 4, pp. 571–583, 2012.
- [7] F. G. Barr, N. Galili, J. Holick, J. A. Biegel, G. Rovera, and B. S. Emanuel, "Rearrangement of the PAX3 paired box gene in the paediatric solid tumour alveolar rhabdomyosarcoma," *Nature Genetics*, vol. 3, no. 2, pp. 113–117, 1993.
- [8] R. J. Davis, C. M. D'Cruz, M. A. Lovell, J. A. Biegel, and F. G. Barr, "Fusion of PAX7 to FKHR by the variant t(1;13)(p36;q14) translocation in alveolar rhabdomyosarcoma," *Cancer Research*, vol. 54, no. 11, pp. 2869–2872, 1994.
- [9] A. M. Morrison, S. L. Nutt, C. Thévenin, A. Rolink, and M. Busslinger, "Loss- and gain-of-function mutations reveal an important role of BSAP (Pax-5) at the start and end of B cell differentiation," *Seminars in Immunology*, vol. 10, no. 2, pp. 133–142, 1998.
- [10] T. G. Kroll, P. Sarraf, L. Pecciarini et al., "PAX8-PPAR γ 1 fusion in oncogene human thyroid carcinoma," *Science*, vol. 289, no. 5483, pp. 1357–1360, 2000.
- [11] G. Cazzaniga, M. Daniotti, S. Tosi et al., "The paired box domain gene PAX5 is fused to ETV6/TEL in an acute lymphoblastic leukemia case," *Cancer Research*, vol. 61, no. 12, pp. 4666–4670, 2001.
- [12] A. R. Marques, C. Espadinha, A. L. Catarino et al., "Expression of PAX8-PPAR γ 1 rearrangements in both follicular thyroid carcinomas and adenomas," *The Journal of Clinical Endocrinology & Metabolism*, vol. 87, no. 8, pp. 3947–3952, 2002.
- [13] R. G. Harris, E. White, E. S. Phillips, and K. A. Lillycrop, "The expression of the developmentally regulated proto-oncogene Pax-3 is modulated by N-Myc," *The Journal of Biological Chemistry*, vol. 277, no. 38, pp. 34815–34825, 2002.
- [14] S. Du, E. J. Lawrence, D. Strzelecki et al., "Co-expression of alternatively spliced forms of PAX3, PAX7, PAX3-FKHR and PAX7-FKHR with distinct DNA binding and transactivation properties in rhabdomyosarcoma," *International Journal of Cancer*, vol. 115, no. 1, pp. 85–92, 2005.
- [15] J. D. Kubic, K. P. Young, R. S. Plummer, A. E. Ludvik, and D. Lang, "Pigmentation PAX-ways: The role of Pax3 in melanogenesis, melanocyte stem cell maintenance, and disease," *Pigment Cell & Melanoma Research*, vol. 21, no. 6, pp. 627–645, 2008.
- [16] K. Tsukamoto, Y. Nakamura, and N. Niikawa, "Isolation of two isoforms of the PAX3 gene transcripts and their tissue-specific alternative expression in human adult tissues," *Human Genetics*, vol. 93, no. 3, pp. 270–274, 1994.
- [17] T. D. Barber, M. C. Barber, T. E. Cloutier, and T. B. Friedman, "PAX3 gene structure, alternative splicing and evolution," *Gene*, vol. 237, no. 2, pp. 311–319, 1999.
- [18] C. J. Parker, S. G. Shawcross, H. Li et al., "Expression of PAX 3 alternatively spliced transcripts and identification of two new isoforms in human tumors of neural crest origin," *International Journal of Cancer*, vol. 108, no. 2, pp. 314–320, 2004.
- [19] Q. Wang, S. Kumar, M. Slevin, and P. Kumar, "Functional analysis of alternative isoforms of the transcription factor PAX3 in melanocytes in vitro," *Cancer Research*, vol. 66, no. 17, pp. 8574–8580, 2006.
- [20] O. Sanchez-Ferras, B. Coutaud, T. D. Samani, I. Tremblay, O. Souchkova, and N. Pilon, "Caudal-related homeobox (Cdx) protein-dependent integration of canonical Wnt signaling on Paired-box 3 (Pax3) neural crest enhancer," *The Journal of Biological Chemistry*, vol. 287, no. 20, pp. 16623–16635, 2012.
- [21] M. D. Goulding, G. Chalepakis, U. Deutsch, J. R. Erselius, and P. Gruss, "Pax-3, a novel murine DNA binding protein expressed during early neurogenesis," *EMBO Journal*, vol. 10, no. 5, pp. 1135–1147, 1991.
- [22] D. Lang, M. M. Lu, L. Huang et al., "Pax3 functions at a nodal point in melanocyte stem cell differentiation," *Nature*, vol. 433, no. 7028, pp. 884–887, 2005.
- [23] F. Relaix, D. Rocancourt, A. Mansouri, and M. Buckingham, "A Pax3/Pax7-dependent population of skeletal muscle progenitor cells," *Nature*, vol. 435, no. 7044, pp. 948–953, 2005.
- [24] A.-H. Monsoro-Burq, E. Wang, and R. Harland, "Mxsl and Pax3 cooperate to mediate FGF8 and WNT signals during Xenopus neural crest induction," *Developmental Cell*, vol. 8, no. 2, pp. 167–178, 2005.
- [25] S. J. Conway, D. J. Henderson, and A. J. Copp, "Pax3 is required for cardiac neural crest migration in the mouse: Evidence from the splotch (Sp(2H)) mutant," *Development*, vol. 124, no. 2, pp. 505–514, 1997.
- [26] M. Olaopa, H.-M. Zhou, P. Snider et al., "Pax3 is essential for normal cardiac neural crest morphogenesis but is not required during migration nor outflow tract septation," *Developmental Biology*, vol. 356, no. 2, pp. 308–322, 2011.
- [27] D. J. Epstein, M. Vekemans, and P. Gros, "splotch (Sp2H), a mutation affecting development of the mouse neural tube, shows a deletion within the paired homeodomain of Pax-3," *Cell*, vol. 67, no. 4, pp. 767–774, 1991.
- [28] L. Pani, M. Horal, and M. R. Loeken, "Rescue of neural tube defects in Pax-3-deficient embryos by p53 loss of function: Implications for Pax-3-dependent development and tumorigenesis," *Genes & Development*, vol. 16, no. 6, pp. 676–680, 2002.
- [29] R. A. Macina, F. G. Barr, N. Galili, and H. C. Riethman, "Genomic organization of the human PAX3 gene: DNA sequence analysis of the region disrupted in alveolar rhabdomyosarcoma," *Genomics*, vol. 26, no. 1, pp. 1–8, 1995.

- [30] L. Xia, Q. Huang, D. Nie et al., "PAX3 is overexpressed in human glioblastomas and critically regulates the tumorigenicity of glioma cells," *Brain Research*, vol. 1521, pp. 68–78, 2013.
- [31] W.-H. Fang, Q. Wang, H.-M. Li, M. Ahmed, P. Kumar, and S. Kumar, "PAX3 in neuroblastoma: Oncogenic potential, chemosensitivity and signalling pathways," *Journal of Cellular and Molecular Medicine*, vol. 18, no. 1, pp. 38–48, 2014.
- [32] R. S. Plummer, C. R. Shea, M. Nelson et al., "PAX3 expression in primary melanomas and nevi," *Modern Pathology*, vol. 21, no. 5, pp. 525–530, 2008.
- [33] E. Frascella, L. Toffolatti, and A. Rosolen, "Normal and rearranged PAX3 expression in human rhabdomyosarcoma," *Cancer Genetics and Cytogenetics*, vol. 102, no. 2, pp. 104–109, 1998.
- [34] T. W. Schulte, J. A. Toretsky, E. Ress, L. Helman, and L. M. Neckers, "Expression of PAX3 in Ewing's sarcoma family of tumors," *Biochemical and Molecular Medicine*, vol. 60, no. 2, pp. 121–126, 1997.
- [35] L. Zhang, L. Xia, L. Zhao et al., "Activation of PAX3-MET pathways due to miR-206 loss promotes gastric cancer metastasis," *Carcinogenesis*, vol. 36, no. 3, pp. 390–399, 2014.
- [36] W. Liu, F. Sui, J. Liu et al., "PAX3 is a novel tumor suppressor by regulating the activities of major signaling pathways and transcription factor FOXO3a in thyroid cancer," *Oncotarget*, vol. 7, no. 34, pp. 54744–54757, 2016.
- [37] C. M. Linardic, "PAX3-FOXO1 fusion gene in rhabdomyosarcoma," *Cancer Letters*, vol. 270, no. 1, pp. 10–18, 2008.
- [38] B. L. Nelms and P. A. Labosky, "Transcriptional Control of Neural Crest Development," *Colloquium Series on Developmental Biology*, vol. 1, no. 1, pp. 1–227, 2010.
- [39] M. Buckingham and F. Relaix, "PAX3 and PAX7 as upstream regulators of myogenesis," *Seminars in Cell & Developmental Biology*, vol. 44, pp. 115–125, 2015.
- [40] G. N. Serbedzija and A. P. McMahon, "Analysis of neural crest cell migration in *spotch* mice using a neural Crest-Specific LacZ reporter," *Developmental Biology*, vol. 185, no. 2, pp. 139–147, 1997.
- [41] M. Zhao, S. C. Isom, H. Lin et al., "Tracing the stemness of porcine skin-derived progenitors (pSKP) back to specific marker gene expression," *Cloning and Stem Cells*, vol. 11, no. 1, pp. 111–122, 2009.
- [42] M. Wu, J. Li, K. A. Engleka et al., "Persistent expression of Pax3 in the neural crest causes cleft palate and defective osteogenesis in mice," *The Journal of Clinical Investigation*, vol. 118, no. 6, pp. 2076–2087, 2008.
- [43] D. J. Henderson, P. Ybot-Gonzalez, and A. J. Copp, "Overexpression of the chondroitin sulphate proteoglycan versican is associated with defective neural crest migration in the Pax3 mutant mouse (*spotch*)," *Mechanisms of Development*, vol. 69, no. 1-2, pp. 39–51, 1997.
- [44] C.-S. Hong and J.-P. Saint-Jeannet, "The activity of Pax3 and Zic1 regulates three distinct cell fates at the neural plate border," *Molecular Biology of the Cell (MBoC)*, vol. 18, no. 6, pp. 2192–2202, 2007.
- [45] T. Sato, N. Sasai, and Y. Sasai, "Neural crest determination by co-activation of Pax3 and Zic1 genes in *Xenopus* ectoderm," *Development*, vol. 132, no. 10, pp. 2355–2363, 2005.
- [46] T. Burstyn-Cohen, J. Stanleigh, D. Sela-Donenfeld, and C. Kalcheim, "Canonical Wnt activity regulates trunk neural crest delamination linking BMP/noggin signaling with G1/S transition," *Development*, vol. 131, no. 21, pp. 5327–5339, 2004.
- [47] L. A. Taneyhill and M. Bronner-Fraser, "Dynamic alterations in gene expression, after Wnt-mediated induction of avian neural crest," *Molecular Biology of the Cell (MBoC)*, vol. 16, no. 11, pp. 5283–5293, 2005.
- [48] H. Nakazaki, A. C. Reddy, B. L. Mania-Farnell et al., "Key basic helix-loop-helix transcription factor genes *Hes1* and *Ngn2* are regulated by Pax3 during mouse embryonic development," *Developmental Biology*, vol. 316, no. 2, pp. 510–523, 2008.
- [49] S. A. Koblar, M. Murphy, G. L. Barrett, A. Underhill, P. Gros, and P. F. Bartlett, "Pax-3 regulates neurogenesis in neural crest-derived precursor cells," *Journal of Neuroscience Research*, vol. 56, no. 5, pp. 518–530, 1999.
- [50] S. J. Conway, R. E. Godt, C. J. Hatcher et al., "Neural crest is involved in development of abnormal myocardial function," *Journal of Molecular and Cellular Cardiology*, vol. 29, no. 10, pp. 2675–2685, 1997.
- [51] S. J. Conway, D. J. Henderson, M. L. Kirby, R. H. Anderson, and A. J. Copp, "Development of a lethal congenital heart defect in the *spotch* (Pax3) mutant mouse," *Cardiovascular Research*, vol. 36, no. 2, pp. 163–173, 1997.
- [52] L. J. Manderfield, K. A. Engleka, H. Aghajanian et al., "Pax3 and hippo signaling coordinate melanocyte gene expression in neural crest," *Cell Reports*, vol. 9, no. 5, pp. 1885–1895, 2014.
- [53] Y. J. Choi, T. J. Yoon, and Y. H. Lee, "Changing expression of the genes related to human hair graying," *European Journal of Dermatology*, vol. 18, no. 4, pp. 397–399, 2008.
- [54] T. M. Lamey, A. Koenders, and M. Ziman, "Pax genes in myogenesis: Alternate transcripts add complexity," *Histology and Histopathology*, vol. 19, no. 4, pp. 1289–1300, 2004.
- [55] J. A. Epstein, J. Li, D. Lang et al., "Migration of cardiac neural crest cells in *Spotch* embryos," *Development*, vol. 127, no. 9, pp. 1869–1878, 2000.
- [56] P. Bailey, T. Holowacz, and A. B. Lassar, "The origin of skeletal muscle stem cells in the embryo and the adult," *Current Opinion in Cell Biology*, vol. 13, no. 6, pp. 679–689, 2001.
- [57] S. J. Odelberg, A. Kollhoff, and M. T. Keating, "Dedifferentiation of mammalian myotubes induced by *msx1*," *Cell*, vol. 103, no. 7, pp. 1099–1109, 2000.
- [58] K. A. Miller, J. Barrow, J. M. Collinson et al., "A highly conserved Wnt-dependent TCF4 binding site within the proximal enhancer of the anti-myogenic *Msx1* gene supports expression within Pax3-expressing limb bud muscle precursor cells," *Developmental Biology*, vol. 311, no. 2, pp. 665–678, 2007.
- [59] A. Karaman and C. Aliagaoglu, "Waardenburg syndrome type 1," *Dermatology online journal*, vol. 12, no. 3, 2003, <https://escholarship.org/uc/item/0r5371ck>.
- [60] M. Ptok and S. Morlot, "Unilateral sensorineural deafness associated with mutations in the PAX3-gene in Waardenburg syndrome type I," *HNO*, vol. 54, no. 7, pp. 557–560, 2006.
- [61] A. P. Read and V. E. Newton, "Waardenburg syndrome," *Journal of Medical Genetics*, vol. 34, no. 8, pp. 656–665, 1997.
- [62] M. Tassabehji, A. P. Read, V. E. Newton et al., "Mutations in the PAX3 gene causing Waardenburg syndrome type 1 and type 2," *Nature Genetics*, vol. 3, no. 1, pp. 26–30, 1993.
- [63] M. Tassabehji, V. E. Newton, K. Leverton et al., "PAX3 gene structure and mutations: Close analogies between waardenburg syndrome and the *Spotch* mouse," *Human Molecular Genetics*, vol. 3, no. 7, pp. 1069–1074, 1994.
- [64] M. Tassabehji, V. E. Newton, X.-Z. Liu et al., "The mutational spectrum in waardenburg syndrome," *Human Molecular Genetics*, vol. 4, no. 11, pp. 2131–2137, 1995.

- [65] G. Van Camp, M. N. Van Thienen, I. Handig et al., "Chromosome 13q deletion with Waardenburg syndrome: Further evidence for a gene involved in neural crest function on 13q," *Journal of Medical Genetics*, vol. 32, no. 7, pp. 531–536, 1995.
- [66] A. Muratovska, C. Zhou, S. He, P. Goodyer, and M. R. Eccles, "Paired-Box genes are frequently expressed in cancer and often required for cancer cell survival," *Oncogene*, vol. 22, no. 39, pp. 7989–7997, 2003.
- [67] T. Glaser, D. S. Walton, and R. L. Maas, "Genomic structure, evolutionary conservation and aniridia mutations in the human PAX6 gene," *Nature Genetics*, vol. 2, no. 3, pp. 232–239, 1992.
- [68] T. Jordan, I. Hanson, D. Zaletayev et al., "The human PAX6 gene is mutated in two patients with aniridia," *Nature Genetics*, vol. 1, no. 5, pp. 328–332, 1992.
- [69] M. Tassabehji, A. P. Read, V. E. Newton et al., "Waardenburg's syndrome patients have mutations in the human homologue of the Pax-3 paired box gene," *Nature*, vol. 355, no. 6361, pp. 635–636, 1992.
- [70] P. Sanyanusin, L. A. Schimmenti, L. A. McNoe et al., "Mutation of the PAX2 gene in a family with optic nerve colobomas, renal anomalies and vesicoureteral reflux," *Nature Genetics*, vol. 9, no. 4, pp. 358–364, 1995.
- [71] M. Bouchard, A. Souabni, M. Mandler, A. Neubüser, and M. Busslinger, "Nephric lineage specification by Pax2 and Pax8," *Genes & Development*, vol. 16, no. 22, pp. 2958–2970, 2002.
- [72] F. Francioso, F. Carinci, L. Tosi et al., "Identification of Differentially Expressed Genes in Human Salivary Gland Tumors by DNA Microarrays 1 Supported by Università di Ferrara, Murst Prin, Carisbo, Carife Grants," *Molecular Cancer Therapeutics*, vol. 1, no. 7, pp. 533–538, 2002.
- [73] N. Chi and J. A. Epstein, "Getting your Pax straight: pax proteins in development and disease," *Trends in Genetics*, vol. 18, no. 1, pp. 41–47, 2002.
- [74] D. Lang, S. K. Powell, R. S. Plummer, K. P. Young, and B. A. Ruggeri, "PAX genes: roles in development, pathophysiology, and cancer," *Biochemical Pharmacology*, vol. 73, no. 1, pp. 1–14, 2007.
- [75] C. C. Maulbecker and P. Gruss, "The oncogenic potential of Pax genes," *EMBO Journal*, vol. 12, no. 6, pp. 2361–2367, 1993.
- [76] M. Jothi, K. Nishijo, C. Keller, and A. K. Mal, "AKT and PAX3-FKHR cooperation enforces myogenic differentiation blockade in alveolar rhabdomyosarcoma cell," *Cell Cycle*, vol. 11, no. 5, pp. 895–908, 2012.
- [77] T. R. Gershon, O. Oppenheimer, S. S. Chin, and W. L. Gerald, "Temporally regulated neural crest transcription factors distinguish neuroectodermal tumors of varying malignancy and differentiation," *Neoplasia*, vol. 7, no. 6, pp. 575–584, 2005.
- [78] F. A. Scholl, J. Kamarashev, O. V. Murmann, R. Geertsen, R. Dummer, and B. W. Schäfer, "PAX3 is expressed in human melanomas and contributes to tumor cell survival," *Cancer Research*, vol. 61, no. 3, pp. 823–826, 2001.
- [79] S.-J. He, G. Stevens, A. W. Braithwaite, and M. R. Eccles, "Transfection of melanoma cells with antisense PAX3 oligonucleotides additively complements cisplatin-induced cytotoxicity," *Molecular Cancer Therapeutics*, vol. 4, no. 6, pp. 996–1003, 2005.
- [80] X. D. Wang, S. C. Morgan, and M. R. Loeken, "Pax3 stimulates p53 ubiquitination and degradation independent of transcription," *PLoS ONE*, vol. 6, no. 12, Article ID e29379, 2011.
- [81] Q. Wang, C. Parker, S. Kumar, and P. Kumar, "Differential PAX3 expression in neuroblastoma," in *Proceedings of the Differential PAX3 expression in neuroblastoma*, vol. 3, p. 271, 2004.
- [82] K. W. Vance and C. R. Goding, "The transcription network regulating melanocyte development and melanoma," *Pigment Cell Research*, vol. 17, no. 4, pp. 318–325, 2004.
- [83] J. A. Blake and M. R. Ziman, "Pax3 transcripts in melanoblast development," *Development, Growth & Differentiation*, vol. 47, no. 9, pp. 627–635, 2005.
- [84] A. K. Kamaraju, C. Bertolotto, J. Chebath, and M. Revel, "Pax3 down-regulation and shut-off of melanogenesis in melanoma B16/F10.9 by interleukin-6 receptor signaling," *The Journal of Biological Chemistry*, vol. 277, no. 17, pp. 15132–15141, 2002.
- [85] C. S. K. Mayanil, D. George, L. Freilich et al., "Microarray Analysis Detects Novel Pax3 Downstream Target Genes," *The Journal of Biological Chemistry*, vol. 276, no. 52, pp. 49299–49309, 2001.
- [86] Q. Wang, S. Kumar, N. Mitsios, M. Slevin, and P. Kumar, "Investigation of downstream target genes of PAX3c, PAX3e and PAX3g isoforms in melanocytes by microarray analysis," *International Journal of Cancer*, vol. 120, no. 6, pp. 1223–1231, 2007.
- [87] J. P. Ginsberg, R. J. Davis, J. L. Bennicelli, L. E. Nauta, and F. G. Barr, "Up-regulation of MET but not neural cell adhesion molecule expression by the PAX3-FKHR fusion protein in alveolar rhabdomyosarcoma," *Cancer Research*, vol. 58, no. 16, pp. 3542–3546, 1998.
- [88] C. M. Margue, M. Bernasconi, F. G. Barr, and B. W. Schäfer, "Transcriptional modulation of the anti-apoptotic protein BCL-XL by the paired box transcription factors PAX3 and PAX3/FKHR," *Oncogene*, vol. 19, no. 25, pp. 2921–2929, 2000.
- [89] P. Y. P. Lam, J. E. Sublett, A. D. Hollenbach, and M. F. Roussel, "The oncogenic potential of the Pax3-FKHR fusion protein requires the Pax3 homeodomain recognition helix but not the Pax3 paired-box DNA binding domain," *Molecular and Cellular Biology*, vol. 19, no. 1, pp. 594–601, 1999.
- [90] M. Bernasconi, A. Remppis, W. J. Fredericks, F. J. Rauscher III, and B. W. Schäfer, "Induction of apoptosis in rhabdomyosarcoma cells through down-regulation of PAX proteins," *Proceedings of the National Academy of Sciences of the United States of America*, vol. 93, no. 23, pp. 13164–13169, 1996.
- [91] Y. Zhang, J. Schwartz, and C. Wang, "Comparative analysis of paired- and homeodomain-specific roles in PAX3-FKHR oncogenesis," *International Journal of Clinical and Experimental Pathology*, vol. 2, no. 4, pp. 370–383, 2009.
- [92] S. J. Xia and F. G. Barr, "Analysis of the transforming and growth suppressive activities of the PAX3-FKHR oncoprotein," *Oncogene*, vol. 23, no. 41, pp. 6864–6871, 2004.
- [93] S. Ichi, V. Boshnjaku, Y.-W. Shen et al., "Role of Pax3 acetylation in the regulation of Hes1 and Neurog2," *Molecular Biology of the Cell (MBoC)*, vol. 22, no. 4, pp. 503–512, 2011.
- [94] M. Shiota, Y. Song, A. Yokomizo et al., "Foxo3a suppression of urothelial cancer invasiveness through twist1, Y-box-binding protein 1, and E-cadherin regulation," *Clinical Cancer Research*, vol. 16, no. 23, pp. 5654–5663, 2010.
- [95] A. D. Marshall, F. Picchione, R. I. K. Galtink, and G. C. Grosveld, "PAX3-FOXO1 induces up-regulation of Noxa sensitizing alveolar rhabdomyosarcoma cells to apoptosis," *Neoplasia*, vol. 15, no. 7, pp. 738–748, 2013.
- [96] E. H. Ahn, "Regulation of target genes of PAX3-FOXO1 in alveolar rhabdomyosarcoma," *Anticancer Research*, vol. 33, no. 5, pp. 2029–2035, 2013.
- [97] Z. Fu and D. J. Tindall, "FOXOs, cancer and regulation of apoptosis," *Oncogene*, vol. 27, no. 16, pp. 2312–2319, 2008.

- [98] P. Hu, K. G. Geles, J.-H. Paik, R. A. DePinho, and R. Tjian, "Codependent Activators Direct Myoblast-Specific MyoD Transcription," *Developmental Cell*, vol. 15, no. 4, pp. 534–546, 2008.
- [99] W. Qiang, Y. Zhao, Q. Yang et al., "ZIC1 is a putative tumor suppressor in thyroid cancer by modulating major signaling pathways and transcription factor FOXO3a," *The Journal of Clinical Endocrinology & Metabolism*, vol. 99, no. 7, pp. E1163–E1172, 2014.

Research Article

Rectal Cancer: Redox State of Venous Blood and Tissues of Blood Vessels from Electron Paramagnetic Resonance and Its Correlation with the Five-Year Survival

A. P. Burlaka ¹, A. V. Vovk,¹ A. A. Burlaka,² M. R. Gafurov ³,
K. B. Iskhakova,³ and S. N. Lukin^{1,4}

¹R.E. Kavetsky institute of Experimental Pathology, Oncology and Radiobiology NAS of Ukraine, Kyiv, Ukraine

²Ukrainian National Cancer Institute, Kyiv, Ukraine

³Kazan Federal University, Kazan, Russia

⁴V. E. Lashkaryov Institute of Semiconductor Physics NAS of Ukraine, Kyiv, Ukraine

Correspondence should be addressed to M. R. Gafurov; marat.gafurov@kpfu.ru

Received 27 February 2018; Revised 27 June 2018; Accepted 19 July 2018; Published 13 August 2018

Academic Editor: Franco M. Buonaguro

Copyright © 2018 A. P. Burlaka et al. This is an open access article distributed under the Creative Commons Attribution License, which permits unrestricted use, distribution, and reproduction in any medium, provided the original work is properly cited.

A role of pro- and antioxidants for reducing rectal cancer (RC) incidence in operative, preoperative, and postoperative treatments is still disputable and controversial. The redox state of venous blood and tissues of blood vessels of 60 patients with RC ($T_{2-4}N_{0-2}M_0G_2$) and 20 donors is studied by means of the conventional and spin-trapping electron paramagnetic resonance (EPR). The intensity of the signals from ceruloplasmin (CP), transferrin (TF), and labile iron pool (LIP) at temperature $T = 77$ K as well as superoxide generation rate and nitric oxide (NO) levels at $T = 300$ K is measured. The reduced CP and TF activity and decreased NO levels increased LIP levels and superoxide-generating rates are detected in blood species. Correlation analysis for the five-year survival rate as a function of the extracted values is done. The results show that the intensities of the corresponding EPR signals from the “native” and “trapped” paramagnetic centers can be potentially used for the understanding of the molecular mechanisms underlying the RC progression and treatment.

1. Introduction

Biological electron transfer (ET) is crucial for the running of the energy processes of the cell. ET is responsible for the growth and apoptosis of cells and, therefore, can play an important role in the progress of the pathological processes. This transfer is mediated by chains of protein-bound redox (reduction-oxidation) units. The basic redox units of blood are ceruloplasmin (CP), transferrin (TF), “free” iron (also known as labile iron pool, LIP), NADPH oxidase, and iNOS of neutrophils and platelets [1]. The activity of the mentioned units can be investigated with electron paramagnetic resonance (EPR, also abbreviated as ESR for electron spin resonance) techniques. The fundamentals of using the EPR techniques for studying organs and tissues of humans and animals in the norm and pathology were established and developed in 1960-80s [2–10]. It seems that this field is

experiencing its second birth in recent years, including numerous applications in cancer related research [11–21].

Various aspects of the EPR utilization in the tumor associated studies with the corresponding references and explanations of the experimental/technical details are given in our publications [11, 13] and additionally for the blood investigations in [22]. From the last one it could be erroneously concluded that EPR of “native” (intrinsic) paramagnetic centers is not a sensitive tool for investigation of blood redox state under the pathological conditions. From other side [23] EPR of 16-doxyl stearic acid as spin probe to measure conformational changes in albumin in blood samples clearly demonstrates its diagnostic utility in patients with cancer including the colorectal cancer (CRC) which comprises rectal cancer (RC) and colon cancer [24]. Changes of intensities of EPR signals in the whole blood corresponding to CP and

TF of breast cancer patients under the influence of radiation therapy are pictured in [25].

Paramagnetic centers in human tissues include primarily the molecular complexes containing iron Fe^{3+} (supplied mainly in transferrin and haemoglobin), copper Cu^{2+} ions (ceruloplasmin), and “free” radicals. Human ceruloplasmin is a glycoprotein present in the blood plasma (about 300 $\mu\text{g}/\text{ml}$ in healthy adult people) with a molecular weight of 132 kDa. CP in EPR spectra of tissues is usually detected as signal from Cu^{2+} ions with the spectral line at $g = 2.05$. Ceruloplasmin is implicated in iron metabolism by catalyzing oxidation of Fe^{2+} and thus facilitating the incorporation of Fe^{3+} into apotransferrin. CP oxidizes four Fe^{2+} ions and is involved in four-electron transfer to oxygen, thus hindering nonenzymatic oxidation of iron producing “free” radicals [26]. Apotransferrin is EPR-silent, but when it bounds Fe^{3+} ions one can observe a distinct EPR signal with $g \approx 4.3$ from the paramagnetic Fe^{3+} ions due to the high-spin (electronic spin $S = 5/2$) iron in TF.

About (3–4) grams of iron is distributed among body compartments. In normal subjects it is all protein bound. About 70 % of the total iron is circulating, largely in erythrocyte haemoglobin. Up to 25 % of iron is stored in cells in the cytosol as ferritin or in the lysosomes as haemosiderin. Only about 0.1 % of the total body iron is circulating in plasma, all bound to TF. “Free” iron is toxic for blood and tissues [26]. In many pathological processes, including the tumor growth, the amount of “free” iron in blood and tissues increases due to the decompartmentalization of Fe ions from the ferritin and destruction of other heme and nonheme proteins. EPR spectra of “free” iron (labile iron pool, LIP) are detected as a broad signal in the vicinity of $g = (2.2 - 2.4)$ [9, 14, 15].

Comparing with the normal counterparts, cancer cells generate more “free” radicals. When “free” radicals are produced in excessive and uncontrollable amounts, they and their derivative products may react with various cellular macromolecules, such as lipids, proteins, and DNA and may modulate gene expression [27, 28]. Redox state and ET disturbances are associated with the synthesis of reactive oxygen species (ROS) and degradation of matrix proteins, with consequent effects on cell survival, invasion, and metastasis [29]. Matrix metalloproteinases (MMPs) are capable of decomposing extracellular matrix proteins, enhancing invasion of cancer cells. Generally, it is assumed that the synthesis and/or activation of MMP is increased by oxidative stress such as that created by activated neutrophils and ROS, for example [29, 30].

Recent data suggest more important and significant roles for neutrophils and platelets in tumor biology. Neutrophil-to-lymphocyte and platelet-to-lymphocyte ratios have been proposed as independent markers of poor prognosis in patients with cancer, including CRC [31]. A role of neutrophils is controversial. At present it is assumed that there are two neutrophil phenotypes, the so-called antitumour N1 neutrophils and protumorigenic N2 neutrophils. The N1 neutrophils show a direct antitumour effect induced by ROS production as well as antibody-dependent cellular cytotoxicity. Meanwhile, N2 neutrophils are thought to facilitate

cancer development via reconstruction of the extracellular matrix, acceleration of angiogenesis and lymphangiogenesis, and immune modulation through protumorigenic cytokine production [32, 33].

In this study, we report the measurements of the redox state of venous blood (also the extracted neutrophils and platelets) of patients with rectal cancer which include EPR of the native paramagnetic centers at liquid nitrogen temperature of $T = 77 \text{ K}$ and spin-trapping EPR of the reactive oxygen/nitrogen species- (ROS/RNS-) superoxide ($\text{O}_2^{\cdot-}$) and nitric oxide (NO) radicals at room temperature (RT) to exhibit the features of the RC redox state in blood and to demonstrate the EPR capabilities for RC research. The results are compared with those obtained on the pieces of the blood vessels from tumor and the superior rectal arteries. It is a continuation of our many faceted works with some preliminary results presented in [34, 35].

2. Materials and Methods

Venous blood of 60 patients who stayed at the Ukrainian National Cancer Institute for treatment (34 men and 26 women, mean age 61 ± 2.3 years) with stage II/III ($T_{2-4}N_{0-2}M_0G_2$ according to the Seventh Edition of the American Joint Committee of Cancer classification [36], where T factor is the degree of wall penetration of the primary tumor; N factor is the status of lymph node metastasis; M factor shows the presence of distant metastasis; and G describes the grade of the cancer) of adenocarcinoma of the rectum was studied. Diagnoses, stage of disease, and presence of metastasis were established according to requirements of the evidence-based medicine (morphologically, in course of corresponding clinical-instrumental checkup). No other diseases were diagnosed within the investigated group. All participants expressed their prior written consent to take part in the research. All procedures followed were in accordance with the ethical standards of the responsible committee on human experimentation (institutional and national) and with the Helsinki Declaration of 1964 and later amendments. Results for the group of 20 practically healthy people (9 men, 11 women at age of 56 ± 4.1 years) served as control values.

0.5 mL from 6 mL of the collected venous blood sample from elbow vein was poured into the test tube with 0.1 mL of anticoagulant Trilon B solution (3%), then frozen, and stored in a special mold in liquid nitrogen for the estimation of CP, TF, and “free” iron levels by EPR at $T = 77 \text{ K}$. The rest (5.5 ml) was used for the determination of NO level and generation rate of $\text{O}_2^{\cdot-}$ radicals in the whole blood, neutrophils, and platelets at RT by using Fe/diethyldithiocarbamate (Fe/DETC) and 1-hydroxy-2,2,6,6-tetramethyl-4-oxo-piperidine hydrochloride (TEMPONE-H) from Sigma-Aldrich as spin traps. Neutrophils were isolated in a double density ($\rho = 1.077 \text{ g}/\text{cm}^3$ and $\rho = 1.119 \text{ g}/\text{cm}^3$) gradient of Ficoll–Verographin at $+4^\circ\text{C}$ by centrifugation at 400g during 45 min [37]. Platelets were extracted after a series of blood centrifugations at $+4^\circ\text{C}$ according to procedure described in [38]. EPR measurements were done by using RE-1307 (USSR, Russia) and Bruker

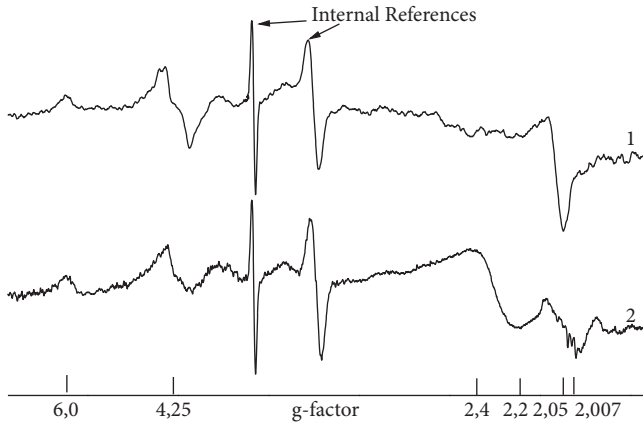


FIGURE 1: Typical EPR spectra of samples of blood of (1) donor and (2) patient with RC at T = 77 K in the units of g-factor. Description and assignment of the obtained EPR features are given in the text. The internal references signals are from the ruby crystals on the wall of EPR cavity for the quantitative analysis of EPR spectra.

ESP-300 (Bruker, Germany) EPR spectrometers (the spectrometers operate at microwave frequency of 9.5 GHz) at room and liquid nitrogen temperatures (T = 77K). Technical details of EPR measurements and sample preparations with spin traps are given elsewhere [11, 13, 15].

Additionally, to follow the changes in the blood circulatory system connected with adenocarcinoma, samples of the superior rectal artery and blood vessels of tumor tissues from 21 RC patients (12 men, 9 women) and 9 peptic ulcer patients (5 men and 4 women, mean age 59.1 ± 2.8 years) obtained during the surgical interference were frozen, stored in a special mold in liquid nitrogen, and investigated.

Statistical analyses were done using GraphPad Prism 6 and Origin 7.5 programs. Difference between the parameters was considered to be reliable for p < 0.05.

3. Results and Discussion

Figure 1 shows the typical EPR spectra of blood samples of donor and patient with RC at liquid nitrogen temperature. To exclude the influence of the resonance frequency onto the shift of the EPR spectra, it is quite common to recalculate and present the spectra in the units of the spectroscopic g-factor rather than magnetic field strength following the simple relation

$$h\nu = g\beta B, \tag{1}$$

where h is Planck constant, ν is a microwave frequency of EPR, β is Bohr constant, and B is a magnetic field strength.

There are lines with g = 2.05, g = 4.25 in spectra 1 and 2 in Figure 1; their intensities correspond to CP activity and TF content, correspondingly. Additionally, signals due to methemoglobin (g = 6.3) and “free” iron (LIP, g=2.2 – 2.4) could be detected.

The results of comparison of EPR intensities for CP, TF, and LIP for donors and RC patients are shown in Figure 2. It follows that CP and TF levels for blood of RC patients are

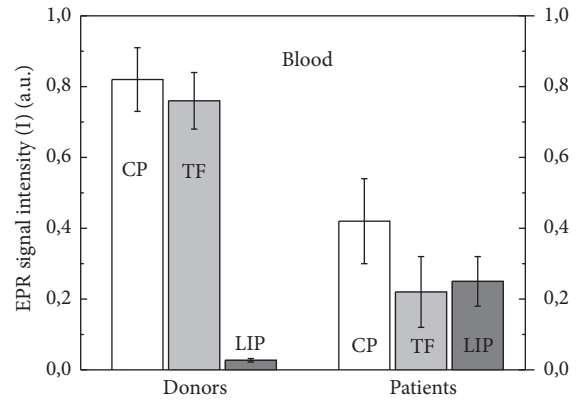


FIGURE 2: Relative intensities (I) of EPR signals corresponding to CP, TF, and LIP in blood of donors (n = 20, 0.82 ± 0.09, 0.76 ± 0.08, and 0.027 ± 0.010, correspondingly) and RC patients (n = 60, 0.42 ± 0.12, 0.22 ± 0.10, and 0.25 ± 0.070, correspondingly). Data are presented as mean ± SEM.

2 and 3 times less than those for donors, respectively, while growth of LIP level in 10 times is observed (p<0.05).

Kaplan–Meier analysis was performed to determine and to compare 5-year survival associated with the CP, TF, and LIP activity/level (Figure 3). The five-year overall survival (OS) of patients with the activity of CP $I_{CP} \geq 0.42$ a.u. (n = 34) was 60%, median survival (SM) was not reached. For the group with $I_{CP} < 0.42$ a.u. (n = 26) OS = 28%, the median time was of 23 months ($\chi^2 = 4.08$, p = 0.044, Figure 3(a)). For $I_{TF} \geq 0.22$ (n = 29), SM was not reached, OS = 60%. For $I_{TF} < 0.22$ (n = 31), the median time was 27 months ($\chi^2 = 3.16$, p = 0.076, Figure 3(b)). For the subgroup with $I_{LIP} < 0.23$ a.u. (n = 33) OS = 58%, SM was not reached; with $I_{LIP} \geq 0.23$ (n = 27) OS = 30%, the median time was 17 months ($\chi^2 = 4.96$, p = 0.026, Figure 3(c)).

Data for the generation rates of superoxide radicals by NADPH oxidase and NO radicals by iNOS of blood neutrophils and platelets are gathered in Table 1. From those, it can be seen that $O_2^{\cdot -}$ generation rate of platelets is of 8-14 times higher than in the control species (p < 0.001).

According to the superoxide generation rate data, the patients may be divided into 3 subgroups with the distinct 5-year survival (Figure 4(a)): (1) with the high activity (> 3.20 nM/10⁵ cells·min, n = 11, mean = 3.45 ± 0.11); (2) with the moderate activity (in the range 2.50 – 3.20, n = 18, mean = 2.75 ± 0.03, p < 0.05); and (3) with the low activity (< 2.5, n = 21, mean = 2.35 ± 0.05, p < 0.05). Five-year OS for subgroup 1 was 39%, SM = 22 months; for subgroups 2 and 3, SM was not reached and OS values are of 56% and 62%, correspondingly ($\chi^2 = 0.88$, p = 0.35).

RC patients have the significantly lower levels of NO production (up 3 times, p < 0.01). For the patients with this value of < 0.41 nM/10⁵ cells·min, OS = 31 %, SM = 23 months while for the values of > 0.41 nM/10⁵ cells·min OS = 66% and SM was not reached ($\chi^2 = 3.11$, p = 0.078).

As concerns NO generation rate of platelets, in the subgroup with the high activity of iNOS (> 0.34 nM/10⁵ cells·min) OS = 64%, SM was not reached, and in the

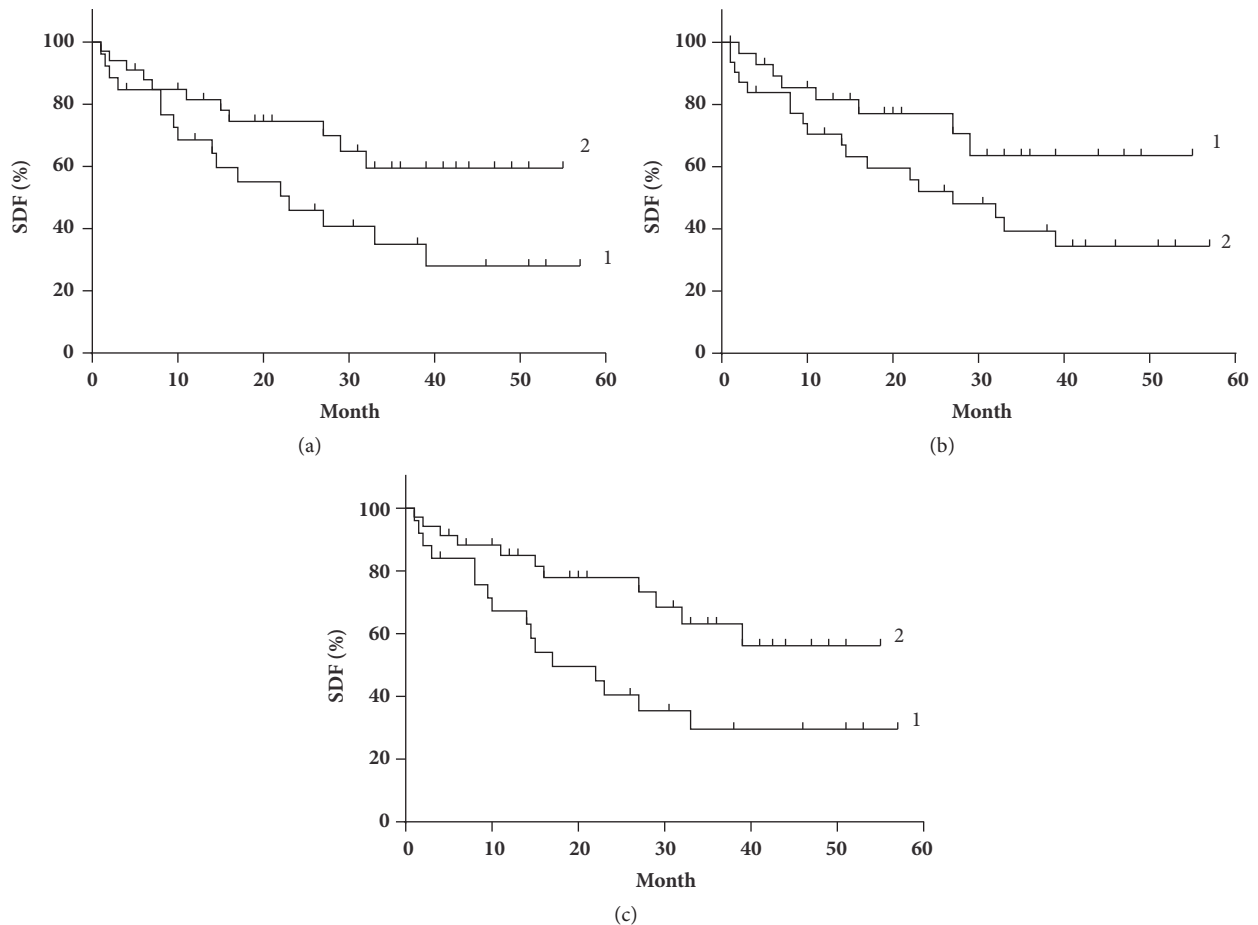


FIGURE 3: Survival distribution functions (SDF) depending on (a) CP activity in blood for $I_{CP} < 0.42$ a.u. (curve 1) and $I_{CP} > 0.42$ a.u. (curve 2); (b) TF level in blood for $I_{TF} \geq 0.22$ a.u. (curve 1) and $I_{TF} < 0.22$ a.u. (curve 2); (c) LIP level for $I_{LIP} < 0.23$ a.u. (curve 1) and $I_{LIP} \geq 0.23$ (curve 2).

TABLE 1: Superoxide and NO generation rates in blood platelets and neutrophils of RC patients and control group; NO levels in tumor blood vessels and tissues of adjacent rectum artery.

	$O_2^{\cdot-}$		NO			
	mean \pm SEM	range	mean SEM (control)	mean \pm SEM	range	mean \pm SEM (control)
Blood, nM/10 ⁵ cells·min						
Platelets	2.67 \pm 0.08	1.75-3.95	0.25 \pm 0.01	0.34 \pm 0.01	0.25 - 0.49	1.51 \pm 0.02
Neutrophils	0.336 \pm 0.010	0.22-0.48	0.230 \pm 0.004	0.41 \pm 0.11	0.15-0.49	1.45 \pm 0.02
$n_1= 18$	0.240 \pm 0.003					
$n_2= 44$	0.36 \pm 0.01	0.25-0.48				

subgroup with the low activity of iNOS (≤ 0.34 nM/10⁵ cells·min) SM = 29 months ($p = 0.4$, Figure 4(b)).

Data for the superoxide generation rate by neutrophils allow dividing the five-year survival results into two groups: one (30% from 60 patients) with the same values as for the control one and the rest (2) with 1.5-2 times ($p < 0.01$) higher values. It is in correspondence with the dual role of neutrophils in tumor progression (see the Introduction section, [31–33]). For the statistical analysis we have divided the investigated group into two subgroups: (1) with the $O_2^{\cdot-}$

generation rate > 0.31 nM/10⁵ cells·min ($n = 28$) for which OS = 40% and SM = 39 months were observed; and (2) with the $O_2^{\cdot-}$ generation rate < 0.31 nM/10⁵ cells·min ($n = 32$) for which OS = 78 % and SM was not reached ($\chi^2 = 4.1$, $p = 0.043$, data are not presented graphically). As concerns nitric oxide, no statistically significant correlation between the neutrophils' NO levels and five-year survival was found ($\chi^2 = 2.3$, $p = 0.13$).

Significant alterations of the redox state observed in the blood species suggest that the corresponding changes could also be obtained in the tumor tissues and arteries that feed the

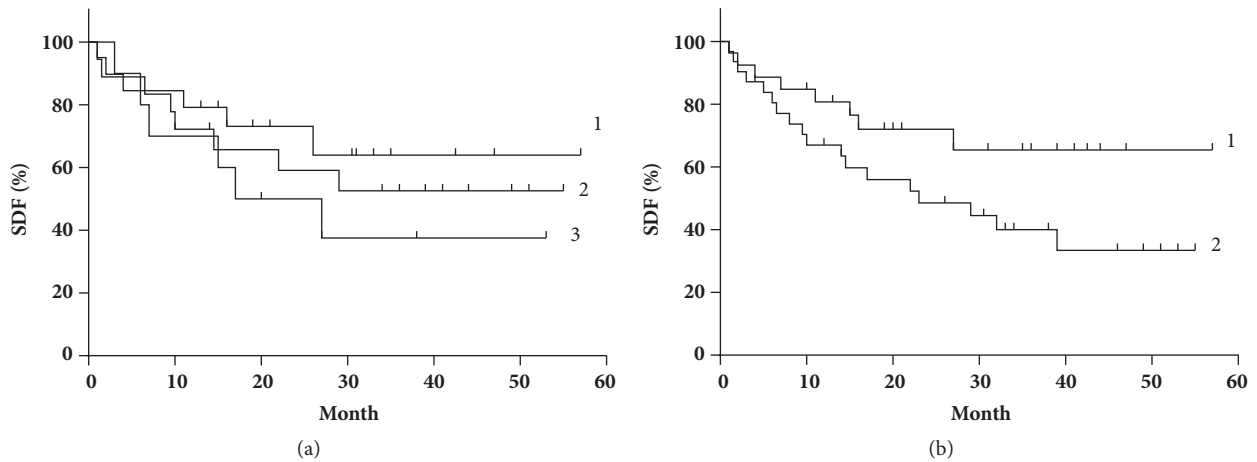


FIGURE 4: Survival distribution functions (SDF) depending on (a) superoxide-generating activity of NADP:N-oxidase of platelets: 1 - <math> < 2,35 \text{ nM}/10^5 \text{ cells}\cdot\text{min}</math>; 2 - $(2.5 - 3.0) \text{ nM}/10^5 \text{ cells}\cdot\text{min}$; 3 - $> 3.20 \text{ nM}/10^5 \text{ cells}\cdot\text{min}$; $p = 0,35$; (b) NO-generative activity of platelets 1 - $> 0.34 \text{ nM}/10^5 \text{ cells}\cdot\text{min}$; 2 - $\leq 0.34 \text{ nM}/10^5 \text{ cells}\cdot\text{min}$.

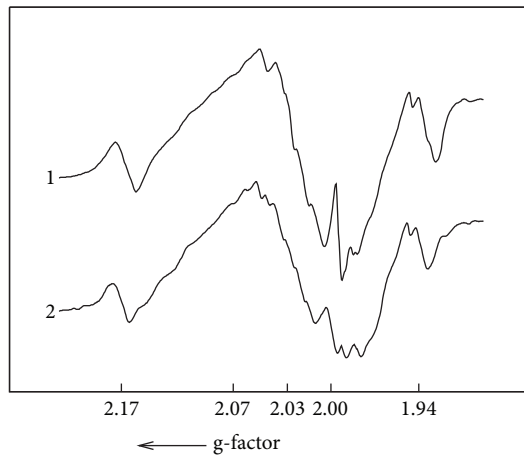


FIGURE 5: Parts of EPR spectra of blood vessels from rectum tumor (1) and from the superior rectum artery (2) in the vicinity of $g\text{-factor} \approx 2$.

tumor tissues. EPR spectra from the blood vessels of tumor and vessels from the nearby tissues of RC patients are shown in Figure 5. The main feature of the EPR for RC tissues is a signal with $g = 2.03$. The intensity of this signal corresponds to the level of NO-FeS protein complexes formed during the interaction of NO• with FeS-proteins of the respiratory chain of mitochondrial membranes, in particular with proteins of N and S clusters in NADPH-ubiquinone reductase and succinate dehydrogenase, respectively [13]. In the vessels of tumors, high levels of NO-FeS-protein complexes ($1.8 \pm 0.11 \text{ a.u.}$, $m = 26$) are found in comparison with the upper rectal artery ($0.58 \pm 0.05 \text{ a.u.}$, $n = 26$) and control group (artery tissues of the peptic ulcer patients, $0.15 \pm 0.02 \text{ a.u.}$, $n = 9$) (the nature of other signals presented in Figure 5 is described in detail in [13]).

We have measured the nitric oxide concentrations in the vessels by the spin-trapping technique. The obtained data are presented in Figures 6 and 7. As follows, in contrast to the

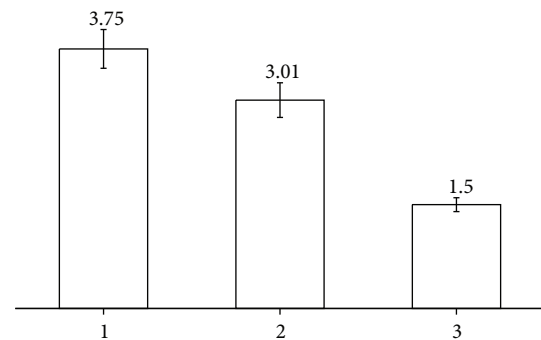


FIGURE 6: Concentration of NO in vessels from (1) tumor ($n = 26$, 3.75 ± 0.28); (2) superior rectum artery of RC patients ($n = 26$, 3.01 ± 0.25); and (3) superior rectum artery from peptic ulcer patients ($n = 9$, 1.5 ± 0.1). Data are presented as mean \pm SEM in the units of nM/g of tissue.

blood species, NO levels in the arteries of RC patients are higher than in the peptic ulcer patients' tissues ($p < 0.01$, Figure 6). Correlation between the NO concentration from the spin-trapping EPR and intensity of EPR signal with $g = 2.03$ in the tissues of tumor vessels becomes apparent from Figure 7 ($r = 0.84$, $p < 0.05$). It shows that the intensity of the intrinsic EPR signal at $g = 2.03$ can serve (at least in some cases) as a measure of NO amount without applying the expansive spin traps while EPR itself could be exploited as an indicator of pathological changes. No reliable correlation between the NO levels in the investigated tissues and survival rates was established.

As can be seen, the NO production in RC tissues is high and in correspondence with our previous observations for other tumor types [11-13]. Let us now discuss the possible mechanisms which lead to the lowering of the levels of NO and superoxide overproduction in the blood species of RC patients (the feasible ways of changing of the copper and iron related EPR signals are extensively reviewed in the Introduction section). The main generating source for the

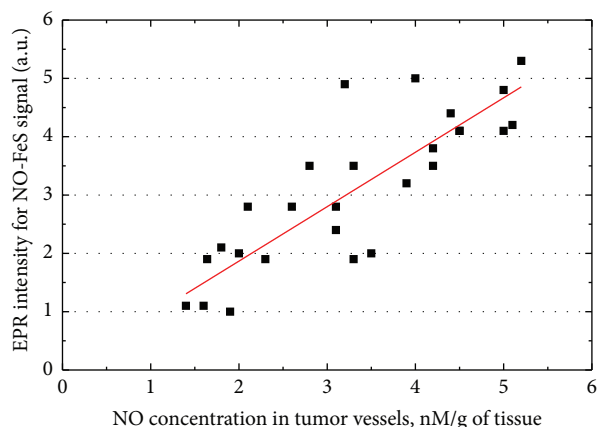


FIGURE 7: Correlation between the relative intensity of the intrinsic EPR signal at $g = 2.03$ and NO concentration derived from the spin-trapping measurements in tumor vessels of RC patients (T3N1M0G2). The straight line is drawn with a slope of 0.93.

nitric oxide generation is the inducible nitric oxide synthase (iNOS). NOS enzymes are complex oxido-reductases with the potential to produce ROS as well as, or instead of, NO. Specifically, for NO production, the NOS enzymes require the cofactor tetrahydrobiopterin (BH4). BH4 participates in electron transfer during the two-step oxidation of L-arginine to L-citrulline via an *N*-hydroxyarginine intermediate. In the absence of BH4, NOS enzymes are unable to generate NO by oxidation of L-arginine and become “uncoupled,” whereby reduction of molecular oxygen, driven by electron flow from the NOS reductase domain, can generate superoxide or other ROS [39–42].

4. Conclusion

The growth of adenocarcinoma of RC patients (T2-4N0-2M0G2) is accompanied by the changes in the redox state of blood. Namely, CP activity and TF levels decrease, resulting in appearing of “free” iron and increase of its level. The results show the feasibility of using EPR of the intrinsic paramagnetic centers for the relative simple investigation of blood redox state. Status of the redox-forming parts of blood correlates with the five-year survival rate.

Simultaneously, due to the alteration of NADP-N-oxidase and iNOS superoxide- and NO- generative activities of neutrophils and platelets, the nitric oxide generation activity reduces while the superoxide generation rate grows. Though a relationship between the superoxide generation rate and the five-year survival rates is found, no reliable correlation between the NO levels in the investigated blood species, artery tissues, and survival is established. It emphasizes anew that the link between the NO levels and biological response should be further extensively studied [40].

Data Availability

The data used to support the findings of this study are available from the corresponding author upon request.

Disclosure

A part of this work is done in the framework of the cooperation agreement between the R.E. Kavetsky Institute and Kazan Federal University and supported by the Program of Competitive Growth of Kazan Federal University (“5-100”).

Conflicts of Interest

The authors declare that there are no conflicts of interest regarding the publication of this paper.

Acknowledgments

The authors appreciate a support of Professor Vasyl Chekhun (Kyiv) and Dr. Sergei Nikitin (Kazan) for the incarnation of this Agreement and Dr. Sergei Orlinskii and Dr. Georgy Mamin (Kazan) for the helpful discussion and healthy criticism.


References

- [1] M. Mittal, M. R. Siddiqui, K. Tran, S. P. Reddy, and A. B. Malik, “Reactive oxygen species in inflammation and tissue injury,” *Antioxidants & Redox Signaling*, vol. 20, no. 7, pp. 1126–1167, 2014.
- [2] J. R. Mallard and M. Kent, “Electron spin resonance in biological tissues,” *Physics in Medicine and Biology*, vol. 14, no. 3, pp. 373–396, 1969.
- [3] A. F. Vanin, L. V. Vakhnina, and A. G. Chetverikov, “Nature of the EPR signals of a new type found in cancer tissues,” *Biophysics*, vol. 15, no. 6, pp. 1082–1089, 1970.
- [4] N. M. Emanuel, R. E. Kavetskii, B. N. Tarusov, and E. P. Sidorik, “Cancer Biophysics,” *Naukova dumka, Kyiv*, 1976.
- [5] A. A. Konstantinov and E. K. Ruuge, “Semiquinone Q in the respiratory chain of electron transport particles: Electron spin resonance studies,” *FEBS Letters*, vol. 81, no. 1, pp. 137–141, 1977.
- [6] N. M. Emanuel, “Physical, biochemical and biophysical bases for creation of new effective anticancer agents,” *Pure and Applied Chemistry*, vol. 52, no. 1, pp. 11–32, 1980.
- [7] P. L. Gutierrez and H. M. Swartz, “Paramagnetic changes in cancer: Growth of Walker 256 carcinoma studied in frozen and lyophilized tissues,” *British Journal of Cancer*, vol. 39, no. 1, pp. 24–34, 1979.
- [8] J. I. Azhipa, “Medical-biological aspects in electron paramagnetic resonance method applications,” *Nauka*, 1983.
- [9] M. K. Pulatova, G. T. Rikhireva, and Z. V. Kuropteva, “Electron Spin Resonance in Molecular Radiobiology,” *Energoatomizdat*, 1989.
- [10] R. G. Saifutdinov, L. I. Larina, T. I. Vakul’skaya, and M. G. Voronkov, *Electron Paramagnetic Resonance in Biochemistry and Medicine*, Springer, NY, USA, 2001.
- [11] A. P. Burlaka, I. I. Ganusevich, S. N. Lukin, M. R. Gafurov, and E. P. Sidorik, “Superoxide-and NO-Dependent Mechanisms of the Reprogramming of Bone Marrow Cells by Tumor Cells,” *Applied Magnetic Resonance*, vol. 45, no. 11, pp. 1261–1273, 2014.
- [12] A. P. Burlaka, I. I. Ganusevich, M. R. Gafurov, S. M. Lukin, and E. P. Sidorik, “Stomach cancer: interconnection between the redox state, activity of MMP-2, MMP-9 and stage of tumor growth,” *Cancer Microenvironment*, vol. 9, no. 1, pp. 27–32, 2016.

- [13] A. P. Burlaka, M. R. Gafurov, K. B. Iskhakova et al., "Electron paramagnetic resonance in the experimental oncology: implementation examples of the conventional approaches," *BioNanoScience*, vol. 6, no. 4, pp. 431–436, 2016.
- [14] S. V. Yurtaeva, V. N. Efimov, N. I. Silkin et al., "Magnetic Resonance of Ferritin Crystalline Particles in Tumor Tissue," *Applied Magnetic Resonance*, vol. 42, no. 3, pp. 299–311, 2012.
- [15] A. P. Burlaka, I. I. Ganusevich, M. R. Gafurov, S. N. Lukin, and E. P. Sidorik, "Electron paramagnetic resonance study of tumor affected bone marrow," *Cancer Microenvironment*, vol. 6, no. 3, pp. 273–276, 2013.
- [16] E. A. Preoteasa, G. Schianchi, and D. C. Giori, "EPR Detection of Possible Superparamagnetic Polyiron Nanoparticles and Free Radicals in the Blood Serum of Patients with Homozygous β -Thalassemia," *Applied Magnetic Resonance*, vol. 45, no. 6, pp. 537–571, 2014.
- [17] S. Mrakic-Sposta, M. Gussoni, M. Montorsi, S. Porcelli, and A. Vezzoli, "A quantitative method to monitor reactive oxygen species production by electron paramagnetic resonance in physiological and pathological conditions," *Oxidative Medicine and Cellular Longevity*, vol. 2014, Article ID 306179, pp. 1–10, 2014.
- [18] Y. Chelyshev, M. Gafurov, I. Ignatyev et al., "Paramagnetic manganese in the atherosclerotic plaque of carotid arteries," *BioMed Research International*, vol. 2016, Article ID 3706280, 7 pages, 2016.
- [19] P. Olczyk, K. Komosinska-Vashev, P. Ramos, Ł. Mencner, K. Olczyk, and B. Pilawa, "Application of Numerical Analysis of the Shape of Electron Paramagnetic Resonance Spectra for Determination of the Number of Different Groups of Radicals in the Burn Wounds," *Oxidative Medicine and Cellular Longevity*, vol. 2017, 2017.
- [20] K. E. Prosser and C. J. Walsby, "Electron Paramagnetic Resonance as a Tool for Studying the Mechanisms of Paramagnetic Anticancer Metalloodrugs," *European Journal of Inorganic Chemistry*, vol. 2017, no. 12, pp. 1573–1585, 2017.
- [21] S. B. Lohan, S. Ahlberg, A. Mensch et al., "EPR Technology as Sensitive Method for Oxidative Stress Detection in Primary and Secondary Keratinocytes Induced by Two Selected Nanoparticles," *Cell Biochemistry and Biophysics*, vol. 75, no. 3-4, pp. 359–367, 2017.
- [22] T. Kubiak, R. Krzyminiwski, and B. Dobosz, "EPR Study of Paramagnetic Centers in Human Blood," *Current Topics in Biophysics*, vol. 36, no. 1, pp. 7–13, 2013.
- [23] S. C. Kazmierczak, A. Gurachevsky, G. Matthes, and V. Muravsky, "Electron spin resonance spectroscopy of serum albumin: a novel and new test for cancer diagnosis and monitoring," *Clinical Chemistry*, vol. 52, no. 11, pp. 2129–2134, 2006.
- [24] Z. Liu, W. Zhang, S. Fan, L. Wang, and L. Jiao, "Changes in the electron paramagnetic resonance spectra of albumin-associated spin-labeled stearic acid as a diagnostic parameter of colorectal cancer," *World Journal of Surgical Oncology*, vol. 11, p. 223, 2013.
- [25] R. Krzyminiwski, B. Dobosz, and T. Kubiak, "The influence of radiotherapy on ceruloplasmin and transferrin in whole blood of breast cancer patients," *Radiation and Environmental Biophysics*, vol. 56, no. 4, pp. 345–352, 2017.
- [26] M. A. Crook, *Clinical Biochemistry and Metabolic Medicine*, CRC Press, Boca Raton, 8th edition, 2012.
- [27] S. Lin, Y. Li, A. A. Zamyatnin, J. Werner, and A. V. Bazhin, "Reactive oxygen species and colorectal cancer," *Journal of Cellular Physiology*, vol. 233, no. 7, pp. 5119–5132, 2018.
- [28] M. Perse, "Oxidative stress in the pathogenesis of colorectal cancer: Cause or consequence?" *BioMed Research International*, vol. 2013, Article ID 725710, 9 pages, 2013.
- [29] D. B. Graves, "The emerging role of reactive oxygen and nitrogen species in redox biology and some implications for plasma applications to medicine and biology," *Journal of Physics D: Applied Physics*, vol. 45, no. 26, Article ID 263001, 2012.
- [30] K. Kessenbrock, V. Plaks, and Z. Werb, "Matrix metalloproteinases: regulators of the tumor microenvironment," *Cell*, vol. 141, no. 1, pp. 52–67, 2010.
- [31] C. Pedrazzani, G. Mantovani, E. Fernandes et al., "Assessment of neutrophil-to-lymphocyte ratio, platelet-to-lymphocyte ratio and platelet count as predictors of long-term outcome after R0 resection for colorectal cancer," *Scientific Reports*, vol. 7, no. 1, 2017.
- [32] Z. Granot and J. Jablonska, "Distinct functions of neutrophil in cancer and its regulation," *Mediators of Inflammation*, vol. 2015, Article ID 701067, pp. 1–11, 2015.
- [33] W. Liang and N. Ferrara, "The complex role of Neutrophils in tumor angiogenesis and metastasis," *Cancer Immunology Research*, vol. 4, no. 2, pp. 83–91, 2016.
- [34] V. V. Golotyuk and A. P. Burlaka, "The Influence of the Radiotherapy on the State of The Ceruloplasmin-Transferrin System and Free Iron Combinations' Levels in the Blood of Rectal Cancer Patients," vol. 3, 2014.
- [35] V. V. Golotyuk and A. P. Burlaka, "Redox-dependent markers for response to neoadjuvant radiotherapy for rectal cancer," *Pharma Innovation*, vol. 3, no. 6, pp. 24–27, 2014.
- [36] American Joint Committee on Cancer, *AJCC Cancer Staging Manual*, Springer, NY, USA, 2010.
- [37] S. V. Shirshv and E. M. Kuklina, "Specific features of neutrophil response to chorionic gonadotropin related to sex and the phase of the menstrual cycle," *Human Physiology*, vol. 27, no. 2, pp. 247–252, 2001.
- [38] A. A. Qureshi, C. W. Karpen, N. Qureshi, C. J. Papasian, D. C. Morrison, and J. D. Folts, "Tocotrienols-induced inhibition of platelet thrombus formation and platelet aggregation in stenosed canine coronary arteries," *Lipids in Health and Disease*, vol. 10, article no. 58, 2011.
- [39] U. Förstermann and W. C. Sessa, "Nitric oxide synthases: regulation and function," *European Heart Journal*, vol. 33, no. 7, pp. 829–837, 2012.
- [40] F. Vanini, K. Kashfi, and N. Nath, "The dual role of iNOS in cancer," *Redox Biology*, vol. 6, pp. 334–343, 2015.
- [41] D. J. Stuehr, "Mammalian nitric oxide synthases," *Biochimica et Biophysica Acta*, vol. 1411, no. 2-3, pp. 217–230, 1999.
- [42] J. Vasquez-Vivar, P. Martasek, and B. Kalyanaraman, "Superoxide generation from nitric oxide synthase: role of cofactors and protein interaction," in *Biological Magnetic Resonance*, pp. 75–91, Kluger, 2004.

Research Article

Histogram Analysis of Perfusion Parameters from Dynamic Contrast-Enhanced MR Imaging with Tumor Characteristics and Therapeutic Response in Locally Advanced Rectal Cancer

Dong Myung Yeo ¹, Soon Nam Oh ², Moon Hyung Choi,² Sung Hak Lee,³ Myung Ah Lee,⁴ and Seung Eun Jung ²

¹Department of Radiology, Daejeon St. Mary's Hospital, The Catholic University of Korea, Republic of Korea

²Departments of Radiology, Seoul St. Mary's Hospital, The Catholic University of Korea, Republic of Korea

³Hospital Pathology, Seoul St. Mary's Hospital, The Catholic University of Korea, Republic of Korea

⁴Division of Oncology, Department of Internal Medicine, Seoul St. Mary's Hospital, The Catholic University of Korea, Republic of Korea

Correspondence should be addressed to Soon Nam Oh; hiohnsn@gmail.com

Received 9 February 2018; Revised 22 July 2018; Accepted 7 August 2018; Published 13 August 2018

Academic Editor: Franco M. Buonaguro

Copyright © 2018 Dong Myung Yeo et al. This is an open access article distributed under the Creative Commons Attribution License, which permits unrestricted use, distribution, and reproduction in any medium, provided the original work is properly cited.

Purpose. To explore the role of histogram analysis of perfusion parameters from dynamic contrast-enhanced magnetic resonance imaging (DCE-MRI) based on entire tumor volume in discriminating tumor characteristics and predicting therapeutic response in rectal cancer. **Materials and Methods.** Thirty-seven DCE-MRIs of locally advanced rectal cancer patients who received chemoradiation therapy (CRT) before surgery were analyzed by pharmacokinetic model for quantification and histogram analysis of perfusion parameters. The results were correlated with tumor characteristics including EGFR expression, KRAS mutation, and CRT response based on the pathologic tumor regression grade (TRG). **Results.** The area under the contrast agent concentration-time curve (AUC) skewness was significantly lower in patients with node metastasis. The v_p histogram parameters were significantly higher in group with perineural invasion (PNI). The receiver operating characteristics (ROC) curve analyses showed that mode v_p revealed the best diagnostic performance of PNI. The values of K^{trans} and k_{ep} were significantly higher in the group with KRAS mutation. ROC curve analyses showed that mean and mode K^{trans} demonstrated excellent diagnostic performance of KRAS mutation. DCE-MRI parameters did not demonstrate statistical significance in correlating with TRG. **Conclusion.** These preliminary results suggest that a larger proportion of higher AUC skewness was present in LN metastasis group and a higher v_p histogram value was present in rectal cancer with PNI. In addition, K^{trans} and k_{ep} histogram parameters showed difference according to the KRAS mutation, demonstrating the utility of the histogram of perfusion parameters derived from DCE-MRI as potential imaging biomarkers of tumor characteristics and genetic features.

1. Introduction

Perfusion parameters from dynamic contrast-enhanced magnetic resonance imaging (DCE-MRI) based on pharmacokinetic modeling have been investigated as promising imaging biomarkers to assess tumor biologic properties and behaviors and to monitor and predict therapeutic effects on the basis of tumor perfusion. Among them, the widely used perfusion parameters extracted from the two-compartment pharmacokinetic Tofts model [1] have K^{trans} [volume transfer constant between blood plasma and the extravascular

extracellular space (EES), which is determined by blood flow and vascular permeability], k_{ep} (rate constant or reflux rate between blood plasma and EES, $k_{ep} = K^{trans}/v_e$), v_e (fractional EES volume), v_p (fractional plasma volume), and area under the contrast agent concentration-time curve (AUC, total amount of contrast agent).

In rectal cancer, change in K^{trans} after neoadjuvant chemoradiation therapy (CRT) in locally advanced rectal cancer has been correlated with pathologically favorable responses in previous studies [2, 3]. In addition, the initial

K^{trans} measured by preoperative DCE-MRI was also reported to be a useful marker in predicting good response to neoadjuvant CRT [2, 4]. However, contradictory findings have also been reported. Kim et al. [3] found no significant difference in the initial value or change in perfusion parameters between good responders and nonresponders of CRT or between pathologic complete responders and noncomplete responders. Furthermore, correlations of TNM stage with perfusion parameters also showed discrepant results [5, 6]. Based on these previous studies, there are many factors that influence the variable results of tumor perfusion analysis using DCE-MRI such as intrinsic limits in a simplified pharmacokinetic model, measurement error of arterial input function, difference among postprocessing software, small number of cases, sampling bias of region of interest (ROI), or inherent tumor heterogeneity [7, 8]. In order to reduce and avoid sampling bias and to overcome limited results arising from intrinsic tumor heterogeneity, entire lesion-ROI analysis has been demonstrated to be more a reproducible method with low interobserver variability [8, 9]. Furthermore, histogram analysis of the entire tumor can provide direct information on the heterogeneity of the tumor using the value of each pixel or voxel. In recent studies, histogram analysis based on MRI has been performed in various areas of cancer research [10–13]. To our knowledge, volume-based histogram analysis of perfusion maps in rectal cancer has not been well demonstrated in the literature. The purpose of our study was to explore the role of histogram analysis of DCE-MRI based on entire tumor volume in discriminating tumor characteristics and predicting neoadjuvant CRT response.

2. Materials and Methods

2.1. Patient Population. The institutional review board approved this retrospective study, and patient informed consent was waived. From December 2011 to March 2015, 167 consecutive patients with locally advanced rectal cancer (stages II (cT3-4, N0, M0) and III (cT1-4, N+, M0) were treated with CRT at our institution. The inclusion criteria for our study were biopsy-proven adenocarcinoma of the rectum treated with neoadjuvant CRT followed by resection of the tumor, adequate MR examinations to delineate the rectal cancer that included sequences to obtain a perfusion map before CRT, and availability of detailed surgical and histopathologic reports. In total, 37 met these inclusion criteria and formed the population of this study. There were 25 men and 12 women. The median age was 61 years (range, 29–84 years). The other 130 patients were excluded for no obtainment of MR sequences for perfusion map ($n = 96$), image distortion by motion or metallic artifact ($n = 21$), and inadequate histopathologic reports ($n = 13$). Preoperative MR imaging including sequences to produce perfusion map was not performed for the following reasons: other MR equipment which was not available to produce perfusion map was used ($n = 74$), and patients were not expected to be treated neoadjuvant CRT after understaging by computed tomography and colonoscopy ($n = 22$).

Among this cohort, one patient was reported elsewhere; it was addressed whether only mean values of quantitative

parameters derived from DCE-MRI are correlated with angiogenesis and biologic aggressiveness of rectal cancer using other software [14]. All included patients underwent CRT within a month after MRI (median 10, range 0–25 days) and underwent complete resection of the tumor as follows: lower anterior resection ($n = 28$), proctosigmoidectomy ($n = 4$), abdominoperineal resection ($n = 3$), proctocolectomy ($n = 1$), and endoscopic resection ($n = 1$). Radiation therapy of 50.4 Gy was delivered to the pelvis in 36 patients and 45 Gy was delivered in one patient. Twenty-two patients were treated with 5-fluorouracil plus leucovorin and 15 patients with capecitabine.

2.2. MR Imaging Techniques. All MRI studies were performed using a 3T MR scanner (Magnetom Verio; Siemens Medical Solutions, Erlangen, Germany) with six-channel phased-array surface coil (Body Matrix) combined with up to six elements of the integrated spine coil. Before MR scanning, approximately 50–100 mL of sonography transmission gel was administered for appropriate distension of the rectum, which assisted in delineating the tumor, particularly in small tumors. The MR images were obtained using the following sequences. First, a sagittal image was obtained with a T2-weighted fast spin-echo sequence. A plane perpendicular to the long axis of the rectal cancer was selected for axial scanning, covering the rectum with the lower edge at least 10 cm below the symphysis pubis and the upper edge below the sacral promontory.

Then, an oblique axial T1-weighted fast spin-echo sequence (TR/TE of 750/10; flip angle of 150° ; field of view [FOV] of 200×200 mm; matrix size of 320×224 ; 2 NEX; slice thickness of 5 mm with no gap; and acquisition time of 4 minutes 31 seconds) and an oblique axial T2-weighted fast spin-echo sequence (TR/TE of 4000/118; flip angle of 140° ; FOV of 200×200 mm; spectral width of 363 Hz/pixel; matrix size of 320×224 ; 2 NEX; slice thickness of 5 mm with no gap; acquisition time of 3 minutes 27 seconds) were applied. Diffusion-weighted MR images were acquired on the sagittal and oblique axial planes using the single shot-echo planar imaging technique with b of 0, 500, and 1000 seconds/ mm^2 ; TR/TE of 6100/83; FOV of 200 mm; matrix size of 104×73 ; 2 NEX; slice thickness of 5 mm with no slice gap; and an acquisition time of 2 minutes 30 seconds. DCE-MRI included two precontrast T1-weighted volumetric interpolated breath-hold examinations (3D VIBE, TR/TE of 5.1/1.8, FOV 250×250 mm, matrix 192×138 , 20 axial slices [slice thickness, 5 mm]) with different flip angles (2° , 15°) to determine the T1 relaxation time in the tissue before the arrival of contrast agent. This imaging was followed by a DCE series with fat suppression on the axial plane with TR/TE of 4.3/1.47; flip angle of 15° ; slice thickness of 5.0 mm; acquisition time of 4 minute 35 seconds; and an intravenous bolus injection of 0.1 mmol/kg gadobutol (Gadovist, Schering, Berlin, Germany) at a rate of 3 mL/s, followed by a 25 mL saline flush.

2.3. Image Analysis. Perfusion parametric maps were obtained using dedicated DCE-MRI software (Olea Sphere; Olea Medical Solutions, La Ciotat, France) with Tofts model implementation [1, 15].

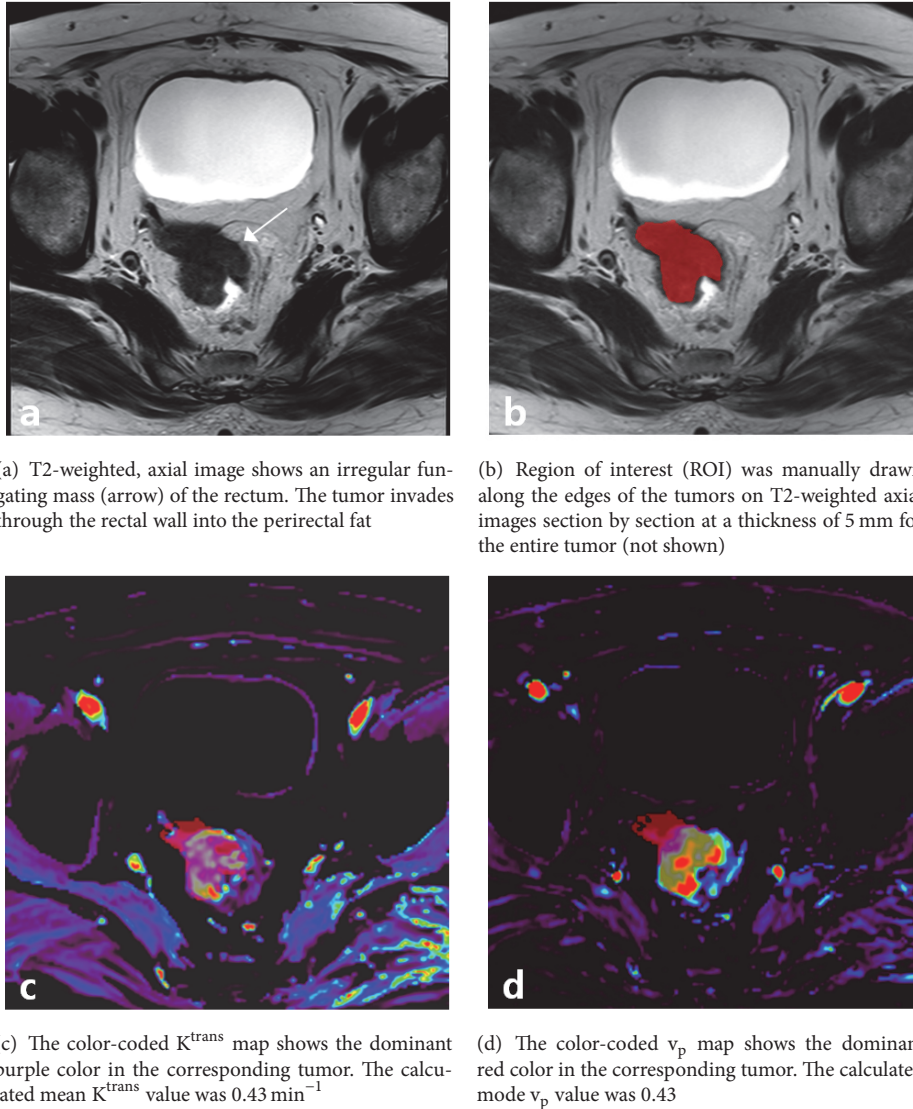


FIGURE 1: Rectal carcinoma in a 66-year-old female patient with perineural invasion and KRAS gene mutation (+).

The arterial input function was selected automatically using a cluster analysis algorithm individually.

For voxel-wise histogram analysis of DCE-MRI perfusion parameters, tumor ROIs were manually drawn along the edges of the tumors on T2-weighted axial images section by section at a thickness of 5 mm for the entire tumor, while avoiding areas of necrosis/cystic area or hemorrhage by two abdominal radiologists (S.N.O and M.H.C with 16 and 6 years of experience) independently. ROIs were copied and pasted over automatically driven perfusion maps from the software. Then, the following histogram analysis values of each perfusion parameter were derived: mean; minimum; maximum; standard deviation (SD); mode (the value exhibiting the highest peak on the histogram); skewness; kurtosis; 10th, 20th, 30th, 40th, 50th, 60th, 70th, 80th, and 90th percentiles (the nth percentile is the point at which n% of the voxel values that form the histogram are found to the left) of the DCE-MRI parameters, composed of the

volume transfer constant between the blood plasma and EES (K^{trans} , min^{-1}); the rate constant between EES and the blood plasma (k_{ep} , min^{-1}); volume of EES space per unit volume of tissue (v_e); fractional blood-plasma volume (v_p); and AUC ($\text{mM}\cdot\text{s}$). Skewness represents the degree of asymmetry of a distribution. Negative skewness indicates that the distribution is concentrated on the right of the figure, and positive skewness indicates the converse distribution pattern. Kurtosis represents the sharpness of the peaked of the distribution. Higher kurtosis indicates a sharper peak.

Representative cases for histogram analysis of DCE-MRI are shown in Figures 1 and 2.

2.4. Histopathologic Analysis. Histopathologic information was obtained from pathology reports. We assessed morphological factors, including depth of invasion (T stage), lymph node metastasis (N stage), and the presence of lymphatic,

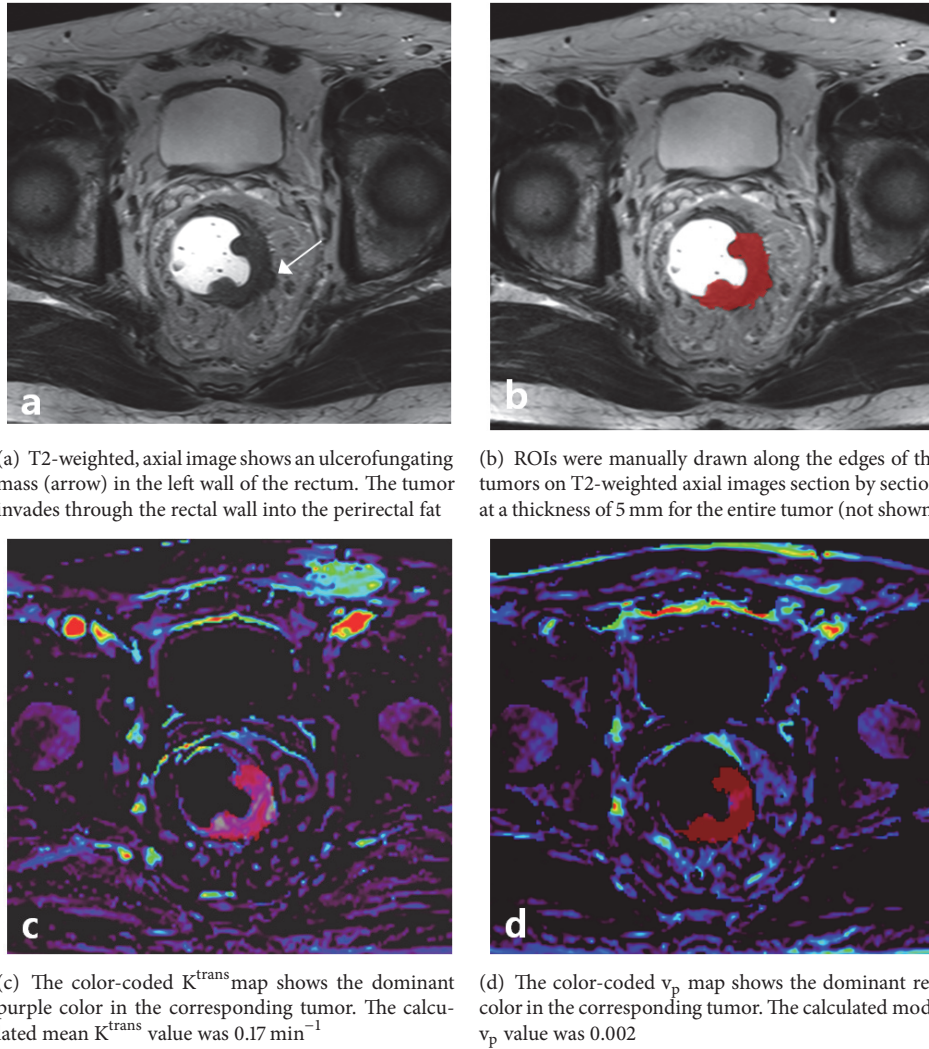


FIGURE 2: Rectal carcinoma in a 63-year-old male patient without perineural invasion and KRAS gene mutation (-).

vascular, and perineural invasion (PNI) as well as biologic markers including expression of EGFR, KRAS gene mutations, and tumor regression grade (TRG) as described by Dworak et al.[16], indicating pathologic grading of regression following neoadjuvant CRT. Tumor regression was classified according to the following five grades: Grade 0, no regression; Grade 1, dominant tumor mass with obvious fibrosis and/or vasculopathy; Grade 2, dominantly fibrotic changes with few tumor cells or groups (easy to find); Grade 3, very few (difficult to find microscopically) tumor cells in fibrotic tissue with or without mucous substance; and Grade 4, no tumor cells, only fibrotic mass (total regression or response).

2.5. Statistical Analysis. Statistical analyses were performed using statistical software R version 3.2.1[17] and MedCalc, version 11.5.0.0 [MedCalc, Mariakerke, Belgium]). To assess interobserver reliability of the DCE-MRI parameters, measurements were analyzed using the intraclass correlation coefficient (lower than 0.40, poor agreement; 0.40–0.75, fair to good agreement; and higher than 0.75, excellent

agreement). The cases were assigned to groups based on histologic results including depth of invasion (T stage), lymph node metastasis (negative versus positive), lymphovascular invasion (negative versus positive), PNI (negative versus positive), EGFR expression (negative versus positive), and KRAS gene mutation (negative versus positive). To assess neoadjuvant CRT response predictability, the patients were also divided into groups of TRG nonresponders (Grades 0, 1, and 2) and TRG responders (Grades 3 and 4) and complete response (CR) group and non-CR group. The values from histogram analysis of DCE-MRI parameters (K^{trans} , k_{ep} , v_e , v_p , and AUC; mean, minimum, maximum, SD, mode, skewness, kurtosis, 10th, 20th, 30th, 40th, 50th, 60th, 70th, 80th, and 90th percentile value) are compared between the groups using the Mann–Whitney U test with the moonBook package [18].

For the parameters that demonstrated statistically significant difference between the groups, receiver operating characteristics (ROC) curve analysis was performed to calculate the sensitivity, specificity, and diagnostic accuracy.

TABLE 1: Interobserver intraclass correlation coefficient for measurements of perfusion parameters.

Parameter	K^{trans}	v_p	AUC	k_{ep}	v_e
Mean	0.971 (0.943, 0.985)	0.995 (0.990, 0.997)	0.982 (0.965, 0.991)	0.993 (0.987, 0.997)	0.996 (0.993, 0.998)
Minimum	0.435 (0.129, 0.665)	0.414 (0.104, 0.651)	0.665 (0.435, 0.814)	0.747 (0.559, 0.863)	0.889 (0.794, 0.942)
10th percentile	0.264 (-0.065, 0.542)	0.973 (0.948, 0.986)	0.907 (0.826, 0.952)	0.977 (0.955, 0.988)	0.998 (0.996, 0.999)
20th percentile	0.254 (-0.077, 0.534)	0.985 (0.970, 0.992)	0.925 (0.859, 0.961)	0.967 (0.936, 0.983)	0.998 (0.995, 0.999)
30th percentile	0.413 (0.103, 0.650)	0.989 (0.979, 0.995)	0.936 (0.879, 0.967)	0.979 (0.960, 0.989)	0.998 (0.997, 0.999)
40th percentile	0.788 (0.623, 0.886)	0.993 (0.986, 0.996)	0.970 (0.941, 0.984)	0.987 (0.974, 0.993)	0.997 (0.995, 0.999)
50th percentile	0.928 (0.863, 0.963)	0.995 (0.990, 0.997)	0.981 (0.963, 0.991)	0.987 (0.974, 0.993)	0.998 (0.996, 0.999)
60th percentile	0.993 (0.986, 0.996)	0.997 (0.994, 0.998)	0.982 (0.964, 0.991)	0.990 (0.981, 0.995)	0.994 (0.988, 0.997)
70th percentile	0.996 (0.993, 0.998)	0.996 (0.993, 0.998)	0.991 (0.982, 0.995)	0.991 (0.982, 0.995)	0.991 (0.982, 0.995)
80th percentile	0.996 (0.993, 0.998)	0.994 (0.988, 0.997)	0.995 (0.989, 0.997)	0.993 (0.986, 0.996)	0.977 (0.955, 0.988)
90th percentile	0.996 (0.991, 0.998)	0.995 (0.991, 0.998)	0.996 (0.992, 0.998)	0.994 (0.988, 0.997)	0.994 (0.988, 0.997)
Maximum	0.970 (0.941, 0.984)	0.972 (0.947, 0.986)	1.000	0.997 (0.994, 0.999)	1.000
Standard deviation	0.981 (0.965, 0.989)	0.993 (0.987, 0.996)	0.962 (0.931, 0.979)	0.996 (0.992, 0.998)	0.961 (0.930, 0.979)
Mode	0.965 (0.933, 0.982)	0.925 (0.856, 0.962)	0.957 (0.912, 0.978)	0.835 (0.700, 0.912)	0.998 (0.996, 0.999)
Skewness	0.955 (0.913, 0.977)	0.969 (0.940, 0.984)	0.950 (0.904, 0.974)	0.990 (0.980, 0.995)	0.988 (0.978, 0.994)
Kurtosis	0.888 (0.792, 0.941)	0.935 (0.877, 0.966)	0.920 (0.849, 0.958)	0.984 (0.968, 0.992)	0.967 (0.936, 0.983)

Note. Data in parentheses are 95% confidence intervals.

3. Results

3.1. Correlation with Prognostic Histologic Results and DCE-MRI Parameters. Histogram analysis measurements of perfusion parameters showed overall excellent interreader agreement except for some minimum or lower percentile measurements. Table 1 summarizes the interobserver agreement correlation coefficients using the corresponding intraclass correlation coefficients.

Comparisons of DCE-MRI parameters of rectal cancer by group, classified according to histologic results and molecular biology, are summarized in Table 2.

In patients with lymph node metastasis, AUC skewness was significantly lower than that in patients without lymph node metastasis (-0.4; median [-0.7,-0.2; interquartile range] versus -0.2 [-0.3,0.1], $p = 0.016$). Therefore, a larger proportion of higher AUC values were present in the nodal metastasis group compared to the group with nonnodal metastasis. The area under the ROC curve (A_z) of AUC skewness was 0.744 (95% CI: 0.565-0.922; sensitivity 69.2%, specificity 79.2%) for reader 1 and 0.753 (95% CI: 0.583-0.923; sensitivity 69.2%, specificity 75.0%) for reader 2. AUC kurtosis and v_p kurtosis also showed higher values in the nodal metastasis group, which was represented by a sharper histogram peak, in reader 1 only.

The v_p -associated histogram values (mean, 10th–80th percentile, skewness, kurtosis, and mode) showed statistically significant correlation with PNI. ROC curve analyses revealed that mode v_p showed the best diagnostic performance of PNI (A_z of mode v_p 0.859; 95% CI: 0.698-1; sensitivity 87.5%, specificity 81.5% for reader 1; A_z of mode v_p 0.783; 95% CI: 0.591-0.976; sensitivity 62.5%, specificity 89.3% for reader 2).

The K^{trans} (mean, SD, 50th–90th percentile, and mode) and k_{ep} histogram values (mean, 30th–90th percentile, and kurtosis) were significantly higher in the group with KRAS

gene mutation and v_e kurtosis was lower in KRAS-mutated than in nonmutated tumors. ROC curve analyses showed that mean K^{trans} and mode K^{trans} demonstrated excellent diagnostic performance of KRAS gene mutation (A_z of mean K^{trans} 0.788, 95% CI: 0.610-0.967; sensitivity 76.9%, specificity 81.2%; A_z of mode K^{trans} 0.793, 95% CI: 0.624-0.963; sensitivity 100%, specificity 56.2% for reader 1).

Other histologic (T stage, lymphatic invasion, and vascular invasion) and immunohistochemical (EGFR expression) results were not associated with any difference in DCE-MRI parameters.

3.2. Correlation with Treatment Response after Neoadjuvant CRT and DCE-MRI Parameters. Of the total 37 patients, 10 were in TRG 1, 19 were in TRG 2, 1 was in TRG 3, and 7 were in TRG 4 (CR). The mean K^{trans} values of the responder and nonresponders groups were similar (0.4; median [0.3, 0.5; interquartile range] versus 0.4[0.3, 0.5], $p = 0.685$). The mean k_{ep} was lower in the TRG responder group compared to the TRG nonresponder group, but the difference was not statistically significant (1.0 ± 0.5 versus 1.0 ± 0.3 , $p = 0.760$).

The mean K^{trans} and mean k_{ep} were lower in the CR group compared to the non-CR group (0.3[0.3; 0.4] versus 0.4[0.3; 0.5], $p = 0.461$; 1.0 [0.9,1.0] versus 1.2 [0.8; 1.4], $p = 0.332$, respectively), but the differences were not statistically significant. No other DCE-MRI parameter histogram analysis values were significantly correlated with CRT treatment response. The mean, maximum, skewness, and kurtosis of K^{trans} and k_{ep} , based on TRG and CR, are summarized in Table 3.

4. Discussion

The aim of the present study was to explore the role of histogram analysis of model-based perfusion parameters from DCE-MRI in rectal cancer for discriminating tumor

TABLE 2: Correlation of histogram analysis of perfusion parameters with biologic aggressiveness.

	Parameter	Reader 1				Reader 2			
		Yes (n = 24)	No (n = 13)	P value*	A _z [†]	Yes (n = 24)	No (n = 13)	P value*	A _z [†]
Biologic aggressiveness	AUC skewness	-0.4 (-0.7;-0.2)	-0.2 (-0.3;0.1)	0.016	0.744	-0.4(-0.6;-0.2)	-0.2(-0.3;0.2)	0.012	0.753
	AUC kurtosis	-0.1 (-0.5;0.1)	-0.6 (-0.9;-0.1)	0.036	0.712	-0.4 (-0.6;0.2)	-0.6(-0.8;-0.1)	0.098	0.667
	v _p kurtosis	-0.2 (-0.6;0.4)	0.4 (-0.1;1.6)	0.036	0.712	-0.3 (-0.5;0.2)	0.5 (-0.2;1.7)	0.052	0.696
PNI		Yes (n = 8)	No (n = 29)	P value	A _z [*]	Yes (n = 8)	No (n = 29)	P value	A _z [*]
	v _p mean	0.3 (0.2;0.3)	0.1 (0.1;0.2)	0.042	0.737	0.3 (0.2;0.3)	0.1 (0.1;0.2)	0.046	0.733
	v _p 10th percentile	0.1 (0.1;0.1)	0.0 (0.0;0.0)	0.011	0.797	0.1 (0.1;0.1)	0.0 (0.0;0.0)	0.013	0.789
	v _p 20th percentile	0.1 (0.1;0.2)	0.1 (0.0;0.1)	0.022	0.767	0.2 (0.1;0.2)	0.1 (0.0;0.1)	0.035	0.746
	v _p 30th percentile	0.2 (0.1;0.2)	0.1 (0.0;0.1)	0.024	0.763	0.2 (0.1;0.2)	0.1 (0.1;0.1)	0.039	0.741
	v _p 40th percentile	0.2 (0.2;0.3)	0.1 (0.0;0.1)	0.027	0.759	0.2 (0.1;0.3)	0.1 (0.1;0.1)	0.042	0.737
	v _p 50th percentile	0.3 (0.2;0.3)	0.1 (0.1;0.2)	0.029	0.754	0.3 (0.2;0.3)	0.1 (0.1;0.2)	0.035	0.746
	v _p 60th percentile	0.3 (0.2;0.4)	0.2 (0.1;0.2)	0.032	0.750	0.3 (0.2;0.4)	0.1 (0.1;0.2)	0.035	0.746
	v _p 70th percentile	0.4 (0.2;0.4)	0.2 (0.1;0.2)	0.035	0.746	0.4 (0.2;0.4)	0.2 (0.1;0.2)	0.039	0.741
	v _p 80th percentile	0.4 (0.3;0.5)	0.2 (0.2;0.3)	0.046	0.733	0.4 (0.3;0.5)	0.2 (0.2;0.3)	0.042	0.746
	v _p skewness	0.4 (0.1;0.5)	0.8 (0.6;1.3)	0.022	0.767	0.3 (0.2;0.6)	0.8 (0.6;1.3)	0.020	0.772
	v _p kurtosis	-0.4 (-0.7;-0.1)	0.4 (-0.2;1.4)	0.018	0.776	-0.4 (-0.7;-0.1)	0.4 (-0.3;1.6)	0.035	0.746
	v _p mode	0.2 (0.1;0.4)	0.0 (0.0;0.1)	0.002	0.859	0.1 (0.1;0.3)	0.0 (0.0;0.1)	0.016	0.783
	KRAS mutation		Yes (n = 13)	No (n = 16)	P value	A _z [*]	Yes (n = 13)	No (n = 16)	P value
K ^{trans} mean		0.5 (0.4;0.5)	0.3 (0.2;0.4)	0.009	0.788	0.5 (0.4;0.5)	0.3 (0.2;0.4)	0.010	0.784
K ^{trans} SD		0.3 (0.3;0.5)	0.2 (0.1;0.3)	0.020	0.755	0.3 (0.3;0.5)	0.2 (0.1;0.4)	0.035	0.731
K ^{trans} 50th percentile		0.4 (0.2;0.5)	0.2 (0.2;0.3)	0.039	0.726	0.4 (0.2;0.5)	0.2 (0.2;0.3)	0.048	0.716
K ^{trans} 60th percentile		0.5 (0.3;0.6)	0.3 (0.2;0.4)	0.035	0.731	0.5 (0.4;0.5)	0.3 (0.2;0.4)	0.048	0.716
K ^{trans} 70th percentile		0.6 (0.4;0.7)	0.4 (0.3;0.5)	0.028	0.740	0.6 (0.4;0.7)	0.4 (0.3;0.5)	0.032	0.736
K ^{trans} 80th percentile		0.8 (0.5;0.9)	0.5 (0.3;0.6)	0.014	0.769	0.8 (0.5;0.9)	0.5 (0.3;0.6)	0.023	0.750
K ^{trans} 90th percentile		0.8 (0.8;1.4)	0.6 (0.4;0.9)	0.023	0.750	0.9 (0.8;1.3)	0.6 (0.4;0.9)	0.039	0.726
K ^{trans} mode		1.3 (0.8;1.8)	0.6 (0.0;1.1)	0.007	0.793	1.3 (0.8;1.8)	0.6 (0.1;1.1)	0.007	0.793
k _{ep} mean		1.4 (1.2; 1.5)	0.9 (0.3;1.3)	0.018	0.760	1.3 (1.2; 1.5)	1.0 (0.3;1.3)	0.044	0.721
k _{ep} 30th percentile		0.7 (0.5;0.8)	0.5 (0.2;0.7)	0.025	0.745	0.7 (0.6;0.8)	0.5 (0.2;0.6)	0.032	0.736
k _{ep} 40th percentile		0.9 (0.8;1.1)	0.6 (0.2;0.8)	0.028	0.740	0.9 (0.8;1.1)	0.7 (0.2;0.8)	0.028	0.740
k _{ep} 50th percentile		1.1 (0.9;1.4)	0.8 (0.2;1.0)	0.018	0.760	1.1 (1.0;1.2)	0.8 (0.2;1.0)	0.039	0.726
k _{ep} 60th percentile		1.4 (1.1;1.6)	0.9 (0.3;1.2)	0.020	0.755	1.4 (1.2;1.5)	1.0 (0.3;1.3)	0.035	0.731
k _{ep} 70th percentile	1.8 (1.4;1.8)	1.1 (0.3; 1.5)	0.028	0.740	1.7 (1.4;1.9)	1.2 (0.4;1.5)	0.032	0.736	
k _{ep} 80th percentile	2.1 (1.8;2.5)	1.4 (0.4;1.9)	0.016	0.764	2.1 (1.7;2.7)	1.5 (0.4;2.0)	0.032	0.736	
k _{ep} 90th percentile	2.7 (2.4;3.1)	1.9 (0.6;2.7)	0.025	0.745	2.7 (2.3;3.1)	1.9 (0.6;2.8)	0.048	0.716	
v _e kurtosis	0.5 (-0.6;1.9)	1.3 (0.9;5.1)	0.035	0.731	0.4 (-0.6;1.4)	2.0 (0.7;5.6)	0.018	0.760	

Note. All figures of perfusion parameters in the above table have been rounded to one decimal place and are presented as median value (interquartile range) according to the data distribution.

Numbers in bold are statistically significant P-values. Parameters in bold are high in area under the ROC curve.

AUC, area under the concentration curve; PNI, perineural invasion; SD, standard deviation.

*Determined with the Mann-Whitney U test.

†Az= area under the ROC curve.

characteristics and predicting CRT response. Our results showed that histogram values from DCE-MRI parameters correlated with prognostic factors including LN metastasis, PNI, and KRAS gene mutation. The histogram analysis values of DCE-MRI parameters were not correlated with pathologic CRT response.

Previous studies have reported discrepant results regarding the correlation of TNM staging and DCE-MRI parameters. Yao et al. suggested that K^{trans} positively correlates with LN metastasis [5]. However, Kim et al. reported no

relationship between TN staging and K^{trans} and v_e [6]. In our study, K^{trans}, k_{ep}, and v_e revealed no correlation with TNM staging, and the AUC data of the group with nodal metastasis demonstrated wider spread to the right of the mean compared to that of the group with nonnodal metastasis, illustrating that a larger proportion of patients with nodal metastasis had higher AUC values than patients without nodal metastasis.

To the best of our knowledge, there have been no studies regarding the correlations between the PNI of rectal cancer and DCE-MRI parameters. Our present study showed a

TABLE 3: Correlation with treatment response of neoadjuvant chemoradiotherapy after rectal cancer.

Treatment Response	Parameter	Reader 1			Reader 2		
		TRG0,1,2(n=29)	TRG 3,4 (n=8)	P value*	TRG0,1,2(n=29)	TRG3,4 (n=8)	P value*
TRG	K^{trans} mean	0.4 (0.3;0.5)	0.4 (0.3;0.5)	0.685	0.4 (0.3;0.5)	0.4 (0.3;0.4)	0.854
	K^{trans} maximum	1.3 (0.7;1.8)	0.9 (0.7;1.5)	0.685	1.3 (0.7;1.8)	0.9 (0.7;1.5)	0.605
	K^{trans} skewness	0.9 (0.2;1.6)	0.8 (0.1;1.5)	0.912	0.8 (0.3;1.6)	0.8 (0.1;1.6)	0.912
	K^{trans} kurtosis	0.4 (-0.9;2.1)	-0.1 (-1.2;1.9)	0.507	0.2 (-0.9;2.7)	-0.2 (-1.1;2.5)	0.825
	k_{ep} mean	1.2 (0.8;1.4)	1.0 (0.9;1.1)	0.685	1.1 (0.7;1.3)	1.0(0.9;1.1)	0.483
	k_{ep} maximum	3.3 (2.7;4.0)	3.5 (2.7;4.2)	1.000	3.5 (2.7;4.0)	3.5 (2.7;4.2)	0.971
	k_{ep} skewness	1.3 (0.9;1.7)	1.3 (0.9;1.8)	0.971	1.3 (0.9;1.7)	1.4 (0.9;1.8)	0.941
	k_{ep} kurtosis	1.1 (0.2;4.1)	2.1 (-0.1;3.9)	0.941	1.3 (0.3;3.6)	2.2 (-0.1;4.0)	0.941
CR		CR (n=7)	nonCR (n=30)	P value	CR (n=7)	nonCR (n=30)	P value
	K^{trans} mean	0.3 (0.3;0.4)	0.4 (0.3;0.5)	0.461	0.4 (0.3;0.4)	0.4 (0.3;0.5)	0.587
	K^{trans} maximum	1.0 (0.7;1.5)	1.2 (0.7;1.8)	0.816	1.0 (0.7;1.5)	1.2 (0.7;1.8)	0.727
	K^{trans} skewness	1.0 (0.4;1.5)	0.8 (0.1; 1.6)	0.670	1.0 (0.4;1.6)	0.8 (0.1;1.6)	0.614
	K^{trans} kurtosis	0.3 (-0.8;1.9)	0.3(-0.9;2.1)	0.907	0.1 (-0.8;2.5)	0.1(-0.9;2.7)	0.786
	k_{ep} mean	1.0 (0.9;1.0)	1.2 (0.8;1.4)	0.332	0.9 (0.9;1.0)	1.2 (0.7;1.4)	0.201
	k_{ep} maximum	3.8 (2.9; 4.2)	3.3 (2.7;4.0)	0.756	3.8 (2.9;4.2)	3.4 (2.7;4.0)	0.786
	k_{ep} skewness	1.5 (1.1;1.8)	1.3 (0.7;1.7)	0.510	1.6 (1.2;1.8)	1.3 (0.8;1.7)	0.438
k_{ep} kurtosis	3.1 (0.8;3.9)	1.1(-0.5;4.1)	0.535	3.1 (0.9;4.0)	1.3(-0.5;3.6)	0.535	

Note. TRG, tumor regression grade; TRG0, no regression; TRG1, dominant tumor mass with obvious fibrosis and/or vasculopathy; TRG2, dominantly fibrotic changes with few tumor cells or groups; TRG3, very few tumor cells in fibrotic tissue with or without mucous substance; TRG4, no tumor cells, only fibrotic mass; TRG nonresponders (Grades 0,1, and 2) and TRG responders (Grades 3 and 4); CR, complete response.

All figures of perfusion parameters in the above table have been rounded to one decimal place and are presented as median value (interquartile range) according to the data distribution.

*Determined with the Mann-Whitney U test.

significant correlation between PNI and v_p . The presence of PNI in rectal cancer is associated with a significantly worse prognosis [19, 20], indicating that a high v_p is a poor prognostic factor.

In patients with metastatic colorectal cancer, treatment using EGFR-directed antibodies such as cetuximab or panitumumab is recommended. However, KRAS (exon2 or nonexon2) or NRAS mutations are known to be resistant to EGFR-targeting agents; therefore, anti-EGFR therapy cannot be used in patients with RAS gene mutations. In the present study, there were no patients with NRAS mutation, and 13 patients (44. 8%, 13/29) with KRAS mutation. Most histogram values of K^{trans} and k_{ep} were higher in the KRAS mutation group. In our previous study, there was also a higher mean K^{trans} in the group with KRAS mutation, although the difference did not reach statistical significance[14]. However, the present study showed statistical significance of higher K^{trans} and k_{ep} correlating with presence of aKRAS gene mutation. It is well known that the mutant KRAS oncogene can induce or strongly upregulate various proangiogenic factors such as vascular endothelial growth factor/vascular permeability factor (VEGF/VPF) and transforming growth factors β (TGF- β) or α (TGF- α) in a cascade manner. Although the precise mechanism has not been discovered, the current study suggests the possibility of MRI-derived perfusion parameters reflecting an event at the genetic level of tumorigenesis[21, 22].Although further studies of clinical validity with a larger sample size are required, K^{trans} or k_{ep} may be important imaging biomarkers in predicting

an individual’s response to anti-EGFR therapy, even before genotyping.

Contrary to the significant results regarding the usefulness of mean K^{trans} for response assessment or prediction of CRT in previous studies[2–4, 23], our study demonstrated no correlation of histogram values of K^{trans} , k_{ep} , or v_e with CRT response. However, several studies have reported similar results. Lim et al.[2]demonstrated that K^{trans} was not predictive of TRG, and Kim et al. [3] also reported that K^{trans} , k_{ep} , and v_e are not useful to assess or predict CR. Furthermore, Intven et al. [23] revealed that changes in K^{trans} after CRT have no additive value for response assessment in the combination study of T2-weighted MR volumetry, diffusion-weighted MR imaging, and DCE-MRI. Further studies with larger sample sizes are needed to investigate clinical validation and additive values of perfusion MRI for response assessment or prediction of CRT.

Our study has several limitations. First, this is a retrospective study and therefore has an unavoidable selection bias. Second, the sample size was relatively small and was thus insufficient to suggest optimal threshold values of DCE-MRI parameters for predicting prognosis. Third, we did not analyze the MRI after CRT and thus cannot assess the changes in perfusion parameters after CRT. However, in a clinical setting, there is actually less interest in assessing treatment response after CRT compared to predicting response before CRT. For this reason, we performed this study to explore the role of DCE-MRI in predicting treatment response before CRT. These preliminary results suggest that

a larger proportion of higher AUC skewness was present in LN metastasis group and a higher v_p histogram value was present in rectal cancer with PNI. In addition, K^{trans} and k_{ep} histogram parameters showed difference according to the KRAS mutation, demonstrating the utility of the histogram of perfusion parameters derived from DCE-MRI as potential imaging biomarkers of tumor characteristics and genetic features.

Data Availability

This study is based on medical images of patients. Sharing data is believed to be a possible source of legal and ethical issues. The software used for image analysis is currently commercially available.

Conflicts of Interest

The authors have no conflicts of interest with regard to this study.

Acknowledgments

This study was funded by Ministry of Education, Republic of Korea (2016R1D1A1B03932876).

References

- [1] P. S. Tofts, G. Brix, D. L. Buckley et al., "Estimating kinetic parameters from dynamic contrast-enhanced T1-weighted MRI of a diffusible tracer: standardized quantities and symbols," *Journal of Magnetic Resonance Imaging*, vol. 10, no. 3, pp. 223–232, 1999.
- [2] J. S. Lim, D. Kim, S.-E. Baek et al., "Perfusion MRI for the prediction of treatment response after preoperative chemoradiotherapy in locally advanced rectal cancer," *European Radiology*, vol. 22, no. 8, pp. 1693–1700, 2012.
- [3] S. H. Kim, J. M. Lee, S. N. Gupta, J. K. Han, and B. I. Choi, "Dynamic contrast-enhanced MRI to evaluate the therapeutic response to neoadjuvant chemoradiation therapy in locally advanced rectal cancer," *Journal of Magnetic Resonance Imaging*, vol. 40, no. 3, pp. 730–737, 2014.
- [4] T. Tong, Y. Sun, M. J. Gollub et al., "Dynamic contrast-enhanced MRI: Use in predicting pathological complete response to neoadjuvant chemoradiation in locally advanced rectal cancer," *Journal of Magnetic Resonance Imaging*, vol. 42, no. 3, pp. 673–680, 2015.
- [5] W. W. Yao, H. Zhang, B. Ding et al., "Rectal cancer: 3D dynamic contrast-enhanced MRI; correlation with microvascular density and clinicopathological features," *La Radiologia Medica*, vol. 116, no. 3, pp. 366–374, 2011.
- [6] Y.-E. Kim, J. S. Lim, J. Choi et al., "Perfusion parameters of dynamic contrast-enhanced magnetic resonance imaging in patients with rectal cancer: Correlation with microvascular density and vascular endothelial growth factor expression," *Korean Journal of Radiology*, vol. 14, no. 6, pp. 878–885, 2013.
- [7] T. Heye, M. S. Davenport, J. J. Horvath et al., "Reproducibility of dynamic contrast-enhanced MR imaging: Part I. Perfusion characteristics in the female pelvis by using multiple computer-aided diagnosis perfusion analysis solutions," *Radiology*, vol. 266, no. 3, pp. 801–811, 2013.
- [8] T. Heye, E. M. Merkle, C. S. Reiner et al., "Reproducibility of dynamic contrast-enhanced MR imaging part II. Comparison of intra- and interobserver variability with manual region of interest placement versus semiautomatic lesion segmentation and histogram analysis," *Radiology*, vol. 266, no. 3, pp. 812–821, 2013.
- [9] V. Goh, S. Halligan, A. Gharpuray, D. Wellsted, J. Sundin, and C. I. Bartram, "Quantitative assessment of colorectal cancer tumor vascular parameters by using perfusion CT: influence of tumor region of interest," *Radiology*, vol. 247, no. 3, pp. 726–732, 2008.
- [10] S. H. Cho, G. C. Kim, Y.-J. Jang et al., "Locally advanced rectal cancer: Post-chemoradiotherapy ADC histogram analysis for predicting a complete response," *Acta Radiologica*, vol. 56, no. 9, pp. 1042–1050, 2015.
- [11] H. J. Baek, H. S. Kim, N. Kim, Y. J. Choi, and Y. J. Kim, "Percent change of perfusion skewness and kurtosis: a potential imaging biomarker for early treatment response in patients with newly diagnosed glioblastomas," *Radiology*, vol. 264, no. 3, pp. 834–843, 2012.
- [12] S. Woo, J. Y. Cho, S. Y. Kim, and S. H. Kim, "Histogram analysis of apparent diffusion coefficient map of diffusion-weighted mri in endometrial cancer: A preliminary correlation study with histological grade," *Acta Radiologica*, vol. 55, no. 10, pp. 1270–1277, 2014.
- [13] E. Kluza, E. D. Rozeboom, M. Maas et al., "T2 weighted signal intensity evolution may predict pathological complete response after treatment for rectal cancer," *European Radiology*, vol. 23, no. 1, pp. 253–261, 2013.
- [14] D.-M. Yeo, S. N. Oh, C.-K. Jung et al., "Correlation of dynamic contrast-enhanced MRI perfusion parameters with angiogenesis and biologic aggressiveness of rectal cancer: Preliminary results," *Journal of Magnetic Resonance Imaging*, vol. 41, no. 2, pp. 474–480, 2015.
- [15] P. S. Tofts and A. G. Kermode, "Measurement of the blood-brain barrier permeability and leakage space using dynamic MR imaging. 1. Fundamental concepts," *Magnetic Resonance in Medicine*, vol. 17, no. 2, pp. 357–367, 1991.
- [16] O. Dworak, L. Keilholz, and A. Hoffmann, "Pathological features of rectal cancer after preoperative radiochemotherapy," *International Journal of Colorectal Disease*, vol. 12, no. 1, pp. 19–23, 1997.
- [17] R. C. T. R: A language and environment for statistical computing. R Foundation for Statistical Computing, Vienna, Austria, 2014, <http://www.R-project.org/>.
- [18] K.-W. Moon, *R statistics and graphs for medical papers*. Hanaare Seoul, 2015.
- [19] N. Kniijn, S. C. Mogk, S. Teerenstra, F. Simmer, and I. D. Nagtegaal, "Perineural invasion is a strong prognostic factor in colorectal cancer," *The American Journal of Surgical Pathology*, vol. 40, no. 1, pp. 103–112, 2016.
- [20] C. Liebig, G. Ayala, J. Wilks et al., "Perineural invasion is an independent predictor of outcome in colorectal cancer," *Journal of Clinical Oncology*, vol. 27, no. 31, pp. 5131–5137, 2009.
- [21] J. Rak, J. Filmus, G. Finkenzeller, S. Grugel, D. Marmé, and R. S. Kerbel, "Oncogenes as inducers of tumor angiogenesis," *Cancer and Metastasis Reviews*, vol. 14, no. 4, pp. 263–277, 1995.
- [22] F. Okada, J. W. Rak, B. St. Croix et al., "Impact of oncogenes in tumor angiogenesis: Mutant K-ras up-regulation of

vascular endothelial growth factor/vascular permeability factor is necessary, but not sufficient for tumorigenicity of human colorectal carcinoma cells,” *Proceedings of the National Academy of Sciences of the United States of America*, vol. 95, no. 7, pp. 3609–3614, 1998.

- [23] M. Intven, O. Reerink, and M. E. P. Philippens, “Dynamic contrast enhanced MR imaging for rectal cancer response assessment after neo-adjuvant chemoradiation,” *Journal of Magnetic Resonance Imaging*, vol. 41, no. 6, pp. 1646–1653, 2015.

Research Article

Bioinformatics Analysis Reveals Most Prominent Gene Candidates to Distinguish Colorectal Adenoma from Adenocarcinoma

Nina Hauptman , Emanuela Boštjančič , Margareta Žlajpah, Branislava Ranković, and Nina Zidar

Institute of Pathology, Faculty of Medicine, University of Ljubljana, Ljubljana, Slovenia

Correspondence should be addressed to Nina Hauptman; nina.hauptman@mf.uni-lj.si

Received 2 March 2018; Accepted 30 July 2018; Published 6 August 2018

Academic Editor: Renato Franco

Copyright © 2018 Nina Hauptman et al. This is an open access article distributed under the Creative Commons Attribution License, which permits unrestricted use, distribution, and reproduction in any medium, provided the original work is properly cited.

Colorectal cancer (CRC) is one of the leading causes of death by cancer worldwide. Bowel cancer screening programs enable us to detect early lesions and improve the prognosis of patients with CRC. However, they also generate a significant number of problematic polyps, e.g., adenomas with epithelial misplacement (pseudoinvasion) which can mimic early adenocarcinoma. Therefore, biomarkers that would enable us to distinguish between adenoma with epithelial misplacement (pseudoinvasion) and adenoma with early adenocarcinomas (true invasion) are needed. We hypothesized that the former are genetically similar to adenoma and the latter to adenocarcinoma and we used bioinformatics approach to search for candidate genes that might be potentially used to distinguish between the two lesions. We used publicly available data from Gene Expression Omnibus database and we analyzed gene expression profiles of 252 samples of normal mucosa, colorectal adenoma, and carcinoma. In total, we analyzed 122 colorectal adenomas, 59 colorectal carcinomas, and 62 normal mucosa samples. We have identified 16 genes with differential expression in carcinoma compared to adenoma: *COL12A1*, *COL1A2*, *COL3A1*, *DCN*, *PLAU*, *SPARC*, *SPON2*, *SPPI*, *SULF1*, *FADS1*, *GOS2*, *EPHA4*, *KIAA1324*, *LITDI*, *PCKSL1*, and *C11orf96*. In conclusion, our *in silico* analysis revealed 16 candidate genes with different expression patterns in adenoma compared to carcinoma, which might be used to discriminate between these two lesions.

1. Introduction

Colorectal cancer (CRC) is developed by multistep process from normal epithelium to adenoma and adenocarcinoma, which can eventually metastasize to different organs [1]. The model of development of CRC was introduced in 1990, where *APC*, *KRAS*, *TP53*, and *DCC* were proposed as genes promoting the progression of CRC [2]. Since, many studies have investigated underlying molecular mechanisms of CRC. It is accepted that CRC arises from accumulation of genetic and epigenetic events that alter signaling in pathways, such as Wnt, PIK3CA, and TGF- β . Three major accepted pathways in the pathogenesis of CRC are chromosome instability pathway, microsatellite instability pathway, and CpG island methylator phenotype. There are many CRCs that lack the changes described in above pathways, suggesting that other mechanisms are involved in the development of CRC [1].

CRC is one of the leading causes of death by cancer worldwide. In Europe, CRC is the second and the third cause of death by cancer in men and women, respectively [3]. Five-year survival for patients with early CRC is 90%, while for patients with advanced CRC, survival drops to only 8-12% [4]. The prognosis can improve significantly with the introduction of population screening. Bowel cancer screening programs enable us to detect early lesions, including adenomas and adenomas with early adenocarcinoma (malignant polyps). However, they also generate a significant number of problematic polyps which contain dysplastic glands in the submucosa. This phenomenon has been referred to as epithelial misplacement (pseudoinvasion). It can be the result of a torsion or intraluminal trauma of large pedunculated polyps of the distal colon, or it may be a consequence of a previous biopsy. Adenomas with epithelial misplacement (pseudoinvasion) can be difficult to distinguish from adenomas

with early adenocarcinoma [5–7]. The correct diagnosis is crucial for the choice of optimal treatment. For adenoma and adenoma with epithelial misplacement, endoscopic removal is sufficient, whereas malignant adenomas (early carcinomas) may require surgical treatment, since they are capable of metastasizing [7].

Despite well-defined morphologic features of epithelial misplacement and early invasion, there are a significant number of lesions with ambiguous features leading to divergent diagnostic opinions among pathologists [7]. Biomarkers that would enable to distinguish between adenoma with epithelial misplacement (pseudoinvasion) and adenoma with early adenocarcinoma (true invasion) are needed. We hypothesized that the former is genetically similar to adenoma and the latter to adenocarcinoma and we used bioinformatics approach to search for candidate genes that might be potentially used to distinguish between the two lesions.

Gene expression in CRC was widely studied by microarray technique, usually comparing carcinomas to normal mucosa tissue, studying microsatellite instable CRC, or establishing CRC subtypes based on gene expression patterns [8–10]. Some of the studies have focused on the gene expression difference between colorectal adenomas and carcinomas [11–15]. The downside of these studies is limitation in number of samples. Our goal was to minimize any variabilities arising from different microarrays and procedures, to identify the genes and subsequently pathways associated with adenoma progression to carcinoma. Due to the aim of the study, we have chosen five different sets of data, containing normal, adenoma, and carcinoma samples, where two of them were not published yet.

2. Materials and Methods

2.1. Microarray Data. Several projects (GSE10714, GSE37364, GSE41657, GSE50114, and GSE50115) with gene expression profiles of colon normal, adenoma, and carcinoma samples were downloaded from the public functional genomics data repository-Gene Expression Omnibus database (GEO, <http://www.ncbi.nlm.nih.gov/geo>) of the National Center for Biotechnology Information (NCBI). In total, 7 CRC, 5 adenomas, and 3 normal mucosa specimens were included in GSE10714, while 27 CRC, 29 adenomas, and 38 normal mucosa specimens were included in GSE37364 (both on platform GPL570 Affymetrix Human Genome U133 Plus 2.0 array). GSE41657 was composed of 25 CRC, 51 adenomas, 12 normal mucosa samples, and GSE50114 combined with GSE50115 contained 9 CRC, 37 adenoma, and 9 normal mucosa samples (all three on platform GPL6480 Agilent Whole Human Genome Microarray 4x44K G4112F). In total, 252 samples of colonic biopsies, including 62 normal, 122 adenomas, and 59 CRC samples, were included in this study.

2.2. Data Processing. For all projects, the original data files were downloaded and further normalized in R language (<https://www.r-project.org/>). For projects on Affymetrix arrays (GSE10714, GSE37364) package *affy* was used to convert CEL files into expression data using robust multichip average function, which performs background correction

and normalization in one step [16]. For projects on Agilent arrays (GSE41657, GSE50114, and GSE50115) package *limma* was used to perform background correction and normalization between arrays [17]. After data normalization gene filter was used to remove probes that had intensity less than 100 in more than 20% of samples in each project.

Differentially expressed genes (DEG) were identified on probe level using *limma* package in R for each individual project [18]. We constructed three contrast matrices (adenoma compared to normal, carcinoma compared to adenoma, and carcinoma compared to normal) for each GEO project. The cut-off conditions were set to adjusted p value < 0.05 and absolute value of log fold change (log FC) > 1.5. Every comparison (adenoma compared to normal, carcinoma compared to adenoma, and carcinoma compared to normal) was overlapped among the projects to obtain the DEGs common to all projects.

2.3. Functional Analysis and Protein-Protein Interactions Network. For functional analysis and construction of protein-protein interactions (PPI) network, the Search Tool for the Retrieval of Interacting Genes (STRING) database was employed (<https://string-db.org/>). PPI network analysis is one of the important tools for interpretation of molecular mechanisms in the process of carcinogenesis. STRING offers integrative tools for uncovering the biological meaning behind large sets of genes, providing besides constructing PPI networks and also functional and pathway enrichment analysis. Gene ontology (GO) analysis including biological process, molecular function, and cellular component and Kyoto Encyclopedia of Genes and Genomes (KEGG) pathway enrichment analysis were conducted for selected DEGs with STRING. The statistical significance threshold was set to $p < 0.05$.

In this study, we constructed PPI networks of DEGs for carcinoma compared to normal, adenoma compared to normal, and carcinoma compared to adenoma. The PPI network was constructed under the cut-off of interaction score of 0.4. Visualization of all three networks together was done in Cytoscape version 3.5.1 (<http://www.cytoscape.org/>).

3. Results

Data from each microarray was separately analyzed to obtain DEGs for each comparison, carcinoma compared to normal, adenoma compared to normal, and carcinoma compared to adenoma. We identified 172 genes overlapping in all projects for carcinoma compared to normal (568 in GSE10714, 845 in GSE37364, 1057 in GSE41657, and 806 in GSE50114 combined with GSE50115), 137 genes overlapping in all projects for adenoma compared to normal (530 in GSE10714, 412 in GSE37364, 927 in GSE41657, and 555 in GSE50114 combined with GSE50115), and 26 genes overlapping in all projects for carcinoma compared to adenoma (252 in GSE10714, 392 in GSE37364, 116 in GSE41657, and 348 in GSE50114 combined with GSE50115) (Figure 1). We also constructed heatmap with union of all genes differentially expressed in every individual project, to confirm that samples belong to three distinct

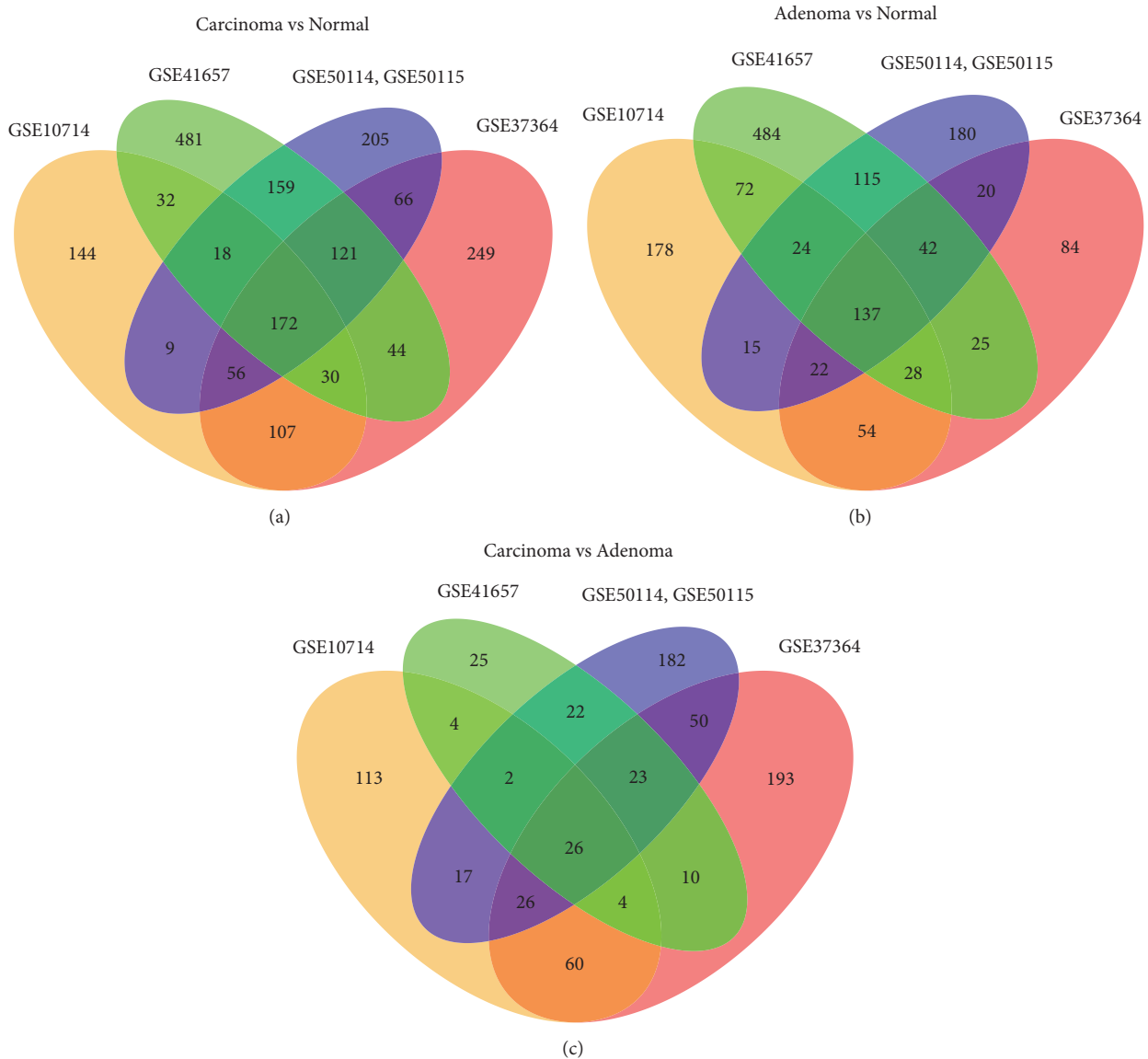


FIGURE 1: Identification of differentially expressed genes in gene expression datasets (GSE10714, GSE37364, GSE41657, GSE50114, and GSE50115) and their overlaps.

groups, namely, carcinoma, adenoma, and normal mucosa samples (Figure 2).

In order to investigate our selected DEGs, we overlapped the genes in each comparison, to obtain the unique set of genes characteristic for each comparison (Supplementary Figure 1). As expected, the most DEGs were found in carcinoma compared to normal mucosa group (172), somewhat less in adenoma compared to normal group (137), and just 26 DEGs in carcinoma compared to adenoma group (Supplementary Table 1). Interestingly, there were no DEG common to all three comparisons.

3.1. Protein-Protein Interaction Networks. The PPI network was constructed on the basis of STRING database and visualized using Cytoscape software. Figure 3 represents network of genes differentially expressed in our analysis. In the whole

network, the top hub genes are IGF1 (21), MYC (20), FN1 (14), CXCL12 (14), GCG (13), AGT (10), and BCL2 (10). The number in brackets represents the number of interaction each gene has with other genes in network.

We identified top hub genes in each group, where there are at least four connections for a gene. In adenoma compared to normal top hub genes are APOE (7), NR3C1 (4), and NMU (4), in carcinoma compared to normal top hub genes are AGT (10), BCL2 (10), AURKA (9), MMP3 (6), CDC6 (6), TPX2 (6), PRKACB (6), UB2C (5), SULT1A1 (4), KLF4 (4), ECT2 (4), and MMP1 (4), and in carcinoma compared to adenoma top hub genes are COL3A1 (6), COL1A2 (6), SPARC (5), DCN (5), and SPPI (4).

3.2. Functional Enrichment Analysis. The top five significant terms of GO and KEGG enrichment analysis are presented

TABLE 1: Gene ontology and Kyoto Encyclopedia of Genes and Genomes (KEGG) analysis of differentially expressed genes in each comparison group.

Pathway ID	Pathway description	Number of observed genes	FDR	Number of genes up/down regulated
Carcinoma vs normal				
Biological process				
GO.0001932	Regulation of protein phosphorylation	29	7.58E-05	16↑/13↓
GO.0006730	One-carbon metabolic process	7	7.58E-05	1↑/6↓
GO.0006820	Anion transport	17	0.000315	4↑/13↓
GO.0009719	Response to endogenous stimulus	30	0.000315	8↑/22↓
GO.0015701	Bicarbonate transport	6	0.000315	0↑/6↓
Cellular component				
GO.0005576	Extracellular region	63	9.38E-05	14↑/49↓
GO.0031982	Vesicle	53	0.000163	12↑/41↓
GO.0031988	Membrane-bounded vesicle	52	0.000163	12↑/40↓
GO.0044421	Extracellular region part	55	0.000163	13↑/42↓
GO.0070062	Extracellular exosome	42	0.00196	9↑/31↓
Molecular function				
GO.0004089	Carbonate dehydratase activity	5	0.0001	0↑/5↓
GO.0003824	Catalytic activity	70	0.000147	15↑/55↓
GO.0005179	Hormone activity	7	0.00231	2↑/5↓
GO.0005488	Binding	106	0.00306	35↑/71↓
GO.0008237	Metallopeptidase activity	9	0.00509	3↑/6↓
KEGG				
910	Nitrogen metabolism	5	5.28E-05	0↑/5↓
4964	Proximal tubule bicarbonate reclamation	4	0.00167	0↑/4↓
4976	Bile secretion	6	0.00167	0↑/6↓
5204	Chemical carcinogenesis	6	0.00167	0↑/6↓
4972	Pancreatic secretion	6	0.00513	0↑/6↓
Adenoma vs normal				
Biological process				
GO.0006820	Anion transport	15	5.23E-05	3↑/12↓
GO.0006730	One-carbon metabolic process	5	2.40E-03	0↑/5↓
GO.0015701	Bicarbonate transport	5	0.0024	0↑/5↓
GO.0015711	Organic anion transport	11	0.0024	3↑/8↓
GO.0006811	Ion transport	17	0.0359	3↑/14↓
Cellular component				
GO.0005576	Extracellular region	47	4.53E-06	10↑/37↓
GO.0005615	Extracellular space	23	1.15E-05	6↑/17↓
GO.0044421	Extracellular region part	41	1.15E-05	8↑/33↓
GO.0031988	Membrane-bounded vesicle	37	0.000128	6↑/31↓
GO.0098589	Membrane region	19	0.000128	5↑/14↓
Molecular function				
GO.0004089	Carbonate dehydratase activity	4	0.00115	0↑/4↓
KEGG				
910	Nitrogen metabolism	4	1.89E-04	0↑/4↓
4976	Bile secretion	6	0.000189	1↑/5↓
4964	Proximal tubule bicarbonate reclamation	4	0.000204	0↑/4↓
Carcinoma vs adenoma				
Biological process				
GO.0022617	Extracellular matrix disassembly	6	3.11E-05	6↑/0↓
GO.0030198	Extracellular matrix organization	8	3.11E-05	8↑/0↓
GO.0009888	Tissue development	11	0.0017	8↑/3↓
GO.0060279	Positive regulation of ovulation	2	0.0128	2↑/0↓
GO.0018149	Peptide cross-linking	3	0.0138	3↑/0↓

TABLE 1: Continued.

Pathway ID	Pathway description	Number of observed genes	FDR	Number of genes up/down regulated
Cellular component				
GO.0005615	Extracellular space	14	4.03E-08	11↑/3↓
GO.0044420	Extracellular matrix component	6	5.01E-06	6↑/0↓
GO.0098644	Complex of collagen trimers	3	0.00151	3↑/0↓
GO.0005581	Collagen trimer	4	0.00166	4↑/0↓
GO.0044421	Extracellular region part	14	0.00637	10↑/4↓
Molecular function				
GO.0050840	Extracellular matrix binding	3	0.0478	3↑/0↓
KEGG				
4512	Extracellular-receptor interaction	4	0.00111	4↑/0↓
4510	Focal adhesion	4	0.0155	4↑/0↓
4974	Protein digestion and absorption	3	0.0155	3↑/0↓
5146	Amoebiasis	3	0.0219	3↑/0↓
4151	PI3K-Akt signaling pathway	4	0.0461	4↑/0↓

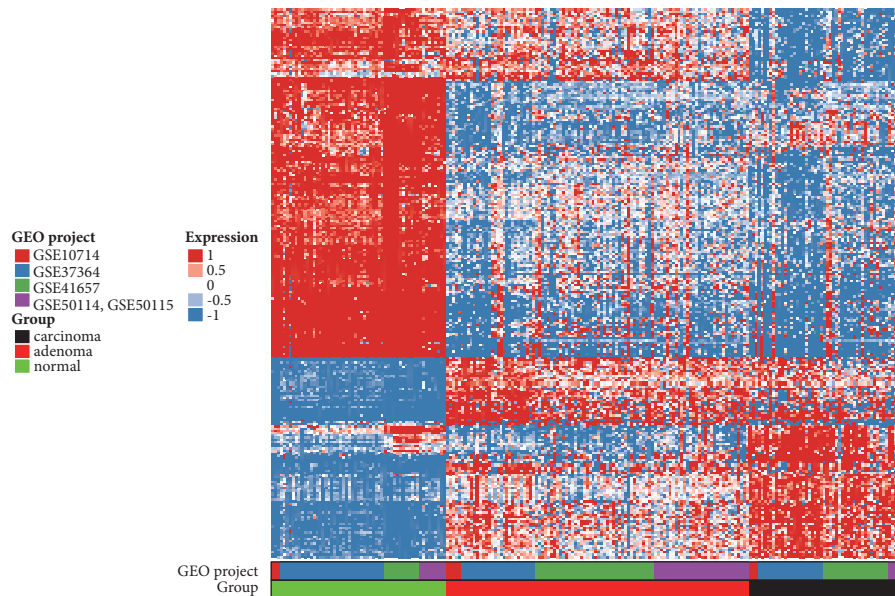


FIGURE 2: Heatmap of union of genes differentially expressed in each dataset (GSE10714, GSE37364, GSE41657, GSE50114, and GSE50115).

in Table 1, while all terms can be viewed in Supplementary Table 2. The group carcinoma compared to normal exhibits enrichment in biological process of regulation of protein phosphorylation, one-carbon metabolic process, anion transport, response to endogenous stimulus, and bicarbonate transport. As for molecular function, these genes are enriched in carbonate dehydratase activity, catalytic activity, hormone activity, binding, and metalloproteinase activity. Cellular function is enriched for genes which are included in extracellular region, vesicle, membrane-bounded vesicle, extracellular region part, and extracellular exosome. The biological processes enriched in adenoma compared to normal group were anion transport, one-carbon metabolic process, bicarbonate transport, organic anion transport, and ion transport. In this group, only one molecular function term was enriched, namely, carbonate dehydratase activity. Genes

were enriched in cellular component of extracellular region, extracellular space, extracellular region part, membrane-bounded vesicle, and membrane region. It is interesting that in both described groups of carcinoma compared to normal and adenoma compared to normal the same KEGG pathways were enriched, i.e., nitrogen metabolism, bile secretion, and proximal tubule bicarbonate reclamation. Additionally, in cancer compared to normal group two more KEGG pathways were found, namely, chemical carcinogenesis and pancreatic secretion.

3.3. *Carcinoma Compared to Adenoma.* The most interesting is the comparison between adenoma and carcinoma. Construction of contrast matrix enables us to compare the two groups, yet we have no information about the third group. To compare all three groups, we constructed a figure of

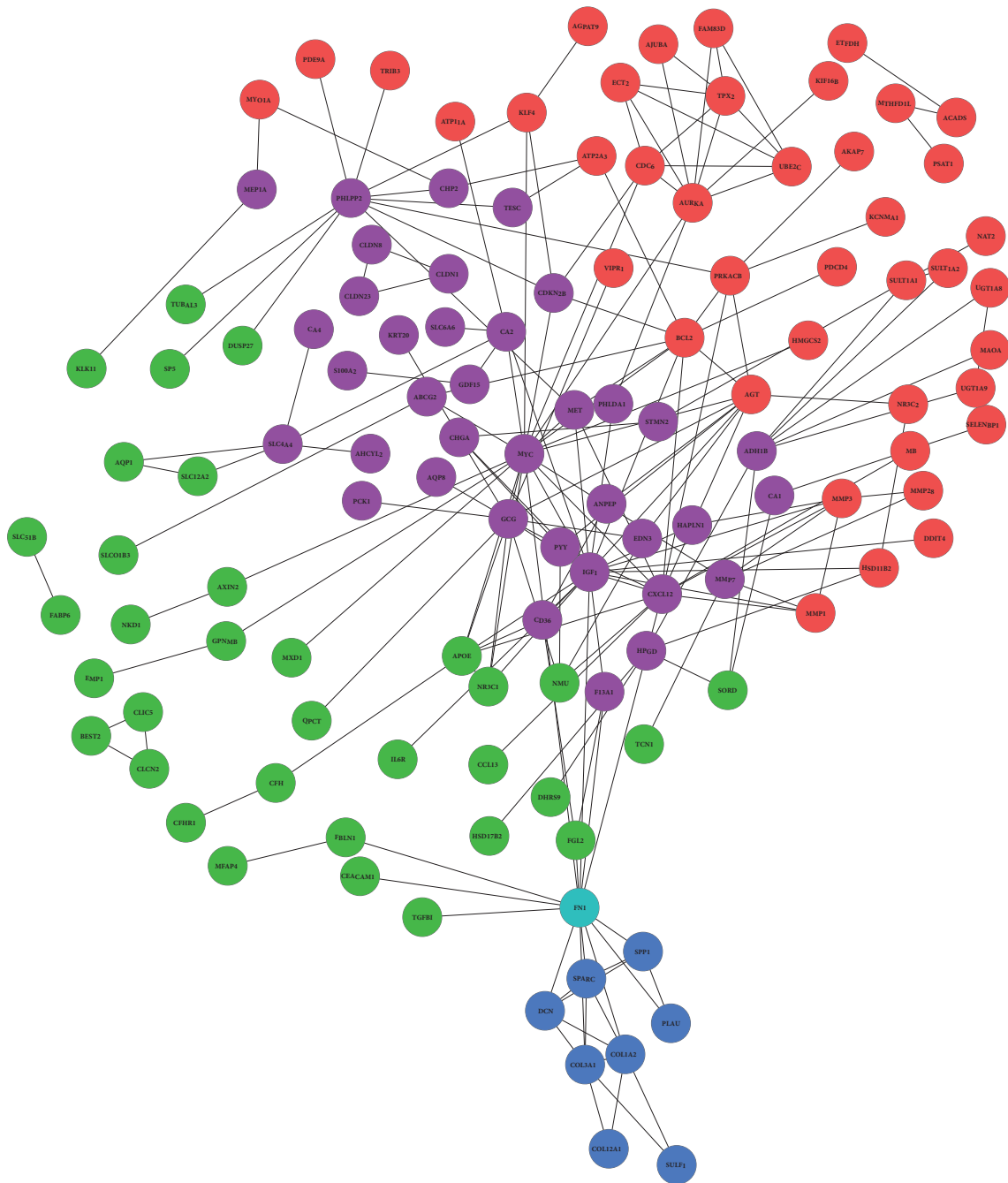


FIGURE 3: The protein-protein interactions (PPI) network of differentially expressed genes (DEGs) for each comparison. Red, green, and blue hubs represent carcinoma compared to normal, adenoma compared to normal, and carcinoma compared to adenoma, respectively. Purple hubs represent genes which are common to carcinoma compared to normal and adenoma compared to normal groups, while turquoise represents genes common to adenoma compared to normal and carcinoma compared to adenoma groups.

logarithmic average intensity values, comparing normal, adenoma, and carcinoma samples (Figure 4). The figure shows that the 16 genes unique to carcinoma compared to adenoma group are also distinguishable from average intensities of normal samples. There are four types of changes in expression. *COL12A1* follows the first pattern and has similar expression in normal and adenoma, while in carcinoma the expression is elevated. The other pattern is that expression is similar in

normal and adenoma, and reduced expression is observed in carcinoma. Genes that follow this pattern are *KIAA1324* and *PCKS1*. *EPHA4* and *LITD1* follow the third pattern, which higher expression in adenoma and lower in normal and carcinoma. All the other genes *C11orf96*, *COL1A2*, *COL3A1*, *DCN*, *FADS1*, *G0S2*, *PLAU*, *SPARC*, *SPON2*, *SPPI*, and *SULF1* follow the fourth pattern, where expression is decreased in adenoma and increased in normal and carcinoma.

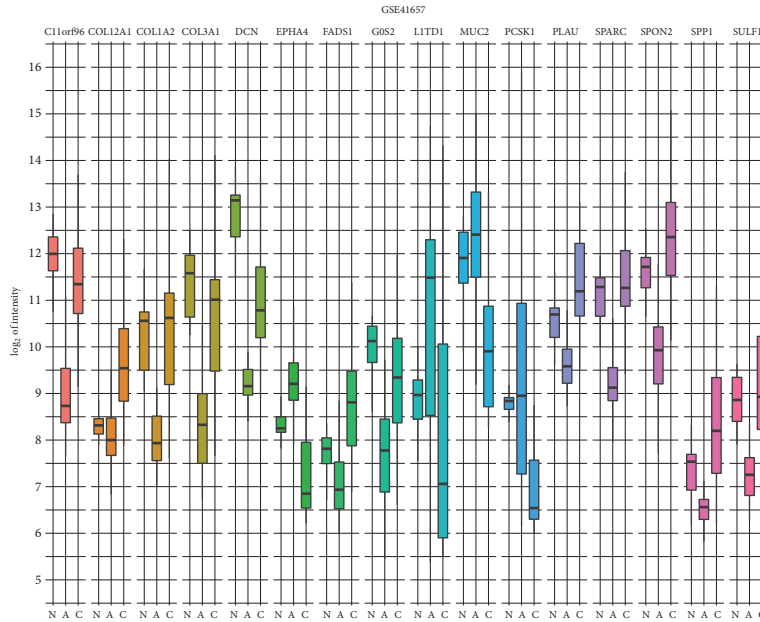


FIGURE 4: Logarithmic values of average intensities for normal (N), adenoma (A), and carcinoma (C) samples for GSE41657. Logarithmic values of average intensities for GSE37364, GSE10714, GSE50114, and GSE50115 can be found in Supplementary Figure 2.

4. Discussion

The CRC can arise through the progression of adenoma, which is the consequence of genetic and epigenetic events in epithelial cells. Some microarray studies have already identified gene expression profiles of adenoma and carcinoma [11, 19–24]. However, a study conducted by Nannini et al. revealed there is a rather weak overlap of gene expression profiles among different studies. They assigned this to several reasons: technical variability arising from collection of samples, protocols used for sample preparation, type of microarray used and subsequent data analysis pipeline used, and lack of large scale study [25]. We overcame some of these limitations by using more datasets on two different platforms, Affymetrix Human Genome U133 Plus 2.0 array and Agilent Whole Human Genome Microarray 4x44K G4112F. We used four raw datasets of microarray gene expression studies (GSE10714–Gambo et al. [19], GSE37364–Valcz et al. [26], GSE41657, GSE50114 and GSE50115—the latter three unpublished) and conducted our procedure of normalization, summation, and filtration, irrespective of procedures supplied by authors of the data.

The aim of this study was to investigate the differences in gene expression profiles of colorectal adenoma compared to adenocarcinoma, using normal mucosa samples as the reference. Our analysis showed many changes occur in adenoma compared to the normal group, suggesting that adenoma is an intermediate state between normal and carcinoma, although not all the changes found in carcinoma were found in adenoma. We identified 16 gene expression patterns unique to carcinoma compared to adenoma, suggesting that these 16 genes have a role in promoting progression of adenoma to carcinoma. Some of these genes have already been reported in

adenoma compared to carcinoma, such as *SPON2* [15], *SPPI*, and *SPARC* [11], which is validation for our own analysis.

Functional analysis of genes in carcinoma compared to adenoma group revealed that the most significant biological processes and KEGG pathways are connected to extracellular matrix (ECM). Top two significant biological processes in this comparison are ECM disassembly and the other ECM organization; furthermore the top KEGG pathway is ECM-receptor interaction. Genes involved in these two biological process pathways are similar; *COL12A1*, *COL1A2*, *COL3A1*, *DCN*, *FNI*, and *SPPI* are involved in ECM disassembly and the same genes with addition of *SPARC* and *SULF1* are involved in ECM organization (Supplementary Table 2). Genes involved in these pathways are all upregulated in carcinoma compared to adenoma, indicating that the process of ECM organization is involved in the progression of adenoma to carcinoma.

The ECM is a superstructure, which has a supportive role, but on the other hand, it also delivers signals to cells, which determines their behavior. Therefore, the EMC is directly involved in process of EMT during malignant transformation and plays a major role in the pathology of cancer [27]. Results of our analysis show that nine out of 16 genes, which showed differential expression in carcinoma compared to adenoma, are components of ECM. These genes are all three collagen genes, *DCN*, *PLAU*, *SPARC*, *SPON2*, *SPPI*, and *SULF1*. They all showed an increase in expression in carcinoma compared to adenoma in our study.

Two collagen I proteins (*COL1A1*, *COL1A2*) were found significantly upregulated in cancer group compared to normal tissue. The study revealed higher expression of collagen I in stage II tumors, suggesting that the activation of collagen I is an early event in CRC progression. The finding suggests that expression of collagen I is higher at early stages of CRC and

that collagen I is needed for tumor invasiveness [28]. Studies on cell lines suggest that adherence to collagen I promotes intracellular signaling pathways, including AKT pathways; furthermore collagen I was demonstrated to induce EMT-like changes, associated with tumor progression and metastasis [29, 30]. Expression of *COL3A1* gene was shown to be upregulated in CRC compared to normal controls. Wang et al. used Kaplan-Meier survival analysis to show that increased *COL3A1* protein in cancer epithelial cells predicted a worse prognosis [31]. The study was expanded to plasma samples, where soluble extracellular protein *COL3A1* was also significantly higher in patients with CRC compared to normal controls. Also, *COL3A1* was found to promote CRC cell proliferation by activating AKT signaling pathway [31]. One study used microarray data (GSE20219) and experimentally validated *COL12A1* gene. Its expression continuously increased from normal, through adenoma to carcinoma. Moreover, expression of *COL12A1* was reported to clearly distinguish between normal, adenoma, and carcinoma group and may have further diagnostic potential [32]. Besides collagens, EMC contains also other proteins, such as proteoglycans, sulfatases, and phosphoproteins. DCN is a fibril-associated proteoglycan, found in EMC. Although upregulated when compared carcinoma to adenoma, the overall expression of *DCN* is downregulated when carcinoma to normal and adenoma to normal is compared. The role of *DCN* both in vivo and in vitro suggested that its role is tumor suppressive in stromal and epithelial cells [33]. A negative correlation between the immunoreactivity of *DCN* and malignant potential was observed [34].

The *PLAU* is a urokinase-like plasminogen activator (uPA), which is secreted serine protease that converts plasminogen into active plasmin. Binding of uPA to its receptor, uPA-R, activates its proteolytic activity, which promotes ECM degradation and subsequently the invasion and migration of tumor cells. The *PLAU* is found to be upregulated in CRC. Furthermore, increased activity of the plasmin/plasminogen system leads to tumor budding, which is also significantly related to lymph node metastasis [35]. SPARC is a member of the family of matricellular proteins, a calcium-binding protein. Studies have shown that *SPARC* expression in mesenchymal and stromal cells (MSC) was significantly higher compared to expression in cancer cells and in normal mucosa tissues. Low expression of *SPARC* is an independent unfavorable prognostic factor of colorectal cancer [36]. Another secreted ECM protein is SPON2, which belongs to mindin/Fspondin family. Spondin proteins play important role in different signaling pathways, important in cancer. SPON2 is found to be upregulated in many cancers, including CRC. SPON2 was also tested as a biomarker in plasma of CRC patients, where it was upregulated and downregulated after surgery was performed, indicating SPON2 to be associated with tumor burden [37]. SPP1 is phosphoprotein found upregulated in many cancers, including CRC. It was found to promote cell proliferation and metastasis by activating EMT [38]. The last ECM component that was significantly differentially expressed between adenoma and carcinoma is sulfatase, *SULF1*. Sulfatases are overexpressed in CRC and contribute to cell proliferation, migration, and invasion [39].

Other genes are not connected to ECM but are included in the progression of carcinoma. Two more genes had increased expression in carcinoma compared to adenoma, and these are *FADS1* and *G0S2*. *FADS1* is a member of the fatty acid desaturase gene family and has been suggested to regulate inflammation by modifying the metabolite profiles of fatty acids, which may influence the progression of cancer. Decreased expression of *FADS1* benefits development and growth of cancer cells, whereas increased expression was observed to be a protective factor in esophageal squamous cell carcinoma (ESCC). Decreased expression was associated with poor prognosis in patients with ESCC [40]. Expression of *G0S2* is downregulated in a wide variety of cancer cell types and has the properties of tumor suppressor. The upregulation of *G0S2* has shown a significant reduction in tumor cell growth and motility. Since the *G0S2* is a negative regulator of triglyceride catabolism, an altered lipid metabolism is present in transformation of cells from normal to cancerous [41].

The last four genes in our study were downregulated in carcinoma compared to adenoma, and those are *EPHA4*, *KIAA1324*, *LITD1*, and *PCKS1*. Upregulation of *EPHA4* was observed in various cancers, including CRC. The study shows that activated *EPHA4* is associated with highly aggressive EMT-like phenotype. Also, activation of *EPHA4* reduced E-cadherin expression and controlled cell migration and invasion through PI3K signaling [42]. The *KIAA1324* is a transmembrane protein, also known as EIG121 (estrogen-induced gene 121). It was shown that *KIAA1324* acts as a tumor suppressor in gastric cancer cell lines, where the induction of *KIAA1324* gene expression significantly reduced tumor size [43]. *LITD1* is RNA-binding protein, which is highly expressed in pluripotent cells. Depletion of *LITD1* leads to reduction in levels of OCT4 and NANOG and increased differentiation in human embryonic stem cells (hESCs). *LITD1* is required for self-renewal of hESCs and is reported as one of the key regulators of stem cell fate [44]. One study reported an increased expression of *PSKCI* in nasal polyps compared to the normal nasal mucosa. Furthermore, they showed that increased expression of *PSKCI* induces EMT-like process in airway epithelial cells. The cell lines displayed a morphological transformation from typical epithelial-like shape to an elongated, spindle morphology. The overexpression in *PSKCI* resulted in an enhanced cell proliferation and exhibits a significant increase in cell migration after wounding. Also the cells displayed reduced expression of epithelial markers and increased expression of mesenchymal markers [45].

In conclusion, distinguishing adenomas with epithelial misplacement (pseudoinvasion) from adenomas with early carcinomas (true invasion) is of great importance, in order to choose the optimal treatment. For this purpose, we identified 16 candidate genes with different expression patterns in adenoma compared to carcinoma, with a potential to discriminate between these two lesions, which will be the basis of our future work, where we will experimentally validate genes on selected tissue sections of adenomas with epithelial misplacement and adenomas with early carcinomas.

Data Availability

The data used to support the findings of this study are available from the corresponding author upon request.

Conflicts of Interest

The authors declare that they have no conflicts of interest.

Acknowledgments

The authors would like to thank Daša Jevšinek Skok, Ph.D., (Institute of Pathology, Faculty of Medicine, University of Ljubljana) for designing Figure 3. The authors acknowledge the financial support from the Slovenian Research Agency through research core funding no. P3-0054. Nina Hauptman acknowledges the financial support from the Slovenian Research Agency through Project no. Z3-6797.

Supplementary Materials

Supplementary 1. Supplementary Figures: Figure 1 shows the number of genes differentially expressed in each comparison and their intersection; Figure 2 shows the logarithmic values of average intensities for normal, adenoma, and carcinoma samples for (a) GSE10714, (b) GSE37364, (c) GSE50114 and GSE50115.

Supplementary 2. Supplementary Table 1 shows a list of genes common in each comparison and their expressions for each project.

Supplementary 3. Supplementary Table 2 shows gene ontology and KEGG of differentially expressed genes in each comparison group.

References

- [1] C. Balch, J. B. Ramapuram, and A. K. Tiwari, "The Epigenomics of Embryonic Pathway Signaling in Colorectal Cancer," *Frontiers in Pharmacology*, vol. 8, 2017.
- [2] E. R. Fearon and B. Vogelstein, "A genetic model for colorectal tumorigenesis," *Cell*, vol. 61, no. 5, pp. 759–767, 1990.
- [3] M. Malvezzi, G. Carioli, P. Bertuccio et al., "European cancer mortality predictions for the year 2017, with focus on lung cancer," *Annals of Oncology*, vol. 28, no. 5, pp. 1117–1123, 2017.
- [4] H. Cao, E. Xu, H. Liu, L. Wan, and M. Lai, "Epithelial-mesenchymal transition in colorectal cancer metastasis: A system review," *Pathology - Research and Practice*, vol. 211, no. 8, pp. 557–569, 2015.
- [5] N. A. Shepherd and R. K. L. Griggs, "Bowel cancer screening-generated diagnostic conundrum of the century: Pseudoinvasion in sigmoid colonic polyps," *Modern Pathology*, vol. 28, pp. S88–S94, 2015.
- [6] N. C. Panarelli, T. Somarathna, W. S. Samowitz et al., "Diagnostic Challenges Caused by Endoscopic Biopsy of Colonic Polyps: A Systematic Evaluation of Epithelial Misplacement with Review of Problematic Polyps from the Bowel Cancer Screening Program, United Kingdom," *The American Journal of Surgical Pathology*, vol. 40, no. 8, pp. 1075–1083, 2016.
- [7] R. K. L. Griggs, M. R. Novelli, D. S. A. Sanders et al., "Challenging diagnostic issues in adenomatous polyps with epithelial misplacement in bowel cancer screening: 5 years' experience of the Bowel Cancer Screening Programme Expert Board," *Histopathology*, vol. 70, no. 3, pp. 466–472, 2017.
- [8] M. Sheffer, M. D. Bacolod, O. Zuk et al., "Association of survival and disease progression with chromosomal instability: A genomic exploration of colorectal cancer," *Proceedings of the National Academy of Sciences of the United States of America*, vol. 106, no. 17, pp. 7131–7136, 2009.
- [9] D. Barras, E. Missiaglia, P. Wirapati et al., "BRAF V600E mutant colorectal cancer subtypes based on gene expression," *Clinical Cancer Research*, vol. 23, no. 1, pp. 104–115, 2017.
- [10] M. Bianchini, E. Levy, C. Zucchini et al., "Comparative study of gene expression by cDNA microarray in human colorectal cancer tissues and normal mucosa," *International Journal of Oncology*, vol. 29, pp. 83–94, 2006.
- [11] O. Galamb, F. Sipos, S. Spisak et al., "Potential biomarkers of colorectal adenoma-dysplasia-carcinoma progression: mRNA expression profiling and in situ protein detection on TMAs reveal 15 sequentially upregulated and 2 downregulated genes," *Cellular Oncology*, vol. 31, pp. 19–29, 2009.
- [12] M. Skrzypczak, K. Goryca, T. Rubel et al., "Modeling oncogenic signaling in colon tumors by multidirectional analyses of microarray data directed for maximization of analytical reliability," *PLoS ONE*, vol. 5, no. 10, Article ID e13091, 2010.
- [13] H. Tang, Q. Guo, C. Zhang et al., "Identification of an intermediate signature that marks the initial phases of the colorectal adenoma-carcinoma transition," *International Journal of Molecular Medicine*, vol. 26, no. 5, pp. 631–641, 2010.
- [14] A. H. Sillars-Hardebol, B. Carvalho, M. De Wit et al., "Identification of key genes for carcinogenic pathways associated with colorectal adenoma-to-carcinoma progression," *Tumor Biology*, vol. 31, no. 2, pp. 89–96, 2010.
- [15] B. Carvalho, A. H. Sillars-Hardebol, C. Postma et al., "Colorectal adenoma to carcinoma progression is accompanied by changes in gene expression associated with ageing, chromosomal instability, and fatty acid metabolism," *Cellular Oncology*, vol. 35, no. 1, pp. 53–63, 2012.
- [16] L. Gautier, L. Cope, B. M. Bolstad, and R. A. Irizarry, "Affy—analysis of Affymetrix GeneChip data at the probe level," *Bioinformatics*, vol. 20, no. 3, pp. 307–315, 2004.
- [17] M. E. Ritchie, B. Phipson, D. Wu et al., "limma powers differential expression analyses for RNA-seq and microarray studies," *Nucleic Acids Research*, 2015.
- [18] G. K. Smyth, "Linear models and empirical Bayes methods for assessing differential expression in microarray experiments," *Statistical Applications in Genetics and Molecular Biology*, vol. 3, no. 1, article 3, 2004.
- [19] O. Galamb, F. Sipos, N. Solymosi et al., "Diagnostic mRNA expression patterns of inflamed, benign, and malignant colorectal biopsy specimen and their correlation with peripheral blood results," *Cancer Epidemiology, Biomarkers & Prevention*, vol. 17, no. 10, pp. 2835–2845, 2008.
- [20] O. Kitahara, Y. Furukawa, T. Tanaka et al., "Alterations of gene expression during colorectal carcinogenesis revealed by cDNA microarrays after laser-capture microdissection of tumor tissues and normal epithelia," *Cancer Research*, vol. 61, no. 9, pp. 3544–3549, 2001.
- [21] S. Lechner, U. Müller-Ladner, B. Renke, J. Schölmerich, J. Rüschoff, and F. Kullmann, "Gene expression pattern of laser microdissected colonic crypts of adenomas with low grade dysplasia," *Gut*, vol. 52, no. 8, pp. 1148–1153, 2003.

- [22] D. A. Notterman, U. Alon, A. J. Sierk, and A. J. Levine, "Transcriptional gene expression profiles of colorectal adenoma, adenocarcinoma, and normal tissue examined by oligonucleotide arrays," *Cancer Research*, vol. 61, no. 7, pp. 3124–3130, 2001.
- [23] E. Staub, J. Groene, M. Heinze et al., "Genome-wide expression patterns of invasion front, inner tumor mass and surrounding normal epithelium of colorectal tumors," *Molecular Cancer*, vol. 6, article no. 79, 2007.
- [24] A. H. Wiese, J. Auer, S. Lassmann et al., "Identification of gene signatures for invasive colorectal tumor cells," *Cancer Epidemiology*, vol. 31, no. 4, pp. 282–295, 2007.
- [25] M. Nannini, M. A. Pantaleo, A. Maleddu, A. Astolfi, S. Formica, and G. Biasco, "Gene expression profiling in colorectal cancer using microarray technologies: Results and perspectives," *Cancer Treatment Reviews*, vol. 35, no. 3, pp. 201–209, 2009.
- [26] G. Valcz, Á. V. Patai, A. Kalmár et al., "Myofibroblast-Derived SFRP1 as Potential Inhibitor of Colorectal Carcinoma Field Effect," *PLoS ONE*, vol. 9, no. 11, p. e106143, 2014.
- [27] G. Tzanakakis, R.-M. Kavasi, K. Voudouri et al., "Role of the extracellular matrix in cancer-associated epithelial to mesenchymal transition phenomenon," *Developmental Dynamics*, vol. 247, no. 3, pp. 368–381, 2017.
- [28] X. Zou, B. Feng, T. Dong et al., "Up-regulation of type I collagen during tumorigenesis of colorectal cancer revealed by quantitative proteomic analysis," *Journal of Proteomics*, vol. 94, pp. 473–485, 2013.
- [29] S. C. Kirkland, "Type i collagen inhibits differentiation and promotes a stem cell-like phenotype in human colorectal carcinoma cells," *British Journal of Cancer*, vol. 101, no. 2, pp. 320–326, 2009.
- [30] L. Krasny, N. Shimony, K. Tzukert et al., "An in-vitro tumour microenvironment model using adhesion to type i collagen reveals Akt-dependent radiation resistance in renal cancer cells," *Nephrology Dialysis Transplantation*, vol. 25, no. 2, pp. 373–380, 2010.
- [31] X. Wang, Z. Tang, D. Yu et al., "Epithelial but not stromal expression of collagen alpha-1(III) is a diagnostic and prognostic indicator of colorectal carcinoma," *Oncotarget*, vol. 7, no. 8, 2016.
- [32] M. Mikula, T. Rubel, J. Karczmarski, K. Goryca, M. Dadlez, and J. Ostrowski, "Integrating proteomic and transcriptomic high-throughput surveys for search of new biomarkers of colon tumors," *Functional & Integrative Genomics*, vol. 11, no. 2, pp. 215–224, 2011.
- [33] X. Bi, N. M. Pohl, Z. Qian et al., "Decorin-mediated inhibition of colorectal cancer growth and migration is associated with E-cadherin *in vitro* and in mice," *Carcinogenesis*, vol. 33, no. 2, pp. 326–330, 2012.
- [34] K. Augoff, J. Rabczynski, R. Tabola, L. Czaplá, K. Ratajczak, and K. Grabowski, "Immunohistochemical study of decorin expression in polyps and carcinomas of the colon," *Medical Science Monitor*, vol. 14, no. 10, pp. CR530–CR535, 2008.
- [35] B. Märkl, I. Renk, D. V. Oruzio et al., "Tumour budding, uPA and PAI-1 are associated with aggressive behaviour in colon cancer," *Journal of Surgical Oncology*, vol. 102, no. 3, pp. 235–241, 2010.
- [36] J. Liang, H. Wang, H. Xiao et al., "Relationship and prognostic significance of SPARC and VEGF protein expression in colon cancer," *Journal of Experimental & Clinical Cancer Research*, vol. 29, no. 1, p. 71, 2010.
- [37] Q. Zhang, X. Wang, J. Wang et al., "Upregulation of spondin-2 predicts poor survival of colorectal carcinoma patients," *Oncotarget*, vol. 6, no. 17, 2015.
- [38] C. Xu, L. Sun, C. Jiang et al., "SPP1, analyzed by bioinformatics methods, promotes the metastasis in colorectal cancer by activating EMT pathway," *Biomedicine & Pharmacotherapy*, vol. 91, pp. 1167–1177, 2017.
- [39] C. M. Vicente, M. A. Lima, E. A. Yates, H. B. Yates, and L. Toma, "Enhanced tumorigenic potential of colorectal cancer cells by extracellular sulfatases," *Molecular Cancer Research*, vol. 13, no. 3, pp. 510–523, 2015.
- [40] Y. Du, S.-M. Yan, W.-Y. Gu et al., "Decreased expression of FADS1 predicts a poor prognosis in patients with esophageal squamous cell carcinoma," *Asian Pacific Journal of Cancer Prevention*, vol. 16, no. 12, pp. 5089–5094, 2015.
- [41] R. Zagani, W. El-Assaad, I. Gamache, and J. G. Teodoro, "Inhibition of adipose triglyceride lipase (ATGL) by the putative tumor suppressor GOS2 or a small molecule inhibitor attenuates the growth of cancer cells," *Oncotarget*, vol. 6, no. 29, pp. 28282–28295, 2015.
- [42] P. G. de Marcondes and J. A. Morgado-Díaz, "The Role of EphA4 Signaling in Radiation-Induced EMT-Like Phenotype in Colorectal Cancer Cells," *Journal of Cellular Biochemistry*, vol. 118, no. 3, pp. 442–445, 2017.
- [43] J. M. Kang, S. Park, S. J. Kim et al., "KIAA1324 suppresses gastric cancer progression by inhibiting the oncoprotein GRP78," *Cancer Research*, vol. 75, no. 15, pp. 3087–3097, 2015.
- [44] E. Närvä, N. Rahkonen, M. R. Emani et al., "RNA-binding protein LITD1 interacts with LIN28 via RNA and is required for human embryonic stem cell self-renewal and cancer cell proliferation," *Stem Cells*, vol. 30, no. 3, pp. 452–460, 2012.
- [45] S.-N. Lee, D.-H. Lee, M. H. Sohn, and J.-H. Yoon, "Over-expressed proprotein convertase 1/3 induces an epithelial-mesenchymal transition in airway epithelium," *European Respiratory Journal*, vol. 42, no. 5, pp. 1379–1390, 2013.

Research Article

Plasma Chemokine CCL2 and Its Receptor CCR2 Concentrations as Diagnostic Biomarkers for Breast Cancer Patients

Emilia Lubowicka ¹, Andrzej Przyłipiak¹, Monika Zajkowska ², Barbara Maria Piskór,¹
Paweł Malinowski,³ Wojciech Fiedorowicz,³ and Sławomir Ławicki²

¹Department of Esthetic Medicine, Medical University of Białystok, 15-267 Białystok, Poland

²Department of Biochemical Diagnostics, Medical University of Białystok, 15-269 Białystok, Poland

³Department of Oncological Surgery, Białystok Oncology Center, Białystok, 15-276 Białystok, Poland

Correspondence should be addressed to Emilia Lubowicka; emila_lubowicka@wp.pl

Received 23 March 2018; Revised 21 June 2018; Accepted 22 July 2018; Published 30 July 2018

Academic Editor: Franco M. Buonaguro

Copyright © 2018 Emilia Lubowicka et al. This is an open access article distributed under the Creative Commons Attribution License, which permits unrestricted use, distribution, and reproduction in any medium, provided the original work is properly cited.

The aim of this study was to investigate plasma levels and applicability of CCL2, CCR2, and tumor marker CA 15-3 in breast cancer (BC) patients and in relation to the control groups: patients with benign breast tumor and healthy subjects. Plasma levels of tested parameters were determined by enzyme-linked immunosorbent assay (ELISA) and CA 15-3 by Chemiluminescent Microparticle Immunoassay (CMIA). The median levels of CCL2 in entire group of BC were significantly higher compared to the control groups, similarly as median levels of CA 15-3. CCR2 is a negative marker whose levels were significantly lower in BC group compared to healthy women. The concentration of CCL2 in BC increases with advancing tumor stage, while a median level of CCR2 decreases with advancing stage. CCL2 showed the highest value of sensitivity (SE) (64.95%) in entire BC group and also in early stages of disease. The highest specificity (SP) was obtained by CA 15-3 (85.71%). The area under the ROC curve (AUC) of CCR2 (0.7304) was the largest of all the tested parameters (slightly lower than CA 15-3) in the entire BC group, but a maximum range was obtained for the combination of all tested parameters with CA 15-3 (0.8271). In early stages of BC the highest AUC of all tested parameters was observed in CCL2 or CCR2 (stage I: 0.6604 and 0.6564; respectively; stage II: 0.7768, respectively, for CCR2). The findings of this study suggest that there may be applicability of CCL2, CCR2 in diagnosis of BC patients, particularly in conjunction with CA 15-3.

1. Introduction

Breast cancer is one of the most frequent malignancies in women around the world, with a higher incidence in developed countries and greatest relative mortality in less developed countries [1, 2]. Tumor growth and metastasis are regulated at least partially by chemokine-chemokine receptor interactions. The family currently includes more than 50 members of the human chemokines and the corresponding 20 chemokine receptors and they are classified into several groups depending on composition of a conserved cysteine motif present on the ligand [3, 4].

Chemokines are a family of small soluble proteins involved not only in inflammation but also in important physiological and pathological processes, such as cancer progression and metastasis [5]. Carcinogenesis is thought to

intensify by prolonged inflammation providing a microenvironment that is ideal for cancer development and growth [6]. Many cancer cells, including breast cancer cells, express chemokines and chemokine receptors [7].

Among more than 50 human chemokines, CC-chemokine ligand 2 (CCL2) is of particular importance. CCL2, also known as monocyte chemoattractant protein-1 (MCP-1), belongs to the CC family of chemokines. CCL2 is produced by variety of cell types, not only by tumor cells but also by stromal cells such as monocytes, fibroblasts, and endothelial cells [8]. The activity of CCL2 is mediated through its binding to the receptor CCR2 [9]. CCR2 is a receptor that binds other chemokines, particularly CCL8, CCL7, and CCL13 consistent with their structural similarity to CCL2. This flexibility in chemokine-receptor interaction may lead to different biological functions, depending on the particular chemokine

TABLE 1: Characteristics of breast cancer patients and control group.

Study group		Number of patients	
EXAMINED GROUPS	Breast cancer patients	Ductal adenocarcinoma 100	
	Median age (range)	57 (21-84)	
	Tumor stage	I	34
		II	41
		III and IV	25
	Menopausal status:		
	(i) premenopausal	22	
(ii) postmenopausal	78		
CONTROL GROUPS	Benign breast tumor group	35	
		adenoma 12	
		fibroadenoma 23	
	Median age (range)	39 (21-63)	
	Menopausal status:		
	(i) premenopausal	12	
	(ii) postmenopausal	23	
	Healthy women	35	
	Median age (range)	37 (21-58)	
	Menopausal status:		
(i) premenopausal	15		
(ii) postmenopausal	20		

and receptor pair engaged, or may produce similar effects, suggesting that most of chemokines have redundant or similar functions with other known chemokines [10]. Both CCL2 and its receptor CCR2 have been detected in most tumors, including those of the breast, endometrium, colon, and prostate [11–15].

The aim of the current study was to determine the plasma levels of CCL2, CCR2 and the levels of the commonly accepted tumor marker (CA 15-3) in 3 groups: (1) the breast cancer patients group; (2) the benign breast tumor group; and (3) the control group consisting of healthy women. We evaluated the plasma levels of these markers in different stages of breast cancer. Additionally, we defined the criteria for the diagnosis based on investigated marker set. Obtained data may be helpful in both determining the clinical applicability of the analyzed parameters (separately and in conjunction) in the diagnosis of breast cancer and in the differentiation of its subtypes.

2. Material and Methods

2.1. Human Subjects. Table 1 shows the examined and control groups. The study comprised 100 patients with breast cancer (BC) who were referred to the Department of Oncology, Medical University of Białystok, Poland, between 2015 and 2017. Tumor classification and staging were determined in accordance with the International Union against Cancer Tumor-Node-Metastasis (UICC-TNM) classification in all

cases. Breast cancer histopathology was established in all cases by tissue biopsy of the mammary tumor or after surgery from tumor cancer tissues (all patients with *ductal adenocarcinoma*). Written consent including participants' own statements regarding their medical history (i.e., data related to reproductive history, personal or family history of cancer, general health issues: hospitalization or surgery, and use of medications) and lifestyle habits including smoking was obtained from all the subjects. None of the patients had received chemo- or radiotherapy before blood sample collection. The pretreatment staging procedures included physical and blood examinations, mammography, mammary ultrasound scanning, breast core biopsies, and chest X-rays. In addition, radioisotopic bone scans, the examination of bone marrow aspirates, and CT scans of the brain and chest were performed where necessary.

The control groups included 35 patients with benign breast tumors (*adenoma*, *fibroadenoma*) and 35 healthy, untreated women who underwent mammary gland examination performed by a gynecologist prior to blood sample collection. In addition, mammary ultrasound scanning was performed in all cases. Benign breast tumor histopathology was established in all cases by tissue biopsy of the mammary tumor or after surgery.

We have selected a control group in the best way and exclude women with other diseases that could influence the quality of our research. From the control group we had to exclude people with inflammatory conditions, cardiovascular disorders, and other accompanying diseases. For this reason, the number of patients with benign breast tumor was chosen according to the number of healthy subjects.

The study was approved by the local Ethics Committee (R-I-002/51/2015) and all the patients gave their informed consent for participation in the study.

2.2. Plasma Collection and Storage. Venous blood samples were collected from each patient. Blood was collected into EDTA tubes (S-Monovette, SARSTEDT, Germany), centrifuged 1000 xg for 15 min at 2–8°C to obtain plasma samples, and stored at –85°C until assayed.

2.3. Measurement of CCL2, CCR2, and CA 15-3. The tested parameters (CCL2 and CCR2) were measured with enzyme-linked immunosorbent assay (ELISA) (CCL2-R&D systems, Abingdon, United Kingdom; CCR2-EIAab Science, Wuhan, China), according to the manufacturer's instructions. ELISA system can specifically and selectively detect soluble chemokine receptors [16–18]. Plasma concentration of CA 15-3 was measured by chemiluminescent microparticle immunoassay (CMIA) (Abbott, Chicago, IL, USA). The intra-assay coefficient of variation (CV%) of CA 15-3 is reported to be 2.2% at a mean concentration of 27.0 U/mL, SD=0.6. CCL2 is reported to be 4.7% at a mean concentration of 364 pg/mL, SD=17.1 and CCR2 is reported to be ≤ 7.3%. The inter-assay coefficient of variation (CV%) of CA 15-3 is reported to be 2.6% at a mean concentration of 27.0 U/ml, SD=0.7. CCL2 is reported to be 5.8% at a mean concentration of 352 pg/mL, SD=20.5 and CCR2 to be ≤10.9%. The value of intra- and interassay CVs were calculated by the manufacturers and

TABLE 2: Plasma levels of examined parameters and CA 15-3 in patients with breast cancer and in control groups.

Groups tested	CCL2 (pg/mL)	CCR2 (ng/mL)	CA 15-3 (U/mL)
Breast cancer (median, range)			
Stage I	192.81 (36.68-438.58) ^{b/f}	1.34 (0.11-8.17) ^{a/f}	17.15 (6.20-50.30) ^{a/b/f}
Stage II	227.22 (1.45-1631.48) ^{b/f}	0.93 (0.05-6.16) ^{a/b/f}	17.60 (4.40-48.10) ^{a/b/f}
Stage III and IV	398.55 (99.12-592.30) ^{a/b/c/d/f}	0.92 (0.34-3.81) ^{a/b/f}	27.75 (8.90-250.00) ^{a/b/c/d/f}
Total group	228.34 (1.45-1631.48) ^{a/b/f}	0.96 (0.05-8.17) ^{a/f}	19.20 (4.40-250.00) ^{a/b/f}
Control groups (median, range)			
Benign breast tumor	118.64 (37.37-489.88) ^e	1.82 (0.05-7.67) ^e	14.00 (5.20-20.70)
Healthy women	155.17 (70.58-440.06)	3.45 (0.84-22.60)	13.40 (6.30-28.40)
Total control group	130.64 (37.37-489.88)	2.30 (0.05-22.60)	13.60 (5.20-28.40)

Notes:^astatistically significant when patients with BC compared with healthy women. ^bStatistically significant when patients with BC compared with benign breast tumor group. ^cStatistically significant when patients with BC stages III and IV compared with patients with BC stage I. ^dStatistically significant when patients with BC stages III and IV compared with patients with BC stage II. ^eStatistically significant when patients with benign breast tumor compared with healthy women. ^fStatistically significant when patients with BC compared with total control group.

enclosed in the reagent kits. The assay does not exhibit cross-reactivity or interference with numerous human cytokines and other growth factors. Duplicate samples were assessed for each patient.

2.4. Statistical Analysis. Statistical analysis was performed using STATISTICA 12.0 (StatSoft, Tulsa, OK, USA). Preliminary statistical analysis (using the Shapiro-Wilk test) revealed that the tested parameters and tumor marker levels did not follow a normal distribution. Consequently, the statistical analysis between the groups was performed by using the Mann-Whitney U test, the Kruskal-Wallis test, and a multivariate analysis of various data by the post hoc Dwass-Steel-Critchlow-Fligner test. Statistically significant differences were defined as comparisons resulting in $p < 0.05$. Diagnostic sensitivity (SE) and specificity (SP) were calculated. The *cut-off* values were calculated by Youden's index (as a criterion for selecting the optimum cut-off point) and each of the tested parameters was as follows: CCL2: 183.19 pg/mL; CCR2: 1.49 ng/mL; and CA 15-3: 16.85 U/mL. In the analyses of both diagnostic performance (SE, SP) and ROC curve, healthy subjects and benign breast tumor group were used as a control group. The construction of the ROC curves was performed using the GraphRoc program for Windows (Windows, Royal, AR, USA) and the areas under the ROC curve (AUC) were calculated to evaluate the diagnostic accuracy and to compare AUC for all tested parameters separately and in combination with the commonly used tumor marker (CA 15-3).

3. Results

Table 2 presents the median and the range of plasma levels of the investigated parameters and CA 15-3 in examined groups. The median levels of CCL2 and CA 15-3 in the entire group of BC were significantly higher than in the healthy patients group ($p < 0.05$ in all cases). Moreover, the median levels of CCR2 in the group of BC were significantly lower when compared to the healthy subjects ($p < 0.001$). We also noticed that the median of CCL2 levels in stages III and IV

was significantly higher when compared to healthy group ($p < 0.001$). In the case of CCR2, the median of plasma levels in all stages of BC was significantly lower when compared to healthy subjects ($p < 0.001$ in all cases). However, the concentrations of commonly accepted tumor marker (CA 15-3) in all stages of BC were significantly higher than in the healthy volunteers.

The statistical test also showed the similar relationship between the entire group of BC and patients with benign breast tumors. The concentrations of CCL2 and CA 15-3 in the group of BC were significantly higher than in the benign breast tumors ($p < 0.001$). We also observed that the median of CCL2 and commonly accepted tumor marker (CA 15-3) levels in all stages of BC were significantly higher when compared to benign breast tumors. However, the concentration of CCR2 in stages II, III, and IV of BC was significantly lower when compared to the patients with benign breast tumors.

The CCL2 ELISA data showed that plasma levels of CCL2 were significantly increased in the entire BC group compared to the total control group (benign breast tumor and healthy subjects) ($p < 0.001$), similarly as the median levels of CA 15-3 ($p < 0.001$). However, the concentration of CCR2 in patients with breast cancer was significantly lower than entire control group ($p < 0.001$). The same relationships were observed in all stages of BC ($p < 0.05$ in all cases).

Furthermore, the concentration of CCL2 in BC group increases with advancing tumor stage. We detected significantly higher plasma levels of CCL2 and commonly accepted tumor marker CA 15-3 in the comparison of stages III and IV to stage I ($p < 0.001$) and to stage II ($p = 0.001$).

We also noticed statistical differences between the concentrations of CCL2 and CCR2 in patients with benign breast tumors and healthy controls ($p < 0.05$). However, CA 15-3 did not show statistical difference in plasma levels between two studied control groups. This demonstrates possible chance of using CCL2 and CCR2 in differentiation between benign breast tumor and healthy women.

Table 3 shows the diagnostic criteria: sensitivity (SE), specificity (SP), predictive value of a positive test result (PPV),

TABLE 3: Diagnostic criteria of tested parameters and in combined analysis with CA 15-3 in breast cancer patients.

Tested parameters	Diagnostic criteria (%)	Breast cancer			
		Stage I	Stage II	Stage III/IV	Total group
CCL2	SE	58.82	58.54	86.36	64.95
	SP	73.02	73.02	73.02	73.02
	PPV	54.05	58.54	52.78	78.75
	NPV	76.67	73.02	93.88	57.50
CCR2	SE	55.88	58.50	77.27	61.86
	SP	73.02	73.02	73.02	73.02
	PPV	52.78	58.54	50.00	77.92
	NPV	75.41	73.02	90.20	55.42
CA 15-3	SE	50.00	53.66	86.36	59.79
	SP	85.71	85.71	85.71	85.71
	PPV	65.38	70.97	67.86	86.57
	NPV	76.06	73.97	94.74	58.06
CCL2+ CA 15-3	SE	73.53	70.73	95.45	77.32
	SP	63.49	63.49	63.49	63.49
	PPV	52.08	55.77	47.73	76.53
	NPV	81.63	76.92	97.56	64.52
CCR2+ CA 15-3	SE	70.59	82.93	86.36	79.38
	SP	65.08	65.08	65.08	65.08
	PPV	52.17	60.71	46.34	77.78
	NPV	80.39	85.42	93.18	67.21
CCL2+CCR2+ CA 15-3	SE	85.29	92.68	95.45	90.72
	SP	44.44	44.44	44.44	44.44
	PPV	45.31	52.05	37.50	71.54
	NPV	84.85	90.32	96.55	75.68

and predictive value of a negative test result (NPV) in breast cancer patients. The sensitivity of the tested parameters in the total cancer group was higher for CCL2 (64.95%) than for CCR2 (61.86%) and higher than for routinely used tumor marker CA 15-3 (59.79%). A maximum diagnostic sensitivity (90.72%) was obtained for the combination of CCL2 and CCR2 with CA 15-3. Among all the parameters, the highest SE in early stages of cancer was observed for CCL2 (in stage I of BC: 58.82%, in stage II: 58.54%). The combined use of the tested parameters with CA 15-3 resulted in an increase of SE in every stage of BC. The diagnostic SP of the tested parameters was the highest for CA 15-3 (85.71%) in the entire group of breast cancer patients. Moreover, in all stages of cancer, CA 15-3 has the highest specificity (85.71% in all cases).

Among the examined parameters, the predictive value of a positive test result in the group of BC patients was the highest for CCL2 (78.75%) in comparison to CCR2 (77.92%) but was lower than PPV for CA 15-3 (86.57%). The highest PPV values in all stages of cancer were observed for CA 15-3 (65.38%, 70.97%, and 67.86%, respectively). The predictive value of a negative test result in the group of BC was higher for CCL2 (57.50%) than for CCR2 (55.42%) and was slightly lower than NPV for CA 15-3 (58.06%). The combination of CCL2 or CCR2 with antigen CA 15-3 resulted in an increase in the NPV. The highest NPV values in other stages of BC (II, III, and IV) were observed for CA 15-3 (70.97% and 94.74%, respectively). The combination of CCL2 or CCR2

with antigen CA 15-3 resulted in an increase in the NPV in all stages of cancer.

The relationship between the diagnostic SE and SP is illustrated by the ROC curve (Table 4). The AUC indicates the possible clinical usefulness of a tumor marker and its diagnostic power. We have noticed that the AUC for CA 15-3 (0.7354) in entire group of BC was slightly larger than for CCR2 (0.7304) and CCL2 (0.7154). Moreover, areas under the ROC curve for all parameters were significantly larger in comparison to AUC=0.5 (borderline of the diagnostic usefulness of the test) ($p<0.001$ in all cases). The combination of CCL2 or CCR2 with CA 15-3 resulted in an increase in areas under the ROC curve in all cases (0.7771 and 0.7879; respectively). A maximum range in the entire BC group was obtained for the combination of all the studies parameters (0.8271; $p<0.001$) (Figure 1).

The AUC of CCL2 presented noticeable increase with the BC stage advancement, in parallel to CA 15-3 AUC. In stage I of BC the highest AUC of all the tested parameters was presented by CCL2 (0.6604) and it was the parameter which was significantly larger in comparison to AUC= 0.5 ($p=0.0097$), correspondingly to CCR2 ($p=0.0074$) and CA 15-3 ($p=0.0266$) (Figure 2). In stage II of BC the highest AUC of all tested parameters was observed in CCR2 (0.7768; $p<0.001$); importantly it was higher than that of CA 15-3 (0.7163). Moreover, the AUCs for CCL2 and CCR2, CA 15-3, were significantly higher in comparison to AUC =0.5

TABLE 4: Diagnostic criteria of ROC curve for tested parameters and CA 15-3.

Tested parameters	AUC	SE	95% C.I. (AUC)	p (AUC=0.5)
<i>ROC criteria in breast cancer (total group)</i>				
CCL2	0.7154	0.0410	0.635-0.796	<0.001
CCR2	0.7304	0.0412	0.650-0.811	<0.001
CA 15-3	0.7354	0.0389	0.659-0.812	<0.001
CCL2+ CA 15-3	0.7771	0.0363	0.706-0.848	<0.001
CCR2+ CA 15-3	0.7879	0.0349	0.719-0.856	<0.001
CCL2+ CCR2+ CA 15-3	0.8271	0.0316	0.765-0.889	<0.001
<i>ROC criteria in breast cancer (I stage)</i>				
CCL2	0.6604	0.0620	0.539-0.782	0.0097
CCR2	0.6564	0.0584	0.542-0.771	0.0074
CA 15-3	0.6452	0.0655	0.517-0.774	0.0266
CCL2+ CA 15-3	0.6783	0.0620	0.557-0.800	0.0040
CCR2+ CA 15-3	0.7031	0.0606	0.584-0.822	<0.001
CCL2+ CCR2+ CA 15-3	0.7367	0.0575	0.624-0.849	<0.001
<i>ROC criteria in breast cancer (II stage)</i>				
CCL2	0.6615	0.0625	0.539-0.784	0.0097
CCR2	0.7768	0.0479	0.683-0.871	<0.001
CA 15-3	0.7163	0.0551	0.608-0.824	<0.001
CCL2+ CA 15-3	0.7575	0.0541	0.652-0.863	<0.001
CCR2+ CA 15-3	0.7940	0.0448	0.706-0.882	<0.001
CCL2+ CCR2+ CA 15-3	0.8317	0.0416	0.750-0.913	<0.001
<i>ROC criteria in breast cancer (III and IV stages)</i>				
CCL2	0.8983	0.0417	0.817-0.980	<0.001
CCR2	0.7605	0.0570	0.649-0.872	<0.001
CA 15-3	0.9098	0.0426	0.826-0.993	<0.001
CCL2+ CA 15-3	0.9654	0.0184	0.929-1.001	<0.001
CCR2+ CA 15-3	0.9076	0.0437	0.822-0.993	<0.001
CCL2+ CCR2+ CA 15-3	0.9582	0.0248	0.909-1.007	<0.001

p: statistically significantly larger AUC compared to AUC=0.5.

($p=0.0097$; $p=0.0074$; $p=0.0266$; respectively) (Figure 3). In stages III and IV of BC the highest AUC from all the tested parameters was observed for CA 15-3 (0.9098; $p<0.001$) and of note, it was slightly higher than for CCR2 (0.8983; $p<0.001$). Additionally, the AUCs for CCL2 and CCR2, CA 15-3, were significantly larger in comparison to AUC =0.5 ($p<0.001$ in all cases). The combination of CCL2 or CCR2 with antigen CA 15-3 resulted in an increase in the AUCs in all cases (Figure 4).

4. Discussion

Recent studies have showed that chemokines family and their receptors play crucial roles in the development of breast cancer, including tumor growth, migration, and angiogenesis [19–21]. Moreover, they influence the infiltration of leukocytes into any tissue, including tumors [22]. Out of all the known chemokines, breast cancer cells express the CCL2 chemokine, the receptor of which is CCR2 [23]. CCL2 may promote breast cancer cell development by many mechanisms. CCL2 mainly binds to CCR2 receptor, but other receptors including CCR4 can also be involved in activation of signaling pathways [20]. As an important component in

the tumor microenvironment, leukocytes in cancer stroma support tumor growth and facilitate metastatic dissemination [24]. CCL2 recruits CCR2-expressing inflammatory monocytes to facilitate breast tumor metastasis [25]. However, CCL2-CCR4 signaling also regulates the migration and infiltration of T regulatory cells to tumor sites [26].

CCL2 (MCP-1) is proinflammatory chemokine; therefore, studies have demonstrated its overexpression or increased serum levels and resultant promotion of tumor growth in breast [27–29]. The data presented here reveals that breast cancer patients have a significantly higher level of plasma CCL2 and commonly used tumor marker CA 15-3 than control groups. Moreover, the concentration of CCR2 in the group of BC was significantly lower when compared to the healthy subjects. There have been studies showing that MCP-1 median (range) serum level was markedly elevated in cancer patients versus controls [30]. In the study by Dwyer et al. [31] the ELISA method was used to detect MCP-1 serum levels in 125 BC patients and 86 age-matched controls. Results of the study revealed that BC patients showed higher levels of MCP-1, but the difference was not statistically significant. One of the findings in our study was that of a statistically significantly

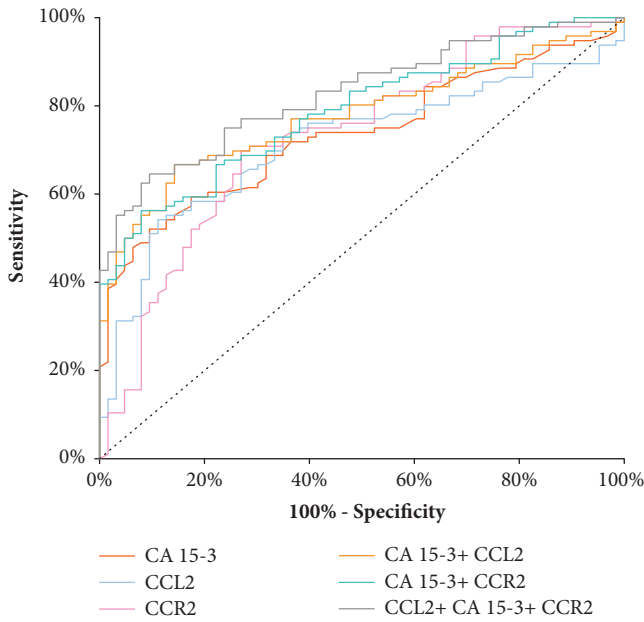


FIGURE 1: Diagnostic criteria of ROC curve for tested parameters and in combination with CA 15-3 in entire BC group.

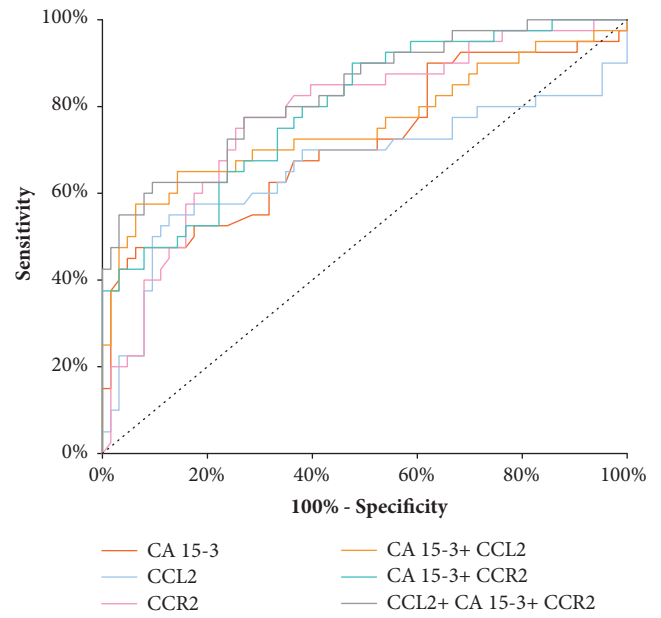


FIGURE 3: Diagnostic criteria of ROC curve for tested parameters and in combination with CA 15-3 in stage II of BC.

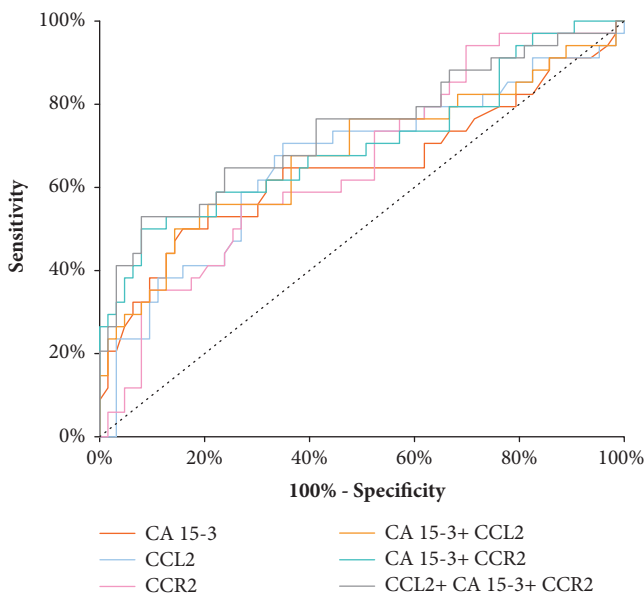


FIGURE 2: Diagnostic criteria of ROC curve for tested parameters and in combination with CA 15-3 in stage I of BC.

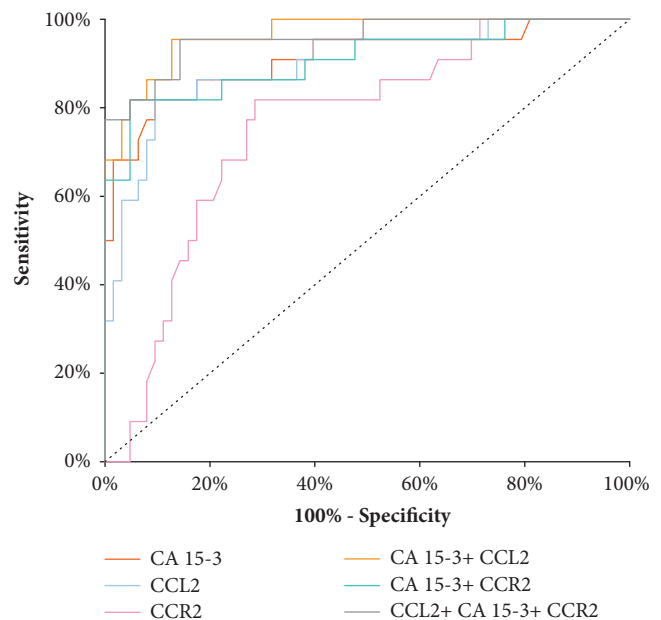


FIGURE 4: Diagnostic criteria of ROC curve for tested parameters and in combination with CA 15-3 in stage III and IV of BC.

increase of plasma CCL2 concentration in breast cancer patients compared to benign breast tumors. We are able to establish CCL2 as differentiation maker between malignant and benign breast diseases. Additionally, CCL2 and CCR2 levels may be useful in differentiation between benign breast tumor and healthy women. The work of Lebrecht and her coworkers [11] in the 2004 show the analysis of serum MCP-1 level in patients with invasive breast cancer, ductal carcinoma *in situ*, benign breast lesions, and healthy women.

The authors failed to show any significant differences in the serum chemokine levels of these four groups.

However, the limitations of this study (smaller number of patients in control groups than patients with breast cancer) make it important to confirm our results on a larger group of these patients but the numbers of healthy subjects and patients with benign breast cancer are large enough for regular statistic evaluation.

Interestingly, we observed significant increase of CCL2 serum levels in cancer patients based on stage of disease compared with entire control group. In some studies, elevated expression or serum levels of CCL2 have been strongly associated with advanced stage of disease in BC [30, 32–34]. There is some evidence to suggest that high levels of tumor-associated macrophages (TAMs) correlate with poor prognosis in breast cancer, and it has been suggested that the relationship between high levels of CCL2 chemokine and poor prognosis is mediated by the recruitment of TAMs into the tumor microenvironment [25, 35]. TAMs contribute to tumor progression also by producing chemokine CCL2, which leads to the elevated angiogenic profile attributed to this chemokine [36, 37].

In the present study, we defined the diagnostic criteria (sensitivity and specificity) of all tested parameters. The ability of a test to correctly classify an individual as diseased is called the diagnostic sensitivity. In our study, the sensitivity of CCL2 was the highest of all the tested parameters (64.95%) in entire BC group. Additionally, a maximum diagnostic sensitivity (90.72%) was obtained for the combination of CCL2 and CCR2 with CA 15-3. Specificity is the ability of a test to correctly classify an individual as disease-free. Our results showed that the diagnostic specificity was the highest for CA 15-3 (85.71%). According to our knowledge, there are no studies of the diagnostic criteria (sensitivity and specificity) of CCL2 and CCR2 serum or plasma levels in breast cancer patients. The results of the study on the role of CCL2 in various cancers indicated that specificity and sensitivity were 80.00% and 85.00% for CCL2 to differentiate CNS (central nervous system) tumor patients from nontumoral individuals [38]. In our previous study in BC [39], which comprised other cytokines (M-CSF and VEGF) in breast cancer patients, the highest SE value was found for VEGF (76.25%) and it was higher than M-CSF (60%).

The ROC curve illustrates the relationship between diagnostic sensitivity and specificity. The area under the ROC curve indicates the clinical applicability of a tumor marker. To date, there are no reports of the diagnostic usefulness of CCL2 and CCR2 serum or plasma levels in breast cancer patients. According to this study, the ROC area of CA 15-3 (0.7354) was the largest of all the tested parameters in the group of BC and slightly larger than for CCR2 (0.7304) and CCL2 (0.7154). Moreover, ROC curve analysis using the combination CCL2+CCR2+CA 15-3 (AUC = 0.8271) showed an interesting improvement in BC diagnosis as compared with CCL2 or CCR2 alone. In the paper by Koper et al. [38], the area under the ROC curve for CCL2 (AUC=0.793) in differentiation between CNS tumor patients and nontumoral individuals was slightly larger than ours [38]. The results obtained from the experiments conducted with pleural liquids showed that AUC value for CCL2 was 0.7912 to differentiate MPM (malignant pleural mesothelioma) from ADCA (adenocarcinomas) and BPE (benign pleural effusions) [40]. The right direction of the diagnostic power assessment is a combined analysis of the tested parameters, which was demonstrated also in our previous studies on other cytokines (M-CSF, VEGF) in breast cancer patients [41, 42]. In our previous study in BC [39], which comprised other cytokines

(M-CSF and VEGF) in breast cancer patients, the highest AUC value was found for VEGF (0.729) and it was higher than M-CSF (0.645). We have verified that CCL2 and CCR2 may be more applicable and useful than M-CSF. However, the ROC area of VEGF was larger than CCL2, and the same relationship was observed in our previous papers [41, 43]

The complete and current state of knowledge leads to the conclusion that increased levels of chemokines in plasma may help tumor cells to migrate and invade. In this study, we are trying to draw attention to a CCL2 chemokine and its receptor CCR2, the levels of which are statistically significantly different in breast cancer patients compared to control groups. Additionally, CCL2 and CCR2 levels may be useful in differentiation between benign breast tumor and healthy women. The area under ROC curve was the highest for the combination of CCL2 and CCR2 with commonly accepted tumor marker, which indicates a possible clinical significance of plasma CCL2 and CCR2 measurements in the diagnosis of BC. The findings of this study suggest there may be applicability of CCL2 and CCR2 in diagnosis of BC patients, particularly in conjunction with CA 15-3.

Data Availability

The data used to support the findings of this study are available from the corresponding author upon request.

Ethical Approval

The study was approved by the local Ethics Committee in Medical University of Bialystok (R-I-002/51/2015). This work was conducted in accordance with the Declaration of Helsinki (1964).

Consent

All the patients gave their informed consent for study participation.

Conflicts of Interest

The authors declare that they have no conflicts of interest.

Acknowledgments

This research was financed by grants for Medical University of Bialystok (N/ST/MN/17/001/2230; N/ST/ZB/17/001/2230; and N/ST/ZB/17/002/2230) from the Polish Ministry of Science and Higher Education.

References



- [1] M. Ghoncheh, Z. Pournamdar, and H. Salehiniya, "Incidence and Mortality and Epidemiology of Breast Cancer in the World," *Asian Pacific Journal of Cancer Prevention*, vol. 17, no. S3, pp. 43–46, 2016.
- [2] L. A. Torre, F. Bray, R. L. Siegel, J. Ferlay, and J. Lortet-Tieulent, "Global cancer statistics, 2012," *A Cancer Journal for Clinicians*, vol. 65, no. 2, pp. 87–108, 2015.

- [3] S. J. Allen, S. E. Crown, and T. M. Handel, "Chemokine: receptor structure, interactions, and antagonism," *Annual Review of Immunology*, vol. 25, pp. 787–820, 2007.
- [4] A. Zlotnik and O. Yoshie, "The Chemokine Superfamily Revisited," *Immunity*, vol. 36, no. 5, pp. 705–712, 2012.
- [5] F. R. Balkwill, "The chemokine system and cancer," *The Journal of Pathology*, vol. 226, no. 2, pp. 148–157, 2012.
- [6] F. Balkwill and A. Mantovani, "Inflammation and cancer: back to Virchow?" *The Lancet*, vol. 357, no. 9255, pp. 539–545, 2001.
- [7] L. M. Coussens and Z. Werb, "Inflammation and cancer," *Nature*, vol. 420, no. 6917, pp. 860–867, 2002.
- [8] S. L. Deshmane, S. Kremlev, S. Amini, and B. E. Sawaya, "Monocyte chemoattractant protein-1 (MCP-1): an overview," *Journal of Interferon & Cytokine Research*, vol. 29, no. 6, pp. 313–326, 2009.
- [9] L. Borsig, M. J. Wolf, M. Roblek, A. Lorentzen, and M. Heikenwalder, "Inflammatory chemokines and metastasis-Tracing the accessory," *Oncogene*, vol. 33, no. 25, pp. 3217–3224, 2014.
- [10] D. Rossi and A. Zlotnik, "The biology of chemokines and their receptors," *Annual Review of Immunology*, vol. 18, pp. 217–243, 2000.
- [11] A. Lebrecht, C. Grimm, T. Lantzsich et al., "Monocyte chemoattractant protein-1 serum levels in patients with breast cancer," *Tumor Biology*, vol. 25, no. 1-2, pp. 14–17, 2004.
- [12] R. Attar, B. Agachan, S. B. Kuran et al., "Association of CCL2 and CCR2 gene variants with endometrial cancer in Turkish women," *In Vivo*, vol. 24, no. 2, pp. 243–248, 2010.
- [13] A. M. Szczepanik, M. Siedlar, M. Szura et al., "Preoperative serum chemokine (C-C motif) ligand 2 levels and prognosis in colorectal cancer," *Polskie Archiwum Medycyny Wewnętrznej*, vol. 125, no. 6, pp. 443–451, 2015.
- [14] E. Chun, S. Lavoie, M. Michaud et al., "CCL2 Promotes colorectal carcinogenesis by enhancing polymorphonuclear myeloid-derived suppressor cell population and function," *Cell Reports*, vol. 12, no. 2, pp. 244–257, 2015.
- [15] R. D. Loberg, L. L. Day, J. Harwood et al., "CCL2 is a potent regulator of prostate cancer cell migration and proliferation," *Neoplasia*, vol. 8, no. 7, pp. 578–586, 2006.
- [16] A. Tsimanis, A. Kalinkovich, and Z. Bentwich, "Soluble chemokine CCR5 receptor is present in human plasma," *Immunology Letters*, vol. 96, no. 1, pp. 55–61, 2005.
- [17] D. A. Klaus, R. Seemann, F. Roth-Walter et al., "Plasma levels of chemokine ligand 20 and chemokine receptor 6 in patients with sepsis," *European Journal of Anaesthesiology*, vol. 33, no. 5, pp. 348–355, 2016.
- [18] M. Łukaszewicz-Zajac, B. Mroczko, M. Kozłowski, and M. Szmitkowski, "The Serum Concentrations of Chemokine CXCL12 and Its Specific Receptor CXCR4 in Patients with Esophageal Cancer," *Disease Markers*, vol. 2016, Article ID 7963895, 7 pages, 2016.
- [19] S. Ali and G. Lazennec, "Chemokines: novel targets for breast cancer metastasis," *Cancer and Metastasis Reviews*, vol. 26, no. 3-4, pp. 401–420, 2007.
- [20] G. Soria and A. Ben-Baruch, "The inflammatory chemokines CCL2 and CCL5 in breast cancer," *Cancer Letters*, vol. 267, no. 2, pp. 271–285, 2008.
- [21] L. V. Rhodes, S. P. Short, N. F. Neel et al., "Cytokine receptor CXCR4 mediates estrogen-independent tumorigenesis, metastasis, and resistance to endocrine therapy in human breast cancer," *Cancer Research*, vol. 71, no. 2, pp. 603–613, 2011.
- [22] G. Lazennec and A. Richmond, "Chemokines and chemokine receptors: new insights into cancer-related inflammation," *Trends in Molecular Medicine*, vol. 16, no. 3, pp. 133–144, 2010.
- [23] S. M. Potter, R. M. Dwyer, M. C. Hartmann et al., "Influence of stromal-epithelial interactions on breast cancer in vitro and in vivo," *Breast Cancer Research and Treatment*, vol. 131, no. 2, pp. 401–411, 2012.
- [24] D. Hanahan and L. M. Coussens, "Accessories to the crime: functions of cells recruited to the tumor microenvironment," *Cancer Cell*, vol. 21, no. 3, pp. 309–322, 2012.
- [25] B. Qian, J. Li, H. Zhang et al., "CCL2 recruits inflammatory monocytes to facilitate breast-tumour metastasis," *Nature*, vol. 475, no. 7355, pp. 222–225, 2011.
- [26] H. Nishikawa and S. Sakaguchi, "Regulatory T cells in tumor immunity," *International Journal of Cancer*, vol. 127, no. 4, pp. 759–767, 2010.
- [27] G. Soria, N. Yaal-Hahoshen, E. Azenshtein et al., "Concomitant expression of the chemokines RANTES and MCP-1 in human breast cancer: a basis for tumor-promoting interactions," *Cytokine*, vol. 44, no. 1, pp. 191–200, 2008.
- [28] H. Saji, M. Koike, T. Yamori et al., "Significant correlation of monocyte chemoattractant protein-1 expression with neovascularization and progression of breast carcinoma," *Cancer*, vol. 92, no. 5, pp. 1085–1091, 2001.
- [29] M. Mestdagt, M. Polette, G. Buttice et al., "Transactivation of MCP-1/CCL2 by β -catenin/TCF-4 in human breast cancer cells," *International Journal of Cancer*, vol. 118, no. 1, pp. 35–42, 2006.
- [30] Z. A. Dehqanzada, C. E. Storrer, M. T. Hueman et al., "Assessing serum cytokine profiles in breast cancer patients receiving a HER2/neu vaccine using luminex technology," *Oncology Reports*, vol. 17, no. 3, pp. 687–694, 2007.
- [31] R. M. Dwyer, S. M. Potter-Beirne, K. A. Harrington et al., "Monocyte chemotactic protein-1 secreted by primary breast tumors stimulates migration of mesenchymal stem cells," *Clinical Cancer Research*, vol. 13, no. 17, pp. 5020–5027, 2007.
- [32] G. Luboshits, S. Shina, O. Kaplan et al., "Elevated expression of the CC chemokine regulated on activation, normal T cell expressed and secreted (RANTES) in advanced breast carcinoma," *Cancer Research*, vol. 59, no. 18, pp. 4681–4687, 1999.
- [33] T. Valković, K. Lučin, M. Krstulja, R. Dobi-Babić, and N. Jonjić, "Expression of monocyte chemotactic protein-1 in human invasive ductal breast cancer," *Pathology - Research and Practice*, vol. 194, no. 5, pp. 335–340, 1998.
- [34] T. Valković, D. Fučkar, S. Štifter et al., "Macrophage level is not affected by monocyte chemotactic protein-1 in invasive ductal breast carcinoma," *Journal of Cancer Research and Clinical Oncology*, vol. 131, no. 7, pp. 453–458, 2005.
- [35] J. M. Low-Marchelli, V. C. Ardi, E. A. Vizcarra, N. van Rooijen, J. P. Quigley, and J. Yang, "Twist1 induces CCL2 and recruits macrophages to promote angiogenesis," *Cancer Research*, vol. 73, no. 2, pp. 662–671, 2013.
- [36] L. M. Arendt, J. McCready, P. J. Keller et al., "Obesity promotes breast cancer by CCL2-mediated macrophage recruitment and angiogenesis," *Cancer Research*, vol. 73, no. 19, pp. 6080–6093, 2013.
- [37] E. C. Keeley, B. Mehrad, and R. M. Strieter, "Chemokines as mediators of tumor angiogenesis and neovascularization," *Experimental Cell Research*, vol. 317, no. 5, pp. 685–690, 2011.
- [38] O. M. Koper, J. Kamińska, K. Sawicki et al., "Cerebrospinal fluid and serum IL-8, CCL2, and ICAM-1 concentrations in

- astrocytic brain tumor patients,” *Irish Journal of Medical Science*, pp. 1–9, 2017.
- [39] M. Zajkowska, E. K. Głażewska, G. E. Będkowska, P. Chorąży, M. Szmitkowski, and S. Ławicki, “Diagnostic Power of Vascular Endothelial Growth Factor and Macrophage Colony-Stimulating Factor in Breast Cancer Patients Based on ROC Analysis,” *Mediators of Inflammation*, vol. 2016, Article ID 5962946, 8 pages, 2016.
- [40] C. Blanquart, F. Gueugnon, J.-M. Nguyen et al., “CCL2, galectin-3, and SMRP combination improves the diagnosis of mesothelioma in pleural effusions,” *Journal of Thoracic Oncology*, vol. 7, no. 5, pp. 883–889, 2012.
- [41] S. Ławicki, M. Zajkowska, E. K. Głażewska, G. E. Będkowska, and M. Szmitkowski, “Plasma levels and diagnostic utility of VEGF, MMP-9, and TIMP-1 in the diagnosis of patients with breast cancer,” *OncoTargets and Therapy*, vol. 9, pp. 911–919, 2016.
- [42] S. Ławicki, M. Zajkowska, E. K. Głażewska, G. E. Będkowska, and M. Szmitkowski, “Plasma levels and diagnostic utility of M-CSF, MMP-2 and its inhibitor TIMP-2 in the diagnostics of breast cancer patients,” *Clinical Laboratory*, vol. 62, no. 9, pp. 1661–1669, 2016.
- [43] S. Ławicki, M. Zajkowska, E. K. Głażewska, G. E. Będkowska, and M. Szmitkowski, “Plasma levels and diagnostic utility of VEGF, MMP-2 and TIMP-2 in the diagnostics of breast cancer patients,” *Biomarkers*, vol. 22, no. 2, pp. 157–164, 2017.

Research Article

Mutational Profile of Metastatic Breast Cancer Tissue in Patients Treated with Exemestane Plus Everolimus

Claudia Omarini ¹, **Maria Elisabetta Filieri**,¹ **Stefania Bettelli**,²
Samantha Manfredini,² **Shaniko Kaleci**,² **Cecilia Caprera**,² **Cecilia Nasso**,¹
Monica Barbolini,¹ **Giorgia Guaitoli**,¹ **Luca Moschetti**,¹ **Antonino Maiorana**,²
Pier Franco Conte,³ **Stefano Cascinu**,¹ and **Federico Piacentini** ¹

¹Division of Medical Oncology, Department of Medical and Surgical Sciences for Children & Adults, University Hospital of Modena, Italy

²Division of Pathological Anatomy, Department of Diagnostic, Clinical Medicine and Public Health, University Hospital of Modena, Italy

³Department of Surgery, Oncology, and Gastroenterology, University of Padova, Italy

Correspondence should be addressed to Claudia Omarini; claudia.omarini@gmail.com

Received 7 March 2018; Accepted 10 July 2018; Published 24 July 2018

Academic Editor: Franco M. Buonaguro

Copyright © 2018 Claudia Omarini et al. This is an open access article distributed under the Creative Commons Attribution License, which permits unrestricted use, distribution, and reproduction in any medium, provided the original work is properly cited.

Background. Everolimus has been shown to overcome endocrine resistance in hormone receptor positive advanced breast cancer patients. Predictive biomarkers of everolimus efficacy have been investigated in primary breast cancer tissue without finding univocal results. The goal of this study was to investigate the mutational burden in the metastatic site of endocrine-resistant tumors treated with everolimus plus exemestane. **Patients and Methods.** Mass Array Sequenom platform was used to analyse genetic status of 18 cancer-related genes in 25 archival tumor specimens from metastatic lesions and available primary matched breast cancer tissue of patients treated with everolimus and exemestane for advanced disease. An exploratory analysis of everolimus efficacy in terms of progression free survival benefit and single gene mutation was carried out. **Results.** The overall detection rate of mutation was 30% and 38% from metastatic and primary breast cancer samples, respectively. AKT1^{E17K} was the most frequent mutated gene. No primary breast cancer and matched relapse maintained the same mutation profile. Considering molecular pathways, the most of the genes belong to PI3K pathway (AKT1^{E17K}, PI3KCA^{E545K}, and KIT^{G565R,S709F}). In patients with detected mutations in breast and/or recurrence tissue the median PFS was 5,6 months while in the subgroup of patients with no mutations the median PFS was 7,5 months. **Conclusions.** The mutational status of breast cancer recurrence allows the identification of some genes potentially correlating tumor response/resistance to everolimus. The most frequently mutated genes were involved in the PI3K/AKT/mTOR pathway highlighting that the deregulation of this pathway in the relapse plays a crucial role in the mechanisms of everolimus resistance/sensitivity. Owing to the small sample size and the retrospective nature of the study, these correlations need to be validated in a large prospective study.

1. Introduction

Breast cancer (BC) is the most common malignant tumor in women. More than 70% of BCs are hormone receptor positive (HR+) and human epidermal growth factor receptor 2 negative (HER2-) and potentially benefit from endocrine therapies [1]. However, approximately 25% of these tumors fail to respond to hormonal treatment because of the *novo* or acquired resistance [2]. In the last decade, new targeted

therapies have been investigated, with the aim of improving treatment efficacy in patients progressed on endocrine therapy. The double-blinded randomized placebo control, phase III BOLERO-2 study, demonstrated that everolimus plus exemestane improved progression free survival (PFS) compared with exemestane alone in HR+ HER2- advanced BC that recurred or progressed during/after nonsteroidal aromatase inhibitors [3].

Actually, the main challenge is the identification of biomarkers able to predict which patients can benefit from the addition of targeted agents (such as everolimus) to hormonal treatment. A large number of preclinical and clinical studies tried to identify predictive biomarkers of everolimus sensitivity in endocrine resistance population. Several pre-clinical analyses have suggested how the presence of mutation in PI3KCA/AKT/mTOR (*phosphatidylinositol 3-kinase/protein kinase B/mammalian target of rapamycin*) pathway as well as PTEN (*phosphatase and tensin homolog*) gene loss detected on primary BC tissue correlates with everolimus benefit [4, 5]. However, the following clinical trials in BC patients did not confirm the correlation between PI3KCA/PTEN status and clinical response [6–8]. This discordance could be in part justified by the different mutational status between primary tumors and metastatic site. To the best of our knowledge, there are no data regarding the gene mutation status in metastatic tissue and tumor sensitivity to everolimus.

The main purpose of this study was to investigate the mutational burden in the metastatic site of endocrine-resistant patients treated with everolimus plus exemestane in our Institution. We used a panel of 18 genes known to be involved in the mechanism of endocrine and targeted treatments resistance. Moreover, we analysed the gene mutation status of the available matched primary tumors.

2. Materials and Methods

2.1. Patient Population and Samples. We retrospectively identified fifty patients with HR+ HER2- metastatic BC progressed on/after endocrine therapies and treated with exemestane plus everolimus in routine clinical practice at the Modena Cancer Centre. All these patients wrote an informed consent to study enrolment. Clinical and pathological characteristics were collected from informatic archives. PFS on everolimus and exemestane was defined as the time elapsed between treatment initiation and first documented progression disease/death. Thirty-one patients performed a biopsy of the local or distant recurrence; twenty-five of these patients had stored paraffin blocks of metastatic tissue suitable for gene analysis. In nineteen cases, the matched primary BC was available too (Figure 1). Metastatic site biopsy was performed before starting the combination treatment in all the patients.

2.2. Gene Analysis. Gene analysis was performed in Molecular Biology Laboratory of Modena Pathology Department. DNA was extracted from formalin-fixed and paraffin-embedded (FFPE) metastatic and primary BC tissues. The FFPE tissues were cut and stained with haematoxylin and eosin and a pathologist selected sections containing more than 30 % tumor cells. Genomic DNA was isolated from unstained 10 μm -sections using QIAamp DNA Mini kit (QIAGEN). The DNA concentration in the samples was quantified using a spectrophotometer TrineanXpose and they were diluted to a final concentration of 20 $\text{ng}/\mu\text{l}$. DNA samples were analysed by OncoCarta v2.0 panel using Mass Array Sequenom platform following the manufacturer's protocols (<http://agenabio.com>). This panel is able to detect 152

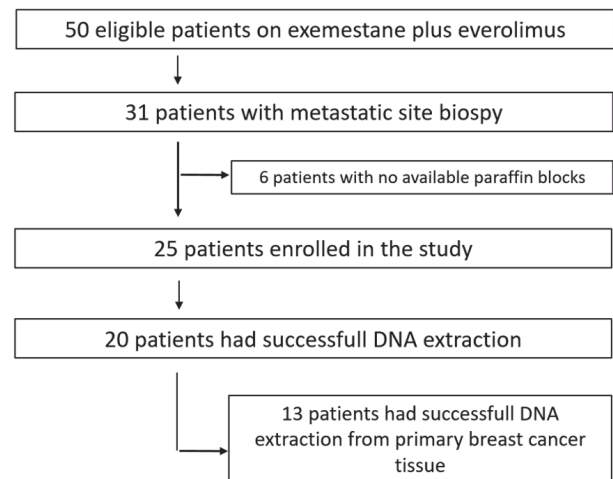


FIGURE 1: Flowchart of the study population.

somatic mutations across 18 oncogenes and tumor suppressors (AKT1, BRAF, CTNNB1, FBX4, FBXW7, FGFR2, FGFR3, GNAQ, KIT, KRAS, MAP2K1, MAP2K2, NRAS, PDGFR α , PIK3CA, PTPN11, SOS1, and TP53). The panel consists of 12 multiplexed wells that are run on each sample using 40 ng of input DNA from FFPE tissue. The polymerase chain reaction amplification and primer extension were performed using the OncoCarta Panel v2.0 reagents. The detection and quantify mutation frequencies are $\geq 10\%$. Twenty patients had successful DNA extraction from the metastatic site useful for gene analysis. In thirteen cases, we had successful DNA extraction from the matched primary BCs too.

3. Results

3.1. Study Population. Twenty-five patients have been enrolled in the study. Four patients were diagnosed with de novo metastatic BC, while all the other cases relapsed in spite of adjuvant treatments. All the patients progressed on/after aromatase inhibitors and received at least two previous lines of (chemo- or hormonal-) therapies for advanced disease. The median age at the time to start everolimus plus exemestane was 54 years (range 50-67). Regarding the tumor burden at the beginning of everolimus and exemestane, four patients had only bone disease and two patients only loco-regional recurrence (chest wall and/or lymph nodes), while all other patients presented visceral disease (liver and/or lung). Tumors characteristics of both metastatic site and primary BC are reported in Table 1. According to 13th St Gallen International Breast Cancer Conference classification, seventeen patients relapsed as luminal B-like disease (HR+, HER2-, Mib1 $\geq 20\%$), and eight were luminal A-like BCs (HR+, Mib1 $<20\%$). Primary BC was luminal B-like in twelve patients, whereas luminal A-like in the other ones. Of note, in two patients the BC subtypes changed from luminal A-like to luminal B-like from primary breast disease to relapse, whereas in other two cases it changed from luminal B-like to luminal A-like from breast sample to metastasis. At the time of analysis, all the patients had progressed on everolimus and

TABLE 1: Tumors characteristics of metastatic site and matched primary breast cancer.

	Site of biopsy	Relapse	Primary tumor
		relapse characteristics	Primary tumor characteristics
Patient 1	liver	CDI ER90%, PgR 5%, Mib1 30%, HER2 1+	CDI ER100%, PgR60%, MIB1 25%, HER2 1+
Patient 2	breast	CDI ER60%, PgR 95%, Mib1 10%, HER2 1+	CDI ER98%, PgR98%, MIB1 15%, HER2 1+
Patient 3	liver	CDI ER40%, PgR30%, Mib1 40%, HER2 0	CDI ER98%, PgR70%, MIB1 30%, HER2 1+
Patient 4	liver	CDI ER100%, PgR 50%, Mib1 40%, HER2 1+	CDI ER100%, PgR80%, MIB1 25%, HER2 1+
Patient 5	chest wall	CDI ER 99%, PgR70%, Mib1 15%, HER2 0+	CDI ER 99%, PgR 70%, MIB1 15%, HER2 1+
Patient 6	liver	CDI ER 95%, PgR2%, Mib1 25%, HER2 1+	CDI ER 85%, PgR 70%, MIB1 35%, HER2 1+
Patient 7	lung	CDI ER 85%, PgR25%, Mib1 15%, HER2 1+	CDI ER 80%, PgR 60%, MIB1 25%, HER2 0+
Patient 8	breast	CDI ER 100%, PgR100%, Mib1 30%, HER2 1+	CDI ER 100%, PgR 100%, MIB1 35%, HER2 1+
Patient 9	liver	CDI ER 99%, PgR99%, Mib1 50%, HER2 1+	CDI ER 80%, PgR 60%, MIB1 25%, HER2 0+
Patient 10	liver	CDI ER 90%, PgR60%, Mib1 22%, HER2 1+	CDI ER 50%, PgR 50%, Mib1 10%, HER2 1+
Patient 11	liver	CDI ER 80%, PgR0%, Mib1 40%, HER2 1+	CDI ER 90%, PgR 50%, MIB1 25%, HER2 1+
Patient 12	skin	CDI ER 99%, PgR50%, Mib1 25%, HER2 1+	not applicable
Patient 13	bone	CDI ER 70%, PgR0%, Mib1 35%, HER2 0+	CDI ER 80%, PgR 60%, MIB1 25%, HER2 0+
Patient 14	bone	CDI ER 50%, PgR5%, Mib1 25%, HER2 0+	not applicable
Patient 15	liver	CDI ER 100%, PgR10%, Mib1 20%, HER2 1+	not applicable
Patient 16	lymph node	CDI ER 70%, PgR0%, Mib1 25%, HER2 1+	CDI ER 90%, PgR 80%, MIB1 8%, HER2 0+
Patient 17	liver	CDI ER 95%, PgR80%, Mib1 15%, HER2 0+	CDI ER 100%, PgR 100%, MIB1 15%, HER2 0+
Patient 18	lung	CDI ER 90%, PgR2%, Mib1 30%, HER2 1+	CDI ER 50%, PgR 65%, MIB1 25%, HER2 0+
Patient 19	lung	CDI ER 95%, PgR25%, Mib1 10%, HER2 1+	CDI ER 60%, PgR 10%, MIB1 25%, HER2 1+
Patient 20	lung	CDI ER 75%, PgR50%, Mib1 10%, HER2 1+	CDI ER 75%, PgR 20%, MIB1 15%, HER2 0+
Patient 21	bone	CDI ER 95%, PgR65%, Mib1 25%, HER2 1+	not applicable
Patient 22	bone	CDI ER 95%, PgR95%, Mib1 10%, HER2 1+	CDI ER 100%, PgR 85%, MIB1 3%, HER2 0+
Patient 23	liver	CDI ER 90%, PgR25%, Mib1 40%, HER2 0+	not applicable
Patient 24	lung	CDI ER 50%, PgR50%, Mib1 30%, HER2 1+	CDI ER 70%, PgR 50%, MIB1 25%, HER2 1+
Patient 25	lymph node	CDI ER 100%, PgR5%, Mib1 15%, HER2 0+	not applicable

exemestane. Median PFS was 6,6 months (range from 1 to 17 months).

3.2. Gene Mutations on Metastatic Site. Among twenty-five patients enrolled, twenty had successful DNA extraction from FFPE metastatic site. In six of these patients, the biopsy was performed on the local/regional recurrence site (breast, chest wall, or lymph nodes). In nine cases, the biopsy was performed on liver recurrence, in three patients on lung metastasis, and in two cases on the spinal bone lesions.

In all but one case the mutations were detected in the visceral recurrence (liver or lung) (Figure 2). Gene mutations were identified in 6 out of 20 patients analysed (30%). All but one of them had only one mutated gene (BRAF, CTNNB1, FBXW7, KIT, or PT53). Only patient 6 presented two mutations: one on PI3KCA and one on AKT1, respectively (Table 2). Considering molecular pathways, the most of the detected genes belong to PI3K pathway (AKT1, KIT, PI3KCA, and PT53), APC pathway (CTNNB1, FBXW7, and PT53), and MAP and RAS pathways (AKT1 and KIT; AKT1 and BRAF, respectively).

3.3. Gene Mutations on Primary Breast Cancer. Primary BC tissue was available in nineteen patients but only in thirteen cases the DNA was successfully extracted. The overall detection rate of mutations in the primary BC was 38% (5 out of

13 patients). A single gene mutation was identified in four out of thirteen patients analysed. Only patient 7 presented three mutations in three different genes: FBX4, PI3KCA, and KIT. Two patients presented the same mutation on AKT1: E17K. Other two cases had a single mutation on MAP2K1 and FBXW7, respectively. Considering molecular pathways, the most of the mutated genes belong to PI3K pathway (AKT1, KIT, and PI3KCA), APC pathway (FBXW7 and FBX4), and MAP and RAS pathways (AKT1 and MAP2K1; AKT1 and KIT, respectively) (Table 2).

3.4. Correlation between Gene Mutations on Metastatic and Primary Breast Cancer. The metastatic and the matched primary BC tissues were profiled in eight patients; in three of them no mutation has been detected in both samples. No primary BC and matched relapse maintained the same mutation profile. Two patients acquired AKT1^{E17K} mutation in the metastatic sites, while two patients lost the mutation detected in the primary tissue. In patient 18 a single mutation on a different gene was detected in primary tissue (FBXW7^{R479Q}) and in the recurrence one (MAP2K1^{D67N}) (Table 2).

Overall AKT1 was the most frequent mutated gene, with the same mutation E17K (one in the metastatic tissue and two in the relapse ones). Similarly, the E545K was the only mutation detected in PI3K gene. Mutations in KIT, PI3KCA,

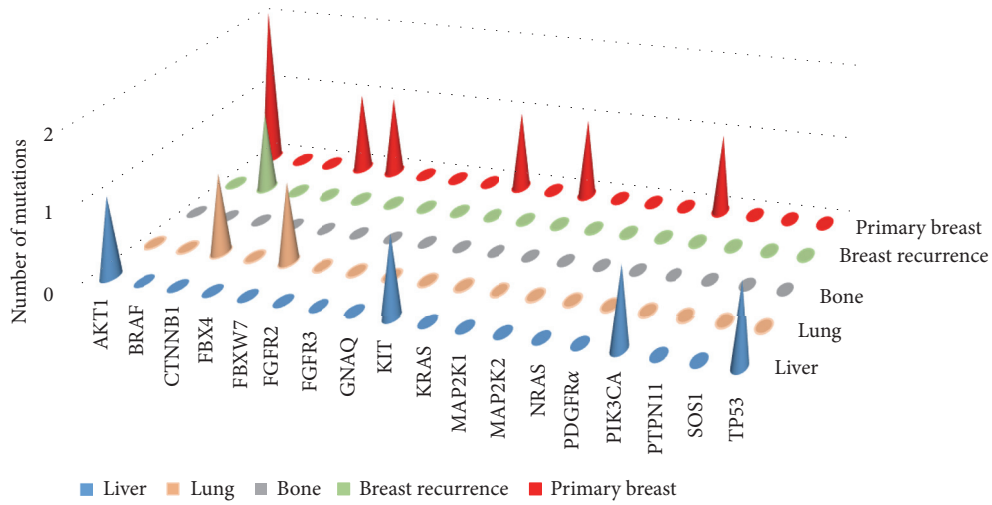


FIGURE 2: Oncogene mutations across metastatic and primary breast cancer site.

TABLE 2: Mutations detected in relapse tissue and in primary breast cancer.

	Relapse mutations			Primary tumor mutations		
	status	gene	mutation	status	gene	mutation
Patient 1	wild type			<i>not available</i>		
Patient 2	mutated	BRAF	R444W	<i>not available</i>		
Patient 3	wild type			<i>not available</i>		
Patient 4	wild type			<i>not available</i>		
Patient 5	wild type			<i>not available</i>		
Patient 6	mutated	PIK3CA AKT1	E545K E17K	<i>not available</i>		
Patient 7	<i>not available</i>			mutated	FBX4 PIK3CA KIT	G30N E545K S709F
Patient 8	wild type			<i>not available</i>		
Patient 9	mutated	TP53	R273H	wild type		
Patient 10	wild type			mutated	AKT1	E17K
Patient 11	wild type			wild type		
Patient 12	wild type			<i>not available</i>		
Patient 13	wild type			mutated	AKT1	E17K
Patient 14	wild type			<i>not available</i>		
Patient 15	mutated	KIT	G565R	<i>not available</i>		
Patient 16	wild type			wild type		
Patient 17	<i>not available</i>			wild type		
Patient 18	mutated	FBXW7	R479Q	mutated	MAP2K1	D67N
Patient 19	wild type			wild type		
Patient 20	mutated	CTNNB1	S45F	wild type		
Patient 21	<i>not available</i>			wild type		
Patient 22	<i>not available</i>			mutated	FBXW7	R465C
Patient 23	wild type			<i>not available</i>		
Patient 24	<i>not available</i>			wild type		
Patient 25	wild type			<i>not available</i>		

TABLE 3: Correlation between mutations detected in primary tumor or relapse tissue and PFS on everolimus and exemestane.

	Mutations in primary tumor or relapse tissue	PFS (months)
Patient 1	wild type	3
Patient 2	mutated (BRAF)	6
Patient 3	wild type	4
Patient 4	wild type	5
Patient 5	wild type	2
Patient 6	mutated (PIK3CA; AKT1)	15
Patient 7	mutated (FBX4; PIK3CA; KIT)	3
Patient 8	wild type	17
Patient 9	mutated (TP53)	1
Patient 10	mutated (AKT1)	3
Patient 11	wild type	5
Patient 12	wild type	9
Patient 13	mutated (AKT1)	2
Patient 14	wild type	9
Patient 15	mutated (KIT)	3
Patient 16	wild type	8
Patient 17	wild type	13
Patient 18	mutated (MAP2K1; FBXW7)	6
Patient 19	wild type	5
Patient 20	mutated (CTNNB1)	8
Patient 21	wild type	12
Patient 22	mutated (FBXW7)	5
Patient 23	wild type	5
Patient 24	wild type	13
Patient 25	wild type	2

and FBXW7 were detected in both primary BC and relapse. Regarding molecular pathways, the most of the genes belong to PI3K, MAP, and APC pathways, with four mutated genes involved in each pathway.

In patients with detected mutations in breast and/or recurrence tissue, the median PFS was 5,6 months (range from 1 to 15 months), while in the subgroup of patients with no mutations the median PFS was 7,5 months (range from 2 to 17 months) (Table 3).

4. Discussion

Everolimus is a selective inhibitor of mTOR, a multiprotein complex controlled by mitogenic positive signal (mediated through PI3K/AKT pathway) and by negative regulators (such as PTEN) [9]. Receptors tyrosine kinase signalling and/or acquired mutation in genes involved in PI3K/AKT pathway can activate constitutively this complex [9, 10]. Hormone resistance models have shown that tumors can lose endocrine responsiveness through activation of PI3K/AKT/mTOR [11]. The combination of mTOR inhibitors such as everolimus and endocrine therapy can restore hormone sensitivity to previously resistant tumors cells [12]. Everolimus has been mainly investigated in combination with tamoxifen in TAMRAD trial and with exemestane in BOLERO2 trial [3, 13]. The combination significantly reduced the risk of disease

progression and improved the clinical benefit rate compared with endocrine therapy alone in metastatic BC patients resistant to aromatase inhibitors. Translational studies of these two trials tried to find biomarkers able to predict a patient's positive response or resistance to everolimus [6, 7]. In spite of preclinical evidence showing a predictive role of specific genetic aberrations in the PI3K/AKT/mTOR pathway [14, 15], clinical data failed to confirm the correlation between a specific mutation status in the primary BC tissue and sensitivity/resistance to everolimus.

On these premises, we analysed a panel of 18 genes known to be involved in endocrine and targeted treatment resistance in metastatic BC samples. Our study is the only one that performed the gene analysis in metastatic tissue of endocrine resistance BC patients before starting everolimus. That is extremely important considering that during the natural history of the disease, metastases can acquire different biological profiles as compared to their matched primary tumor [16, 17].

In our analysis, the overall detection rate of mutations was 30%. Most of detected genes belong to PI3K pathway, supporting this pathway as a key-point in endocrine resistance BCs. The mutated genes in PI3K pathway were PI3KCA, AKT1, KIT, and PT53. All these genes are known to be involved in BC progression and metastatization [18]. Several preclinical studies have shown how PI3KCA and AKT1 mutations were able to activate PI3K pathway and to be driver

of BC progression. In particular, PI3KCA is mutated and/or amplified in ~30% of BCs [19]. In the TAMRAD study 45 primary tumor samples of BC were screening for mutation status. No relationship between PI3K mutations and everolimus efficacy was found. The overall detection rate of mutations was 22%. Nine patients (5 in tamoxifen/everolimus arm and 4 in tamoxifen alone arm) had a PI3K mutation: two in the exons 9 (mutation E542K) and seven in exon 20 (mutation H1047R) [7]. Furthermore, the BOLERO-2 study failed to identify any specific gene mutation associated with a greater benefit from everolimus, in both tumor tissue and plasma cell-free DNA. Gene analyses were performed on 302 FFPE archival tumor tissue. The genes most frequently mutated were PI3KCA (47.6%), CCND1 (31.3%), TP53 (23.3%), and FGFR1 (18.1%). None of these genes such as the pathways alteration of which they were components predicted the PFS benefit with everolimus. However, quantitative differences in everolimus benefit were observed between patients subgroup defined by the exon specific mutation in PI3KCA genes. In particular, patients with the PI3KCA exon 9 (helical domain) mutation had greater PFS benefit compared with those with exon 20 (kinase domain) mutation [6]. The relationship between the PI3KCA exon 9 status and the efficacy of everolimus was investigated and confirmed in the subgroup analysis of the Phase II study of neoadjuvant everolimus plus letrozole in HR+ BC [20]. Interestingly, in our analysis *patient 6* with both PI3KCA^{E545K} (exon 9) and AKT1^{E17K} mutation experienced the greatest benefit from everolimus treatment with a PSF of 15 months.

Notably, the activating mutations in AKT gene are reported in 1.4%–8% of BCs, exclusively in HR+ tumors [21]. AKT1^{E17K} is the most commonly reported mutation. This mutation increases gene activity by promoting constitutive localization of AKT1 to the plasmatic membrane [22]. In vitro studies have shown how high levels of pAKT were predictor of sensitivity to everolimus [21]. In our series, *patient 10* and *patient 13* with AKT1^{E17K} mutation only in the primary BC had an extremely poor PFS on everolimus (5 and 2 months, respectively).

Regarding TP53, another gene involved PI3K pathway, in vitro evidence has shown how R273H mutation enhanced proliferation, invasion, and drug resistance [23]. RNA analysis confirmed how TP53^{R273H} mutants had the apoptosis pathway less active than TP53 wild type ones [23]. In accordance with this finding, *Patient9* with TP53^{R273H} mutation detected in the metastatic liver biopsy rapidly progressed on the combination treatment (PFS = 1 month).

Less evidence is available regarding the predictive role of the other mutated genes. In our series, poor PFS were achieved by *patient 2* with BRAF^{R444W}, *patient 15* with KIT^{G565R}, and *patient 18* with FBXW7^{R479Q} mutation (6, 3, and 5 months, respectively). These findings are consistent with available data in literature deriving from preclinical evidence but not specifically on BC [24–26]. Globally, median PFS in our population was higher in wild type patients compared with mutated ones. This finding is in accordance with the conclusions of the BOLERO2 investigators where patients with no alteration or a single genetic alteration received a greater PFS benefit from everolimus.

Considering the correlation between gene mutation status in the metastatic and matched BC tissue, no patient maintained the same mutation profile. In contrast with our evidence are the data from the mutational analysis performed in the metastatic tissue of 56 patients enrolled in the BOLERO2. In this subgroup analysis, the genetic profile of metastatic and primary tumors was generally similar, with a statistically increased mutation rates for ESRI, MDM2, and DNMT3A in the metastatic samples [6]. This discordance could be justified by the fact that our population was highly pretreated. In fact, it should be noted that all our patients received at least two lines of treatment for metastatic disease before starting everolimus and more than 80% of them were treated with chemotherapy for advance disease compared to 26% in BOLERO2 study. The discordance between the mutational profile of metastatic and primary BC tissue further stresses the importance of the biopsy of the metastatic site in order to catch important molecular markers that can evolve during the disease progression. Finally, the high rate of mutations detected in the primary BCs tissue (5 of 13 analysed patients, 38%) could highlight a more aggressive behaviour of these tumors and the subsequent relapse in spite of the adjuvant treatments.

Nevertheless, our study presents three major limitations. The first is the small sample size due to preanalytic bias in DNA extraction. Furthermore, a possible sampling bias must be taken into account due to the heterogeneity of the metastatic disease, where different areas of the same lesion may show different genomic profiles [27, 28]. Finally, our study focused on gene mutations, but the recent evidence underline how microRNA expression, protein expression, and abnormalities in DNA methylation may influence the response/resistance to antitumor treatments, independently from genes profile [29, 30].

5. Conclusion

The mutational status of BC recurrence allows the identification of some genes potentially correlating to tumor response/resistance to everolimus plus exemestane. The most frequently mutated genes among those investigated were involved in the PI3K/AKT/mTOR pathway. It is likely that the deregulation of this pathway in the relapse plays a crucial role in the mechanisms of everolimus resistance/sensitivity. Owing to the small sample size and the retrospective nature of the study, these correlations are purely exploratory and need to be validated in large prospective studies. Future research should be directed not only on the analysis of genes profile but also on the RNA expression, proteins level, and epigenetic alteration.

Data Availability

The data regarding RNA extraction/concentration/purity are available from the corresponding author upon request.

Conflicts of Interest

The authors declare that there are no conflicts of interest regarding the publication of this paper.

Acknowledgments

This study was funded by Progetto Ricerca Finalizzata 2009 (RF 2009-1472600).

References

- [1] E. Dalmau, A. Armengol-Alonso, M. Muñoz, and M. Á. Seguí-Palmer, "Current status of hormone therapy in patients with hormone receptor positive (HR+) advanced breast cancer," *The Breast*, vol. 23, no. 6, pp. 710–720, 2014.
- [2] E. A. Musgrove and R. L. Sutherland, "Biological determinants of endocrine resistance in breast cancer," *Nature Reviews Cancer*, vol. 9, no. 9, pp. 631–643, 2009.
- [3] J. Baselga et al., "Everolimus in postmenopausal hormone-receptor-positive advanced breast cancer," *The New England Journal of Medicine*, vol. 366, no. 6, pp. 520–529, 2012.
- [4] E. Paplomata and R. O'Regan, "The PI3K/AKT/ mTOR pathway in breast cancer: targets, trials and biomarkers," *Therapeutic Advances in Medical Oncology*, vol. 6, no. 4, pp. 154–166, 2014.
- [5] N. Margariti, S. B. Fox, A. Bottini, and D. Generali, "Overcoming breast cancer drug resistance with mTOR inhibitors". Could it be a myth or a real possibility in the short-term future?" *Breast Cancer Research and Treatment*, vol. 128, no. 3, pp. 599–606, 2011.
- [6] G. N. Hortobagyi et al., "Correlative Analysis of Genetic Alterations and Everolimus Benefit in Hormone Receptor-Positive, Human Epidermal Growth Factor Receptor 2-Negative Advanced Breast Cancer: Results From BOLERO-2," *Journal of Clinical Oncology*, vol. 34, no. 5, pp. 419–426, 2016.
- [7] I. Treilleux, M. Arnedos, C. Cropet et al., "Translational studies within the TAMRAD randomized GINECO trial: evidence for mTORC1 activation marker as a predictive factor for everolimus efficacy in advanced breast cancer," *Annals of Oncology*, vol. 26, no. 1, pp. 120–125, 2014.
- [8] M. E. Moynahan, D. Chen, W. He et al., "Correlation between PIK3CA mutations in cell-free DNA and everolimus efficacy in HR+, HER2-advanced breast cancer: Results from BOLERO-2," *British Journal of Cancer*, vol. 116, no. 6, pp. 726–730, 2017.
- [9] C. K. Yip, K. Murata, T. Walz, D. M. Sabatini, and S. A. Kang, "Structure of the human mTOR complex I and its implications for rapamycin inhibition," *Molecular Cell*, vol. 38, no. 5, pp. 768–774, 2010.
- [10] R. Katso, K. Okkenhaug, K. Ahmadi, S. White, J. Timms, and M. D. Waterfield, "Cellular function of phosphoinositide 3-kinase: implications for development, immunity, homeostasis, and cancer," *Annual Review of Cell and Developmental Biology*, vol. 17, pp. 615–675, 2001.
- [11] L. H. Saal, K. Holm, M. Maurer et al., "PIK3CA mutations correlate with hormone receptors, node metastasis, and ERBB2, and are mutually exclusive with PTEN loss in human breast carcinoma," *Cancer Research*, vol. 65, no. 7, pp. 2554–2559, 2005.
- [12] T. W. Miller, B. T. Hennessy, A. M. González-Angulo et al., "Hyperactivation of phosphatidylinositol-3 kinase promotes escape from hormone dependence in estrogen receptor-positive human breast cancer," *The Journal of Clinical Investigation*, vol. 120, no. 7, pp. 2406–2413, 2010.
- [13] T. Bachelot, C. Bourcier, C. Cropet et al., "Randomized phase II trial of everolimus in combination with tamoxifen in patients with hormone receptor-positive, human epidermal growth factor receptor 2-negative metastatic breast cancer with prior exposure to aromatase inhibitors: a GINECO study," *Journal of Clinical Oncology*, vol. 30, no. 22, pp. 2718–2724, 2012.
- [14] V. Serra, B. Markman, M. Scaltriti et al., "NVP-BEZ235, a dual PI3K/mTOR inhibitor, prevents PI3K signaling and inhibits the growth of cancer cells with activating PI3K mutations," *Cancer Research*, vol. 68, no. 19, pp. 8022–8030, 2008.
- [15] A. M. Gonzalez-Angulo and G. R. Blumenschein, "Defining biomarkers to predict sensitivity to PI3K/Akt/mTOR pathway inhibitors in breast cancer," *Cancer Treatment Reviews*, vol. 39, no. 4, pp. 313–320, 2013.
- [16] L. Ding et al., "Genome remodelling in a basal-like breast cancer metastasis and xenograft," *Nature*, vol. 464, no. 7291, pp. 999–1005, 2010.
- [17] M. V. Dieci, F. Piacentini, M. Dominici et al., "Quantitative expression of estrogen receptor on relapse biopsy for ER-positive breast cancer: Prognostic impact," *Anticancer Research*, vol. 34, no. 7, pp. 3657–3662, 2014.
- [18] F. Janku et al., "PIK3CA mutations in advanced cancers: characteristics and outcomes," *Oncotarget*, vol. 3, no. 12, pp. 1566–1575, 2012.
- [19] F. Ahmad, A. Badwe, G. Verma, S. Bhatia, and B. R. Das, "Molecular evaluation of PIK3CA gene mutation in breast cancer: Determination of frequency, distribution pattern and its association with clinicopathological findings in Indian patients," *Medical Oncology*, vol. 33, no. 7, article no. 74, 2016.
- [20] J. Baselga et al., "Phase II randomized study of neoadjuvant everolimus plus letrozole compared with placebo plus letrozole in patients with estrogen receptor-positive breast cancer," *Journal of Clinical Oncology*, vol. 27, no. 16, pp. 2630–2637, 2009.
- [21] M. Rudolph, T. Anzeneder, A. Schulz et al., "AKT1E17K mutation profiling in breast cancer: Prevalence, concurrent oncogenic alterations, and blood-based detection," *BMC Cancer*, vol. 16, no. 1, article no. 622, 2016.
- [22] K. Stemke-Hale, A. M. Gonzalez-Angulo, A. Lluch et al., "An integrative genomic and proteomic analysis of PIK3CA, PTEN, and AKT mutations in breast cancer," *Cancer Research*, vol. 68, no. 15, pp. 6084–6091, 2008.
- [23] M. Gasco, S. Shami, and T. Crook, "The p53 pathway in breast cancer," *Breast Cancer Research*, vol. 4, no. 2, pp. 70–76, 2002.
- [24] R. Simon, S. Panussis, R. Maurer et al., "KIT (CD117)-Positive Breast Cancers Are Infrequent and Lack KIT Gene Mutations," *Clinical Cancer Research*, vol. 10, no. 11, pp. 178–183, 2004.
- [25] G. Wei, Y. Wang, P. Zhang, J. Lu, and J.-H. Mao, "Evaluating the prognostic significance of FBXW7 expression level in human breast cancer by a meta-analysis of transcriptional profiles," *Journal of Cancer Science & Therapy*, vol. 4, no. 9, pp. 299–305, 2012.
- [26] A. L. Cohn, B.-M. Day, S. Abhyankar, E. McKenna, T. Riehl, and I. Puzanov, "Brafv600 mutations in solid tumors, other than metastatic melanoma and papillary thyroid cancer, or multiple myeloma: A screening study," *OncoTargets and Therapy*, vol. 10, pp. 965–971, 2017.
- [27] N. Navin, J. Kendall, J. Troge et al., "Tumour evolution inferred by single-cell sequencing," *Nature*, vol. 472, no. 7341, pp. 90–95, 2011.
- [28] M. Gerlinger et al., "Intratumor Heterogeneity and Branched Evolution Revealed by Multiregion Sequencing," *The New England Journal of Medicine*, vol. 366, no. 10, pp. 883–892, 2012.

- [29] S. Badve and H. Nakshatri, "Breast-cancer stem cells-beyond semantics," *The Lancet Oncology*, vol. 13, no. 1, pp. e43–e48, 2012.
- [30] Y. K. Chae, A. A. Davis, S. Jain et al., "Concordance of genomic alterations by next-generation sequencing in tumor tissue versus circulating tumor DNA in breast cancer," *Molecular Cancer Therapeutics*, vol. 16, no. 7, pp. 1412–1420, 2017.

Research Article

The Thomsen-Friedenreich Antigen-Specific Antibody Signatures in Patients with Breast Cancer

Oleg Kurtenkov ¹, Kaire Innos,² Boris Sergejev,¹ and Kersti Klaamas ¹

¹Department of Oncology and Immunology, National Institute for Health Development, Hiiu 42, 11619 Tallinn, Estonia

²Department of Epidemiology and Biostatistics, National Institute for Health Development, Hiiu 42, 11619 Tallinn, Estonia

Correspondence should be addressed to Oleg Kurtenkov; oleg.kurtenkov@tai.ee

Received 14 March 2018; Accepted 3 July 2018; Published 15 July 2018

Academic Editor: Franco M. Buonaguro

Copyright © 2018 Oleg Kurtenkov et al. This is an open access article distributed under the Creative Commons Attribution License, which permits unrestricted use, distribution, and reproduction in any medium, provided the original work is properly cited.

Alterations in the glycosylation of serum total immunoglobulins show these antibodies to have a diagnostic potential for cancer but the disease-related Abs to the tumor-associated antigens, including glycans, have still poorly been investigated in this respect. We analysed serum samples from patients with breast carcinoma ($n = 196$) and controls ($n = 64$) for the level of Thomsen-Friedenreich (TF) antigen-specific antibody isotypes, their sialylation, interrelationships, and the avidity by using ELISA with the synthetic TF-polyacrylamide conjugate as an antigen and the sialic acid-specific *Sambucus nigra* agglutinin (SNA) and ammonium thiocyanate as a chaotrope. An increased sialylation of IgG and IgM, but a lower SNA reactivity of IgA TF antibodies, and a higher level and avidity of the TF-specific IgA were found in cancer patients. Other cancer-related signatures were the highly significant increase of the IgG/IgA ratio and the very low SNA/IgA index in cancer, including patients with an early stage of the disease. These changes showed a good diagnostic potential with about 80% accuracy. Thus, the level of naturally occurring anti-TF antigen antibodies, their sialylation profile, isotype distribution, and avidity displayed cancer-specific changes that could serve as novel noninvasive Ab-based biomarkers for early breast cancer.

1. Introduction

The altered glycosylation often observed in cancer cells leads to the expression of modified glycopeptide epitopes, as well as tumor-associated glycans (TAG) that may be autoimmunogenic and recognized by autoantibodies [1–8]. A broad spectrum of natural and adaptive anti-glycan Abs is present in human serum in health and disease, showing a rather stable level over time in healthy people [2, 4, 9–12]. There is strong evidence that a majority of them is a result of the innate and adaptive immune response to microbial carbohydrates [13–15].

The immunoreactive Thomsen-Friedenreich glycoantigen, TF, CD176 (Gal β 1-3GalNAc α -O-Ser/Thr (Core 1) structure) is expressed in about 90% of all human carcinomas but not in healthy tissues [2, 16]. The level of naturally occurring TF-specific Abs is usually decreased in cancer and is associated with tumor progression and patient survival [9, 17–19], suggesting the important role of anti-TF Abs in tumor immunosurveillance. Both murine and humanized MAbs to

TF showed in vitro and in vivo activity towards TF-positive human breast cancer cell lines and in a human breast cancer xenograft model in SCID mice [20].

Immunoglobulins (Igs) are glycosylated molecules and it is now clear that the N-glycans of the Fc-fragment strongly influence IgG-Fc γ receptor interactions and thus the Fc-mediated effector mechanisms [21, 22]. Several studies have demonstrated that agalactosylated IgGs show an increased inflammatory activity, whereas sialylated Abs display an anti-inflammatory effect [23–25].

Compared to healthy individuals, there is a marked change of serum IgG glycosylation in individuals with autoimmune diseases, infections, and tumors [26–29], including breast cancer [29, 30]. The serum IgG glycosylation profiling has showed a diagnostic and prognostic potential in various malignancies [27, 31], including breast [30, 32]. However, it is important to note that the total serum IgG glycosylation may significantly differ from that of antigen-specific Abs [28], suggesting the presence of disease-specific IgG changes of potential clinical importance.

TABLE 1: The characteristics of groups under investigation.

Group	N (females)	Median age (range)
Donors	64	53 (24 - 75)
Breast cancer patients	196	62 (23 - 91)
stage 0	14	65 (29 - 82)
stage 1	50	59 (32 - 79)
stage 2a	28	59 (23 - 80)
stage 2b	29	60 (35 - 79)
stage 3a	29	58 (31 - 78)
stage 3b	9	74 (69 - 79)
stage 3c	30	67 (50 - 91)
stage 4	7	54 (38 - 71)

The glycodiversity of Abs is now a topic of interest because of the important role of glycans in the functional behavior of Abs and a possibility of constructing Ab glycoforms with the predicted potential [33, 34]. Although it is well established that antibodies are very heterogeneous by glycosylation and functionally very limited data are available on the glycodiversity of Abs to tumor-associated antigens, including TAG and of the currently used cancer biomarkers, only a few studies have been reported on the analysis of disease-specific anti-TAG Abs polymorphism, including glycosylation [35–37].

We recently established the increased α 2,6 sialylation of TF-specific Abs in patients with gastric and colon cancer [36, and unpublished]. Moreover, some changes showed a good diagnostic potential and association with long-term survival in patients. However, it remains unclear whether this is characteristic of only gastrointestinal cancer. In the present study, we show that the levels of anti-TF antigen Abs, sialylation profile, isotypes distribution, and avidity reveal cancer-specific changes also in patients with breast cancer and can serve as diagnostic biomarkers.

2. Material and Methods

2.1. Subjects. Serum samples were taken from patients with newly diagnosed histologically verified breast carcinoma and healthy blood donors (Table 1). The investigation was carried out in accordance with the ICH GCP Standards and approved by Tallinn Medical Research Ethics Committee, Estonia. A written informed consent was obtained from each subject under study. Tumor staging was based on the histopathological (pTNM) classification of malignant tumors. The serum samples were stored in aliquots at -20°C until use.

2.2. TF-Specific Antibody Assay. The levels of anti-TF IgG, IgM, and IgA were determined by the enzyme-linked immunosorbent assay (ELISA) as described elsewhere [37] with some modifications. The plates (NUNC Maxisorp, Denmark) were coated with a synthetic TF-polyacrylamide conjugate (TF-PAA, Lectinity, Russia; 10 mol% of carbohydrate) in the carbonate buffer, pH 9.6. After the overnight incubation, triple washing and blocking with a Superblock solution

(Pierce, USA) for 30 min at 25°C , the serum samples diluted 1:25 in PBS-0.05% Tween (Tw) were applied for 1.5 h at 25°C . After the subsequent washing with PBS-Tw, the level of bound anti-TF Abs was determined using the alkaline phosphatase (AP) conjugated goat anti-human IgG, IgM (Sigma, USA), or IgA (Dako, USA) and developed with p-nitrophenylphosphate disodium hexahydrate (pNPP, Sigma, USA). The absorbance values were read at 405 nm (Tecan Reader, Austria). The optical density value (OD) of control wells (blank: a Superblock solution instead of serum) was subtracted from that of Ab-coated wells and each sample was analysed in duplicate. To standardize the assay, standard serum (A) was included in each plate for IgG determination and lectin binding measurement. The interassay variations were minimized by using the correction factor (CF): $\text{CF} = 1 / (\text{standard serum A values} - \text{blank}) \times 100$. The results were expressed in relative units (RU): $\text{RU} = \text{sample OD value} \times \text{CF}$.

2.3. SNA Lectin Reactivity of TF-Specific Antibodies. The lectin reactivity of TF glycoform-specific antibodies was measured in a similar way, except that the binding of the neuraminic acid (sialic acid) specific Sambucus nigra agglutinin (SNA) to the absorbed anti-TF antibodies was determined as described earlier [37]. The biotinylated SNA (Vector Laboratories, Inc., USA) in 10 mmol/L Hepes, 0.15 mol/L NaCl, 0.1 mmol/L CaCl_2 , pH 7.5 was applied at a concentration of $5 \mu\text{g}/\text{mL}$ for 1.5 h at 25°C . The bound lectin was detected with a streptavidin-AP conjugate (Dako, USA) and pNPP (Sigma, USA). The OD of control wells (no serum sample) was subtracted from that of Ab-coated wells to determine the lectin binding. Each sample was analysed in duplicate. The value of the SNA binding to all TF-specific Abs and the ratio of SNA binding to the level of TF-specific IgG, IgM, and IgA (SNA/Ig index) were determined.

2.4. Avidity of TF-Specific Antibodies. The avidity of anti-TF IgG, IgM, and IgA antibodies was determined by ELISA as described previously [38] with minimal changes. The plates were coated with the synthetic TF-polyacrylamide conjugate in the carbonate buffer, pH 9.6, $5 \mu\text{g}$ per well. After the overnight incubation at $+4^{\circ}\text{C}$, washing with PBS-0.05% Tw and blocking with the Superblock solution as above, the serum (diluted 1:25 in PBS-0.05% Tw) was applied for 1.5 hr at 25°C . After subsequent washing ammonium thiocyanate (NH_4SCN) as a dissociating agent was added at a concentration of 1.25 mol/L for 15 min at $+25^{\circ}\text{C}$. The bound antibodies were detected with the alkaline phosphatase conjugated goat anti-human IgG, IgM or IgA, and pNPP. The absorbance values were read at 405 nm. The relative avidity index (AI) was calculated for each sample and expressed as the percentage of reactivity remaining in the thiocyanate-treated wells in relation to that of untreated wells (PBS-Tw instead of chaotrope).

2.5. Statistical Analysis. The results were analysed using the nonparametric Mann-Whitney U test or Student's t-test, where appropriate, and the Pearson two-tailed correlation. The receiver operator characteristic (ROC) curve analysis was

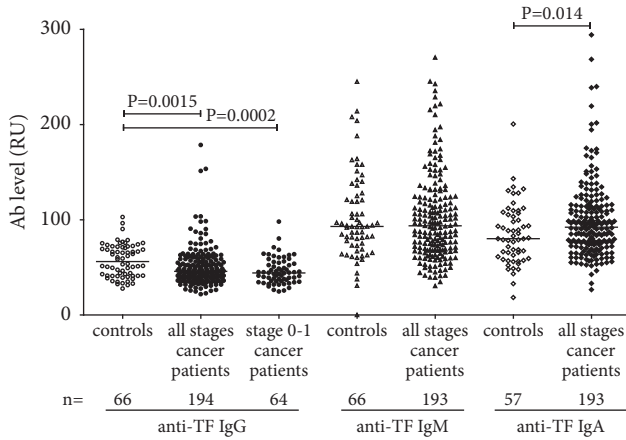


FIGURE 1: The level of TF-specific IgG, IgM, and IgA antibodies in controls and breast cancer patients. Each dot represents one individual and the group median is indicated by horizontal lines. P values were calculated by the Mann–Whitney U test and are shown for significant differences.

used to evaluate the sensitivity and specificity of changes found in colon cancer patients, as well as the accuracy of diagnostics. The respective difference between the groups was considered to be significant when $P \leq 0.05$. All calculations were performed using the GraphPad Prism 5 and SPSS 15.0 software.

3. Results

3.1. Anti-TF IgG, IgM, and IgA Antibody Levels. A significantly lower level of serum TF-specific IgG was found in cancer patients at all stages of the disease ($P=0.0015$), including early 0+1 stages ($P=0.0002$) (Figure 1).

The anti-TF-IgM level was significantly lower only in stage 3b+3c patients ($P=0.040$). In contrast, an increase of the IgA Ab level was detected. No significant correlation between the levels of anti-TF antibodies of different Ig isotypes was observed in both patients and controls: IgG versus IgM, $r = -0.1$; IgG or IgM versus IgA $r = 0.23$ and 0.31 ($P > 0.05$). However, the ratio IgG/IgM was significantly lower in cancer patients than in controls ($P=0.019$), including stages 0-3a ($P=0.0076$) (Figure 2). A similar decrease of IgG/IgA ratio ($P < 0.0001$) was found in cancer patients with a more pronounced decrease at very early stages (0-1). No difference in IgM/IgA ratio ($P=0.41$) between patients and controls was found.

Thus, the level of some anti-TF Ab isotypes and their interrelations demonstrate significant changes in patients with breast cancer.

3.2. SNA Reactivity. A significantly higher SNA binding to anti-TF Abs (a pool of all Ig isotypes) in cancer patients compared with controls was established ($P=0.0005$), including stage 1 patients ($P=0.001$) (Figure 3).

The SNA/IgG index was significantly higher in cancer patients ($P=0.0012$) and was observed at all stages of the disease (Figure 4). In contrast, the SNA/IgA index demonstrated a marked decrease in the cancer group (< 0.0001)

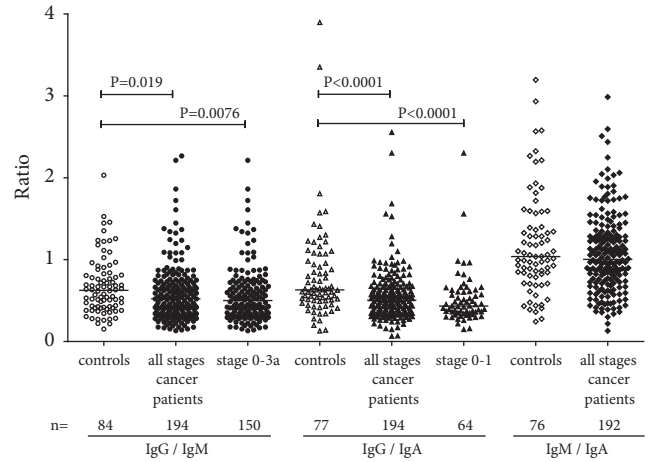


FIGURE 2: Different anti-TF antibody isotype ratios in cancer patients and controls. P values are shown for significant differences.

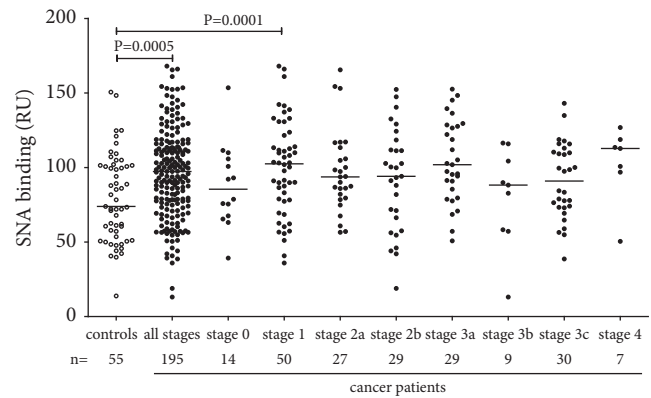


FIGURE 3: The binding of SNA lectin to TF-specific antibodies in the serum samples of cancer patients and controls. The group median is indicated by horizontal lines. P values are shown for significant differences.

irrespective of the disease stage especially in early cancer ($P < 0.0001$ for stage 0+1 patients). The SNA/IgM index revealed no significant difference between patients and the controls though a slight trend to increased values was detected ($p=0.12$).

These findings show that all anti-TF Ab isotypes contribute to cancer-related changes of the SNA reactivity of TF-specific Abs. It appears that IgG and IgM are responsible for the increase of SNA lectin binding in cancer.

3.3. Avidity of Anti-TF Abs in Breast Cancer Patients and Controls. No changes in the avidity of anti-TF IgG ($P=0.604$) and IgM ($P=0.67$) were found in cancer patients unlike controls, while the IgA Abs exhibited significantly higher avidity index values ($P=0.0109$) especially at the earlier stages of the disease ((1-3 a; $P=0.0007$) (Figure 5). In both cancer patients and controls, the IgG Abs showed a much higher avidity compared with IgM and IgA: $P < 0.0001$ in all comparisons. A significant negative correlation between the SNA binding and the avidity of anti-TF IgM, IgA and, to a lesser extent, IgG

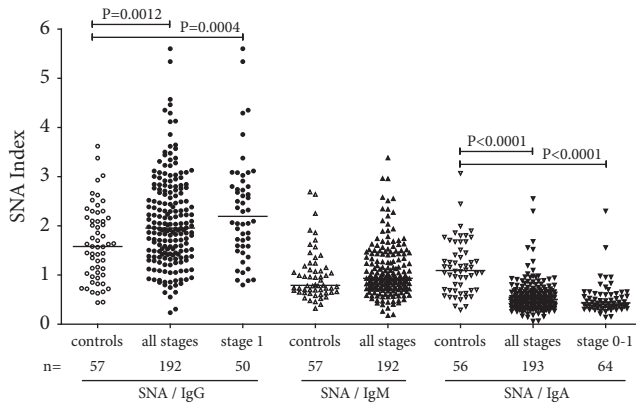


FIGURE 4: The anti-TF IgG, IgM, and IgA SNA indexes in patients and controls. P values are shown for significant differences.

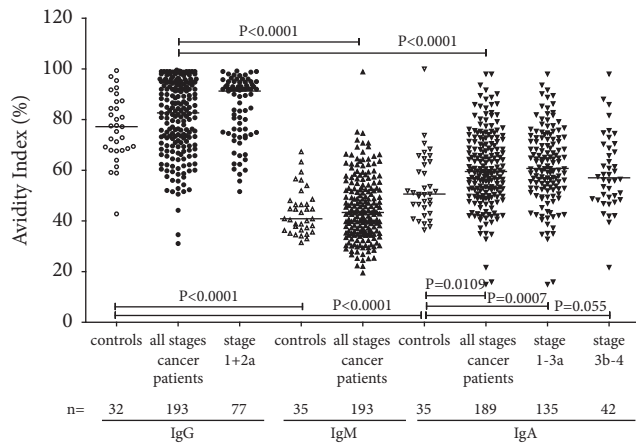


FIGURE 5: The avidity of anti-TF IgG, IgM, and IgA antibodies in controls and cancer patients.

($P=0.03$) was found in cancer patients (Figure 6). A similar trend was established in controls for IgM ($r=-0.31$, $P=0.08$) but not for IgG and IgA ($P=0.75$ and 0.23 , respectively).

Thus, a higher avidity of TF-specific IgA Abs was found in breast cancer patients. An increased SNA reactivity of anti-TF antibodies in breast cancer patients was associated with the prevalence of the lower avidity TF-specific antibodies.

3.4. Diagnostic Potential. The cancer-associated anti-TF Ab diversity differences were analysed by the Receiver Operator Curve (ROC) analysis to assess their possible potential for cancer-noncancer group discrimination (Table 2, Figure 7).

More informative data were noted about the highly significant decrease of the SNA/IgA index, which demonstrated an about 77% accuracy of diagnostics also at the very early stages of breast cancer (0+1) (Figure 7(b)) when the sensitivity was 62.5% even at 90% specificity (Table 2). In addition, the increased avidity of anti-TF IgA Abs revealed a rather high sensitivity and specificity for cancer (75% and 82.2%, respectively, with a 80.8% accuracy of diagnostics). Despite the significant difference between patients and controls,

the other parameters presented in Table 2 show diagnostic accuracy (ACC) values below 70%.

Thus, the lower SNA reactivity of anti-TF IgA antibodies (as evaluated by the SNA/IgA index), and their higher avidity demonstrated a rather good ability to discriminate patients with breast cancer from healthy controls already at the early stages of the disease.

4. Discussion

Unlike traditional tumor markers which are soluble proteins shed by bulky tumors, serum autoantibodies (AAbs) to TAAs are often detectable already at the early stages of cancer [38, 39]. It has been shown that the measurement of serum AAbs to a single specific TAA is usually of little value for breast cancer diagnosis [39, 40], whereas the analysis of Abs to a tailor-made panel of TAAs shows a promising diagnostic potential [41–43]. Contrary to the adaptive antibodies the naturally occurring Abs to TAA, including those to the TF antigen, are always present in the circulation, thus representing a universal and convenient target for analysis of their structural and functional alteration in neoplasia.

We proceeded from the assumption that cancer-specific signatures of anti-TF Abs may be due to their local modification by the inflammatory tumor microenvironment *in situ*. Moreover, the cancer-related changes may concern only a specific subset/glyco-subset of Abs but, at the same time, determine the main or entire functional activity and clinically important effects.

In the present study, a significant decrease of TF-specific IgG level was found already at the early stages of breast cancer. We have previously observed similar changes in patients with other cancers [9, 44, 45]. Unexpectedly, the IgA level was significantly elevated (Figure 1).

This is in contrast to our previous studies in patients with stomach, and colon cancer who showed no appreciable changes of serum IgA level [36, and unpublished] like many other natural and adaptive antibody levels in breast cancer patients [12, 39]. Notable, compared with Ab levels, the ratio between different Ab isotypes showed more pronounced differences between cancer patients, including those at the early stage of the disease (Figure 2), and controls, being highly significant for IgG/IgM and especially for IgG/IgA.

For all Ig subclasses, a low level of galactosylation and sialylation of the total serum IgG has been shown to be associated with various pathologies such as autoimmune diseases, cancer, and increased inflammation [25, 27–29, 35]. We established an increased binding of SNA to a pool of all isotypes of anti-TF Abs at all stages of cancer (Figure 3). Changes in the binding of sialic acid-specific lectin SNA to anti-TF antibodies reveal isotype-specific features. In fact, contrary to IgG and IgM, the IgA sialylation (SNA/IgA index) was very low ($P<0.0001$) in breast cancer patients, including stage 0-1 patients (Figure 4).

The low sialylation of TF-specific IgA Abs and their higher avidity in breast cancer patients revealed the best diagnostic potential (Table 2, Figure 7) with an about of 80% accuracy of diagnostics. We suggest that it is not the antibody level *per se* but rather the proportion of sialylated Abs among

TABLE 2: Receiver operating characteristic (ROC) curves analysis for distinguishing cancer patients from controls.

Parameter	stage	Sensitivity (95% CI)	Specificity (95% CI)	ROC Curve Area (95% CI)	P Value	ACC	Sensitivity at 90% Specificity
IgG/IgM ratio	all	60.3% (47.2% - 72.4%)	60.8% (53.6% - 67.7%)	0.636 (55.9% - 71.4%)	0.0012	0.603	26.8%
IgG/IgM ratio	0-3a	60.3% (47.2% - 72.4%)	64.7% (56.5% - 72.3%)	0.651 (57.2% - 73.1%)	0.0005	0.620	28.7%
IgG/IgA ratio	all	60.7% (46.8% - 73.5%)	58.8% (51.5% - 65.8%)	0.636 (54.8% - 72.3%)	0.0020	0.592	17.0%
IgG/IgA ratio	0-1	66.1% (52.2% - 72.2%)	65.6% (52.7% - 77.1%)	0.690 (59.4% - 78.7%)	0.0003	0.658	21.9%
SNA binding	all	63.6% (49.5% - 76.2%)	60.5% (53.3% - 67.4%)	0.658 (57.6% - 74.0%)	0.0003	0.612	23.1%
SNA binding	1-2a, b	63.6% (49.6% - 76.2%)	61.3% (51.4% - 70.6%)	0.659 (57.1% - 74.7%)	0.0009	0.621	24.5%
SNA/IgG index	all	66.7% (49.0% - 81.4%)	65.3% (58.1% - 72.0%)	0.706 (61.0% - 80.3%)	< 0.0001	0.651	32.1%
SNA/IgG index	0+1	69.4% (51.8% - 83.7%)	70.3% (57.6% - 81.1%)	0.754 (65.2% - 85.5%)	< 0.0001	0.700	39.1%
SNA/IgA index	all	58.3% (40.8% - 74.5%)	80.3% (74.0% - 85.7%)	0.793 (71.0% - 87.7%)	< 0.0001	0.769	49.2%
SNA/IgA index	0+1	58.3% (40.8% - 74.5%)	87.5% (76.9% - 94.5%)	0.833 (74.7% - 91.8%)	< 0.0001	0.770	62.5%
IgA avidity index	1-3a	75.0% (56.6% - 88.5%)	82.2% (74.4% - 88.3%)	79.7% (70.1% - 89.3%)	< 0.0001	0.808	33.3%

The diagnostic sensitivity, specificity, and accuracy for representative parameters studied at different stages of cancer. The area under the curve (AUC) with 95% confidence interval (CI), the accuracy of diagnostics (ACC), and P values are presented. AUC: the area under the receiver operator curve (ROC).

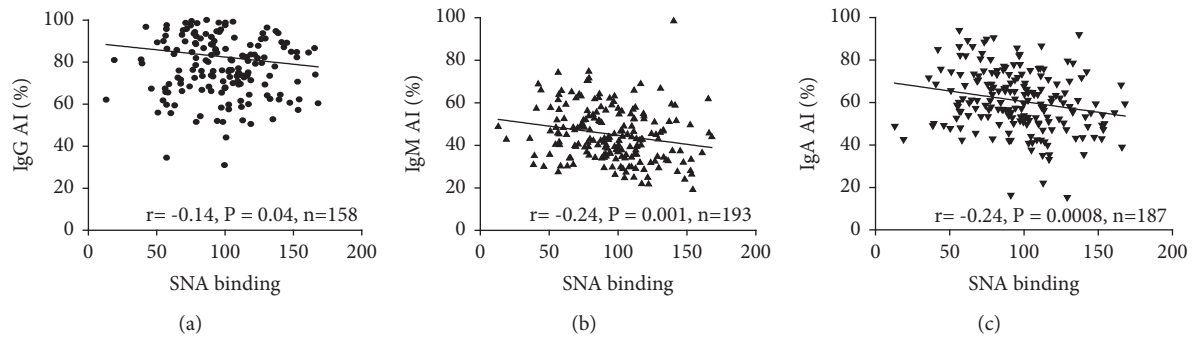


FIGURE 6: The correlation between the SNA lectin binding and the avidity of anti-TF IgG, IgM, and IgA in breast cancer patients.

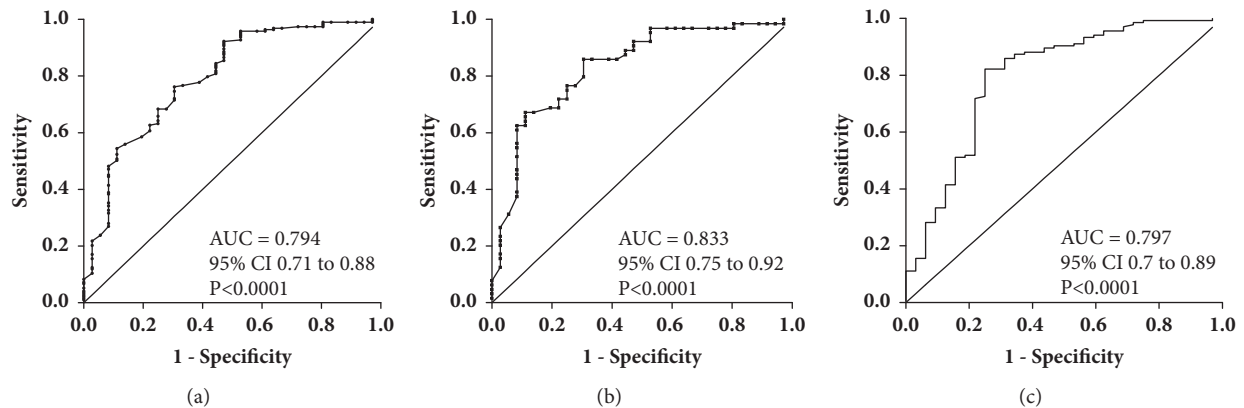


FIGURE 7: A receiver operator characteristic (ROC) curve analysis for anti-TF IgA-related parameters// SNA/IgA index and the avidity of IgA. (a) SNA/IgA index for all cancer patients; (b) SNA/IgA index for patients with 0-1 stage of cancer; (c) IgA avidity index for all breast cancer patients. The area under the ROC curve represents the diagnostic accuracy of changes in cancer.

various isotypes that is more informative. Since all isotypes may compete for SNA binding, these findings need to be further specified by using purified TF-specific Ab isotypes and their ability to interact with SNA in health and cancer. The findings of the present study as well as our recent data on gastric and colon cancer support the idea that the increased sialylation of the total serum anti-TF Abs (a pool of all isotypes) is a common phenomenon in cancer despite the differences observed between various Ig isotypes. Notable, these changes are quite opposite to those found in patients with autoimmune conditions [46] where the IgG agalactosylation and asialylation are typical changes, at least for total IgG. Thus, the glycosylation profile could be an informative marker for the discrimination between these two conditions. In our opinion the antigen-specific Abs deserve more attention because their glycoprofile and functional characteristics may appreciably differ from those of total serum immunoglobulins. It has been demonstrated that the sialylation level of IgG antibodies to rheumatoid arthritis-(RA-) associated antigens but not to other IgG Abs control the arthritogenicity of RA-associated IgG [47]. Specifically, the higher sialylated IgG suppressed the development of collagen-induced arthritis. The disease-specific IgG from serum and glycopeptides attached to the IgG Fc region have been analysed by mass spectrometry and their good ability

to distinguish gastric cancer from benign gastric conditions was demonstrated with a sensitivity and specificity above 80% [48]. There is evidence that the immune system drives Ab glycosylation in an antigen-specific manner [49]. Although factors contributing to the differences in the disease-specific Ab glycosylation remain not completely understood, our data support the idea that the glycoprofiling of disease-relevant autoantibodies may be a more promising way for the search of novel Ab-based biomarkers than the analysis of total serum immunoglobulins.

A general conclusion that can be drawn from our findings is that naturally occurring Abs to tumor-associated TF glyco-topes display cancer-specific changes that are observed already at the early stages of breast cancer. Importantly, these changes of TF-specific Abs may concern only a particular, i.e., higher sialylated subset of Abs. We suppose that the combined approach which takes into account the level of TF-specific Abs, their glycosylation profile, the relative proportions of different isotypes of Abs, their glyco-subsets, and functional characteristics has potential to be further developed into a novel noninvasive naturally occurring Ab-based methodology to cancer diagnostics and prognostics. This concept can be extended to other conditions (autoimmunity, infections) where structural and functional characterization of disease-specific Ab subsets would be of clinical importance.

Data Availability

Data may be available upon request through the corresponding author.

Conflicts of Interest

The authors declare that there are no conflicts of interest regarding the publication of this paper.

Acknowledgments

This work was supported by the Estonian Research Council Grant PUT371.

References

- [1] G. F. Springer, "T and Tn, general carcinoma autoantigens," *Science*, vol. 224, no. 4654, pp. 1198–1206, 1984.
- [2] G. F. Springer, "Immunoreactive T and Tn epitopes in cancer diagnosis, prognosis, and immunotherapy," *Journal of Molecular Medicine*, vol. 75, no. 8, pp. 594–602, 1997.
- [3] S. Hakomori, "Aberrant glycosylation in tumors and tumor-associated carbohydrate antigens," *Advances in Cancer Research*, vol. 52, pp. 257–331, 1989.
- [4] H. P. Vollmers and S. Brändlein, "Natural antibodies and cancer," *Journal of Autoimmunity*, vol. 29, no. 4, pp. 295–302, 2007.
- [5] U. M. Abd Hamid, L. Royle, R. Saldova et al., "A strategy to reveal potential glycan markers from serum glycoproteins associated with breast cancer progression," *Glycobiology*, vol. 18, no. 12, pp. 1105–1118, 2008.
- [6] H. H. Wandall, O. Blixt, M. A. Tarp et al., "Cancer biomarkers defined by autoantibody signatures to aberrant O-glycopeptide epitopes," *Cancer Research*, vol. 70, no. 4, pp. 1306–1313, 2010.
- [7] S. Kobold, T. Lütken, Y. Cao, C. Bokemeyer, and D. Atanackovic, "Autoantibodies against tumor-related antigens: incidence and biologic significance," *Human Immunology*, vol. 71, no. 7, pp. 643–651, 2010.
- [8] B. Monzavi-Karbassi, A. Pashov, and T. Kieber-Emmons, "Tumor-Associated Glycans and Immune Surveillance," *Vaccines*, vol. 1, no. 2, pp. 174–203, 2013.
- [9] O. Kurtenkov, K. Klaamas, S. Mensdorff-Pouilly, L. Miljukhina, L. Shljapnikova, and V. Chužmarov, "Humoral immune response to MUC1 and to the Thomsen-Friedenreich (TF) glyco- tope in patients with gastric cancer: relation to survival," *Acta Oncologica*, vol. 46, no. 3, pp. 316–323, 2007.
- [10] R. Schwartz-Albiez, "Naturally occurring antibodies directed against carbohydrate tumor antigens," *Advances in Experimental Medicine and Biology*, vol. 750, pp. 27–43, 2012.
- [11] N. V. Bovin, "Natural antibodies to glycans," *Biochemistry (Moscow)*, vol. 78, no. 7, pp. 786–797, 2013.
- [12] M. Díaz-Zaragoza, R. Hernández-Ávila, R. Viedma-Rodríguez, D. Arenas-Aranda, and P. Ostoa-Saloma, "Natural and adaptive IgM antibodies in the recognition of tumor-associated antigens of breast cancer (Review)," *Oncology Reports*, vol. 34, no. 3, pp. 1106–1114, 2015.
- [13] G. F. Springer and H. Tegtmeier, "Origin of anti-Thomsen-Friedenreich (T) and Tn agglutinins in man and in white leghorn chicks," *British Journal of Haematology*, vol. 47, no. 3, pp. 453–460, 1981.
- [14] U. Galili, R. E. Mandrell, R. M. Hamadeh, S. B. Shohet, and J. M. Griffiss, "Interaction between human natural anti- α -galactosyl immunoglobulin G and bacteria of the human flora," *Infection and Immunity*, vol. 56, no. 7, pp. 1730–1737, 1988.
- [15] N. R. Khasbiullina and N. V. Bovin, "Hypotheses of the origin of natural antibodies: A glyco-biologist's opinion," *Biochemistry (Moscow)*, vol. 80, no. 7, pp. 820–835, 2015.
- [16] U. Karsten and S. Goletz, "What controls the expression of the core-1 (Thomsen - Friedenreich) glyco- tope on tumor cells?" *Biochemistry (Moscow)*, vol. 80, no. 7, pp. 801–807, 2015.
- [17] L.-G. Yu, "The oncofetal Thomsen-Friedenreich carbohydrate antigen in cancer progression," *Glycoconjugate Journal*, vol. 24, no. 8, pp. 411–420, 2007.
- [18] E. Smorodin, B. Sergeev, K. Klaamas, V. Chuzmarov, and O. Kurtenkov, "The relation of the level of serum anti-TF, -Tn and -alpha-gal IgG to survival in gastrointestinal cancer patients," *International Journal of Medical Sciences*, vol. 10, no. 12, pp. 1674–1682, 2013.
- [19] E. P. Smorodin and B. L. Sergeev, "The level of IgG antibodies reactive to TF, Tn and alpha-Gal polyacrylamide-glycoconjugates in breast cancer patients: relation to survival," *Experimental Oncology*, vol. 38, no. 2, pp. 117–121, 2016.
- [20] S. Tati, J. C. Fisk, J. Abdullah et al., "Corrigendum to "Humanization of JAA-F11, a Highly Specific Anti-Thomsen-Friedenreich Pancarcinoma Antibody and In Vitro Efficacy Analysis" [Neoplasia 19.9 (2017) 716-733] (S1476558617302270) (10.1016/j.neo.2017.07.001)," *Neoplasia (United States)*, vol. 20, no. 1, p. 118, 2018.
- [21] F. Nimmerjahn and J. V. Ravetch, "Antibodies, Fc receptors and cancer," *Current Opinion in Immunology*, vol. 19, no. 2, pp. 239–245, 2007.
- [22] T. S. Raju, "Terminal sugars of Fc glycans influence antibody effector functions of IgGs," *Current Opinion in Immunology*, vol. 20, no. 4, pp. 471–478, 2008.
- [23] M. D. Kazatchkine and S. V. Kaveri, "Immunomodulation of autoimmune and inflammatory diseases with intravenous immune globulin," *The New England Journal of Medicine*, vol. 345, no. 10, pp. 747–755, 2001.
- [24] Y. Kaneko, F. Nimmerjahn, and J. V. Ravetch, "Anti-inflammatory activity of immunoglobulin G resulting from Fc sialylation," *Science*, vol. 313, no. 5787, pp. 670–673, 2006.
- [25] S. Böhm, I. Schwab, A. Lux, and F. Nimmerjahn, "The role of sialic acid as a modulator of the anti-inflammatory activity of IgG," *Seminars in Immunopathology*, vol. 34, no. 3, pp. 443–453, 2012.
- [26] A. S. Mehta, R. E. Long, M. A. Comunale et al., "Increased levels of galactose-deficient anti-Gal immunoglobulin G in the sera of hepatitis C virus-infected individuals with fibrosis and cirrhosis," *Journal of Virology*, vol. 82, no. 3, pp. 1259–1270, 2008.
- [27] K. Kodar, J. Stadlmann, K. Klaamas, B. Sergeev, and O. Kurtenkov, "Immunoglobulin G Fc N-glycan profiling in patients with gastric cancer by LC-ESI-MS: relation to tumor progression and survival," *Glycoconjugate Journal*, vol. 29, no. 1, pp. 57–66, 2012.
- [28] K. Shade and R. Anthony, "Antibody Glycosylation and Inflammation," *Antibodies*, vol. 2, no. 4, pp. 392–414, 2013.
- [29] S. Ren, Z. Zhang, C. Xu et al., "Distribution of IgG galactosylation as a promising biomarker for cancer screening in multiple cancer types," *Cell Research*, vol. 26, no. 8, pp. 963–966, 2016.
- [30] N. Kawaguchi-Sakita, K. Kaneshiro-Nakagawa, M. Kawashima et al., "Serum immunoglobulin G Fc region N-glycosylation profiling by matrix-assisted laser desorption/ionization mass

- spectrometry can distinguish breast cancer patients from cancer-free controls," *Biochemical and Biophysical Research Communications*, vol. 469, no. 4, pp. 1140–1145, 2016.
- [31] K. Kodar, O. Kurtenkov, and K. Klaamas, "The thomsen-friedenreich antigen and α Gal-specific human IgG glycoforms: concanavalin a reactivity and relation to survival of cancer patients," *Immunological Investigations*, vol. 38, no. 8, pp. 704–717, 2009.
- [32] M. Stuchlová Horynová, M. Raška, H. Clausen, and J. Novak, "Aberrant O-glycosylation and anti-glycan antibodies in an autoimmune disease IgA nephropathy and breast adenocarcinoma," *Cellular and Molecular Life Sciences*, vol. 70, no. 5, pp. 829–839, 2013.
- [33] T. Li, D. J. DiLillo, S. Bournazos, J. P. Giddens, J. V. Ravetch, and L. Wang, "Modulating IgG effector function by Fc glycan engineering," *Proceedings of the National Academy of Sciences of the United States of America*, vol. 114, no. 13, pp. 3485–3490, 2017.
- [34] X. Yu, M. J. E. Marshall, M. S. Cragg, and M. Crispin, "Improving Antibody-Based Cancer Therapeutics Through Glycan Engineering," *BioDrugs*, vol. 31, no. 3, pp. 151–166, 2017.
- [35] K. Kodar, J. Izotova, K. Klaamas, B. Sergeev, L. Järvekülg, and O. Kurtenkov, "Aberrant glycosylation of the anti-Thomsen-Friedenreich glycotope immunoglobulin G in gastric cancer patients," *World Journal of Gastroenterology*, vol. 19, no. 23, pp. 3573–3582, 2013.
- [36] Oleg Kurtenkov, Jelena Izotova, Kersti Klaamas, and Boris Sergeev, "Increased Sialylation of Anti-Thomsen-Friedenreich Antigen (CD176) Antibodies in Patients with Gastric Cancer: A Diagnostic and Prognostic Potential," *BioMed Research International*, vol. 2014, Article ID 830847, pp. 1–11, 2014.
- [37] Oleg Kurtenkov and Kersti Klaamas, "Hidden IgG Antibodies to the Tumor-Associated Thomsen-Friedenreich Antigen in Gastric Cancer Patients: Lectin Reactivity, Avidity, and Clinical Relevance," *BioMed Research International*, vol. 2017, Article ID 6097647, pp. 1–11, 2017.
- [38] C.-K. Heo, Y. Y. Bahk, and E.-W. Cho, "Tumor-associated autoantibodies as diagnostic and prognostic biomarkers," *BMB Reports*, vol. 45, no. 12, pp. 677–685, 2012.
- [39] Jérôme Lacombe, Alain Mangé, and Jérôme Solassol, "Use of Autoantibodies to Detect the Onset of Breast Cancer," *Journal of Immunology Research*, vol. 2014, Article ID 574981, pp. 1–8, 2014.
- [40] W. Liu, I. G. De La Torre, M. C. Gutiérrez-Rivera et al., "Detection of autoantibodies to multiple tumor-associated antigens (TAAs) in the immunodiagnosis of breast cancer," *Tumor Biology*, vol. 36, no. 2, pp. 1307–1312, 2015.
- [41] L. Zhong, K. Ge, J. Zu et al., "Autoantibodies as potential biomarkers for breast cancer," *Breast Cancer Research*, vol. 10, no. 3, article R40, 2008.
- [42] E. Piura and B. Piura, "Autoantibodies to Tumor-Associated Antigens in Breast Carcinoma," *Journal of Oncology*, vol. 2010, pp. 1–14, 2010.
- [43] Y. Liu, Y. Liao, L. Xiang et al., "A panel of autoantibodies as potential early diagnostic serum biomarkers in patients with breast cancer," *International Journal of Clinical Oncology*, vol. 22, no. 2, pp. 291–296, 2017.
- [44] O. Kurtenkov, L. Miljukhina, J. Smorodin et al., "Natural IgM and IgG antibodies to Thomsen-Friedenreich (T) antigen in serum of patients with gastric cancer and blood donors—relation to Lewis (a,b) histo-blood group phenotype," *Acta Oncologica*, vol. 38, no. 7, pp. 939–943, 1999.
- [45] O. Kurtenkov, K. Klaamas, K. Rittenhouse-Olson et al., "IgG immune response to tumor-associated carbohydrate antigens (TF, Tn, α Gal) in patients with breast cancer: Impact of neoadjuvant chemotherapy and relation to the survival," *Experimental Oncology*, vol. 27, no. 2, pp. 136–140, 2005.
- [46] R. Plomp, L. R. Ruhaak, H. Uh et al., "Subclass-specific IgG glycosylation is associated with markers of inflammation and metabolic health," *Scientific Reports*, vol. 7, no. 1, 2017.
- [47] Y. Ohmi, W. Ise, A. Harazono et al., "Sialylation converts arthritogenic IgG into inhibitors of collagen-induced arthritis," *Nature Communications*, vol. 7, Article ID 11205, 2016.
- [48] D. Zhang, B. Chen, Y. Wang et al., "Disease-specific IgG Fc N-glycosylation as personalized biomarkers to differentiate gastric cancer from benign gastric diseases," *Scientific Reports*, vol. 6, no. 1, 2016.
- [49] A. E. Mahan, M. F. Jennewein, T. Suscovich et al., "Antigen-Specific Antibody Glycosylation Is Regulated via Vaccination," *PLoS Pathogens*, vol. 12, no. 3, Article ID e1005456, 2016.

Review Article

Targeting CD36 as Biomarker for Metastasis Prognostic: How Far from Translation into Clinical Practice?

Ana-Maria Enciu ^{1,2}, Eugen Radu ^{1,2}, Ionela Daniela Popescu ¹,
Mihail Eugen Hinescu ^{1,2} and Laura Cristina Ceafalan ^{1,2}

¹Victor Babes National Institute of Pathology, 99-101 Splaiul Independentei, Sector 5, 050096 Bucharest, Romania

²Carol Davila University of Medicine and Pharmacy, No. 8 B-dul Eroilor Sanitari, Sector 5, 050474, Bucharest, Romania

Correspondence should be addressed to Eugen Radu; eugen.radu@umfcd.ro and Mihail Eugen Hinescu; mhinescu@yahoo.com

Received 23 March 2018; Accepted 21 May 2018; Published 4 July 2018

Academic Editor: Valli De Re

Copyright © 2018 Ana-Maria Enciu et al. This is an open access article distributed under the Creative Commons Attribution License, which permits unrestricted use, distribution, and reproduction in any medium, provided the original work is properly cited.

Metastasis requires cellular changes related to cell-to-cell and cell-to-matrix adhesion, immune surveillance, activation of growth and survival signalling pathways, and epigenetic modifications. In addition to tumour cells, tumour stroma is also modified in relationship to the primary tumour as well as to distant metastatic sites (forming a metastatic niche). A common denominator of most stromal partners in tumour progression is CD36, a scavenger receptor for fatty acid uptake that modulates cell-to-extracellular matrix attachment, stromal cell fate (for adipocytes, endothelial cells), TGF β activation, and immune signalling. CD36 has been repeatedly proposed as a prognostic marker in various cancers, mostly of epithelial origin (breast, prostate, ovary, and colon) and also for hepatic carcinoma and gliomas. Data gathered in preclinical models of various cancers have shown that blocking CD36 might prove beneficial in stopping metastasis spread. However, targeting the receptor in clinical trials with thrombospondin mimetic peptides has proven ineffective, and monoclonal antibodies are not yet available for patient use. This review presents data to support CD36 as a potential prognostic biomarker in cancer, its current stage towards achieving *bona fide* biomarker status, and knowledge gaps that must be filled before further advancement towards clinical practice.

1. Introduction

Metastasis is a rather inefficient process if the number of circulating tumour cells is to be compared with the number of clinically overt metastatic sites [1]. From vascular invasion to secondary site tumour initiation, a cell can go through changes in cell-to-cell and cell-to-matrix adhesion profile, face immune surveillance systems, activate growth and survival signalling pathways, and undergo epigenetic modifications. To be effective, these changes must occur in a time-dependent manner, modifying the cell phenotype for survival in new microenvironments. Under these conditions, how much of the primary tumour is recapitulated in a metastasis? And how can we predict whether or when a primary tumour would seed secondary sites?

Perhaps surprisingly, scrutinizing the less investigated stromal tumour tissue—or the modern and reinvented “stromal metastatic niche”—could provide some answers. The

metastatic niche has been defined as “extracellular matrix, nonmalignant cells, and the signalling molecules they produce” [2]. Different in composition and less characterized than its counterpart—the primary tumour niche—the stromal metastatic niche recently underwent a shift in perspective to a “premetastatic niche,” prepared in advance by conditioned infiltrating monocytes. This premetastatic niche, as yet unoccupied by tumour cells, is thought to create a tumour friendly environment to enhance the survival chances of invading cells [3].

A common denominator of most stromal partners playing a role in tumour progression is expression of CD36—a scavenger receptor for fatty acid (FA) uptake that modulates cell-to-extracellular matrix attachment, stromal cell fate (for adipocytes, endothelial cells), TGF β activation, and immune signalling [4]. Unlike its well-known and better-studied binding partners (thrombospondins (TSPs) 1 and 2) but with controversial involvement in cancer progression, CD36 is

increasingly emerging as a prognostic marker associated with the metastatic process. Even more so, its presence seems not to be limited to tumour stroma, as the number of reports describing it on tumour cells is increasing.

Several gaps remain in CD36-related knowledge. Learning from paths travelled in understanding other receptors as cancer-related biomarkers, one can argue that there are still plenty of blank spots on the CD36 cancer-related map. In cancer studies, CD36 is investigated mostly in relationship with TSPs, a family of matrix proteins acting as ligands, and most data are related to TSP interactions and, to a lesser extent, TGF β . Only a handful of papers have been published directly addressing CD36, almost all measuring levels of expression in relationship to tumour growth and metastasis. Furthermore, lessons from myeloproliferative diseases and gliomas suggest that mutated receptors do not require a ligand to be active. In the case of CD36, constitutive activation, regardless of TSP expression within the tumour or tumour niche, could be largely overlooked if the main focus falls on the ligand rather than the receptor.

In addition, a parallel analysis of stromal CD36 versus tumour CD36 is usually missing from the scientific argument in most original articles. Last, but not least, studies in animal models using athymic mice remove a key player from the stroma, the immune cell, yielding an incomplete tumour–stroma interaction panel.

What is the ultimate goal in CD36 research? One size fits all? Probably not. That pattern has not yet been the case for any molecular intervention in diagnostics, prognostics, or therapy. However, the chase for a single but efficient antimetastatic molecular target is justifiable from several perspectives. First and foremost, time is gained for diagnostic and therapeutic intervention. Second, absence of metastases will translate into an absence of cellular polymorphisms derived from environmental change. Thus, molecular therapies addressing the primary tumour could have a greater impact on relapse and survival rates.

How far is CD36 from validated status as a biomarker and what type of biomarker would best fit are the questions the present review will attempt to answer, after analysing the evidence tying CD36 to the metastatic process and the translation into knowledge towards clinical practice.

2. CD36 Distribution and Functions in Normal Tissues

CD36, also known as platelet glycoprotein (GP) 4/, FA translocase (FAT)/, scavenger receptor class B member 3 (SCARB3)/, GP88, GPIIB, or GPIV [5], is an integral membrane GP encoded by the CD36 gene and belonging to the scavenger receptor family. The intracellular trafficking of the molecule requires different degrees of glycosylation, with the heavy glycosylated protein being exposed on the cell membrane [6, 7]. When exposed, CD36 may associate with other transmembrane proteins, such as integrins (β 1, β 2, and β 5) and tetraspanins (CD9, CD81) [8]. Its intracellular domains associate with members of the src family of tyrosine kinases, such as fyn, lyn, and, yes, a molecular interaction

most probably mediated by lipids in the context of lipid rafts [9]. Supramolecular assembly of CD36 into nanoclusters at the plasma membrane, even in the absence of ligands, is important for downstream fyn signalling [10]. The extracellular domain binds to a vast array of ligands, which accounts for the diversity of signal transduction outcomes: (i) adhesive glycoproteins of the TSP family [11]; (ii) collagenic proteins (collagens I and IV) [5]; (iii) lipid ligands (anionic or oxidized phospholipids –PL), native and oxidized lipoproteins [8], FAs; and (iv) peptides such as hexarelin or fibrillar A β amyloid species [12].

As a surface protein, CD36 is widely distributed. Found on platelets and monocytes/macrophages, it is involved in cellular activation. It not only mediates the initial binding of platelets on extracellular matrix protein like collagen I [5] and TSP-1 but also triggers signal transduction, inducing an oxidative burst in monocytes [13]. In addition, it is present on erythrocytes, where it mediates adherence of *Plasmodium falciparum*-infected erythrocytes.

CD36 expression was also detected in differentiated adipocytes [14]. *In vitro* studies proved that CD36 is located in lipid rafts, along with caveolin-1, mediating FA uptake [15]. Both functional studies with CD36 cross-linking agents and disruption of lipid rafts stop the transport of long-chain FAs [14].

In skeletal muscle, CD36 expression on the cell surface is an important mechanism for FA uptake and short-term regulation through subcellular redistribution [16]. However, CD36 is also found in the mitochondria, where it is responsible for FA oxidation [17]. CD36 expression is regulated by both insulin and contraction, which promotes the translocation of intracellular stored CD36 to the plasma membrane. Increased expression can contribute to lipid accumulation in heart and skeletal muscle [18].

CD36 also has been described on endothelial cells of human dermis, but only in the microvasculature and not in the large vessels [19] and in caveolin-rich membranes isolated from lung endothelium [20]. It is also present on normal mammary epithelial cells [21], which prompted its investigation in breast cancer, as discussed below.

Another type of epithelial cell expressing CD36 is the taste receptor cell within lingual taste buds in tongue of rodents [22], pigs, and humans [23]. CD36 expression is restricted to only the lingual papillae where it has been localized at the apical side of the circumvallate [22] and foliate taste buds [23]. Its expression is lipid-mediated, changing the attraction for fat during a meal [24]. Only lipid discrimination is affected in CD36-null mice [22].

CD36 is expressed in the brush border membrane of duodenal and jejunal enterocytes [25] in both mice and humans [26]. Moreover, early after lipid ingestion, CD36 disappears from the luminal side of intestinal villi [27]. Similar to adipocytes, CD36 is located in lipid rafts, where it colocalizes with caveolin-1. *In vitro* studies showed that caveolin-1 is required for the transport of CD36 to the apical membrane, thus regulating its surface availability for FA uptake [28]. Moreover, brush border caveolae provide the absorptive surface for dietary FA. Studies performed on

caveolin-1 knockout mice proved that FA absorption was compromised and the animals could not gain weight [25].

Also at the intestinal level, CD36 was detected on enteroendocrine cells secreting secretin and cholecystokinin in the mucosa of the duodenum, jejunum, and proximal ileum on both apical membranes and cytosolic granules [29].

In mouse liver, CD36 is expressed on hepatocytes, endothelial cells, and Kupffer cells [30] and the expression is increased by starvation [8] and aging, especially when associated with a high-fat diet. Insulin increases CD36 expression in the liver [31] by activating PPAR γ , an upstream regulator of CD36 expression. Enhanced expression and subsequent fat uptake and triglyceride (TG) accumulation may accelerate progression of nonalcoholic fatty liver disease [32], insulin resistance, and type 2 diabetes [33].

In the normal brain, CD36 expression is low, but it is upregulated upon stroke due to monocyte-macrophage infiltration. It appears that CD36 contributes to acute ischemic brain injury during the inflammatory phase and is involved in phagocytosis during the recovery phase [7].

In ovary, CD36 is found on serous ovarian epithelial cells [34], contributing to angiogenesis and folliculogenesis [35].

3. Functions of CD36: Lessons Learned from the CD36 Knockout Mouse Model

CD36 was first identified as platelet GPIV, due to thrombocytes' ability to bind TSP [36]. Later, its overlapping structure with leukocyte differentiation antigen CD36 was demonstrated [37]. In the following years, its role in platelet activation [38] and cell adhesion [39] was investigated. Not long after, its involvement in translocation of long-chain FAs was reported [40].

Febbraio and collaborators have played an important role in understanding CD36 functions by creating mice with a null mutation in the CD36 gene through targeted homologous recombination [41]. The animal model was subsequently used by a large number of researchers, with 528 citations recorded to date (ISI Web of Science Core Collection, searched on March 13, 2018). Some of the significant insights provided by CD36 $^{-/-}$ mouse experiments include regulation of CD36 by PPAR- γ [42] inhibition of angiogenesis *in vitro* and *in vivo*; induction of apoptosis by TSP-1 via activation of CD36, p59fyn, caspase-3-like proteases, and p38 mitogen-activated protein kinases [43]; understanding of atherosclerotic lesion development [44, 45] contribution to uptake and use long-chain FAs [46] diet response [47], serving as an advanced glycation end-products receptor [48] orosensory perception of long-chain FAs [49]. Conversely, mice were also engineered to overexpress CD36 in specific tissues by using the promoter of the muscle creatine kinase gene, resulting in enhanced FA oxidation, reduced plasma TGs and FAs, and increased plasma glucose and insulin [50].

More recent mouse experimental models include double-knockout animals for CD36 and other genes such as leptin [51], tyrosine-protein kinase Mer [52], liver-specific signal transducer and activator of transcription (STAT)5 [53], scavenger receptor-A [54], scavenger receptor class B type I [55],

heart-specific lipoprotein lipase [56], apolipoprotein E [57], and liver-type FA-binding protein [58].

The CD36 molecular structure includes two transmembrane domains located near both ends of the molecule, joined by a large extracellular region [59]; the transmembrane domains continue with small intracellular tails that are palmitoylated [60] and are important in localizing CD36 within caveolae and lipid rafts [61]. The N-glycosylated extracellular region has a binding site for TSP-1 (residues 93–120) [62] and one site for competitive binding of FA and oxidized low-density lipoprotein (ox)LDL/oxidized glycerophospholipids (residues: 150–168) [63, 64] that can bind hexarelin, one of several growth hormone-releasing peptides [65], and PfEMP1 proteins of the malaria parasite [66]. Neculai et al. [67] found, through an analogy with the crystal structure of structurally related LIMP-2 that they described, a notable feature of the CD36 extracellular domain: a tunnel, mainly comprising hydrophobic residues, spanning its entire length and apparently able to selectively transfer cholesterol esters from the extracellular environment to the outer leaflet of the cell membrane. Thus, future, more detailed structural studies of CD36 could provide actionable targets for therapies for diseases involving this molecule and its numerous, highly variable binding partners.

Other studies have contributed to identifying and understanding the role of CD36 association with other membrane or intracellular molecules. An interesting example is the discovery of CD36 as a regulator of Toll-like receptors 4 and 6 heterodimer assembly that can subsequently trigger inflammatory signalling in microglia [68]. Such data suggest that CD36 can make a major contribution to sterile inflammation in response to atherogenic lipids and amyloid-beta.

Interesting avenues of research might also be opened by a few recent studies that identified a role for noncoding RNA molecules in CD36 expression regulation with functional consequences. miR-758-5p decreases lipid accumulation in foam cells via regulating CD36-mediated cholesterol uptake [69], long noncoding RNA MALAT1 regulates oxLDL-induced CD36 expression via activating β -catenin [70], and uc.372, an ultraconserved RNA belonging to the class of long noncoding RNAs, regulates expression of genes related to lipid synthesis and uptake, including CD36, via suppression of specific miR molecule maturation [71].

Following data gathered from these models and others not mentioned here, the involvement in lipid metabolism and cell-to-matrix adhesion has been confirmed for various cell types, and other functions that are site-specific have been identified and are presented briefly below.

3.1. Lipid Scavenger Receptor and Subsequent Impact on Lipid Metabolism. CD36 has long been known as a scavenger receptor able to bind oxidized LDL (oxLDL) and HDL (oxHDL) [72, 73] but also native lipoprotein molecules [74]. CD36 is involved in high-affinity FA uptake and processing and eventually lipid accumulation and metabolic dysfunction under excessive supply [8]. First found on monocytes and platelets, CD36 is also responsible for uptake of long-chain FA into muscle and adipose tissues and across the

brush border [25]. Ligand binding activates phospholipase C, increases cytosolic Ca concentration, and activates chylomicron production [27]. CD36 also regulates the secretion of hepatic very LDL (VLDL), which may explain the correlation between CD36 protein expression and serum levels of VLDL lipid, particle number, and apolipoprotein B in humans [75]. CD36 deletion decreases VLDL output *in vivo* by increasing prostaglandins D2, F2, and E2 synthesis in the liver [51].

CD36 is a key factor in acute and adaptive regulation of muscle FA oxidation in response to a chronic metabolic stimulus and for the selection of skeletal muscle fuel under basal conditions, during acute exercise, or after muscle training [76]. In heart muscle, CD36 impacts adaptation of myocardial rhythm to energy deprivation [77]. During fasting, CD36 null mice have abnormal myocardial Ca²⁺ dynamics, phospholipid composition, and cAMP levels and associated conduction anomalies with a high incidence of sudden death [77]. Moreover, recent data have shown that myocardial CD36-mediated signal transduction activates FA β -oxidation [8].

Pathology Impact. Following the interaction of oxLDL with CD36 on intimal transmigrated macrophages, oxLDLs are internalized. They bind to the nuclear hormone receptor PPAR γ followed by the upregulation of CD36, which amplifies oxLDL uptake and foam cell formation [78]. Moreover, by stimulation of cytokine production, intima is further infiltrated and atherosclerotic lesion is formed [8].

3.2. Cell-to-Matrix Attachment. CD36 can bind to extracellular matrix proteins, such as collagen [5] and thrombospondin 2 in platelets and various cell lines. It also binds to TSP-1, but at concentrations higher than physiological, possibly reached in overdeveloped cancerous stromal tissue. CD47 is required for CD36 activation under TSP-1 ligation [79]. In endothelial cells, TSP binding triggers apoptosis, a mechanism bypassed in cancer, where it favours angiogenesis and tumour growth, as discussed later.

4. CD36 as an Early Biomarker for Metastatic Cancer

The term “biomarker” came into frequent use from the 1970s [80] and is currently defined as a “characteristic that is measured as an indicator of normal biological processes, pathogenic processes, or responses to an exposure or intervention, including therapeutic interventions” [81]. A candidate biomarker should provide measurable features, accuracy in indication for a physiologic or pathogenic mechanism, or pharmacological response to a therapeutic approach. According to the US Food and Drug Administration, an ideal biomarker should be highly sensitive and specific for a certain disease, safe, and easily measured in any biological sample, cost-effective, and able to yield accurate results [82].

Correlated with invasion of tumours and metastasis, CD36 has been repeatedly proposed as a prognostic marker in various types of cancers, mostly of epithelial origin. In the following section, we discuss the results that build up the case

for CD36 as an “early prognostic marker in metastasis” and review its progress towards clinical validation.

4.1. Preclinical Studies. To be considered as a potential biomarker of metastatic cancer, CD36 must respect the first rule of biomarkers—to exhibit a constant change in disease versus health, in this case, in metastatic cancer versus normal paired control tissue. Indeed, the expression of CD36 has been demonstrated to be *increased* in human tumour cell lines, human biopsies from ovarian tumours [83], gastric cancer [84], glioblastoma [85], and oral squamous carcinoma [86]. In contrast, consistent with data from tumour growth mechanism studies, CD36 has been reported to be *decreased* in endothelial cells, as a bypass program of its antiangiogenic effect [87].

Most preclinical studies address CD36 indirectly, in the context of TSP binding. These studies exploit the antiangiogenic effect of TSP 1 and 2 via CD36 signalling, by using recombinant proteins, or TSR peptides, to compensate for loss of TSP in tumour cells. Controversies arose when migration and invasion of cancer cells seemed to be promoted although the primary tumour responded to treatment. A TSP-1 null/breast cancer mouse model demonstrated reduced pulmonary metastases, although there was no impact on primary tumour growth, indicative of effects on the metastatic [88]. The same group demonstrated that inclusion of the RFK sequence in the TSP recombinant protein impacts positively metastases reduction, but in relation to TGF β activation [88], and that, to some extent, loss of CD36 binding to TSP is compensated by the RFK sequence, in terms of antitumour effect. Another study on a mouse model of breast cancer, using a TSP-2-derived recombinant protein, reported both inhibition of primary tumour growth and reduction of lymph node and lung metastasis. Although the primary effect was positively correlated with CD36-induced mitochondrial apoptosis in endothelial cells and decreased neoangiogenesis; an antimetastatic effect was correlated with the RFK sequence and TGF β activation [89].

Results with another mouse model of metastatic breast cancer indicated that although CD36 expression in the whole primary tumour was downregulated, this alteration was related to loss of stromal receptor. This hypothesis was confirmed by normal expression of CD36 on isolated tumour cells [90].

In metastatic prostate cancer, CD36 was activated in tumour cells, which led to increased cell migration and invasion, linked to downstream activation of MAPK [91].

Ovarian tumour cells harvested from ascites of patients also express CD36, which was used by Wang et al. as a target for TSP-1-induced apoptosis and subsequent tumour shrinkage in a mouse xenograft model [92]. A recent study showed upregulation of CD36 in metastatic *versus* primary human ovarian tumours; moreover, blocking CD36 with monoclonal antibodies resulted in reduced tumour burden in a mouse xenograft model [83]. Furthermore, Russell et al. found that combined therapy with thrombospondin-1 type I repeats (3TSR) and chemotherapy induces regression and improves survival in a mouse model of ovarian cancer [93].

TABLE 1: Involvement of CD36 in various types of cancer—data from human sample studies.

Type of cancer	Location within the tumour	Contribution of CD36	Refs
Breast cancer	Stroma tissue Decreased endothelial expression Tumour cells	Angiogenesis	[90] [87]
Prostate cancer	Tumour cells	Activation of MAPK signalling, pro-invasion	[91]
Ovarian cancer	Tumour cells harvested from patient ascites	Pro-metastatic	[92]
Colon cancer	Not specified	Decreased expression in metastatic cancer	[96]
Oral squamous cell carcinoma	Tumour cells	Favours lymph node and lung metastasis	[86]
Acute myeloid leukaemia	Tumour cells	Part of immunophenotyping panel used for patient stratification	[95]
Glioblastoma	Tumour cells	Maintenance of stemness features, tumour initiation	[85]
Hepatocellular carcinoma	Not mentioned	Increased CD36 is associated with epithelial-to-mesenchymal transduction	[101]

These results suggest that CD36 might offer an interesting therapy target, besides its putative biomarker role.

CD36 has been reported on glioblastoma cells as well, in a specific subset of stem-like cells, with role in stemness preservation and tumour initiation [85].

Recently, a study addressed directly the involvement of CD36 in tumour growth and metastasis, by overexpressing CD36 in oral squamous carcinoma cell lines. Tumour cells were then transplanted into immune-competent mice, showing significantly increased metastatic potential over their wild-type counterparts. Conversely, knocking CD36 down led to zero lymph node invasions. The same antimetastatic effect was obtained with CD36- targeting antibodies. While metastasis was prevented, or if already present, significantly reduced, primary lesions were not affected by the treatment [86]. Unlike previous reports, the work of Pascual et al. highlighted a possible cooperation between adipose tissue and tumour cells via CD36, which favours a predominantly lipidic metabolism. The link between increased lipidic profile and tumour progression was also highlighted in an obese mouse model of breast cancer [87]. The authors reported CD36 expression on some, but not all tumour cells, as well as downregulation of CD36 expression on endothelium of neovessels, presumably due to repressed CD36 gene transcription via PDK1-FOXO1 activation by lysophosphatidic acid.

The model that can be delineated so far is that a high CD36 level correlates with metastatic cancers and thus is poorly prognostic. However, blocking CD36 in a tumour system composed of tumour cells and stromal niche would equally affect both populations. An earlier work of deFillipis et al. [94] proposes that loss of CD36 in the pretumoural breast stroma creates a milieu favourable for tumour initiation or progression. Thus, targeting CD36 to prevent metastasis would have a protumorigenic impact on the surrounding

stroma. Add to this the proangiogenic effect on the tumour itself, and the outcome will be, very likely, a thriving primary tumour that is possibly nonmetastatic.

These results highlight the importance of integration of models in a correct spatial context, in which stromal niches and tumour cells interact. From this perspective, which part is more important for metastasis? And, in consequence, which population of cells should be targeted in studies aiming at validation of CD36 as a prognostic biomarker (see Figure 1)? Which population holds greater prognostic value: CD36+ tumour cells, as proposed by Pascual et al., or CD36-depleted stroma, as proposed by deFillipis et al.?

Unfortunately, these aspects have not yet been covered by clinical studies, as discussed in the next section, although CD36 is emerging as a candidate prognostic biomarker in different types of epithelial cancers, alone or in panels with other proteins.

4.2. Human Studies. Data from animal models and *in vitro* human tumour cell lines point to CD36 as a metastasis-related indicator, prompting investigations on a larger scale in human tumour samples (Table 1). One of the first mentions of CD36 as a possible biomarker for cancer prognostics dates more than 15 years, when it was included in a panel of immunophenotyping for high risk for acute myeloblastic leukaemia [95].

In a study of inflammation and cancer, Rachidi et al. used a reductive approach by considering all epithelial cancers as oncoinflammatory events and looking for a common signature. Although CD36 did not meet the criteria for all seven types of cancers studied, a high CD36 gene expression level was proposed as a poor prognostic marker in colon and ovarian cancer when assessed in panel with other proteins [96].

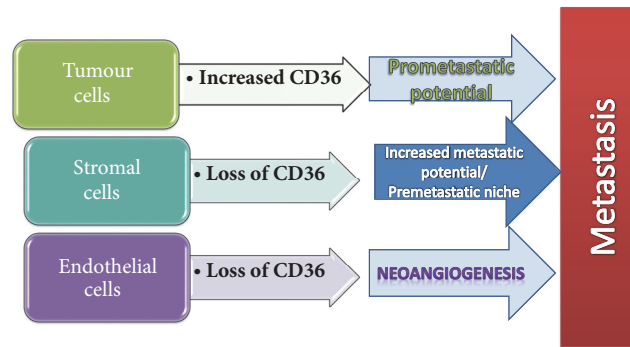


FIGURE 1: Involvement of CD36 in the metastatic process, related to the main three components of any tumour niche: the tumour cells, stromal cells, and vascularisation. CD36 expression in tumours prone to metastasis is different in each compartment, as demonstrated by animal models and pathology studies in patient samples.

Wang et al. found that 97% of ovarian cancers express CD36, as do 100% of lymph node metastases. Furthermore, the receptor's expression was increased with disease progression [92]. CD36 was also detected in liposarcoma and prostate and breast tumours; in the last type, translocation of the protein from the cytoplasm to cell membrane was related to oestrogen signalling [97].

Firm confirmation of the relationship between CD36 and metastasis came from a study of over 2500 cases of different types of cancers (a “pan-cancer” study) in which genes involved in metabolic rewiring towards aerobic glycolysis and *de novo* FA synthesis were assessed in metastatic tumours compared to primary tumours. The CD36 gene was frequently amplified in metastatic tumours and survival rates in the high-copy-number group were reduced when compared with low-copy-number patients [98].

5. Clinical Trials

Direct targeting of CD36 in tumour pathology has not yet been addressed in cancer-related clinical trials. Rather, its ability to bind TSP1 and modulate antiangiogenic responses was exploited therapeutically. Several clinical trials tested TSP-1 peptidomimetics specifically binding to CD36, but they were discontinued for lack of response or severe adverse effects [79]. Data gathered in preclinical models of various types of cancers taught that blocking CD36 might prove beneficial in stopping metastases from spreading. Lessons learned from other fields of successful clinical research show that humanized monoclonal antibodies are a valid option (reviewed in [99]). But a recent commentary estimates that development of antibodies against CD36, to be used in clinical trials, would take at least 4 years [100].

Continuing the pipeline of TSP peptidomimetics, in line with the lipid scavenger function of CD36, apolipoprotein A-I-mimetic peptides are being tested in preclinical trials, but mostly for noncancerous pathologies [102–104].

CD36 has been and continues to be investigated as a possible biomarker in metabolic diseases (obesity, insulin resistance, and diabetes type 2), cardiovascular diseases, and autoimmune/inflammatory conditions (Table 2).

The hope is that data gathered from these clinical trials will be highly informative about the pharmacological profile and side-effects of various types of CD-36 related compounds, for further repurposing in cancer therapy.

6. Future Perspectives in CD36-Related Tumour Biology

Plenty of data have been gathered to demonstrate CD36 involvement in metastasis spreading and, yet, novel and exciting avenues are still opening. Along with new reports of CD36 involvement in normal mitochondrial function [105], one could ask how CD36 increase impacts tumour cells energetic metabolism and the effect of CD 36 inhibition on bystander cells.

Further on, based on tumour animal models, the next step would be translation to human pathology. This process has already started, at least at the bioinformatics level, contributing to acknowledgment of CD36 as a possible prognostic biomarker for metastatic cancer, by compiling data from repositories and meta-analyses. So far, high levels of CD36 have been proposed as a poor prognostic marker for colon and ovarian cancer [96] as well as for breast cancer, lung small cell carcinoma, and urinary bladder carcinoma [86].

If the molecule is to be included in further clinical trials, validation in large cohorts remains to be accomplished, along with clarifications in some grey areas, such as site of detection of CD36 (stromal cells versus tumour cells) and proper quantification.

Conflicts of Interest

The authors declare that they have no conflicts of interest.

TABLE 2: Clinical trials investigating CD36 expression.

No	Conditions	Title	Interventions	Identifier
1	Healthy Young/Elderly	Effects of Native Whey or Milk Supplementation on Adaptations to 12 Weeks of Strength Training in Young and Elderly Anabolic Effects of Whey and Casein After Strength Training in Young and Elderly	Dietary Supplement: Native whey Dietary Supplement: Milk Other: Strength training Strength training Dietary Supplement: Milk 1% Dietary Supplement: Whey protein concentrate 80 Dietary Supplement: Native whey	NCT03033953 NCT02968888
2	Taste Sensitivity/Fatty Acid Type	Fatty Acid Taste Thresholds: Caproic, Lauric, Oleic, Linoleic, Linolenic		NCT01996566
3	Obesity/Metabolic Syndrome	CD36 and Human Fat Taste Perception Metabolic and Cardiovascular Impact of CD36 Deficiency in African Americans Study 8: Fat Perception in Humans (09-0873) Study 19: Metabolically Normal and Metabolically Abnormal Obesity	No intervention	NCT02699567 NCT02126735 NCT01128400 NCT01184170
4	Insulin Resistance Endothelial Dysfunction	CD36 in Nutrient Delivery and Its Dysfunction	Behavioral: overfeeding Sildenafil Citrate (Viagra)	NCT03012386
5	Type 2 Diabetes or Obesity Without Diabetes	Search for Biological Markers of Orosensory Perception of Fatty Acids in Healthy Subjects and Possible Modifications in Patients With Type 2 Diabetes and in Obese Non-diabetic Patients.	Other: Measure the threshold of detection for linoleic acid Other: Oral stimulation tests Other: Venous blood samples Other: Samples for genetic studies (ancillary study)	NCT02028975
6	Moderate Hypertriglycerolemic Subjects	Intervention With n3 LC-PUFA-supplemented Yogurt	Dietary Supplement: n3 long chain polyunsaturated fatty acids	NCT01244048
7	Diabetes Mellitus, Type 2 Dyslipidemia Associated With Type II Diabetes Mellitus Percutaneous Coronary Intervention	Effects of Evolocumab on Platelet Reactivity in Patients With Diabetes Mellitus After Elective Percutaneous Coronary Intervention	Drug: Evolocumab Drug: Placebo	NCT03258281
	Resistance Diabetes Cancer Obesity Inflammation	Study 14: Diet and Metabolic Inflammation	Other: Diet A Other: Diet B	NCT02539355
	Renal Failure Chronic Requiring Hemodialysis Metabolic Syndrome Diabetes Mellitus Type 2 Hyperlipidemia	Study 16: Salusin-alpha - a New Factor in the Pathogenesis of Lipid Abnormalities in Hemodialysis Patients	Drug: Atorvastatin	NCT01448174
	Cardiovascular Abnormalities	Study 13: A Study of Immunological Biomarkers as Predictors of Cardiovascular Events	Other: blood tests	NCT02894060
	Coronary Artery Disease	Polymorphisms in CD36 and STAT3 Genes and Different Dietary Interventions Among Patients With Coronary Artery Disease	Dietary Supplement: Olive oil Dietary Supplement: Nuts Dietary Supplement: Control diet	NCT02202265
	Thrombocytopenia	Study 5: Identification of Donors of CD36-Deficient Platelets Among Japanese Individuals on the NIH Campus	None	NCT00015639
	Idiopathic Thrombocytopenic Purpura	The Effect of Eltrombopag on the Expression of Platelet Collagen Receptor GPVI in Pediatric ITP.	Drug: Eltrombopag Drug: conventional	NCT03412188

TABLE 2: Continued.

No	Conditions	Title	Interventions	Identifier
	Myelodysplastic Syndromes	Study 22: Azacitidine and Erythropoietin Versus Azacitidine Alone for Patients With Low-Risk Myelodysplastic Syndromes	Azacitidine Drug: Erythropoietin Drug: Azacitidine (Monotherapy)	NCT00379912
	Rheumatoid Arthritis	Study 7: A New Mode of Action of Anti-TNF; Reverse Signaling, in Rheumatoid Arthritis	Diagnostic Test: Blood test	NCT03216928
	Rheumatoid Arthritis	Atherosclerosis in Rheumatoid Arthritis and Lupus: Restoring Cholesterol Balance		NCT01180361
	SLE Rheumatoid Arthritis Healthy Subjects	Study 15: Efferocytosis and Genomic Polymorphism in Autoimmune Diseases		NCT00364728
	HIV Infections	Study 12: Maraviroc 300 mg Twice Daily in HIV Negative Male Volunteers	Drug: Maraviroc	NCT00771823

Acknowledgments

This work was partially supported by Core Program, implemented with the support of MRI [Projects nos. 18.21-01.01, 18.21-02.01, and 18.21-01.06].

References

- [1] J. Massagué and A. C. Obenauf, "Metastatic colonization by circulating tumour cells," *Nature*, vol. 529, no. 7586, pp. 298–306, 2016.
- [2] J. P. Sleeman, "The metastatic niche and stromal progression," *Cancer and Metastasis Reviews*, vol. 31, no. 3-4, pp. 429–440, 2012.
- [3] A. Irmisch and J. Huelsken, "Metastasis: new insights into organ-specific extravasation and metastatic niches," *Experimental Cell Research*, vol. 319, no. 11, pp. 1604–1610, 2013.
- [4] R. L. Silverstein and M. Febbraio, "CD36, a scavenger receptor involved in immunity, metabolism, angiogenesis, and behavior," *Science Signaling*, vol. 2, no. 72, article re3, 16 pages, 2009.
- [5] N. N. Tandon, U. Kralisz, and G. A. Jamieson, "Identification of glycoprotein IV (CD36) as a primary receptor for platelet-collagen adhesion," *The Journal of Biological Chemistry*, vol. 264, no. 13, pp. 7576–7583, 1989.
- [6] M. Alessio, L. De Monte, A. Scirea, P. Gruarin, N. N. Tandon, and R. Sitia, "Synthesis, processing, and intracellular transport of CD36 during monocytic differentiation," *The Journal of Biological Chemistry*, vol. 271, no. 3, pp. 1770–1775, 1996.
- [7] M. S. Woo, J. Yang, C. Beltran, and S. Cho, "Cell surface CD36 protein in monocyte/macrophage contributes to phagocytosis during the resolution phase of ischemic stroke in mice," *The Journal of Biological Chemistry*, vol. 291, no. 45, pp. 23654–23661, 2016.
- [8] M. Y. Pepino, O. Kuda, D. Samovski, and N. A. Abumrad, "Structure-function of CD36 and importance of fatty acid signal transduction in fat metabolism," *Annual Review of Nutrition*, vol. 34, pp. 281–303, 2014.
- [9] R. F. Thorne, E. G. Law, C. A. Elith, K. J. Ralston, R. C. Bates, and G. F. Burns, "The association between CD36 and Lyn protein tyrosine kinase is mediated by lipid," *Biochemical and Biophysical Research Communications*, vol. 351, no. 1, pp. 51–56, 2006.
- [10] J. M. Githaka, A. R. Vega, M. A. Baird, M. W. Davidson, K. Jaqaman, and N. Touret, "Ligand-induced growth and compaction of CD36 nanoclusters enriched in Fyn induces Fyn signaling," *Journal of Cell Science*, vol. 129, no. 22, pp. 4175–4189, 2016.
- [11] A. S. Asch, S. Silbiger, E. Heimer, and R. L. Nachman, "Thrombospondin sequence motif (CSVTCG) is responsible for CD36 binding," *Biochemical and Biophysical Research Communications*, vol. 182, no. 3, pp. 1208–1217, 1992.
- [12] Y. M. Park, "CD36, a scavenger receptor implicated in atherosclerosis," *Experimental & Molecular Medicine*, vol. 46, no. 6, article e99, 2014.
- [13] C. Trezzini, T. W. Jungi, M. O. Spycher, F. E. Maly, and P. Rao, "Human monocytes CD36 and CD16 are signaling molecules. Evidence from studies using antibody-induced chemiluminescence as a tool to probe signal transduction," *The Journal of Immunology*, vol. 71, no. 1, pp. 29–37, 1990.
- [14] J. Pohl, A. Ring, Ü. Korkmaz, R. Ehehalt, and W. Stremmel, "FAT/CD36-mediated long-chain fatty acid uptake in adipocytes requires plasma membrane rafts," *Molecular Biology of the Cell (MBoC)*, vol. 16, no. 1, pp. 24–31, 2005.
- [15] R. P. Souto, G. Vallega, J. Wharton, J. Vinten, J. Trantum-Jensen, and P. F. Pilch, "Immunopurification and characterization of rat adipocyte caveolae suggest their dissociation from insulin signaling," *The Journal of Biological Chemistry*, vol. 278, no. 20, pp. 18321–18329, 2003.
- [16] J. J. Luiken, D. J. Dyck, X. Han et al., "Insulin induces the translocation of the fatty acid transporter FAT/CD36 to the plasma membrane," *American Journal of Physiology-Endocrinology and Metabolism*, vol. 282, no. 2, pp. E491–E495, 2002.
- [17] V. Bezaire, C. R. Bruce, G. J. F. Heigenhauser et al., "Identification of fatty acid translocase on human skeletal muscle mitochondrial membranes: Essential role in fatty acid oxidation," *American Journal of Physiology-Endocrinology and Metabolism*, vol. 290, no. 3, pp. E509–E515, 2006.
- [18] D. P. Y. Koonen, J. F. C. Glatz, A. Bonen, and J. J. F. P. Luiken, "Long-chain fatty acid uptake and FAT/CD36 translocation in heart and skeletal muscle," *Biochimica et Biophysica Acta (BBA) - Molecular and Cell Biology of Lipids*, vol. 1736, no. 3, pp. 163–180, 2005.
- [19] R. A. Swerlick, K. H. Lee, T. M. Wick, and T. J. Lawley, "Human dermal microvascular endothelial but not human umbilical vein endothelial cells express CD36 in vivo and in vitro," *The Journal of Immunology*, vol. 148, no. 1, pp. 78–83, 1992.
- [20] M. Krieger, "Charting the fate of the "good cholesterol": identification and characterization of the high-density lipoprotein receptor SR-BI," *Annual Review of Biochemistry*, vol. 68, pp. 523–558, 1999.
- [21] D. E. Greenwalt, O. Y. So, N. Jiwani, and K. W. K. Watt, "PAS IV, an Integral Membrane Protein of Mammary Epithelial Cells, Is Related to Platelet and Endothelial Cell CD36 (GP IV)," *Biochemistry*, vol. 29, no. 30, pp. 7054–7059, 1990.
- [22] F. Laugerette, P. Passilly-Degrace, B. Patris et al., "CD36 involvement in orosensory detection of dietary lipids, spontaneous fat preference, and digestive secretions," *The Journal of Clinical Investigation*, vol. 115, no. 11, pp. 3177–3184, 2005.
- [23] P. J. Simons, J. A. Kummer, J. J. F. P. Luiken, and L. Boon, "Apical CD36 immunolocalization in human and porcine taste buds from circumvallate and foliate papillae," *Acta Histochemica*, vol. 113, no. 8, pp. 839–843, 2011.
- [24] C. Martin, P. Passilly-Degrace, D. Gaillard, J.-F. Merlin, M. Chevrot, and P. Besnard, "The lipid-sensor candidates CD36 and GPR120 are differentially regulated by dietary lipids in mouse taste buds: impact on spontaneous fat preference," *PLoS ONE*, vol. 6, no. 8, Article ID e24014, 2011.
- [25] S. Siddiqi, A. Sheth, F. Patel, M. Barnes, and C. M. Mansbach II, "Intestinal caveolin-1 is important for dietary fatty acid absorption," *Biochimica et Biophysica Acta*, vol. 1831, no. 8, pp. 1311–1321, 2013.
- [26] M. V. T. Lobo, L. Huerta, N. Ruiz-Velasco et al., "Localization of the lipid receptors CD36 and CLA-1/SR-BI in the human gastrointestinal tract: Towards the identification of receptors mediating the intestinal absorption of dietary lipids," *Journal of Histochemistry & Cytochemistry*, vol. 49, no. 10, pp. 1253–1260, 2001.
- [27] T. T. T. Tran, H. Poirier, L. Clément et al., "Luminal lipid regulates CD36 levels and downstream signaling to stimulate chylomicron synthesis," *The Journal of Biological Chemistry*, vol. 286, no. 28, pp. 25201–25210, 2011.
- [28] A. Ring, S. Le Lay, J. Pohl, P. Verkade, and W. Stremmel, "Caveolin-1 is required for fatty acid translocase (FAT/CD36) localization and function at the plasma membrane of mouse embryonic





- fibroblasts," *Biochimica et Biophysica Acta (BBA) - Molecular and Cell Biology of Lipids*, vol. 1761, no. 4, pp. 416–423, 2006.
- [29] S. Sundaresan, R. Shahid, T. E. Riehl et al., "CD36-dependent signaling mediates fatty acid-induced gut release of secretin and cholecystokinin," *The FASEB Journal*, vol. 27, no. 3, pp. 1191–1202, 2013.
- [30] L. Malerød, L. Juvet, T. Gjøen, and T. Berg, "The expression of scavenger receptor class B, type I (SR-BI) and caveolin-1 in parenchymal and nonparenchymal liver cells," *Cell and Tissue Research*, vol. 307, no. 2, pp. 173–180, 2002.
- [31] P. Steneberg, A. G. Sykaras, F. Backlund, J. Straseviciene, I. Söderström, and H. Edlund, "Hyperinsulinemia enhances hepatic expression of the fatty acid transporter Cd36 and provokes hepatosteatosis and hepatic insulin resistance," *The Journal of Biological Chemistry*, vol. 290, no. 31, pp. 19034–19043, 2015.
- [32] F. Sheedfar, M. M. Y. Sung, M. Aparicio-Vergara et al., "Increased hepatic CD36 expression with age is associated with enhanced susceptibility to nonalcoholic fatty liver disease," *AGING*, vol. 6, no. 4, pp. 281–295, 2014.
- [33] D. P. Y. Koonen, R. L. Jacobs, and M. Febbraio, "Increased hepatic CD36 expression contributes to dyslipidemia associated with diet-induced obesity," *Diabetes*, vol. 56, no. 12, pp. 2863–2871, 2007.
- [34] J. J. Petrik, P. A. Gentry, J.-J. Feige, and J. LaMarre, "Expression and localization of thrombospondin-1 and -2 and their cell-surface receptor, CD36, during rat follicular development and formation of the corpus luteum," *Biology of Reproduction*, vol. 67, no. 5, pp. 1522–1531, 2002.
- [35] K. Osz, M. Ross, and J. Petrik, "The thrombospondin-1 receptor CD36 is an important mediator of ovarian angiogenesis and folliculogenesis," *Reproductive Biology and Endocrinology*, vol. 12, no. 1, article no. 21, 2014.
- [36] A. S. Asch, J. Barnwell, R. L. Silverstein, and R. L. Nachman, "Isolation of the thrombospondin membrane receptor," *The Journal of Clinical Investigation*, vol. 79, no. 4, pp. 1054–1061, 1987.
- [37] N. N. Tandon, R. H. Lipsky, W. H. Burgess, and G. A. Jamieson, "Isolation and characterization of platelet glycoprotein IV (CD36)," *The Journal of Biological Chemistry*, vol. 264, no. 13, pp. 7570–7575, 1989.
- [38] M. L. Aiken, M. H. Ginsberg, V. Byers-Ward, and E. F. Plow, "Effects of OKM5, a monoclonal antibody to glycoprotein IV, on platelet aggregation and thrombospondin surface expression," *Blood*, vol. 76, no. 12, pp. 2501–2509, 1990.
- [39] N. N. Tandon, C. F. Ockenhouse, N. J. Greco, and G. A. Jamieson, "Adhesive functions of platelets lacking glycoprotein IV (CD36)," *Blood*, vol. 78, no. 11, pp. 2809–2813, 1991.
- [40] C. M. Harmon and N. A. Abumrad, "Binding of sulfosuccinimidyl fatty acids to adipocyte membrane proteins: Isolation and amino-terminal sequence of an 88-kD protein implicated in transport of long-chain fatty acids," *Journal of Membrane Biology*, vol. 133, no. 1, pp. 43–49, 1993.
- [41] M. Febbraio, N. A. Abumrad, D. P. Hajjar et al., "A null mutation in murine CD36 reveals an important role in fatty acid and lipoprotein metabolism," *The Journal of Biological Chemistry*, vol. 274, no. 27, pp. 19055–19062, 1999.
- [42] A. Chawla, Y. Barak, L. Nagy, D. Liao, P. Tontonoz, and R. M. Evans, "PPAR- γ dependent and independent effects on macrophage-gene expression in lipid metabolism and inflammation," *Nature Medicine*, vol. 7, no. 1, pp. 48–52, 2001.
- [43] B. Jiménez, O. V. Volpert, S. E. Crawford, M. Febbraio, R. L. Silverstein, and N. Bouck, "Signals leading to apoptosis-dependent inhibition of neovascularization by thrombospondin-1," *Nature Medicine*, vol. 6, no. 1, pp. 41–48, 2000.
- [44] M. Febbraio, E. A. Podrez, J. D. Smith et al., "Targeted disruption of the class B scavenger receptor CD36 protects against atherosclerotic lesion development in mice," *The Journal of Clinical Investigation*, vol. 105, no. 8, pp. 1049–1056, 2000.
- [45] M. P. Young, M. Febbraio, and R. L. Silverstein, "CD36 modulates migration of mouse and human macrophages in response to oxidized LDL and may contribute to macrophage trapping in the arterial intima," *The Journal of Clinical Investigation*, vol. 119, no. 1, pp. 136–145, 2009.
- [46] C. T. Coburn, J. Knapp F.F., M. Febbraio, A. L. Beets, R. L. Silverstein, and N. A. Abumrad, "Defective uptake and utilization of long chain fatty acids in muscle and adipose tissues of CD36 knockout mice," *The Journal of Biological Chemistry*, vol. 275, no. 42, pp. 32523–32529, 2000.
- [47] T. Hajri, X. X. Han, A. Bonen, and N. A. Abumrad, "Defective fatty acid uptake modulates insulin responsiveness and metabolic responses to diet in CD36-null mice," *The Journal of Clinical Investigation*, vol. 109, no. 10, pp. 1381–1389, 2002.
- [48] N. Ohgami, R. Nagai, M. Ikemoto et al., "CD36, a member of the class B scavenger receptor family, as a receptor for advanced glycation end products," *The Journal of Biological Chemistry*, vol. 276, no. 5, pp. 3195–3202, 2001.
- [49] D. Gaillard, F. Laugerette, N. Darcel et al., "The gustatory pathway is involved in CD36-mediated orosensory perception of long-chain fatty acids in the mouse," *The FASEB Journal*, vol. 22, no. 5, pp. 1458–1468, 2008.
- [50] A. Ibrahim, A. Bonen, W. D. Blinn et al., "Muscle-specific overexpression of FAT/CD36 enhances fatty acid oxidation by contracting muscle, reduces plasma triglycerides and fatty acids, and increases plasma glucose and insulin," *The Journal of Biological Chemistry*, vol. 274, no. 38, pp. 26761–26766, 1999.
- [51] F. Nassir, O. L. Adewole, E. M. Brunt, and N. A. Abumrad, "CD36 deletion reduces VLDL secretion, modulates liver prostaglandins, and exacerbates hepatic steatosis in ob/ob mice," *Journal of Lipid Research*, vol. 54, no. 11, pp. 2988–2997, 2013.
- [52] S. Dehn and E. B. Thorp, "Myeloid receptor CD36 is required for early phagocytosis of myocardial infarcts and induction of Nr4a1-dependent mechanisms of cardiac repair," *The FASEB Journal*, vol. 32, no. 1, pp. 254–264, 2018.
- [53] A. Hosui, T. Tatsumi, H. Hikita et al., "Signal transducer and activator of transcription 5 plays a crucial role in hepatic lipid metabolism through regulation of CD36 expression," *Hepatology Research*, vol. 9, pp. 5–15, 2016.
- [54] C. Blanchet, G. Jouvion, C. Fitting, J.-M. Cavaillon, and M. Adib-Conquy, "Protective or deleterious role of scavenger receptors SR-A and CD36 on host resistance to *Staphylococcus aureus* depends on the site of infection," *PLoS ONE*, vol. 9, no. 1, Article ID e87927, 2014.
- [55] T. Q. Truong, D. Aubin, L. Falstrault, M. R. Brodeur, and L. Brissette, "SR-BI, CD36, and caveolin-1 contribute positively to cholesterol efflux in hepatic cells," *Cell Biochemistry & Function*, vol. 28, no. 6, pp. 480–489, 2010.
- [56] K. G. Bharadwaj, Y. Hiyama, Y. Hu et al., "Chylomicron- and VLDL-derived lipids enter the heart through different pathways: In vivo evidence for receptor- and non-receptor-mediated fatty acid uptake," *The Journal of Biological Chemistry*, vol. 285, no. 49, pp. 37976–37986, 2010.
- [57] D. Harb, K. Bujold, M. Febbraio, M. G. Sirois, H. Ong, and S. Marleau, "The role of the scavenger receptor CD36 in regulating mononuclear phagocyte trafficking to atherosclerotic lesions

- and vascular inflammation,” *Cardiovascular Research*, vol. 83, no. 1, pp. 42–51, 2009.
- [58] Y. Xie, V. Cifarelli, T. Pietka et al., “Cd36 knockout mice are protected against lithogenic diet-induced gallstones,” *Journal of Lipid Research*, vol. 58, no. 8, pp. 1692–1701, 2017.
- [59] M. Febbraio, D. P. Hajjar, and R. L. Silverstein, “CD36: a class B scavenger receptor involved in angiogenesis, atherosclerosis, inflammation, and lipid metabolism,” *The Journal of Clinical Investigation*, vol. 108, no. 6, pp. 785–791, 2001.
- [60] N. Tao, S. J. Wagner, and D. M. Lublin, “CD36 is palmitoylated on both N- and C-terminal cytoplasmic tails,” *The Journal of Biological Chemistry*, vol. 271, no. 37, pp. 22315–22320, 1996.
- [61] F. J. O. Rios, M. Ferracini, M. Pecenin et al., “Uptake of oxLDL and IL-10 production by macrophages requires PAFR and CD36 recruitment into the same lipid rafts,” *PLoS ONE*, vol. 8, no. 10, Article ID e76893, 2013.
- [62] S. F. A. Pearce, J. Wu, and R. L. Silverstein, “Recombinant GST/CD36 fusion proteins define a thrombospondin binding domain: Evidence for a single calcium-dependent binding site on CD36,” *The Journal of Biological Chemistry*, vol. 270, no. 7, pp. 2981–2986, 1995.
- [63] M. Takai, Y. Kozai, S. Tsuzuki et al., “Unsaturated long-chain fatty acids inhibit the binding of oxidized low-density lipoproteins to a model CD36,” *Bioscience, Biotechnology, and Biochemistry*, vol. 78, no. 2, pp. 238–244, 2014.
- [64] S. Tsuzuki, M. Yamasaki, Y. Kozai et al., “Assessment of direct interaction between CD36 and an oxidized glycerophospholipid species,” *The Journal of Biochemistry*, vol. 162, no. 3, pp. 163–172, 2017.
- [65] A. Demers, N. McNicoll, M. Febbraio et al., “Identification of the growth hormone-releasing peptide binding site in CD36: a photoaffinity cross-linking study,” *Biochemical Journal*, vol. 382, no. 2, pp. 417–424, 2004.
- [66] F.-L. Hsieh, L. Turner, J. R. Bolla, C. V. Robinson, T. Lavstsen, and M. K. Higgins, “The structural basis for CD36 binding by the malaria parasite,” *Nature Communications*, vol. 7, 2016.
- [67] D. Neculai, M. Schwake, M. Ravichandran et al., “Structure of LIMP-2 provides functional insights with implications for SR-BI and CD36,” *Nature*, vol. 504, no. 7478, pp. 172–176, 2013.
- [68] C. R. Stewart, L. M. Stuart, K. Wilkinson et al., “CD36 ligands promote sterile inflammation through assembly of a Toll-like receptor 4 and 6 heterodimer,” *Nature Immunology*, vol. 11, no. 2, pp. 155–161, 2010.
- [69] B. Li, L. Xia, J. Liu et al., “miR-758-5p regulates cholesterol uptake via targeting the CD36 3'UTR,” *Biochemical and Biophysical Research Communications*, vol. 494, no. 1-2, pp. 384–389, 2017.
- [70] N. Huangfu, Z. Xu, W. Zheng, Y. Wang, J. Cheng, and X. Chen, “LncRNA MALAT1 regulates oxLDL-induced CD36 expression via activating β -catenin,” *Biochemical and Biophysical Research Communications*, vol. 495, no. 3, pp. 2111–2117, 2018.
- [71] J. Guo, W. Fang, L. Sun et al., “Ultraconserved element uc.372 drives hepatic lipid accumulation by suppressing miR-195/miR4668 maturation,” *Nature Communications*, vol. 9, no. 1, 2018.
- [72] G. Endemann, L. W. Stanton, K. S. Madden, C. M. Bryant, R. T. White, and A. A. Protter, “CD36 is a receptor for oxidized low density lipoprotein,” *The Journal of Biological Chemistry*, vol. 268, no. 16, pp. 11811–11816, 1993.
- [73] R. F. Thorne, N. M. Mhaidat, K. J. Ralston, and G. F. Burns, “CD36 is a receptor for oxidized high density lipoprotein: Implications for the development of atherosclerosis,” *FEBS Letters*, vol. 581, no. 6, pp. 1227–1232, 2007.
- [74] D. Calvo, D. Gómez-Coronado, Y. Suárez, M. A. Lasunción, and M. A. Vega, “Human CD36 is a high affinity receptor for the native lipoproteins HDL, LDL, and VLDL,” *Journal of Lipid Research*, vol. 39, no. 4, pp. 777–788, 1998.
- [75] L. Love-Gregory, R. Sherva, T. Schappe et al., “Common CD36 SNPs reduce protein expression and may contribute to a protective atherogenic profile,” *Human Molecular Genetics*, vol. 20, no. 1, pp. 193–201, 2011.
- [76] J. T. McFarlan, Y. Yoshida, S. S. Jain et al., “In vivo, fatty acid translocase (CD36) critically regulates skeletal muscle fuel selection, exercise performance, and training-induced adaptation of fatty acid oxidation,” *The Journal of Biological Chemistry*, vol. 287, no. 28, pp. 23502–23516, 2012.
- [77] T. A. Pietka, M. S. Sulkin, O. Kuda et al., “CD36 protein influences myocardial Ca²⁺ homeostasis and phospholipid metabolism: Conduction anomalies in CD36-deficient mice during fasting,” *The Journal of Biological Chemistry*, vol. 287, no. 46, pp. 38901–38912, 2012.
- [78] S. O. Rahaman, D. J. Lennon, M. Febbraio, E. A. Podrez, S. L. Hazen, and R. Silverstein, “A CD36-dependent signaling cascade is necessary for macrophage foam cell formation,” *Cell Metabolism*, vol. 4, no. 3, pp. 211–221, 2006.
- [79] A. Jeanne, C. Schneider, L. Martiny, and S. Dedieu, “Original insights on thrombospondin-1-related antireceptor strategies in cancer,” *Frontiers in Pharmacology*, vol. 6, 2015.
- [80] J. M. Yuhas, A. P. Li, A. O. Martinez, and A. J. Ladman, “A simplified method for production and growth of multicellular tumor spheroids,” *Cancer Research*, vol. 37, no. 10, pp. 3639–3643, 1977.
- [81] FDA-NIH Biomarker Working Group, *BEST (Biomarkers, Endpoints, and other Tools) Resource*, Food and Drug Administration (US), Silver Spring (MD), 2016.
- [82] K. K. Jain, “Technologies for Discovery of Biomarkers,” in *The Handbook of Biomarkers*, Springer New York, New York, NY, USA, 2017.
- [83] A. Ladanyi, A. Mukherjee, H. A. Kenny et al., “Adipocyte-induced CD36 expression drives ovarian cancer progression and metastasis,” *Oncogene*, vol. 37, no. 17, pp. 2285–2301, 2018.
- [84] H. Kashihara, M. Shimada, K. Yoshikawa et al., “Correlation between thrombospondin-1 expression in non-cancer tissue and gastric carcinogenesis,” *Anticancer Research*, vol. 37, no. 7, pp. 3547–3552, 2017.
- [85] J. S. Hale, B. Otvos, M. Sinyuk et al., “Cancer stem cell-specific scavenger receptor 36 drives glioblastoma progression,” *Stem Cells*, vol. 32, no. 7, pp. 1746–1758, 2014.
- [86] G. Pascual, A. Avgustinova, S. Mejetta et al., “Targeting metastasis-initiating cells through the fatty acid receptor CD36,” *Nature*, vol. 541, no. 7635, pp. 41–45, 2017.
- [87] L. Dong, Y. Yuan, C. Opansky et al., “Diet-induced obesity links to ER positive breast cancer progression via LPA/PKD-1-CD36 signaling-mediated microvascular remodeling,” *Oncotarget*, vol. 8, no. 14, pp. 22550–22562, 2017.
- [88] K. O. Yee, C. M. Connolly, M. Duquette, S. Kazerounian, R. Washington, and J. Lawler, “The effect of thrombospondin-1 on breast cancer metastasis,” *Breast Cancer Research and Treatment*, vol. 114, no. 1, pp. 85–96, 2009.
- [89] M. Koch, F. Hussein, A. Woeste et al., “CD36-mediated activation of endothelial cell apoptosis by an N-terminal recombinant fragment of thrombospondin-2 inhibits breast cancer growth

- and metastasis in vivo," *Breast Cancer Research and Treatment*, vol. 128, no. 2, pp. 337–346, 2011.
- [90] C. N. Johnstone, Y. E. Smith, Y. Cao et al., "Functional and molecular characterisation of EO771.LMB tumours, a new C57BL/6-mouse-derived model of spontaneously metastatic mammary cancer," *DISEASE MODELS & MECHANISMS*, vol. 8, no. 3, pp. 237–251, 2015.
- [91] P.-C. Chen, C.-H. Tang, L.-W. Lin et al., "Thrombospondin-2 promotes prostate cancer bone metastasis by the up-regulation of matrix metalloproteinase-2 through down-regulating miR-376c expression," *Journal of Hematology & Oncology*, vol. 10, no. 1, article no. 33, 2017.
- [92] S. Wang, A. Blois, T. El Rayes et al., "Development of a prosaposin-derived therapeutic cyclic peptide that targets ovarian cancer via the tumor microenvironment," *Science Translational Medicine*, vol. 8, no. 329, Article ID 329ra34, 2016.
- [93] S. Russell, M. Duquette, J. Liu, R. Drapkin, J. Lawler, and J. Petrik, "Combined therapy with thrombospondin-1 type I repeats (3TSR) and chemotherapy induces regression and significantly improves survival in a preclinical model of advanced stage epithelial ovarian cancer," *The FASEB Journal*, vol. 29, no. 2, pp. 576–588, 2015.
- [94] R. A. DeFilippis, H. Chang, N. Dumont et al., "CD36 repression activates a multicellular stromal program shared by high mammographic density and tumor tissues," *Cancer Discovery*, vol. 2, no. 9, pp. 826–839, 2012.
- [95] R. O. Casasnovas, F. K. Slimane, R. Garand et al., "Immunological classification of acute myeloblastic leukemias: relevance to patient outcome," *Leukemia*, vol. 17, no. 3, pp. 515–527, 2003.
- [96] S. M. Rachidi, T. Qin, S. Sun, W. J. Zheng, and Z. Li, "Molecular profiling of multiple human cancers defines an inflammatory cancer-associated molecular pattern and uncovers KPNA2 as a uniform poor prognostic cancer marker," *PLoS ONE*, vol. 8, no. 3, Article ID e57911, 2013.
- [97] N. B. Kuemmerle, E. Rysman, P. S. Lombardo et al., "Lipoprotein lipase links dietary fat to solid tumor cell proliferation," *Molecular Cancer Therapeutics*, vol. 10, no. 3, pp. 427–436, 2011.
- [98] A. Nath and C. Chan, "Genetic alterations in fatty acid transport and metabolism genes are associated with metastatic progression and poor prognosis of human cancers," *Scientific Reports*, vol. 6, Article ID 18669, 2016.
- [99] J. T. Pento, "Monoclonal antibodies for the treatment of cancer," *Anticancer Research*, vol. 37, no. 11, pp. 5935–5939, 2017.
- [100] H. Ledford, "Fat fuels cancer's spread in mice," *Nature*, 2016.
- [101] A. Nath, I. Li, L. R. Roberts, and C. Chan, "Elevated free fatty acid uptake via CD36 promotes epithelial-mesenchymal transition in hepatocellular carcinoma," *Scientific Reports*, vol. 5, Article ID 14752, 2015.
- [102] A. C. P. Souza, A. V. Bocharov, I. N. Baranova et al., "Antagonism of scavenger receptor CD36 by 5A peptide prevents chronic kidney disease progression in mice independent of blood pressure regulation," *Kidney International*, vol. 89, no. 4, pp. 809–822, 2016.
- [103] H. Yokoi and M. Yanagita, "Targeting the fatty acid transport protein CD36, a class B scavenger receptor, in the treatment of renal disease," *Kidney International*, vol. 89, no. 4, pp. 740–742, 2016.
- [104] A. V. Bocharov, T. Wu, I. N. Baranova et al., "Synthetic amphipathic helical peptides targeting CD36 attenuate lipopolysaccharide-induced inflammation and acute lung injury," *The Journal of Immunology*, vol. 197, no. 2, pp. 611–619, 2016.
- [105] C. M. Anderson, M. Kazantzis, J. Wang et al., "Dependence of brown adipose tissue function on CD36-mediated coenzyme Q uptake," *Cell Reports*, vol. 10, no. 4, pp. 505–515, 2015.

Research Article

Mutational Analysis of Oncogenic AKT1 Gene Associated with Breast Cancer Risk in the High Altitude Ecuadorian Mestizo Population

Andrés López-Cortés ¹, Paola E. Leone ¹,
Byron Freire-Paspuel,^{2,3} Nathaly Arcos-Villacís,^{3,4} Patricia Guevara-Ramírez ¹,
Felipe Rosales,⁵ and César Paz-y-Miño ¹

¹Centro de Investigación Genética y Genómica, Facultad de Ciencias de la Salud Eugenio Espejo, Universidad Tecnológica Equinoccial, Avenue Mariscal Sucre, 170129 Quito, Ecuador

²Escuela de Medicina, Facultad de Ciencias de la Salud, Universidad de las Américas, Avenue de los Granados, 170125 Quito, Ecuador

³Departamento de Ciencias de la Vida, Universidad de las Fuerzas Armadas (ESPE), Avenue General Rumiñahui, 1715231B Sangolquí, Ecuador

⁴The James Black Centre, Cardiovascular Division, King's College London, BHF Centre of Excellence, 125 Coldharbour Lane, London SE5 9NU, UK

⁵Departamento de Patología, Hospital Oncológico Solon Espinosa Ayala, Avenue Eloy Alfaro, 170138 Quito, Ecuador

Correspondence should be addressed to César Paz-y-Miño; cesar.pazymino@ute.edu.ec

Received 19 March 2018; Revised 17 May 2018; Accepted 30 May 2018; Published 3 July 2018

Academic Editor: Franco M. Buonaguro

Copyright © 2018 Andrés López-Cortés et al. This is an open access article distributed under the Creative Commons Attribution License, which permits unrestricted use, distribution, and reproduction in any medium, provided the original work is properly cited.

Breast cancer is the leading cause of cancer-related death among women worldwide. AKT1 encodes the kinase B alpha protein. The rs121434592, rs12881616, rs11555432, rs11555431, rs2494732, and rs3803304 single nucleotide polymorphisms have been identified in the AKT1 kinase gene. Activated AKT1 phosphorylates downstream substrates regulating cell growth, metabolism, apoptosis, angiogenesis, and drug responses. It is essential to know how breast cancer risk is associated with histopathological and immunohistochemical characteristics and genotype polymorphisms in a high altitude Ecuadorian mestizo population. This is a retrospective case-control study. DNA was extracted from 185 healthy and 91 affected women who live 2,800 meters above sea level. Genotypes were determined by genomic sequencing. We found a possible association between the noncoding intronic variant rs3803304 and breast cancer risk development: GG (odds ratio [OR] = 5.2; 95% confidence interval [CI] = 1.3-20.9; $P \leq 0.05$; $Q > 0.05$). Regarding pathologic characteristics, we found significant risk between estrogen receptor, progesterone receptor, and HER2 status and molecular subtypes ($P \leq 0.001$; $Q \leq 0.05$). On the other hand, we did not find risk between variants and histopathological characteristics. Despite the small sample size, we found that the intronic variant, AKT1 rs3803304, may act as a predictive biomarker in the risk of developing breast cancer in the high altitude Ecuadorian mestizo population.

1. Introduction

Breast cancer (BC) in women involves the progressive accumulation of genetic, hereditary, hormonal, and environmental factors representing a significant health problem worldwide [1]. BC is the leading cause of cancer-related death among women (521,541 cases) and the most commonly diagnosed cancer (1,679,076 cases) [2]. The areas with a higher incidence of BC per each 100,000 inhabitants are

Western Europe (89.9), Oceania (85.5), and Northern Europe (76.7), while South America has a lower incidence (44.3) [3]. In Ecuador, the incidence rate of BC has reached up to 32.7 in 2012 [4].

The molecular subtyping of the progesterone receptor (PR), estrogen receptor (ER), and HER2 status coupled with the histopathological classification (noninvasive or “*in situ*” carcinoma and invasive or infiltrating carcinoma) generates five different subtypes: luminal A (ER+ and/or

PR+, HER2-, or low Ki67), luminal B (ER+ and/or PR+, HER2+, or HER2- with high Ki67), HER2-enriched (ER-, PR-, or HER2+), basal-like (ER-, PR-, HER2-, cytokeratin 5/6+, and/or HER1+), and normal-like (ER+ and/or PR+, HER2-, low Ki67, prognosis slightly worse than luminal A) [5–7].

Approximately 10% of BC cases correspond to hereditary factors with germline mutations in BRCA1, BRCA2, TP53, E-Cadherin, STK11, PTEN, ATM, and CHEK2 genes, while 90% of mammary tumors are adenocarcinomas with the presence of somatic mutations in high-penetrance genes such as PIK3CA, AKT1, SF3B1, GATA3, MLL3, CDH1, MAP3K1, NCOR1, MAP2K4, and MACF1 [5, 8–10]. All breast cancer's driver genes are fully detailed in the Cancer Genome Interpreter and the Pan-Cancer Atlas [11, 12]. Regarding the AKT subfamily, it is made up of three isoforms in mammals: AKT1, AKT2, and AKT3. AKT1 is located in the 14q32.33 position and has 14 exons that include a reading frame of 1443 base pairs (bp). AKT1 encodes the kinase B alpha (PKB α) protein of 480 amino acids and 55686 Daltons. PKB α contains an N-terminal pleckstrin homology (PH) domain, a short α -helical linker, a kinase domain (KD), and a regulatory motif [13, 14]. Various cytokines, hormones, and growth factors activate AKT1 by binding their cognate receptor tyrosine kinase (RTK), GPCR, or cytokine receptor and triggering activation of the PI3K kinase, which generates PIP3 [15, 16]. AKT1 binds PIP3 through its PH domain, resulting in translocation of AKT1 to the membrane. The mTOR-riCTOR complex (mTORC2) phosphorylates AKT1 within the carboxy terminus at S473 and PDK1 phosphorylates AKT1 within its activation loop at T308 [16, 17]. Activated AKT1 phosphorylates a large number of downstream substrates that play a crucial role in regulating cell growth, metabolism, proliferation, apoptosis, angiogenesis, and drug responses [18–21].

The E17K rs121434592, E319G rs12881616, L357P rs11555432, P388T rs11555431, rs2494732, and rs3803304 single nucleotide polymorphisms (SNPs) have been identified in the AKT1 kinase gene [22]. The E17K variant generates a conformational change in the PH domain of the AKT1 protein, making it possible to join the protein and the cell membrane, causing the process of intracellular phosphorylation [23]. The E319G, L357P, and P388T variants are located in the kinase domain (KD), and the rs2494732 and rs3803304 variants are placed in intronic regions (Figure 1). Consequently, dysregulation in cell proliferation, survival, and growth drives progressive transformation of normal cells towards a malignant phenotype [18, 24–27]. Aberrant AKT signaling is the underlying defect found in several pathologies such as esophageal cancer [28], head and neck cancer [29], and non-small cell lung cancer [30].

The objective was to determine the risk of breast cancer associated with histopathological and immunohistochemical characteristics and genetic polymorphisms in a high altitude Ecuadorian mestizo population.

2. Materials and Methods

2.1. Study Subjects. The Bioethics Committee of our institution, conducted following the Declaration of Helsinki,

approved this retrospective case-control study. It comprised a total of 276 Ecuadorian mestizo women who live 2,800 meters above sea level (masl) and were included into the analysis. Concerning the individuals with BC, 91 samples from tumor tissue embedded in paraffin with luminal A, luminal B, HER2-enriched, and basal-like subtypes were obtained from the Pathology Department at Solon Espinosa Ayala Oncologic Hospital. Affected individuals were diagnosed with BC between 2008 and 2011. Each case history conferred relevant information such as age, affected breast, surgical margins, tumor stage (T1-T4), pTNM (tumor, node, and metastasis) classification, histopathological and molecular classification, ER status, PR status, and HER2 status. With regard to the control group, 185 peripheral blood samples from individuals of the mestizo population with no family or personal history of cancer or smoking history were selected at random from our sample collection. Thus, the matching of cases to controls presented similar age (54.0 versus 52.3 years), age at menopause (47.4 versus 46.7 years), age at menarche (14.2 versus 14.6 years), age at first live birth (26.8 versus 26.2 years), mean number of live births (2.5 versus 2.5), and breast cancer in first-degree relative (3.1 versus 2.1 percent), respectively. Furthermore, all participants included in the study signed their respective informed consent.

2.2. DNA Extraction and Purification. DNA extraction and purification of control and case individuals were performed using the Wizard Genomic DNA Purification Kit (Promega, Madison, WI) and the PureLink Genomic DNA Kit (Invitrogen, Carlsbad, CA), respectively. The DNA of the healthy individuals was extracted from peripheral blood samples and presented an average concentration of 135 ng/ μ l. Meanwhile, the DNA of the affected individuals, which presented an average concentration of 84 ng/ μ l, was extracted from ten sections (5 μ m) of formalin-fixed paraffin-embedded breast tumor tissue previously cut with a microtome CUT 6062 (SLEE, Mainz, Germany). Both calculations were obtained using NanoDrop 2000 (Thermo Scientific, Waltham, MA).

2.3. Amplification and Genotyping. Genotyping was performed using DNA sequencing analysis. A final volume of 20 μ l was used for each PCR reaction for AKT1 SNPs. Each reaction consisted of 16.2 μ l of Milli-Q water, 2 μ l of DNA template (10 ng/ μ l), 0.2 μ M of each deoxynucleotide triphosphate (dNTP's), 3 mM of MgCl₂, 0.05 U of Taq DNA polymerase, 2.5 μ l of 10X buffer (500 mM of KCl, 200 mM of Tris-HCl, pH = 8.4), and 0.4 μ M of forward (FW) and reverse (RV) primers detailed in Table 1.

The SNPs E17K rs121434592 (G>A) (198 bp), L357P rs11555432 (T>C) (142 bp), E319G rs12881616 (A>G) (186 bp), and P388T rs11555431 (C>A) (171 bp) presented in exonic regions and rs3803304 (C>G) (171 bp) and rs2494732 (C>T) (171 bp) presented in intronic regions were amplified through the polymerase chain reaction (PCR) technique. Supplementary Table 2 details the genetic variants analyzed in this study. The PCR program started with an initial denaturation stage lasting 5 minutes at 94°C, followed by 35 cycles of 50 seconds at 94°C, 50 seconds at different annealing temperatures

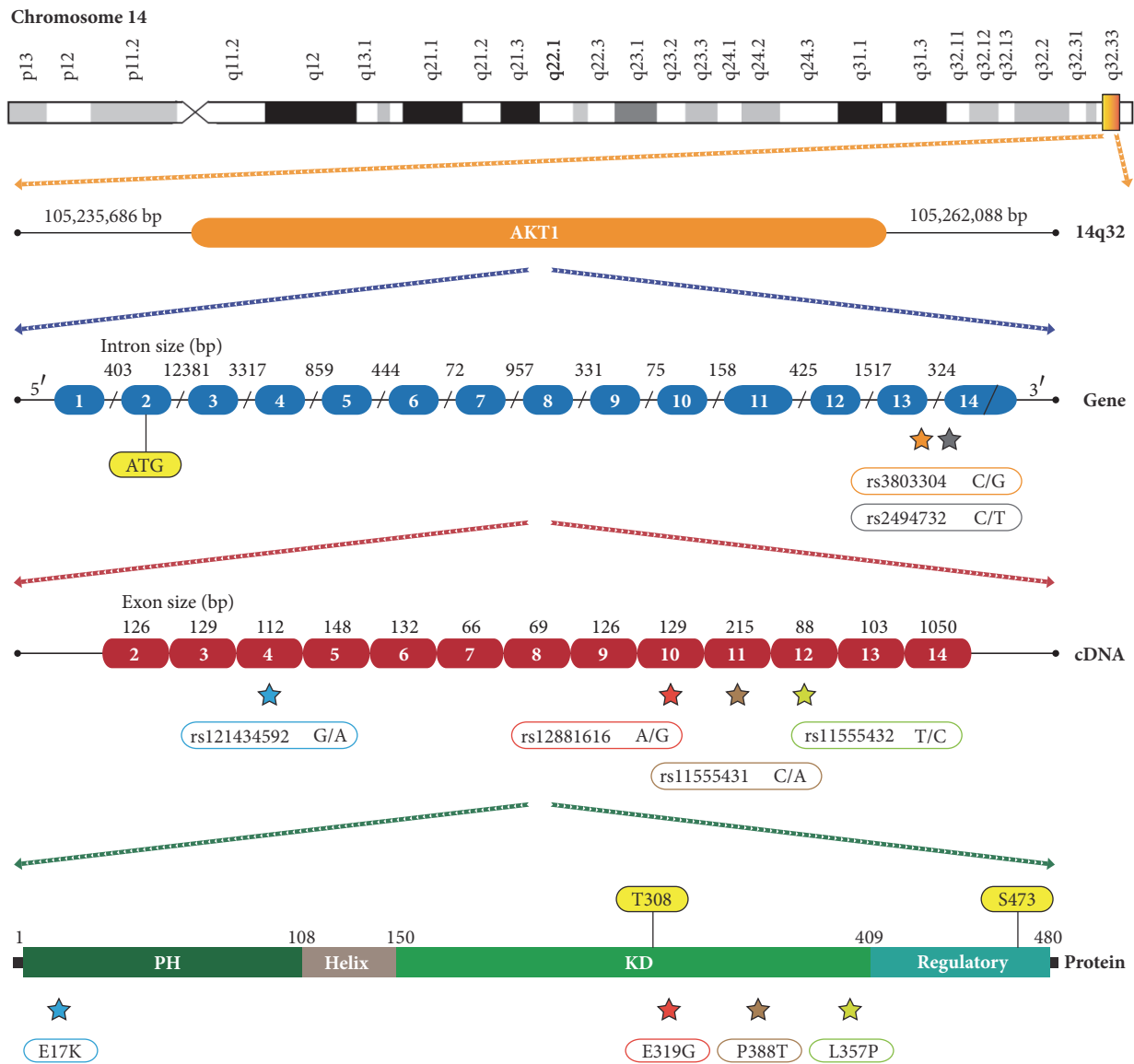


FIGURE 1: Location of the rs121434592, rs12881616, rs11555432, rs11555431, rs2494732, and rs3803304 variants in chromosome 14 in the AKT1 gene.

(Table 1), 45 seconds at 70°C, and a final elongation for 3 minutes at 72°C. Each run was completed using a Sure Cycler 8800 thermocycler (Agilent, Santa Clara, CA). The amplified fragment was then separated by electrophoresis in 2% agarose gels stained with ethidium bromide and was observed in an ImageQuant 300 transilluminator (General Electric, Fairfield, SC).

Genotyping was performed using DNA sequencing analysis through Genetic Analyzer 3130 (Applied Biosystems, Austin, TX). The final volume of the reaction was 12 µl and contained 2.8 µl of Milli-Q water, 2 µl of 5X buffer, 1 µl of primer FW (3.2 pmol), 1 µl of BigDye Terminator v3.1 sequencing standard (Applied Biosystems, Austin, TX), and 3 µl of PCR product (3 to 10 ng). Once the product was amplified, it was then purified using Agencourt CleanSEQ (Beckman Coulter, Miami, FL). The amplification program

consisted of 3 minutes at 96°C, followed by 30 cycles of 10 seconds at 96°C, 5 seconds at 50°C, and 4 minutes at 60°C. Finally, sequence analysis was performed using Sequencing Analysis Software 5.3.1 (Applied Biosystems, Austin, TX), and the alignment with sequences from GenBank (AKT1 NC.000014.9) was performed using Seq-Scape Software v2.6 (Applied Biosystems, Austin, TX) [7].

2.4. Statistical Analysis. The information from the clinical records of the patients was collected and stored in a database. Allelic and genotypic frequencies of the AKT1 SNPs were calculated; also Hardy-Weinberg equilibrium was determined by using a tool available on the Internet (<http://www.oege.org/software/hwe-mr-calc.shtml>) [31]. With the use of IBM SPSS Statistics 22 software (SPSS Inc., Chicago, IL), chi-square (χ^2), and odds ratio (OR) (with a

TABLE 1: Primer sequences, annealing temperatures, and genetic variations.

Polymorphisms	Primer sequences	Annealing temperatures	Location	Fragment (bp)
rs121434592 E17K	FW 5'- GGC CAA GGG GAT ACT TAC GC -3' RV 5'- AGG GTC TGA CGG GTA GAG TG -3'	60	Exon 4	198
rs11555432 L357P	FW 5'- CCT TCT TGA GCA GCC CTG AA -3' RV 5'- TAC GAG ATG ATG TGC GGT CG -3'	56.5	Exon 12	142
rs12881616 E319G	FW 5'- CAG AGA GGA CAC AGC ATT GCG -3' RV 5'- ACA AGG ACG GGC ACA TTA AGA -3'	60.5	Exon 10	186
rs11555431 P388T	FW 5'- CAA GGA CAT CAA GCT TTG GCT -3' RV 5'- AAG TCC TTG CTT TCA GGG CT -3'	61	Exon 11	171
rs3803304	FW 5'- CAA GGA CAT CAA GCT TTG GCT -3' RV 5'- AAG TCC TTG CTT TCA GGG CT -3'	61	Intron 13	171
rs2494732	FW 5'- CAA GGA CAT CAA GCT TTG GCT -3' RV 5'- AAG TCC TTG CTT TCA GGG CT -3'	61	Intron 13	171

bp, base pairs.

95% confidence interval [CI] and 2 x 2 contingency table), tests were applied to determine the association between the risk of developing BC, the SNPs, histopathological characteristics, and immunohistochemical characteristics. $P < 0.05$ was considered statistically significant. Consequently, the false discovery rate (FDR) Benjamini/Hochberg correction was performed in order to obtain Q values.

3. Results

The distribution of baseline characteristics in all patients with BC is shown in Table 2 and is fully detailed in Supplementary Table 1. Regarding age of diagnosis, 72.7% of luminal B individuals, 58.5% of luminal A, 56.3% of basal-like, 36.4% of HER2-enriched, and 57.1% of all cases presented were 50 years old or older. The right breast was affected in 57.1% of all cases, from which 72.6% presented luminal B, 58.5% luminal A, 50% basal-like, and 45.5% HER2-enriched. Regarding T stage, 93.8% of basal-like individuals, 77% of luminal A, 72.7% of HER2-enriched, 54.5% of luminal B, and 76.9% of all cases presented T1-T2 stage. Positive LN status was presented in 51.6% of all cases. Negative ER status was presented in 35.2% of all cases, from which 100% of basal-like individuals, 100% of HER2-enriched, 9.1% of luminal B, and 7.5% of luminal A did not present this receptor ($P \leq 0.001$; $Q \leq 0.05$). Regarding PR status, a total of 39.6% presented a negative PR status, of which 100% was basal-like, 90.9% was HER2-enriched and luminal B, and 79.2% was luminal A ($P \leq 0.001$; $Q \leq 0.05$). Overall, 70.3% presented negative HER2-enriched status, of which 100% was basal-like, 79.2% was luminal A, and 54.5% was luminal B ($P \leq 0.001$; $Q \leq 0.05$). Finally, 67% of all cases presented positive and 33% presented negative surgical margins.

Frequency of mutations in the AKT1 gene in breast cancer subtypes is detailed in Table 2 and genotype distribution and allele frequencies of AKT1 mutations in cases and controls are detailed in Table 3. The E17K AA homozygous genotype had a frequency of 0.02 in cases and 0.00 in control and was present in 2/91 affected individuals (2.2%) and 6.25% of basal-like

type ($P > 0.05$; $Q > 0.05$). The E319G GG, L357P CC, and P388T AA genotypes had a frequency of 0.00 in cases and controls and were present in 0/91 affected individuals (0%). The rs2494732 TT mutant genotype had a frequency of 0.14 in cases and 0.22 in controls and was present in 13/91 affected individuals (14.29%) and 36.4% of HER individuals ($P > 0.05$; $Q > 0.05$). The rs3803304 mutant homozygous genotype had a frequency of 0.08 in cases and 0.02 in controls and was present in 7/91 affected individuals (7.7%) and 18.2% of HER individuals ($P > 0.05$; $Q > 0.05$), whereas the rs3803304 CG heterozygous genotype was significantly different among the four subtypes ($P \leq 0.05$; $Q \leq 0.05$), where luminal B had the highest percentage (63.6%). Finally, the alleles of the rs2494732 and rs3803304 SNPs presented Hardy-Weinberg equilibrium.

The association between rs2494732 and rs3803304 polymorphisms and the risk of developing BC is detailed in Table 4. Regarding variant rs2494732, the CT genotype presented an odds ratio (OR) of 0.6 (95% CI = 0.3-1.0; $P > 0.05$; $Q > 0.05$); the TT genotype presented an OR of 0.4 (95% CI = 0.2-0.9; $P \leq 0.05$; $Q > 0.05$); and the combination of CT+TT presented an OR of 0.5 (95% CI = 0.3-0.9; $P \leq 0.05$; $Q > 0.05$). Regarding the rs3803304 intronic variant, the CG genotype presented an OR of 1.1 (95% CI = 0.6-1.9; $P > 0.05$; $Q > 0.05$); the GG genotype presented an OR of 5.2 (95% CI = 1.3-20.9; $P \leq 0.05$; $Q > 0.05$); and the combination of CG+GG presented an OR of 1.3 (95% CI = 0.8-2.2; $P > 0.05$; $Q > 0.05$). The OR in the remaining polymorphisms was not calculated due to low and nonexisting frequency in the study population.

The association between the rs3803304 and rs2494732 polymorphisms and the histopathological and immunohistochemical characteristics is detailed in Table 5. Regarding the affected breast, tumor stage, LN status, ER status, PR status, HER2 status, and surgical margins, no statistically significant differences ($P > 0.05$; $Q > 0.05$) were found in relation to the genetic polymorphisms. Additionally, data of control individuals is fully detailed in Supplementary Table 3.

TABLE 2: Distribution (*n*, %) of baseline characteristics (at diagnosis) and frequency of AKT1 mutations in patients with all breast cancer subtypes.

	Luminal A		Luminal B		HER2-enriched		Basal-like		All		<i>P</i> value	FDR Q value
	<i>n</i>	%	<i>n</i>	%	<i>n</i>	%	<i>n</i>	%	<i>n</i>	%		
Age at diagnosis												
<35	1	1.9	0	0.0	1	9.1	0	0.0	2	2.2	Reference	
35-49	21	39.6	3	27.3	6	54.5	7	43.75	37	40.7	<i>P</i> > 0.05	Q > 0.05
≥50	31	58.5	8	72.7	4	36.4	9	56.25	52	57.1	<i>P</i> > 0.05	Q > 0.05
Affected breast												
Right	31	58.5	8	72.7	5	45.5	8	50.0	52	57.1	<i>P</i> > 0.05	Q > 0.05
Left	22	41.5	3	27.3	6	54.5	8	50.0	39	42.9		
T stage												
T1-T2	41	77.36	6	54.5	8	72.7	15	93.75	70	76.92	Reference	
T3-T4	9	16.98	5	45.5	3	27.3	1	6.25	18	19.78	<i>P</i> > 0.05	Q > 0.05
T0, X	3	5.66	0	0.0	0	0.0	0	0.00	3	3.30	<i>P</i> > 0.05	Q > 0.05
LN status												
+	28	52.8	3	27.3	9	81.8	7	43.75	47	51.6	<i>P</i> > 0.05	Q > 0.05
-	25	47.2	8	72.7	2	18.2	9	56.25	44	48.4		
ER status												
+	49	92.5	10	90.9	0	0.0	0	0.0	59	64.8	<i>P</i> ≤ 0.001	Q ≤ 0.05
-	4	7.5	1	9.1	11	100	16	100	32	35.2		
PR status												
+	53	100	1	9.1	1	9.1	0	0.0	55	60.4	<i>P</i> ≤ 0.001	Q ≤ 0.05
-	0	0.0	10	90.9	10	90.9	16	100	36	39.6		
HER2 status												
+	11	20.8	5	45.5	11	100	0	0.0	27	29.7	<i>P</i> ≤ 0.001	Q ≤ 0.05
-	42	79.2	6	54.5	0	0.0	16	100	64	70.3		
Surgical margins												
+	33	62.3	8	72.7	7	63.6	13	81.25	61	67.0	<i>P</i> > 0.05	Q > 0.05
-	20	37.7	3	27.3	4	36.4	3	18.75	30	33.0		
rs121434592 E17K												
GG	52	98.1	11	100	11	100	15	93.75	89	97.8	Reference	
GA	0	0.0	0	0.0	0	0.0	0	0.0	0	0.0	-	-
AA	1	1.9	0	0.0	0	0.0	1	6.25	2	2.2	<i>P</i> > 0.05	Q > 0.05
rs12881616 E319G												
AA	53	100	11	100	11	100	16	100	91	100	Reference	
AG	0	0.0	0	0.0	0	0.0	0.0	0.0	0	0.0	-	-
GG	0	0.0	0	0.0	0	0.0	0.0	0.0	0	0.0	-	-
rs11555432 L357P												
TT	53	100	11	100	11	100	16	100	91	100	Reference	
TC	0	0.0	0	0.0	0	0.0	0.0	0.0	0	0.0	-	-
CC	0	0.0	0	0.0	0	0.0	0.0	0.0	0	0.0	-	-
rs11555431 P388T												
CC	53	100	11	100	11	100	16	100	91	100	Reference	
CA	0	0.0	0	0.0	0	0.0	0.0	0.0	0	0.0	-	-
AA	0	0.0	0	0.0	0	0.0	0.0	0.0	0	0.0	-	-
rs2494732												
CC	24	45.3	5	45.45	6	54.5	6	37.5	41	45.05	Reference	
CT	24	45.3	4	36.36	1	9.1	8	50.0	37	40.66	<i>P</i> > 0.05	Q > 0.05
TT	5	9.4	2	18.18	4	36.4	2	12.5	13	14.29	<i>P</i> > 0.05	Q > 0.05

TABLE 2: Continued.

	Luminal A		Luminal B		HER2-enriched		Basal-like		All		<i>P</i> value	FDR Q value
	<i>n</i>	%	<i>n</i>	%	<i>n</i>	%	<i>n</i>	%	<i>n</i>	%		
rs3803304												
CC	31	58.5	4	36.4	4	36.4	15	93.8	54	59.3	Reference	
CG	18	34.0	7	63.6	5	45.5	0	0.0	30	33.0	<i>P</i> ≤ 0.05	<i>Q</i> ≤ 0.05
GG	4	7.5	0	0.0	2	18.2	1	6.3	7	7.7	<i>P</i> > 0.05	<i>Q</i> > 0.05

LN, lymph node; ER, estrogen receptor; PR, progesterone receptor; HER, human epidermal growth factor receptor; FDR, false discovery rate.

TABLE 3: Genotype distribution and allele frequency of AKT1 mutations in cases and controls.

Mutations	Genotypes	Genotypic frequency			Allele frequency		
		Cases	Controls	All	Cases	Controls	All
rs121434592 E17K	GG	0.98	1.00	0.99	0.98	1.00	0.99
	GA	0.00	0.00	0.00			
	AA	0.02	0.00	0.01	0.02	0.00	0.01
rs12881616 E319G	AA	1.00	1.00	1.00	1.00	1.00	1.00
	AG	0.00	0.00	0.00			
	GG	0.00	0.00	0.00	0.00	0.00	0.00
rs11555432 L357P	TT	1.00	1.00	1.00	1.00	1.00	1.00
	TC	0.00	0.00	0.00			
	CC	0.00	0.00	0.00	0.00	0.00	0.00
rs11555431 P388T	CC	1.00	1.00	1.00	1.00	1.00	1.00
	CA	0.00	0.00	0.00			
	AA	0.00	0.00	0.00	0.00	0.00	0.00
rs2494732	CC	0.45	0.30	0.34	0.65	0.54	0.57
	CT	0.41	0.48	0.46			
	TT	0.14	0.22	0.20	0.35	0.46	0.43
rs3803304	CC	0.59	0.65	0.63	0.76	0.82	0.80
	CG	0.33	0.33	0.33			
	GG	0.08	0.02	0.04	0.24	0.18	0.20

4. Discussion

During the last decade, breast cancer genome-wide association studies (GWAS) have identified ~80 loci with small-to-moderate effects on OR ranging from 1.05 to 1.53 [10, 32–34]. Studying SNPs is crucial to fully understand breast cancer biology, as well as for the development of novel therapeutics for cancer treatment and for providing methods for prevention and early diagnosis [35]. The most studied populations have been Asian, European, and African. However, Latin American populations have been poorly studied, making genetic characterization essential to better understand the development of BC [7, 36].

Mounting evidence exists that activation of AKT proteins is important in cancer development [14]. Hyperactivation of the AKT pathway has been detected in up to 50% of all human tumors and is closely associated with chemoresistance [37]. Therefore, AKT has been an attractive target for anticancer drug discovery [38]. In particular, genetic alterations of the AKT genes have been demonstrated in many human tumors, including breast, colorectal, and ovarian cancers [39]. Concerning BC, the activating mutations of AKT1

gene have not been widely reported, the first being a study conducted in a female Latin American mestizo population from a high altitude (2,800 masl). It is noteworthy that this retrospective research presented a limited number of cases. However, it gives us relevant information about BC risk and its association with genotype polymorphisms of the AKT1 gene.

The E17K (rs121434592) point mutation in the pleckstrin homology domain of the AKT1 gene is the major point mutation that has been reported in the literature. In 2007, Carpten et al. evaluated the complete coding regions of AKT family members for mutations in genomic DNA from clinical tumour specimens representing breast (*n* = 61), colorectal (*n* = 51), and ovarian (*n* = 50) cancers [39]. Analysis of these samples revealed a unique mutation in the PH domain of AKT1 which results in a lysine substitution for glutamic acid at amino acid 17. E17K was identified in 5 of 51 (8%) breast, 3 of 51 (6%) colorectal, and 1 of 50 (2%) ovarian cancers. Although the sample size was insufficient to document statistical significance, the lack of coincidence of these mutations indicates that the AKT1 mutation (E17K) is sufficient for pathological activation of the PI3K/AKT

TABLE 4: Association between rs2494732 and rs3803304 polymorphisms and breast cancer risk among cases and controls.

Mutations	Genotypes	Cases (<i>n</i> = 91), <i>n</i> (%)	Controls (<i>n</i> = 185), <i>n</i> (%)	OR	95% CI	<i>P</i> value	FDR Q value
rs2494732	CC ^a	41 (45)	56 (30)	1.0		Reference	
	CT	37 (41)	89 (48)	0.6	0.3 – 1.0	<i>P</i> > 0.05	Q > 0.05
	TT	13 (14)	40 (22)	0.4	0.2 – 0.9	<i>P</i> ≤ 0.05	Q > 0.05
	CT+TT	50 (55)	129 (70)	0.5	0.3 – 0.9	<i>P</i> ≤ 0.05	Q > 0.05
rs3803304	CC ^a	54 (59)	121 (65)	1.0		Reference	
	CG	30 (33)	61 (33)	1.1	0.6 – 1.9	<i>P</i> > 0.05	Q > 0.05
	GG	7 (8)	3 (2)	5.2	1.3 – 20.9	<i>P</i> ≤ 0.05	Q > 0.05
	CG+GG	37 (41)	64 (35)	1.3	0.8 – 2.2	<i>P</i> > 0.05	Q > 0.05

OR, odds ratio; CI, confidence interval; FDR, false discovery rate.

^aReferences.

pathway [40]. In 2008, Stemke-Hale et al. published that E17K mutation was detected in only 6 of 418 breast cancers (1.4%), where all of them presented ER+ and PR+ [41]. In that year, Kim et al. identified the E17K mutation in 4 of 93 (4.3%) invasive ductal carcinomas [42]. In 2014, Shanti et al. used different genomic algorithms (SIFT, Polyphen 2.0, I-Mutant 2.0, and SNPs&GO) for prioritization of high-risk missense mutations in coding regions of AKT1 gene. They revealed that mutations such as E17S, E319G, L357P, and P388T were probably damaging and these mutations should be considered alongside E17K in the therapeutic development of AKT inhibitors to treat human cancer [22]. In the high altitude Ecuadorian mestizo population, the E17K mutation was found in 2 of 91 individuals (2.2%), where one of them was luminal A and the other one was basal-like (Table 2). In spite of the low percentage found in our population, it is known that the E17K (rs121434592) substitution decreases the sensitivity to an allosteric kinase inhibitor, so this mutation may have important clinical utility for AKT drug development [43].

According to the analysis of prioritization of Shanti et al., the E319G (rs12881616), L357P (rs11555432), and P388T (rs11555431) exonic variants are high-risk missense mutations of the AKT1 gene [22]. Nevertheless, these variants are 100% present in their normal homozygous state in this study due to a small sample size of the high altitude Ecuadorian mestizo population. On the other hand, the analysis of the rs2494732 and rs3803304 intronic variants was carried out. As for the rs2494732 variant, the CT genotype is found in 40.66% of the affected population with a higher percentage in the basal-like subtype (50%) and luminal A subtype (45.3%), whereas the TT genotype is found in 14.29% of the affected population with a higher percentage in the luminal A subtype (9.4%) and HER2-enriched subtype (36.4%). The OR statistical test determined that the rs2494732 variant did not present risk with the development of breast cancer in the CT heterozygous genotypes (OR = 0.6, 95% CI = 0.3-1.0; *P* > 0.05; Q > 0.05) or TT mutant homozygous genotypes (OR = 0.4, 95% CI = 0.2-0.9; *P* ≤ 0.05; Q > 0.05), just as found in the Chinese Han population with basocellular skin cancer (OR = 1.00, 95% CI = 0.5-2.2; *P* > 0.05) [41]. As a matter of fact,

in this population, the T mutant allele presented a higher allele frequency (0.46) in controls than in cases (0.35), and the C normal allele had a higher allele frequency in cases (0.65) than in controls (0.54). These results prove that the presence of mutations in the rs2494732 variant is related to a protective factor in the development of breast cancer and is associated with better general survival with a hazard ratio (HR) of 0.59 (95% CI = 0.40-0.86; *P* ≤ 0.05) and progression-free survival with a HR of 0.74 (95% CI = 0.53-1.03; *P* > 0.05) in a Korean population with non-small cell lung cancer [30]. Concerning the rs3803304 variant, the CG genotype is found in 33.0% of the affected population with a higher percentage in the luminal B subtype (63.6%) and HER subtype (45.5%), whereas the GG genotype is found in 7.7% of the affected population with higher percentage in the HER2-enriched subtype (18.2%) and luminal A subtype (7.5%). The OR statistical test determined that the rs3803304 variant presented a possible risk with the development of breast cancer in individuals with the GG mutant homozygous genotype (OR = 5.2, 95% CI = 1.3-20.9; *P* ≤ 0.05; Q > 0.05). In this mestizo population, the C normal allele presented a higher allele frequency in controls (0.82) than in cases (0.76), and the G mutant allele had a higher allele frequency in cases (0.24) than in controls (0.18). There is a statistically significant difference between the rs3803304 CG heterozygous genotype and the four subtypes (*P* ≤ 0.05; Q ≤ 0.05), where the luminal B subtype was present in 63.6%. Nevertheless, it has been observed that US individuals with esophageal cancer and the rs3803304 CG genotype presented a better response to treatments with chemoradiotherapy (OR = 0.5, 95% CI = 0.25-0.99; *P* ≤ 0.05) [28]. The results suggest that the rs3803304 variant is capable of regulating DNA transcription mechanisms and, therefore, it is capable of causing risk in the development of breast cancer in the Ecuadorian mestizo population living at high altitudes.

Regarding the rs3803304 variant that presented risk associated with the development of breast cancer, the CG+GG combined genotypes were present in 11.4% of tumor stage T3-T4, in 20.9% of negative LN status, in 12.1% of negative ER status, in 14.3% of negative PR status, and in 24.2% of negative HER2 status. However, there was no statistically

TABLE 5: Association of genotypes with histopathological and immunohistochemical characteristics.

Variables	rs3803304		rs2494732	
	CC	CG+GG	CC	CT+TT
Affected breast				
Right	28 (30.8)	24 (26.4)	24 (26.4)	28 (30.8)
Left	26 (28.6)	13 (14.3)	17 (18.7)	22 (24.2)
OR (95% CI)	0.6 (0.2-1.4)		1.1 (0.5-3.6)	
P value	$P > 0.05, Q > 0.05$		$P > 0.05, Q > 0.05$	
Tumor stage ^a				
T1-T2	43 (48.9)	27 (30.7)	32 (36.4)	38 (43.2)
T3-T4	8 (9.1)	10 (11.4)	7 (7.9)	11 (12.5)
OR (95% CI)	1.9 (0.7-5.7)		1.3 (0.5-3.8)	
P value	$P > 0.05, Q > 0.05$		$P > 0.05, Q > 0.05$	
LN status				
+	29 (31.9)	18 (19.8)	22 (24.1)	25 (27.5)
-	25 (27.5)	19 (20.9)	19 (20.9)	25 (27.5)
OR (95% CI)	1.2 (0.5-2.8)		1.2 (0.5-2.6)	
P value	$P > 0.05, Q > 0.05$		$P > 0.05, Q > 0.05$	
ER status				
+	33 (36.3)	26 (28.6)	26 (28.6)	33 (36.3)
-	21 (23.1)	11 (12.1)	15 (16.5)	17 (18.7)
OR (95% CI)	0.7 (0.3-1.6)		0.9 (0.4-2.1)	
P value	$P > 0.05, Q > 0.05$		$P > 0.05, Q > 0.05$	
PR status				
+	31 (34.1)	24 (26.4)	25 (27.5)	30 (33.0)
-	23 (25.3)	13 (14.3)	16 (17.6)	20 (22.0)
OR (95% CI)	0.7 (0.3-1.7)		1.0 (0.4-2.4)	
P value	$P > 0.05, Q > 0.05$		$P > 0.05, Q > 0.05$	
HER2 status				
+	12 (13.2)	15 (16.5)	11 (8.8)	16 (20.9)
-	42 (46.2)	22 (24.2)	30 (25.3)	34 (45.1)
OR (95% CI)	0.4 (0.2-1.0)		0.8 (0.3-1.9)	
P value	$P > 0.05, Q > 0.05$		$P > 0.05, Q > 0.05$	
Surgical margins				
+	33 (36.3)	28 (30.8)	25 (27.5)	36 (39.6)
-	21 (23.1)	9 (9.9)	16 (17.6)	14 (15.4)
OR (95% CI)	0.5 (0.1-1.3)		0.6 (0.3-1.5)	
P value	$P > 0.05, Q > 0.05$		$P > 0.05, Q > 0.05$	

LN, lymph node; PR, progesterone receptor; ER, estrogen receptor; HER, human epidermal growth factor receptor.

^aAnalyses of 88 individuals.

significant association between these combined genotypes and the histopathological characteristics ($P > 0.05$; $Q \leq 0.05$).

According to our results, the noncoding region rs3803304 variant may act as a predictive biomarker in the risk of developing breast cancer in the high altitude Ecuadorian mestizo population. Nevertheless, sample size should be increased in future analysis to enrich statistical tests. In conclusion, this study as well as our previous genetic studies on MTHFR in breast and prostate cancer [7, 44, 45], EGFR in lung cancer [46], and GPX-1 in bladder cancer [47] is an important contribution in order to integrate pharmacogenetics in clinical practice in Ecuador and Latin America [48, 49].

Data Availability

All data generated or analyzed during this study are included in this published article and its supplementary information files. Supplementary table 1 and table 3 detail clinical data of cases and controls, respectively. Clinical data is structured by genotype information, estrogen status, progesterone status, HER2/neu status, molecular subtypes, age at diagnosis, affected breast, surgical margins, lymph node status, and tumor stage. Supplementary table 2 details information about polymorphisms, nucleotide change, and amino acid change. All these data support the conclusions of the study.

Conflicts of Interest

The authors declare that they have no conflicts of interest.

Supplementary Materials

Supplementary Table 1: genotypes and clinical data of cases. **Supplementary Table 2:** genetic variants. **Supplementary Table 3:** genotypes and clinical data of controls. (*Supplementary Materials*)

References

- [1] S. Tuzlali, *Pathology of Breast Cancer. In: Breast Disease: Diagnosis and Pathology*, 2015.
- [2] Uk CR, "Worldwide cancer statistics. Cancer Res," *Cancer Res*, 2014.
- [3] A. Jemal, F. Bray, M. M. Center, J. Ferlay, E. Ward, and D. Forman, "Global cancer statistics," *CA: A Cancer Journal for Clinicians*, vol. 61, no. 2, pp. 69–90, 2011.
- [4] GLOBOCAN, "Breast Cancer Estimated Incidence, Mortality and Prevalence Worldwide in 2012".
- [5] R. Kumar, A. Sharma, and R. K. Tiwari, "Application of microarray in breast cancer: An overview," *Journal of Pharmacy and Bioallied Sciences*, vol. 4, no. 1, pp. 21–26, 2012.
- [6] S. Banerji, K. Cibulskis, C. Rangel-Escareno et al., "Sequence analysis of mutations and translocations across breast cancer subtypes," *Nature*, vol. 486, no. 7403, pp. 405–409, 2012.
- [7] A. López-Cortés, C. Echeverría, F. Oña-Cisneros et al., "Breast cancer risk associated with gene expression and genotype polymorphisms of the folate-metabolizing MTHFR gene: a case-control study in a high altitude Ecuadorian mestizo population," *Tumor Biology*, vol. 36, no. 8, pp. 6451–6461, 2015.
- [8] M. R. G. Taylor, M. Špirek, K. R. Chaurasiya et al., "Rad51 paralogs remodel pre-synaptic Rad51 filaments to stimulate homologous recombination," *Cell*, vol. 162, no. 2, pp. 271–286, 2015.
- [9] E. Honrado, A. Osorio, J. Palacios, and J. Benitez, "Pathology and gene expression of hereditary breast tumors associated with BRCA1, BRCA2 and CHEK2 gene mutations," *Oncogene*, vol. 25, no. 43, pp. 5837–5845, 2006.
- [10] D. C. Koboldt, R. S. Fulton, M. D. McLellan et al., "Comprehensive molecular portraits of human breast tumours," *Nature*, vol. 490, no. 7418, pp. 61–70, 2012.
- [11] D. Barh and M. Gunduz, "A Comprehensive Pan-Cancer Molecular Study of Gynecologic and Breast Cancers," *Cancer Cell*, 2018.
- [12] D. Tamborero, C. Rubio-Perez, J. Deu-Pons, MP. Schroeder, A. Vivancos, and A. Rovira, "Cancer Genome Interpreter Annotates The Biological And Clinical Relevance Of Tumor Alterations," *bioRxiv*, 2017.
- [13] B. Vanhaesebroeck and D. R. Alessi, "The PI3K-PDK1 connection: more than just a road to PKB," *Biochemical Journal*, vol. 346, part 3, pp. 561–576, 2000.
- [14] D. Hanahan and R. A. Weinberg, "Hallmarks of cancer: the next generation," *Cell*, vol. 144, no. 5, pp. 646–674, 2011.
- [15] S. Zhang and D. Yu, "PI(3)king apart PTEN's role in cancer," *Clinical Cancer Research*, vol. 16, no. 17, pp. 4325–4330, 2010.
- [16] E. Dazert and M. N. Hall, "mTOR signaling in disease," *Current Opinion in Cell Biology*, vol. 23, no. 6, pp. 744–755, 2011.
- [17] R. Zoncu, A. Efeyan, and D. M. Sabatini, "mTOR: from growth signal integration to cancer, diabetes and ageing," *Nature Reviews Molecular Cell Biology*, vol. 12, no. 1, pp. 21–35, 2011.
- [18] J. Chen, P. Shao, Q. Cao et al., "Genetic variations in a PTEN/AKT/mTOR axis and prostate cancer risk in a Chinese population," *PLoS ONE*, vol. 7, no. 7, Article ID e40817, 2012.
- [19] L.-Z. Liu, X.-D. Zhou, G. Qian, X. Shi, J. Fang, and B.-H. Jiang, "AKT1 amplification regulates cisplatin resistance in human lung cancer cells through the mammalian target of rapamycin/p70s6K1 pathway," *Cancer Research*, vol. 67, no. 13, pp. 6325–6332, 2007.
- [20] L. S. Faried, A. Faried, T. Kanuma et al., "Expression of an activated mammalian target of rapamycin in adenocarcinoma of the cervix: A potential biomarker and molecular target therapy," *Molecular Carcinogenesis*, vol. 47, no. 6, pp. 446–457, 2008.
- [21] X. Yang, M. Fraser, U. M. Moll, A. Basak, and B. K. Tsang, "Akt-mediated cisplatin resistance in ovarian cancer: modulation of p53 action on caspase-dependent mitochondrial death pathway," *Cancer Research*, vol. 66, no. 6, pp. 3126–3136, 2006.
- [22] V. Shanthi, R. Rajasekaran, and K. Ramanathan, "Computational identification of significant missense mutations in AKT1 gene," *Cell Biochemistry and Biophysics*, vol. 70, no. 2, pp. 957–965, 2014.
- [23] C. Parikh, V. Janakiraman, W.-I. Wu et al., "Disruption of PH-kinase domain interactions leads to oncogenic activation of AKT in human cancers," *Proceedings of the National Academy of Sciences of the United States of America*, vol. 109, no. 47, pp. 19368–19373, 2012.
- [24] S. Dimmeler, I. Fleming, B. Fisslthaler, C. Hermann, R. Busse, and A. M. Zeiher, "Activation of nitric oxide synthase in endothelial cells by Akt-dependent phosphorylation," *Nature*, vol. 399, no. 6736, pp. 601–605, 1999.
- [25] O. N. Ozes, L. D. Mayo, J. A. Gustin, S. R. Pfeffer, L. M. Pfeffer, and D. B. Donner, "NF- κ B activation by tumour necrosis factor requires the Akt serine-threonine kinase," *Nature*, vol. 401, no. 6748, pp. 82–85, 1999.
- [26] I. Mende, S. Malstrom, P. N. Tschlis, P. K. Vogt, and M. Aoki, "Oncogenic transformation induced by membrane-targeted Akt2 and Akt3," *Oncogene*, vol. 20, no. 32, pp. 4419–4423, 2001.
- [27] L. Wei, Y. Yang, and Q. Yu, "Tyrosine kinase-dependent, phosphatidylinositol 3 β -kinase, and mitogen-activated protein kinase-independent signaling pathways prevent lung adenocarcinoma cells from anoikis," *Cancer Research*, vol. 61, no. 6, pp. 2439–2444, 2001.
- [28] M. A. T. Hildebrandt, H. Yang, M.-C. Hung et al., "Genetic variations in the PI3K/PTEN/AKT/mTOR pathway are associated with clinical outcomes in esophageal cancer patients treated with chemoradiotherapy," *Journal of Clinical Oncology*, vol. 27, no. 6, pp. 857–871, 2009.
- [29] K. Pfisterer, A. Fusi, K. Klinghammer, M. Knödler, A. Nonnenmacher, and U. Keilholz, "PI3K/PTEN/AKT/mTOR polymorphisms: Association with clinical outcome in patients with head and neck squamous cell carcinoma receiving cetuximab-docetaxel," *Head & Neck*, vol. 37, no. 4, pp. 471–478, 2015.
- [30] M. J. Kim, H.-G. Kang, S. Y. Lee et al., "AKT1 polymorphisms and survival of early stage non-small cell lung cancer," *Journal of Surgical Oncology*, vol. 105, no. 2, pp. 167–174, 2012.
- [31] S. Rodriguez, T. R. Gaunt, and I. N. M. Day, "Hardy-Weinberg equilibrium testing of biological ascertainment for Mendelian randomization studies," *American Journal of Epidemiology*, vol. 169, no. 4, pp. 505–514, 2009.

- [32] K. Michailidou, P. Hall, and A. Gonzalez-Neira, "Large-scale genotyping identifies 41 new loci associated with breast cancer risk," *Nature Genetics*, vol. 45, no. 4, pp. 353–361, 2013.
- [33] D. F. Easton, K. A. Pooley, A. M. Dunning et al., "Genome-wide association study identifies novel breast cancer susceptibility loci," *Nature*, vol. 447, no. 7148, pp. 1087–1093, 2007.
- [34] A. Siddiq, F. J. Couch, G. K. Chen et al., "A meta-analysis of genome-wide association studies of breast cancer identifies two novel susceptibility loci at 6q14 and 20q11," *Human Molecular Genetics*, vol. 21, no. 24, pp. 5373–5384, 2012.
- [35] L. J. Engle, C. L. Simpson, and J. E. Landers, "Using high-throughput SNP technologies to study cancer," *Oncogene*, vol. 25, no. 11, pp. 1594–1601, 2006.
- [36] L. Fejerman, N. Ahmadiyeh, D. Hu et al., "Genome-wide association study of breast cancer in Latinas identifies novel protective variants on 6q25," *Nature Communications*, vol. 5, article no. 5260, 2014.
- [37] D. A. Altomare and J. R. Testa, "Perturbations of the AKT signaling pathway in human cancer," *Oncogene*, vol. 24, no. 50, pp. 7455–7464, 2005.
- [38] K. A. West, S. S. Castillo, and P. A. Dennis, "Activation of the PI3K/Akt pathway and chemotherapeutic resistance," *Drug Resistance Updates*, vol. 5, no. 6, pp. 234–248, 2002.
- [39] J. D. Carpten, A. L. Faber, C. Horn et al., "A transforming mutation in the pleckstrin homology domain of AKT1 in cancer," *Nature*, vol. 448, no. 7152, pp. 439–444, 2007.
- [40] Y. Yu, R. E. Savage, S. Eathiraj et al., "Targeting AKT1-E17K and the PI3K/AKT pathway with an allosteric AKT inhibitor, ARQ 092," *PLoS ONE*, vol. 10, no. 10, Article ID 0140479, 2015.
- [41] K. Stemke-Hale, A. M. Gonzalez-Angulo, A. Lluch et al., "An integrative genomic and proteomic analysis of PIK3CA, PTEN, and AKT mutations in breast cancer," *Cancer Research*, vol. 68, no. 15, pp. 6084–6091, 2008.
- [42] M. S. Kim, E. G. Jeong, N. J. Yoo, and S. H. Lee, "Mutational analysis of oncogenic AKT E17K mutation in common solid cancers and acute leukaemias," *British Journal of Cancer*, vol. 98, no. 9, pp. 1533–1535, 2008.
- [43] Y. Wang, L. Lin, H. Xu et al., "Genetic variants in AKT1 gene were associated with risk and survival of OSCC in Chinese Han Population," *Journal of Oral Pathology & Medicine*, vol. 44, no. 1, pp. 45–50, 2015.
- [44] A. López-Cortés, G. Jaramillo-Koupermann, and M. J. Muñoz, "Genetic polymorphisms in MTHFR (C677T, A1298C), MTR (A2756G) and MTRR (A66G) genes associated with pathological characteristics of prostate cancer in the ecuadorian population," *The American Journal of the Medical Sciences*, vol. 346, no. 6, pp. 447–454, 2013.
- [45] A. López-Cortés, A. Cabrera-Andrade, C. Salazar-Ruales et al., "Genotyping the high altitude mestizo ecuadorian population affected with prostate cancer," *BioMed Research International*, vol. 2017, 2017.
- [46] C. Paz-y-Miño, A. López-Cortés, M. J. Muñoz, A. Cabrera, B. Castro, and M. E. Sánchez, "Incidence of the L858R and G719S mutations of the epidermal growth factor receptor oncogene in an Ecuadorian population with lung cancer," *Cancer Genetics and Cytogenetics*, vol. 196, no. 2, pp. 201–203, 2010.
- [47] C. Paz-y-Miño, M. J. Muñoz, A. López-Cortés et al., "Frequency of polymorphisms pro198leu in GPX-1 gene and ile58thr in MnSOD gene in the altitude ecuadorian population with bladder cancer," *Oncology Research : Featuring Preclinical and Clinical Cancer Therapeutics*, vol. 18, no. 8, pp. 395–400, 2010.
- [48] L. Quinones, M. Lavanderos, J. Cayun et al., "Perception of the Usefulness of Drug/Gene Pairs and Barriers for Pharmacogenomics in Latin America," *Current Drug Metabolism*, vol. 15, no. 2, pp. 202–208, 2014.
- [49] A. López-Cortés, S. Guerrero, M. Redal, A. Alvarado, and L. Quiñones, "State of Art of Cancer Pharmacogenomics in Latin American Populations," *International Journal of Molecular Sciences*, vol. 18, no. 6, p. 639, 2017.

Review Article

Clinically Correlated MicroRNAs in the Diagnosis of Non-Small Cell Lung Cancer: A Systematic Review and Meta-Analysis

Min Jiang ^{1,2}, Xuelian Li,² Xiaowei Quan ², Xiaoying Li ², and Baosen Zhou ^{1,2}

¹Department of Clinical Epidemiology and Center of Evidence-Based Medicine, The First Affiliated Hospital, China Medical University, Shenyang, Liaoning 110001, China

²Department of Epidemiology, School of Public Health, China Medical University, Shenyang 110122, China

Correspondence should be addressed to Baosen Zhou; bszhou@cmu.edu.cn

Received 5 February 2018; Revised 30 April 2018; Accepted 7 June 2018; Published 28 June 2018

Academic Editor: Maria L. Tornesello

Copyright © 2018 Min Jiang et al. This is an open access article distributed under the Creative Commons Attribution License, which permits unrestricted use, distribution, and reproduction in any medium, provided the original work is properly cited.

(1) *Background.* Non-small cell lung cancer (NSCLC) has a high mortality rate. MiRNAs have been found to be diagnostic biomarkers for NSCLC. However, controversial results exist. We conducted this meta-analysis to evaluate the diagnostic value of miRNAs for NSCLC. (2) *Methods.* Databases and reference lists were searched. Pooled sensitivity (SEN), specificity (SPE), and area under the curve (AUC) were applied to examine the general diagnostic efficacy, and subgroup analysis was also performed. (3) *Results.* Pooled SEN, SPE, and AUC were 85%, 88%, and 0.93, respectively, for 71 studies. Multiple miRNAs (AUC: 0.96) obtained higher diagnostic value than single miRNA (AUC: 0.86), and the same result was found for Caucasian population (AUC: 0.97) when compared with Asian (AUC: 0.91) and Caucasian/African population (AUC: 0.92). MiRNA had higher diagnostic efficacy when participants contained both smokers and nonsmokers (AUC is 0.95 for imbalanced group and 0.91 for balanced group) than when containing only smokers (AUC: 0.90). Meanwhile, AUC was 0.91 for both miR-21 and miR-210. (4) *Conclusions.* Multiple miRNAs such as miR-21 and miR-210 could be used as diagnostic tools for NSCLC, especially for the Caucasian and nonsmoking NSCLC.

1. Introduction

Lung cancer is the principal cause of cancer-associated deaths among males both in developed and in developing countries, and it has exceeded the breast cancer becoming the major cause of cancer-related deaths in females in the developed countries [1]. Non-small cell lung cancer (NSCLC) is a major type of lung cancer that is responsible for 85% lung cancer-associated deaths. Smoking has been recognized as a primary environmental risk factor of lung cancer. However, only a small number of smokers will develop into lung cancer patients.

MicroRNA is a group of 19–22 nucleotide, small, single-stranded, and conserved noncoding RNA that acts as a regulator of gene expression at both the posttranscriptional and the translational levels through acting on the 3'-untranslated region (UTR) of messenger RNA (mRNA) [2]. MiRNAs play important roles in various biological processes associated with the tumorigenesis such as the cellular proliferation,

differentiation, metabolism, and apoptosis [3, 4]. It is available to isolate the miRNAs from the clinical specimens including the plasma, serum, sputum, and tissue. Meanwhile, it has a high stability. Due to these advantages, the miRNAs are increasingly becoming an ideal tool for the detection of NSCLC.

Recently, a series of articles have shown that different miRNAs might be applied to detect the NSCLC [5–7]. For example, miR-21, an oncogenic miRNA, has been shown to be overexpressed in lung cancer as well as other various human tumors [8]. Upregulation of miR-21 could promote the tumorigenesis of lung cancer through inhibiting the apoptosis process and negatively regulating the Ras/MEK/ERK signal pathway [9]. High miR-210 expression was correlated with the increased lymph node metastasis and a poor prognosis in patients with NSCLC [10]. Both these two, miR-21 and miR-210, have been explored to be used as diagnostic tools for NSCLC, no matter whether they are applied in combination with other miRNAs or alone [11–14]. However,

as a result of the small sample sizes, the different miRNAs profiling, and the differences of the specimen and ethnicity, inconsistencies existed among studies that had examined the diagnostic value of miR-21, miR-210, and other miRNAs for NSCLC. Therefore, a meta-analysis was performed to assess the performance of miRNAs in the detection for NSCLC.

2. Materials and Methods

2.1. Search Strategy. Our meta-analysis was based on the Preferred Reporting Items for Systematic Reviews and Meta-Analyses (PRISMA). We searched PubMed, Google Scholar, Chinese National Knowledge Infrastructure (CNKI), Embase, and Medline to find all associated articles in order to investigate the potential utility of miRNAs as diagnostic tools for NSCLC. The combination of the Medical Subject Headings (MeSH) and the keywords (“lung neoplasm” OR “lung malignancy” OR “lung cancer”) AND (“miRNA” OR “microRNAs”) AND (“ROC curve” OR “sensitivity” OR “specificity” OR “diagnosis”) was used (updated to April 5, 2017). The reference lists of the reviews were also searched to obtain all the acceptable articles.

2.2. Study Selection. A series of criteria were applied for study inclusion and exclusion. For inclusion, the criteria were as follows: (1) patients with NSCLC; (2) the type of the controls being healthy controls (HC) or patients with benign pulmonary diseases (BPD); (3) assessing the diagnostic value of the miRNAs; (4) the possibility of extracting or calculating TP, FP, FN, and TN from the articles. For exclusion, the criteria were as follows: (1) studies that were duplicate publications, reviews, or unrelated; (2) studies without complete data.

2.3. Data Collection and Quality Assessment. Two authors collected the data independently as follows: the first author, publication year, and participant demographic characteristics (ethnicity, sample size, mean or median age, smoking status, the types of the controls, and the testing method of controls and cancer); types of the specimen; miRNA profiling and the data used for this meta-analysis (SEN, SPE, TP, FP, FN, and TN). The quality of these articles were assessed with the QUADAS-2 guidelines [15].

2.4. Statistical Analysis. All the statistical analyses were conducted by RevMan 5.3 (version 1.4) software and STATA 11.0 (STATA-Corp, College Station, TX, version 11.0) software. The heterogeneity among the selected studies was assessed through the Q test and the I^2 value [16]. The P value for the Q test being less than 0.05 or the $I^2 \geq 50\%$ demonstrated that there was heterogeneity among the included studies. The pooled SPE $[TN/(FP+TN)]$, SEN $[TP/(FN+TP)]$, diagnostic odds ratio (DOR) $[PLR/NLR]$, the negative likelihood ratio (NLR) $[(1-SPE)/SPE]$, the positive likelihood ratio (PLR) $[(SEN)/(1-SEN)]$, and their 95% confidence intervals (95% CIs) were evaluated by a bivariate random-effect-regression model. The SROC curve was constructed and the AUC value was calculated too. A Fagan nomogram was also constructed to evaluate the clinical utility of miRNAs in the

diagnosis of NSCLC. Subgroup analyses (grouped by miRNA profiling: single and multiple; smoking status: only smokers, smokers, and nonsmokers (imbalanced between groups), smokers and nonsmokers (balanced between groups), and unknown smoking status; specimen: serum, plasma, whole blood/blood cell, and not blood; ethnicity: Asian, Caucasian, and Caucasian/African; control-type: BPD, HC, and BPD/HC; stage: early stage and no early stage; and case number: large (≥ 50) and small (< 50)) and meta-regression analysis were used to identify the potential sources of the heterogeneity. The Deeks' funnel plot asymmetry test was also applied to explore the publication bias, with the P value less than 0.01 considered significant [17].

3. Results

3.1. Literature Search and the Studies' Characteristics. As shown in Figure 1(a), 2594 eligible articles were included, of which 2145 articles were removed as unrelated and duplicate articles. And then 370 reviews were also excluded, leaving 79 articles with full texts, and another 21 articles were then removed through carefully reading: 14 articles met the exclusion criteria and 7 articles did not have the complete data. Ultimately, 58 articles [5–7, 11–14, 18–68] with 71 studies published from 2009 to 2017 including 9,099 participants (5111 cases with NSCLC and 3988 controls from the healthy individuals and the patients with the benign pulmonary disease (BPD)) were included. The main characteristics of these 71 studies were shown in Table 1. Wang Y's article [7], Fan LH's article [52], Nadal E's article [45], Tang DF's article [32], Razzak R's article [14], Wang W's article [68], Yu L's article [19], and Xing LX's article [18] included 2 studies. Bediaga's article [28] included 3 studies, Wang C's article [46] included 4 studies, and the remaining articles [5, 6, 11–13, 20–27, 29–31, 33–44, 47–51, 53–67] included 1 study, respectively. Meanwhile, there were 18 studies [13, 14, 28, 31, 33, 45, 46, 48, 54, 56, 63, 65, 66] performed in Caucasian, 11 studies [18, 19, 21, 23, 27, 29, 30, 38, 44] performed in Caucasian/African, and 1 study [26] performed in African populations; the remaining studies were performed in Asian populations. A total of 50 studies detected the miRNAs in blood such as the whole blood, plasma, serum, and peripheral blood mononuclear cells (PBMC) [6, 7, 11, 20–24, 26, 29–35, 37, 39–42, 44–47, 49–54, 56–64, 66–68], while the remaining studies were detected in nonblood samples (7 tissue [5, 25, 28, 55, 68], 1 pleural effusion [43], 12 sputum [12, 14, 18, 19, 27, 36, 38, 48, 65], and 1 BAL [13]). We evaluated 45 studies for assessing the diagnostic value of multiple miRNAs and 26 studies [5, 6, 11, 20, 22, 24–26, 33–37, 39–41, 43, 47, 50, 51, 55, 57, 58, 60, 67, 68] of single miRNA.

The quantitative real-time polymerase chain reaction (qRT-PCR) and digital polymerase chain reaction (digital PCR) were used in these studies to test the expression levels of different miRNAs, and the most common reference miRNAs were RNU6B, miR-39, and miR-16. Quality of the enrolled studies summarized in Figure 1(b) was generally good.

3.2. Pooled Diagnostic Performance. Significant heterogeneity was obtained since I^2 values for SEN and SPE were

TABLE 1: The main features of 71 included studies in this meta-analysis.

Study ID	Ethnicity	Specimen	Case N	Age	Control N	Age	Type of control	Stage	MIRNA profiling	SEN (%)	SPE (%)	Reference miRNA	microRNA assay	Smoking status*
Zhang H 2017	Asian	plasma	129	59.6	83	60.0	HC	I-II	miR-145, miR-20a, miR-21, miR-223	81.8	90.1	miR-16	qRT-PCR	3
Halvorsen A 2016	Caucasian	serum	100	62.6	58	57.6	HC	I-IV	miR-429, miR-205, miR-200b, miR-203, miR-12, miR-34b	88.0	71.0	miR-220, miR-19b, U6	qRT-PCR	3
TaiMei C2016	Asian	blood	110	65.0	52	65.7	HC	I-III	20 miRNAs ^a	89.1	100	miR-159a, U6	qRT-PCR	4
Su KL 2016	Asian	plasma	100	NA	100	NA	HC	I-III	miR-195, miR-182, miR-183, miR-210, miR-126	78.0	86.0	miR-39	qRT-PCR	3
Zhu WY 2016	Asian	plasma	112	58.5	40	57.9	HC	I-III	miR-532, miR-628, miR-425	81.3	100	U6	qRT-PCR	2
Jiang LP 2016	Asian	tissue	154	54.9	63	57.8	BPD	I-IV	miR-26b	79.9	79.4	U6	qRT-PCR	3
Wang Y 2016	Asian	plasma	82	NA	91	NA	HC	I-II	miR-532, miR-628, miR-425	91.5	97.8	miR-39	qRT-PCR	4
Wang Y 2016	Asian	plasma	36	NA	43	NA	HC	I-II	miR-532, miR-628, miR-425	97.2	95.3	miR-39	qRT-PCR	4
Fan LH 2016	Asian	serum	94	60.5	58	58.1	HC	I-III	miR-15b, miR-16, miR-20a	86.2	91.4	NA	qRT-PCR	4
Fan LH 2016	Asian	serum	70	59.7	54	58.0	HC	I-III	miR-15b, miR-16, miR-20a	94.3	94.2	NA	FQDs	4
Sun L 2016	Asian	plasma	87	60.7	96	53.8	HC,BPD	I-IV	miR-30a	61.0	84.3	U6	qRT-PCR	4
Su Y 2016	Asian	sputum	144	66.3	171	65.2	BPD	I	miR-21, miR-31, miR-210	81.5	85.9	U6	qRT-PCR	1
Gao X 2016	Asian	plasma	30	61.1	30	60.2	HC	I	miR-324, miR-1285	93.3	90.0	miR-39	qRT-PCR	4
Wang X 2016	Asian	plasma	59	55.9	59	57.6	BPD	I-III	miR-486	83.1	78.0	miR-16	qRT-PCR	4
Wei J 2016	Asian	plasma	63	61.0	30	57.0	HC	I-IV	miR-21	76.2	70.0	miR-16	qRT-PCR	3
Razzak 2016	Caucasian	sputum	22	68	10	58	HC,BPD	III-IV	miR-21, miR-210, miR-372	64	100	U6	qRT-PCR	4

TABLE I: Continued.

Study ID	Ethnicity	Specimen	Case N	Age	Control N	Age	Type of control	Stage	MIRNA profiling	SEN (%)	SPE (%)	Reference miRNA	microRNA assay	Smoking status*
Razzak 2016	Caucasian	sputum	21	70	10	58	HC,BPD	I-II	miR-21, miR-210, miR-372	67	90	U6	qRT-PCR	4
Leidinger P 2016	Caucasian	blood	74	NA	20	NA	HC	I-III	miR-720, miR-29c, miR-199a, miR-378a,let-7f	91.0	98.0	U24,U48	qRT-PCR	4
Wang WZ 2016	Asian	tissue	15	57	16	58	HC	I-IV	miR-182, miR-10a, miR-301b, miR-1244, miR-301a, miR-135b, miR-224, miR-21 miR-1244	93.3	93.8	miR-16	qRT-PCR	4
Wang WZ 2016	Asian	serum	54	NA	15	NA	HC	I-IV	miR-21, miR-143, miR-155, miR-210, miR-373 miR-483,	81.5	80	miR-39	qRT-PCR	4
Kim JL O 2015	Caucasian	BAL	21	70	10	59	HC,BPD	I-II	miR-193a, miR-25, miR-214, miR-7	85.7	100	U6	qRT-PCR	4
Wang C 2015	Asian	serum	19	61.8	19	62.1	HC	I-IV	miR-483, miR-193a, miR-25, miR-214, miR-7	100	84	let-7d/g/i	qRT-PCR	4
Li WS 2015	Asian	plasma	11	59	11	55	HC	I-III	miR-486	90.9	81.8	miR-39, U44	qRT-PCR	4
Wang C 2015	Asian	serum	63	61.9	63	59.7	HC	I-IV	miR-193a, miR-25, miR-214, miR-7 miR-483,	89.0	68.0	let-7d/g/i	qRT-PCR	4
Wang C 2015	Caucasian	serum	108	67.2	56	63.7	BPD	I-IV	miR-193a, miR-25, miR-214, miR-7	95.0	95.0	let-7d/g/i	qRT-PCR	4
Wang C 2015	Caucasian	serum	108	67.2	48	58.5	HC	I-IV	miR-483, miR-193a, miR-25, miR-214, miR-7	95.0	84.0	let-7d/g/i	qRT-PCR	4
Nadal E 2015	Caucasian	serum	70	67.5	22	67.0	HC,BPD	I-III	miR-141, miR-200b, miR-193b	96.0	95.0	U6	qRT-PCR	2
Nadal E 2015	Caucasian	serum	84	65.5	23	60.0	HC,BPD	I-III	miR-141, miR-200b, miR-193b	97.0	96.0	U6	qRT-PCR	2
Guo WG 2015	Asian	plasma	126	NA	50	NA	HC	I-IV	mir-204	76.0	82.0	U6	qRT-PCR	4

TABLE I: Continued.

Study ID	Ethnicity	Specimen	Case N	Age	Control N	Age	Type of control	Stage	MIRNA profiling	SEN (%)	SPE (%)	Reference miRNA	microRNA assay	Smoking status*
Ma J 2015	Caucasian, African	PBMC	84	64.1	69	62.4	BPD	I-IV	miR-19b, miR-29b, miR-148a, miR-148b, miR-152	72.6	82.6	miR-423-3p	qRT-PCR	2
Li L 2015	Asian	serum	36	56.0	30	58.0	HC,BPD	I-IV	miR-141, miR-21, miR-145, miR-152, miR-148a, miR-148b, miR-21	72.2	90.0	U6	qRT-PCR	4
Zhang XL 2015	Asian	tissue	125	61.0	125	61.0	HC	I-IV	miR-141	64.8	64.8	miR-191, miR-103	qRT-PCR	3
Zhao W 2015	Asian	serum	80	57.6	60	55.4	HC	NA	miR-21	73.8	71.7	U6	qRT-PCR	4
Wang RJ 2015	Asian	serum	70	64.4	70	63.7	HC	NA	miR-145, miR-152, miR-148a, miR-148b, miR-21	92.8	61.4	miR-39	qRT-PCR	3
Yang JS 2015	Asian	serum	152	NA	300	NA	HC	I-IV	miR-21, miR-31, miR-210	96.0	91.0	U6	qRT-PCR	3
Xing LX 2015	Caucasian	sputum	67	66.4	69	64.9	BPD	I-II	miR-192	82.1	88.4	U6, miR-16	qRT-PCR	4
Liu CM 2015	Asian	Pleural effusion	61	53.8	70	54.4	BPD	NA	miR-152	61.3	79.5	U6	qRT-PCR	2
Dou HL 2015	Asian	plasma	120	63.2	360	NA	HC	I-IV	miR-10b	86.0	81.3	U6	digital PCR	4
Yang YL 2015	Asian	PBMC	74	62.5	52	61.8	HC	I-IV	miR-31, miR-210	86.5	76.9	miR-16	qRT-PCR	3
Li N 2014	Caucasian, African	sputum	35	68.9	40	65.7	HC	I	miR-429, miR-499, miR-328, 8 miRNAs ^b , 8 miRNAs ^b , 8 miRNAs ^b	65.7	85.0	NA	qRT-PCR	4
Zhu W 2014	Asian	serum	70	59.0	48	NA	HC	I-IV	miR-429	54.3	81.2	U6, U48	qRT-PCR	4
LI M 2014	Asian	serum	514	NA	54	NA	HC	I-IV	miR-499	73.7	92.7	miR-39	qRT-PCR	3
Uliivi P 2013	Caucasian	blood	86	68.0	24	65.0	HC	I-II	miR-328	70.0	83.0	U38B,U58A	qRT-PCR	4
Bediaga 2013	Caucasian	tissue	45	66.4	45	66.4	HC	I-IV	8 miRNAs ^b	100	97.8	4miRNAs ^c	qRT-PCR	3
Bediaga 2013	Caucasian	tissue	47	67.8	47	67.8	HC	I-IV	8 miRNAs ^b	97.5	96.3	4miRNAs ^c	qRT-PCR	3
Bediaga 2013	Caucasian	tissue	22	68.4	22	68.4	HC	I-IV	8 miRNAs ^b	100	95.0	4miRNAs ^c	qRT-PCR	3
Anjuman 2013	Caucasian, African	sputum	39	65.6	42	62.3	BPD	I	miR-210, miR-31	61.5	90.5	U6	qRT-PCR	4
Tang DF 2013	Asian	plasma	62	64.8	60	66.0	HC	I-III	miR-21, miR-145, miR-155	69.4	78.3	U6	qRT-PCR	1

TABLE I: Continued.

Study ID	Ethnicity	Specimen	Case N	Age	Control N	Age	Type of control	Stage	MIRNA profiling	SEN (%)	SPE (%)	Reference miRNA	microRNA assay	Smoking status*
Tang DF 2013	Asian	plasma	34	65.2	32	66.4	HC	I-III	miR-21, miR-145, miR-155	76.5	81.3	U6	qRT-PCR	1
Mozzoni 2013	Caucasian	plasma	54	69.1	46	64.1	BPD	I-III	miR-21, miR-486	87.0	86.5	miR-16	qRT-PCR	4
ZENG XL 2013	Asian	PBMC	64	58.9	26	54.4	HC	I-IV	miR-143	75.0	92.3	U6	qRT-PCR	4
Yang XQ 2013	Asian	sputum	24	60.5	24	57.8	BPD	I-IV	let-7a	87.5	83.3	U6	digital PCR	4
Ma J 2013	Caucasian, African	plasma	36	66.7	38	64.6	HC	I	miR-21, miR-335	71.8	80.6	NA	qRT-PCR	4
Cazzoli R 2013	Caucasian, African	plasma	50	66.1	30	64.8	BPD	I	miR-151a, miR-30a, miR-200b, miR-629, miR-100, miR-154 miR-182	96.0	60.0	let7a	qRT-PCR	2
Abd-E 2013	African	Serum	65	54.1	37	50.1	HC	I-II	miR-152, miR-145, miR-199a, miR-24,	100	86.5	SNORD68	qRT-PCR	4
Sanfiorenzo C 2013	Caucasian	plasma	52	65.1	10	68.9	BPD	I-III	miR-20a, miR-25 miR-21, miR-143, miR-155, miR-210, miR-372 miR-494, miR-22, miR-200b miR-125b miR-15b, miR-27b	90.9	83.3	miR-192, miR-16	qRT-PCR	4
Roa Wilson H 2012	Caucasian	sputum	24	68.8	6	44.7	HC	I-II	miR-21, miR-143, miR-155, miR-210, miR-372 miR-494, miR-22, miR-200b miR-125b miR-15b, miR-27b	83.3	100	U6	qRT-PCR	4
Li GJ 2012	Asian	plasma	16	NA	14	NA	BPD	I	miR-21, miR-143, miR-155, miR-210, miR-372 miR-494, miR-22, miR-200b miR-125b miR-15b, miR-27b	85.3	94.5	18S	qRT-PCR	4
Ma YX 2012	Asian	serum	193	NA	110	NA	HC	I-IV	miR-21, miR-143, miR-155, miR-210, miR-372 miR-494, miR-22, miR-200b miR-125b miR-15b, miR-27b	78.2	66.4	NA	qRT-PCR	4
Hennessey P 2012	Caucasian, African	serum	55	68.2	75	65.7	HC	I-IV	miR-21, miR-143, miR-155, miR-210, miR-372 miR-494, miR-22, miR-200b miR-125b miR-15b, miR-27b	100	84.0	miR-16	qRT-PCR	4
ZengXL 2012	Asian	PBMC	34	NA	26	54.4	HC	I-IV	miR-150	87.5	69.2	U6	qRT-PCR	4
Zhao M 2012	Asian	tissue	55	NA	55	NA	HC	I-IV	miR-29a	49.1	85.5	U6	qRT-PCR	3
Shen J 2011	Caucasian, African	plasma	34	68.0	29	66.0	HC	I-IV	miR-21, miR-126, miR-210, miR-486	91.7	96.6	miR-16	qRT-PCR	1
Jeong H 2011	Asian	blood	35	67.0	30	60.0	HC	I-IV	let-7a	90.3	90.3	U6	qRT-PCR	4
Wei J 2011	Asian	plasma	77	59.6	36	56.4	HC	I-IV	miR-21	61.0	83.3	miR-16	qRT-PCR	3
Liu S 2011	Asian	plasma	130	53.1	170	57.5	HC	I-III	miR-126	46.4	90	NA	qRT-PCR	3

TABLE I: Continued.

Study ID	Ethnicity	Specimen	Case N	Age	Control N	Age	Type of control	Stage	MIRNA profiling	SEN (%)	SPE (%)	Reference miRNA	microRNA assay	Smoking status*
Yu L 2010	Caucasian, African	sputum	36	68.2	36	66.7	HC	I	miR-486, miR-21, miR-200b, miR-375	80.6	91.7	U6	qRT-PCR	4
Yu L 2010	Caucasian, African	sputum	64	67.0	58	65.0	HC	I-IV	miR-486, miR-21, miR-200b, miR-375	70.3	80.0	U6	qRT-PCR	3
Xing LX 2010	Caucasian, African	sputum	48	67.5	48	65.9	HC	I	miR-205, miR-210, miR-708	73.0	96.0	U6	qRT-PCR	4
Xing LX 2010	Caucasian, African	sputum	67	68.0	55	65.0	HC	I-IV	miR-205, miR-210, miR-708	72.0	95.0	U6	qRT-PCR	3
Keller Andreas 2009	Caucasian	blood	17	64.2	19	37.9	HC	I-III	24miRNAs ^d	92.5	98.1	NA	qRT-PCR	4

^amiR-451, miR-1290, miR-636, miR-30c, miR-22-3p, miR-19b, miR-486-5p, miR-20b, miR-93, miR-34b, miR-185, miR-126-5p, miR-93-3p, miR-1274a, miR-142-5p, miR-628-5p, miR-486-3p, miR-425, miR-645, miR-24; ^bmiR-96, miR-450a, miR-183, miR-9, miR-577, Let-7i, miR-27b and miR-34a; ^cmiR-26a, miR-140-5p, miR-195, miR-30b; ^dmiR-126, miR-423, miR-15a, let-7d, let-7i, miR-22, miR-98, miR-19a, miR-20b, miR-324, miR-574, miR-195, miR-25, let-7e, let-7c, let-7a, let-7f, let-7g, miR-140, miR-339, miR-361, miR-1283, miR-18a, miR-26b; * 1: only smokers; 2: smokers and nonsmokers (smoking status was imbalanced between groups); 3: smokers and nonsmokers (smoking status was balanced between groups); 4: unknown smoking status.

N: number; HC: healthy control; BPD: benign pulmonary disease; miR: microRNA; SEN: sensitivity; SPE: specificity; FQDs: fluorescence quantum dots; BAL: bronchoalveolar lavage.

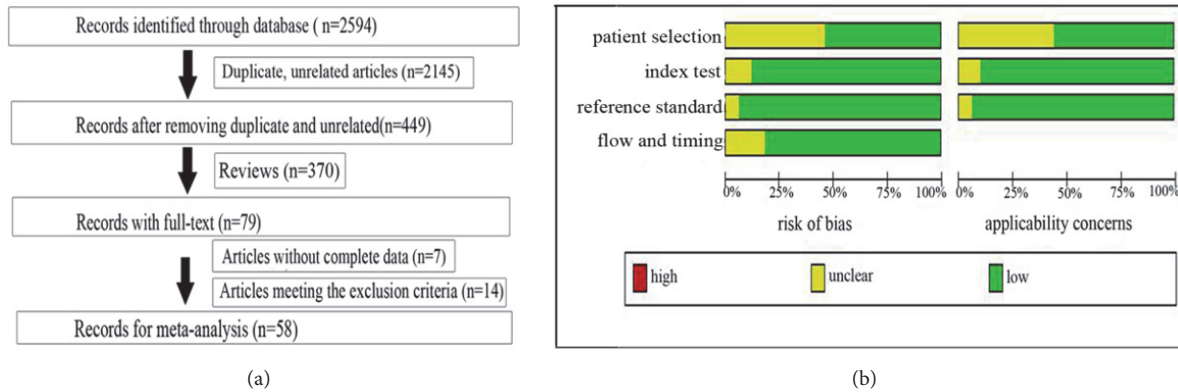


FIGURE 1: Flow chart of this meta-analysis of miRNAs in NSCLC detection (a) and the quality of these included articles according to the QUADAS-2 guidelines: proportion of articles with risk of bias (left) and proportion of articles with concerns regarding applicability (right) (b).

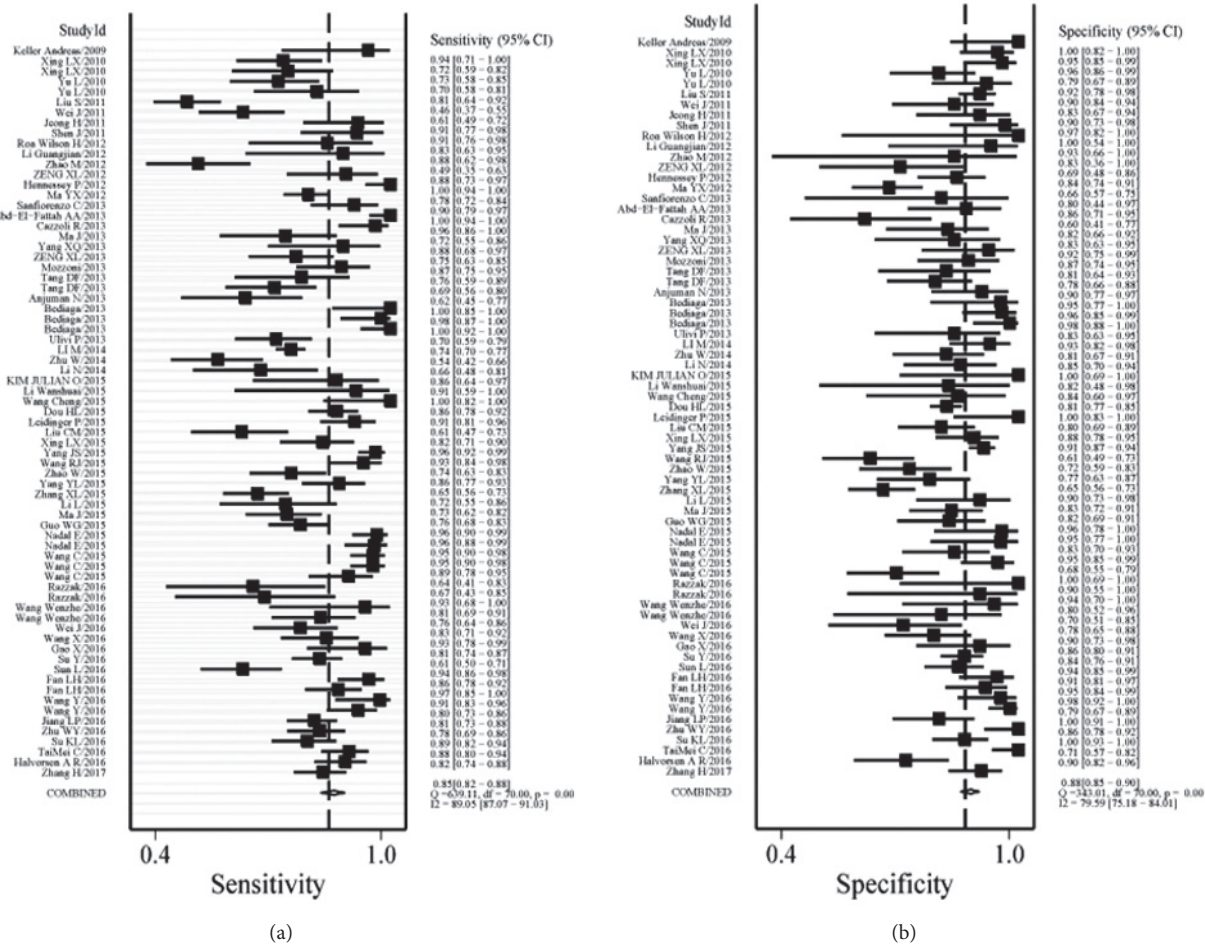


FIGURE 2: Forest plots of SEN and SPE for the NSCLC diagnosis. Both the SEN and SPE of each study were shown by squares with the 95% confidence interval shown by the error bars.

89.05% (95% CI: 87.07-91.03%) and 79.59% (95% CI: 75.18-84.01%), respectively. Therefore, a random-effect model was conducted for this study. Results indicated the pooled SEN and SPE for these 71 studies were 85% (95% CI: 82-88%) and 88% (95% CI: 85-90%), respectively (Figure 2). The PLR and NLR were 6.9 (95% CI: 5.6-8.4) and 0.17 (95% CI:

0.14-0.21), respectively (Figure 3), the DOR was 40 (95% CI: 28-58), and the AUC was 0.93 (95% CI: 0.90-0.95) (Figure 4(a)).

3.3. *Publication Bias.* Results of the Deeks' funnel plot asymmetry test showed that the publication bias did not exist in

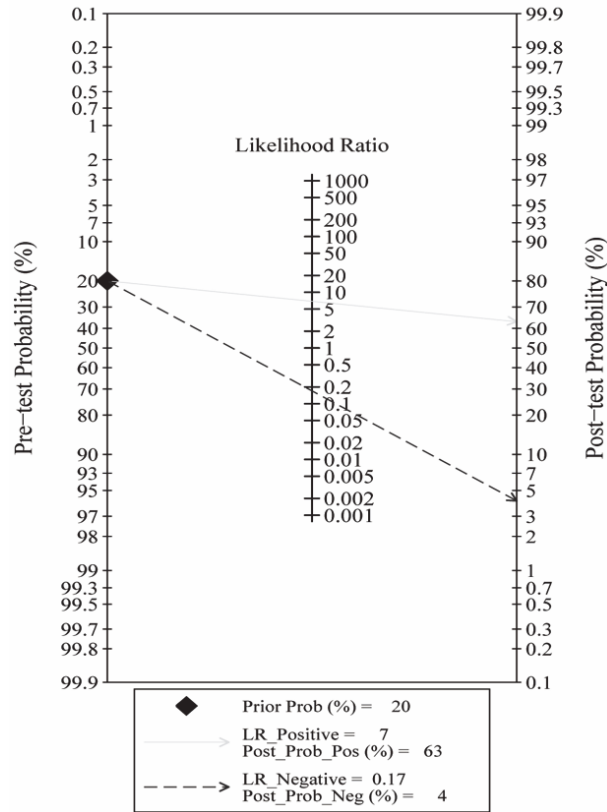


FIGURE 3: Fagan plot of PLR and NLR to evaluate the clinical utility of miRNAs for diagnosis of NSCLC.

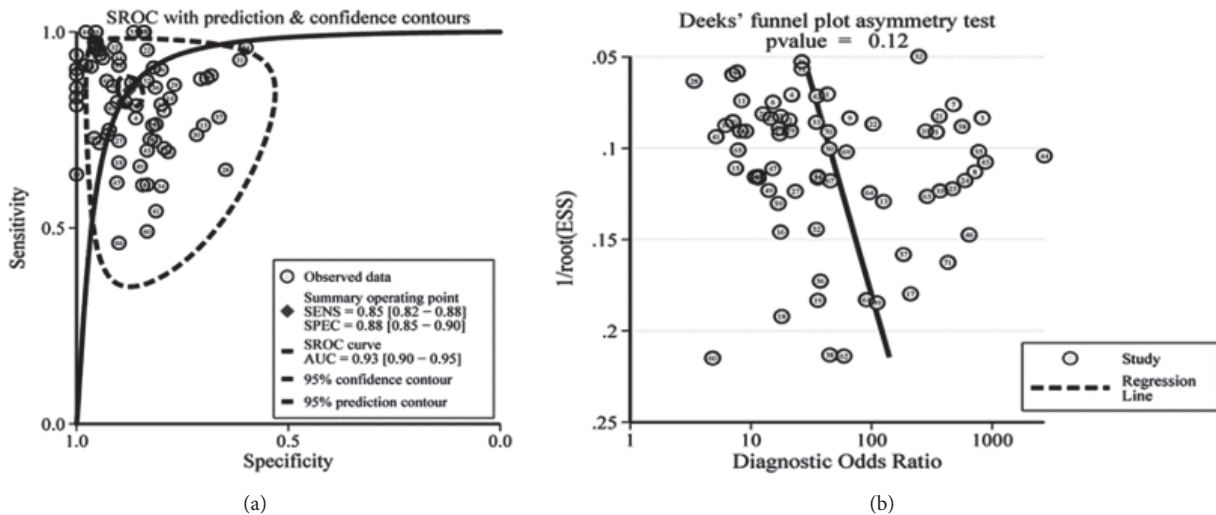


FIGURE 4: SROC curve of the miRNAs as diagnostic tools for NSCLC (a) and the Deeks' test for assessing the publication bias for miRNAs in the detection of NSCLC (b).

these studies as the funnel plot was symmetry (Figure 4(b)) and P value equaled 0.12.

3.4. Subgroup Analyses and Meta-Regression Analysis. Results of the meta-regression analysis demonstrated that the heterogeneity might be explained by miRNA profiling

($P < 0.001$) and case number ($P < 0.05$) for SPE and by miRNA profiling ($P < 0.01$) for SEN as described in Figure 5. The subgroup analyses were also conducted and the results were presented in Table 2. For the subgroups of smoking status, compared with the subgroup of only smokers (SEN: 80% (95% CI: 70-87%), SPE: 86% (95% CI: 77-91%), and AUC:

TABLE 2: Subgroup analyses for the selected studies.

Subgroups	No	SEN [95%CI]	SPE [95%CI]	PLR[95%CI]	NLR [95%CI]	DOR[95%CI]	AUC [95%CI]
MiR profiling							
single	26	0.77[0.71-0.82]	0.80[0.77-0.84]	3.9[3.3-4.7]	0.28[0.22-0.36]	14[10-20]	0.86[0.82-0.88]
multiple	45	0.88[0.85-0.91]	0.91[0.88-0.93]	10.0[7.5-13.3]	0.13[0.10-0.17]	79[50-126]	0.96[0.93-0.97]
Smoking status							
only smokers	4	0.80[0.70-0.87]	0.86[0.77-0.91]	5.6[3.2-9.9]	0.23[0.14-0.38]	24[9-66]	0.90[0.87-0.92]
S+NS (imbalanced)*	6	0.88[0.74-0.95]	0.90[0.73-0.97]	9.2[3.0-28.2]	0.13[0.05-0.31]	71[14-360]	0.95[0.93-0.97]
S+NS (balanced) *	18	0.83[0.74-0.90]	0.86[0.80-0.90]	5.9[3.9-8.8]	0.19[0.12-0.32]	30[13-69]	0.91[0.88-0.93]
unknown status	43	0.86[0.82-0.89]	0.88[0.85-0.91]	7.3[5.7-9.4]	0.16[0.12-0.21]	46[30-70]	0.93[0.91-0.95]
Specimen							
plasma	22	0.82[0.76-0.87]	0.87[0.83-0.90]	6.3[4.6-8.5]	0.20[0.15-0.28]	31[18-52]	0.92[0.89-0.94]
serum	19	0.91[0.86-0.95]	0.85[0.79-0.89]	6.1[4.3-8.5]	0.10[0.06-0.17]	60[28-128]	0.94[0.91-0.95]
Whole blood/blood cell	9	0.84[0.78-0.89]	0.92[0.80-0.97]	10.9[3.9-30.3]	0.17[0.11-0.26]	64[17-234]	0.92[0.89-0.94]
not blood	21	0.80[0.72-0.86]	0.89[0.85-0.93]	7.5[4.9-11.7]	0.22[0.16-0.32]	34[16-71]	0.92[0.89-0.94]
Ethnicity							
Asian	41	0.82[0.77-0.85]	0.86[0.82-0.88]	5.7[4.5-7.2]	0.21[0.17-0.27]	27[18-40]	0.91[0.88-0.93]
Caucasian	18	0.91[0.86-0.95]	0.92[0.87-0.96]	12[7.0-20.4]	0.09[0.06-0.15]	127[54-302]	0.97[0.95-0.98]
Caucasian/African	12	0.85[0.72-0.93]	0.87[0.81-0.91]	6.6[4.6-9.4]	0.17[0.09-0.33]	39[17-88]	0.92[0.89-0.94]
Control-type							
BPD	13	0.84[0.77-0.89]	0.84[0.80-0.88]	5.3[4.1-6.8]	0.19[0.13-0.28]	27[16-46]	0.90[0.87-0.92]
HC	50	0.86[0.82-0.89]	0.88[0.85-0.91]	7.4[5.7-9.5]	0.16[0.12-0.21]	47[30-74]	0.94[0.91-0.95]
BPD, HC	8	0.81[0.67-0.90]	0.91[0.79-0.96]	8.8[3.4-22.9]	0.21[0.11-0.40]	42[9-187]	0.93[0.90-0.95]
Stage							
I-II	18	0.84[0.78-0.89]	0.90[0.86-0.93]	8.3[5.8-11.9]	0.17[0.12-0.25]	48[27-87]	0.94[0.91-0.96]
I-IV	50	0.86[0.82-0.89]	0.88[0.84-0.90]	6.5[5.4-8.7]	0.16[0.13-0.22]	42[27-66]	0.93[0.90-0.95]
No. of cases							
small	25	0.88[0.82-0.92]	0.91[0.88-0.94]	10.0[7.1-14.2]	0.14[0.09-0.21]	74[38-143]	0.95[0.93-0.97]
large	46	0.84[0.79-0.87]	0.86[0.82-0.88]	5.8[4.6-7.2]	0.19[0.15-0.24]	31[20-46]	0.91[0.89-0.94]
MiR-210	12	0.77[0.72-0.81]	0.93[0.88-0.96]	11.0[6.2-19.4]	0.25[0.20-0.31]	44[22-87]	0.91[0.88-0.93]
MiR-21	16	0.82[0.77-0.86]	0.87[0.84-0.89]	6.3[5.0-8.1]	0.21[0.15-0.28]	31[19-50]	0.91[0.88-0.93]

No: the number of the studies; HC: healthy control; BPD: benign pulmonary disease; SEN: sensitivity; SPE: specificity; PLR: positive likelihood ratio; NLR:negative likelihood ratio; DOR: diagnostic odds ratio; AUC:area under the curve; no. of case: small (<50) and large (≥50).

* S: smokers; NS: nonsmokers; imbalanced: the smoking status was imbalanced between groups; balanced: the smoking status was balanced between groups.

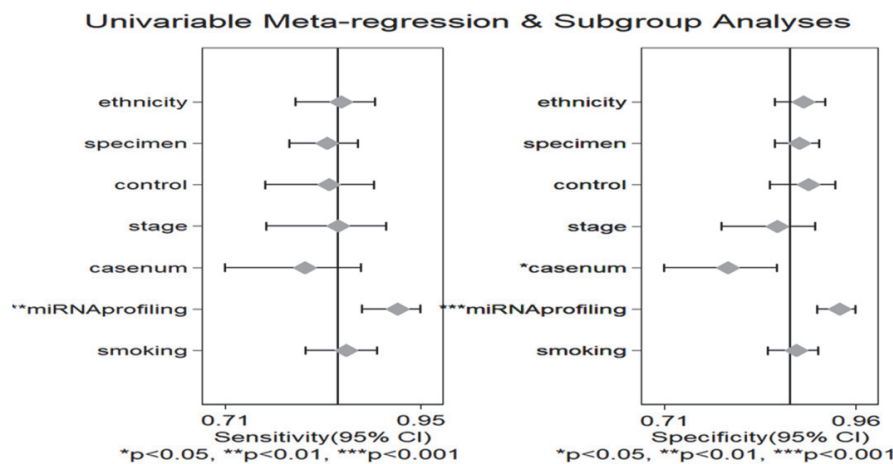


FIGURE 5: Forest plots for the meta-regression analysis: SEN and SPE. The factors included miRNA profiling, smoking status, specimen, ethnicity, type of control, case number, and stage.

0.90 (95% CI: 0.87-0.92)), miRNAs had a higher diagnostic efficacy in the subgroups of smokers and nonsmokers (SEN: 88% (95% CI: 74-95%), SPE: 90% (95% CI: 73-97%), and AUC: 0.95 (95% CI: 0.93-0.97) for imbalanced groups and SEN: 83% (95% CI: 74-90%), SPE: 86% (95% CI: 80-90%), and AUC: 0.91 (95% CI: 0.88-0.93) for balanced groups). Subgroup analysis by specimen showed that studies with serum samples exhibited higher diagnostic accuracy with SEN: 91% (95% CI: 86-95%), SPE: 85% (95% CI: 79-89%), and AUC: 0.94 (95% CI: 0.91-0.95) than studies with plasma samples with the SEN: 82% (95% CI: 76-87%), SPE: 87% (95% CI: 83-90%), and AUC: 0.92 (95% CI: 0.89-0.94) and not bleeding samples with the SEN: 80% (95% CI: 72-86%), SPE: 89% (95% CI: 85-93%), and AUC: 0.92 (95% CI: 0.89-0.94), respectively. When compared with the large sample size, miRNA might be a better diagnostic tool for small sample size with SEN: 88% (95% CI: 82-92%), SPE: 91% (95% CI: 88-94%), and AUC: 0.95 (95% CI: 0.93-0.97). In the subgroups for the ethnicity, the miRNAs obtained a better diagnostic value in the Caucasian populations with the SEN: 91% (95% CI: 86-95%), SPE: 92% (95% CI: 87-96%), and AUC: 0.97 (95% CI: 0.95-0.98), respectively, when compared with the Asian populations with the SEN: 82% (95% CI: 77-85%), SPE: 86% (95% CI: 82-88%), and AUC: 0.91 (95% CI: 0.88-0.93), respectively, and the Caucasian/African populations with SEN: 85% (95% CI: 72-93%), SPE: 87% (95% CI: 81-91%), and AUC: 0.92 (95% CI: 0.89-0.94), respectively. In the subgroups of the miRNAs profiling, the multiple miRNAs had a higher accuracy for diagnosing the NSCLC with SEN: 88% (95% CI: 85-91%), SPE: 91% (95% CI: 88-93%), and AUC: 0.96 (95% CI: 0.93-0.97), respectively, when compared with the single miRNA with the SEN: 77% (95% CI: 71-82%), SPE: 80% (95% CI: 77-84%), and AUC: 0.86 (95% CI: 0.82-0.88), respectively. miRNAs had a higher value to distinguish the NSCLC patients from healthy individuals with the SEN: 86% (95% CI: 82-89%), SPE: 88% (95% CI: 85-91%), and AUC: 0.94 (95% CI: 0.91-0.95) than controls with benign pulmonary disease with SEN: 84% (95% CI: 77-89%), SPE: 84% (95% CI: 80-88%), and AUC: 0.90 (95% CI: 0.87-0.92). Compared with other miRNAs, miR-210 and miR-21 were more often used as diagnostic tools. However, they were usually associated with other miRNAs. The sensitivity, specificity, and AUC were, respectively, 77% (95% CI: 72-81%), 93% (95% CI: 88-96%), and 0.91 (95% CI: 0.88-0.93) for miR-210 with other miRNAs. The sensitivity, specificity, and AUC of miR-21 with other miRNAs were, respectively, 82% (95% CI: 77-86%), 87% (95% CI: 84-89%), and 0.91 (95% CI: 0.88-0.93).

4. Discussion

Due to the high mortality rate and low survival rate of NSCLC, there is an urgent need for the accurate detection method for the early detection of NSCLC especially for the nonsmoking NSCLC patients. Although miRNAs may have a high diagnostic accuracy according to the previous articles, the clinical utility of the miRNA for diagnosing NSCLC remains controversial. Compared with the previous meta-analyses [69–71], there were more studies and participants included in this meta-analysis. Our analysis showed the

pooled SEN was 85% (95% CI: 82-88%), the pooled SPE was 88% (95% CI: 85-90%), and the AUC was 0.93 (95% CI: 0.90-0.95), suggesting that miRNAs had pretty high diagnostic value for NSCLC. Our results also showed that the pooled DOR was 40 (95% CI: 28-58), indicating that for an individual proved positive by miRNAs the chance of having NSCLC is 40 times higher than the negative ones. For the subgroup analyses, higher accuracy was observed in the multiple miRNA profiling when compared with the single miRNA, which was consistent with the previous conclusions [69–71]. MiRNAs might have a higher diagnostic efficacy for the nonsmoking NSCLC patients compared with the smoking ones. Meanwhile, differences were also observed among the Caucasian, Asian, and Caucasian/African populations. This result could be supported by the Wang H's article [71]. Furthermore, miRNAs from serum samples exhibited higher diagnostic value than miRNAs from other specimen. These results meant that combinations of various miRNAs may be better diagnostic tools than the single miRNA, and miRNA isolated from serum could have a higher diagnostic value for the Caucasian populations when compared with the Asian and Caucasian/African populations. Among the different multiple miRNAs, miR-210 and miR-21 associated with other miRNAs could be used for the detection of NSCLC. However, there were still some limitations that could not be neglected in this meta-analysis such as the heterogeneity among these 71 studies, the different methods in miRNA profiling, the possibility that some articles are missed or not published online.

5. Conclusions

Our meta-analysis showed the practicability of miRNAs for diagnosing NSCLC and demonstrated that the multiple miRNAs might have a relatively high diagnostic value for NSCLC compared with the single miRNA diagnosis. miR-210 and miR-21 could be used as effective tools through combining with other miRNAs. In addition, miRNAs, especially isolated from serum, had a better diagnostic accuracy in Caucasian populations than the Asian populations as well as the Caucasian/African populations. When compared with the smoking NSCLC patients, miRNAs might have a higher diagnostic efficacy for the nonsmoking ones. However, studies on the large samples are still demanded to verify our results.

Abbreviations

miRNA:	MicroRNA
NSCLC:	Non-small cell lung cancer
SEN:	Sensitivity
SPE:	Specificity
SROC:	Summary receiver operating characteristic
AUC:	The area under the SROC curve
mRNA:	Messenger RNA
3'-UTR:	3'-untranslated region
BPD:	Benign pulmonary disease
HC:	Healthy Control
CNKI:	Chinese national knowledge infrastructure

PLR:	Positive likelihood ratio
NLR:	Negative likelihood ratio
DOR:	Diagnostic odds ratio
TP:	True positive
FP:	False positive
FN:	False negative
TN:	True negative
qRT-PCR:	Quantitative real-time polymerase chain reaction
PBMC:	Peripheral blood mononuclear cells
PRISMA:	Preferred Reporting Items for Systematic Reviews and Meta-Analyses
BAL:	Bronchoalveolar lavage.

Conflicts of Interest

The authors declare that there are no potential conflicts of interest.

Authors' Contributions

Baosen Zhou, Xuelian Li, and Min Jiang conceived and designed this study. Min Jiang and Xiaoying Li searched the literature and analyzed the data. Xiaowei Quan contributed to the analysis tools and the statistical analysis. Min Jiang and Baosen Zhou wrote and revised the paper.

Acknowledgments

This study was supported by the National Natural Science Foundation of China (no. 81502878) and the Doctoral Research Project of Liaoning Province (no. 201601117).

References

- [1] L. A. Torre, F. Bray, R. L. Siegel, J. Ferlay, and J. Lortet-Tieulent, "Global cancer statistics, 2012," *CA: A Cancer Journal for Clinicians*, vol. 65, no. 2, pp. 87–108, 2015.
- [2] M. Lagos-Quintana, R. Rauhut, W. Lendeckel, and T. Tuschl, "Identification of novel genes coding for small expressed RNAs," *Science*, vol. 294, no. 5543, pp. 853–858, 2001.
- [3] S. P. Nana-Sinkam and C. M. Croce, "Non-coding RNAs in cancer initiation and progression and as novel biomarkers," *Molecular Oncology*, vol. 5, no. 6, pp. 483–491, 2011.
- [4] G. A. Calin and C. M. Croce, "MicroRNA signatures in human cancers," *Nature Reviews Cancer*, vol. 6, no. 11, pp. 857–866, 2006.
- [5] X. Zhang, P. Li, and M. Rong, "MicroRNA-141 is a biomarker for progression of squamous cell carcinoma and adenocarcinoma of the lung: clinical analysis of 125 patients," *The Tohoku Journal of Experimental Medicine*, vol. 235, no. 3, pp. 161–169, 2015.
- [6] X. Wang, X. Zhi, Y. Zhang, G. An, and G. Feng, "Role of plasma MicroRNAs in the early diagnosis of non-small-cell lung cancers: a case-control study," *Journal of Thoracic Disease*, vol. 8, no. 7, pp. 1645–1652, 2016.
- [7] Y. Wang, H. Zhao, X. Gao et al., "Identification of a three-miRNA signature as a blood-borne diagnostic marker for early diagnosis of lung adenocarcinoma," *Oncotarget*, vol. 7, no. 18, pp. 26070–26086, 2016.
- [8] B. Wang and Q. Zhang, "The expression and clinical significance of circulating microRNA-21 in serum of five solid tumors," *Journal of Cancer Research and Clinical Oncology*, vol. 138, no. 10, pp. 1659–1666, 2012.
- [9] M. E. Hatley, D. M. Patrick, M. R. Garcia et al., "Modulation of K-Ras-dependent lung tumorigenesis by MicroRNA-21," *Cancer Cell*, vol. 18, no. 3, pp. 282–293, 2010.
- [10] J. Osugi, Y. Kimura, Y. Owada et al., "Prognostic Impact of Hypoxia-Inducible," *Journal of Oncology*, vol. 2015, pp. 1–8, 2015.
- [11] J. Wei, L.-K. Liu, W. Gao et al., "Reduction of plasma MicroRNA-21 is associated with chemotherapeutic response in patients with non-small cell lung cancer," *Chinese Journal of Cancer Research*, vol. 23, no. 2, pp. 123–128, 2011.
- [12] Y. Su, M. A. Guarnera, H. Fang, and F. Jiang, "Small non-coding RNA biomarkers in sputum for lung cancer diagnosis," *Molecular Cancer*, vol. 15, no. 1, article no. 36, 2016.
- [13] J. O. Kim, S. Gazala, R. Razzak et al., "Non-small cell lung cancer detection using microRNA expression profiling of bronchoalveolar lavage fluid and sputum," *Anticancer Research*, vol. 35, pp. 1873–1880, 2015.
- [14] R. Razzak, E. Bédard, J. Kim et al., "MicroRNA expression profiling of sputum for the detection of early and locally advanced non-small-cell lung cancer: a prospective case-control study," *Current Oncology*, vol. 23, no. 2, p. 86, 2016.
- [15] P. F. Whiting, A. W. S. Rutjes, M. E. Westwood et al., "Quadas-2: a revised tool for the quality assessment of diagnostic accuracy studies," *Annals of Internal Medicine*, vol. 155, no. 8, pp. 529–536, 2011.
- [16] J. P. T. Higgins, S. G. Thompson, J. J. Deeks, and D. G. Altman, "Measuring inconsistency in meta-analyses," *British Medical Journal*, vol. 327, no. 7414, pp. 557–560, 2003.
- [17] J. J. Deeks, P. Macaskill, and L. Irwig, "The performance of tests of publication bias and other sample size effects in systematic reviews of diagnostic test accuracy was assessed," *Journal of Clinical Epidemiology*, vol. 58, no. 9, pp. 882–893, 2005.
- [18] L. Xing, N. W. Todd, L. Yu, H. Fang, and F. Jiang, "Early detection of squamous cell lung cancer in sputum by a panel of microRNA markers," *Modern Pathology*, vol. 23, no. 8, pp. 1157–1164, 2010.
- [19] L. Yu, N. W. Todd, L. Xing et al., "Early detection of lung adenocarcinoma in sputum by a panel of microRNA markers," *International Journal of Cancer*, vol. 127, no. 12, pp. 2870–2878, 2010.
- [20] H. C. Jeong, E. K. Kim, J. H. Lee, J. M. Lee, H. Nayoo, and J. K. Kim, "Aberrant expression of let-7a miRNA in the blood of non-small cell lung cancer patients," *Molecular Medicine Reports*, vol. 4, no. 2, pp. 383–387, 2011.
- [21] J. Shen, Z. Liu, N. W. Todd et al., "Diagnosis of lung cancer in individuals with solitary pulmonary nodules by plasma microRNA biomarkers," *BMC Cancer*, vol. 11, article 374, 2011.
- [22] S. Liu and J. Yang, "Application of plasma circulation microRNA - 126 to diagnosis of non - small cell lung cancer," *Medical Journal of National Defending Forces in Southwest China*, vol. 21, pp. 1280–1283, 2011.
- [23] P. T. Hennessey, T. Sanford, A. Choudhary et al., "Serum microRNA biomarkers for detection of non-small cell lung cancer," *PLoS ONE*, vol. 7, no. 2, Article ID e32307, 2012.
- [24] M. Yuxia, T. Zhennan, and Z. Wei, "Circulating miR-125b is a novel biomarker for screening non-small-cell lung cancer and predicts poor prognosis," *Journal of Cancer Research and Clinical Oncology*, vol. 138, no. 12, pp. 2045–2050, 2012.

- [25] M. Zhao, X. Shen, P. Zhan, T. Lv, H. Liu, and Y. Song, "Expression of miRNA-29a in non-small cell lung cancer and clinical significance," *Chinese Clinical Oncology*, vol. 17, pp. 428–432, 2012.
- [26] A. A. Abd-El-Fattah, N. A. H. Sadik, O. G. Shaker, and M. L. Aboulftouh, "Differential microRNAs expression in serum of patients with lung cancer, pulmonary tuberculosis, and pneumonia," *Cell Biochemistry and Biophysics*, vol. 67, no. 3, pp. 875–884, 2013.
- [27] N. Anjuman, N. Li, M. Guarnera, S. A. Stass, and F. Jiang, "Evaluation of lung flute in sputum samples for molecular analysis of lung cancer," *linical and Translational Medicine*, vol. 2, article 15, 2013.
- [28] N. G. Bediaga, M. P. A. Davies, A. Acha-Sagredo et al., "A microRNA-based prediction algorithm for diagnosis of non-small lung cell carcinoma in minimal biopsy material," *British Journal of Cancer*, vol. 109, no. 9, pp. 2404–2411, 2013.
- [29] R. Cazzoli, F. Buttitta, M. di Nicola et al., "MicroRNAs derived from circulating exosomes as noninvasive biomarkers for screening and diagnosing lung cancer," *Journal of Thoracic Oncology*, vol. 8, no. 9, pp. 1156–1162, 2013.
- [30] J. Ma, N. Li, M. Guarnera, and F. Jiang, "Quantification of Plasma miRNAs by Digital PCR for Cancer Diagnosis," *Biomarker Insights*, vol. 8, p. BMI.S13154, 2013.
- [31] P. Mozzoni, I. Banda, M. Goldoni et al., "Plasma and EBC microRNAs as early biomarkers of non-small-cell lung cancer," *Biomarkers*, vol. 18, no. 8, pp. 679–686, 2013.
- [32] D. Tang, Y. Shen, M. Wang et al., "Identification of plasma microRNAs as novel noninvasive biomarkers for early detection of lung cancer," *European Journal of Cancer Prevention*, vol. 22, no. 6, pp. 540–548, 2013.
- [33] P. Ulivi, G. Foschi, M. Mengozzi et al., "Peripheral blood miR-328 expression as a potential biomarker for the early diagnosis of NSCLC," *International Journal of Molecular Sciences*, vol. 14, no. 5, pp. 10332–10342, 2013.
- [34] X. L. Zeng, S. Y. Zhang, J. F. Zheng, H. Yuan, and Y. Wang, "Altered miR-143 and miR-150 expressions in peripheral blood mononuclear cells for diagnosis of non-small cell lung cancer," *Chinese Medical Journal*, vol. 126, pp. 4510–4516, 2013.
- [35] Z. Wang, X. Zhang, H. Bai et al., "EML4-ALK Rearrangement and Its Clinical Significance in Chinese Patients with Advanced Non-Small Cell Lung Cancer," *Oncology*, vol. 83, no. 5, pp. 248–256, 2012.
- [36] X. Yang, Y. Zhang, B. Sun et al., "Diagnostic value of the detection of MicroRNAs in sputum of patients with non-small cell lung cancer," *Journal of Clinical Pulmonary Medicine*, vol. 18, pp. 226–229, 2013.
- [37] M. Li, Q. Zhang, L. Wu et al., "Serum miR-499 as a novel diagnostic and prognostic biomarker in non-small cell lung cancer," *Oncology Reports*, vol. 31, no. 4, pp. 1961–1967, 2014.
- [38] N. Li, J. Ma, M. A. Guarnera, H. Fang, L. Cai, and F. Jiang, "Digital PCR quantification of miRNAs in sputum for diagnosis of lung cancer," *Journal of Cancer Research and Clinical Oncology*, vol. 140, no. 1, pp. 145–150, 2014.
- [39] W. Zhu, J. He, D. Chen et al., "Expression of miR-29c, miR-93, and miR-429 as potential biomarkers for detection of early stage non-small lung cancer," *PLoS ONE*, vol. 9, no. 2, Article ID e87780, 2014.
- [40] H. Dou, Y. Wang, G. Su, and S. Zhao, "Decreased plasma let-7c and miR-152 as noninvasive biomarker for non-small-cell lung cancer," *International Journal of Clinical and Experimental Medicine*, vol. 8, pp. 9291–9298, 2015.
- [41] W. Guo, Y. Zhang, Y. Zhang et al., "Decreased expression of MIR-204 in plasma is associated with a poor prognosis in patients with non-small cell lung cancer," *International Journal of Molecular Medicine*, vol. 36, no. 6, pp. 1720–1726, 2015.
- [42] L. Li, Y. Y. Chen, Li. SQ, C. Huang, and Y. Z. Qin, "Expression of miR-148/152 family as potential biomarkers in non-small-cell lung cancer," *Medical Science Monitor*, vol. 21, pp. 1155–1161, 2015.
- [43] C. Liu, C. Wang, F. Chen, H. Yu, J. Wang, and J. Yang, "Combined detection of pleural effusion cell DNA aneuploidy and microRNA-192 and its related factors in diagnosis of non-small cell lung cancer," *China Journal of Modern Medicine*, vol. 25, pp. 26–30, 2015 (Chinese).
- [44] J. Ma, Y. Lin, M. Zhan, D. L. Mann, S. A. Stass, and F. Jiang, "Differential miRNA expressions in peripheral blood mononuclear cells for diagnosis of lung cancer," *Laboratory Investigation*, vol. 95, no. 10, pp. 1197–1206, 2015.
- [45] E. Nadal, A. Truini, A. Nakata et al., "A Novel Serum 4-microRNA Signature for Lung Cancer Detection," *Scientific Reports*, vol. 5, Article ID 12464, 2015.
- [46] C. Wang, M. Ding, M. Xia et al., "A Five-miRNA Panel Identified From a Multicentric Case-control Study Serves as a Novel Diagnostic Tool for Ethnically Diverse Non-small-cell Lung Cancer Patients," *EBioMedicine*, vol. 2, no. 10, pp. 1377–1385, 2015.
- [47] R. J. Wang, Y. H. Zheng, P. Wang, and J. Z. Zhang, "Serum miR-125a-5p, miR-145 and miR-146a as diagnostic biomarkers in non-small cell lung cancer," *International Journal of Clinical and Experimental Pathology*, vol. 8, pp. 765–771, 2015.
- [48] L. Xing, J. Su, M. A. Guarnera et al., "Sputum microRNA biomarkers for identifying lung cancer in indeterminate solitary pulmonary nodules," *Clinical Cancer Research*, vol. 21, no. 2, pp. 484–489, 2015.
- [49] J.-S. Yang, B.-J. Li, H.-W. Lu et al., "Serum miR-152, miR-148a, miR-148b, and miR-21 as novel biomarkers in non-small cell lung cancer screening," *Tumor Biology*, vol. 36, no. 4, pp. 3035–3042, 2015.
- [50] Y.-L. Yang, L.-P. Xu, F.-L. Zhuo, and T.-Y. Wang, "Prognostic value of microRNA-10b overexpression in peripheral blood mononuclear cells of nonsmall-cell lung cancer patients," *Tumor Biology*, vol. 36, no. 9, pp. 7069–7075, 2015.
- [51] W. Zhao, J. J. Zhao, L. Zhang et al., "Serum miR-21 level: a potential diagnostic and prognostic biomarker for non-small cell lung cancer," *International Journal of Clinical and Experimental Medicine*, vol. 8, pp. 14759–14763, 2015.
- [52] L. Fan, H. Qi, J. Teng et al., "Identification of serum miRNAs by nano-quantum dots microarray as diagnostic biomarkers for early detection of non-small cell lung cancer," *Tumor Biology*, vol. 37, no. 6, pp. 7777–7784, 2016.
- [53] X. Gao, Y. Wang, H. Zhao et al., "Plasma miR-324-3p and miR-1285 as diagnostic and prognostic biomarkers for early stage lung squamous cell carcinoma," *Oncotarget*, vol. 7, no. 37, 2016.
- [54] A. R. Halvorsen, M. Bjaanaes, M. LeBlanc et al., "A unique set of 6 circulating microRNAs for early detection of non-small cell lung cancer," *Oncotarget*, vol. 7, no. 24, pp. 37250–37259, 2016.
- [55] L.-P. Jiang, Z.-T. Zhu, and C.-Y. He, "Expression of miRNA-26b in the diagnosis and prognosis of patients with non-small-cell lung cancer," *Future Oncology*, vol. 12, no. 9, pp. 1105–1115, 2016.
- [56] P. Leidinger, T. Brefort, C. Backes et al., "High-throughput qRT-PCR validation of blood microRNAs in non-small cell lung cancer," *Oncotarget*, vol. 7, no. 4, pp. 4611–4623, 2016.

- [57] K. Su, T. Zhang, Y. Wang, and G. Hao, "Diagnostic and prognostic value of plasma microRNA-195 in patients with non-small cell lung cancer," *World Journal of Surgical Oncology*, vol. 14, no. 1, 2016.
- [58] L. Sun, Y. Chen, Q. Su et al., "Increased plasma miRNA-30a as a biomarker for non-small cell lung cancer," *Medical Science Monitor*, vol. 22, pp. 647–655, 2016.
- [59] M. C. Tai, K. Yanagisawa, M. Nakatochi et al., "Blood-borne miRNA profile-based diagnostic classifier for lung adenocarcinoma," *Scientific Reports*, vol. 6, no. 1, 2016.
- [60] J. Wei, W. Gao, C.-J. Zhu et al., "Identification of plasma microRNA-21 as a biomarker for early detection and chemosensitivity of non-small cell lung cancer," *Chinese Journal of Cancer*, vol. 30, no. 6, pp. 407–414, 2011.
- [61] W. Zhu, K. Zhou, Y. Zha et al., "Diagnostic value of serum miR-182, miR-183, miR-210, and miR-126 levels in patients with early-stage non-small cell lung cancer," *PLoS ONE*, vol. 11, no. 4, Article ID e0153046, 2016.
- [62] H. Zhang, F. Mao, T. Shen et al., "Plasma miR-145, miR-20a, miR-21 and miR-223 as novel biomarkers for screening early-stage non-small cell lung cancer," *Oncology Letters*, vol. 13, no. 2, pp. 669–676, 2017.
- [63] A. Keller, P. Leidinger, A. Borries et al., "MiRNAs in lung cancer - Studying complex fingerprints in patient's blood cells by microarray experiments," *BMC Cancer*, vol. 9, article no. 1471, p. 353, 2009.
- [64] G. Li, Y. Huang, Y. He et al., "Study of miRNA Signatures as Biomarkers for Early Stage Nonsmoking Female Lung Cancer of Xuanwei Country of Yunnan Province," *Cancer prevention and control research*, vol. 39, pp. 802–806, 2012.
- [65] W. H. Roa, J. O. Kim, R. Razzak et al., "Sputum microRNA profiling: a novel approach for the early detection of non-small cell lung cancer," *Clinical & Investigative Medicine*, vol. 35, no. 5, pp. E271–E281, 2012.
- [66] C. Sanfiorenzo, M. I. Ilie, A. Belaid et al., "Two panels of plasma microRNAs as non-invasive biomarkers for prediction of recurrence in resectable NSCLC," *PLoS ONE*, vol. 8, no. 1, Article ID e54596, 2013.
- [67] W. Li, Y. Wang, Q. Zhang et al., "MicroRNA-486 as a biomarker for early diagnosis and recurrence of non-small cell lung cancer," *PLoS ONE*, vol. 11, no. 1, 2016.
- [68] W. Wang, W. Li, M. Ding et al., "Identification of miRNAs as non-invasive biomarkers for early diagnosis of lung cancers," *Tumor Biology*, vol. 37, no. 12, pp. 16287–16293, 2016.
- [69] L. Chen and H. Jin, "MicroRNAs as novel biomarkers in the diagnosis of non-small cell lung cancer: a meta-analysis based on 20 studies," *Tumor Biology*, vol. 35, no. 9, pp. 9119–9129, 2014.
- [70] Y. Huang, Q. Hu, Z. Deng, Y. Hang, J. Wang, and K. Wang, "MicroRNAs in body fluids as biomarkers for non-small cell lung cancer: a systematic review," *Technology in Cancer Research & Treatment*, vol. 13, no. 3, pp. 277–287, 2014.
- [71] H. Wang, S. Wu, L. Zhao, J. Zhao, J. Liu, and Z. Wang, "Clinical use of microRNAs as potential non-invasive biomarkers for detecting non-small cell lung cancer: A meta-analysis," *Respirology*, vol. 20, no. 1, pp. 56–65, 2015.

Review Article

Cystathionine β -Synthase in Physiology and Cancer

Haoran Zhu,^{1,2} Shaun Blake,^{1,2} Keefe T. Chan,¹
Richard B. Pearson ^{1,2,3,4} and Jian Kang ¹

¹Division of Research, Peter MacCallum Cancer Centre, 305 Grattan Street, Melbourne, Victoria 3000, Australia

²Sir Peter MacCallum Department of Oncology, Australia

³Department of Biochemistry and Molecular Biology, University of Melbourne, Parkville, Victoria 3052, Australia

⁴Department of Biochemistry and Molecular Biology, Monash University, Clayton, Victoria 3168, Australia

Correspondence should be addressed to Richard B. Pearson; rick.pearson@petermac.org

Received 23 March 2018; Accepted 29 May 2018; Published 28 June 2018

Academic Editor: Maria L. Tornesello

Copyright © 2018 Haoran Zhu et al. This is an open access article distributed under the Creative Commons Attribution License, which permits unrestricted use, distribution, and reproduction in any medium, provided the original work is properly cited.

Cystathionine β -synthase (CBS) regulates homocysteine metabolism and contributes to hydrogen sulfide (H_2S) biosynthesis through which it plays multifunctional roles in the regulation of cellular energetics, redox status, DNA methylation, and protein modification. Inactivating mutations in CBS contribute to the pathogenesis of the autosomal recessive disease CBS-deficient homocystinuria. Recent studies demonstrating that CBS promotes colon and ovarian cancer growth in preclinical models highlight a newly identified oncogenic role for CBS. On the contrary, tumor-suppressive effects of CBS have been reported in other cancer types, suggesting context-dependent roles of CBS in tumor growth and progression. Here, we review the physiological functions of CBS, summarize the complexities regarding CBS research in oncology, and discuss the potential of CBS and its key metabolites, including homocysteine and H_2S , as potential biomarkers for cancer diagnosis or therapeutic targets for cancer treatment.

1. Introduction

Cystathionine β -synthase (CBS) catalyzes the condensation of homocysteine (Hcy) with serine to form cystathionine, which is the initial and rate-limiting step in the transsulfuration pathway. Cystathionine is subsequently cleaved by the enzyme cystathionine gamma-lyase (CTH) to form cysteine, a precursor of glutathione. Besides this canonical pathway, CBS also participates in the desulfuration reactions that contribute to endogenous hydrogen sulfide (H_2S) production (Figure 1). Thus, CBS acting mainly through control of Hcy and H_2S metabolism exerts diverse biological functions including mitochondrial bioenergetics, redox homeostasis, DNA methylation and protein modification. Deregulation of CBS and the associated alterations in Hcy and/or H_2S levels leads to a wide range of pathological disturbances in the cardiovascular, immune, and central nervous systems and contributes to disease development, such as CBS-deficient homocystinuria (CBSDH). It is now becoming clear that CBS activity also plays an important but complex role in cancer

biology. This review focuses on the current understanding of the functional role of CBS and the derived metabolites Hcy and H_2S in cancer pathogenesis and provides insight into the development of novel prognostic markers and therapeutic approaches for cancer patients.

2. CBS Protein Structure and Biological Functions

The human CBS gene encodes a protein of 551 amino acids. The crystal structure of the active form of human CBS, formed by four of 63-kDa subunits, has been fully characterized [1, 2]. Each subunit consists of three structural domains. The N-terminal domain binds to the cofactor heme, which is required for successful protein folding and assembly but not necessary for catalytic activity [3]. The catalytic domain encompasses a binding site for another cofactor, pyridoxal-phosphate (PLP) [4]. The C-terminal regulatory domain contains two CBS motifs (CBS1 and CBS2) that dimerize to form a Bateman domain. This domain is responsible for CBS

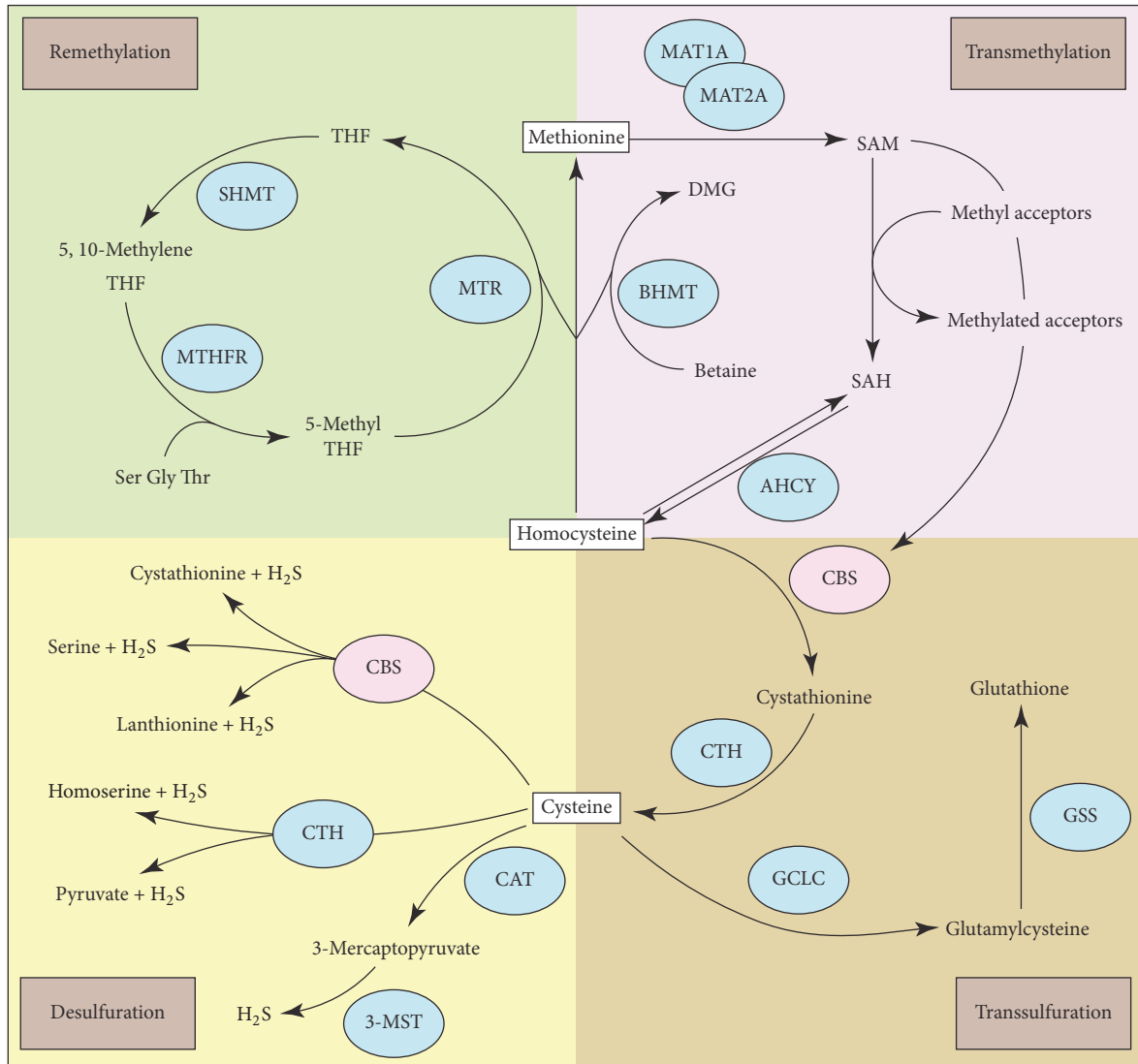


FIGURE 1: *Metabolic reactions catalyzed by CBS.* CBS catalyzes the condensation of homocysteine (Hcy) with serine to form cystathionine which is subsequently cleaved by cystathionine gamma-lyase (CTH) to form cysteine, a precursor of glutathione. CBS also catalyzes the production of H₂S. In addition to CBS, CTH and 3-mercaptopyruvate sulfurtransferase (3-MST) are also involved in the conversion of cysteine to H₂S. Homocysteine is another key CBS-derived metabolite and is linked to the metabolism of methionine. Methionine is converted to homocysteine via S-adenosyl methionine (SAM) and S-adenosyl homocysteine (SAH), releasing a methyl group that is used in numerous methylation reactions. SAM is an allosteric activator of CBS. 3-MST, 3-mercaptopyruvate sulfurtransferase; AHCY, adenosylhomocysteinase; BHMT, betaine-homocysteine methyltransferase; CAT, cysteine aminotransferase; CBS, cystathionine β -synthase; CTH, cystathionine gamma-lyase; GCLC, gamma-glutamylcysteine synthetase; GSS, glutathione synthetase; MAT1A/2A, methionine adenosyltransferase 1A/2A; MTHFR, methylenetetrahydrofolate reductase; MTR, 5-methyltetrahydrofolate-homocysteine methyltransferase; SAM, S-adenosyl methionine; SAH, S-adenosyl homocysteine; SHMT, serine hydroxymethyltransferase.

subunit tetramerization and contains the binding sites for the allosteric activator S-adenosylmethionine (SAM) [1, 5, 6]. In the native quaternary structure, the access of substrates to the catalytic core is occluded by the C-terminal regulatory motifs and the binding of SAM induces a conformational change that improves the access of the substrates to the catalytic site [2]. The autoinhibitory function of the C-terminal regulatory domain is relieved by the C-terminal truncation that generates a 45 kDa isoform with higher basal catalytic activity than the full-length form [1].

CBS is predominantly expressed in the brain, liver, kidney, and pancreas. It is mainly a cytosolic enzyme, but localization in the nucleus [7] and mitochondria [8] had been detected in specific cell types. CBS can be translocated to the mitochondria in response to hypoxia [9] or nucleolar stress [10]. CBS expression is regulated at multiple levels upon different stimuli. For example, hormonal regulation by glucocorticoids increases CBS expression at the transcriptional level in liver cells, a process that may be perturbed by insulin administration through binding to an

insulin-sensitive sequence localized on the CBS promoter [11]. In addition, testosterone can regulate CBS expression and activity in renal tissue [12]. Growth/differentiation factors such as EGF, TGF- α , cAMP, and dexamethasone induced CBS protein expression in mouse astrocytes [13]. Hypoxia upregulated CBS expression either via hypoxia-inducible factor- (HIF-) 1 at the transcriptional level [14] or decreased degradation of CBS protein by Lon proteases in the mitochondria [9]. Besides HIF-1, the zinc finger transcription factor SPI binds to the CBS gene promoter, establishing its role as a key regulator of CBS expression [15, 16]. Furthermore, CBS activity may be enhanced via posttranslational regulation through S-glutathionylation [17] or inhibited via epigenetic downregulation of CBS expression through promoter methylation [18, 19].

CBS plays a critical role in Hcy elimination. Patients with CBS deficiency exhibit elevated Hcy plasma levels at excess of 200 μ M compared to 5-15 μ M in healthy adults [20]. CBS-deficient homocystinuria (CBSDH) is an autosomal recessive metabolic disease, resulting from inactivating mutations in the CBS gene. CBSDH patients present multiple pathologic changes in the eye, skeleton, central nervous, and vascular systems. Common symptoms in CBSDH patients include thrombosis, osteoporosis, and impaired mental cognitive development (reviewed in [21-23]). Administration of high doses of the PLP precursor, pyridoxine, or vitamin B₆ is common treatment that ameliorates approximately 50% of clinical symptoms. To date, 164 pathogenic genetic variants have been identified (<http://cbs.lf1.cuni.cz/mutations.php>) of which the predominant mutations are missense mutations. c.833 T > C (p.I278T) is the most frequent mutation detected in many European populations [24]. The I278T missense mutation and many of the less prevalent mutations likely affect the folding or stability of the CBS protein [25] whereas some mutations such as mutant D444N, a missense mutation in the C-terminal regulatory domain, showed an approximately twofold increase in basal CBS activity but impaired response to SAM stimulation [2]. The pathophysiology of CBS deficiency is still not fully understood. As well as the accumulation of Hcy, CBS defects lead to increased concentrations of methionine and S-adenosyl-L-homocysteine (SAH) and depletion of cystathionine and cysteine. These perturbations may act in concert with high Hcy to promote the development and progression of CBSDH (reviewed in [26]).

Accordingly, extensive studies in the mouse models of CBS deficiency showed mice with homozygotic CBS deletion (CBS^{-/-}) died within 4 weeks after birth due to severe hepatic dysfunction and exhibited extremely high levels of circulating Hcy (reviewed in [26, 27]). Wang et al. showed that the neonatal lethality could be rescued by decreasing circulating Hcy levels in a transgenic mouse model with inducible CBS expression [28]. They further found that there may be a threshold effect with Hcy, meaning that moderately lowering homocysteinemia can improve mouse viability during the neonatal period [29]. In support of the Hcy threshold effect, CBS^{+/-} heterozygote mice were fully viable with a 3-fold increase of Hcy levels compared to the 8-fold increase in homozygous mice [30].

3. Homocysteine and H₂S, the Major CBS-Derived Metabolites

3.1. Homocysteine. Hcy is a sulfur-containing nonproteinogenic amino acid linked to the metabolism of methionine and cysteine. Methionine is converted to Hcy via S-adenosyl methionine (SAM) and SAH, releasing a methyl group that is used in numerous methylation reactions. Hcy can reform Met by the remethylation pathway either via 5-methyltetrahydrofolate-homocysteine methyltransferase (MTR, 5-methyltetrahydrofolate as the methyl group donor) or betaine-homocysteine methyltransferase (BHMT, betaine as the methyl group donor) (Figure 1). Hcy is also irreversibly metabolized by CBS to cystathionine that subsequently converts to cysteine via CTH in the transsulfuration pathway (Figure 1). Hcy metabolism mainly occurs in the liver and conversion to cystathionine by CBS is a major elimination route of Hcy [31].

Hyperhomocysteinemia (HHcy) is recognized as an independent risk factor for atherosclerotic vascular disease [32]. HHcy may result from mutations in genes encoding enzymes of Hcy biosynthesis and metabolism or deficiencies of vitamin cofactors including vitamin B₁₂ and B₆ [33]. The molecular mechanisms underlying HHcy-induced atherosclerosis are complex and multifactorial (Figure 2). Elevated Hcy concentration reduces nitric oxide (NO) bioavailability and causes oxidative stress. HHcy also leads to formation of Hcy thiolactone as a result of error-prone editing by the methionyl-tRNA synthase [34]. This Hcy derivative can cause protein N-homocysteinylation in which the thioester group of thiolactone binds to the lysine residues in proteins, consequently impairing protein function, resulting in unfolded protein response and endoplasmic reticulum stress (reviewed in [35, 36]). Moreover, an elevated Hcy level could lead to accumulation of SAH, a competitive inhibitor of most methyltransferases, consequently inducing DNA hypomethylation [37]. Through this epigenetic mechanism, Hcy has been reported to inhibit endothelial cell growth by decreasing the expression of cyclin A [38], fibroblast growth factor 2 [39], and hTERT expression [40] and by upregulation of platelet-derived growth factors and P66shC [41].

HHcy has also been implicated in the pathogenesis of cancer. Increased release of Hcy by tumor cells is related to their rapid proliferation rate [42]. Hcy accumulation results from defects in methionine synthesis, leading to a methionine-dependent malignant phenotype [43]. A meta-analysis revealed the association of elevated circulating Hcy levels with increased overall risk of cancer [44]. A higher Hcy plasma level has been detected in the patients with hepatocellular carcinoma (HCC) [44] and head and neck squamous cell carcinoma [45]. Although the mechanisms underlying this association between elevated Hcy levels and malignant transformation are unclear, a recent study proposed a mechanism linking Hcy to lipid metabolism and HCC [46]. It demonstrated that Hcy transcriptionally upregulated CYP2J2, a cytochrome P450 (CYP) epoxygenase by stimulating DNA demethylation and increasing SPI/AP1 activity on the promoter of CYP2J2, which promotes epoxyeicosatrienoic acid synthesis and hepatocellular tumorigenesis.

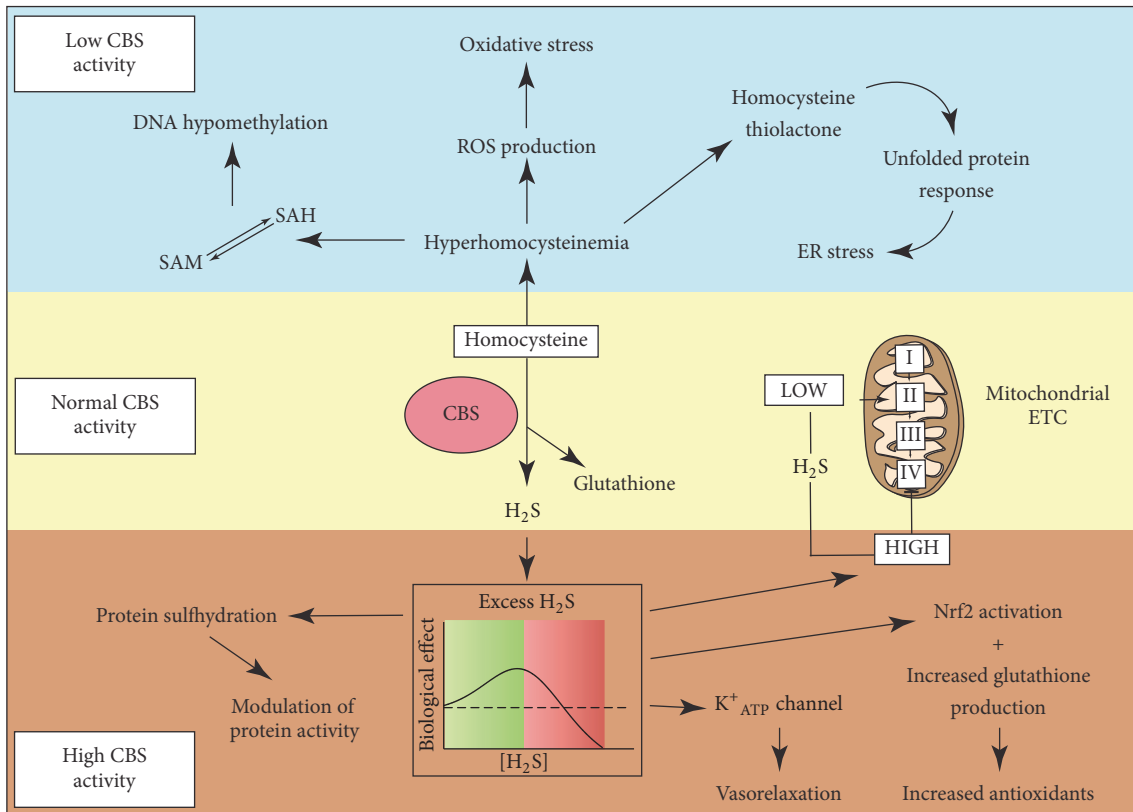


FIGURE 2: Potential mechanisms underlying CBS deregulation with alterations of homocysteine and H_2S levels in cancer pathogenesis. CBS deficiency causes hyperhomocysteinemia. Elevated Hcy concentration can increase reactive oxygen species (ROS) production and induce oxidative stress. Hyperhomocysteinemia also leads to formation of homocysteine thiolactone as a result of error-prone editing by the methionyl-tRNA synthase. This homocysteine derivative can cause protein N-homocysteinylation that impairs protein function, resulting in an unfolded protein response and endoplasmic reticulum (ER) stress. The elevated Hcy level can lead to accumulation of S-adenosyl homocysteine (SAH), a competitive inhibitor of most methyltransferases, consequently inducing DNA hypomethylation and affecting gene transcription. CBS-driven endogenous H_2S production maintains mitochondrial respiration and ATP synthesis, promotes antioxidant production by enhancing Nrf2 activation and increasing glutathione production, and modulates protein activity via protein sulfhydration. Secreted H_2S can cause vasodilation via activation of ATP-sensitive K^+ channels.

3.2. H_2S . Like nitric oxide and carbon monoxide, H_2S is a diffusible gaseous transmitter in the human body and is mainly synthesized during cysteine metabolism and excreted as urinary sulfates by the kidney (reviewed in [47]). CBS catalyzes the production of H_2S via at least three pathways including (i) converting cysteine to serine and H_2S , (ii) condensing cysteine and Hcy to yield cystathionine and H_2S , and (iii) condensing two cysteine molecules to lanthionine and H_2S (Figure 1). In addition to CBS, CTH and 3-mercaptopyruvate sulfurtransferase (3-MST) are also involved in the conversion of cysteine to H_2S (Figure 1).

While H_2S has diverse biological functions in the nervous, cardiovascular, and immune systems, the pathological role of H_2S in cancer biology has attracted substantial attention in recent years. CBS-driven endogenous H_2S production has been reported to support tumor growth by (i) maintaining mitochondrial respiration and ATP synthesis, (ii) stimulating cell proliferation and survival, (iii) redox balance, and (iv) vasodilation (Figure 2). H_2S modulates mitochondrial functions and cellular bioenergetics in a

concentration-dependent manner. At low concentrations, H_2S acts as a mitochondrial electron donor to mitochondrial complex II, resulting in bioenergetic stimulation [48, 49]. At higher concentrations, H_2S acts as a mitochondrial poison via the inhibition of cytochrome *c* oxidase in mitochondrial complex IV [50]. H_2S stimulates cell proliferation through activation of specific kinase pathways (e.g., MAPK and PI3K/Akt) and inhibition of selective phosphatases such as PTEN and PTP1B [51–53]. Modulation of protein activity by H_2S either occurs via protein sulfhydration (reviewed in [54]) or intracellular formation of polysulfides by H_2S followed by oxidative inactivation of proteins [55, 56]. The sulfhydration of nuclear factor kappa B (NF- κ B) by H_2S has also been shown to inhibit apoptosis and may be of particular relevance to cancer cell survival [57]. The protective effect of H_2S from oxidative stress has been extensively studied in endothelial cells and neurons [58–62]. Studies showed H_2S inhibited H_2O_2 -mediated mitochondrial dysfunction by preserving the protein expression levels and activity of key antioxidant enzymes, inhibiting reactive oxygen species

(ROS) production and lipid peroxidation [60]. Additionally, these effects may be associated with sulfhydration of Keap1 and activation of Nrf2 [61] or increasing the production of the antioxidant glutathione. Vasorelaxation is one of the first recognized biological effects of H₂S. The mechanisms of H₂S-mediated vasodilation include the activation of ATP-sensitive K⁺ channels, inhibition of phosphodiesterases, and a synergy with NO (reviewed in [63]).

H₂S-donating compounds deliver H₂S exogenously, including fast H₂S donors such as sulfate salts (e.g., NaHS and Na₂S) and naturally occurring compounds (e.g., the garlic constituent diallyl trisulfide, sulforaphane, erucin, and iberin) and slow H₂S-releasing synthetic moieties such as GYY4137 (reviewed in [64]). The cellular response to exogenous H₂S released by the donors has been considered as a biphasic response, in which low H₂S concentrations (or low H₂S production rates) showed enhancement of cell proliferation rates and cell viability whereas high H₂S caused deleterious/adverse effects in cells [50, 65]. This biphasic cellular response is consistent with the special action model of H₂S on mitochondrial respiration described above, that is, stimulation of mitochondrial respiration at low levels and inhibition at high levels. This bell-shape pharmacology of H₂S may, at least in part, explain the inconsistent results of the effect of exogenous H₂S in colon cancer cell line HCT116 reported by different groups including a growth inhibitory effect (using NaHS at 400 μM and 800 μM) by the Deng lab [66] and a growth stimulatory effect (using NaHS at 30-300 μM) by the Szabo lab [49, 65, 67].

4. CBS and Cancer

4.1. Promoting Tumor Growth by Activation of CBS. Elevated expression of CBS in tumor tissues or cell lines has been reported in colon [49, 68], ovarian [8], prostate [69], and breast cancer [70], compared to adjacent normal tissue or nontransformed cells. A series of studies from the Hellmich group characterized the oncogenic role of CBS in colon cancer [49, 68, 71]. Through modification of CBS expression (overexpression or RNAi knockdown) or CBS activity (allosteric activator SAM or the inhibitor aminooxyacetate) in the HCT116 colon cancer cell line, they demonstrated that CBS promoted cancer cell proliferation. The antiproliferative effect observed by silencing or inhibiting CBS was recapitulated in the xenograft mouse models and patient-derived tumor xenografts [49]. CBS not only promotes tumor growth and progression but also initiates tumor formation [68]. Overexpression of CBS in adenoma-like colonic epithelial cell line NCM356 enhanced cell proliferative, anchorage-independent growth and invasive capability *in vitro* and tumorigenicity *in vivo*. Mice heterozygous for CBS showed fewer numbers of mutagen-induced aberrant crypt foci than wild-type controls. Through a similar approach, Bhattacharyya et al. [8] reported that CBS knockdown inhibited cell proliferation and suppressed tumor growth in an orthotopic mouse model of cisplatin-resistant ovarian cancer. Interestingly, in breast cancer silencing CBS did not affect cell proliferation in culture but significantly attenuated tumor growth in a xenograft mouse model [70].

The protumorigenic effect of CBS occurs through an autocrine mechanism by regulation of bioenergetics, antioxidant capacity, and apoptosis-related pathways. Targeting CBS genetically or pharmacologically impairs cellular bioenergetics through inhibiting mitochondrial electron transport, oxidative phosphorylation, and glycolysis. H₂S was identified to be responsible for such metabolic and bioenergetic rewiring in colon cancer cells, as CBS expression and activity correlated with H₂S production and exogenous H₂S stimulated cell proliferation and bioenergetics [49]. Systematic metabolomic analysis of CBS-overexpressing NCM356 cells uncovered an anabolic metabolic phenotype with significantly enhanced glycolysis, nucleotide synthesis, and lipogenesis, which is thought to promote malignant transformation [68]. CBS may also promote tumor cell survival by increasing cell intrinsic antioxidant capacity. Ovarian cancer cells depleted of CBS showed enhanced ROS production. Antioxidant glutathione, but not H₂S, fully rescued viability of CBS-depleted cells, suggesting that the effect of CBS in ovarian cancer cells is mediated through regulation of ROS production by glutathione [8]. Similarly, reduced glutathione abundance was observed in breast cancer cells upon CBS silencing and was accompanied by decreased Nrf2 expression [72]. CBS downregulation reduced antioxidant capacity and enhanced the sensitivity of cancer cells to chemotherapeutic drugs. The cytoprotective effect of CBS is also associated with regulation of NF-κB and p53 apoptosis-related signaling [8]. A recent study further suggested CBS is involved in nucleolar stress-induced apoptosis [10]. The authors demonstrated that treatment of p53^{-/-} colon cancer cells with 5-fluorouracil caused nucleolar stress, which led to accumulation of the ribosome-free form of ribosomal protein L3 (rpL3). rpL3 decreased CBS protein abundance through suppression of SPI-mediated CBS gene transcription and increase of CBS protein degradation by translocation of CBS into mitochondria. Decreased CBS abundance and, in turn, reduction of H₂S production have been suggested to contribute to mitochondrial cytochrome C release and induction of the intrinsic cell death pathway [10].

In addition to autocrine regulation, CBS acts via a paracrine mechanism to modulate the tumor microenvironment including stimulating angiogenesis and vasodilation via H₂S production and release as reported in colon and ovarian cancer xenografts [8, 49] and regulating macrophage activation in breast cancer xenograft mouse models [70].

4.2. CBS Associated Oncogenesis Is Tumor Type-Specific. Unlike in colon, ovarian, and breast cancer, CBS does not appear to have a functional role in melanoma [73]. CBS expression is absent in dysplastic nevi, detected in only 25% of primary melanoma samples, and unregulated in four of five melanoma cell lines examined. More importantly, modulation of CBS expression had a minimal effect on melanoma cell proliferation [73].

Downregulation of CBS through promoter methylation has been observed in multiple gastric cancer cell lines and four colon cancer cell lines (including HCT116) [74]. However, the biological consequence of CBS epigenetic silencing in gastric cancer has not been determined. Evidence from

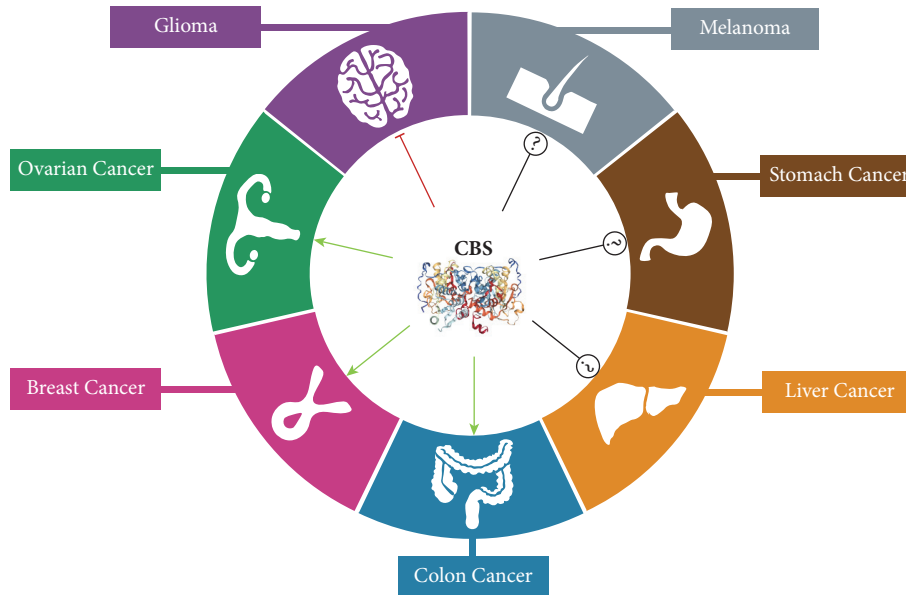


FIGURE 3: CBS associated oncogenesis is tumor type-specific. Activation of CBS promotes tumor growth in colon, ovarian, and breast cancer but suppresses tumor growth in glioma. The role of CBS in liver cancer, gastric cancer, and melanoma is still conflicting and inconclusive.

glioma supports a tumor-suppressive role for CBS [75]. CBS deficiency in U87-MG glioma cells did not affect cell proliferation in 2D culture but increased colony formation in soft agar, indicative of enhanced anchorage-independent growth. Consistently, CBS knockdown decreased tumor latency in U87-MG xenografts and increased tumor volume in an orthotopic model. Enhanced glioma tumorigenicity upon CBS loss was associated with upregulation of HIF-2 α protein level and HIF-2 α -dependent transcriptional activation of angiopoietin like 4 (ANGPTL4) and vascular endothelial growth factor A (VEGFA). The lack of function or suppression of tumor growth by CBS in certain tumor types indicates that CBS associated oncogenesis is tumor-specific (Figure 3).

4.3. Conflicting Role of CBS in Hepatocellular Carcinoma. Clinical evidence from patient samples strongly supports a negative regulatory role for CBS in hepatocellular carcinoma (HCC). Downregulation of CBS expression and activity contributes to the pathogenesis of multiple liver diseases (Reviewed in [76]). Analysis of 120 HCC specimens found that CBS mRNA was markedly lower in tumor tissues than surrounding noncancerous liver [77]. Reduced CBS expression was significantly correlated with the poor clinic pathological parameters including tumor stage, Edmondson grade, alpha-fetoprotein (AFP) level, and overall survival. Further data analysis suggested that the expression level of CBS mRNA could be used as a prognostic marker for overall survival especially in patients with low AFP levels [77]. Diminished CBS levels were also detected in the tumor tissues from the mouse model of HCC [78–80]. Further supporting the tumor-suppressive role for CBS, exogenous H₂S induced autophagy and apoptosis in HCC cells through the PI3K/Akt/mTOR pathway [81].

Intriguingly, distinct from this clinical data, a recent study showed that several HCC cell lines exhibited higher CBS expression than normal liver cells HL-7702 and QSG-7701 [82]. Both genetic (by siRNA) and pharmacological (by AOAA) inhibition of CBS in the SMMC-7721 HCC cell line with reduced H₂S production decreased cell viability and enhanced ROS production *in vitro*. Another study showing that the PI3K/AKT pathway regulated the CTH/H₂S to promote HCC proliferation also supports the oncogenic role of H₂S in HCC [53]. Clearly, the biological function of CBS in liver cancer is complex and requires further investigation.

5. CBS in Cancer Therapy

Consistent with the complex roles of CBS in cancer biology described above, it is also becoming evident that both the activators and inhibitors of CBS have antitumor activity in different cancer models. This genetic context dependence determines different types of cancer will display distinct efficacy and toxicity profiles in response to CBS-based targeted therapies.

5.1. CBS Inhibitors. Aminoxyacetate (AOAA) is currently considered as the most potent CBS inhibitor compared with the other drugs such as trifluoroalanine and hydroxylamine [65]. It has shown antitumor actions in the mouse xenograft models of colon [49] and breast cancer [83] and patient-derived colon cancer xenografts [49]. Decreased H₂S level in plasma was detected in a colon xenograft mouse model treated with AOAA while the drug effect on circulating Hcy level was not investigated. While these antitumor responses are encouraging, the therapeutic effect of CBS inhibition requires further investigation as AOAA is actually not

selective for CBS [65, 84]. The pharmacological action of AOAA is not limited to suppression of the CBS/ H₂S axis. It binds irreversibly to the cofactor PLP, and therefore, in addition to CBS, it inhibits other PLP-dependent enzymes such as CTH, 3-MST, and glutamate oxaloacetate transaminase 1 (GOT1). AOAA has been reported to target CTH preferentially over CBS (IC₅₀ 8.52 μM for CBS versus 1.09 μM for CTH) [85]. Furthermore, inhibition of GOT1 by AOAA disrupted the malate/aspartate shuttle, decreased glucose-derived carbon flux into mitochondrial tricarboxylic acid cycle, and ATP synthesis [83].

To identify new CBS inhibitors, two groups performed small-molecule screening [86, 87]. The Barrios group [87] and the Wu group [86] used recombinant CBS enzymes and employed fluorescent H₂S readouts to screen a composite library of 1900 compounds and a chemical library consisting of 20,000 compounds, respectively. Several compounds showed some selectivity for CBS compared with CTH with IC₅₀ 20-50 μM. However, as the studies did not use AOAA as a reference in the screen, whether these drugs are superior to AOAA in terms of potency and selectivity remains unknown.

5.2. CBS Activator S-Adenosyl-L-Methionine (SAM). SAM is a vital molecule for transmethylation and transsulfuration reactions. It is the principle methyl-donor for DNA, amino acid, protein, and lipid methyltransferase and a key precursor for glutathione and polyamine synthesis (reviewed by [88]). It is synthesized from methionine and ATP by methionine adenosyltransferase (MAT, Figure 1). SAM, as an allosteric activator, modulates CBS activity by inducing a conformational change in the C-terminus of CBS that facilitates the entrance of substrates into the catalytic site of the enzyme [1]. Although SAM has been used for treatment of osteoarthritis [89], depression [90], and liver diseases [88], the clinical evidence for its efficacy in these diseases is still inconclusive. Recent data support the concept of using SAM as a chemopreventive agent in HCC and colon cancer, consistent with the proposed tumor-suppressive role of CBS in HCC. The *Mat1a* knockout mice spontaneously develop HCC supporting the fact that hepatic SAM deficiency predisposes to HCC [91]. In several rodent models of HCC, administration of SAM is effective in preventing liver carcinogenesis [92, 93]. One phase II clinical trial is evaluating SAM as a potential chemoprevention agent in patients with hepatitis C cirrhosis [94]. SAM also showed a similar chemoprevention effect in an inflammation induced colon cancer mouse model [95]. In addition to chemoprevention, SAM exerted a proapoptotic effect in liver (at 0.2 mM over 5 days) [96], gastric (10 μM over 7 days) [97], and colon cancer cells (ranging from 0.25 to 5 mM for 24 hours) [98]. Interestingly, similar to the conflicting data regarding CBS function and effects of H₂S donors in colon cancer, the Szabo group [71] reported a biphasic response to SAM in colon cancer cells. At low concentrations for the short-time period (0.1-1 mM for 12 hours or 0.1 mM for 24 hours), SAM induced a stimulatory effect on CBS activation, H₂S production, and cell proliferation, while at higher concentrations or chronic exposure (0.1-5 mM after 24 hours) the inhibitory effects became more prominent and were not attenuated by CBS silencing, suggesting nonspecificity or

toxicity [71]. Therefore, more work in multiple experiment models is required to better define the role of SAM/CBS axis in cancer pathogenesis.

6. CBS in Cancer Prognosis

With the identification of the pathogenic role of CBS in cancer, the use of CBS as a prognostic and predictive biomarker is becoming attractive. As described above, the negative correlation of CBS expression with the pathologic parameters in HCC indicates its potential as a prognostic marker in HCC [77]. Modulation of CBS activity can be indicated by the changes of Hcy and/or H₂S levels. The potential prognostic values of Hcy in cancer have been extensively studied [99–101]. However, the biological sources of Hcy were not defined in these studies and, thus, the link between the levels of Hcy and CBS function remains unknown. Nevertheless, significant progress in the detection and quantitation of Hcy from patient samples has been made in recent years. Methods of measuring plasma Hcy have evolved from ion-exchange chromatography to high-performance liquid chromatography (HPLC), gas-chromatography mass spectrometry, liquid chromatography-electrospray tandem mass spectrometry (LC-MS/MS), and fluorescence polarization immunoassay (FPIA) [102]. In terms of H₂S, elevated H₂S in exhaled breath or its degraded form in urine in cancer patients provides support for the clinical utility of H₂S as a marker of cancer [101]. However, in order to determine the prognostic and predictive values of H₂S in cancer, development of the methods that can accurately measure H₂S levels in the circulation or in the targeted organs is imperative.

7. Summary and Future Directions

A functional role for CBS in tumor biology is supported by (i) clinical evidence of altered CBS expression level and CBS-derived Hcy and H₂S levels in cancer patients; (ii) preclinical studies showing dysregulation of CBS function and activity in cancer cell culture and animal models; (iii) mechanistic investigations linking CBS to cancer-related cellular and molecular changes and signaling pathways. The distinct biological effects of CBS alterations in different cancer models reveal the complexity of CBS signaling in cancer pathogenesis. The contradictory role of CBS in cancer biology (Figure 3) is possibly due to the existence of alternative Hcy and H₂S metabolic pathways, and multiple modes of regulation of CBS expression and activity by hormones, growth factors, and other metabolites. Therefore, the functional role of CBS is determined by the distinct metabolic and genetic profiles in different types of cancer and is context-dependent. Furthermore, the current conflicting data adds an additional layer of complexity, indicating that multiple experimental and analytical approaches as well as in-depth mechanistic investigations are required to clarify the role of CBS in cancer biology.

Increased understanding of the role of the CBS-controlled network in cancer biology will greatly promote the development of pharmacological reagents targeting CBS and the identification of appropriate patient populations. CBS acts

through two main metabolites Hcy and H₂S, which have important physiological roles in specific tissues such as the liver, brain, and blood vessels. Given its central metabolic role, it is possible that CBS-based targeted therapy may cause side effects due to accumulation of unfavorable metabolites. For example, CBS inhibitors may elevate Hcy levels with potential risk for developing HHcy. Therefore, further studies will be required to define the therapeutic windows of the novel CBS targeting agents. Additional investigations are clearly required to better elucidate the complex role of CBS in malignant transformation including (i) characterizing the role of CBS-related metabolic signaling in cancer pathogenesis including but not limited to CBS, Hcy, H₂S, and the related enzymes; (ii) determining the interaction of tumor cell-derived CBS and its metabolites with the microenvironment; (iii) identifying biomarkers of CBS-based therapies in clinical samples and cancer models. Certainly, a greater appreciation for the complexity of CBS in cancer biology will give rise to new prospective biomarkers or targets for cancer.

Conflicts of Interest

The authors declare that there are no conflicts of interest regarding the publication of this paper.

Authors' Contributions

Richard B. Pearson and Jian Kang contributed equally to this work.

Acknowledgments

The authors apologize to the authors of many primary research papers that were not cited here due to space constraints but whose work influenced their understanding substantially. This work was supported by the National Health and Medical Research Council (NHMRC) of Australia project and program grants and Cancer Council Victoria. Researchers were funded by NHMRC Fellowships (Richard B. Pearson), a Melbourne International Research Scholarship (Haoran Zhu), and Research Training Program Scholarship (the University of Melbourne) (Shaun Blake).

References

- [1] J. Ereño-Orbea, T. Majtan, I. Oyenarte, J. P. Kraus, and L. A. Martínez-Cruza, "Structural basis of regulation and oligomerization of human cystathionine β -synthase, the central enzyme of transsulfuration," *Proceedings of the National Academy of Sciences of the United States of America*, vol. 110, no. 40, pp. E3790–E3799, 2013.
- [2] J. Ereño-Orbea, T. Majtan, I. Oyenarte, J. P. Kraus, and L. A. Martínez-Cruz, "Structural insight into the molecular mechanism of allosteric activation of human cystathionine β -synthase by S-adenosylmethionine," *Proceedings of the National Academy of Sciences of the United States of America*, vol. 111, no. 37, pp. E3845–E3852, 2014.
- [3] T. Majtan, L. R. Singh, L. Wang, W. D. Kruger, and J. P. Kraus, "Active cystathionine β -synthase can be expressed in heme-free systems in the presence of metal-substituted porphyrins or a chemical chaperone," *The Journal of Biological Chemistry*, vol. 283, no. 50, pp. 34588–34595, 2008.
- [4] M. Meier, M. Janosik, V. Kery, J. P. Kraus, and P. Burkhard, "Structure of human cystathionine β -synthase: a unique pyridoxal 5'-phosphate-dependent heme protein," *EMBO Journal*, vol. 20, no. 15, pp. 3910–3916, 2001.
- [5] V. Kery, L. Poneleit, and J. P. Kraus, "Trypsin cleavage of human cystathionine β -synthase into an evolutionarily conserved active core: Structural and functional consequences," *Archives of Biochemistry and Biophysics*, vol. 355, no. 2, pp. 222–232, 1998.
- [6] K.-H. Jhee, P. McPhie, and E. W. Miles, "Domain architecture of the heme-independent yeast cystathionine β -synthase provides insights into mechanisms of catalysis and regulation," *Biochemistry*, vol. 39, no. 34, pp. 10548–10556, 2000.
- [7] O. Kabil, Y. Zhou, and R. Banerjee, "Human cystathionine β -synthase is a target for sumoylation," *Biochemistry*, vol. 45, no. 45, pp. 13528–13536, 2006.
- [8] S. Bhattacharyya, S. Saha, K. Giri et al., "Cystathionine Beta-Synthase (CBS) Contributes to Advanced Ovarian Cancer Progression and Drug Resistance," *PLoS ONE*, vol. 8, no. 11, Article ID e79167, 2013.
- [9] H. Teng, B. Wu, K. Zhao, G. Yang, L. Wu, and R. Wang, "Oxygen-sensitive mitochondrial accumulation of cystathionine β -synthase mediated by Lon protease," *Proceedings of the National Academy of Sciences of the United States of America*, vol. 110, no. 31, pp. 12679–12684, 2013.
- [10] V. Pagliara, A. Saide, E. Mitidieri et al., "5-FU targets rpL3 to induce mitochondrial apoptosis via cystathionine- β -synthase in colon cancer cells lacking p53," *Oncotarget*, vol. 7, no. 31, pp. 50333–50348, 2016.
- [11] S. Ratnam, K. N. Maclean, R. L. Jacobs, M. E. Brosnan, J. P. Kraus, and J. T. Brosnan, "Hormonal regulation of cystathionine β -synthase expression in liver," *The Journal of Biological Chemistry*, vol. 277, no. 45, pp. 42912–42918, 2002.
- [12] V. Vitvitsky, A. Prudova, S. Stabler, S. Dayal, S. R. Lentz, and R. Banerjee, "Testosterone regulation of renal cystathionine β -synthase: Implications for sex-dependent differences in plasma homocysteine levels," *American Journal of Physiology-Renal Physiology*, vol. 293, no. 2, pp. F594–F600, 2007.
- [13] Y. Enokido, E. Suzuki, K. Iwasawa, K. Namekata, H. Okazawa, and H. Kimura, "Cystathionine β -synthase, a key enzyme for homocysteine metabolism, is preferentially expressed in the radial glia/astrocyte lineage of developing mouse CNS," *The FASEB Journal*, vol. 19, no. 13, pp. 1854–1856, 2005.
- [14] N. Takano, Y.-J. Peng, G. K. Kumar et al., "Hypoxia-inducible factors regulate human and rat cystathionine beta-synthase gene expression," *Biochemical Journal*, vol. 458, no. 2, pp. 203–211, 2014.
- [15] K. N. Maclean, E. Kraus, and J. P. Kraus, "The Dominant Role of Sp1 in Regulating the Cystathionine β -Synthase -1a and -1b Promoters Facilitates Potential Tissue-specific Regulation by Kruppel-like Factors," *The Journal of Biological Chemistry*, vol. 279, no. 10, pp. 8558–8566, 2004.
- [16] Y. Ge, M. A. Konrad, L. H. Matherly, and J. W. Taub, "Transcriptional regulation of the human cystathionine β -synthase -1b basal promoter: Synergistic transactivation by transcription factors NF-Y and Sp1/Sp3," *Biochemical Journal*, vol. 357, no. 1, pp. 97–105, 2001.
- [17] W.-N. Niu, P. K. Yadav, J. Adamec, and R. Banerjee, "S-glutathionylation enhances human cystathionine β -synthase








- activity under oxidative stress conditions," *Antioxidants & Redox Signaling*, vol. 22, no. 5, pp. 350–361, 2015.
- [18] F. Qi, Y. Zhou, Y. Xiao et al., "Promoter demethylation of cystathionine- β -synthetase gene contributes to inflammatory pain in rats," *PAIN*, vol. 154, no. 1, pp. 34–45, 2013.
- [19] H.-H. Zhang, J. Hu, Y.-L. Zhou et al., "Promoted interaction of nuclear factor- κ B with demethylated cystathionine- β -synthetase gene contributes to gastric hypersensitivity in diabetic rats," *The Journal of Neuroscience*, vol. 33, no. 21, pp. 9028–9038, 2013.
- [20] W. D. Kruger, L. Wang, K. H. Jhee, R. H. Singh, and L. J. Elsas II, "Cystathionine β -Synthase Deficiency in Georgia (USA): Correlation of Clinical and Biochemical Phenotype with Genotype," *Human Mutation*, vol. 22, no. 6, pp. 434–441, 2003.
- [21] M. Meier, J. Oliveriusova, J. P. Kraus, and P. Burkhard, "Structural insights into mutations of cystathionine β -synthase," *Biochimica et Biophysica Acta (BBA) - Proteins and Proteomics*, vol. 1647, no. 1-2, pp. 206–213, 2003.
- [22] M. Yamanishi, O. Kabil, S. Sen, and R. Banerjee, "Structural insights into pathogenic mutations in heme-dependent cystathionine- β -synthase," *Journal of Inorganic Biochemistry*, vol. 100, no. 12, pp. 1988–1995, 2006.
- [23] A. A. M. Morris, V. Kozich, S. Santra et al., "Guidelines for the diagnosis and management of cystathionine beta-synthase deficiency," *Journal of Inherited Metabolic Disease*, vol. 40, no. 1, pp. 49–74, 2017.
- [24] V. E. Shih, J. M. Fringer, R. Mandell et al., "A missense mutation (I278T) in the cystathionine β -synthase gene prevalent in pyridoxine-responsive homocystinuria and associated with mild clinical phenotype," *American Journal of Human Genetics*, vol. 57, no. 1, pp. 34–39, 1995.
- [25] E. W. Miles and J. P. Kraus, "Cystathionine β -synthase: Structure, function, regulation, and location of homocystinuria-causing mutations," *The Journal of Biological Chemistry*, vol. 279, no. 29, pp. 29871–29874, 2004.
- [26] W. D. Kruger, "Cystathionine β -synthase deficiency: Of mice and men," *Molecular Genetics and Metabolism*, vol. 121, no. 3, pp. 199–205, 2017.
- [27] M. Watanabe, J. Osada, Y. Aratani et al., "Mice deficient in cystathionine β -synthase: animal models for mild and severe homocyst(e)inemia," *Proceedings of the National Academy of Sciences of the United States of America*, vol. 92, no. 5, pp. 1585–1589, 1995.
- [28] L. Wang, K.-H. Jhee, X. Hua, P. M. DiBello, D. W. Jacobsen, and W. D. Kruger, "Modulation of cystathionine β -synthase level regulates total serum homocysteine in mice," *Circulation Research*, vol. 94, no. 10, pp. 1318–1324, 2004.
- [29] S. Gupta, J. Kühnisch, A. Mustafa et al., "Mouse models of cystathionine β -synthase deficiency reveal significant threshold effects of hyperhomocysteinemia," *The FASEB Journal*, vol. 23, no. 3, pp. 883–893, 2009.
- [30] N. Tyagi, N. Qipshidze, U. Sen, W. Rodriguez, A. Ovechkin, and S. C. Tyagi, "Cystathionine beta synthase gene dose dependent vascular remodeling in murine model of hyperhomocysteinemia," *International Journal of Physiology, Pathophysiology and Pharmacology*, vol. 3, no. 3, pp. 210–222, 2011.
- [31] K. Robert, J. Nehmé, E. Bourdon et al., "Cystathionine β synthase deficiency promotes oxidative stress, fibrosis, and steatosis in mice liver," *Gastroenterology*, vol. 128, no. 5, pp. 1405–1415, 2005.
- [32] L. M. Graham, L. E. Daly, H. M. Refsum et al., "Plasma homocysteine as a risk factor for vascular disease: The European Concerted Action Project," *Journal of the American Medical Association*, vol. 277, no. 22, pp. 1775–1781, 1997.
- [33] S. Brustolin, R. Giugliani, and T. M. Félix, "Genetics of homocysteine metabolism and associated disorders," *Brazilian Journal of Medical and Biological Research*, vol. 43, no. 1, pp. 1–7, 2010.
- [34] H. Jakubowski, "Proofreading in vivo: Editing of homocysteine by methionyl-tRNA synthetase in *Escherichia coli*," *Proceedings of the National Academy of Sciences of the United States of America*, vol. 87, no. 12, pp. 4504–4508, 1990.
- [35] W. K. C. Lai and M. Y. Kan, "Homocysteine-induced endothelial dysfunction," *Annals of Nutrition and Metabolism*, vol. 67, no. 1, pp. 1–12, 2015.
- [36] X. C. Wang, W. T. Sun, C. M. Yu et al., "ER stress mediates homocysteine-induced endothelial dysfunction: modulation of IKCa and SKCa channels," *Atherosclerosis*, vol. 242, no. 1, pp. 191–198, 2015.
- [37] S. Zhou, Z. Zhang, and G. Xu, "Notable epigenetic role of hyperhomocysteinemia in atherogenesis," *Lipids in Health and Disease*, vol. 13, no. 1, article no. 134, 2014.
- [38] M. S. Jamaluddin, I. Chen, F. Yang et al., "Homocysteine inhibits endothelial cell growth via DNA hypomethylation of the cyclin A gene," *Blood*, vol. 110, no. 10, pp. 3648–3655, 2007.
- [39] P.-Y. Chang, S.-C. Lu, C.-M. Lee et al., "Homocysteine inhibits arterial endothelial cell growth through transcriptional down-regulation of fibroblast growth factor-2 involving G protein and DNA methylation," *Circulation Research*, vol. 102, no. 8, pp. 933–941, 2008.
- [40] D. Zhang, X. Sun, J. Liu, X. Xie, W. Cui, and Y. Zhu, "Homocysteine accelerates senescence of endothelial cells via DNA hypomethylation of human telomerase reverse transcriptase," *Arteriosclerosis, Thrombosis, and Vascular Biology*, vol. 35, no. 1, pp. 71–78, 2015.
- [41] C.-S. Kim, Y.-R. Kim, A. Naqvi et al., "Homocysteine promotes human endothelial cell dysfunction via site-specific epigenetic regulation of p66shc," *Cardiovascular Research*, vol. 92, no. 3, pp. 466–475, 2011.
- [42] C.-F. Sun, T. R. Haven, T.-L. Wu, K.-C. Tsao, and J. T. Wu, "Serum total homocysteine increases with the rapid proliferation rate of tumor cells and decline upon cell death: A potential new tumor marker," *Clinica Chimica Acta*, vol. 321, no. 1-2, pp. 55–62, 2002.
- [43] P. Cavuoto and M. F. Fenech, "A review of methionine dependency and the role of methionine restriction in cancer growth control and life-span extension," *Cancer Treatment Reviews*, vol. 38, no. 6, pp. 726–736, 2012.
- [44] D. Zhang, X. Wen, W. Wu, Y. Guo, and W. Cui, "Elevated homocysteine level and folate deficiency associated with increased overall risk of carcinogenesis: Meta-analysis of 83 case-control studies involving 35,758 individuals," *PLoS ONE*, vol. 10, no. 5, Article ID e0123423, 2015.
- [45] G. Almadori, F. Bussu, J. Galli et al., "Serum folate and homocysteine levels in head and neck squamous cell carcinoma," *Cancer*, vol. 94, no. 4, pp. 1006–1011, 2002.
- [46] D. Zhang, J. Lou, X. Zhang et al., "Hyperhomocysteinemia results from and promotes hepatocellular carcinoma via CYP450 metabolism by CYP2J2 DNA methylation," *Oncotarget*, vol. 8, no. 9, pp. 15377–15392, 2017.
- [47] C. Szabo, "Gasotransmitters in cancer: From pathophysiology to experimental therapy," *Nature Reviews Drug Discovery*, vol. 15, no. 3, pp. 185–203, 2016.

- [48] E. Lagoutte, S. Mimoun, M. Andriamihaja, C. Chaumontet, F. Blachier, and F. Bouillaud, "Oxidation of hydrogen sulfide remains a priority in mammalian cells and causes reverse electron transfer in colonocytes," *Biochimica et Biophysica Acta (BBA) - Bioenergetics*, vol. 1797, no. 8, pp. 1500–1511, 2010.
- [49] C. Szabo, C. Coletta, C. Chao et al., "Tumor-derived hydrogen sulfide, produced by cystathionine- β -synthase, stimulates bioenergetics, cell proliferation, and angiogenesis in colon cancer," *Proceedings of the National Academy of Sciences of the United States of America*, vol. 110, no. 30, pp. 12474–12479, 2013.
- [50] C. Szabo, C. Ransy, K. Módis et al., "Regulation of mitochondrial bioenergetic function by hydrogen sulfide. Part I. Biochemical and physiological mechanisms," *British Journal of Pharmacology*, vol. 171, no. 8, pp. 2099–2122, 2014.
- [51] W.-J. Cai, M.-J. Wang, P. K. Moore, H.-M. Jin, T. Yao, and Y.-C. Zhu, "The novel proangiogenic effect of hydrogen sulfide is dependent on Akt phosphorylation," *Cardiovascular Research*, vol. 76, no. 1, pp. 29–40, 2007.
- [52] P. Manna and S. K. Jain, "Hydrogen sulfide and L-cysteine increase phosphatidylinositol 3,4,5-trisphosphate (PIP3) and glucose utilization by inhibiting phosphatase and tensin homolog (PTEN) protein and activating phosphoinositide 3-kinase (PI3K)/serine/threonine protein kinase (AKT)/protein kinase Czeta/lambda (PKCzeta/lambda) in 3T3L1 adipocytes," *The Journal of Biological Chemistry*, vol. 286, no. 46, pp. 39848–39859, 2011.
- [53] P. Yin, C. Zhao, Z. Li et al., "Sp1 is involved in regulation of cystathionine γ -lyase gene expression and biological function by PI3K/Akt pathway in human hepatocellular carcinoma cell lines," *Cellular Signalling*, vol. 24, no. 6, pp. 1229–1240, 2012.
- [54] B. D. Paul and S. H. Snyder, "H₂S signalling through protein sulfhydration and beyond," *Nature Reviews Molecular Cell Biology*, vol. 13, no. 8, pp. 499–507, 2012.
- [55] R. Greiner, Z. Pálkás, K. Báseš et al., "Polysulfides link H₂S to protein thiol oxidation," *Antioxidants & Redox Signaling*, vol. 19, no. 15, pp. 1749–1765, 2013.
- [56] Y. Kimura, Y. Mikami, K. Osumi, M. Tsugane, J.-I. Oka, and H. Kimura, "Polysulfides are possible H₂S-derived signaling molecules in rat brain," *The FASEB Journal*, vol. 27, no. 6, pp. 2451–2457, 2013.
- [57] N. Sen, B. D. Paul, M. M. Gadalla et al., "Hydrogen sulfide-linked sulfhydration of NF- κ B mediates its antiapoptotic actions," *Molecular Cell*, vol. 45, no. 1, pp. 13–24, 2012.
- [58] P. B. L. Pun, J. Lu, E. M. Kan, and S. Mochhala, "Gases in the mitochondria," *Mitochondrion*, vol. 10, no. 2, pp. 83–93, 2010.
- [59] K. Suzuki, G. Olah, K. Modis et al., "Hydrogen sulfide replacement therapy protects the vascular endothelium in hyperglycemia by preserving mitochondrial function," *Proceedings of the National Academy of Sciences of the United States of America*, vol. 108, no. 33, pp. 13829–13834, 2011.
- [60] Y.-D. Wen, H. Wang, S.-H. Kho et al., "Hydrogen sulfide protects HUVECs against hydrogen peroxide induced mitochondrial dysfunction and oxidative stress," *PLoS ONE*, vol. 8, no. 2, Article ID e53147, 2013.
- [61] G. Yang, K. Zhao, and Y. Ju, "Hydrogen sulfide protects against cellular senescence via S-sulfhydration of keap1 and activation of Nrf2," *Antioxidants & Redox Signaling*, vol. 18, no. 15, pp. 1906–1919, 2013.
- [62] S. Koike, Y. Ogasawara, N. Shibuya, H. Kimura, and K. Ishii, "Polysulfide exerts a protective effect against cytotoxicity caused by t-butylhydroperoxide through Nrf2 signaling in neuroblastoma cells," *FEBS Letters*, vol. 587, no. 21, pp. 3548–3555, 2013.
- [63] R. Wang, "Physiological implications of hydrogen sulfide: a whiff exploration that blossomed," *Physiological Reviews*, vol. 92, no. 2, pp. 791–896, 2012.
- [64] K. Kashfi and K. R. Olson, "Biology and therapeutic potential of hydrogen sulfide and hydrogen sulfide-releasing chimeras," *Biochemical Pharmacology*, vol. 85, no. 5, pp. 689–703, 2013.
- [65] M. R. Hellmich, C. Coletta, C. Chao, and C. Szabo, "The therapeutic potential of cystathionine β -synthetase/hydrogen sulfide inhibition in cancer," *Antioxidants & Redox Signaling*, vol. 22, no. 5, pp. 424–448, 2015.
- [66] Z. W. Lee, J. Zhou, C.-S. Chen et al., "The slow-releasing Hydrogen Sulfide donor, GYY4137, exhibits novel anti-cancer effects in vitro and in vivo," *PLoS ONE*, vol. 6, no. 6, Article ID e21077, 2011.
- [67] W.-J. Cai, M.-J. Wang, L.-H. Ju, C. Wang, and Y.-C. Zhu, "Hydrogen sulfide induces human colon cancer cell proliferation: Role of Akt, ERK and p21," *Cell Biology International*, vol. 34, no. 6, pp. 565–572, 2010.
- [68] C. M. Phillips, J. R. Zatarain, M. E. Nicholls et al., "Upregulation of cystathionine- β -synthase in colonic epithelia reprograms metabolism and promotes carcinogenesis," *Cancer Research*, vol. 77, no. 21, pp. 5741–5754, 2017.
- [69] H. Guo, J.-W. Gai, Y. Wang, H.-F. Jin, J.-B. Du, and J. Jin, "Characterization of hydrogen sulfide and its synthases, cystathionine β -synthase and cystathionine γ -lyase, in human prostatic tissue and cells," *Urology*, vol. 79, no. 2, pp. 483.e1–483.e5, 2012.
- [70] S. Sen, B. Kawahara, D. Gupta et al., "Role of cystathionine β -synthase in human breast Cancer," *Free Radical Biology & Medicine*, vol. 86, pp. 228–238, 2015.
- [71] K. Módis, C. Coletta, A. Asimakopoulou et al., "Effect of S-adenosyl-L-methionine (SAM), an allosteric activator of cystathionine- β -synthase (CBS) on colorectal cancer cell proliferation and bioenergetics in vitro," *Nitric Oxide: Biology and Chemistry*, vol. 41, pp. 146–156, 2014.
- [72] B. Kawahara, T. Moller, K. Hu-Moore et al., "Attenuation of Antioxidant Capacity in Human Breast Cancer Cells by Carbon Monoxide through Inhibition of Cystathionine β -Synthase Activity: Implications in Chemotherapeutic Drug Sensitivity," *Journal of Medicinal Chemistry*, vol. 60, no. 19, pp. 8000–8010, 2017.
- [73] E. Panza, P. De Cicco, C. Armogida et al., "Role of the cystathionine γ lyase/hydrogen sulfide pathway in human melanoma progression," *Pigment Cell & Melanoma Research*, vol. 28, no. 1, pp. 61–72, 2015.
- [74] H. Zhao, Q. Li, J. Wang et al., "Frequent epigenetic silencing of the folate-metabolising gene cystathionine-beta-synthase in gastrointestinal Cancer," *PLoS ONE*, vol. 7, no. 11, Article ID e49683, 2012.
- [75] N. Takano, Y. Sarfraz, D. M. Gilkes et al., "Decreased expression of cystathionine β -synthase promotes glioma tumorigenesis," *Molecular Cancer Research*, vol. 12, no. 10, pp. 1398–1406, 2014.
- [76] L. K. Sarna, Y. L. Siow, and O. Karmin, "The CBS/CSE system: A potential therapeutic target in NAFLD?" *Canadian Journal of Physiology and Pharmacology*, vol. 93, no. 1, pp. 1–11, 2015.
- [77] J. Kim, S. J. Hong, J. H. Park et al., "Expression of cystathionine β -synthase is downregulated in hepatocellular carcinoma and associated with poor prognosis," *Oncology Reports*, vol. 21, no. 6, pp. 1449–1454, 2009.
- [78] M. A. Avila, C. Berasain, L. Torres et al., "Reduced mRNA abundance of the main enzymes involved in methionine metabolism in human liver cirrhosis and hepatocellular carcinoma," *Journal of Hepatology*, vol. 33, no. 6, pp. 907–914, 2000.

- [79] A. Prudova, Z. Bauman, A. Braun, V. Vitvitsky, S. C. Lu, and R. Banerjee, "S-adenosylmethionine stabilizes cystathionine β -synthase and modulates redox capacity," *Proceedings of the National Academy of Sciences of the United States of America*, vol. 103, no. 17, pp. 6489–6494, 2006.
- [80] D. F. Calvisi, M. M. Simile, S. Ladu et al., "Altered methionine metabolism and global DNA methylation in liver cancer: relationship with genomic instability and prognosis," *International Journal of Cancer*, vol. 121, no. 11, pp. 2410–2420, 2007.
- [81] S. S. Wang, Y. H. Chen, N. Chen et al., "Hydrogen sulfide promotes autophagy of hepatocellular carcinoma cells through the PI3K/Akt/mTOR signaling pathway," *Cell Death & Disease*, vol. 8, no. 3, Article ID e2688, 2017.
- [82] H. Jia, J. Ye, J. You, X. Shi, W. Kang, and T. Wang, "Role of the cystathionine β -synthase/H₂S system in liver cancer cells and the inhibitory effect of quinolone-indolone conjugate QIC2 on the system," *Oncology Reports*, vol. 37, no. 5, pp. 3001–3009, 2017.
- [83] J. M. Thornburg, K. K. Nelson, B. F. Clem et al., "Targeting aspartate aminotransferase in breast cancer," *Breast Cancer Research*, vol. 10, no. 5, article no. R84, 2008.
- [84] K. Módis, E. M. Bos, E. Calzia et al., "Regulation of mitochondrial bioenergetic function by hydrogen sulfide. Part II. Pathophysiological and therapeutic aspects," *British Journal of Pharmacology*, vol. 171, no. 8, pp. 2123–2146, 2014.
- [85] A. Asimakopoulou, P. Panopoulos, C. T. Chasapis et al., "Selectivity of commonly used pharmacological inhibitors for cystathionine β synthase (CBS) and cystathionine γ lyase (CSE)," *British Journal of Pharmacology*, vol. 169, no. 4, pp. 922–932, 2013.
- [86] Y. Zhou, J. Yu, X. Lei et al., "High-throughput tandem-microwell assay identifies inhibitors of the hydrogen sulfide signaling pathway," *Chemical Communications*, vol. 49, no. 100, pp. 11782–11784, 2013.
- [87] M. K. Thorson, T. Majtan, J. P. Kraus, and A. M. Barrios, "Identification of Cystathionine β -Synthase Inhibitors Using a Hydrogen Sulfide Selective Probe," *Angewandte Chemie International Edition*, vol. 52, no. 17, pp. 4641–4644, 2013.
- [88] S. C. Lu and J. M. Mato, "S-adenosylmethionine in liver health, injury, and cancer," *Physiological Reviews*, vol. 92, no. 4, pp. 1515–1542, 2012.
- [89] A. W. Rutjes, E. Nüesch, S. Reichenbach, and P. Jüni, "S-Adenosylmethionine for osteoarthritis of the knee or hip.," *Cochrane Database of Systematic Reviews (Online)*, no. 4, p. CD007321, 2009.
- [90] I. Galizia, L. Oldani, K. Macritchie et al., "S-adenosyl methionine (SAMe) for depression in adults," *Cochrane Database of Systematic Reviews*, vol. 2016, no. 10, Article ID CD011286, 2016.
- [91] M. L. Martínez-Chantar, F. J. Corrales, L. A. Martínez-Cruz et al., "Spontaneous oxidative stress and liver tumors in mice lacking methionine adenosyltransferase 1A," *The FASEB Journal*, vol. 16, no. 10, pp. 1292–1294, 2002.
- [92] R. M. Pascale, M. M. Simile, M. R. D. Miglio et al., "Chemoprevention by s-adenosyl-l-methionine of rat liver carcinogenesis initiated by 1,2-dimethylhydrazine and promoted by orotic acid," *Carcinogenesis*, vol. 16, no. 2, pp. 427–430, 1995.
- [93] S. C. Lu, K. Ramani, X. Ou et al., "S-adenosylmethionine in the chemoprevention and treatment of hepatocellular carcinoma in a rat model," *Hepatology*, vol. 50, no. 2, pp. 462–471, 2009.
- [94] T. R. Morgan, "Chemoprevention of hepatocellular carcinoma in chronic hepatitis C," *Recent Results in Cancer Research*, vol. 188, pp. 85–99, 2011.
- [95] T. W. H. Li, H. Yang, H. Peng, M. Xia, J. M. Mato, and S. C. Lu, "Effects of S-adenosylmethionine and methylthioadenosine on inflammation-induced colon cancer in mice," *Carcinogenesis*, vol. 33, no. 2, pp. 427–435, 2012.
- [96] Y. Wang, Z. Sun, and M. Szyf, "S-adenosyl-methionine (SAM) alters the transcriptome and methylome and specifically blocks growth and invasiveness of liver cancer cells," *Oncotarget*, vol. 8, no. 67, pp. 111866–111881, 2017.
- [97] J. Luo, Y.-N. Li, F. Wang, W.-M. Zhang, and X. Geng, "S-adenosylmethionine inhibits the growth of cancer cells by reversing the hypomethylation status of c-myc and H-ras in human gastric cancer and colon cancer," *International Journal of Biological Sciences*, vol. 6, no. 7, pp. 784–795, 2010.
- [98] T. W. H. Li, Q. Zhang, P. Oh et al., "S-adenosylmethionine and methylthioadenosine inhibit cellular FLICE inhibitory protein expression and induce apoptosis in colon cancer cells," *Molecular Pharmacology*, vol. 76, no. 1, pp. 192–200, 2009.
- [99] L. L. Wu and J. T. Wu, "Hyperhomocysteinemia is a risk factor for cancer and a new potential tumor marker," *Clinica Chimica Acta*, vol. 322, no. 1-2, pp. 21–28, 2002.
- [100] Y. Özkan, S. Yardim-Akaydin, H. Firat, E. Çalişkan-Can, S. Ardiç, and B. Şimşek, "Usefulness of homocysteine as a cancer marker: Total thiol compounds and folate levels in untreated lung cancer patients," *Anticancer Research*, vol. 27, no. 2, pp. 1185–1189, 2007.
- [101] M. R. Hellmich and C. Szabo, "Hydrogen sulfide and cancer," *Handbook of Experimental Pharmacology*, vol. 230, pp. 233–241, 2015.
- [102] H. J. Powers and S. J. Moat, "Developments in the measurement of plasma total homocysteine," *Current Opinion in Clinical Nutrition & Metabolic Care*, vol. 3, no. 5, pp. 391–397, 2000.

Research Article

PATRI, a Genomics Data Integration Tool for Biomarker Discovery

G. Ukmar ¹, **G. E. M. Melloni** ², **L. Radrizzani** ¹, **P. Rossi**,³ **S. Di Bella** ¹,
M. R. Pirchio,³ **M. Vescovi**,⁴ **A. Leone**,¹ **M. Callari** ⁵, **M. Cesarini**,² **A. Somaschini**,¹
G. Della Vedova ², **M. G. Daidone**,⁵ **M. Pettenella**,⁴ **A. Isacchi**,¹ and **R. Bosotti** ¹

¹NMS Oncology, Nerviano Medical Sciences Srl, Nerviano, Italy

²University of Milano Bicocca, Milano, Italy

³Icona Srl, Cinisello Balsamo, Italy

⁴Parametric Design Biotech, Gessate, Italy

⁵Fondazione IRCCS Istituto Nazionale dei Tumori, Milano, Italy

Correspondence should be addressed to R. Bosotti; roberta.bosotti@nervianoms.com

Received 20 March 2018; Accepted 29 May 2018; Published 28 June 2018

Academic Editor: Maria L. Tornesello

Copyright © 2018 G. Ukmar et al. This is an open access article distributed under the Creative Commons Attribution License, which permits unrestricted use, distribution, and reproduction in any medium, provided the original work is properly cited.

The availability of genomic datasets in association with clinical, phenotypic, and drug sensitivity information represents an invaluable source for potential therapeutic applications, supporting the identification of new drug sensitivity biomarkers and pharmacological targets. Drug discovery and precision oncology can largely benefit from the integration of treatment molecular discriminants obtained from cell line models and clinical tumor samples; however this task demands comprehensive analysis approaches for the discovery of underlying data connections. Here we introduce PATRI (Platform for the Analysis of TRanslational Integrated data), a standalone tool accessible through a user-friendly graphical interface, conceived for the identification of treatment sensitivity biomarkers from user-provided genomics data, associated with information on sample characteristics. PATRI streamlines a translational analysis workflow: first, baseline genomics signatures are statistically identified, differentiating treatment sensitive from resistant preclinical models; then, these signatures are used for the prediction of treatment sensitivity in clinical samples, via random forest categorization of clinical genomics datasets and statistical evaluation of the relative phenotypic features. The same workflow can also be applied across distinct clinical datasets. The ease of use of the PATRI tool is illustrated with validation analysis examples, performed with sensitivity data for drug treatments with known molecular discriminants.

1. Introduction

The recognition of cancer as a genetic disease has raised in recent years huge “omics” efforts that have generated extensive molecular information on cancer cell lines and tumor samples, along with clinical characterization and drug sensitivity information. These data are often accessible through public resources, such as CCLE [1, 2], TCGA Research Network [3], ExpO [4], and ICGC [5], to name a few. As a consequence, a number of initiatives, often at global scale, have taken advantage of this unprecedented opportunity, such as the Cancer Therapeutics Response Portal (CTRP) [6–8], linking publicly available cancer cell

line features to small-molecule sensitivity for the discovery of patient-matched cancer therapeutics, or the i2b2 (Informatics for Integrating Biology and the Bedside)-tranSMART Foundation, a platform and a community aimed at integrating clinical and translational research data, providing “open-source, open-data” resources for precision medicine [9, 10]. In translational research, treatment sensitivity biomarkers are key to decision-making, for the identification and definition of patient populations susceptible to therapy benefits. In recent years, the search for biomarkers has indeed raised a huge community effort [1–3, 11–15] and a stimulating debate around the drug sensitivity issue [16–20]. Cancer cell lines can recapitulate many of the molecular alterations

driving tumor drug sensitivity [11]: for this reason, molecular characterization of experimental preclinical models has been widely used in support to all phases of drug discovery and development, for the identification of potential targets and for the exploration of several molecular aspects, such as drug sensitivity contexts, mechanisms of action, or issues in treatment responsiveness. Correlation between multiple baseline cancer genomics data and relative drug sensitivity has been explored in a number of public resources, such as CellMiner [12, 21], Genomics Drug Sensitivity in cancer (GDSC) [13, 22], or CancerDP [23, 24], where data can be enriched for compound and/or cell line numerosity but cannot be extended to user-supplied genomics or compound sensitivity data, which would be fundamental for new drug development.

Biomarkers resulting from the complex task of complementing cancer preclinical findings with clinical knowledge have found application as prognostic or diagnostic indicators, favoring the design of companion diagnostics for targeted drugs and facilitating therapeutic developments [28]. This is the case, for instance, of *KRAS* gene mutations in the observed resistance to cetuximab and panitumumab treatment in colorectal cancers samples [29, 30] or of rearranged *Abl* in the sensitivity to imatinib in acute myeloid leukemia [31] and of afatinib, gefitinib, and erlotinib in *EGFR* mutated tumors [32, 33]. Other examples are the sensitivity to vemurafenib in *BRAF* mutated tumors [34] or to lapatinib in amplified/overexpressed *Her2* (*ERBB2*) positive tumors [35], as well as the sensitivity to inhibitors of *ALK*, *ROS1*, and *TRK* (*NTRK1-2-3*) in tumors harboring activating rearrangements of these kinases [36, 37]. Indeed, gene rearrangements with kinase catalytic domains often result in the anomalous overexpression of kinase targets, driven by the partner gene, which can be identified by protein or RNA expression analysis as indirect readout [38, 39]. Especially in the targeted drug field, determination of patient eligibility for a certain treatment is sometimes only possible by performing a specific molecular assay on clinical specimens; however, other peculiar phenotypic characteristics measured in treatment susceptible individuals might be used to aid in the process of patient population selection. An example is the frequent association of the presence of *ALK* rearrangements in lung tumors with patients' young age, male gender, and nonsmoking history [40, 41].

The aim of our work was to provide a flexible and quick solution to streamline an analysis workflow for the search of potential treatment biomarkers across preclinical and clinical datasets and to make it accessible for application to user-provided genomics and treatment sensitivity data. For this purpose, we designed the “Platform for the Analysis of Translational Integrated data” (PATRI) tool, requiring data imported by users and integrating this workflow with an intuitive user-friendly graphical interface. First, drug response information is required to set up statistical analyses for the identification of potential drug sensitivity baseline genomic traits in cell lines (“Translational” workflow) or in tumor samples (“Clinical” workflow); lists of resulting relevant markers can then be used to predict genomics responsiveness in annotated datasets of tumor samples, which are stratified

into putative “Sensitive” or “Resistant” populations by the algorithm and correlated with the respective relevant clinical characteristics.

PATRI is conceived for basic end-users and is freely distributed as a virtual machine, portable on Windows, Linux, and MacOS platforms. The PATRI tool is accessible for open download at <https://www.parametricdesign.bio/>.

2. Materials and Methods

2.1. PATRI Database and Structure Implementation. In PATRI, the Database Management System (DBMS) implementation was based on MariaDB. The database schema (Suppl. Fig. 1) was designed to include cross-referenced tables for Cell Line and Clinical Sample genomics data (gene expression, somatic mutation, and copy number) and respective sample annotations, each with fixed and customizable fields. Upload of data input was predisposed as tab-delimited text files, previously formatted to mirror the destination tables. Detailed descriptions and instructions can be found in the *PATRI Platform User's Guide* (Suppl. File) and in the *PATRI Platform Installation and Configuration Guide* (Suppl. File) downloadable documents. Export of analysis results was enabled as tab-delimited text files. All PATRI functions were made accessible through a web graphical user interface developed using Joomla and Zend Frameworks. Statistical analysis libraries from CRAN [42] and Bioconductor R [43, 44] were integrated and interactive graphing functions were introduced using Google Charts [45]. PATRI is provided for download at <https://www.parametricdesign.bio/> as an Oracle VM Virtual Box file, populated with an artificial demonstration dataset, which can be removed and replaced with the desired data following instructions in the *PATRI Platform User's Guide* (Suppl. File).

2.2. Statistical Methods. The PATRI tool integrates selected libraries from CRAN [42] and Bioconductor R [43] for the statistical analysis of molecular data, according to the different genomics data types. Before statistical analysis of defined “Sensitive” versus “Resistant” sample groups, complexity reduction of the input genomics data is performed via a stepwise filtering procedure to remove background noise, i.e., all genes with no significant variation across samples. Briefly, all the genes appearing constant across conditions are removed from the data (i.e., never mutated or always mutated genes; all genes with identical “loss”, “normal”, or “gain” copy number type definition across samples; all genes with \log_2 expression below a user-selectable threshold value). In addition, a calculation of a point-biserial Pearson's correlation between sensitive/resistant cell lines or clinical samples and each gene is also applied, followed by removal of poorly correlated genes (default absolute value cut-off: 0.1).

For all accepted data types, i.e., gene expression, copy number, and mutation, a custom implementation of the Elastic Net algorithm [46] originally used in Barretina J et al. [1] was included, applicable if both “Sensitive” and “Resistant” groups are composed of a minimum of 4 samples each. The Elastic Net is a regularization and variable

selection method favoring the selection of strongly correlated predictors, particularly useful for data matrices in which the number of features (genes) is much bigger than the number of subjects (samples). The relative robustness of a selected gene is represented by the final ranking, reported as the percentage of times a molecular feature is retained in the model across 100 runs, accompanied by the average beta value across runs. Additionally, for the detection of differentially expressed genes, we introduced testing procedures such as ANOVA and Limma [47], particularly suited for small sample groups [48]; ANOVA was included also for copy number analysis. Resulting p values and log₂ fold change measures are reported and used to rank the molecular features. For the detection of mutated genes, statistical tests based on hypergeometric distribution and odds ratio measures were also implemented. The above algorithms can be applied starting from cell line genomics data (“Translational” workflow) or from tumor sample genomics data (“Clinical” workflow).

Buttons and slide bars are provided to enable sorting and manual filtering of the obtained gene lists, differentiating “Sensitive” and “Resistant” cell lines or clinical samples, based on statistical significance or fold change differences. Putative “biomarker” gene lists can then be quickly evaluated in the available annotated clinical sample data to categorize them into predicted “biomarker sensitive” or “biomarker resistant” cases and to extract relevantly differentiating clinical descriptive parameters in a single button click. First, a reversed classification algorithm based on “random forest” [49] is launched, applying a majority voting approach to assign clinical samples to the most likely category (“Sensitive” or “Resistant”), based on the status of the candidate biomarkers of the starting filtered gene list. One hundred thousand classification trees are run in parallel, using the entire spectrum of identified biomarkers for the random forest classification model. Then, the resulting “Sensitive” and “Resistant” assigned clinical samples are immediately tested for association with specific patient clinical annotations with a two-tail nonparametric Mann–Whitney test for continuous variables (like age, number of cigarettes, etc.) and a multiple-category Chi-square test for categorical variables (tumor subtype, grade, etc.). Associated clinical features are displayed in a table, ranked based on significance p values: visualization of each tested variable is enabled as a boxplot or a barplot, respectively. A heatmap, clustered both on molecular features and on samples, is reported with clustering distances calculated with Hamming distance for mutations and with Ward’s method for copy number and gene expression. For available time-to-event survival data, a separate classical two-tail log-rank test between predicted sensitive and resistant samples can be run, with visualization via Kaplan–Meier survival curves.

2.3. Cell Line Compound Treatment. Cell lines were grown in the appropriate culture media as recommended by vendors and treated with increasing doses of the tested compounds. Drug sensitivity data were expressed as the micromolar concentration of the compound at which cell proliferation is reduced by 50% (IC₅₀). All cell lines were authenticated by STR analysis (AmpFISTR® Identifiler® PCR Amplification Kit, Applied Biosystems, Foster City, CA, USA) using the

GeneMarker HID v 2.4.0 software (Soft Genetics, State College, PA, USA) and comparative analysis was performed with CLIFF (Cell Line Identity Finding by Fingerprinting, [50]).

2.4. Datasets and Analysis Workflows for PATRI Validation. Genomics data for 1036 cell lines were imported from CCLE [51]; mutation data were converted into binary information (wild type or mutated genes); cell line compound sensitivity was assessed in-house. Annotated TCGA clinical genomic datasets [3], comprising gene expression, copy number, mutation data, and clinical sample descriptions, were obtained from cBioportal [52, 53] for breast cancer (Breast Invasive Carcinoma (TCGA, “Provisional”), 1017 samples) and melanoma (Skin Cutaneous Melanoma (TCGA, “Provisional”), 478 samples); none of the datasets contained treatment response information for the considered drugs. Two lymphoma gene expression datasets for 20 (GSE14879) and 130 (GSE19069) samples, respectively, were downloaded from Gene Expression Omnibus (GEO) [54], with clinical annotations derived from the respective descriptive publications [25, 26]; the two datasets were not merged due to the discrepancy of the available clinical sample information and were utilized to test the “Clinical” analysis workflow. Txt tables were created with cell line names and the respective “Sensitive” or “Resistant” labels, assigned based on a threshold IC₅₀ of 1 μM for all the tested compounds. For the lymphoma GEO14879 clinical dataset, no entrectinib treatment response could be available, so drug sensitivity was presumed for the 5 ALK-positive samples, arbitrarily defined as “Sensitive” responders to ALK inhibition only to simulate a “Clinical” workflow analysis. Statistical analysis was launched on the selected cell lines or clinical samples using all the algorithms in PATRI for all the available genomics data types; only the relevant molecular signature results, filtered based on the indicated p value and/or log fold change thresholds, are discussed in the manuscript. The filtered lists were then used to categorize the indicated clinical samples into “Sensitive” and “Resistant” and to explore the resulting statistically relevant sample annotations, ranked based on significance (p value).

3. Results and Discussion

3.1. Design and Implementation of PATRI. The identification of sensitivity markers implicated in cancer treatment response is fundamental to support patient population definition in the clinics and is well established for a number of approved kinase inhibitors drugs that are selectively active in tumors harboring activating mutations or rearrangements of their target genes, such as vemurafenib in BRAF mutated tumors [34], lapatinib in amplified/overexpressed ERBB2 (Her2) positive tumors [35], and entrectinib in ALK rearranged tumors [37]. We focused on building an intuitive tool for use in drug discovery pipelines to immediately link relevant molecular markers from cell line drug treatment models with clinical features associated with tumor sample genomics data, for the quick exploration of potential population therapeutic biomarkers. For this purpose, we have developed



FIGURE 1: **PATRI graphical user interface: welcome and login page.** Screenshot of the PATRI welcome and login home page. See also text and Supplementary File.

PATRI (Platform for the Analysis of TRanslational Integrated data), an open-source tool offering a flexible genomic data integration resource to basic end-users for the identification of predictive biomarkers of differential sensitivity to drugs or any other treatments, such as siRNA or CRISPR-Cas9, starting from user-provided data. Central to the design was the ease of use, through an intuitive graphical user interface, based on a simple workflow of streamlined data analysis, extraction, and visualization procedures, directly correlating biomarkers identified in cell line or tumor sample genomics data to clinical information, aided by the introduction of mouseover and pop-up interactive options. PATRI is a web-based application (Figure 1) with a client-server architecture, as detailed in the PATRI Installation and Configuration Guide (Suppl. File), built on a relational database supporting data mining activities. The downloadable tool is initially populated with a “test” database for demonstration purposes that can be removed and replaced with the desired data. Free codes and analysis packages were utilized for the implementation of all PATRI components to enable distribution as an open-source tool and, possibly, custom code implementation.

Figure 2 schematically illustrates the conceptual “Translational” and “Clinical” workflows in PATRI, with full functionalities detailed in Suppl. Fig. 2-7 and in the PATRI Platform User’s Guide (Suppl. File). A “Translational” workflow is available to obtain putative treatment biomarkers starting from cell line genomics data that can be used to categorize clinical samples into “biomarker sensitive” and “biomarker resistant” samples and to simultaneously obtain significantly correlated clinical characteristics for patient stratification (Figure 2(a)). Similarly, starting from clinical genomic datasets (“Clinical” workflow, Figure 2(b)), PATRI allows analysis and correlation of putative treatment response genomics markers from a test tumor sample population to the clinical characteristics of a second clinical sample cohort. Briefly, after import of the desired baseline (pretreatment)

genomics data for cell line models and clinical samples, users will define opposite groups of “Sensitive” and “Resistant” cell lines or “responder” and “nonresponder” tumor samples based on available treatment sensitivity information. PATRI automatically retrieves and associates the genomics data and descriptions to the list of provided samples. By a mouse click, single or multiple predefined statistical tests can be chosen and launched for analysis of the selected sets of gene expression, copy number, and gene variant analyses data (Suppl. Fig. 3-4), including the Elastic Net option [1, 46] for all the three types of data. The resulting lists of significant sensitivity biomarker genes are displayed in separate tabs with sorting buttons and slide bars, allowing data filtering; the tool also enables quick export of results and graphical visualization through different charting options supporting mouseover and zooming functions (Suppl. Fig. 5), such as interactive Volcano plots, dendrograms, or scatter plots integrating data by color shades and dot sizes. Filtered sensitivity biomarkers obtained at this point for cell lines can be immediately connected to clinical data imported into PATRI, to investigate the presence of molecularly discriminated clinical subpopulations: one mouse click starts simultaneous classification of clinical tumor samples, based on the respective molecular status of the selected filtered biomarkers, as potentially “Resistant” or “Sensitive” to the drug, via an adaptation of the random forest classifier algorithm [49], together with a stratification of associated clinical sample characteristics, ranked based on statistical significance (Suppl. Fig. 6-7). Graphical representation and data export upon mouse clicking allow exploration of the identified clinical features associated with tumor genomics data (Suppl. Fig. 7) and permit rapid identification of particularly discriminating clinical features potentially defining patient subpopulations, which might be used in support of patient selection for clinical trials. Thanks to the flexibility of sample description fields in the PATRI database, along

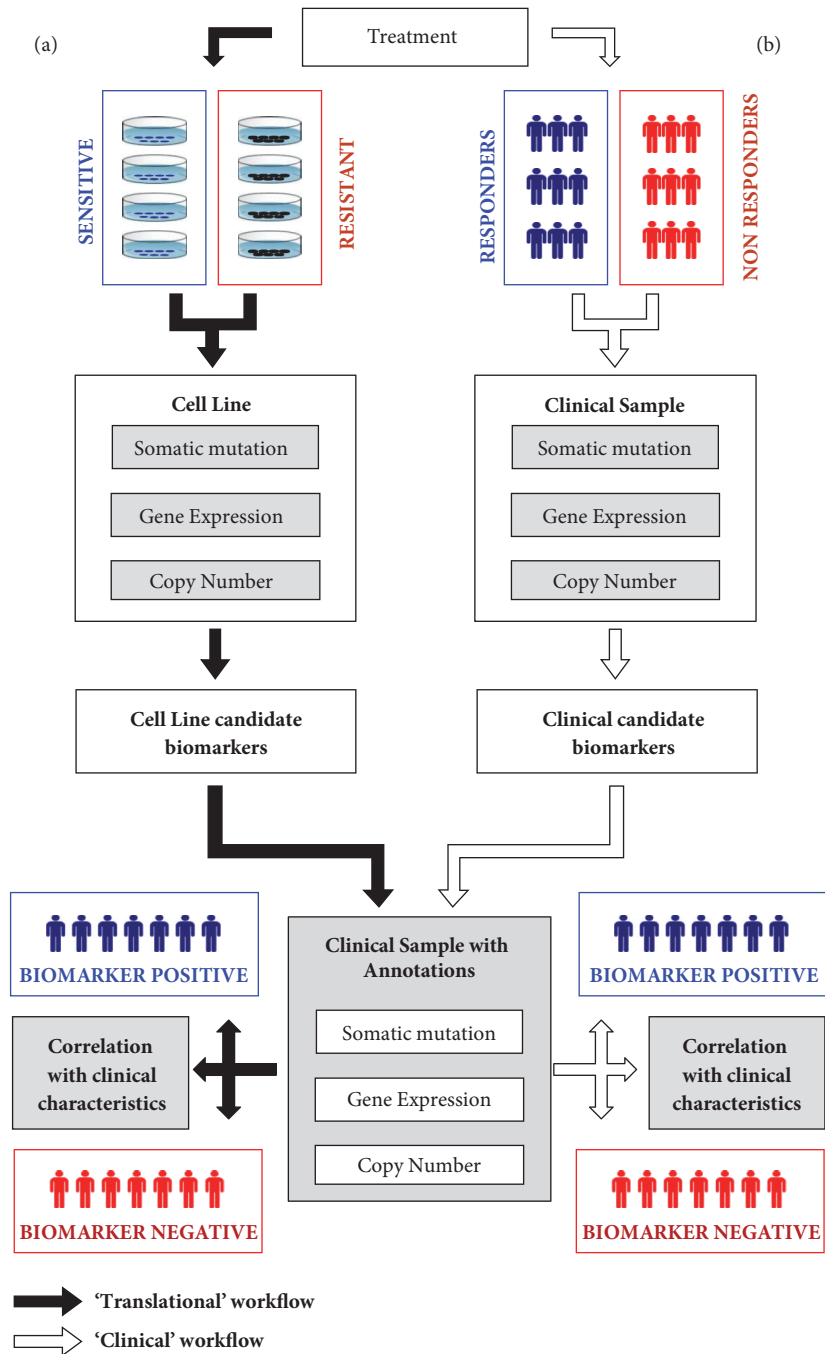


FIGURE 2: **PATRI analysis workflows.** Schematic representation of the PATRI tool analysis workflows. (a) “Translational” workflow (black arrows), executing a statistical identification of candidate baseline genomics biomarkers starting from defined treatment “Sensitive” versus “Resistant” cell line groups, through categorization of “biomarker sensitive” versus “biomarker resistant” clinical samples in the annotated clinical dataset, based on the selected gene candidates, with simultaneous identification of statistically correlated differentiating characteristics. (b) “Clinical” workflow (white arrows), executing the same operations as in the “Translational” workflow, starting from defined treatment “Sensitive” (responder) versus “Resistant” (nonresponder) tumor samples in pretreatment clinical genomics datasets.

with cell lines or clinical samples, the tool might similarly accept data from patient-derived cancer models, such as PDXs and PDOs (patient-derived xenografts and organoids, respectively) that more closely mirror the architecture and

cellular heterogeneity of human tumors [55–57], increasingly available with associated clinical/genomic data sets and annotations thanks to a number of recent international initiatives (e.g., Human Cancer Model Initiative (HCMI)

[58], EurOPDX Consortium [59], or Public Repository of Xenografts (PROXe) [60], to name a few) [61–63].

3.2. Validation of PATRI. For the validation of the tool, we generated in-house cell growth inhibition sensitivity data (IC₅₀) on panels of cancer cell lines treated with the well-known targeted drugs lapatinib, vemurafenib, or entrectinib and tested PATRI for the ability to identify significant treatment sensitivity-related molecular markers through the “Translational” workflow (Figure 2(a)), using data from CCLE [1, 51], TCGA [3], and Gene Expression Omnibus (GEO) [54] resources.

Lapatinib [35] is a dual EGFR and ERBB2 inhibitor, currently approved in the clinics for the treatment of ERBB2 amplified breast cancers in combination with capecitabine or letrozole [64]. In our analysis, ERBB2 kinase gene amplification and overexpression were correctly identified by PATRI within a group of lapatinib sensitive versus resistant breast cancer cell lines (Figure 3(a)) tested in our labs. Concomitant amplification and overexpression of a number of additional genes, correlating with lapatinib treatment sensitivity, were also observed (Figures 3(b) and 3(c)). Many of these genes, such as *GRB7*, *PGAP3*, *STARD3*, and *MIEN1*, have been reported to be coamplified and overexpressed with ERBB2 in breast tumors in the “ERBB2 amplicon”, located on the long arm of chromosome 17 (17q12), neighboring the ERBB2 coding sequence [65–68]. STRING analysis [27] of the 17 differentially expressed genes in Figure 3(b) (obtained by ANOVA expression analysis, p value $>10^{-4}$, \log_2 FC $> |1.5|$) revealed a considerable number of known or predicted protein interactions, supporting the functional interconnections in the selected list (not shown). Using the “Translational” workflow implemented in PATRI, the above marker list was used to categorize potentially “Sensitive” or “Resistant” cases in a panel of breast cancer clinical samples from TCGA data collection with the respective associated clinical feature annotations via random forest classification. In the resulting breast sample hierarchical analysis heatmap, most of the predicted “Sensitive” breast cancer samples were clustered in a compact group (Figure 3(d)), characterized by a strong enrichment in Her2 positive tumors as measured by immunohistochemistry (IHC levels = 3+) (Figure 3(e)) having more than 90% cells positive to Her2 staining (not shown), both characteristics clearly associated with ERBB2 overexpression. In addition, chromosome 17 amplification (chromosome 17 signal ratio value) was also among the top ranking clinical annotations differentiating predicted “Sensitive” and “Resistant” samples in the breast cancer dataset (Figure 3(f)). Gene lists obtained from gene expression or copy number alternative analysis algorithms (ANOVA and Elastic Net for both copy number and gene expression, Limma for gene expression) and with different filtering thresholds could all identify groups of “Sensitive” breast cancer samples significantly enriched in Her2 IHC-positive tumors and with marked chromosome 17 amplification among the top ranking clinical reported features in the breast cancer dataset. Interestingly, this result was observed also with the Elastic Net copy number list (not shown), which did not include ERBB2 among the most significant differential genes. This observation prompted us

to test the robustness of the obtained gene signatures after removal of the ERBB2 gene from all the previously evaluated biomarker gene lists. Though with a lower p value, the predictive power was still retained, with a strongly significant enrichment in Her2 IHC-positive and chromosome 17 amplified samples among the predicted “Sensitive” (not shown), likely driven by the other overexpressed and amplified genes from the “ERBB2 amplicon” included in the signature.

Vemurafenib (Zelboraf) is a B-Raf inhibitor approved for the treatment of late-stage melanoma. It selectively inhibits melanoma cells harboring the V600E BRAF activating mutation, being inactive on WT BRAF cells [34]. Using the PATRI workflow, statistical mutation analysis in a small panel of melanoma cell lines showing differential sensitivity to vemurafenib (Figure 4(a)), provided a list of 29 mutated genes (filtered p value >0.1 , \log_{10} odds ratio $> |1|$), among which mutated BRAF was the only feature common to the 3 highly sensitive melanoma cell lines, but also present in the resistant RPMI-7951, harboring a V600E BRAF mutated gene (Figure 4(b)). This cell line has been previously described as a B-Raf inhibitor resistant cell line [69], likely due to a reactivation of the MEK pathway, in which a combined treatment with the AS703026 MEK inhibitor and the PLX4032 BRAF inhibitor could actually overcome this resistance phenotype [69]. In 2 out of 3 BRAF mutated sensitive cell lines, we concomitantly observed a mutation in MutS Homolog 3 (*MSH3*), a gene participating in the mismatch repair (MMR) system. Indeed, BRAF mutations have been observed to frequently occur in colorectal tumors cases with MSI characterized by deficient DNA mismatch repair (dMMR) [70]. Besides, we found the ALPK2 kinase to be preferentially mutated in BRAF wt-vemurafenib resistant melanoma cell lines; mutations in ALPK2 have been proposed to be involved in cutaneous melanoma [71]. Due to the low number of starting cell line samples and the limited concordance of the identified mutational profiles, we focused only on the above BRAF, MSH3, and ALPK2 mutations for the execution of the “Translational” workflow on a set of clinical genomics data for about 470 melanoma samples from the TCGA database [52]. Hierarchical clustering evaluation of the melanoma samples showed a group of predicted “Sensitive” melanoma samples with mutated BRAF and WT ALPK2; only a small fraction of melanoma samples showed mutated MSH3 without a clear clustering pattern (Figure 4(c)). In the majority of melanoma samples, BRAF and ALPK2 molecular alterations appeared to be mutually exclusive; however ALPK2 has been reported among genes that are mutated in significantly higher proportion of melanoma cell lines than in melanoma tumors [72]. We repeated the melanoma clinical analysis using only BRAF for sample classification: the resulting “Sensitive” melanoma group was enriched in primary tumor samples derived from “trunk” rather than other excision sites and from patients with an average lower age as compared to predicted “Resistant” patients (54.3 versus 60.3, Figure 4(d)), in agreement with reported literature [73, 74].

We then considered a panel of lymphoma cell lines formerly tested in our labs for sensitivity to entrectinib ([37] and Figure 5(a)), a new TRKs/ALK/ROS1 inhibitor

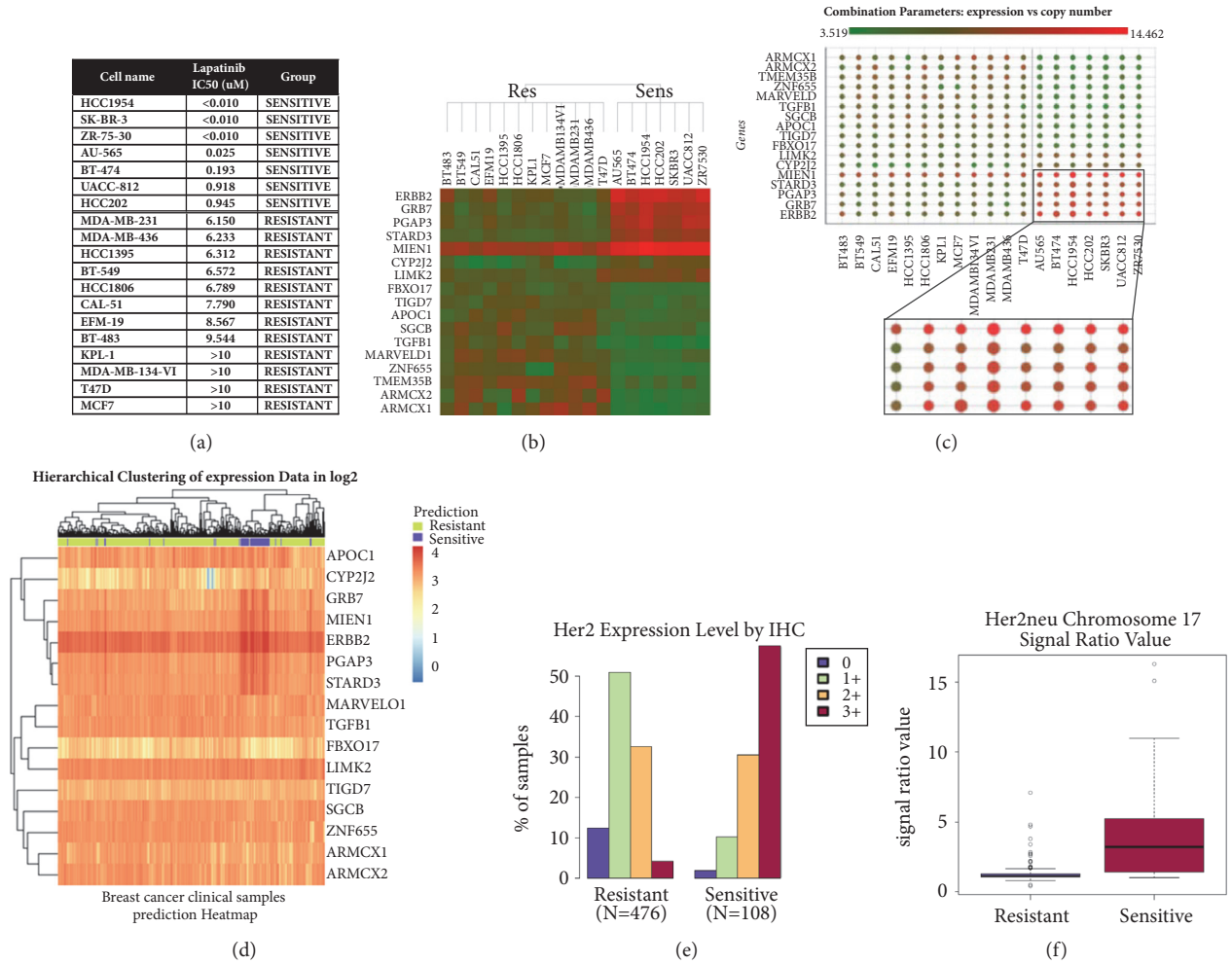


FIGURE 3: “Translational” analysis of lapatinib sensitivity in breast cancer cell lines and clinical samples. Results of PATRI “Translational” analysis workflow performed on a panel of breast cancer cell lines sensitive or resistant to lapatinib treatment and on a panel of 1017 TCGA breast cancer clinical samples. (a) List of treated breast cell lines with respective lapatinib IC50 values. A threshold of 1µM was chosen to define “Sensitive” and “Resistant” cell lines. (b) Heatmap dendrogram of 17 markers differentiating lapatinib sensitive versus resistant breast cell lines, obtained by ANOVA gene expression analysis (p value>10⁻⁴, log2 FC>|1.5|). Significantly high or low expressed genes are highlighted in red and green, respectively. (c) Scatter plot visualization of the identified genes in the different cell lines, combining dot size, representing magnitude of copy number values, and dot color shades, ranging from low (green) to high (red) gene expression values. (d) Heatmap representing hierarchical cluster analysis via random forest categorization of the predicted “Sensitive” or “Resistant” 1071 breast cancer samples, based on the selected genes (with the exception of *TMEM35B*, not represented in the clinical dataset; sample IDs could not be represented on the lower part of the graph). (e-f) Top ranking of significant clinical features (where available) associated with TCGA breast cancer samples, classified as potentially “Sensitive” or “Resistant”. (e) Histogram representing distribution of clinically evaluated Her2 immunohistochemistry levels (0-3+) in the predicted “Sensitive” and “Resistant” clinical sample groups. The displayed data correspond to the column “Her2 IHC score” in the TCGA Breast Invasive Carcinoma “Provisional” Clinical Data annotation file. (f) Box plot representing the clinically assessed average signal value for chromosome 17 amplification in predicted “Sensitive” (4.28) and “Resistant” (1.32) clinical sample groups. The displayed data correspond to the column “Her2 cent 17 ratio” in the TCGA Breast Invasive Carcinoma “Provisional” Clinical Data annotation file.

currently showing great promise in phase I/II clinical trials on tumors driven by rearrangements of one of these kinases [37, 75]. The panel included 4 anaplastic large cell lymphoma (ALCL) cell lines, all harboring the nucleophosmin *NPM-ALK* rearrangement [76], and all extremely sensitive to treatment with entrectinib. In the PATRI gene expression analysis of the 4 sensitive versus 7 resistant lymphoma cell lines with Limma, *ALK* resulted as the most statistically significant overexpressed kinase (Figures 5(b) and 5(c)). The

most differentially expressed genes (p value<10⁻⁷, logFC> |5|, Figures 5(b) and 5(c)) found in the entrectinib sensitive lymphoma cell lines were subjected to STRING analysis [27] and resulted to be significantly networked with *ALK* (Figure 5(d)) and found to be transcriptionally regulated in *ALK* activated pathways [[26, 77–80] and reviewed in [81, 82]]. “Translational” analysis of these markers in two distinct gene expression clinical non-Hodgkin’s lymphoma datasets (GSE14879, 20 samples [25], and GSE19069, 130

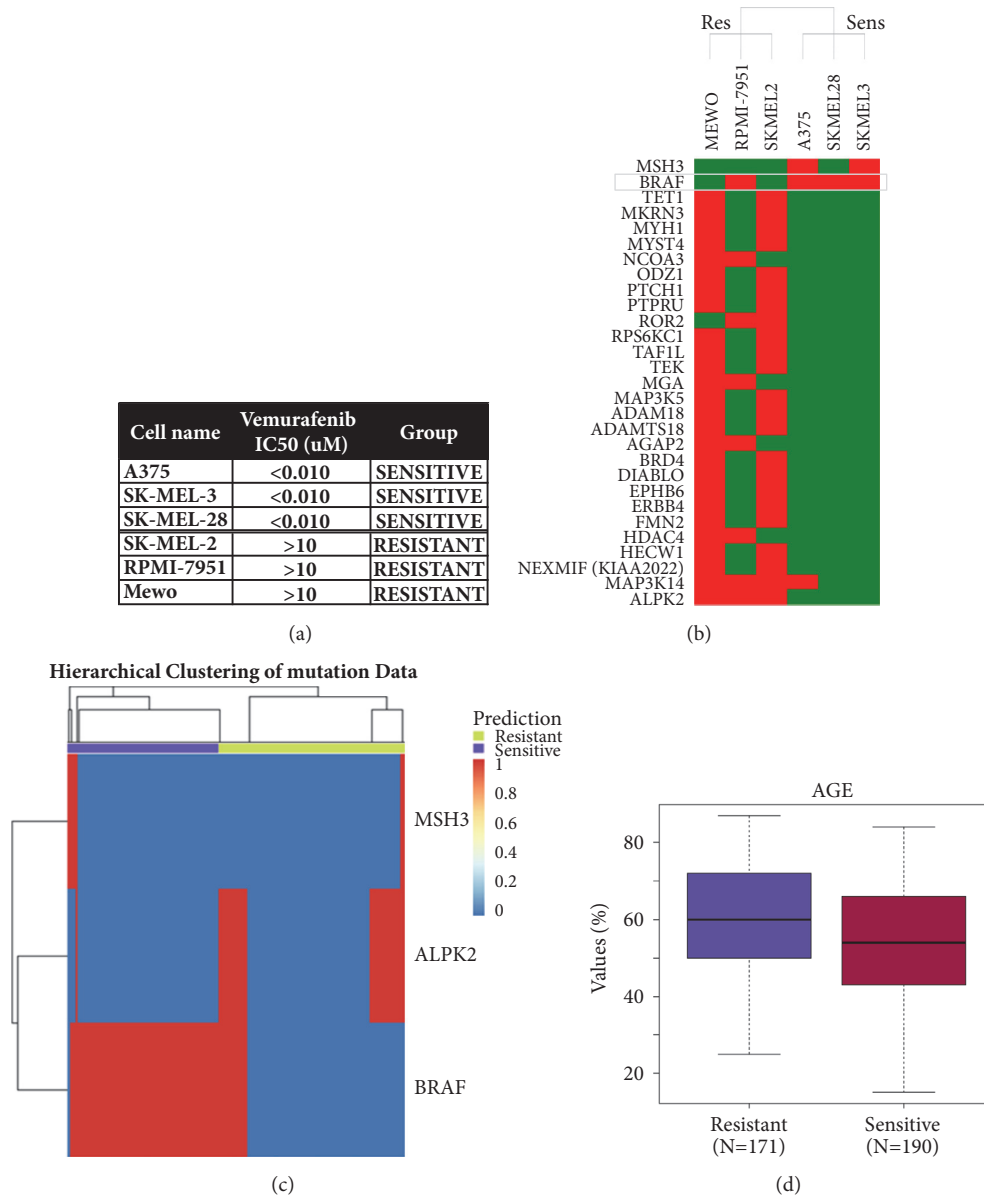


FIGURE 4: “Translational” analysis of vemurafenib sensitivity in melanoma cell lines and clinical samples. Results of PATRI “Translational” analysis workflow performed on a panel of melanoma cell lines sensitive or resistant to vemurafenib treatment and on a panel of 478 TCGA melanoma clinical samples. (a) List of melanoma cell lines with respective vemurafenib IC50 values. A threshold of $1\mu\text{M}$ was chosen to define “Sensitive” and “Resistant” cell lines. (b) Heatmap dendrogram for the results of PATRI odds ratio mutational analysis in “Sensitive” versus “Resistant” melanoma cell lines. Red, mutated genes; green, wild type genes. (c) Heatmap representing hierarchical cluster mutation analysis via random forest categorization of the predicted “Sensitive” or “Resistant” 478 melanoma TCGA samples, based on 3 selected mutated genes: *BRAF*, *MSH3*, *ALPK2* (sample IDs could not be represented on the lower part of the graph). (d) Box plot representing the reported age distribution in predicted “Sensitive” (avg. 54.3) and “Resistant” (avg. 60.3) clinical melanoma sample groups. The displayed data correspond to the column “Age” in the TCGA Skin Cutaneous Melanoma (TCGA, Provisional) Clinical Data annotation file.

samples [26]) correctly predicted and clustered the 5 ALK-positive ALCL samples from GSE14879 (Figure 5(e)), with immunohistochemistry positivity features for ALK (Figure 5(f)) and PRF1 (not shown) and younger age (Figure 5(g)) ranking with highest statistical significance. Interestingly, a comparable result was achieved with a 22-gene list obtained with ANOVA gene expression analysis (p value $< 10^{-5}$, $\log_{2}\text{FC} > |4.5|$) not containing ALK, though with a less defined

heatmap “Sensitive” versus “Resistant” cluster pattern (not shown). In GSE14879, predicted “Sensitive” samples included most of the ALK-positive ALCL samples and also included 5 Peripheral T-Cell lymphoma, unspecified (PTCL-NOS) samples, however displaying again ALK-positive diagnosis and lower age among the top ranking significant clinical associated parameters (not shown). Mutational analysis of the entrectinib-treated lymphoma cell line panel did not provide

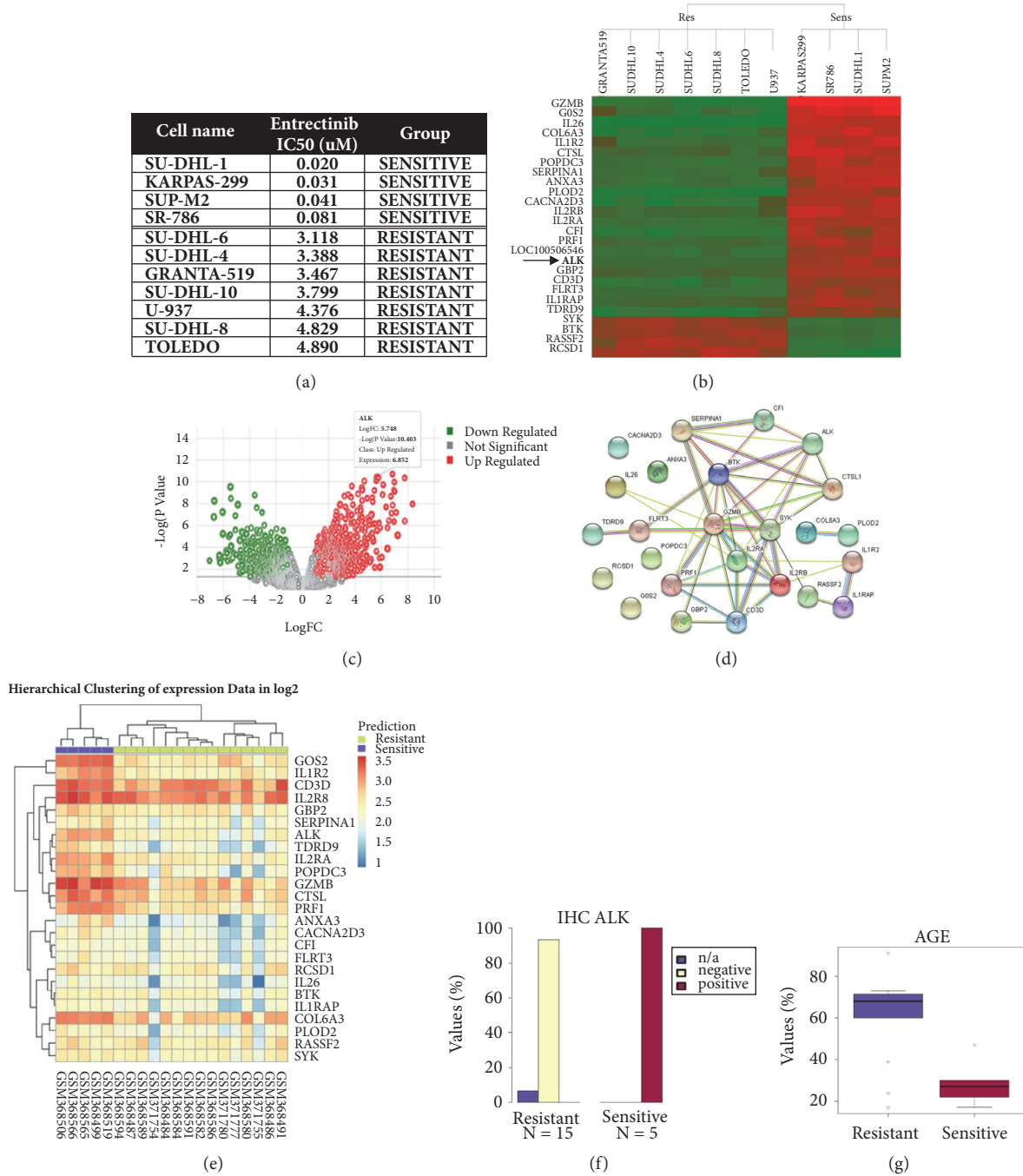


FIGURE 5: “Translational” analysis of entrectinib sensitivity in lymphoma cell lines and clinical samples. Results of PATRI “Translational” analysis workflow performed on a panel of lymphoma cell lines sensitive or resistant to entrectinib treatment and on two panels of 20 and 130 lymphoma clinical samples (GSE14879 [25] and GSE19069 [26], respectively). (a) List of lymphoma cell lines with respective entrectinib IC50 values. A threshold of $1\mu\text{M}$ was chosen to define “Sensitive” and “Resistant” cell lines. (b) Heatmap dendrogram of 26 markers differentiating entrectinib sensitive versus resistant lymphoma cell lines, obtained by Limma gene expression analysis (p value $< 10^{-7}$, $\log\text{FC} > |5|$). Significantly high or low expressed genes are highlighted in red and green, respectively. (c) Volcano plot visualizing significance and magnitude of gene expression differences in sensitive versus resistant conditions, with pop-up indicating ALK expression level. Significantly high or low expressed genes (p value < 0.05 , $\log\text{FC} > |1|$) are highlighted in red and green, respectively. (d) Results from STRING analysis [27] showing the protein-protein interaction network connecting the identified genes (STRING interaction score: 0.150). (e) Heatmap representing hierarchical cluster analysis via random forest categorization of the predicted “Sensitive” or “Resistant” GSE14879 lymphoma samples, based on the selected genes (sample IDs are represented on the lower part of the graph). (f-g) Top ranking of significant clinical features associated with GSE14879 lymphoma samples, classified as potentially “Sensitive” or “Resistant”. (f) Histogram representing distribution of clinically assessed ALK immunohistochemistry (IHC) positivity (reported in [25]) in the predicted “Sensitive” and “Resistant” sample groups. (g) Box plot representing the distribution of the reported age [25] in predicted “Sensitive” (avg. 21.6) and “Resistant” (avg. 61.3) lymphoma sample groups.

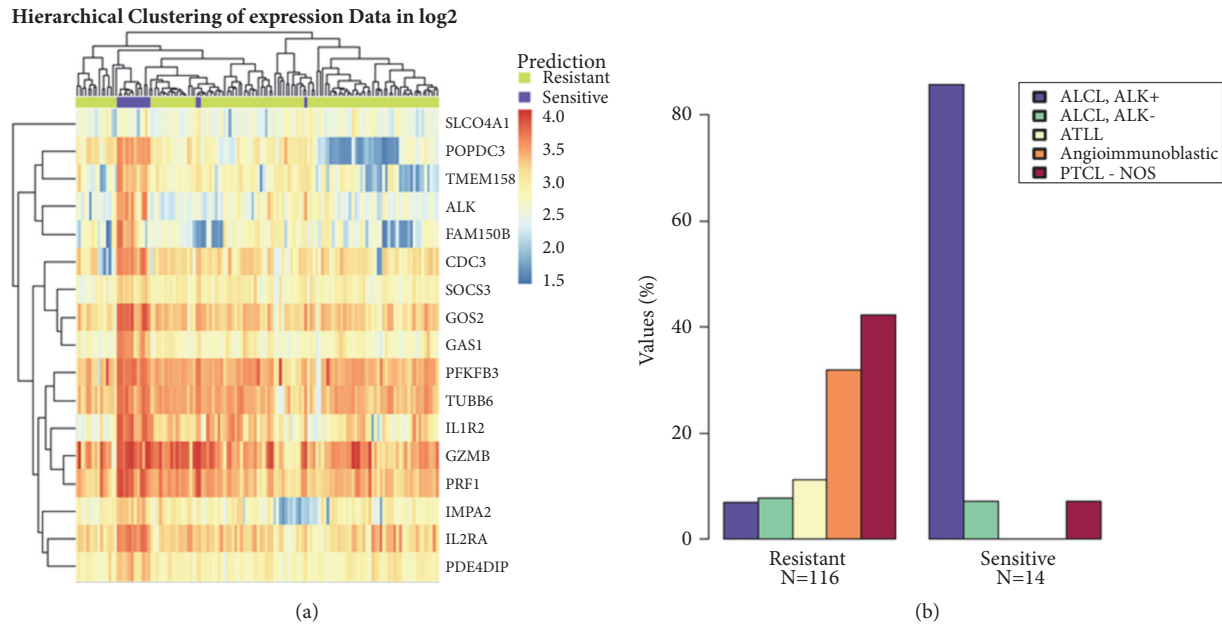


FIGURE 6: Simulation of “Clinical” analysis workflow based on presumed ALK inhibitor sensitivity in lymphoma clinical samples. Results of PATRI “Clinical” analysis workflow, simulated using two panels of lymphoma clinical samples. The 5 ALK-positive ALCL samples in the GSE14879 dataset (sample IDs: GSM368499, GSM368506, GSM368519, GSM368565, and GSM368566) were presumed to be ALK inhibitor responders and set as “Sensitive” samples only for validation purposes, using the PATRI available gene expression analysis algorithms. (a) Heatmap representing hierarchical cluster analysis via random forest categorization of the predicted “Sensitive” or “Resistant” 130 samples in the lymphoma GSE19069 dataset (sample IDs could not be represented on the lower part of the graph), starting from a filtered 17-gene expression biomarker list obtained by Limma analysis of the GSE14879 dataset (p value $< 10^{-10}$, $\log_{FC} > |1|$). (b) Histogram representing lymphoma diagnosis distribution for the 14 predicted “Sensitive” and the 116 “Resistant” lymphoma samples from the GSE19069 dataset (ALCL, ALK+: anaplastic large cell lymphoma ALK-positive; ALCL, ALK-: anaplastic large cell lymphoma ALK-negative; PTCL-NOS: peripheral T-cell lymphoma, unspecified; ATLL: adult T-cell leukemia/lymphoma; Angioimmunoblastic: angioimmunoblastic T-cell lymphoma).

significant results, while copy number analysis with ANOVA revealed only two markers with significant microalterations, namely, TCR gamma alternate reading frame protein (*TARP*) loss and ADAM metalloproteinase domain 6 pseudogene (*ADAM6*) gain in entrectinib sensitive, ALK-positive cell lines. The significance of these two markers could not be explored using the PATRI translational workflow, since only gene expression data were available for the same samples in the two lymphoma clinical datasets.

The same lymphoma clinical datasets were also used to simulate a “Clinical” workflow analysis, presuming the 5 ALK-positive ALCL samples in the GSE14879 dataset as ALK inhibitor treatment “responder” patient samples for validation purposes. PATRI biomarker analysis was executed with Limma and a filtered 17-gene list (p value $< 10^{-10}$, $\log_{FC} > |1|$) was used for exploration and sensitivity prediction in the lymphoma GSE19069 dataset (Figure 6(a)), resulting in the prediction of 14 “Sensitive” lymphoma samples mostly containing ALK-positive ALCL samples, with top ranking clinical annotations for ALK-positive ALCL diagnosis (Figure 6(b)) and younger age (not shown). The provided results illustrate the feasibility of the PATRI “Clinical” analysis workflow for the quick evaluation and the comparison of “training versus test” dataset biomarker analysis correlations for all available clinical datasets with consistent phenotypic annotations.

4. Conclusion

In this work, we describe PATRI, a freely available standalone tool conceived as a biomarker data analysis “starter kit” for basic users, enabling flexible storage, analysis, and complementation of preclinical and clinical baseline genomics data for correlation with treatment sensitivity, allowing the exploration of potential predictive therapeutical biomarkers.

The current version of the tool design, along with widely accepted algorithms and graphical representations, introduces a “Translational” workflow, supporting rapid clinical evaluation of putative preclinical therapeutic response biomarkers in annotated clinical genomics datasets, based on random forest categorization in parallel with phenotypic significance analysis. The same workflow can also be applied across distinct clinical datasets (“Clinical” workflow).

We have proposed examples of use of PATRI with in-house sensitivity data from representative targeted drugs with well-established mutated or overexpressed biomarkers; however, PATRI might also be applied to support the identification of new relevant biomarkers and indicators of sensitivity in other types of treatments, such as RNA interference or CRISPR/Cas9 screenings, as well as for the evaluation of their frequency and relevance in the clinics.

The PATRI structure can be integrated with further analysis methods, available as R packages, making the tool

a suitable platform for future implementation of innovative analysis approaches in biomarker discovery, such as the integration of novel prediction algorithms [83–86], possibly supporting also the identification of synergistic combinations [87], or the handling of confounding factors in preclinical cancer model variability [88]. One easy adaptation might be, for example, the emerging promising field of the identification of splicing gene isoforms or transcriptomics biomarkers as novel predictors of drug response [89].

Data Availability

All the data used in the paper are publicly available and have been referenced accordingly. The produced analysis results are only for validation purposes; if requested we can provide them as stated in the present Data Statement.

Disclosure

The current address of M. Callari is Cancer Research UK Cambridge Institute, University of Cambridge, UK, and of G. E. M. Melloni is Harvard Medical School, Boston, MA, USA.

Conflicts of Interest

The authors declare that there are no conflicts of interest regarding the publication of this paper.

Authors' Contributions

G. Ukmar, G. E. M. Melloni, and L. Radrizzani contributed equally to the work.

Acknowledgments

This work was supported by a grant under the call R&S Regione Lombardia-MIUR (DDUO n.7128/2011), Project ID 30255458. The authors would like to acknowledge Antonella Zambon, Francesca D'Aiuto, Dario Ballinari, Matteo Dugo, Franco Mele, Silvana Canevari, and Giovanni Corrao for support and helpful discussion and Emanuela Scacheri, Giorgio Nepa, and Valeria Anselmi for project management support.

Supplementary Materials

The Supplementary File to “PATRI, a Genomics Data Integration Tool for Biomarker Discovery”, by Ukmar, G. et al., contains the following 3 sections: (1) Supplementary Figures 1-7 (Supplementary Figure 1: PATRI database scheme; Supplementary Figure 2: PATRI graphical user interface: Analysis windows; Supplementary Figure 3: PATRI graphical user interface: “New Analysis” algorithm selection windows; Supplementary Figure 4: PATRI graphical user interface: “Selected Analysis” results window; Supplementary Figure 5: PATRI graphical user interface: Graphing options; Supplementary Figure 6: PATRI graphical user interface: Clinical Samples windows; Supplementary Figure 7: PATRI graphical

user interface: Clinical Samples Analysis results and graphing options); (2) PATRI Installation and Configuration Guide, Version 1.0; (3) PATRI Platform User's Guide, Version 1.0. (*Supplementary Materials*)

References

- [1] J. Barretina, G. Caponigro, N. Stransky et al., “The Cancer Cell Line Encyclopedia enables predictive modelling of anticancer drug sensitivity,” *Nature*, vol. 483, no. 7391, pp. 603–607, 2012.
- [2] S. A. Forbes, D. Beare, H. Boutselakis et al., “COSMIC: Somatic cancer genetics at high-resolution,” *Nucleic Acids Research*, vol. 45, no. 1, pp. D777–D783, 2017.
- [3] TCGA Research Network, <http://cancergenome.nih.gov/>.
- [4] The Expression Project for Oncology (ExpO), <http://www.intgen.org/research-services/biobanking-experience/expo/>.
- [5] International Cancer Genome Consortium, <http://icgc.org/> and <https://dcc.icgc.org/>.
- [6] Cancer Therapeutics Response Portal (CTRP), <https://portals.broadinstitute.org/ctrp/>.
- [7] M. G. Rees, B. Seashore-Ludlow, J. H. Cheah et al., “Correlating chemical sensitivity and basal gene expression reveals mechanism of action,” *Nature Chemical Biology*, vol. 12, no. 2, pp. 109–116, 2016.
- [8] B. Seashore-Ludlow, M. G. Rees, J. H. Cheah et al., “Harnessing connectivity in a large-scale small-molecule sensitivity dataset,” *Cancer Discovery*, vol. 5, no. 11, pp. 1210–1223, 2015.
- [9] i2b2-transSMART Foundation, <http://transmartfoundation.org/>.
- [10] M. Bierkens, W. van der Linden, K. van Bochove et al., “transSMART,” *Journal of Clinical Bioinformatics*, vol. 5, no. Suppl 1, p. S9, 2015.
- [11] F. Iorio, T. A. Knijnenburg, D. J. Vis et al., “A landscape of Pharmacogenomic Interactions in Cancer,” *Cell*, vol. 166, no. 3, pp. 740–754, 2016.
- [12] U. T. Shankavaram, S. Varma, D. Kane et al., “CellMiner: A relational database and query tool for the NCI-60 cancer cell lines,” *BMC Genomics*, vol. 10, article no. 277, 2009.
- [13] W. Yang, J. Soares, P. Greninger et al., “Genomics of Drug Sensitivity in Cancer (GDSC): A resource for therapeutic biomarker discovery in cancer cells,” *Nucleic Acids Research*, vol. 41, no. 1, pp. D955–D961, 2013.
- [14] Y. Qin, A. P. Conley, E. A. Grimm, J. Roszik, and A. Rishi, “A tool for discovering drug sensitivity and gene expression associations in cancer cells,” *PLoS ONE*, vol. 12, no. 4, p. e0176763, 2017.
- [15] J. C. Costello, L. M. Heiser, E. Georgii et al., “A community effort to assess and improve drug sensitivity prediction algorithms,” *Nature Biotechnology*, vol. 32, no. 12, pp. 1202–1212, 2014.
- [16] B. Haibe-Kains, N. El-Hachem, N. J. Birkbak et al., “Inconsistency in large pharmacogenomic studies,” *Nature*, vol. 504, pp. 389–393, 2013.
- [17] P. Geeleher, E. R. Gamazon, C. Seoighe, N. J. Cox, and R. S. Huang, “Consistency in large pharmacogenomic studies,” *Nature*, vol. 540, no. 7631, pp. E1–E2, 2016.
- [18] J. P. Mpindi, B. Yadav, P. Östling et al., “Consistency in drug response profiling,” *Nature*, vol. 540, no. 7631, pp. E5–E6, 2016.
- [19] Z. Safikhani, N. El-Hachem, P. Smirnov et al., “Safikhani et al. reply,” *Nature*, vol. 540, no. 7631, pp. E2–E4, 2016.
- [20] Z. Safikhani, N. El-Hachem, P. Smirnov et al., “Safikhani et al. reply,” *Nature*, vol. 540, no. 7631, pp. E11–E12, 2016.

- [21] CellMiner, <https://discover.nci.nih.gov/cellminer/home.do>.
- [22] Genomics Drug Sensitivity in cancer (GDSC), <http://www.cancerrxgene.org/>.
- [23] CancerDP, Prioritization of Anticancer Drugs, <http://crdd.osdd.net/raghava/cancerdp/>.
- [24] S. Gupta, K. Chaudhary, R. Kumar et al., "Prioritization of anticancer drugs against a cancer using genomic features of cancer cells: A step towards personalized medicine," *Scientific Reports*, vol. 6, Article ID 23857, 2016.
- [25] S. Eckerle, V. Brune, C. Döring et al., "Gene expression profiling of isolated tumour cells from anaplastic large cell lymphomas: Insights into its cellular origin, pathogenesis and relation to Hodgkin lymphoma," *Leukemia*, vol. 23, no. 11, pp. 2129–2138, 2009.
- [26] J. Iqbal, D. D. Weisenburger, T. C. Greiner et al., "Molecular signatures to improve diagnosis in peripheral T-cell lymphoma and prognostication in angioimmunoblastic T-cell lymphoma," *Blood*, vol. 115, no. 5, pp. 1026–1036, 2010.
- [27] D. Szklarczyk, A. Franceschini, S. Wyder et al., "STRING v10: protein-protein interaction networks, integrated over the tree of life," *Nucleic Acids Research*, vol. 43, pp. D447–D452, 2015.
- [28] J. D. Twomey, N. N. Brahme, and B. Zhang, "Drug-biomarker co-development in oncology – 20 years and counting," *Drug Resistance Updates*, vol. 30, pp. 48–62, 2017.
- [29] H.-C. Hsu, T. K. Thiam, Y.-J. Lu et al., "Mutations of KRAS/NRAS/BRAF predict cetuximab resistance in metastatic colorectal cancer patients," *Oncotarget*, vol. 7, no. 16, pp. 22257–22270, 2016.
- [30] K. Knickelbein and L. Zhang, "Mutant KRAS as a critical determinant of the therapeutic response of colorectal cancer," *Genes & Diseases*, vol. 2, no. 1, pp. 4–12, 2015.
- [31] H. Kantarjian, S. O'Brien, E. Jabbour et al., "Improved survival in chronic myeloid leukemia since the introduction of imatinib therapy: a single-institution historical experience," *Blood*, vol. 119, no. 9, pp. 1981–1987, 2012.
- [32] J. C.-H. Yang, Y.-L. Wu, M. Schuler et al., "Afatinib versus cisplatin-based Chemotherapy for EGFR mutation-positive lung adenocarcinoma (LUX-Lung 3 and LUX-Lung 6): analysis of overall survival data from two randomised, phase 3 trials," *The Lancet Oncology*, vol. 16, no. 2, pp. 141–151, 2015.
- [33] M. Burotto, E. E. Manasanch, J. Wilkerson, and T. Fojo, "Gefitinib and erlotinib in metastatic non-small cell lung cancer: A meta-analysis of toxicity and efficacy of randomized clinical trials," *The Oncologist*, vol. 20, no. 4, pp. 400–410, 2015.
- [34] G. Bollag, J. Tsai, J. Zhang et al., "Vemurafenib: The first drug approved for BRAF-mutant cancer," *Nature Reviews Drug Discovery*, vol. 11, no. 11, pp. 873–886, 2012.
- [35] M. F. Press, R. S. Finn, D. Cameron et al., "HER-2 gene amplification, HER-2 and epidermal growth factor receptor mRNA and protein expression, and lapatinib efficacy in women with metastatic breast cancer," *Clinical Cancer Research*, vol. 14, no. 23, pp. 7861–7870, 2008.
- [36] M. M. Awad and A. T. Shaw, "ALK inhibitors in non-small cell lung cancer: Crizotinib and beyond," *Clinical Advances in Hematology and Oncology*, vol. 12, no. 7, pp. 429–439, 2014.
- [37] E. Ardini, M. Menichincheri, P. Banfi et al., "Entrectinib, a Pan-TRK, ROS1, and ALK inhibitor with activity in multiple molecularly defined cancer indications," *Molecular Cancer Therapeutics*, vol. 15, no. 4, pp. 628–639, 2016.
- [38] A. Sartore-Bianchi, E. Ardini, R. Bosotti et al., "Sensitivity to Entrectinib Associated with a Novel LMNA-NTRK1 Gene Fusion in Metastatic Colorectal Cancer," *Journal of the National Cancer Institute*, vol. 108, no. 1, Article ID djv306, 2016.
- [39] P. Erben, D. Gosenca, M. C. Müller et al., "Screening for diverse PDGFRA or PDGFRB fusion genes is facilitated by generic quantitative reverse transcriptase polymerase chain reaction analysis," *Haematologica*, vol. 95, no. 5, pp. 738–744, 2010.
- [40] P. L. Chia, T. John, A. Dobrovic, and P. Mitchell, "Prevalence and natural history of ALK positive non-small-cell lung cancer and the clinical impact of targeted therapy with ALK inhibitors," *Journal of Clinical Epidemiology*, vol. 6, pp. 423–432, 2014.
- [41] A. T. Shaw and B. Solomon, "Anaplastic lymphoma kinase (ALK) fusion oncogene positive non-small cell lung cancer."
- [42] The Comprehensive R Archive Network, <https://cran.r-project.org/>.
- [43] Bioconductor, <https://www.bioconductor.org/>.
- [44] R. C. Gentleman, V. J. Carey, D. M. Bates et al., "Bioconductor: open software development for computational biology and bioinformatics," *Genome Biology*, vol. 5, no. 10, 2004.
- [45] Google Charts, <https://developers.google.com/chart/>.
- [46] H. Zou and T. Hastie, "Regularization and variable selection via the elastic net," *Journal of the Royal Statistical Society: Series B (Statistical Methodology)*, vol. 67, no. 2, pp. 301–320, 2005.
- [47] R. C. Gentleman, V. Carey, W. Hübner, R. Irizarry, and R. Dudoit, *Bioinformatics and Computational Biology Solutions Using R and Bioconductor*, Springer, New York, NY, USA, 2005.
- [48] M. E. Ritchie, B. Phipson, D. Wu et al., "limma powers differential expression analyses for RNA-sequencing and microarray studies," *Nucleic Acids Research*, 2015.
- [49] L. Breiman, "Random forests," *Machine Learning*, vol. 45, no. 1, pp. 5–32, 2001.
- [50] A. Somaschini, N. Amboldi, A. Nuzzo et al., "Cell line identity finding by fingerprinting, an optimized resource for short tandem repeat profile authentication," *Genetic Testing and Molecular Biomarkers*, vol. 17, no. 3, pp. 254–259, 2013.
- [51] Cancer Cell Line Encyclopedia (CCLE), https://portals.broadinstitute.org/ccle_legacy/home.
- [52] cBioportal, <http://www.cbioportal.org/>.
- [53] J. Gao, B. A. Aksoy, and U. Dogrusoz, "Integrative analysis of complex cancer genomics and clinical profiles using the cBioPortal," *Science Signaling*, vol. 6, no. 269, p. 11, 2013.
- [54] Gene Expression Omnibus (GEO), <https://www.ncbi.nlm.nih.gov/geo/>.
- [55] L. Pompili, M. Porru, and C. Caruso, "Patient-derived xenografts: a relevant preclinical model for drug development," *Journal of Experimental Clinical Cancer Research*, vol. 35:189, pp. 10–1186, 2016.
- [56] D. Koller, P. Yu, and R. E. Pollock, "Patient-Derived Xenografts use in Cancer: A Review," *Clinics in Surgery*, vol. 1:1277, 2016.
- [57] G. Li, "Patient-derived xenograft models for oncology drug discovery," *Journal of Cancer Metastasis and Treatment*, vol. 1, no. 1, 2015.
- [58] Human Cancer Model Initiative (HCMI), <https://ocg.cancer.gov/programs/HCMI>.
- [59] EurOPDX Consortium, <http://europdx.eu/>.
- [60] Public Repository of Xenografts (PRoXe), <http://www.proxe.org/>.
- [61] T. Guo, P. Kouvonen, C. C. Koh et al., "Rapid mass spectrometric conversion of tissue biopsy samples into permanent quantitative digital proteome maps," *Nature Medicine*, vol. 21, no. 4, pp. 407–413, 2015.

- [62] A. T. Byrne, D. G. Alf erez, F. Amant et al., "Interrogating open issues in cancer precision medicine with patient-derived xenografts," *Nature Reviews Cancer*, vol. 17, no. 4, pp. 254–268, 2017.
- [63] E. C. Townsend, M. A. Murakami, A. Christodoulou et al., "The Public Repository of Xenografts Enables Discovery and Randomized Phase II-like Trials in Mice," *Cancer Cell*, vol. 29, no. 4, pp. 574–86, 2016.
- [64] J. Liao, M. Gallas, M. Pegram et al., "Lapatinib: new opportunities for management of breast cancer," *Breast Cancer (Dove Med Press)*, vol. 2, pp. 79–91, 2010.
- [65] F. Sircoulomb, I. Bekhouche, P. Finetti et al., "Genome profiling of ERBB2-amplified breast cancers," *BMC Cancer*, vol. 10, article no. 539, 2010.
- [66] M. Katoh and M. Katoh, "Evolutionary recombination hotspot around GSDML-GSDM locus is closely linked to the oncogenic recombination hotspot around the PPP1R1B-ERBB2-GRB7 amplicon," *International Journal of Oncology*, vol. 24, no. 4, pp. 757–763, 2004.
- [67] P. Kauraniemi and A. Kallioniemi, "Activation of multiple cancer-associated genes at the ERBB2 amplicon in breast cancer," *Endocrine-Related Cancer*, vol. 13, no. 1, pp. 39–49, 2006.
- [68] K.-K. Shiu, D. Wetterskog, A. Mackay et al., "Integrative molecular and functional profiling of ERBB2-amplified breast cancers identifies new genetic dependencies," *Oncogene*, vol. 33, no. 5, pp. 619–631, 2014.
- [69] S. J. Park, S. Hong, J. Moon et al., "The MEK1/2 Inhibitor AS703026 Circumvents Resistance to the BRAF Inhibitor PLX4032 in Human Malignant Melanoma Cells," *The American Journal of the Medical Sciences*, vol. 346, no. 6, pp. 494–498, 2013.
- [70] T. T. Sepp al a, J. P. B ohm, M. Friman et al., "Combination of microsatellite instability and BRAF mutation status for subtyping colorectal cancer," *British Journal of Cancer*, vol. 112, no. 12, pp. 1966–1975, 2015.
- [71] E. D. G. Fleuren, L. Zhang, J. Wu, and R. J. Daly, "The kinome 'at large' in cancer," *Nature Reviews Cancer*, vol. 16, no. 2, pp. 83–98, 2016.
- [72] S. A. Luebker, W. Zhang, and S. A. Koepsell, "Comparing the genomes of cutaneous melanoma tumors to commercially available cell lines," *Oncotarget*, vol. 8, no. 70, pp. 114877–114893, 2017.
- [73] M. S. Lawrence, P. Stojanov, C. H. Mermel et al., "Discovery and saturation analysis of cancer genes across 21 tumour types," *Nature*, vol. 505, no. 7484, pp. 495–501, 2014.
- [74] J. Bauer, P. B uttner, R. Murali et al., "BRAF mutations in cutaneous melanoma are independently associated with age, anatomic site of the primary tumor, and the degree of solar elastosis at the primary tumor site," *Pigment Cell & Melanoma Research*, vol. 24, no. 2, pp. 345–351, 2011.
- [75] A. Drilon, S. Siena, and S. I. Ou, "Safety and Antitumor Activity of the Multitargeted Pan-TRK, ROS1, and ALK Inhibitor Entrectinib: Combined Results from Two Phase I Trials (ALKA-372-001 and STARTRK-1)," *Cancer Discovery*, vol. 7, no. 4, pp. 400–409, 2017.
- [76] S. W. Morris, M. N. Kirstein, M. B. Valentine et al., "Fusion of a kinase gene, ALK, to a nucleolar protein gene, NPM, in non-Hodgkin's lymphoma," *Science*, vol. 263, no. 5151, pp. 1281–1284, 1994.
- [77] R. Piva, L. Agnelli, E. Pellegrino et al., "Gene expression profiling uncovers molecular classifiers for the recognition of anaplastic large-cell lymphoma within peripheral T-cell neoplasms," *Journal of Clinical Oncology*, vol. 28, no. 9, pp. 1583–1590, 2010.
- [78] L. Agnelli, E. Mereu, E. Pellegrino et al., "Identification of a 3-gene model as a powerful diagnostic tool for the recognition of ALK-negative anaplastic large-cell lymphoma," *Blood*, vol. 120, no. 6, pp. 1274–1281, 2012.
- [79] L. Lamant, A. De Reyni es, M.-M. Duplantier et al., "Gene-expression profiling of systemic anaplastic large-cell lymphoma reveals differences based on ALK status and two distinct morphologic ALK + subtypes," *Blood*, vol. 109, no. 5, pp. 2156–2164, 2007.
- [80] H. Matsuyama, H. I. Suzuki, H. Nishimori et al., "miR-135b mediates NPM-ALK-driven oncogenicity and renders IL-17-producing immunophenotype to anaplastic large cell lymphoma," *Blood*, vol. 118, no. 26, pp. 6881–6892, 2011.
- [81] Y. Zeng and A. L. Feldman, "Genetics of anaplastic large cell lymphoma," *Leukemia & Lymphoma*, vol. 57, no. 1, pp. 21–27, 2016.
- [82] M. Boi, E. Zucca, G. Inghirami, and F. Bertoni, "Advances in understanding the pathogenesis of systemic anaplastic large cell lymphomas," *British Journal of Haematology*, vol. 168, no. 6, pp. 771–783, 2015.
- [83] P. Jiang, W. Lee, X. Li et al., "Genome-Scale Signatures of Gene Interaction from Compound Screens Predict Clinical Efficacy of Targeted Cancer Therapies," *Cell Systems*, vol. 6, no. 3, pp. 343–354.e5, 2018.
- [84] F. Azuaje, "Computational models for predicting drug responses in cancer research," *Briefings in Bioinformatics*, vol. 18, no. 5, pp. 820–829, 2017.
- [85] C. De Niz, R. Rahman, X. Zhao, and R. Pal, "Algorithms for drug sensitivity prediction," *Algorithms*, vol. 9, no. 4, 77 pages, 2016.
- [86] R. Rahman, K. Matlock, S. Ghosh, and R. Pal, "Heterogeneity Aware Random Forest for Drug Sensitivity Prediction," *Scientific Reports*, vol. 7, no. 1, 2017.
- [87] D. J. McGrail, C. C. Lin, J. Garnett et al., "Improved prediction of PARP inhibitor response and identification of synergizing agents through use of a novel gene expression signature generation algorithm," *npj Systems Biology and Applications*, vol. 3, no. 1, 2017.
- [88] P. Geeleher, N. J. Cox, and R. S. Huang, "Cancer biomarker discovery is improved by accounting for variability in general levels of drug sensitivity in pre-clinical models," *Genome Biology*, vol. 17, no. 1, 2016.
- [89] Z. Safikhani, P. Smirnov, K. L. Thu et al., "Gene isoforms as expression-based biomarkers predictive of drug response in vitro," *Nature Communications*, vol. 8, no. 1, 2017.

Research Article

Alkaline Phosphatase Kinetics Predict Metastasis among Prostate Cancer Patients Who Experience Relapse following Radical Prostatectomy

Carolyn A. Salter,¹ Jennifer Cullen ,^{2,3} Claire Kuo,² Yongmei Chen,² Lauren Hurwitz,² Adam R. Metwalli,⁴ Jordan Dimitrakoff,⁵ and Inger L. Rosner^{1,2,3}

¹Department of Urology, Walter Reed National Military Medical Center, Bethesda, MD, USA

²Center for Prostate Cancer Disease Research, Rockville, MD, USA

³Department of Surgery, Uniformed Services University of the Health Sciences, Bethesda, MD, USA

⁴Urologic Oncology Branch, National Cancer Institute, National Institute of Health, Bethesda, MD, USA

⁵US Food and Drug Administration Division of Bone, Reproductive and Urologic Products, Silver Spring, MD, USA

Correspondence should be addressed to Jennifer Cullen; jcullen@cpdr.org

Received 26 February 2018; Accepted 6 June 2018; Published 28 June 2018

Academic Editor: Maria L. Tornesello

Copyright © 2018 Carolyn A. Salter et al. This is an open access article distributed under the Creative Commons Attribution License, which permits unrestricted use, distribution, and reproduction in any medium, provided the original work is properly cited.

Introduction. Metastasis prostate cancer (CaP) occurs in a small fraction of patients. Improved prognostication of disease progression is a critical challenge. This study examined alkaline phosphatase velocity (APV) in predicting distant metastasis-free survival (DMFS). **Materials and Methods.** This retrospective cohort study examined CaP patients enrolled in the Center for Prostate Disease Research (CPDR) multicenter national database who underwent RP and experienced BCR (n=1783). BCR was defined as a PSA \geq 0.2 ng/mL at \geq 8 weeks post-RP, followed by at least one confirmatory PSA \geq 0.2 ng/mL or initiation of salvage therapy. APV was computed as the slope of the linear regression line of all alkaline phosphatase (AP) values after BCR and prior to distant metastasis. APV values in the uppermost quartile were defined as “rapid” and compared to the lower three quartiles combined (“slower”). Unadjusted Kaplan Meier (KM) estimation curves and multivariable Cox proportional hazards analysis were used to examine predictors of DMFS. **Results.** Of the 1783 eligible patients who experienced post-RP BCR, 701 (39.3%) had necessary AP data for APV calculation. PSA doubling time (PSADT) and APV were strongly associated ($p=0.008$). No differences in APV were observed across race. In KM analysis, significantly poorer DMFS was observed among the rapid versus slower APV group (Log-rank $p=0.003$). In multivariable analysis, a rapid APV was predictive of a twofold increased probability of DMFS (HR = 2.2; 95% CI = 1.2, 3.9; $p = 0.008$), controlling for key study covariates. **Conclusions.** Building on previous work, this study found that rapid APV was a strong predictor of DMFS for a broader group of CaP patients, those who undergo post-RP BCR who were enrolled in a longitudinal cohort with long-term follow-up and equal health care access. APV is worth considering as a complementary clinical factor for predicting DMFS.

1. Introduction

Prostate cancer (CaP) is the most common nonskin cancer in the United States and the third leading cause of cancer-related death in men with 161,360 new cases and 26,730 deaths estimated in 2017[1]. The majority of men with prostate cancer do not die of their disease [1–3]. Development of distant metastasis is a useful surrogate of prostate cancer specific death. Clinical predictors of CaP progression have

included PSA doubling time (PSADT) and more recently alkaline phosphatase (AP) velocity (APV) [4–6]. AP is a known marker of bone-turnover, specifically osteoblast activity. In prior studies, AP has been shown to be elevated in men with bony metastasis and AP elevation is correlated to metastatic burden [7]

Previous, related research conducted at the Center for Prostate Disease Research (CPDR) evaluated men with castrate-resistant CaP (CRPC) [4, 8]. Alkaline phosphatase

velocity (APV) has also been studied as a means to predict progression in men with CaP. A recent article evaluating the CPDR multicenter national database examined men who had castrate-resistance prostate cancer (CRPC) following androgen deprivation therapy and reported that faster APV was a strong predictor in combination with PSA doubling time (PSADT) in predicting development of distant bone metastasis. A similar study retrospectively evaluated patients enrolled at Memorial Sloan Kettering Cancer Center to confirm findings from the CPDR study. In the MSKCC study, Hammerich *et al.* showed that, among patients with post-RP CRPC who received ADT for an elevated PSA, those who had rapid APV progressed more quickly to bone metastasis and had poorer overall survival compared to those with slower APV [9].

The primary study aim was to examine APV as a predictor of distant metastasis-free survival (DMFS) among men who experienced biochemical recurrence following radical prostatectomy (RP) in the context of an equal access health care system. A secondary aim was to confirm the joint roles of APV with PSADT in predicting DMFS.

2. Methodology

2.1. Study Design and Source of Study Subjects. The study population was comprised of men enrolled in the Institutional Review Board-approved Center for Prostate Disease Research (CPDR) multicenter national database (described in detail previously) [10]. Briefly, patients under suspicion for CaP are eligible for enrolment at five US military and 1 civilian medical center nationwide. A total of 8,041 men with biopsy-confirmed CaP detected between 1989 and 2013 and who underwent RP as primary treatment (i.e., within 6 months of CaP diagnosis) were eligible. The main exclusion criterion was no evidence of BCR during study interval ($n=6,101$). Patients were also excluded if they had less than 1-year follow-up ($n=60$) or if there was M1 disease at presentation ($n=15$) or positive nodal status at diagnosis ($n=82$).

2.2. Demographic, Clinical, Pathologic, and Treatment Information. For each subject, data were obtained on age at CaP diagnosis, age at RP, self-reported race, PSA at diagnosis (ng/mL), D'Amico risk stratum (low, intermediate, and high), pathologic T stage (T2, T3-4), pathologic grade (≤ 6 , 3+4, 4+3, and 8-10), surgical margin status (positive, negative), extracapsular extension or ECE (positive, negative), and seminal vesicle invasion or SVI (positive, negative). PSA doubling time (PSADT) was calculated as previously described by Pound *et al.* [6] using all available PSA values at least 3 months apart after BCR. If the slope of the linear regression line was 0 (i.e., elevated but constant PSA levels) or negative (decreasing PSA levels after an initial increase), the PSADT was set to 10 years (120 months). Detailed information on all treatments received before were obtained and categorized as neoadjuvant pre-RP, adjuvant (post RP but pre-BCR), and salvage (post-BCR).

2.3. Assessment of Alkaline Phosphatase (AP) Kinetics. APV was computed as the slope of the linear regression line of

all alkaline phosphatase (AP) values after RP and prior to METs. APV values in the uppermost quartile were defined as "rapid" and compared to those in the lower 3 quartiles combined. Finally, a kinetics measure of alkaline phosphatase velocity (APV) was calculated by using the slope of the linear regression line of the AP values plotted against time in years. This was computed using all AP values drawn at least 3 months apart and obtained after CRPC developed but before radiographic scan-detected metastasis to bone or other locations (e.g., visceral metastasis). APV was dichotomized at the observed upper quartile of all observed AP values in this study sample (<3.11 versus ≥ 3.11 U/L-year).

2.4. Primary Study Endpoint. The primary study endpoint was distant metastasis-free survival (DMFS). Presence of metastases was ascertained based on complete radiographic scan history (bone scan, CT scan, and MRI), captured as part of ongoing data collection activities for the CPDR multicenter national database. Time to DMFS was calculated as the number of years elapsed from time point of documented BCR to distant metastasis or until end of study period for those who did not experience distant metastasis.

2.5. Statistical Analysis. Descriptive statistics included means and standard deviations (SD), frequencies, and percentages. Student's *t*-tests or Wilcoxon-Mann-Whitney tests were used to compare distributions in continuous patient characteristics, including age and time variables, across APV groups. Mantel Haenzel chi-square tests were used to examine differences in the distributions of categorical variables across APV groups.

Unadjusted Kaplan Meier (KM) estimation curves were used to model time to distant-metastasis-free survival (DMFS) across APV strata and PSADT strata. The log rank test and its associated p-value are reported for KM analyses. Multivariable Cox proportional hazards analyses were used to model DMFS controlling for demographic, clinical, pathologic, treatment, and time covariates. Hazard ratios (HR) and corresponding 95% confidence intervals (CI) and p-values are reported.

All statistical tests are 2-sided (summary alpha error = 0.05), and the decision rule was based on a p-value < 0.05 . All statistical analyses were performed using SAS version 9.3 and R.

3. Results

Of the 1,783 patients who experienced post-RP BCR, sufficient alkaline phosphatase (AP) data were available for 701 (39.3%) subjects. This subset represents the study cohort (Figure 1). There were 63 patients (9%) who developed distant metastases during a mean follow-up time of 10.1 years. Among these 63 metastatic patients, 36 (57.4) were confirmed by bone scan, 24 (38.1%) were confirmed by CT scan, 2 (3.2%) were confirmed by MRI, and 1 patient (1.6%) was detected with a metastasis of CaP to the bladder. Per definition of the APV categorized variable, those with a "rapid" APV accounted for 25% of the cohort and the remaining 75% had a slower APV (Table 1). A majority of patients (62%) received

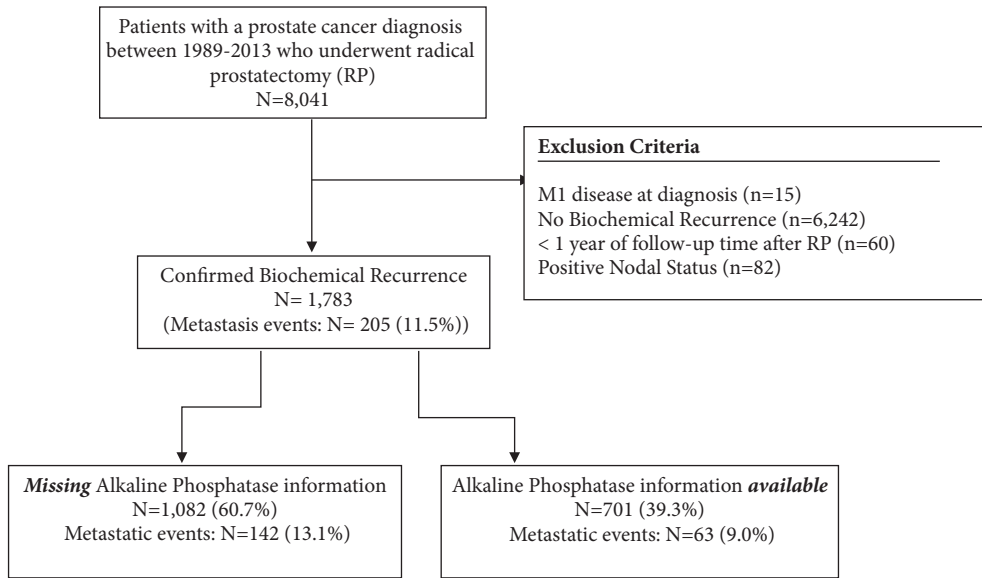


FIGURE 1: Flow diagram of study population selection.

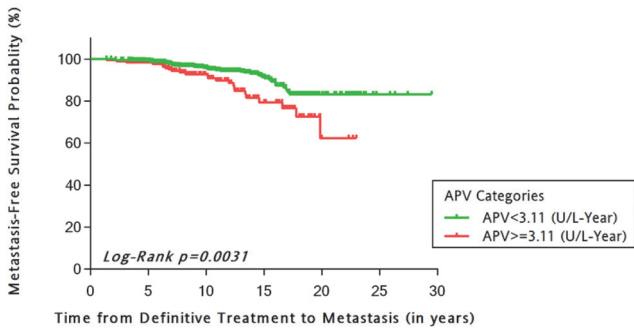


FIGURE 2: Unadjusted Kaplan-Meier estimation curve of distant metastasis-free probability stratified by alkaline phosphatase velocity (APV) categories.

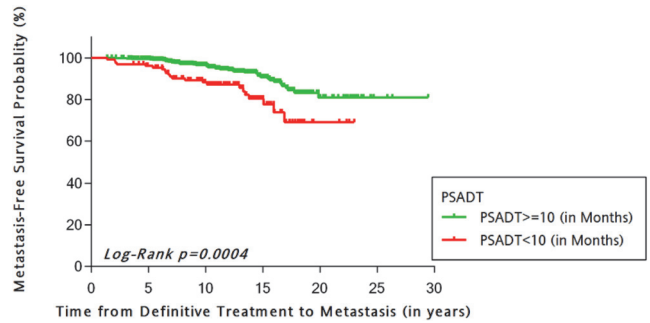


FIGURE 3: Unadjusted Kaplan-Meier estimation curve of distant metastasis-free probability stratified by PSA doubling time (PSADT) categories.

some form of salvage treatment. Chi-square analysis did show a significant association between APV and PSADT categories ($p=0.15$).

Unadjusted Kaplan-Meier estimation curves for DMFS stratified for APV (Figure 2) and PSADT (Figure 3) demonstrated that those with rapid versus slower APV group had poorer DMFS ($p=0.003$) as did patients with faster versus slower PSADT (<10 versus ≥ 10 months) ($p=0.0004$). KM analysis was also performed for PSADT cutpoints by Freedland et al. which demonstrated strong associated with DMFS-free survival ($p<0.0001$). Though there were few observations in the PSADT <3 months category, data are presented for Pound et al. cutpoints.

In multivariable Cox proportional hazards analysis, only rapid APV ($HR_{\geq 3.11 \text{ vs. } < 3.11} = 2.2$; 95% CI=1.2, 3.9; $p=0.008$), PSADT ($HR_{<10 \text{ vs. } \geq 10} = 2.0$; CI=1.1, 3.8; $p=0.03$), and pathological Gleason ($HR_{8-10 \text{ versus } 6} = 2.3$; CI=1.0, 5.1; $p=0.04$) were statistically significant predictors of DMFS (Table 2).

Due to concerns over study bias that might have been caused by missing AP data, preventing calculation of APV, comparisons were made across the subsets of subjects with versus without adequate AP data, across demographic, clinical, pathologic, and treatment variables (Table 3). Among statistically significant differences noted, those *with* versus *without* AP data had a longer follow-up (10.1 versus 7.3 years, $p<0.001$), a greater proportion of salvage treatment (62% versus 50%, $p<0.0001$); a greater proportion of pT2 disease (50% versus 54%, $p=0.01$), and a lower proportion of ECE (38% versus 47%, $p<0.0001$).

4. Discussion

While routine examination of alkaline phosphatase (AP) in prostate cancer care was previously observed, the introduction and widespread use of PSA screening in the late 1980s greatly diminished its clinical use. This study, along with previous and related work, has shown that faster AP kinetics

TABLE 1: Descriptive characteristics of study sample (n=701).

	Study Cohort (N=701)
Continuous Variables	Mean ± SD
Age at CaP Diagnosis (years), Mean ± SD	62.6 ± 6.4
Age at RP (years), Mean ± SD	62.8 ± 6.4
Time from RP to Distant Metastasis (years), Mean ± SD	10.1 ± 4.7
Categorical Variables	N (%)
Distant Metastasis, N (%)	63 (9.0)
Neo- and/or Adjuvant Treatments Received, N (%)	127 (18.1)
Salvage Treatments Received, N (%)	437 (62.3)
PSA Doubling Time (Months), N (%)	
Missing	22 (3.1)
<10	129 (18.4)
≥ 10	550 (78.5)
D'Amico risk stratum, N (%)	
Missing	165 (23.5)
Low	171 (24.4)
Intermediate	199 (28.4)
High	166 (23.7)
Race, N (%)	
Missing	8 (1.1)
African American	163 (23.3)
Caucasian	494 (70.5)
Other	36 (5.1)
PSA at CaP Diagnosis, N (%)	
Missing	126 (18.0)
<10	371 (52.9)
10-20	139 (19.8)
>20	65 (9.3)
Pathologic Gleason Sum, N (%)	
Missing	98 (14.0)
≤6	234 (33.3)
3+4	201 (28.7)
4+3	73 (10.4)
≥ 8	95 (13.6)
Pathological T stage, N (%)	
Missing	15 (2.1)
T2	334 (47.6)
T3-T4	352 (50.3)
Positive Surgical Margin Status, N (%)	311 (44.4)
Positive Extracapsular Extension, N (%)	265 (37.8)
Positive Seminal Vesicle Invasion, N (%)	96 (13.7)

are predictive of poorer metastasis-free survival in distinct subsets of prostate cancer patients.

More recently there has been a renewed interest in using AP to predict disease progression. One study attempted to predict overall survival in men with metastatic CRPC and found that AP was predictive of survival (p= 0.027) whereas

PSA was not (p=0.742) [11]. A similar paper which again used subjects with metastatic CRPC found a median AP of 172. When comparing men with AP ≤ 172 their median survival was 18 months compared to 10 months in men with AP > 172 (p< 0.001) [12]. These data show that, in men with metastatic CRPC, AP levels can be used to predict survival.

TABLE 2: Multivariable Cox proportional hazards analysis of distant metastasis-free survival.

Variable	Hazard Ratio (95% CI)	p-value
Age at RP ¹ (years)	0.99 (0.95, 1.04)	0.78
Time from RP to BCR ² (years)	0.92 (0.81, 1.04)	0.18
Neo- and/or Adjuvant Treatments Received		
Yes vs. No	1.36 (0.69, 2.69)	0.38
Post-BCR² Salvage Treatment Received		
HT Only vs. None	0.94 (0.45, 1.98)	0.87
XRT Only vs. None	0.47 (0.15, 1.41)	0.17
Multi-Treatment* vs. None	1.66 (0.73, 3.79)	0.23
APV³ Upper Quartiles (U/L-Y)		
≥3.11 vs. <3.11	2.18 (1.23, 3.86)	0.008
PSADT⁴(Months)		
<10 vs. ≥10	2.01 (1.07, 3.78)	0.030
Race		
African American vs. Caucasian American & Other	1.07 (0.54, 2.13)	0.84
Pathologic T stage		
pT3-T4 vs. pT2	0.99 (0.47, 2.07)	0.97
Pathologic Gleason Sum		
3+4 vs. ≤6	1.1 (0.53, 2.28)	0.81
4+3 vs. ≤6	0.91 (0.32, 2.58)	0.85
≥8 vs. ≤6	2.29 (1.03, 5.07)	0.042
Surgical Margin Status		
Positive vs. Negative	1.08 (0.53, 2.19)	0.84

¹RP=radical prostatectomy.

²BCR=biochemical recurrence.

³APV=alkaline phosphatase velocity.

⁴PSADT=PSA doubling time.

* Multitreatment refers to combinations of XRT and HT.

Metwalli et al. looked at a similar question and found that, in men with CRPC, faster APV can predict progression to bone metastases. [9]

The current study focused on a time interval in the continuum of CaP treatment that is further upstream than previously examined, by analyzing the role of APV in predicting DMFS in patients who experience post-RP BCR. These data suggests that APV can be used to predict disease progression in numerous stages along trajectory of CaP care, from BCR, to CRPC to metastatic CRPC.

Strengths of this study include the longitudinal, racially diverse patient cohort with long-term patient follow-up in an equal-access health care system. Even though many of these patients were excluded due to lack of alkaline phosphatase data, we still have a large patient cohort to examine the significance of alkaline phosphatase velocity.

Limitations include the retrospective design, precluding the ability to examine temporal changes in short intervals of time on APV and outcome, DMFS. In addition, the role of neoadjuvant, adjuvant, and salvage therapies was limited to categories of any use versus none. Details on duration of use and medication type were beyond the scope of this study. Also, APV was categorized due to nonnormality and strong skew in its data distribution. But identifying an optimal cutpoint that would be useful in other cohorts is a

challenge. In this study, unbiased categories were data-driven, with patients dichotomized into rapid versus slower groups, representing the uppermost quartile versus the lower 3 combined, respectively. This approach is limited and may not be externally generalizable.

5. Conclusions

This study builds on our previous work that demonstrated APV as a strong predictor of distant metastasis-free survival in men with CRPC. This study expanded the study question to a broader group of CaP patients—those who experience post-RP BCR—and demonstrated that APV is a strong predictor of DMFS in this patient subset as well. By examining patients at a time point upstream of CRPC, namely, time of BCR, this study provides support for APV as a tool for improved prognostication of DMFS. Future work should be extended to examine this question among patients undergoing radiation, with or without hormone therapy, who experience biochemical relapse.

Data Availability

For IRB protocol, the authors are not permitted to share raw data files. However, they can provide any collapsed data and statistical information that are requested.

TABLE 3: Comparison of patients with versus without alkaline phosphatase (AP) data needed for calculating AP velocity (APV).

	Alkaline Phosphatase Data Available		p-value
	No (n=1,082)	Yes (n=701)	
Age at CaP¹ Diagnosis (years), Mean \pm SD ²	62.1 \pm 7	62.6 \pm 6.4	0.16
Age at RP³ (years), Mean \pm SD	62.3 \pm 7	62.8 \pm 6.4	0.17
Time from RP³ to Distant Metastasis (years), Mean \pm SD	7.3 \pm 5.4	10.1 \pm 4.7	<.0001
Distant Metastasis , N (%)	142 (13.1)	63 (9)	
Neo- and/or Adjuvant Treatments Received , N (%)	195 (18)	127 (18.1)	0.96
Salvage Treatments Received , N (%)	544 (50.3)	437 (62.3)	<.0001
PSA Doubling Time (Months) , N (%)			0.36
Missing	69 (6.4)	22 (3.1)	
<10	211 (19.5)	129 (18.4)	
\geq 10	802 (74.1)	550 (78.5)	
D'Amico risk stratum , N (%)			0.70
Missing	298 (27.5)	165 (23.5)	
Low	241 (22.3)	171 (24.4)	
Intermediate	283 (26.2)	199 (28.4)	
High	260 (24)	166 (23.7)	
Race , N (%)			0.35
Missing	20 (1.8)	8 (1.1)	
African American	224 (20.7)	163 (23.3)	
Caucasian	790 (73)	494 (70.5)	
Others	48 (4.5)	36 (5.1)	
PSA at CaP Diagnosis , N (%)			0.27
Missing	222 (20.5)	126 (18)	
<10	582 (53.8)	371 (52.9)	
10-20	177 (16.4)	139 (19.8)	
>20	101 (9.3)	65 (9.3)	
Pathologic Gleason Sum , N (%)			0.17
Missing	227 (21)	98 (14)	
\leq 6	328 (30.3)	234 (33.3)	
3+4	249 (23)	201 (28.7)	
4+3	112 (10.4)	73 (10.4)	
\geq 8	166 (15.3)	95 (13.6)	
Pathological T stage , N (%)			0.011
Missing	54 (5)	15 (2.1)	
pT2	436 (40.3)	334 (47.6)	
pT3-T4	592 (54.7)	352 (50.3)	
Positive Surgical Margin Status , N (%)	506 (46.8)	311 (44.4)	0.16
Positive Extracapsular Extension , N (%)	511 (47.2)	265 (37.8)	<.0001
Positive Seminal Vesicle Invasion , N (%)	163 (15.1)	96 (13.7)	0.27

¹CaP = prostate cancer.²SD= standard deviation.³RP = radical prostatectomy.

Disclosure

The opinions or assertions contained herein are the private ones of the author/speaker and are not to be construed as official or reflecting the views of the Department of Defense, the Uniformed Services University of the Health Sciences, or any other agency of the US Government. The views and opinions expressed in the present manuscript do not reflect the views or opinions of the United States Food and Drug Administration or the United States Government. This work was presented as a podium presentation at the American Urological Association (AUA) Annual Meeting in Boston, MA, in May 2017. The direct link to this publication can be found here: <https://www.jurology.com/article/S0022-5347%2817%2930706-1/fulltext>.

Conflicts of Interest

The authors declare that they have no conflicts of interest.

Acknowledgments

This work was performed under the Cooperative Research Agreement Funds with Uniformed Services University for the Health Sciences (Award no. HU0001-10-2-0002).

References

- [1] American Cancer Society, "Cancer Facts and Figures," 2018.
- [2] J.-E. Johansson, O. Andrén, S.-O. Andersson et al., "Natural history of early, localized prostate cancer," *The Journal of the American Medical Association*, vol. 291, no. 22, pp. 2713–2719, 2004.
- [3] D. Schreiber, A. Chhabra, J. Rineer, J. Weedon, and D. Schwartz, "A Population-Based Study of Men with Low-Volume Low-Risk Prostate Cancer: Does African-American Race Predict for More Aggressive Disease?" *Clinical Genitourinary Cancer*, vol. 13, no. 4, pp. e259–e264, 2015.
- [4] A. R. Metwalli, I. L. Rosner, J. Cullen, and et al., "Elevated alkaline phosphatase velocity strongly predicts overall survival and the risk of bone metastases in castrate-resistant prostate cancer," *Urologic Oncology*, vol. 32, no. 6, pp. 761–768, 2014.
- [5] S. J. Freedland, E. B. Humphreys, L. A. Mangold et al., "Risk of prostate cancer-specific mortality following biochemical recurrence after radical prostatectomy," *Journal of the American Medical Association*, vol. 294, no. 4, pp. 433–439, 2005.
- [6] C. R. Pound, A. W. Partin, M. A. Eisenberger, D. W. Chan, J. D. Pearson, and P. C. Walsh, "Natural history of progression after PSA elevation following radical prostatectomy," *Journal of the American Medical Association*, vol. 281, no. 17, pp. 1591–1597, 1999.
- [7] R. J. Cook, R. Coleman, J. Brown et al., "Markers of bone metabolism and survival in men with hormone-refractory metastatic prostate cancer," *Clinical Cancer Research*, vol. 12, no. 11 I, pp. 3361–3367, 2006.
- [8] K. H. Hammerich, T. F. Donahue, I. L. Rosner et al., "Alkaline phosphatase velocity predicts overall survival and bone metastasis in patients with castration-resistant prostate cancer," *Urologic Oncology: Seminars and Original Investigations*, vol. 35, no. 7, pp. 460–460.e28, 2017.
- [9] A. R. Metwalli, I. L. Rosner, J. Cullen et al., "Elevated alkaline phosphatase velocity strongly predicts overall survival and the risk of bone metastases in castrate-resistant prostate cancer," *Urologic Oncology: Seminars and Original Investigations*, vol. 32, no. 6, pp. 761–768, 2014.
- [10] S. A. Brassell, A. Dobi, G. Petrovics, S. Srivastava, and D. McLeod, "The center for prostate disease research (CPDR): A multidisciplinary approach to translational research," *Urologic Oncology: Seminars and Original Investigations*, vol. 27, no. 5, pp. 562–569, 2009.
- [11] O. Smaletz, H. I. Scher, E. J. Small et al., "Nomogram for overall survival of patients with progressive metastatic prostate cancer after castration," *Journal of Clinical Oncology*, vol. 20, no. 19, pp. 3972–3982, 2002.
- [12] S. Halabi, E. J. Small, P. W. Kantoff et al., "Prognostic model for predicting survival in men with hormone-refractory metastatic prostate cancer," *Journal of Clinical Oncology*, vol. 21, no. 7, pp. 1232–1237, 2003.

Research Article

HSP90: A Novel Target Gene of miRNA-628-3p in A549 Cells

Jieli Pan,¹ Fusheng Jiang ,² Jia Zhou,³ Dehong Wu,⁴ Zhenhua Sheng,¹ and Meiya Li ¹

¹Academy of Chinese Medical Sciences, Zhejiang Chinese Medical University, Hangzhou 310053, China

²College of Life Science, Zhejiang Chinese Medical University, Hangzhou 310053, China

³College of Basic Medical Sciences, Zhejiang Chinese Medical University, Hangzhou 310053, China

⁴The Second Affiliated Hospital of Zhejiang Chinese Medical University, Hangzhou 310053, China

Correspondence should be addressed to Meiya Li; lmeiya@126.com

Received 19 March 2018; Accepted 12 April 2018; Published 20 May 2018

Academic Editor: Valli De Re

Copyright © 2018 Jieli Pan et al. This is an open access article distributed under the Creative Commons Attribution License, which permits unrestricted use, distribution, and reproduction in any medium, provided the original work is properly cited.

Lung cancer is one of the leading causes of cancer-related death in the world. MicroRNA- (miR-) 628-3p plays critical roles in many cancers, including lung cancer. We investigated how miR-628-3p affected migration and apoptosis in A549 cells. We used bioinformatics algorithms to predict the miR-628-3p target gene to study the molecular mechanism by which miR-628-3p contributes to lung cancer. Then, we used the luciferase reporter assay to identify whether heat shock protein 90a (*HSP90*) is a direct target of miR-628-3p. Western blotting and quantitative real-time PCR showed that miR-628-3p downregulated *HSP90*a protein expression via a posttranscriptional mechanism. We confirm that miR-628-3p promotes apoptosis and inhibits migration in A549 cells by negatively regulating *HSP90*. Our results may reveal a novel strategy for lung cancer treatment.

1. Introduction

Lung cancer is the most common cancer in the world and is the leading cause of cancer-related deaths [1]. The occurrence and development of lung cancer are a complex, multistep, and multilevel process involving multiple factors, and the mechanism involved remains unknown. Lung cancer has become a challenging topic and hotspot in tumor research. Although research on the early diagnosis and treatment of lung cancer in recent years has become more in depth, the overall prognosis and survival of patients with lung cancer are unsatisfactory; therefore, there is still much to be done in lung cancer research and treatment.

There are many types of lung cancer, among which non-small cell lung cancer (NSCLC) is the main type, accounting for about 75–80% of lung cancer cases [2]. As the symptoms are not apparent and detection is difficult at stage I and II NSCLC, it is mostly diagnosed at the late stages, which reduces the five-year survival rate. Therefore, earlier detection of lung cancer is needed and could lead to more effective management of the disease.

There are a variety of abnormal factors in lung cancer [3, 4]; research into the mechanism of action has been performed at molecular level, but the exact molecular mechanism remains

unclear. With the development of molecular biology technology, the discovery of microRNAs (miRNAs) has opened up a new avenue in lung cancer research and provides new ideas and approaches for diagnosing and treating lung cancer.

miRNAs are a family of naturally occurring, small, endogenous noncoding RNAs that are 18–25 nucleotides in length [5]. miRNAs influence many biological processes, including cell proliferation, apoptosis, development, differentiation, migration, and survival. miRNAs are differentially expressed in cancer and play important roles in regulating gene expression by base-pairing to the complementary sites on the target mRNAs, consequently blocking translation or triggering the degradation of the target mRNAs [6, 7]. Growing evidence has demonstrated the role of miRNAs in many human tumors, including breast [8], ovarian [9], pancreatic [10], thyroid [11], and lung cancers [1].

The altered expression of tissue miRNAs has been associated with many diseases, particularly cancer. In recent years, the role of miR-628-3p in cancer has received increased attention. miR-628-3p is abnormally expressed in many cancers, such as colon [12], gastric [13], and pancreatic cancer [14]. The most recent study, which performed TaqMan low-density DNA microarray comparative analysis of more than 200 cases

TABLE 1: siRNAs against *HSP90* gene.

siRNA	Sequence	Target mRNA sequence
siRNA 1	F: 5'- GCCCUAAGAGACAACUCAAdTdT-3' R: 3'- dTdTTCGGGAUUCUCUGUUGAGUU-5'	5'-GCCCTAAGAGACAACACTCAA-3'
siRNA 2	F: 5'- GGAACGUGAUAAAGAAGUAdTdT-3' R: 3'- dTdTCCUUGCACUAUUUCUUCAU-5'	5'-GGAACGTGATAAAGAAGTA-3'
siRNA 3	F: 5'- GCACCAGAAUGAAGGAGAAdTdT-3' R: 3'- dTdTTCGUGGUCUUACUUCUCUU-5'	5'-GCACCAGAATGAAGGAGAA-3'

of early lung cancer and more than 170 cases of normal human plasma samples, found abnormal high expression miR-628-3p in the lung cancer cases, suggesting that miR-628-3p can be used as a marker of early diagnosis of lung cancer [15]. However, the regulatory mechanism of miRNA in lung cancer is not clear, and more research is needed.

At present, numerous clinical studies have confirmed that the remission rate of molecular targeted drugs in patients with lung cancer is not very high, and drug resistance against targeted drugs is increasing. Therefore, further study of the main target in lung cancer is imperative, and developing lung cancer treatment closely related to miRNA-target research has gradually become a hot research topic. Identifying the target of miR-628-3p and clarifying the mechanism of miR-628-3p would provide new ideas and methods for diagnosing and treating lung cancer.

Heat shock protein 90a (HSP90a), one of the most abundant and conserved chaperone proteins, aids in preserving the integrity and function of numerous client proteins. Plasma HSP90a protein levels are useful as a diagnostic biomarker in lung cancer [16].

In this study, we investigated the relationship between miR-628-3p and HSP90a in A549 lung cancer cells. Moreover, we provide evidence that *HSP90* is a target gene of miR-628-3p in A549 cells.

2. Materials and Methods

2.1. Cell Culture. 293T and A549 cells were cultured in Dulbecco's modified Eagle's medium (Invitrogen, USA) supplemented with 10% (v/v) fetal bovine serum (Gibco, USA) and 1% antibiotics (100 U/mL penicillin and 100 mg/L streptomycin sulfate). All cells were grown in a humidified atmosphere at 37°C with 5% CO₂.

2.2. Oligonucleotide Transfection. miR-628-3p mimics and *HSP90* small interfering RNAs (siRNAs) were designed and synthesized by RiboBio (Guangzhou, China); Table 1 lists their sequences and the targeted mRNAs.

Cells were plated on 6-well plates (Corning, USA) and cultured overnight to 40–60% confluence. Transfection was performed with Lipofectamine 3000 (Invitrogen, USA) according to the manufacturer's protocol. After 48 h, we harvested the cells and detected HSP90 and miR-628-3p by western blotting and quantitative real-time polymerase chain reaction (qRT-PCR), respectively.

2.3. Apoptosis Assay. Apoptosis was determined by annexin V and propidium iodide (PI) staining using an apoptosis

detection kit (556547, BD) according to the manufacturer's instructions. Briefly, A549 cells were transfected with 50 nM NC mimic, miR-628-3p mimic, or *HSP90* siRNAs for 48 h. Then, the cells were washed with 50 mmol/L cold phosphate buffer (pH 7.5), centrifuged at 1200 ×g for 5 min, and suspended in binding buffer.

The treated cells were incubated with annexin V and PI for 15 min at room temperature and then analyzed for annexin V binding affinity within 1 h by flow cytometry (BD Accuri C6).

2.4. RNA Extraction and qRT-PCR. Total RNA from the cells was extracted using TRIzol (Invitrogen) according to the manufacturer's protocol. Complementary DNA (cDNA) was synthesized from 1 μg total RNA with a PrimeScript reverse transcription (RT) reagent kit with genomic DNA (gDNA) Eraser (TaKaRa, China) in a 20 μL volume [mRNA genes, RT primers; miRNA, U6 rRNA, and miRNA-specific primers (Bulge-Loop miRNA quantitative PCR (qPCR) primers, RiboBio)]. Real-time PCR was carried out with SYBR Green I mix reagents (TaKaRa, Dalian, China) in a 20 μL reaction volume (10 μL SYBR Green I mix, 200 mM forward and reverse primer, 1 μL cDNA template) on a 7500 Real-Time PCR System (Applied Biosystems). Each reaction was run in triplicate; the threshold cycle (Ct) data were determined by fixed threshold settings, and the average Ct of triplicate PCR was calculated. The relative miRNA levels were confirmed using the comparative Ct method. The amount of internal control U6-related miRNA was calculated using the equation $2^{-\Delta\Delta Ct}$, in which $\Delta\Delta Ct = (Ct \text{ miRNA} - Ct \text{ U6}) \text{ tumor} - (Ct \text{ miRNA} - Ct \text{ U6}) \text{ control}$. The relative amount of *HSP90* mRNA was normalized to 18s rRNA using a method similar to the one described above.

2.5. Protein Extraction. Cells were washed three times with phosphate-buffered saline (PBS) chilled to 4°C. Whole-cell proteins were extracted with M-PER Mammalian Protein Extraction Reagent (78503, Thermo Fisher Scientific, USA) containing protease and phosphatase inhibitor (Roche, Germany) at 4°C for 30 min. Then, the samples were centrifuged at 14,000 ×g for 10 min, and the supernatant was transferred to a new tube for analysis.

2.6. Automated Western Immunoblotting. Before blotting, the protein was quantified using the bicinchoninic acid (BCA) method. Simple western immunoblotting was performed on a Peggy Sue system (ProteinSimple, California, USA) using a Size Separation Master Kit with Split Buffer (12–230 kDa) according to the manufacturer's standard instruction and

using anti-HSP90 (4877S, CST, USA) and anti- β -actin (4970S, CST, USA) antibodies. Compass software (version 2.7.1, ProteinSimple) was used to program the Peggy Sue and for presentation (and quantification) of the western immunoblots. Output data were displayed from the software-calculated average of seven exposures (5–480 s).

2.7. Luciferase Reporter Assay. We used luciferase reporter assays to verify whether miR-628-3p directly targets the *HSP90* gene and used a pHY-REPORT system (Hanyin Biotechnology, Shanghai, China). Briefly, 46-mer double-stranded oligonucleotides containing the predicted miRNA binding sites in *HSP90* were synthesized and ligated between the *XhoI* and *BamHI* restriction sites of the pHY-REPORT luciferase vector to establish the pLUC-HSP90 vector.

A549 cells were cotransfected with 50 nM miR-628-3p mimic or negative control (NC) mimic in 96-well plates containing 200 ng/ μ L pLUC-HSP90 or pLUC-mutHSP90 plasmid and 10 ng *Renilla* luciferase (internal transfection efficiency control). After 24-h transfection, luciferase activity was detected using a Dual-Luciferase Reporter Assay System (Promega, USA) according to the manufacturer's protocol. Luminescence intensity was read with a microplate luminometer using the corresponding Promega protocol. Transfections were performed in duplicate and repeated three times.

2.8. Wound Healing Assay. An *in vitro* wound healing assay was performed to measure the unidirectional migration of A549 cells. A549 cells (10×10^4 cells/mL) were seeded in 6-well plates and were allowed to grow for 24 h after being transfected with miR-628-3p mimic, NC mimic, or *HSP90* siRNAs. Then, the A549 monolayers were scratch-wounded in a straight line using a 10 μ L pipette tip when cells were 70–80% confluent. Immediately after wounding and after 24 h incubation, the cells were photographed under a microscope (Axio Observer A1, Zeiss, Germany). Migration was calculated as the area of A549 cells that had migrated from the injured edge in to the wound zone. At least four points in each of three random fields were examined for each of three independent wounds. The wound closure (%) was calculated as migrated cell surface area/total surface area \times 100.

2.9. Statistical Analysis. All data are presented as the mean \pm SEM and were analyzed using SPSS16 software. *p* values were calculated using Student's unpaired *t*-test (for two groups) or Z-way analysis of variance (for more than two groups). Statistical significance was taken at $p < 0.05$ and $p < 0.001$.

3. Results

3.1. Screening of miR-628-3p Target Genes. TargetScan (http://www.targetscan.org/mamm_31/) and NCBI (<https://www.ncbi.nlm.nih.gov/>) were used to analyze the information of multiple genes that can bind with miR-628-3p, and we selected nine genes with a high degree of integration: *FAS*, *APAF1*, *XIAP*, *HSP90*, *PIK3R3*, *RIPK1*, *CASP3*, *PMAIP1*, and *AKT2*.

To further screen target genes, miR-628-3p mimic was transfected into 293T cells, and quantitative RT-PCR (qRT-PCR) was used to detect the expression levels of the predicted

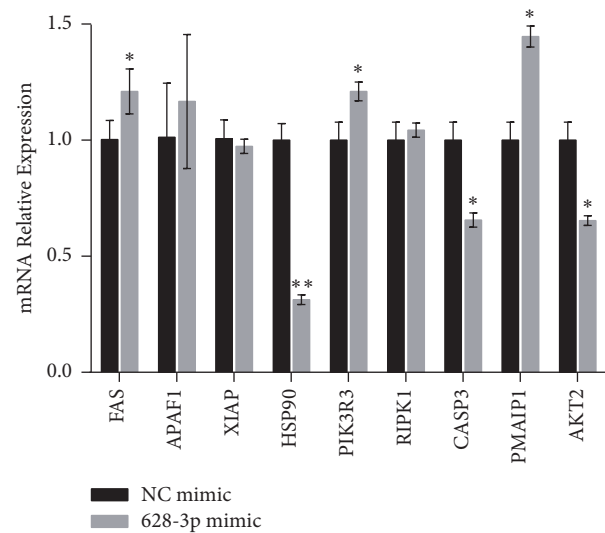


FIGURE 1: miR-628-3p and target gene expression in 293T cells. * $p < 0.05$, ** $p < 0.001$.

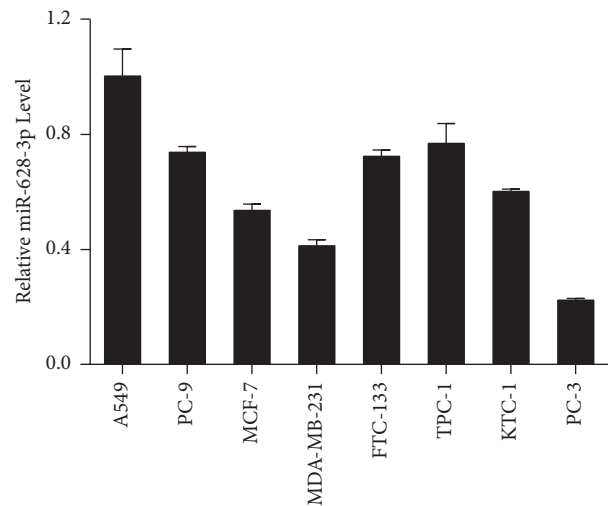


FIGURE 2: miR-628-3p is expressed differentially in different cancer cells. Relative levels of miR-628-3p in A549 cells were normalized against that of the other cell lines. $n = 5$, mean \pm SD.

genes as regulated by miR-628-3p. Figure 1 shows that *FAS*, *PIK3R3*, and *PMAIP1* were upregulated after miR-628-3p mimic transfection, while *HSP90*, *CASP3*, and *AKT1* were downregulated; among the three downregulated genes, *HSP90* was significantly downregulated, so it was selected for further research.

3.2. miR-628-3p Was Expressed High in A549 Cells. We used eight cancer cell lines (A549, PC-9, MCF-7, MDA-MB-231, FTC-133, TPC-1, KTC-1, and PC-3) to select a cell line in which to research the regulatory relationship between *HSP90* and miR-628-3p. miR-628-3p expression levels in the cell lines were compared using qRT-PCR. As miR-628-3p expression was higher in A549 cells than in the other cancer cells (Figure 2), we selected the A549 cell line for further research.

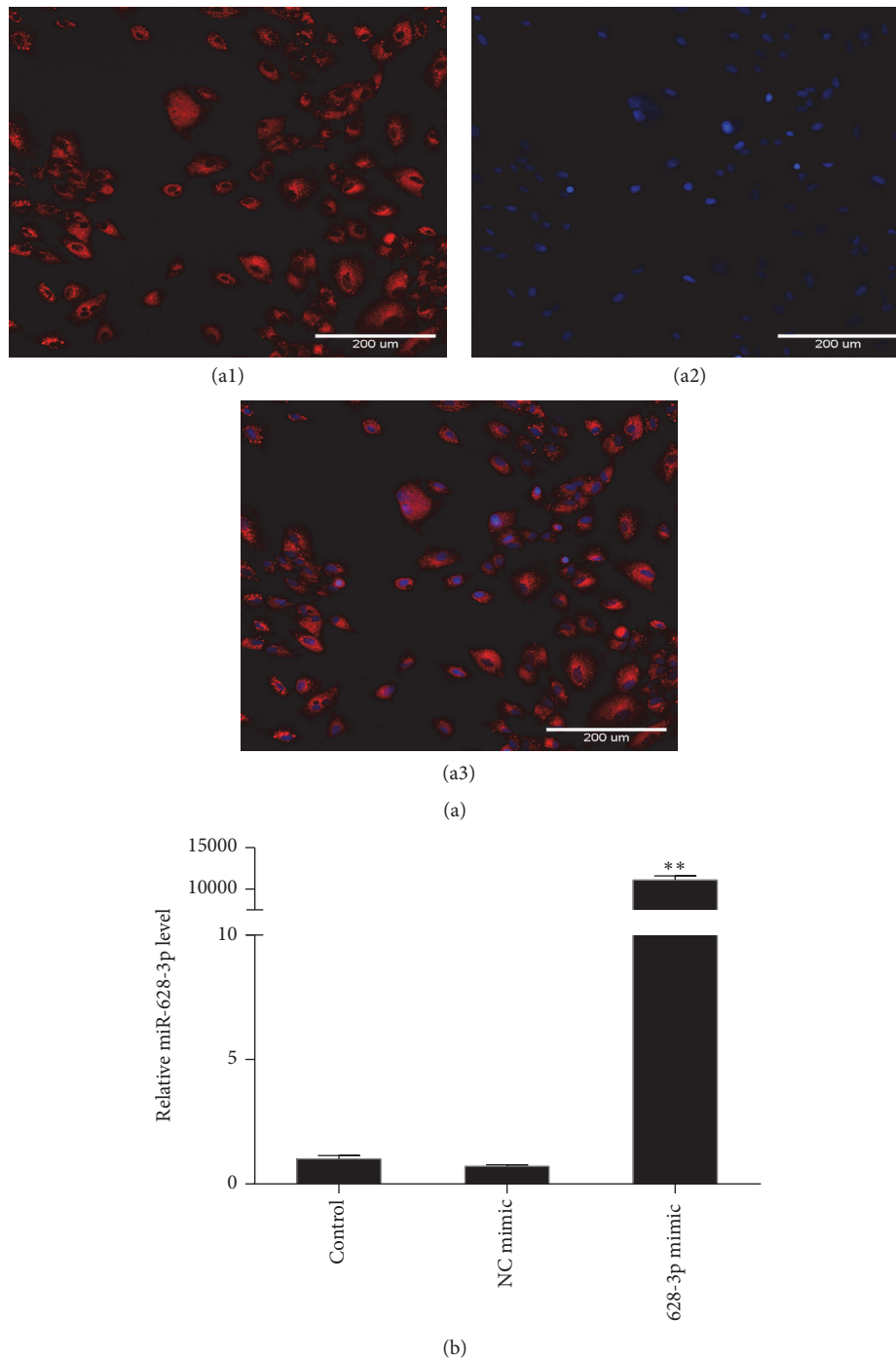


FIGURE 3: (a) Immunofluorescence images of A549 cells transfected with miR-628-3p. (b) Relative miR-628-3p expression levels after transfection in A549 cells. ** $p < 0.001$.

3.3. The Expression of miR-628-3p Was Efficient after Transfection in A549 Cells. Cy3 was used as an indicator to verify the vector transfection efficiency. After 24-h transfection, the cells were photographed by fluorescence microscopy, and each cell emitted red fluorescence (Figure 3(a)), indicating that vector transfection efficiency was very high.

To verify miR-628-3p expression, A549 cells were transfected with miR-628-3p mimic or NC mimic (vector control); the cells that were not transfected with vector were used as the blank control. miR-628-3p expression was detected by fluorescence qPCR (Figure 3(b)), which showed that cells transfected with miR-628-3p mimic had

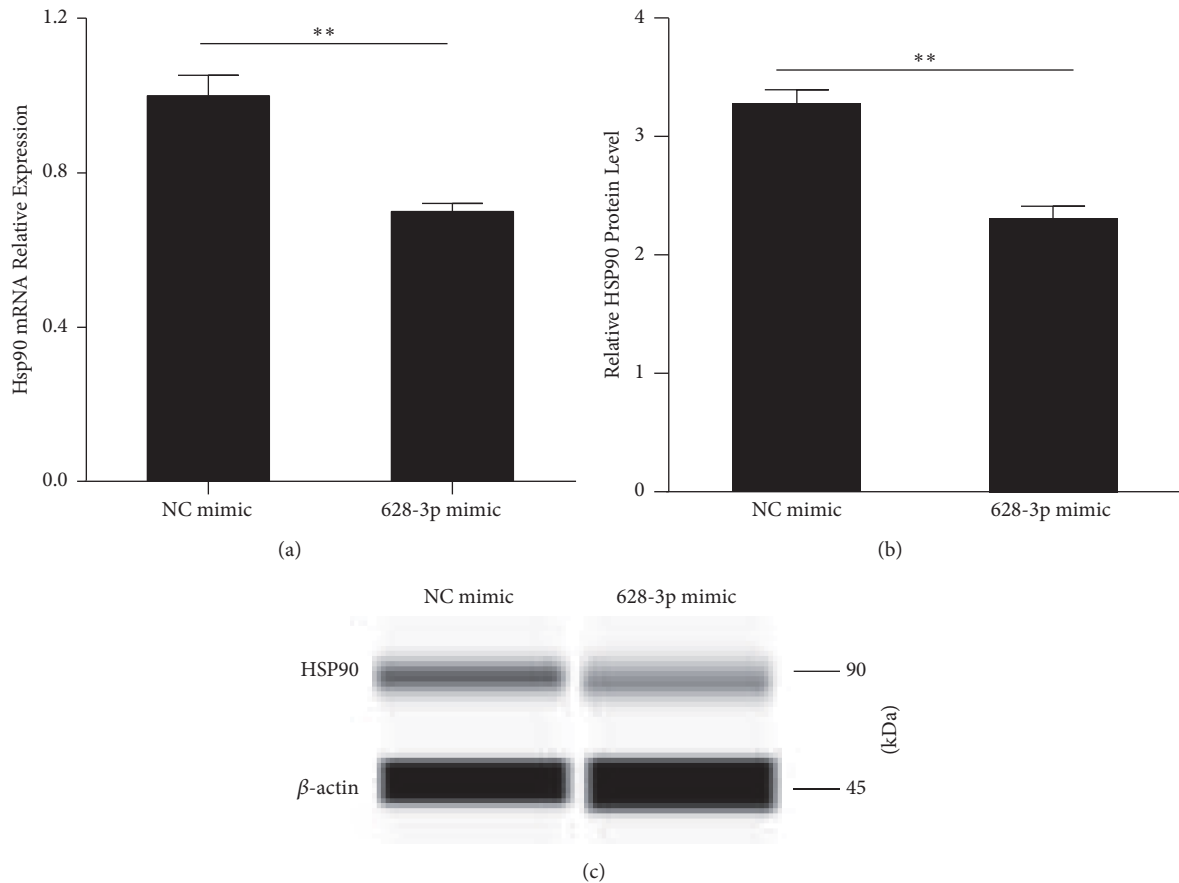


FIGURE 4: (a) *HSP90* mRNA was downregulated in A549 cells transfected with miR-628-3p mimic. The average mRNA expression from the NC group is designated as 1. (b, c) Western blot measurement of HSP90 protein levels after 48-h transfection with miR-628-3p mimic. ** $p < 0.001$.

far higher miR-628-3p expression than the control, indicating that miR-628-3p mimic expression was very efficient.

3.4. HSP90 Protein Was Downregulated in A549 Cells Transfected with miR-628-3p Mimic. Western blotting was used to analyze the regulatory relationship between miR-628-3p and HSP90 in A549 cells following transfection with miR-628-3p mimic or NC mimic. Immunoblotting with antibodies against HSP90 and β -actin showed that miR-628-3p obviously inhibited HSP90 expression (Figure 4), indicating a negative regulatory relationship between miR-628-3p and HSP90.

3.5. miR-628-3p Regulated HSP90 Expression by Targeting Its 3' UTR. Luciferase assay was used to confirm whether the 3' untranslated region (3' UTR) of the predicted target genes had putative miR-628-3p-binding sites. *HSP90* was selected as a potential target gene of miR-628-3p. TargetScan predicted the consequential pairing of the *HSP90* 3' UTR and miR-628-3p (Figure 5(a)), where the dual-luciferase

reporter assay showed that miR-628-3p directly bound to the *HSP90* 3' UTR in A549 cells. To test the *HSP90* putative binding site, we generated a luciferase reporter (pLUC-*HSP90*) and a mutant *HSP90* construct (pLUC-mut*HSP90*) in which the *HSP90* 3' UTR was altered using a site-directed mutagenesis kit. miR-628-3p significantly regulated the luciferase activity of the *HSP90* construct (Figure 5(b)), whereas the mutant construct did not generate luciferase activity. These results indicate that miR-628-3p may regulate *HSP90* expression by targeting its 3' UTR.

3.6. siRNA Transfection Interfered with Downregulated HSP90 Expression. Three siRNAs targeting the *HSP90* gene were transfected into the A549 cells, and the relative mRNA expression was measured 48 h after transfection. siRNA2 is better than the other two siRNAs (Figure 6(a)). HSP90 protein expression was detected by western blotting; siRNA2 interference downregulated HSP90 expression significantly as compared to the other two siRNAs (Figures 6(b) and 6(c)) significantly.

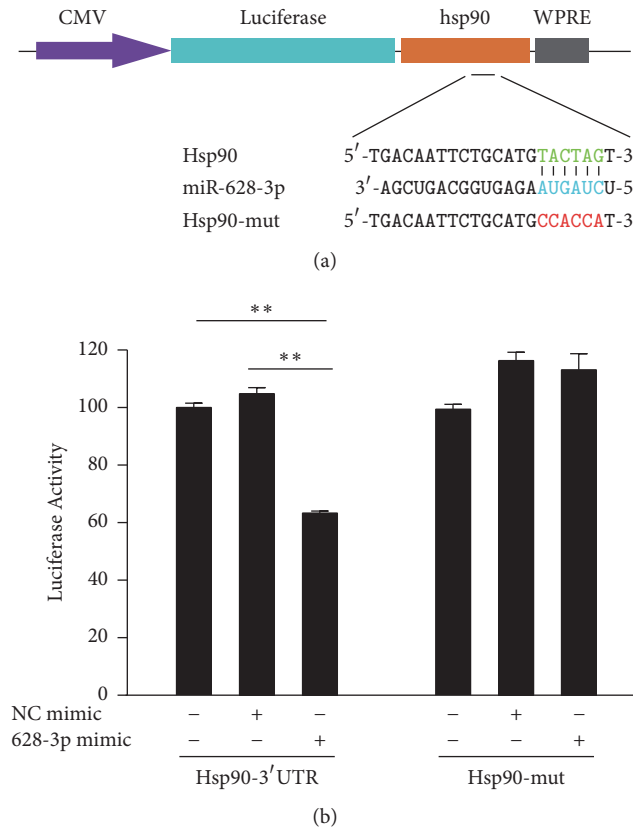


FIGURE 5: *miR-628-3p* directly regulates *HSP90* expression in A549 cells by targeting the *HSP90* 3' UTR. (a) Predicted consequential pairing of *HSP90* 3' UTR and *miR-628-3p* by TargetScan. (b) Luciferase assay in A549 cells. pLUC-*HSP90* vector was cotransfected with *miR-628-3p* mimic or NC mimic. Luciferase activity in pLUC-*HSP90* A549 cells was significantly decreased following ectopic expression of *miR-628-3p* mimic. ** $p < 0.001$.

3.7. *miR-628-3p* Induced Apoptosis in A549 Cell. The rate of apoptosis in the A549 cells was measured by flow cytometry with annexin V and PI staining following 48-h transfection. Figures 7(a) and 7(b) show the percentage of early or late apoptotic cells following transfection with NC mimic and *miR-628-3p* mimic, and Figures 7(c) and 7(d) show the percentage of early or late apoptotic cells following transfection with the control and the three *HSP90* siRNAs. Transfection with *miR-628-3p* mimic and the *HSP90* siRNAs induced apoptosis in the A549 cells.

3.8. *miR-628-3p* Inhibited Migration in A549 Cells. To understand how *miR-628-3p* affects cell migration, A549 cells were transfected with *HSP90* siRNAs or *miR-628-3p* mimic. Transfection with *miR-628-3p* mimic inhibited A549 cell migration (Figures 8(a) and 8(b)), as did transfection with the *HSP90* siRNAs (Figures 8(c) and 8(d)), suggesting that *miR-628-3p* overexpression and interference with *HSP90* expression have the same effect of decreasing A549 cell migration.

4. Discussion

The 2018 US cancer statistics reported an estimated 1,735,350 new cases and 609,640 new deaths from lung and branches cancer in the United States, indicating that lung and branches cancer is the leading cause of death among all tumors in the world [17]. Although the development of diagnostic and prognostic techniques has improved the survival of patients with lung cancer, most patients are diagnosed at the late stage. miRNAs function as tumor suppressors or oncogenes in various human cancers, including lung cancer [18]. Therefore, identifying the tumor-associated miRNAs and their target genes that underlie lung carcinogenesis might reveal novel therapeutic targets.

Some studies have indicated that miRNAs could play an important role in the initiation and progression of lung cancer; for example, overexpression of *miR-21* promotes radiation-resistance of NSCLC [19], *miR-125b* regulates human NSCLC cell apoptosis via the phosphatidylinositol 3-kinase/AKT/glycogen synthase kinase 3 β

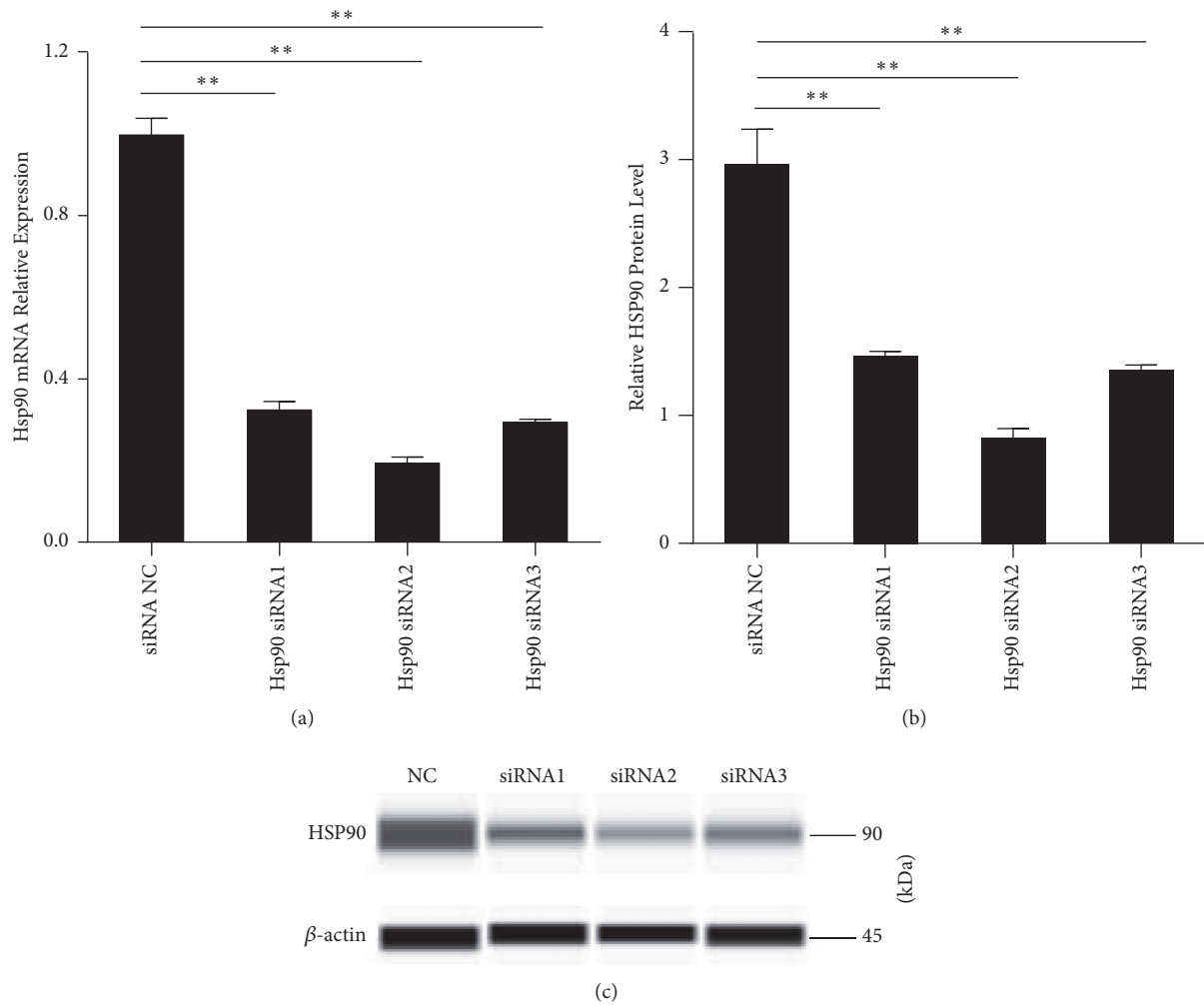


FIGURE 6: (a) qRT-PCR measurement of *HSP90* relative expression after 48-h siRNA transfection. *HSP90* mRNA was downregulated in the siRNA-transfected A549 cells. The average *MIR628-3P* mRNA expression from the NC group is designated as 1. (b, c) Western blot measurement of HSP90 protein after 48-h transfection. HSP90 protein was downregulated in the siRNA-transfected A549 cells. $^{***}P < 0.001$.

(PI3K/AKT/GSK3 β) signaling pathway [20], and miR-9 regulates NSCLC cell invasion and migration by targeting eukaryotic translation initiation factor 5A2 (EIF5A2) [21]; in addition, miR-628-3p and miR-425-3p expression is significantly higher in early-stage lung cancer, and miR-532 expression is significantly lower than in the other types [15]. However, how miR-628-3p functions in lung cancer and which gene it targets are not known. Based on the TargetScan prediction, we selected nine genes with high degree of integration that can bind with miR-628-3p; among the three downregulated genes, *AKT1* has an important role in lung carcinogenesis, and depletion of *AKT1* has antiproliferative and antimigratory effects [22]. miR-9500 represses lung tumorigenesis and metastasis by targeting *AKT1* [23]. *CASP3* is a previously unidentified

target of miR-137 and plays an essential role in miR-137-mediated lung cancer progression [24]. HSP90 plays an essential role in maintaining cellular protein homeostasis by acting as a molecular chaperone to aid in the folding and intracellular trafficking of its protein clients [25]. The in silico prediction indicated that *HSP90* was a potential target of miR-628-3p, and it was significantly downregulated by miR-628-3p, so *HSP90* was selected for further study.

We found that siRNA silencing of *HSP90* or *HSP90* downregulation by miR-628-3p overexpression promoted A549 cell apoptosis and inhibited A549 cell migration. qRT-PCR and western blotting confirmed that miR-628-3p mimic transfection into A549 cells downregulated *HSP90* expression, as did *HSP90* siRNA transfection. In addition,

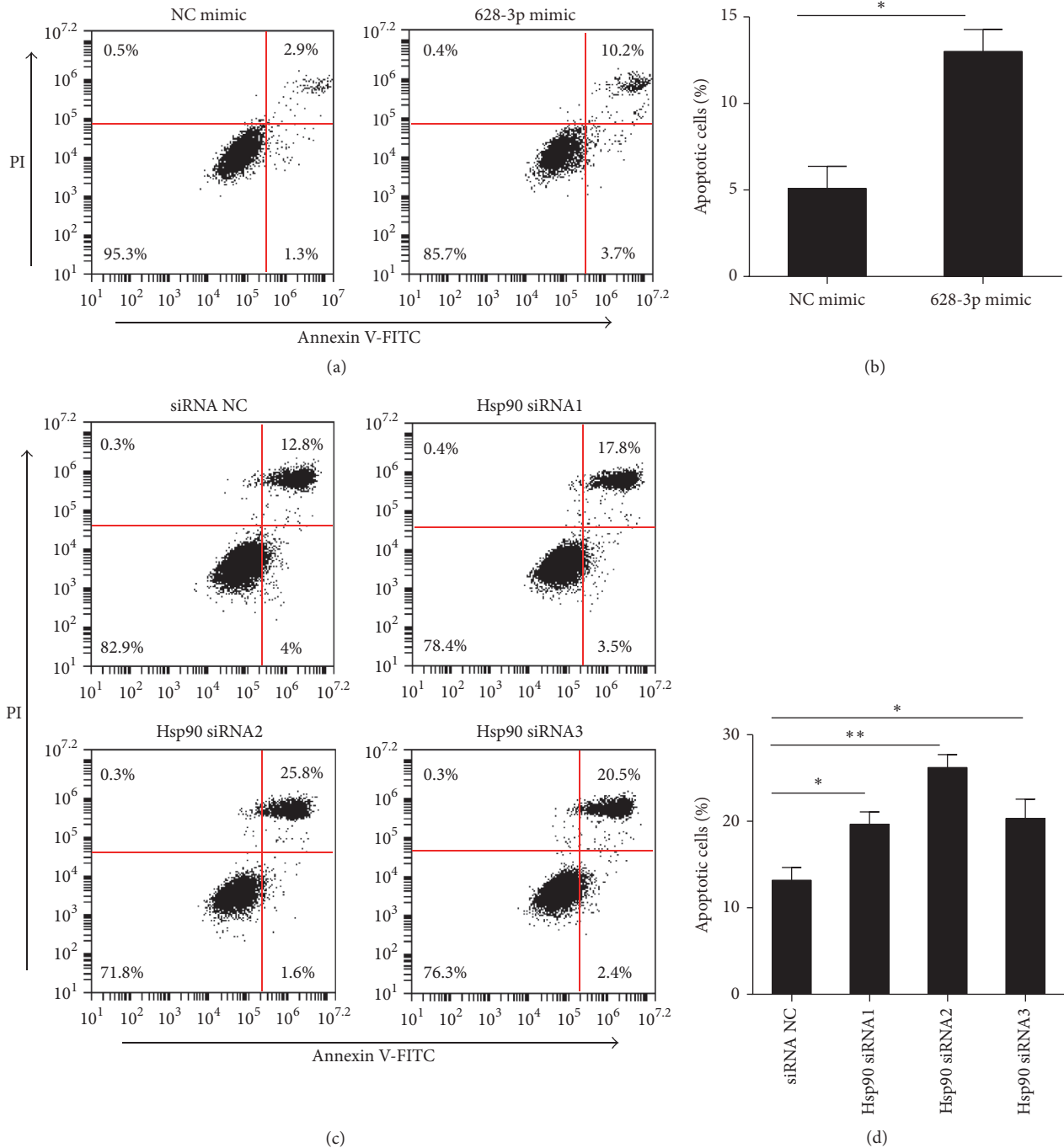


FIGURE 7: *HSP90* expression levels affect A549 cell apoptosis. (a, b) miR-628-3p mimic transfection induced apoptosis in A549 cells. (c, d) *HSP90* siRNA transfection induced apoptosis in A549 cells. * $p < 0.05$, ** $p < 0.001$.

the luciferase assay indicated that miR-628-3p may regulate *HSP90* expression by targeting its 3' UTR.

5. Conclusion

In summary, our results indicate that miR-628-3p promotes A549 cell apoptosis and inhibits A549 cell migration by negatively regulating *HSP90*. Further studies should

consider the relationship between miR-628-3p and *HSP90*, which may reveal a novel therapeutic strategy for lung cancer.

Data Availability

The data used to support the findings of this study are available from the corresponding author upon request.

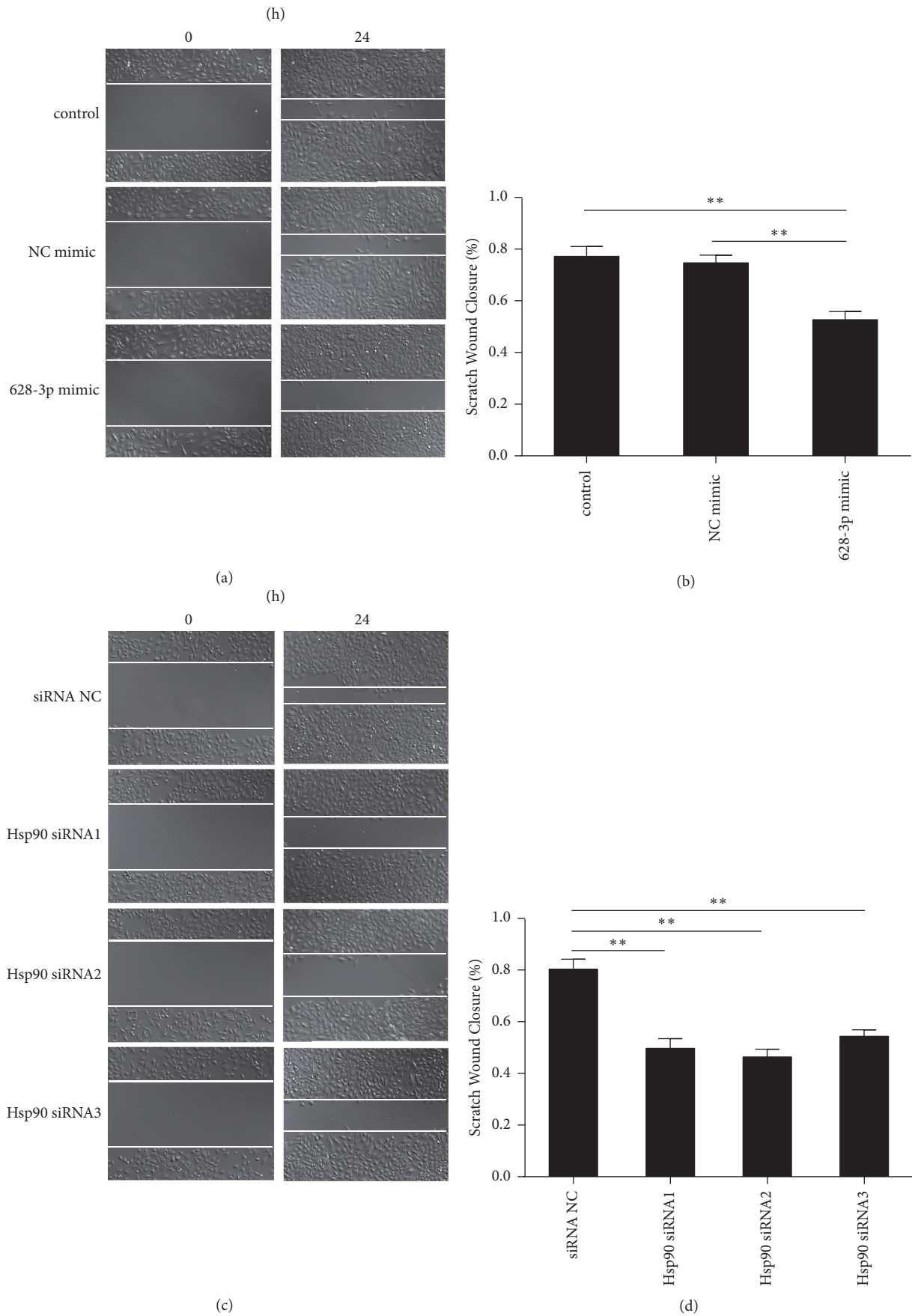


FIGURE 8: RNA interference of HSP90 inhibits wound healing. (a) A549 cells transfected with control, NC mimic, and miR-628-3p mimic photographed at 0 h and 24 h after wounding. (b) Scratch wound closure in A549 cells transfected with control, NC mimic, and miR-628-3p mimic. (c) A549 cells transfected with NC or HSP90 siRNAs photographed at 0 h and 24 h after wounding. (d) Scratch wound closure in A549 cells transfected with NC or HSP90 siRNAs. $**p < 0.001$.

Conflicts of Interest

The authors declare that there are no conflicts of interest regarding the publication of this paper.

Acknowledgments

This work was funded by Science Foundation of Zhejiang Chinese Medical University (no. 2018ZZ12) and the Traditional Chinese Medicine Science Funding of Zhejiang Province (no. 2017ZA064).

References

- [1] L. Yan, J. Ma, Y. Zhu et al., “miR-24-3p promotes cell migration and proliferation in lung cancer by targeting SOX7,” *Journal of Cellular Biochemistry*, 2017.
- [2] S. S. Ramalingam, T. K. Owonikoko, and F. R. Khuri, “Lung cancer: new biological insights and recent therapeutic advances,” *CA: A Cancer Journal for Clinicians*, vol. 61, no. 2, pp. 91–112, 2011.
- [3] S. Al-Saad, E. Richardsen, T. K. Kilvaer et al., “The impact of MET, IGF-1, IGF1R expression and EGFR mutations on survival of patients with non-small-cell lung cancer,” *PLoS ONE*, vol. 12, no. 7, article e0181527, 2017.
- [4] V. Ludovini, A. Flacco, and F. Bianconi, “Concomitant high gene copy number and protein overexpression of IGF1R and EGFR negatively affect disease-free survival of surgically resected non-small-cell-lung cancer patients,” *Cancer Chemotherapy and Pharmacology*, vol. 71, no. 3, pp. 671–680, 2013.
- [5] J. T. Mendell and E. N. Olson, “MicroRNAs in stress signaling and human disease,” *Cell*, vol. 148, no. 6, pp. 1172–1187, 2012.
- [6] H. Lewis, R. Lance, D. Troyer et al., “miR-888 is an expressed prostatic secretions-derived microRNA that promotes prostate cell growth and migration,” *Cell Cycle*, vol. 13, no. 2, pp. 227–239, 2014.
- [7] P. S. Chen, J. L. Su, and M. C. Hung, “Dysregulation of microRNAs in cancer,” *Journal of Biomedical Science*, vol. 19, article 90, 2012.
- [8] E. A. Elghoroury, H. G. ElDine, and S. A. Kamel, “Evaluation of miRNA-21 and miRNA Let-7 as Prognostic Markers in Patients With Breast Cancer,” *Clinical Breast Cancer*, 2017.
- [9] S. Han, J. Zhu, and Y. Zhang, “miR-144 Potentially Suppresses Proliferation and Migration of Ovarian Cancer Cells by Targeting RUNX1,” *Medical Science Monitor Basic Research*, vol. 24, pp. 40–46, 2018.
- [10] A. Li, J. Yu, H. Kim et al., “MicroRNA array analysis finds elevated serum miR-1290 accurately distinguishes patients with low-stage pancreatic cancer from healthy and disease controls,” *Clinical Cancer Research*, vol. 19, no. 13, pp. 3600–3610, 2013.
- [11] Y. Xu, Y.-F. Han, S.-J. Zhu, J.-D. Dong, and B. Ye, “MiRNA-148a inhibits cell growth of papillary thyroid cancer through STAT3 and PI3K/AKT signaling pathways,” *Oncology Reports*, vol. 38, no. 5, pp. 3085–3093, 2017.
- [12] J. Hamfjord, A. M. Stangeland, T. Hughes et al., “Differential Expression of miRNAs in Colorectal Cancer: Comparison of Paired Tumor Tissue and Adjacent Normal Mucosa Using High-Throughput Sequencing,” *PLoS ONE*, vol. 7, no. 4, article e34150, 2012.
- [13] E. Baltruskeviciene, D. Schweigert, V. Stankevicius et al., “Down-regulation of miRNA-148a and miRNA-625-3p in colorectal cancer is associated with tumor budding,” *BMC Cancer*, vol. 17, no. 1, article no. 607, 2017.
- [14] M. I. Qadir and A. Faheem, “miRNA: A Diagnostic and Therapeutic Tool for Pancreatic Cancer,” *Critical Reviews in Eukaryotic Gene Expression*, vol. 27, no. 3, pp. 197–204, 2017.
- [15] Y. Wang, H. Zhao, X. Gao et al., “Identification of a three-miRNA signature as a blood-borne diagnostic marker for early diagnosis of lung adenocarcinoma,” *Oncotarget*, vol. 7, no. 18, pp. 26070–26086, 2016.
- [16] Y. K. Shi, X. Q. Liu, J. T. Lou et al., “Plasma Levels of Heat Shock Protein 90 Alpha Associated with Lung Cancer Development and Treatment Responses,” *Clinical Cancer Research*, vol. 20, no. 23, pp. 6016–6022, 2014.
- [17] R. L. Siegel, K. D. Miller, and D. V. M. Ahmedin Jemal, “Cancer statistics, 2018,” *CA: A Cancer Journal for Clinicians*, vol. 68, no. 1, pp. 7–30, 2018.
- [18] M. Usó, E. Jantus-Lewintre, R. Sirera, R. M. Bremnes, and C. Camps, “MiRNA detection methods and clinical implications in lung cancer,” *Future Oncology*, vol. 10, no. 14, pp. 2279–2292, 2014.
- [19] X. C. Wang, W. Wang, Z. B. Zhang et al., “Overexpression of miRNA-21 promotes radiation-resistance of non-small cell lung cancer,” *Journal of Radiation Oncology*, vol. 8, article 146, 2013.
- [20] Y. Y. Wang, M. Zhao, J. Y. Liu et al., “miRNA-125b regulates apoptosis of human non-small cell lung cancer via the PI3K/Akt/GSK3 beta signaling pathway,” *Oncology Reports*, vol. 38, no. 3, pp. 1715–1723, 2017.
- [21] G. D. Xu, G. F. Shao, Q. L. Pan et al., “MicroRNA-9 regulates non-small cell lung cancer cell invasion and migration by targeting eukaryotic translation initiation factor 5A2,” *American Journal of Translational Research*, vol. 9, no. 2, pp. 478–488, 2017.
- [22] C. X. Xu, H. Jin, J. Y. Shin et al., “Roles of protein kinase B/Akt in lung cancer,” *Frontiers in Bioscience (Elite Ed.)*, vol. 2, pp. 1472–1484, 2010.
- [23] J. K. Yoo, H. Y. Jung, J. M. Lee et al., “The novel miR-9500 regulates the proliferation and migration of human lung cancer cells by targeting Akt1,” *Cell Death Differentiation*, vol. 21, no. 7, pp. 1150–1159, 2014.
- [24] T. J. Su, W. H. Ku, H. Y. Chen et al., “Oncogenic miR-137 contributes to cisplatin resistance via repressing CASP3 in lung adenocarcinoma,” *American Journal of Cancer Research*, vol. 6, no. 6, pp. 1317–1330, 2016.
- [25] L. H. Pearl and C. Prodromou, “Structure and mechanism of the Hsp90 molecular chaperone machinery,” *Annual Review of Biochemistry*, vol. 75, pp. 271–294, 2006.

Research Article

A Predictive Model to Determine the Pattern of Nodal Metastasis in Oral Squamous Cell Carcinoma

B. S. M. S. Siriwardena ¹, I. K. Rambukewela,¹ T. N. Pitakotuwege,¹
M. N. G. P. K. Udagama,¹ P. V. R. Kumarasiri,² and W. M. Tilakaratne¹

¹Department of Oral Pathology, Faculty of Dental Sciences, University of Peradeniya, Peradeniya, Sri Lanka

²Department of Community Medicine, Faculty of Medicine, University of Peradeniya, Peradeniya, Sri Lanka

Correspondence should be addressed to B. S. M. S. Siriwardena; samadarani@yahoo.com

Received 1 December 2017; Revised 5 March 2018; Accepted 5 April 2018; Published 13 May 2018

Academic Editor: Franco M. Buonaguro

Copyright © 2018 B. S. M. S. Siriwardena et al. This is an open access article distributed under the Creative Commons Attribution License, which permits unrestricted use, distribution, and reproduction in any medium, provided the original work is properly cited.

Background. Developing histological prediction models that estimate the probability of developing metastatic deposit will help clinicians to identify individuals who need either radical or prophylactic neck dissection, which leads to better prognosis. Identification of accurate predictive models in oral cancer is important to overcome extensive prophylactic surgical management for neck nodes. Therefore, accurate prediction of metastasis in oral cancer would have an immediate clinical impact, especially to avoid unnecessary radical treatment of patients who are at a low risk of metastasis. **Methods.** Histologically confirmed OSCC cases with neck dissection were used. Interrelation of demographic, clinical, and histological data was done using univariate and multivariate analysis. **Results.** 465 cases were used and presence of metastasis and extracapsular invasion were statistically well correlated with level of differentiation ($p < 0.001$) and pattern of invasion ($p < 0.001$). Multivariate analysis showed level of differentiation, pattern of invasion, and stage as predictors of metastasis. **Conclusions.** The proposed predictive model may provide some guidance for maxillofacial surgeons to decide the appropriate treatment plan for OSCC, especially in developing countries. This model appears to be reliable and simple and may guide surgeons in planning surgical management of neck nodes.

1. Introduction

Developing histological prediction models that estimate the probability of developing metastatic deposit will help clinicians to draw effective treatment plans. That allows the clinician to identify individuals who need either radical or prophylactic neck dissection, which prevents unnecessary undertreatment or overtreatment leading to better prognosis. Oral squamous cell carcinoma (OSCC) is the most frequent malignant tumour of the head and neck region, representing the sixth leading cancer by incidence, and 500000 new cases are reported every year worldwide [1]. In Sri Lanka, it is the commonest cancer among men [2]. Majority of OSCC patients seek treatment at the advanced stage of the disease with subsequent poor prognosis.

Various studies using different statistical models have struggled to predict patients' metastasis and survival by analyzing the relationships between clinicopathological data and

biomarkers (either newly developed or existing ones). However, it is difficult to find out practically successful biomarkers as the patients' survival is related to multiple factors. Therefore, current research direction is to identify various histological characteristics of the tumour which predict prognosis.

Studies indicated that histological tumour differentiation and lymph node metastasis [3] could be good predictors when designing therapeutic strategies for OSCC. Therefore, it is worthwhile to evaluate these potential biological properties and provide predictive information of behavior of the cancer preoperatively.

We have shown with our previous studies that pattern of invasion at the advancing front of the tumour and level of differentiation are some of the individual histological parameters that help to predict regional lymph node metastasis [4, 5]. Apart from histological parameters, tumour staging is one of the commonly used models when deciding the treatment plan [6].

TABLE 1: Relationship of tumour differentiation with age, sex, and tumour site.

	Well-differentiated SCC (%)	Moderately differentiated SCC (%)	Poorly differentiated SCC (%)	Total
Age groups				
20–40	9 (45)	11 (50)	1 (5)	21
41–50	34 (38)	49 (55)	6 (7)	89
51–60	88 (50)	70 (40)	18 (10)	176
61–70	71 (53)	57 (42)	7 (5)	135
71–86	23 (52)	19 (43)	2 (6)	44
Gender				
Male	153	153	23	329
Female	72	53	11	136
Primary site				
BM	104 (60)	58 (33.5)	11 (6.4)	173
FOM	19 (44.2)	24 (55.8)	0 (0)	43
LALR	47 (50.5)	44 (47.3)	2 (2.2)	93
P	6 (25)	11 (45.8)	7 (29)	24
T	43 (38.4)	57 (50.9)	12 (10.7)	112
UALR	6 (30)	12 (60)	2 (10)	20

BM: buccal mucosa, FOM: floor of the mouth, LALR: lower alveolar ridge, P: palate, T: tongue, UALR: upper alveolar ridge.

Despite the fact that significant advances were achieved in surgery and chemotherapy over the past years, OSCC still shows a poor prognosis and lower survival rates [5, 7, 8]. If we have a model that predicts the behavior of the tumour using histopathological characteristics in combination with tumour stage, clinician is in a position to customize their treatment plan which will enhance the survival.

Therefore, we tried to develop a model using clinical and histopathological parameters to predict nodal status in OSCC, as it is difficult to incorporate molecular investigations in daily reporting practices due to lack of facilities in the developing parts of the world, where oral cancer's incidence is much higher.

2. Materials and Methods

We used data from the database of the country's only Head and Neck Pathology Centre, Faculty of Dental Sciences, University of Peradeniya, Sri Lanka. In the present study, we included all the patients with histologically confirmed OSCC who had undergone surgical resection with neck dissection from 1999 to 2012. The tumours have been staged according to TNM classification of UICC (Union for International Cancer Control) [9]. Ethical clearance for the study was obtained from the Faculty Research and Ethical Review Committee (certificate of ethical clearance, number FDS-FRC/2013/01). Informed consent was obtained from all individual participants included in the study before the surgical procedure.

Data in relation to age at first diagnosis, gender, subsites of cancer (buccal mucosa, tongue, upper alveolar ridge, lower alveolar ridge, palate, and floor of the mouth), and clinical stage were collected from patient records. Based on the histopathological reports, pattern of invasion (pattern I, large islands; pattern II, small islands; pattern III, thin strands;

and pattern IV, individual cells), level of tumour differentiation (well-differentiated squamous cell carcinoma, moderately differentiated squamous cell carcinoma, or poorly differentiated squamous cell carcinoma), and nodal status (whether the node is positive or negative for tumour and the presence or absence of extracapsular spread in each node in each level) were recorded. Tumour differentiation was performed according to Bryne and Anneroth's grading criteria that were described in one of our previous studies [5]. The whole group was further divided into young (<40 years) and old (>41 years) groups. This was based on the available literature including our own work [5–7]. Patients with inadequate data such as age gender site and histological materials were excluded from the study. Due to inadequate numbers to perform statistical analysis, tumours from lip, commissure, and retromolar region and histological subtypes such as basaloid, adenoid, adenosquamous, and spindle cell squamous cell carcinomas were also excluded from the study.

Univariate analysis was performed between each two characteristics. Chi Square test was also performed. Multivariate logistic regression was performed to develop the predictive model to identify the level of nodal metastasis. Data were analyzed using SPSS predictive analytics software version 11 for windows.

3. Results

A total of 465 cases with all necessary data were selected for the study. There were 329 males and 136 females with a M : F ratio of 2.6 : 1. The age ranges from 24 to 86 years with a mean age of 57.8 years. More than 50% of the cases were in the age group of 50–70 years at the time of diagnosis and majority of them were males. Buccal mucosa (37.2%) and tongue (24.1%) were the dominant subsites of OSCC in this study (Table 1).

TABLE 2: The relationship between clinicopathological parameters and nodal status in patients with OSCC.

Variable	Frequency (%)	Positive nodes (%)	Extra capsular invasion (%)	<i>p</i> value*
Age				
20–40	21 (4.5)	11 (52.3)	11	NS
41–50	90 (14.35)	42 (46.6)	31	
51–60	177 (38.06)	82 (46.3)	60	
61–70	133 (28.6)	54 (40.6)	40	
71–86	44 (9.4)	19 (43.18)	17	
Gender				
Male	329 (69.8)	149 (45.3)	110	NS
Female	136 (29.2)	60 (44.1)	50	
Primary site				
BM	173 (37.2)	66 (38.15)	53	NS
FOM	43 (9.2)	19 (4.1)	12	
LLR	93 (20)	39 (41.9)	28	
P	24 (5.2)	21 (87.5)	19	
T	112 (24.1)	52 (46.4)	39	
UALR	20 (4.3)	12 (60)	9	
Tumour stage				
1	17 (5.68)	0 (0)	0	0.001
2	54 (18.06)	1 (1.8)	1	
3	98 (32.77)	49 (50)	30	
4	130 (43.47)	87 (66.9)	78	
Tumour differentiation				
Well	225 (48.4)	51 (26.7)	36	0.001
Moderate	206 (44.3)	124 (60.2)	92	
Poor	34 (7.3)	23 (67.7)	20	
Invasive front				
Inv. I	7 (1.5)	0 (0)	0	0.001
Inv. II	142 (30.53)	28 (19.7)	17	
Inv. III	200 (43.01)	102 (51)	76	
Inv. IV	113 (24.3)	79 (69.91)	67	

*Chi-square test. NS: not significant.

Tumour staging is one of the most important factors to predict prognosis. Although documented data is sparse in Sri Lanka, most OSCC patients seek treatment usually in the late stage of the disease. In this study, it was revealed that 43.5% and 32.8% of the patients presented to clinicians at stages 4 and 3, respectively. Well-differentiated and moderately differentiated tumours were significantly common compared to poorly differentiated cancers that represented only 7% of the total sample (Table 2).

The sample was divided into two groups depending on the age as young (<40 years) and old (>40 years). In the present study, more than 95% of the patients were above 40 years of age, which shows that OSCC is mostly a disease of the elderly. Most of the younger group had moderately differentiated tumours compared to the older group who had equal numbers of well-differentiated and moderately differentiated cancers (Table 1). It is interesting to note that the majority of young patients did not have associated habits and the common sites recorded were tongue and floor of the mouth. In the patients with the history of betel chewing habit,

commonly affected site was buccal mucosa followed by lower alveolar ridge irrespective of the age.

Pattern of invasion has an impact on prognosis and was first described by Jakobsson et al. [8] in 1973. We have shown the reliability of predicting metastasis with pattern of invasion in our previous studies [5, 9]. The previous results can be further confirmed with the present study as the sample size is much larger. The present study found the majority of tongue, floor of the mouth, and lower alveolar ridge tumours to have invasive pattern III compared to other sites (Table 2 and Figure 1). Pattern of invasion and metastasis showed statistically significant association ($p < 0.001$) with patterns III and IV revealing higher metastatic rates compared to patterns I and II (Table 2). The relationship between clinicopathological factors and nodal metastases is summarized in Table 2. Presence of metastasis and extracapsular invasion were statistically well correlated with level of differentiation ($p < 0.001$) and pattern of invasion ($p < 0.001$).

We used a multivariate logistic regression model to identify the predictive factors of metastasis. This was done using

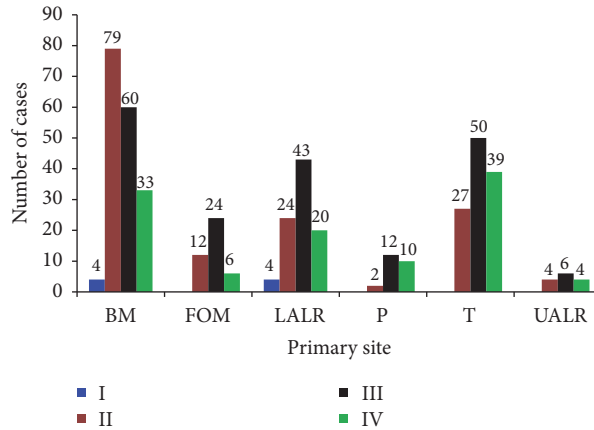


FIGURE 1: BM: buccal mucosa, FOM: floor of the mouth, LALR: lower alveolar ridge, P: palate, T: tongue, UALR: upper alveolar ridge. I, II, III, and IV: pattern of invasion types at the advancing front of the tumour.

TABLE 3: The final regression model identifies differentiation, invasion, and stage as the predictors of the level of positivity in OSCC.

Model		Coefficients ^a		Standardized coefficients Beta	t	Sig.
		Unstandardized coefficients B	Std. error			
(1)	(Constant)	-1.182	.231		-5.123	.000
	stage	.711	.071	.505	10.071	.000
(2)	(Constant)	-2.605	.293		-8.902	.000
	Stage	.620	.067	.440	9.320	.000
	Invasion	.573	.081	.336	7.113	.000
(3)	(Constant)	-2.642	.291		-9.081	.000
	Stage	.611	.066	.434	9.226	.000
	Invasion	.446	.097	.261	4.600	.000
	Differentia	.268	.116	.131	2.322	.021

^aDependent variable: level of nodal positivity. Adjusted R-squared = 0.368; the final regression model (3).

the following variables: invasive pattern, level of differentiation, and tumour stage (Table 3). Level of nodal positivity (levels I–V) was taken as the dependent variable. Although these parameters were proven individually as helpful parameters to plan treatment, there are no documented studies combining these factors to describe a predictive model. We have tried to describe a predictive model using regression analysis in relation to the primary sites of buccal mucosa (Table 4) and tongue. Due to inadequate numbers, only buccal mucosa was considered for the predictive model. A few possible treatment plans for different levels of parameters should be as follows according to the prediction model. It is shown that if a buccal mucosal tumour is in stage 1 (T1N0) or 2 (T2N0) and histological pattern of invasion III or IV predicted nodal positivity goes up to cervical nodal level 3 (Table 4), then the proposed surgical treatment plan should be a selective neck dissection including levels I, II, and III as the minimum. Similarly, for stage 4 buccal cancers with infiltrating pattern IV, the treatment plan should be removal of cervical lymph nodes up to level 5. Further, to elaborate the model, if tumour shows invasive pattern I but stage 3, only up to level I clearance is adequate. Therefore, the

proposed predictive model may provide some guidance for maxillofacial surgeons to decide treatment plan, especially in developing countries, where sophisticated diagnostic tools are least available. The number of cases was inadequate to perform the same for other subsites.

4. Discussion

The prognosis of patients with OSCC is directly related to the presence of lymph node metastasis [9]. A significant percentage of patients with early stages of OSCC have a poor prognosis despite the small size of the tumour [10, 11]. Hence, TNM staging system used in clinical practice does not provide information on the biological characteristics and aggressive clinical behavior of oral SCC.

However, the relationship between prognosis and clinicopathological features of OSCC has not been fully explored in Sri Lankan patients. If it is possible to elucidate potential clinicopathological parameters or predictors of nodal metastasis, they could be used to identify patients for management of neck nodes. Therefore, accurate prediction of metastasis in OSCC would have an immediate clinical impact, especially

TABLE 4: A model developed to predict lymph node metastasis in patients with oral squamous cell carcinoma of buccal mucosa.

	Level 1	Level 2	Level 3	Level 4	Level 5
IP 1 + S 3	✓				
IP 2 + S 1	✓				
IP 2 + S 2	✓				
IP 1 + S 4		✓			
IP 2 + S 3		✓			
IP 3 + S 1		✓			
IP 3 + S 2		✓			
IP 2 + S 4			✓		
IP 3 + S 3			✓		
IP 4 + S 1			✓		
IP 4 + S 2			✓		
IP 3 + S 4				✓	
IP 4 + S 3				✓	
IP 4 + S 4					✓

IP: pattern of invasion; S: stage of the tumour.

to avoid unnecessary radical treatment of patients leading to severe morbidity, despite the fact that they are at a low risk of metastasis.

Oral squamous cell carcinoma displays a wide range of metastatic behaviors that cannot be predicted by a single feature alone such as tumour size, histology, or even individual gene or protein expression/activity. Furthermore, the presence or absence of nodal metastasis consistently shows a statistical correlation with survival [12–16]. Metastasis is a process whereby genetic instability of the primary tumour fuels cell heterogeneity, allowing for a few tumour cells to disseminate cancer at distance [14]. Molecular markers such as HER-2 in breast cancer and chromosomal translocation in lymphomas are useful in planning treatment of above malignancies. However, to date, no molecular marker is used in therapeutic decision-making in OSCC.

In our previous studies, we have shown that there is a significant expression of molecular markers, hypoxia inducible factor-1 α (HIF-1 α) [17, 18], periostin [19], Matrix Metalloproteinase-9 (MMP-9) [20], Vascular Endothelial Growth Factor-C (VEGF-C) [21, 22], epidermal growth factor receptor (EGFR) [23], and β -Catenin [23], in OSCCs, as well as their ability to serve as potential molecules for predicting prognosis and metastasis. Further, it has been stated that the use of molecular markers together with the traditional histological methods may improve the strategy for comprehensive management of patients with OSCC [24]. This may provide a better evaluation of prognosis and the essentiality of elective neck dissection, which on the contrary may reduce the morbidity and cost of the advanced procedures. Further, Cyclin D1 is also positively correlated with nodal metastasis and poorer survival [25].

Although the significance of many of the biomarkers in OSCC has been reported, large prospective studies integrating the most reliable predictive biomarkers for OSCC are crucial to control the variability and for definite clarification

of the prognostic significance of some of these molecular markers [24]. However, the objective of the present study is to propose a predictive model using clinical and histopathological parameters, as most centres in this part of the world have no facilities for molecular diagnostic techniques.

Head and neck surgery is generally considered to be challenging because of complex anatomy with difficulties of access and due to the presence of multiple vital structures. Most of the OSCC patients in this part of the world present to the clinicians at late stages of the disease. These advanced tumours are frequently treated with surgery followed by concurrent chemotherapy and radiation therapy. Neck dissections are associated with significant morbidity, which discourages the use of elective neck dissections. Therefore, a reliable method is needed to predict lymph node metastasis. The mortality and morbidity depend on the extent of surgical intervention. Radical neck dissection invariably leads to significant functional and cosmetic morbidity. Therefore, proper treatment planning is mandatory [26].

Recent advances have been used in the diagnosis and treatment of OSCC including identification of plasma or serum biomarkers, imaging techniques, biological therapy, and surgical techniques. However, these techniques have a little effect on overall survival of cancer [27, 28]. Technologies in functional genomics such as microarray analysis permit qualitative and quantitative biologic investigations on genome-wide scale [29], which is very expensive and cannot be practiced in frequent day-to-day reporting. Therefore, in this study, we were able to elucidate a combination of some histopathological parameters and clinical criteria to predict metastasis.

Detection of cervical lymph node metastasis in OSCC is of utmost importance in terms of surgical planning and prognosis. In this study, we reconfirmed that the pattern of invasion is the most important histological parameter associated with cervical lymph node metastasis. This was supported by other studies showing that patterns III and IV at the invasive front had higher incidence of neck metastasis and poor prognosis than those who had patterns I and II [4, 5]. Degree of tumour differentiation has also been found to correlate with nodal metastasis in OSCC [30]. Our study also confirms the above statement that poorly differentiated tumours show higher metastatic rates.

Tumours involving palate and upper alveolar ridge showed higher metastatic rates compared to other intraoral sites. Although some clinical parameters such as age, gender, and primary site did not reach statistical significance with metastasis, there was an increased tendency of extracapsular invasion in relation to younger patients, female patients, and sites such as tongue, palate, and upper alveolar ridge. There was a positive correlation between pattern of invasion and extracapsular invasion. Similarly, the same relationship was found between stage and extracapsular invasion. Therefore, this information may help to determine the extent of neck dissection and reduce the morbidity associated with unnecessary surgery or irradiation. It has been shown that tumour stage has a marked correlation with prognosis of OSCC [5]. The present study also proved that the stage of a given OSCC is a major factor in predicting metastasis.

Statistical models have always been a helpful tool in modeling disease susceptibility prediction. Logistic regression is a mathematical modeling approach that is used to describe the relationship between several explanatory variables and a dichotomous dependent variable. By using logistic regression, one can predict the outcome from a set of variables that may be continuous, discrete, and dichotomous or a mix of any of these [31]. Predictive regression models characterize the relationship between inputs and outputs using linear equation for linear functions. Interpretations of the logistic regression conclude that pattern of invasion, level of differentiation, and tumour stage have positive contribution to metastatic susceptibility as shown in Table 3. The criteria used for ultimate prediction is the pattern of invasion and tumour stage (TNM), which can be used as a guide to predict nodal metastasis. In the present study, it is clearly indicated that invasive pattern and stage can predict the level of metastasis. Further, for example, if tumour shows invasive pattern I but stage 3, only up to level I clearance is adequate. Similarly, if the tumour is in stage 4 with invasive pattern IV, neck clearance up to level 5 is indicated.

Models based on multiple variables that predict outcome in terms of lymph node metastasis seem to be more accurate than prediction based on single variables [32]. A system proposed by Woolgar and Scott [33] showed that tumour thickness and expression of factor VIII in combination predict nodal metastasis and local recurrence. Similarly, pattern of invasion and immunohistochemical expression of periostin and VEGF-C were also significantly correlated with metastasis [21].

5. Conclusion

Identification of accurate predictive models in OSCC is important to overcome extensive prophylactic surgical management for neck nodes. The therapeutic regimen should be judged by means of not only T classification or stage of the tumour but also evaluation on the histological parameters such as invasive pattern and level of differentiation. In the present study, the proposed predictive model appears to be reliable and simple and may guide the surgeon in planning surgical management of neck nodes for OSCC. Further studies are necessary to identify predictive models in other sites of the oral cavity.

Conflicts of Interest

The authors declare that there are no conflicts of interest.

References

- [1] F. Kamangar, G. M. Dores, and W. F. Anderson, "Patterns of cancer incidence, mortality, and prevalence across five continents: Defining priorities to reduce cancer disparities in different geographic regions of the world," *Journal of Clinical Oncology*, vol. 24, no. 14, pp. 2137–2150, 2006.
- [2] Cancer Registry. National Cancer Control Programme. Government Cancer Institute, Maharagama, Sri Lanka, 2002.
- [3] S. Warnakulasuriya, "Prognostic and predictive markers for oral squamous cell carcinoma: the importance of clinical, pathological and molecular markers," *Saudi Journal of Medicine & Medical Sciences*, vol. 2, no. 1, pp. 12–16, 2014.
- [4] R. Sankaranarayanan, K. Dinshaw, and B. M. Nene, "Cervical and oral cancer screening in India," *Journal of Medical Screening*, vol. 13, supplement 1, pp. S35–38, 2006.
- [5] B. S. M. S. Siriwardena, A. Tilakaratne, E. A. P. D. Amaratunga et al., "Analysis of histopathological and immunohistochemical differences of oral squamous cell carcinoma in young and old patients in Sri Lanka," *Journal of Oral Pathology & Medicine*, vol. 36, no. 6, pp. 357–362, 2007.
- [6] T. Chang, C. Chang, H. Ho et al., "Impact of Young Age on the Prognosis for Oral Cancer: A Population-Based Study in Taiwan," *PLoS ONE*, vol. 8, no. 9, p. e75855, 2013.
- [7] K. B. Pytynia, J. R. Grant, C. J. Etzel, D. Roberts, Q. Wei, and E. M. Sturgis, "Matched analysis of survival in patients with squamous cell carcinoma of the head and neck diagnosed before and after 40 years of age," *Archives of Otolaryngology—Head and Neck Surgery*, vol. 130, no. 7, pp. 869–873, 2004.
- [8] P. A. Jakobsson, C. M. Eneroth, D. Killander, G. Moberger, and B. Mårtensson, "Histologic classification and grading of malignancy in carcinoma of the larynx," *Acta Oncologica*, vol. 12, no. 1, pp. 1–8, 1973.
- [9] W. L. Dissanayaka, G. Pitiyage, P. V. R. Kumarasiri, R. L. P. R. Liyanage, K. D. Dias, and W. M. Tilakaratne, "Clinical and histopathologic parameters in survival of oral squamous cell carcinoma," *Oral Surgery, Oral Medicine, Oral Pathology, Oral Radiology, and Endodontology*, vol. 113, no. 4, pp. 518–525, 2012.
- [10] H. Schliephake, "Prognostic relevance of molecular markers of oral cancer—a review," *International Journal of Oral and Maxillofacial Surgery*, vol. 32, no. 3, pp. 233–245, 2003.
- [11] B. O'Sullivan and J. Shah, "New TNM staging criteria for head and neck tumors," *Seminars in Surgical Oncology*, vol. 21, no. 1, pp. 30–42, 2003.
- [12] M. F. Muñoz-Guerra, "Early stage oral cancer: prognosis with regard to histological grading, intratumorallymphangiogenesis, and the expression of vascular endothelial growth factor-C (VEGF-C)," *Revista Española de Cirugía Oral y Maxilofacial*, vol. 28, pp. 25–40, 2006.
- [13] A. N. Salesiotis and K. J. Cullen, "Molecular markers predictive of response and prognosis in the patient with advanced squamous cell carcinoma of the head and neck: Evolution of a model beyond TNM staging," *Current Opinion in Oncology*, vol. 12, no. 3, pp. 229–239, 2000.
- [14] R. H. Spiro, A. E. Alfonso, H. W. Farr, and E. W. Strong, "Cervical node metastasis from epidermoid carcinoma of the oral cavity and oropharynx. A critical assessment of current staging," *The American Journal of Surgery*, vol. 128, no. 4, pp. 562–567, 1974.
- [15] D. E. Schuller, W. F. McGuirt, B. F. McCabe, and D. Young, "The prognostic significance of metastatic cervical lymph nodes," *The Laryngoscope*, vol. 90, no. 4, pp. 557–570, 1980.
- [16] D. G. Sessions, G. J. Spector, and J. Lenox, "Analysis of treatment results for oral tongue cancer," *The Laryngoscope*, vol. 112, no. 4, pp. 616–625, 2002.
- [17] D. G. Sessions, J. Lenox, G. J. Spector, C. Chao, and O. A. Chaudry, "Analysis of treatment results for base of tongue cancer," *The Laryngoscope*, vol. 113, no. 7, pp. 1252–1261, 2003.
- [18] W. M. Tilakaratne and E. H. Nissanka-Jayasuriya, "Value of HIF-1 α s as an independent prognostic indicator in oral squamous cell carcinoma," *Expert Review of Molecular Diagnostics*, vol. 11, no. 2, pp. 145–147, 2011.

- [19] W. M. Tilakaratne, Z. Iqbal, M. T. Teh et al., "Upregulation of HIF-1 α in malignant transformation of oral submucous fibrosis," *Journal of Oral Pathology & Medicine*, vol. 37, no. 6, pp. 372–377, 2008.
- [20] B. S. M. S. Siriwardena, Y. Kudo, I. Ogawa et al., "Periostin is frequently overexpressed and enhances invasion and angiogenesis in oral cancer," *British Journal of Cancer*, vol. 95, no. 10, pp. 1396–1403, 2006.
- [21] E. M. Deraz, Y. Kudo, M. Yoshida et al., "MMP-10/stromelysin-2 promotes invasion of head and neck cancer," *PLoS ONE*, vol. 6, no. 10, Article ID e25438, 2011.
- [22] B. S. M. S. Siriwardena, Y. Kudo, I. Ogawa, M. N. G. P. K. Udagama, W. M. Tilakaratne, and T. Takata, "VEGF-C is associated with lymphatic status and invasion in oral cancer," *Journal of Clinical Pathology*, vol. 61, no. 1, pp. 103–108, 2008.
- [23] R. Sedivy, J. Beck-Mannagetta, C. Haverkamp, W. Battistutti, and S. Hönigschnabl, "Expression of vascular endothelial growth factor-C correlates with the lymphatic microvessel density and the nodal status in oral squamous cell cancer," *Journal of Oral Pathology & Medicine*, vol. 32, no. 8, pp. 455–460, 2003.
- [24] N. Tanaka, T. Odajima, K. Ogi, T. Ikeda, and M. Satoh, "Expression of E-cadherin, α -catenin, and β -catenin in the process of lymph node metastasis in oral squamous cell carcinoma," *British Journal of Cancer*, vol. 89, no. 3, pp. 557–563, 2003.
- [25] G. R. Thomas, H. Nadiminti, and J. Regalado, "Molecular predictors of clinical outcome in patients with head and neck squamous cell carcinoma," *International Journal of Clinical and Experimental Pathology*, vol. 86, no. 6, pp. 347–363, 2005.
- [26] H. M. Mahdey, A. Ramanathan, S. M. Ismail, M. T. Abraham, M. Jamaluddin, and R. B. Zain, "Cyclin D1 amplification in tongue and cheek squamous cell carcinomas," *Asian Pacific Journal of Cancer Prevention*, vol. 12, no. 9, pp. 2199–2204, 2011.
- [27] S. V. Kane, M. Gupta, A. C. Kakade, and A. D' Cruz, "Depth of invasion is the most significant histological predictor of sub-clinical cervical lymph node metastasis in early squamous carcinomas of the oral cavity," *European Journal of Surgical Oncology*, vol. 32, no. 7, pp. 795–803, 2006.
- [28] J. Kligerman, R. A. Lima, J. R. Soares et al., "Supraomohyoid neck dissection in the treatment of T1/T2 squamous cell carcinoma of oral cavity," *The American Journal of Surgery*, vol. 168, no. 5, pp. 391–394, 1994.
- [29] I. J. Fidler, "The pathogenesis of cancer metastasis: the "seed and soil" hypothesis revisited," *Nature Reviews Cancer*, vol. 3, no. 6, pp. 453–458, 2003.
- [30] S. Mohr, J. M. Stryker, and A. M. Lambowitz, "A DEAD-Box protein functions as an ATP-dependent RNA chaperone in group I intron splicing," *Cell*, vol. 109, no. 6, pp. 769–779, 2002.
- [31] I. J. Fidler and M. L. Kripke, "Metastasis results from preexisting variant cells within a malignant tumor," *Science*, vol. 197, no. 4306, pp. 893–895, 1977.
- [32] P. Roepman, E. de Koning, D. Van Leenen et al., "Dissection of a metastatic gene expression signature into distinct components," *Genome Biology*, vol. 7, no. 12, article no. R117, 2006.
- [33] J. A. Woolgar and J. Scott, "Prediction of cervical lymph node metastasis in squamous cell carcinoma of the tongue/floor of mouth," *Head & Neck*, vol. 17, no. 6, pp. 463–472, 1995.

Research Article

A Comparative Study for Detection of *EGFR* Mutations in Plasma Cell-Free DNA in Korean Clinical Diagnostic Laboratories

Yoonjung Kim ¹, Saem Shin ², and Kyung-A Lee ¹

¹Department of Laboratory Medicine, Yonsei University College of Medicine, Seoul, Republic of Korea

²Department of Laboratory Medicine, Hallym University College of Medicine, Kangnam Sacred Heart Hospital, Seoul, Republic of Korea

Correspondence should be addressed to Kyung-A Lee; kall119@yuhs.ac

Received 4 January 2018; Revised 12 March 2018; Accepted 2 April 2018; Published 8 May 2018

Academic Editor: Valli De Re

Copyright © 2018 Yoonjung Kim et al. This is an open access article distributed under the Creative Commons Attribution License, which permits unrestricted use, distribution, and reproduction in any medium, provided the original work is properly cited.

Liquid biopsies to genotype the epidermal growth factor receptor (*EGFR*) for targeted therapy have been implemented in clinical decision-making in the field of lung cancer, but harmonization of detection methods is still scarce among clinical laboratories. We performed a pilot external quality assurance (EQA) scheme to harmonize circulating tumor DNA testing among laboratories. For EQA, we created materials containing different levels of spiked cell-free DNA (cfDNA) in normal plasma. The limit of detection (LOD) of the cobas® *EGFR* Mutation Test v2 (Roche Molecular Systems) was also evaluated. From November 2016 to June 2017, seven clinical diagnostic laboratories participated in the EQA program. The majority (98.94%) of results obtained using the cobas assay and next-generation sequencing (NGS) were acceptable. Quantitative results from the cobas assay were positively correlated with allele frequencies derived from digital droplet PCR measurements and showed good reproducibility among laboratories. The LOD of the cobas assay was 5~27 copies/mL for p.E746_A750del (exon 19 deletion), 35~70 copies/mL for p.L858R, 18~36 copies/mL for p.T790M, and 15~31 copies/mL for p.A767_V769dup (exon 20 insertion). Deep sequencing of materials (>100,000X depth of coverage) resulted in detection of low-level targets present at frequencies of 0.06~0.13%. Our results indicate that the cobas assay is a reliable and rapid method for detecting *EGFR* mutations in plasma cfDNA. Careful interpretation is particularly important for p.T790M detection in the setting of relapse. Individual laboratories should optimize NGS performance to maximize clinical utility.

1. Introduction

Circulating tumor DNA (ctDNA) carries the same molecular alterations as the tumor itself and can be used to select treatment, assess the emergence of drug resistance, and monitor lung cancer patients in routine clinical practice [1]. The fraction of tumor-derived cell-free DNA (cfDNA) in blood plasma varies according to tumor stage, tumor burden, vascularization of the tumor, biological features of the tumor such as apoptotic rate, and the metastatic potential of the cancer cells [2]. Tumor-derived ctDNA often represents a small percentage of the total cfDNA and can be present at allele fractions as low as 0.01% [3]. Therefore, highly sensitive methodologies have been developed to detect low abundance epidermal growth factor receptor (*EGFR*) mutations, including p.T790M, from cfDNA in non-small cell

lung cancer (NSCLC) patients, although the sensitivities and specificities of the methods vary [4, 5].

A sensitive method is needed to detect the p.T790M mutation in relapsed tumors because of tumor heterogeneity [6]. Recently, several *in vitro* diagnostics (IVD) have been approved by the European Medicines Agency (EMA) and the US Food and Drug Administration (FDA) for detecting *EGFR* mutations in plasma [7]. To ensure optimal quality molecular testing, clinical laboratories should evaluate the technical performance of ctDNA testing according to the standards from formal accreditation bodies, such as Clinical Laboratory Improvement Amendments (CLIA) and ISO 15189 [8, 9]. External quality assessment (EQA) is a way to standardize interlaboratory results and to monitor and improve testing processes across laboratories [10].

In this study, we designed EQA materials to evaluate the limit of detection (LOD) of the cobas *EGFR* Mutation Test v2 (Roche Molecular Systems, Inc., Branchburg, NJ, USA) and Oncomine Lung cfDNA Assay (Thermo Fisher Scientific, Waltham, MA, USA). We also implemented a pilot EQA scheme to assess the interlaboratory comparability of plasma *EGFR* testing results.

2. Materials and Methods

2.1. Preparation of EQA Materials

2.1.1. Pooled Normal Human Plasma (NHP) Preparation. The workflow of the study process is shown in Supplementary Figure S1. Pooled normal human K2 EDTA plasma (NHP) was prepared using residual specimens from healthy individuals and was separated within 4 hours of collection. Negativity for *EGFR* mutation of 2 mL NHP was confirmed using the cobas *EGFR* Mutation Test v2 (Roche Molecular Systems, Inc.). cfDNA was extracted from 2 mL NHP using the MagMAX™ Cell-Free DNA Isolation Kit (Thermo Fisher Scientific) according to the manufacturer's instructions. cfDNA concentration and fragment size distribution were assessed using a 2200 TapeStation Instrument (Agilent Technologies, Santa Clara, CA, USA) with the Agilent D1000 ScreenTape System. Average fragment size was 185 bp, and average cfDNA concentration was 0.106 ng/ μ L. We calculated that there were 1,162 wild-type copies per 2 mL NHP.

2.1.2. EQA Material to Evaluate Assay Sensitivity. To prepare spiked materials with known mutant allele frequencies and mutant DNA copies, Multiplex I cfDNA Reference Standards (Horizon Discovery, Cambridge, UK) were purchased. This set is composed of wild-type cfDNA with mutant allele frequencies of 5%, 1%, 0.1%, and 0%. For each reference standard, copies per μ L of wild-type and mutant DNA were measured using digital droplet PCR and compared with the values provided by the manufacturer (Supplementary Table S1).

Four levels (levels 1 to 4) of spiked NHP (2 mL per sample) were prepared to determine the LOD of the detection assays. Intended mutant allele frequencies were 5%, 2.5%, 1%, and 0.1%, with 4 to 760 mutant copies in a background of about 10,000~16,000 wild-type copies in a spiked NHP samples, depending on the mutation. cfDNA was extracted from 2 mL spiked NHP using MagMAX Cell-Free DNA Isolation Kit (Thermo Fisher Scientific). Concentration and fragment size distribution of cfDNA were assessed using a 2200 TapeStation Instrument (Agilent Technologies). Average fragment size was about 190 bp, and the range of cfDNA was 60.42 ng to 80.18 ng. Details are provided in Supplementary Table S1.

2.1.3. EQA Material to Evaluate Assay Precision. Genomic DNA from cell lines harboring mutations of the *EGFR* gene including p.T790M (HD258), p.L858R (HD254), and p.E746_A750del (HD251) were purchased from Horizon Discovery. To simulate the size distribution of cfDNA, each genomic DNA was fragmented to about 180~190 bp by sonication using a Covaris M220 (330 sec, 0.2% duty, 50 peak

incident power, and 200 cycles/burst; Covaris Inc., Woburn, MA, USA) (Supplementary Table S2 and Supplementary Figure S2). Three spiked NHPs (1 mL per sample) were prepared to evaluate assay precision. Intended mutant allele frequencies were about 5%, with 1,221 to 1,503 mutant copies in a background of nearly 23,000~30,000 wild-type copies in spiked NHP samples, depending on the mutation. cfDNA was extracted from 1 mL spiked NHP using MagMAX Cell-Free DNA Isolation Kit (Thermo Fisher Scientific). Concentration and fragment size distribution of cfDNA were assessed using a 2200 TapeStation Instrument (Agilent Technologies instructions). Average size was 190 bp, and the cfDNA concentration (ng/mL) was 74.5~80.2. Details are provided in Supplementary Table S2. Spiked NHPs were frozen at -70°C until genotyping.

2.2. Validation of EQA Material for LOD Evaluation

2.2.1. cfDNA Extraction from Spiked NHP Samples. cfDNA was extracted from spiked NHP samples using MagMAX Cell-Free DNA Isolation Kit (Thermo Fisher Scientific) for next-generation sequencing and the cobas cfDNA Sample Preparation Kit (Roche Molecular Systems, Inc.) for the cobas *EGFR* assay. cfDNA concentration and purity were assessed using a NanoDrop 1000 spectrometer (Thermo Scientific, Waltham, MA, USA) and a Qubit 2.0 Fluorometer (Life Technologies, Grand Island, NY, USA) using the Qubit™ dsDNA HS Assay Kit. Size and amount of DNA fragments were assessed using a 2200 TapeStation Instrument (Agilent Technologies) with the Agilent D1000 ScreenTape System (Agilent Technologies).

2.2.2. Evaluation of EQA Material Using Next-Generation Sequencing. For next-generation sequencing (NGS), a library was prepared using the Oncomine Lung cfDNA Assay and quantitated using qPCR. Emulsion PCR was performed using the Ion Chef System and Ion AmpliSeq IC 200 Kit (all Thermo Fisher Scientific). Barcoded libraries generated from 20 ng DNA per sample were loaded on an Ion 530 chip and sequenced on the Ion S5 XL System using Ion 520 and Ion 530 Kit-Chef (all Thermo Fisher Scientific). Alignment to the hg19 human reference genome and variant calling were performed using Torrent Suite™ software (Thermo Fisher Scientific). Variant annotation was performed using Ion Reporter™ Software 5.2 (Thermo Fisher Scientific). Torrent Suite software provides molecular coverage depth as well as read coverage depth at target bases to increase detection sensitivity for low-frequency variants [11, 12]. The manufacturer recommends a median read coverage $>25,000\times$ and median molecular coverage $>2,500\times$ to detect a variant with an allele frequency of 0.1%. Measured allele frequency (%) was calculated as mutant coverage depth divided by total coverage depth.

2.2.3. Evaluation of LOD Material Using Real-Time PCR. For the cobas *EGFR* assay, 75 μ L DNA from each sample was loaded into three reaction wells (25 μ L DNA per well). Amplification and detection were performed using the cobas z 480 analyzer (Roche Molecular Systems, Inc.). Data were

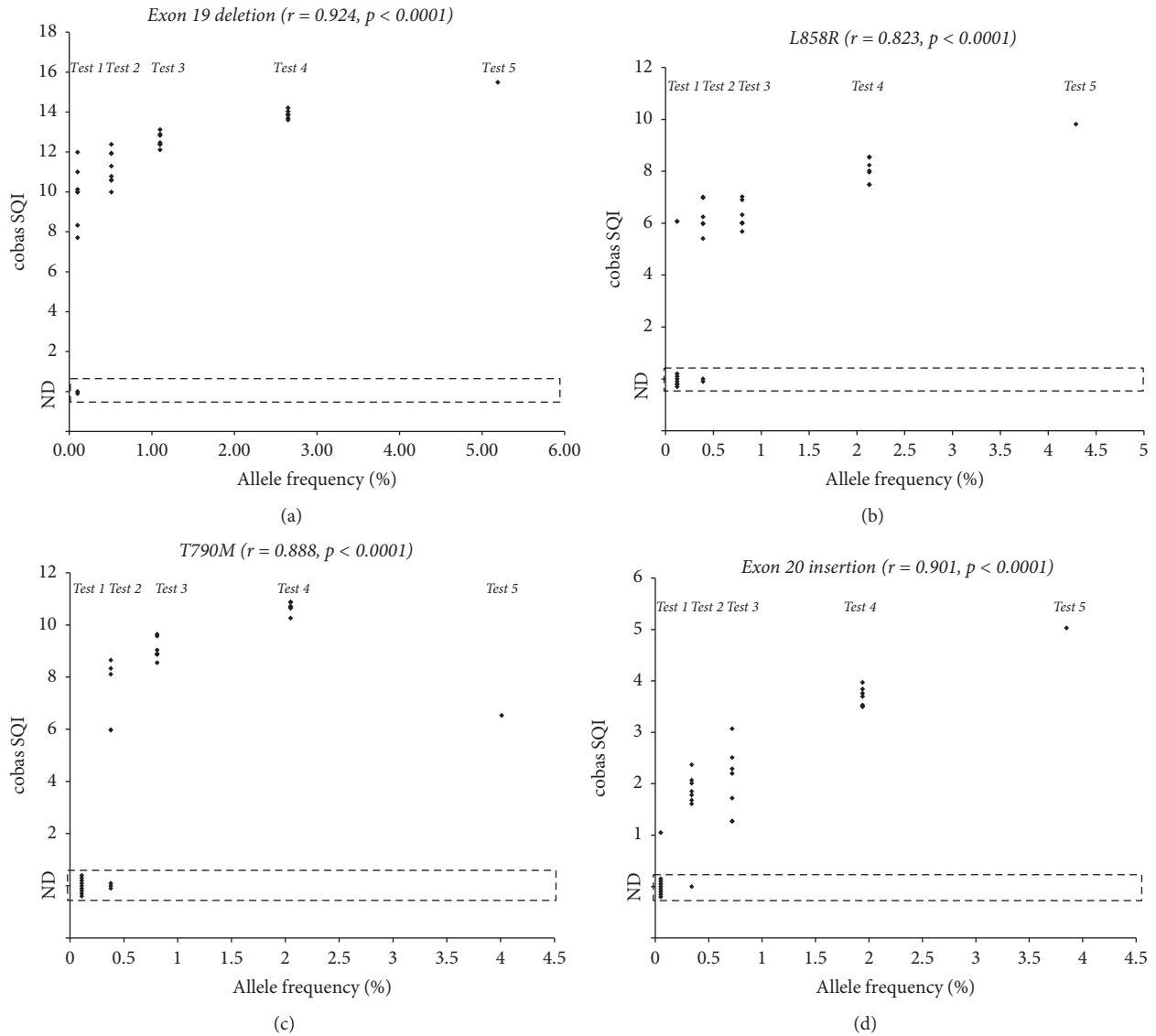


FIGURE 1: Analytical sensitivity of the cobas *EGFR* assay for NHP spiked with five different levels of mutant cfDNA. Copy numbers and frequencies of mutant alleles are provided in Supplementary Table S3. Dots in the figure represent negative measurement (ND) or the SQI value of the positive measurement for (a) p.E746_A750del (exon 19 deletion), (b) p.L858R, (c) p.T790M, and (d) p.A767_V769dup (exon 20 insertion) mutations.

interpreted by the cobas z 480 software if positive and negative controls showed valid results. When a mutation was detected, semiquantitative index (SQI) values for each mutation are reported automatically by the software using the observed threshold cycle for the target mutation. The SQI was developed to measure trends in the amount of mutant cfDNA in a patient [13].

The analytical performance of the cobas *EGFR* assay was additionally evaluated using five NHP samples spiked with different mutant allele frequencies that were made using Multiplex I cfDNA Reference Standards (Horizon Discovery, Cambridge, UK). These test samples had expected mutant allele frequencies of 3.85~5.19%, 1.94~2.65%, 0.72~1.10%, 0.34~0.51%, and 0.05~0.12% (Supplementary Table and Figure 1).

2.3. *Distribution of EQA Material, Data Collection, and Analysis.* Each laboratory director requested the amount of EQA material needed according to the number of methods planned for plasma *EGFR* testing. The number of reactions per test method among participating laboratories was 13. The EQA material set comprised four samples (2 mL, levels 1 to 4) with different mutant allele frequencies (5.0%, 2.5%, 1%, and 0.1%) for LOD analysis, and three samples with different *EGFR* mutations were also provided (1 mL per a reaction, P-1 to P-3).

For each test method, one EQA material set with 2 mL of LOD materials (levels 1 to 4) and 3 mL precision materials (P-1 to P-3) were distributed to each participating laboratory. Materials in barcoded K2 EDTA tubes were shipped to laboratories at 4°C along with a results datasheet to record

qualitative results (detected or not detected) and quantitative results (SQI value from the cobas *EGFR* assay and total/mutant coverage depth from next-generation sequencing) for each mutation. Submitted qualitative results were evaluated as acceptable (positive for expected mutations or negative for unexpected mutations) or unacceptable (negative for expected mutations or positive for unexpected mutations), according to the manufactured and validated target mutations in this study (Table 1 and Supplementary Table S2). LOD level 4 material, which had an expected mutant allele frequency of 0.05~0.12%, was not graded. For the cobas assay, the mean, standard deviation, coefficient of variation (CV), median value, minimum value, and maximum value of data from the peer group and the standard deviation index of the data from the laboratory were provided in the evaluation reports.

2.4. Statistical Analysis. Statistical analysis was performed using SPSS Statistics version 24.0.0 (IBM Corp., Armonk, NY, USA). Correlations between SQI from cobas assay and mutant allele frequency were analyzed using Spearman rank-correlation test. All *p* values were two-sided, and values less than 0.05 were considered significant.

3. Results

3.1. Validation of EQA Materials. EQA materials for LOD evaluation were validated using the Oncomine Lung cfDNA Assay and cobas *EGFR* Mutation Test (Table 1). In a deep sequencing run, all four quality control samples were sequenced with high median coverage depth of more than 86,321X. All target bases showed adequate coverage (>500X). There was sufficient coverage at all target mutations to detect variants with allele frequencies of 0.1% (2,236~4,439X). All targeted mutations were called in levels 1–4 materials at similar allele frequencies to what were expected. cobas assay detected not only all target mutations in levels 1–3 materials but also p.L858R (0.12% allele frequency) and p.E746_A750del (exon 19 deletion; 0.10% allele frequency) in level 4 material.

3.2. Analytical Sensitivity of Real-Time PCR. Analytical sensitivity (LOD) of the cobas *EGFR* assay was assessed using five NHP samples spiked with different amounts of mutated targets (Figure 1 and Supplementary Table S3). Seven of nine cobas assays (77.8%) detected the exon 19 deletion in Test 5 material. All eight measurements of Test 4 material detected the exon 19 deletion. Six (75%), five (62.5%), and seven (87.5%) of eight measurements detected p.L858R, p.T790M, and p.A767_V769dup (exon 20 insertion) mutations in the Test 4 material, respectively. Therefore, the LODs of the cobas *EGFR* assay were determined to be 5~27 copies/mL for exon 19 deletion (0.1~0.5% allele frequency), 35~70 copies/mL for p.L858R (0.4~0.8% allele frequency), 18~36 copies/mL for p.T790M (0.4~0.8% allele frequency), and 15~31 copies/mL for exon 20 insertion (0.3~0.7% allele frequency). For all mutations, SQI values from the cobas assay exhibited a strong positive correlation with the expected mutant allele frequencies derived from digital droplet PCR measurements

(Spearman rank-correlation coefficient, 0.823~0.924; *p* < 0.0001).

3.3. Pilot EQA Scheme. In November 2016, seven clinical laboratories that perform plasma *EGFR* molecular testing were recruited for the pilot EQA scheme (Table 2). In April 2017, EQA materials were made and distributed to each laboratory. A month after distributing the EQA materials, all results were emailed from each laboratory to an organizing director. In June 2017, evaluation reports were distributed to participating laboratories. Plasma *EGFR* testing was performed using an IVD assay and two laboratory-developed tests based on NGS: the cobas *EGFR* assay (*n* = 7), the Oncomine Lung cfDNA Assay on the Ion S5 XL (*n* = 1), and the QIAGEN GeneRead QIAact Actionable Insights Tumor Panel (QIAGEN, Hilden, Germany) on the GeneReader Platform (QIAGEN) (*n* = 1). There were two unacceptable results for NGS of LOD level 3 material (Tables 3 and 5).

3.4. Interlaboratory Comparability of Real-Time PCR Results. All results obtained using the cobas assay were concordant except for detection of *EGFR* exon 19 deletion and p.L858R in LOD level 4 material. Among seven laboratories, only six laboratories had a positive result for exon 19 deletion (detection rate 85.7%) and one laboratory had a positive result for p.L858R (detection rate 14.8%) in level 4 material. p.T790M and exon 20 insertion mutations were not detected in LOD level 4 material by any of the laboratories. The precision of SQI is summarized in Table 4. The cobas assay generally showed good reproducibility with a CV between 1.29% and 7.35% for target mutations. However, for p.T790M and exon 20 insertion, the CV for level 3 and/or level 4 materials (13.1% ~30.98%) was poorer than for the other mutations.

3.5. Interlaboratory Comparison of Next-Generation Sequencing Results. Mutant allele frequencies were calculated from the submitted depth of coverage data from NGS (Table 5). Results from two laboratories were consistent with the expected mutant allele frequencies calculated from absolute allele frequencies measured using digital droplet PCR. In laboratory F (S5XL + Oncomine Lung cfDNA Assay), all expected mutations were detected in level 3 material. Exon 19 deletion and exon 20 insertion mutations were detected at 0.15% (total read coverage depth of 73,836X) and 0.23% (total read coverage depth of 49,234X) in level 4 material, respectively. However, p.T790M and p.L858R mutations were not detected, despite the fact that total read coverage depth was not lower for these loci than other loci (65,455X for p.T790M and 70,849X for p.L858R). In laboratory C (GeneReader + QIAGEN GeneRead QIAact Actionable Insights Tumor Panel), p.T790M and exon 20 insertion mutations were not detected in level 3 material (unacceptable result). None of the four target mutations were detected in level 4 material.

4. Discussion

In this study, we prepared and validated EQA material for *EGFR* mutation detection using cfDNA and evaluated the

TABLE 1: Validation of external quality assurance material using Oncomine Lung cfDNA Assay and cobas EGFR Mutation Test.

EQA materials	EGFR variant	Expected mutant allele frequency (%)	Oncomine Lung cfDNA Assay							cobas EGFR mutation test		
			Number of mapped reads	Percentage of reads on target (%)	Median base coverage depth	Uniformity of base coverage (%)	Target base coverage at 500X (%)	Molecular coverage depth, total/mutant	Measured allele frequency (%) ^a	Read coverage depth, total/mutant	Measured allele frequency (%) ^b	SQL from cobas EGFR mutation test
Level 1	p.L858R	4.29						2999/53	1.77	151533/2489	1.64	9.82
	p.E746_A750del	5.19						4026/118	2.93	88048/1523	1.73	15.49
	p.T790M	4.01	89.72	91374	100	100	3674/117	3.18	97546/3212	3.29	11.93	
Level 2	p.A767_V769dup	3.85						3834/122	3.18	58931/2214	3.76	5.06
	p.L858R	2.13						2843/56	1.97	160148/3418	2.13	7.49
	p.E746_A750del	2.65	89.28	108108	100	100	4174/90	2.16	103525/1216	1.17	13.88	
	p.T790M	2.05					3942/82	2.08	109822/2170	1.98	10.71	
Level 3	p.A767_V769dup	1.94						4349/74	1.70	77146/1661	2.15	3.5
	p.L858R	0.80						2236/6	0.27	122767/477	0.39	6.67
	p.E746_A750del	1.10	87.94	86321	100	100	3533/39	1.10	88048/523	0.59	12.9	
	p.T790M	0.81					3269/31	0.95	92814/927	1.00	9.28	
	p.A767_V769dup	0.72					3655/21	0.57	63023/462	0.73	2.68	
Level 4	p.L858R	0.12						2692/2	0.07	159720/152	0.10	6.07
	p.E746_A750del	0.10	88.17	108397	100	100	3880/4	0.10	110976/117	0.11	9.99	
	p.T790M	0.11					3770/5	0.13	117037/149	0.13	ND	
	p.A767_V769dup	0.05						3877/4	0.10	79331/198	0.25	ND

^a Allele frequency (%) = mutant molecular coverage depth/total molecular coverage depth. ^b Allele frequency (%) = mutant read coverage depth/total read coverage depth. EQA, external quality assurance; SQL, semiquantitative index; ND, not detected.

TABLE 2: Plasma *EGFR* genotyping methods by laboratories participating in pilot external quality assurance.

Laboratories	In vitro diagnostics		Laboratory-developed tests	
	cobas z 480 + cobas <i>EGFR</i> Mutation Test v2	S5XL + Oncomine Lung cfDNA Assay	GeneReader + QIAGEN GeneRead QIAact Actionable Insights Tumor Panel	
A	O			
B	O			
C	O			O
D	O			
E	O			
F	O		O	
G	O			

analytical sensitivity of the cobas *EGFR* assay. According to the package insert, the LOD of the cobas assay using sheared DNA with an average size of 220 bp is less than 0.1% (75 copies/mL for exon 19 deletion, 25 copies/mL for the exon 20 insertion, and 100 copies/mL for p.L858R and p.T790M). In the present study, we confirmed the LODs of the cobas assay for each target mutation. The analytical sensitivities of the cobas assay were not identical for the different target mutations, similar to previous reports [14, 15]. In our pilot EQA, the cobas assay showed a higher detection rate and lower imprecision for exon 19 deletion and p.L858R than for p.T790M and exon 20 insertion. Similarly, in laboratory F that used the Oncomine Lung cfDNA Assay, p.T790M and p.L858R were not detected, despite adequate depth of coverage of the target site compared to other loci. This difference in assay performance according to target mutation might be due to the assay design and characteristics of the target regions [14, 15]. This finding is an important issue for detection of p.T790M in patients who show evidence of tumor progression after prior EGFR-tyrosine kinase inhibitor (TKI) therapy. Previous studies reported that it is challenging to detect the p.T790M mutation in patients with acquired resistance to prior EGFR-TKI therapy due to genomic heterogeneity [16, 17]. Therefore, caution is warranted in the setting of tumor relapse, and additional efforts should be made to optimize the experimental conditions to increase the sensitivity of p.T790M detection.

In our pilot EQA, participating laboratories performed one IVD assay (cobas *EGFR* assay) and two laboratory-developed tests based on NGS. The cobas assay showed reliable and robust test performance in all laboratories. SQI showed a positive correlation with mutant allele frequency derived from digital droplet PCR measurements. This finding is consistent with that of a previous study that evaluated clinical samples with NGS and the cobas assay [13]. Moreover, SQI from the cobas assay was reproducible among laboratories in our pilot EQA. Therefore, SQI could be useful for patient monitoring. About 3 hours of processing time is required for DNA extraction, PCR amplification, and detection in the cobas assay. Thus, this assay can be used for rapid and reliable plasma ctDNA analysis in clinical diagnostic laboratories.

A limitation of this study is the small number of laboratories that participated, especially laboratories performing NGS. It was unclear whether unacceptable responses were due to the performance of specific NGS methods or the laboratory. However, coverage depth results from two laboratories indicate that more read coverage depth is required to detect low-frequency variants in samples. In our validation experiment using the Oncomine Lung cfDNA Assay, all mutations were detected in level 4 material when the coverage depth was more than 100,000X. Our data and previous reports indicate that high coverage depth is essential to improve the detection of low-level targets [18, 19].

Another issue related to NGS is assay turn-around time (TAT). TAT for *EGFR* testing for NSCLC patients is important for drug selection. NGS generally requires more time than IVD, although it differs depending on batch constitution and the platform used. The two laboratories that performed NGS also used an IVD assay. The main advantage of NGS over IVD is scalability for type of mutation and target gene. Using NGS, rare (e.g., the p.C797S resistance mutation [20]) or novel mutations in *EGFR*, as well as other genes, can be identified [21]. Moreover, advanced NGS technology enables detection of not only point mutation but also gene fusions and amplifications [22, 23].

In the era of companion diagnostics, more mutations will be used as predictive markers to determine patient eligibility for molecular-targeted therapies. As a result, rigorous quality controls to avoid inappropriate patient treatment will become increasingly important in clinical diagnostic laboratories. EQA is critical for quality assurance and continuous improvement of individual laboratory performance [9]. Recently, Haselmann et al. have reported EQA scheme for ctDNA analysis of *KRAS* and *BRAF* genotyping, using mutant allele frequency of 0%, 5%, and 10% samples [24]. Digital approaches revealed no error rate, although Sanger sequencing revealed very high error rate around 20%. The authors suggested that method sensitivity correlates with diagnostic accuracy. Another EQA report for blood based *EGFR* p.T790M testing included pyrosequencing, digital PCR, and several allele-specific PCR platforms, using four levels of spiked materials [25]. Although we used limited

TABLE 3: Unacceptable response rate in pilot external quality assurance scheme.

Material ^a	EGFR variant	Acceptable response/total response (n)							NGS (2 laboratories)			Unacceptable response/total response (n)	Unacceptable response rate (%)
		A	B	cobas EGFR Mutation Test (7 laboratories)		F			C	F			
Level 1		4/4	4/4	4/4	4/4	4/4	4/4	4/4	4/4	4/4	4/4	0/36	0.0
Level 2	p.L858R; p.E746_A750del;	4/4	4/4	4/4	4/4	4/4	4/4	4/4	4/4	4/4	4/4	0/36	0.0
Level 3	p.T790M; p.A767_V769dup	4/4	4/4	4/4	4/4	4/4	4/4	4/4	2/4	4/4	4/4	2/36	5.6
Level 4		-/4	-/4	-/4	-/4	-/4	-/4	-/4	-/4	-/4	-/4	Not graded ^b	-
P-1	p.T790M	3/3	3/3	3/3	3/3	3/3	3/3	3/3	3/3	3/3	3/3	0/26 ^c	0.0
P-2	p.L858R	3/3	3/3	3/3	3/3	3/3	3/3	3/3	3/3	3/3	3/3	0/27	0.0
P-3	p.E746_A750del	3/3	3/3	3/3	3/3	3/3	3/3	3/3	3/3	3/3	3/3	0/27	0.0

^aLevel 1~level 4 materials were prepared for a limit of detection and P-1~P-3 materials were prepared for precision evaluation. P-1~P-3 materials were split and run on three replications. ^bFor cobas assay, p.L858R mutation was detected in one among seven laboratories (14.3%), and p.E746_A750del (exon 19 deletion) mutation was detected in six among seven laboratories (85.7%). For NGS, exon 19 deletion and p.A767_V769dup (exon 20 insertion) were detected in laboratory F. ^cOne measurement of P-1 material showed an invalid result in laboratory C. NGS, next-generation sequencing.

TABLE 4: The performance of interlaboratory comparison samples using the cobas EGFR Mutation Assay.

Sample	p.L858R				p.E746_A750del (exon 19 deletion)				p.T790M				p.A767_V769dup (exon 20 insertion)							
	Expected allele frequency (%) ^a	Copies of mutant DNA (μL) ^a	Mean	SD	CV (%)	Expected allele frequency (%) ^a	Copies of mutant DNA (μL) ^a	Mean	SD	CV (%)	Expected allele frequency (%) ^a	Copies of mutant DNA (μL) ^a	Mean	SD	CV (%)	Expected allele frequency (%) ^a	Copies of mutant DNA (μL) ^a	Mean	SD	CV (%)
Level 1	4.29	760	9.91	0.61	6.16	5.19	600	15.14	0.27	1.79	4.01	420	11.28	0.5	4.43	3.85	362	4.52	0.25	5.57
Level 2	4.02	380	8.65	0.5	5.76	4.72	300	14.24	0.18	1.29	3.61	210	10.25	0.59	5.74	3.42	181	3.56	0.47	13.1
Level 3	0.8	140	6.93	0.47	6.79	1.1	108	12.03	0.56	4.63	0.81	72	7.4	1.78	24.08	0.72	62	2.07	0.64	30.98
Level 4	0.12	20	-	-	-	0.1	10	8.91	0.63	7.11	0.11	10	-	-	-	0.05	4	-	-	-
Precision materials	3.0	NP	9.99	0.46	4.61	3.0	NP	15.2	0.27	1.78	3.0	NP	11.03	0.31	2.83	-	-	-	-	-
(P-1-P-3) ^b	3.0	NP	9.77	0.53	5.46	3.0	NP	15.2	0.3	1.95	3.0	NP	11.22	0.49	4.38	-	-	-	-	-
			9.75	0.72	7.35	3.0	NP	15.22	0.32	2.09	3.0	NP	11.19	0.59	5.24	-	-	-	-	-

^aMutant allelic frequency and copies of mutant DNA in materials were adjusted using next-generation sequencing result from information provided by the manufacturer of reference standards. ^b Only positive results from precision materials were summarized in the table. SQI, semiquantitative index; SD, standard deviation; CV, coefficient of variation; NP, not provided.

TABLE 5: Comparison of mutant allelic frequency from two laboratories using different next-generation sequencing platforms.

Sample	p.L858R				p.E746_A750del (exon 19 deletion)				p.T790M				p.A767_V769dup (exon 20 insertion)			
	Expected mutant allele frequency (%)	Lab F Molecular coverage depth, total/mutant (allele frequency, %)	Lab F Read coverage depth, total/mutant (allele frequency, %)	Lab C Read coverage depth, total/mutant (allele frequency, %)	Expected mutant allele frequency (%)	Lab F Molecular coverage depth, total/mutant (allele frequency, %)	Lab F Read coverage depth, total/mutant (allele frequency, %)	Lab C Read coverage depth, total/mutant (allele frequency, %)	Expected mutant allele frequency (%)	Lab F Molecular coverage depth, total/mutant (allele frequency, %)	Lab F Read coverage depth, total/mutant (allele frequency, %)	Lab C Read coverage depth, total/mutant (allele frequency, %)	Expected mutant allele frequency (%)	Lab F Molecular coverage depth, total/mutant (allele frequency, %)	Lab F Read coverage depth, total/mutant (allele frequency, %)	Lab C Read coverage depth, total/mutant (allele frequency, %)
Level 1	4.29	1970/67 (3.40)	74088/2440 (3.29)	4594/171 (3.72)	5.19	3360/131 (3.90)	6099/1272 (2.09)	5819/231 (3.97)	4.01	3182/124 (3.90)	59366/2276 (3.83)	1717/71 (4.14)	3.85	3258/130 (3.99)	38689/1707 (4.41)	1091/30 (2.75)
Level 2	2.13	1755/41 (2.34)	70894/1707 (2.41)	4385/84 (1.92)	2.13	2855/65 (2.28)	61723/753 (1.22)	10001/130 (1.30)	2.05	2680/51 (1.90)	56596/983 (1.74)	2572/87 (3.38)	1.94	2670/53 (1.99)	37564/541 (2.37)	2341/24 (1.03)
Level 3	0.80	1912/15 (0.78)	107664/791 (0.73)	4681/52 (1.11)	1.10	3095/22 (0.71)	94144/378 (0.40)	9416/57 (0.61)	0.81	2902/26 (0.90)	84166/754 (0.90)	ND ^a	0.72	3667/21 (0.57)	57591/541 (0.94)	ND ^a
Level 4	0.12	1804/0 (ND)	70849/0 (ND)	ND ^a	0.10	3158/3 (0.09)	73836/114 (0.15)	ND ^a	0.11	2980/0 (ND)	65455/0 (ND)	ND ^a	0.05	3296/3 (0.09)	49234/115 (0.23)	ND ^a
Precision materials (P-1-P-3) ^b	3.00	2250/89 (3.96)	97519/3743 (3.84)	4067/148 (3.64)	3.00	2306/68 (2.95)	45162/1336 (2.96)	9157/250 (2.73)	3.00	3132/126 (4.02)	60226/1396 (2.32)	2131/111 (5.21)	-	-	-	-
	3.00	2259/94 (4.16)	124662/5042 (4.04)	6335/344 (5.43)	3.00	3326/114 (3.43)	110580/3431 (3.1)	8823/274 (3.11)	3.00	2980/112 (3.76)	88684/3164 (3.57)	2904/126 (4.34)	-	-	-	-
	3.00	2200/72 (3.27)	87890/2799 (3.18)	4638/139 (2.99)	3.00	3462/134 (3.87)	81882/1905 (2.33)	14136/242 (1.71)	3.00	3380/123 (3.64)	89937/3303 (3.67)	Invalid ^c	-	-	-	-

^aCoverage depth was not provided by the laboratory. ^bOnly positive results from precision materials were summarized in the table. ^cOne measurement of P-1 material showed invalid result using next-generation sequencing from a laboratory. ND, not detected.

number of methods of two NGS and one IVD platform, we suggested more delicate means of EQA workflow tailored to ctDNA testing, using strictly designed low-level materials to assess assay sensitivity and precision in individual laboratories. Larger trial including more genotyping platforms including digital PCR with our sample preparation protocol is worthy of further investigation. In our pilot EQA, we used spiked ctDNA samples, which will facilitate standardization and improvement of ctDNA testing practices in clinical diagnostic laboratories.

Conflicts of Interest

The authors declare that there are no conflicts of interest regarding the publication of this paper.

Authors' Contributions

Yoonjung Kim and Saem Shin contributed equally to this work.

Acknowledgments

This study was supported by a grant of the Korean Health Technology R&D Project, Ministry of Health & Welfare, Republic of Korea (A120030).

Supplementary Materials

Supplementary Figure S1: workflow of the pilot external quality assurance scheme. Supplementary Figure S2: electropherograms of DNA sheared by ultrasonication and run on an Agilent D1000 ScreenTape System. Supplementary Table S1: external quality assurance material for evaluation of limit of detection. Supplementary Table S2: external quality assurance material for evaluation of precision. Supplementary Table S3: preparation material for performance evaluation. (*Supplementary Materials*)

References

- [1] M. A. Molina-Vila, C. Mayo-de-las-Casas, A. Giménez-Capitán et al., "Liquid biopsy in non-small cell lung cancer," *Frontiers in Medicine*, vol. 3, p. 69, 2016.
- [2] F. Diehl, K. Schmidt, M. A. Choti et al., "Circulating mutant DNA to assess tumor dynamics," *Nature Medicine*, vol. 14, no. 9, pp. 985–990, 2008.
- [3] S. Volik, M. Alcaide, R. D. Morin, and C. Collins, "Cell-free DNA (cfDNA): Clinical significance and utility in cancer shaped by emerging technologies," *Molecular Cancer Research*, vol. 14, no. 10, pp. 898–908, 2016.
- [4] M. Qiu, J. Wang, Y. Xu et al., "Circulating tumor DNA is effective for the detection of EGFR mutation in non-small cell lung cancer: a meta-analysis," *Cancer Epidemiology, Biomarkers & Prevention*, vol. 24, no. 1, pp. 206–212, 2015.
- [5] J. Luo, L. Shen, and D. Zheng, "Diagnostic value of circulating free DNA for the detection of EGFR mutation status in NSCLC: a systematic review and meta-analysis," *Scientific Reports*, vol. 4, article 6269, 2014.
- [6] R. A. Burrell, N. McGranahan, J. Bartek, and C. Swanton, "The causes and consequences of genetic heterogeneity in cancer evolution," *Nature*, vol. 501, no. 7467, pp. 338–345, 2013.
- [7] G. Siravegna, S. Marsoni, S. Siena, and A. Bardelli, "Integrating liquid biopsies into the management of cancer," *Nature Reviews Clinical Oncology*, vol. 14, no. 9, pp. 531–548, 2017.
- [8] J. O. Westgard and S. A. Westgard, "The quality of laboratory testing today: An assessment of σ metrics for analytic quality using performance data from proficiency testing surveys and the CLIA criteria for acceptable performance," *American Journal of Clinical Pathology*, vol. 125, no. 3, pp. 343–354, 2006.
- [9] E. Dequeker, S. Ramsden, W. W. Grody, T. T. Stenzel, and D. E. Barton, "Quality control in molecular genetic testing," *Nature Reviews Genetics*, vol. 2, no. 9, pp. 717–723, 2001.
- [10] J. H. van Krieken, A. G. Siebers, and N. Normanno, "European Consensus Conference for external quality assessment in molecular pathology," *Annals of Oncology*, vol. 24, no. 8, pp. 1958–1963, 2013.
- [11] S. Islam, A. Zeisel, S. Joost et al., "Quantitative single-cell RNA-seq with unique molecular identifiers," *Nature Methods*, vol. 11, no. 2, pp. 163–166, 2014.
- [12] M. Shugay, O. V. Britanova, E. M. Merzlyak et al., "Towards error-free profiling of immune repertoires," *Nature Methods*, vol. 11, no. 6, pp. 653–655, 2014.
- [13] A. Marchetti, J. F. Palma, L. Felicioni et al., "Early prediction of response to tyrosine kinase inhibitors by quantification of EGFR mutations in plasma of NSCLC patients," *Journal of Thoracic Oncology*, vol. 10, no. 10, pp. 1437–1443, 2015.
- [14] P. O'Donnell, J. Ferguson, J. Shyu et al., "Analytic performance studies and clinical reproducibility of a real-time PCR assay for the detection of epidermal growth factor receptor gene mutations in formalin-fixed paraffin-embedded tissue specimens of non-small cell lung cancer," *BMC Cancer*, vol. 13, article no. 210, 2013.
- [15] T. Xu, X. Kang, X. You et al., "Cross-platform comparison of four leading technologies for detecting EGFR mutations in circulating tumor DNA from non-small cell lung carcinoma patient plasma," *Theranostics*, vol. 7, no. 6, pp. 1437–1446, 2017.
- [16] K. S. Thress, R. Brant, T. H. Carr et al., "EGFR mutation detection in ctDNA from NSCLC patient plasma: a cross-platform comparison of leading technologies to support the clinical development of AZD9291," *Lung Cancer*, vol. 90, no. 3, pp. 509–515, 2015.
- [17] S. Jenkins, J. C.-H. Yang, S. S. Ramalingam et al., "Plasma ctDNA Analysis for Detection of the EGFR T790M Mutation in Patients with Advanced Non-Small Cell Lung Cancer," *Journal of Thoracic Oncology*, vol. 12, no. 7, pp. 1061–1070, 2017.
- [18] J. Uchida, K. Kato, Y. Kukita et al., "Diagnostic accuracy of noninvasive genotyping of EGFR in lung cancer patients by deep sequencing of plasma cell-free DNA," *Clinical Chemistry*, vol. 61, no. 9, pp. 1191–1196, 2015.
- [19] Y. Kukita, J. Uchida, S. Oba et al., "Quantitative identification of mutant alleles derived from lung cancer in plasma cell-free DNA via anomaly detection using deep sequencing data," *PLoS ONE*, vol. 8, no. 11, Article ID e81468, 2013.
- [20] K. S. Thress, C. P. Paweletz, E. Felip et al., "Acquired EGFR C797S mutation mediates resistance to AZD9291 in non-small cell lung cancer harboring EGFR T790M," *Nature Medicine*, vol. 21, no. 6, pp. 560–562, 2015.
- [21] C. W. Bennett, G. Berchem, Y. J. Kim, and V. El-Khoury, "Cell-free DNA and next-generation sequencing in the service of

- personalized medicine for lung cancer,” *Oncotarget* , vol. 7, no. 43, pp. 71013–71035, 2016.
- [22] C. P. Paweletz, A. G. Sacher, C. K. Raymond et al., “Bias-corrected targeted next-generation sequencing for rapid, multiplexed detection of actionable alterations in cell-free DNA from advanced lung cancer patients,” *Clinical Cancer Research*, vol. 22, no. 4, pp. 915–922, 2016.
- [23] S. Cui, W. Zhang, L. Xiong et al., “Use of capture-based next-generation sequencing to detect ALK fusion in plasma cell-free DNA of patients with non-small-cell lung cancer,” *Oncotarget* , vol. 8, no. 2, pp. 2771–2780, 2017.
- [24] V. Haselmann, P. Ahmad-Nejad, W. J. Geilenkeuser et al., “Results of the first external quality assessment scheme (EQA) for isolation and analysis of circulating tumour DNA (ctDNA),” *Clinical Chemistry and Laboratory Medicine*, 2017.
- [25] J. Fassunke, M. A. Ihle, D. Lenze et al., “EGFR T790M mutation testing of non-small cell lung cancer tissue and blood samples artificially spiked with circulating cell-free tumor DNA: results of a round robin trial,” *Virchows Archiv*, vol. 471, no. 4, pp. 509–520, 2017.

Research Article

Mutational Profiling of Non-Small-Cell Lung Cancer Resistant to Osimertinib Using Next-Generation Sequencing in Chinese Patients

Keke Nie,¹ Haiping Jiang,² Chunling Zhang,³ Chuanxin Geng,¹ Xiajuan Xu,³ Ling Zhang,¹ Hao Zhang,⁴ Zhongfa Zhang,¹ Ketao Lan,³ and Youxin Ji³

¹Department of Radiotherapy, Qingdao Cancer Hospital, Qingdao 266042, China

²Department of Oncology, The Affiliated Hospital of Qingdao University, Qingdao 266002, China

³Department of Oncology, The Affiliated Qingdao Central Hospital of Qingdao University, Qingdao 266042, China

⁴Oncology Genemic, Geneplus Beijing, Beijing 100010, China

Correspondence should be addressed to Youxin Ji; 123456789ji@gmail.com

Received 19 December 2017; Revised 23 January 2018; Accepted 6 February 2018; Published 11 March 2018

Academic Editor: Valli De Re

Copyright © 2018 Keke Nie et al. This is an open access article distributed under the Creative Commons Attribution License, which permits unrestricted use, distribution, and reproduction in any medium, provided the original work is properly cited.

Purpose. To identify the somatic mutated genes for optimal targets of non-small-cell lung cancer after resistance to osimertinib treatment. **Patients and Methods.** Study patients all had advanced lung adenocarcinoma and acquired resistance to osimertinib as a second- or third-line treatment. These patients had harboring EGFR T790M mutation before osimertinib treatment, which was confirmed by Amplification Refractory Mutation System (ARMS) PCR or Next-Generation Sequencing (NGS). After resistance to osimertinib treatment, tumor tissue was collected by core needle biopsy. DNA was extracted from 15 × 5 um sliced section of formalin-fixed paraffin-embedded (FFPE) material and NGS was done. The genetic changes were analyzed. **Results.** A total of 9 Chinese patients were studied, 5 females and 4 males, age 51–89 years. After progression with osimertinib treatment, core needle biopsy was performed and next-generation sequencing was performed. Nine patients had harboring 62 point mutations, 2 altered gene copies, 2 amplifications, and 1 EML4-ALK gene fusion. No MET or HER2 amplification was found in this cohort study. Nine patients still maintained initial EGFR 19 del or L858R activating mutations, while 7 of them kept EGFR T790M mutations. Among the 7 patients, 5 had secondary EGFR C797S and/or C797G mutations, which all happened in the same allele with T790M mutation. All patients were treated with targets therapies, chemotherapy, or best supportive care (BSC) in accordance with NGS genetic results and patients' performance status; 7 of them are still alive and 2 of them died of disease progression at last follow-up. **Conclusions.** EGFR C797S/G mutation and the same one presented on the same allele with EGFR T790M mutation were the most common mutation feature and played a key role in resistance to osimertinib in Chinese patients with NSCLC. Tumor cells losing T790M mutation and maintaining EGFR activating mutation might benefit from first-generation EGFR-TKI treatment.

1. Introduction

Epidermal growth factor receptor (EGFR) T790M mutation is the most common genetic change for patients of non-small-cell lung cancer (NSCLC) harboring EGFR after resistance to first-generation EGFR tyrosine kinase inhibitor (TKI) [1]. The substitution of threonine with methionine at amino acid position 790 (T790M), which reduces the ability of ATP-competitive reversible EGFR-TKI binding to EGFR tyrosine kinase domain, results in cancer cells resistant to gefitinib and

erlotinib [1]. Osimertinib (Tagrisso, AZD9291, AstraZeneca) is the only FDA approved drug for lung cancer patients harboring EGFR T790M mutation. After a median of 9.6–11.0 months' remission with osimertinib treatment, tumors will inevitably have progress. Although a lot of studies had been done, the molecular mechanisms of resistance are not yet fully understood [2, 3].

Next-generation sequencing (NGS) is a cost-effective technology capable of screening several genes simultaneously [4]. It is commonly used nowadays for sequencing mutated

TABLE 1: Patients' characteristics.

#	Sex	Age (yrs)	EGFR type	Tissues and genetic testing			
				Before osimertinib		After osimertinib	
1	F	62	L858R	Lung	NGS	Pleura	NGS
2	M	85	19 del	SL	ARMs-PCR	Lung	NGS
3	M	66	19 del	Bone	ARMs-PCR	Lung	NGS
4	F	79	L858R	Lung	ARMs-PCR	Lung	NGS
5	F	89	19 del	Lung	NGS	Lung	NGS
6	F	66	19 del	Serum	ARMs-PCR	Bone	NGS
7	M	56	19 del	Lung	ARMs-PCR	Lung	NGS
8	F	75	19 del	Pleura	ARMs-PCR	Pleura	NGS
9	M	51	19 del	Lung	ARMs-PCR	Lung	NGS
Median		66					

SL denotes supraclavicular lymph node.

tumor genes with tumor tissue or plasma to identify and classify molecular subtypes, to address the unmet need for new drug targets in its category [5]. The mechanism of resistance to osimertinib or other third-generation EGFR-TKI was extremely complicated, and the reported results of mutation sites and/or mutation rates were much different among studies. Phenotype transformation, EGFR new point mutation, pathways activation, or targets loss were the strongest possibilities. Most studies reported that C797S mutation happened in 20–30% of patients after osimertinib initiation [6, 7]. The EGFR C797S mutation conferred resistance to third-generation EGFR-TKI. C797S mutation had been identified in cis or in trans with T790M mutation in tumor specimens from patients who experienced treatment failure with third-generation EGFR-TKIs. C797S and T790M mutation in trans were sensitive to first-generation plus third-generation EGFR-TKI but in cis they would be resistant to all [8]. Therefore, to elicit the mutated driver genes after resistance to third-generation EGFR-TKI is critically important.

2. Material and Methods

Patients enrolled in the study all had histologically confirmed metastatic lung adenocarcinoma. EGFR T790M mutation was confirmed by tumor tissue or serum, which was tested by the ARMS PCR or Next-Generation Sequencing (NGS) before osimertinib treatment. Patients were all treated with osimertinib with a dose of 80 mg oral daily after resistance to gefitinib or erlotinib treatment. Osimertinib acquired resistance was confirmed by CT or PET-CT scan according to RECIST 1.1 [9]. Core needle biopsy (CNB) guided by CT scan was performed. DNA was extracted from 15 × 5 um sliced sections of FFPE tumor tissue. Tumor area was evaluated and confirmed by pathologist. In order to ensure adequacy of sequences and mutation detection, at least 20% tumor area on each slice was set as a minimum. 10 ml blood was drawn and centrifuged for sequencing control and for germline genes mutation test. NGS was performed with HiSeq3000/HiSeq4000 Illumina techniques. 4278 exons of 288 common genes; intron, promoter, and fusion of 38 genes;

and coding area of 728 genes were tested for somatic mutations. 11 germline mutations were also tested. The ultra-deep coverage of genes of interest was 1,000x for tumor tissue and 10,000x for serum.

This study was approved by the Ethics Committee of Affiliated Qingdao Central Hospital of Qingdao University, and Informed consent to reveal patients' medical history for publishing was obtained before submitting this manuscript.

3. Results

A total of 9 Chinese patients were studied. There were 5 female patients and 4 male patients, median age 66-year, range 51–89. All patients were core needle biopsied and adenocarcinomas were confirmed by pathologists; there was no SCLC transformation found. Tissues obtained sources for testing and genetic testing methodologies were listed (Table 1). There were 62 point mutations, 2 altered gene copies, 2 amplifications, and 1 EML4-ALK gene fusion found in these 9 patients (Table 2). No MET or HER2 amplification was found in this cohort study. All the 9 patients still maintained initial EGFR 19 del or L858R activating mutations; meanwhile, 7 of them kept EGFR T790M mutations. Furthermore, among the 7 patients, 5 had secondary EGFR C797S and/or C797G mutations, which all happened in the same allele with T790M mutation. Two patients had EGFR C797G 2389T>G mutations; 1 had EGFR C797S 2390G>C mutation; 1 had EGFR C797S 2389 T>A and 2390 G>C 2 points mutations; and 1 had EGFR C797S 2389 T>A, 2390 G>C 2 points and C797G 2389 T>G mutations. Subjects #1 and #5 had acquired EGFR T790M mutations tested by NGS, but lost them after osimertinib treatment. There were 9 point mutations before osimertinib treatment, which increased to 22 point mutations after resistant to osimertinib. Most pre-osimertinib point mutations could be tested after osimertinib treatment with the exception of T790M mutation and WSCD2 mutation (Table 3). The above 2 patients were treated back with gefitinib, one having had stable disease for 3 months, the other one just started. Subject #3 had a low mutation rate of EML4-ALK fusion and simultaneously had EGFR L858R, T790M mutation, and C797G mutation

TABLE 3: Mutation types and mutant allele fraction (MAF) (%) changes.

#1		#5					
Before osimertinib		After osimertinib		Before osimertinib		After osimertinib	
Mutation	Rate	Mutation	Rates	Mutation	Rates	Mutation	Rates
L858R	42.9	L858R	63.2	19 del	9.6	19 del	2.1
IL7R	19.1	IL7R	31.5	T790M	1.1	PIK3CA	1.8
T790M	5.7	TENM3	27.1	TP53	7.11	TP53	1.7
CCND3	5.8	CCND3	14.3			RNASEL	1.2
WSCD2	5.1	ROS1 (6737 G>A)	2.9			TET2	0.8
FGFR3A	4.1	FGFR3	1.9			MAP3K1	0.8
		XPC	1.5				
		ATM	1.5				
		FAM135B	1.2				
		PALB2	1.1				
		MLL	1				
		ROS1 (1611A>G)	1				
		CDKN2A	0.2				
		Altered copy					
		CDKN2B DEL	0.3				
		CDKN2A DEL	0.2				

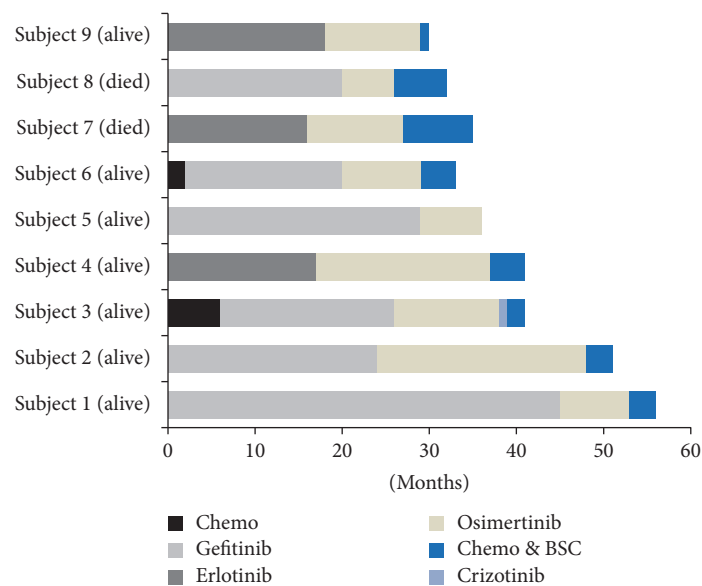


FIGURE 1: Treatment and outcomes.

and was treated with crizotinib but had progression in 1 month. He was treated with pemetrexed for 2 cycles and had a confirmed partial response. Subject #6 had harboring high MAF of EGFR EXON21 (c.2500G>T, p.V834L), 19 del, TP53, T790M, and C797G mutations (91.1%, 85.5%, 85.2%, 61.5%, 36.6%, resp.) and was resistant to gefitinib combined with osimertinib but had stable disease with cisplatin plus pemetrexed chemotherapy. Subject #7 had EGFR C797S (2389 T>A, 2390 G>C) mutations and was treated with erlotinib, osimertinib, and cetuximab but had progression in 2 months and died 6 months later. Subject #8 had EGFR 19 del and T790M and C797S/G mutations and was treated with

BSC and died after 6 months. The other 3 patients were in chemotherapy or BSC at last follow-up on December 15, 2017 (Figure 1).

4. Discussion

Activation of epidermal growth factor receptor (EGFR) triggers antiapoptotic signaling, proliferation, angiogenesis, invasion, and metastasis, which lead to development and progression of NSCLC [10]. Inhibition of EGFR by tyrosine kinase inhibitors such as gefitinib and erlotinib has increased

tumor response and prolonged patients' survival. However, acquired resistance will finally happen, with a progression-free survival (PFS) of around 9–13 months [11, 12]. The substitution of threonine with methionine at amino acid position 790 (T790M), as the second mutation in EGFR, is the most common resistance mechanism and is detected in tumor cells from more than 50–60% of patients after disease progression. This mutation enhances ATP affinity and reduces the ability of ATP-competitive reversible EGFR-TKI binding to EGFR tyrosine kinase domain, which results in cancer cells resistant to gefitinib and erlotinib [1]. Osimertinib is an oral, potent, irreversible EGFR-TKI and inhibits kinase activity of EGFR sensitive mutation and T790M resistant mutation [13, 14]. Osimertinib for second-line treatment in EGFR T790M positive NSCLC was associated with a response rate of 61% and PFS of 9.6 months [13]. But the mechanism of osimertinib resistance is much complicated [6, 7]. Third-generation EGFR-TKIs (WZ 4002, rociletinib, osimertinib) have pyrimidine structure and covalent bond with EGFR Cys797 at ATP binding pocket. Cys797 point mutation (C797S/G/R) intercepts 3rd-generation EGFR-TKIs covalent binding to Cys797 at ATP binding pocket, which results in drug resistance [15, 16]. Thress et al. [17] reported results of 15 patients NGS after osimertinib progression: 6/15 cases acquired the C797S mutations, 5/15 cases maintained the T790M mutations but did not acquire the C797S mutation, and 4/15 cases lost the T790M mutations. In our results, all 5 acquired C797S/G mutations, patients still maintained EGFR T790M mutations, and C797S/G and T790M mutations were in the same allele. In *in vitro* study, tumor cells harboring C797S mutation without T790M mutation are still sensitive to quinazoline-based EGFR inhibitors like gefitinib or erlotinib, and, harboring EGFR C797S in trans with T790M mutations are sensitive to a combination of first- and third-generation EGFR-TKI and in cis are resistant to all current EGFR inhibitors [18, 19].

HER2 or MET amplifications were also reported in osimertinib-resistant NSCLC patients. EGFR T790M mutation and HER2 amplification appeared to be mutually exclusive while MET amplification occurred with or without EGFR T790M mutation [20, 21]. It was hypothesized that tumor heterogeneity, HER2, or MET subclones initiated an independent pathway for tumor progression [17, 22].

There were 2 patients who had acquired low MAF PIK3CA mutations; 1 patient had acquired NOTCH3, IGF1R, and PIK3B mutations. These point mutations are all associated with osimertinib use and might correlate with drug resistance [23], which needs further study to elicit new methods to overcome it.

Small-cell lung cancer transformation is rare in NSCLC patients resistant to EGFR-TKIs treatment. It might preexist before first-/second-/third-generation EGFR-TKIs treatment [24]. So, rebiopsy is critically important in the diagnosis of SCLC transformation after resistance to 3rd-generation EGFR-TKIs.

In our study, 2 patients had been tested by NGS before and after osimertinib treatment. There were 5 point mutations excluding EGFR activating mutation and EGFR T790M mutation before osimertinib treatment. After resistance to

osimertinib, 16 new point mutations were found except loss of T790M mutation and WSCD2 mutation. This phenomenon indicated that the more the lines of EGFR-TKIs therapies were initiated, the more the point mutations would happen. These 2 patients were treated back with gefitinib; 1 had stable disease for 3 months. It was indicated that 1st-generation EGFR-TKI could be used in patients who lost T790M mutation but maintained EGFR 19 del or L858R activating mutation. 1 patient had low rate EML4-ALK gene fusion (0.9%), EGFR 19 del (2.8%), and T790M (4.6%) and C797G (2.6%) mutations and was treated with crizotinib and progressed in 1 month but responded to chemotherapy thereafter. It might be that tumor cells with EML4-ALK gene fusion were too low. Subjects #6 and #7 had high MAF of EGFR 19 del, T790M, and C797S or C797G mutations and were resistant to 1st- and 3rd-generation combination. So, chemotherapy is the optimal treatment for C797S/G in cis with T790M mutation before new drugs can overcome it.

In this study, 5/9 (55.6%) patients had acquired C797S/G mutations, all maintained with T790M mutation in the same allele. In these 5 patients, 3 times of c.2389T>G, 2 times of c.2389T>A, and 3 times of c.2390G>C point mutations were found. The C797S/G mutations were maintained with T790M mutation in cis, and C797S/G mutations happened to be higher than previous report [17]. In the 9 patients, there were a total of 62 point mutations, 2 altered copy numbers, and 2 amplifications, and 1 patient with 2 points C797S (2389 T>A, 2390 G>C) mutations and 1 patient had 2 points C797S and C797G mutations, which made the mechanism of resistance to osimertinib more complicated.

5. Conclusions

Genetic mutation is much complicated after osimertinib treatment in EGFR positive non-small-cell lung cancer. EGFR C797S/G mutation and the same one presented on the same allele with EGFR T790M mutation were the most common mutation feature and played a key role in resistance to osimertinib in Chinese patients with NSCLC. Tumor cells losing T790M mutation and maintaining EGFR activating mutation might be benefit from first-generation EGFR-TKI treatment. To elicit a chemical to overcome EGFR C797S/G point mutation with T790M mutation in the same allele is critically important.

Conflicts of Interest

The authors declare that there are no conflicts of interest regarding the publication of this article.

Authors' Contributions

Keke Nie and Haiping Jiang made equal contributions to this study.

Acknowledgments

The authors sincerely appreciate the superb help by Qing Yan and Ye Wang for genetic consultation at Department of

Central Laboratory, the Affiliated Central Hospital of Qingdao University. They thank Professor Wendy Wang of Feinstein Institute for Medical Research and Professor John Califra in New York for helping in editing the manuscript. This study was supported by Grants from National Health and Family Planning Commission of Peoples Republic of China, Medical Technology Research Center for Health Development Grants W2012FZ007 (Youxin Ji).

References

- [1] K. Suda, R. Onozato, Y. Yatabe, and T. Mitsudomi, "EGFR T790M mutation: A double role in lung cancer cell survival?" *Journal of Thoracic Oncology*, vol. 4, no. 1, pp. 1–4, 2009.
- [2] Y. Yin and J. Li, "Osimertinib in EGFR T790M - Positive lung cancer," *The New England Journal of Medicine*, vol. 376, no. 20, p. 1993, 2017.
- [3] F. H. Knebel, F. Bettoni, A. K. Shimada et al., "Sequential liquid biopsies reveal dynamic alterations of EGFR driver mutations and indicate EGFR amplification as a new mechanism of resistance to osimertinib in NSCLC," *Lung Cancer*, vol. 108, pp. 238–241, 2017.
- [4] I. Vanni, S. Coco, A. Truini et al., "Next-generation sequencing workflow for NSCLC critical samples using a targeted sequencing approach by ion torrent PGM platform," *International Journal of Molecular Sciences*, vol. 16, no. 12, pp. 28765–28782, 2015.
- [5] V. H. Veldore, S. Patil, C. Satheesh et al., "Genomic profiling in a homogeneous molecular subtype of non-small cell lung cancer: an effort to explore new drug targets," *Indian Journal of Cancer*, vol. 52, no. 2, pp. 243–248, 2015.
- [6] A. Oztan, S. Fischer, A. B. Schrock et al., "Emergence of EGFR G724S mutation in EGFR-mutant lung adenocarcinoma post progression on osimertinib," *Lung Cancer*, vol. 111, pp. 84–87, 2017.
- [7] Z. Tang, M. Su, X. Guo et al., "Increased expression of IRE1 α associates with the resistant mechanism of osimertinib (AZD9291)-resistant non-small cell lung cancer HCC827/OSIR cells," *Anti-Cancer Agents in Medicinal Chemistry*, vol. 17, 2017.
- [8] N. Hidaka, E. Iwama, N. Kubo et al., "Most T790M mutations are present on the same EGFR allele as activating mutations in patients with non-small cell lung cancer," *Lung Cancer*, vol. 108, pp. 75–82, 2017.
- [9] L. H. Schwartz, S. Litière, E. De Vries et al., "RECIST 1.1 - Update and clarification: From the RECIST committee," *European Journal of Cancer*, vol. 62, pp. 132–137, 2016.
- [10] J.-Q. Zhu, W.-Z. Zhong, G.-C. Zhang et al., "Better survival with EGFR exon 19 than exon 21 mutations in gefitinib-treated non-small cell lung cancer patients is due to differential inhibition of downstream signals," *Cancer Letters*, vol. 265, no. 2, pp. 307–317, 2008.
- [11] C. Zhou, Y.-L. Wu, G. Chen et al., "Erlotinib versus chemotherapy as first-line treatment for patients with advanced EGFR mutation-positive non-small-cell lung cancer (OPTIMAL, CTONG-0802): a multicentre, open-label, randomised, phase 3 study," *The Lancet Oncology*, vol. 12, no. 8, pp. 735–742, 2011.
- [12] T. S. Mok, Y.-L. Wu, S. Thongprasert et al., "Gefitinib or carboplatin-paclitaxel in pulmonary adenocarcinoma," *The New England Journal of Medicine*, vol. 361, no. 10, pp. 947–957, 2009.
- [13] P. A. Jänne, J. Chih-Hsin Yang, D.-W. Kim et al., "AZD9291 in EGFR inhibitor-resistant non-small-cell lung cancer," *The New England Journal of Medicine*, vol. 372, no. 18, pp. 1689–1699, 2015.
- [14] T. Jiang and C. Zhou, "Clinical activity of the mutant-selective EGFR inhibitor AZD9291 in patients with EGFR inhibitor-resistant non-small cell lung cancer," *Translational Lung Cancer Research*, vol. 3, no. 6, pp. 370–372, 2014.
- [15] Y. Jia, C.-H. Yun, E. Park et al., "Overcoming EGFR(T790M) and EGFR(C797S) resistance with mutant-selective allosteric inhibitors," *Nature*, vol. 534, no. 7605, pp. 129–132, 2016.
- [16] R. Menon, J. Müller, P. Schneider et al., "A Novel EGFR C797 Variant Detected in a Pleural Biopsy Specimen from an Osimertinib-Treated Patient Using a Comprehensive Hybrid Capture-Based Next-Generation Sequencing Assay," *Journal of Thoracic Oncology*, vol. 11, no. 9, pp. e105–e107, 2016.
- [17] K. S. Thress, C. P. Paweletz, E. Felip et al., "Acquired EGFR C797S mutation mediates resistance to AZD9291 in non-small cell lung cancer harboring EGFR T790M," *Nature Medicine*, vol. 21, no. 6, pp. 560–562, 2015.
- [18] Z. Wang, J.-J. Yang, J. Huang et al., "Lung Adenocarcinoma Harboring EGFR T790M and In Trans C797S Responds to Combination Therapy of First- and Third-Generation EGFR TKIs and Shifts Allelic Configuration at Resistance," *Journal of Thoracic Oncology*, 2017.
- [19] D. Ercan, H. G. Choi, C.-H. Yun et al., "EGFR mutations and resistance to irreversible pyrimidine-based EGFR inhibitors," *Clinical Cancer Research*, vol. 21, no. 17, pp. 3913–3923, 2015.
- [20] J. A. Engelman, K. Zejnullahu, T. Mitsudomi et al., "MET amplification leads to gefitinib resistance in lung cancer by activating ERBB3 signaling," *Science*, vol. 316, no. 5827, pp. 1039–1043, 2007.
- [21] Z. Piotrowska, M. J. Niederst, C. A. Karlovich et al., "Heterogeneity Underlies the Emergence of EGFR T790 Wild-Type Clones Following Treatment of T790M-Positive Cancers with a Third-Generation EGFR Inhibitor," *Cancer Discovery*, vol. 5, no. 7, pp. 713–722, 2015.
- [22] D. Planchard, Y. Loriot, F. André et al., "EGFR-independent mechanisms of acquired resistance to AZD9291 in EGFR T790M-positive NSCLC patients," *Annals of Oncology*, vol. 26, no. 10, Article ID mdv319, pp. 2073–2078, 2015.
- [23] S. S. Ramalingam, J. C. Yang, C. K. Lee et al., "Osimertinib As First-Line Treatment of EGFR Mutation-Positive Advanced Non-Small-Cell Lung Cancer," *Journal of Clinical Oncology*, Article ID JCO2017747576, 2017.
- [24] R. Minari, P. Bordi, M. Del Re et al., "Primary resistance to osimertinib due to SCLC transformation: Issue of T790M determination on liquid re-biopsy," *Lung Cancer*, vol. 115, pp. 21–27, 2018.